ISSN

Period.

VOL. 559 NOS. 1 + 2 OCTOBER

3rd Int. Symp. on High Performance Capillary Electrophoresis
San Diego, CA, February 3–6, 1991

JOURNAL OF CHROMATOGRAPHY

INCLUDING ELECTROPHORESIS AND OTHER SEPARATION METHOD

SYMPOSIUM VOLUMES

ELSEVIER

JOURNAL OF CHROMATOGRAPHY

Scope. The *Journal of Chromatography* publishes papers on all aspects of chromatography, electrophoresis and related methods. Contributions consist mainly of research papers dealing with chromatographic theory, instrumental development and their applications. The section *Biomedical Applications*, which is under separate editorship, deals with the following aspects: developments in and applications of chromatographic and electrophoretic techniques related to clinical diagnosis or alterations during medical treatment; screening and profiling of body fluids or tissues with special reference to metabolic disorders; results from basic medical research with direct consequences in clinical practice; drug level monitoring and pharmacokinetic studies; clinical toxicology; analytical studies in occupational medicine.

Submission of Papers. Manuscripts (in English; *four* copies are required) should be submitted to: Editorial Office of *Journal of Chromatography*, P.O. Box 681, 1000 AR Amsterdam, The Netherlands, Telefax (+31-20) 5862 304, or to: The Editor of *Journal of Chromatography, Biomedical Applications*, P.O. Box 681, 1000 AR Amsterdam, The Netherlands. Review articles are invited or proposed by letter to the Editors. An outline of the proposed review should first be forwarded to the Editors for preliminary discussion prior to preparation. Submission of an article is understood to imply that the article is original and unpublished and is not being considered for publication elsewhere. For copyright regulations, see below.

Publication. The *Journal of Chromatography* (incl. *Biomedical Applications*) has 38 volumes in 1991. The subscription prices for 1991 are:

J. Chromatogr. (incl. *Cum. Indexes, Vols. 501–550*) + *Biomed. Appl.* (Vols. 535–572):
Dfl. 7220.00 plus Dfl. 1140.00 (p.p.h.) (total *ca.* US$ 4400.00)

J. Chromatogr. (incl. *Cum. Indexes, Vols. 501–550*) only (Vols. 535–561):
Dfl. 5859.00 plus Dfl. 810.00 (p.p.h.) (total *ca.* US$ 3510.00)

Biomed. Appl. only (Vols. 562–572):
Dfl. 2387.00 plus Dfl. 330.00 (p.p.h.) (total *ca.* US$ 1430.00).

Subscription Orders. The Dutch guilder price is definitive. The US$ price is subject to exchange-rate fluctuations and is given as a guide. Subscriptions are accepted on a prepaid basis only, unless different terms have been previously agreed upon. Subscriptions orders can be entered only by calender year (Jan.–Dec.) and should be sent to Elsevier Science Publishers, Journal Department, P.O. Box 211, 1000 AE Amsterdam, The Netherlands, Tel. (+31-20) 5803 642, Telefax (+31-20) 5803 598, or to your usual subscription agent. Postage and handling charges include surface delivery except to the following countries where air delivery via SAL (Surface Air Lift) mail is ensured: Argentina, Australia, Brazil, Canada, Hong Kong, India, Israel, Japan*, Malaysia, Mexico, New Zealand, Pakistan, PR China, Singapore, South Africa, South Korea, Taiwan, Thailand, USA. * For Japan air delivery (SAL) requires 50% additional charge of the normal postage and handling charge. For all other countries airmail rates are available upon request. Claims for missing issues must be made within three months of our publication (mailing) date, otherwise such claims cannot be honoured free of charge. Back volumes of the *Journal of Chromatography* (Vols. 1–534) are available at Dfl. 208.00 (plus postage). Customers in the USA and Canada wishing information on this and other Elsevier journals, please contact Journal Information Center, Elsevier Science Publishing Co. Inc., 655 Avenue of the Americas, New York, NY 10010, USA, Tel. (+1-212) 633 3750, Telefax (+1-212) 633 3990.

Abstracts/Contents Lists published in Analytical Abstracts, Biochemical Abstracts, Biological Abstracts, Chemical Abstracts, Chemical Titles, Chromatography Abstracts, Clinical Chemistry Lookout, Current Contents/Life Sciences, Current Contents/Physical, Chemical & Earth Sciences, Deep-Sea Research/Part B: Oceanographic Literature Review, Excerpta Medica, Index Medicus, Mass Spectrometry Bulletin, PASCAL-CNRS, Pharmaceutical Abstracts, Referativnyi Zhurnal, Research Alert, Science Citation Index and Trends in Biotechnology.

See inside back cover for Publication Schedule, Information for Authors and information on Advertisements.

0021-9673/91/$03.50

Printed in The Netherlands

For Contents, see p. VII

FOR ADVERTISING INFORMATION PLEASE CONTACT OUR ADVERTISING REPRESENTATIVES

USA/CANADA

Weston Media Associates

Mr. Daniel S. Lipner
P.O. Box 1110, GREENS FARMS, CT 06436-1110
Tel: (203) 261-2500, Fax: (203) 261-0101

GREAT BRITAIN

T.G. Scott & Son Ltd.

Tim Blake
Portland House, 21 Narborough Road
COSBY, Leicestershire LE9 5TA
Tel: (0533) 753-333, Fax: (0533) 750-522
Mr. M. White or Mrs. A. Curtis
30-32 Southampton Street, LONDON WC2E 7HR
Tel: (071) 240 2032, Fax: (071) 379 7155,
Telex: 299181 adsale/g

JAPAN

ESP - Tokyo Branch

Mr. S. Onoda
20-12 Yushima, 3 chome, Bunkyo-Ku
TOKYO 113
Tel: (03) 3836 0810, Fax: (03) 3839-4344
Telex: 02657617

REST OF WORLD

ELSEVIER SCIENCE PUBLISHERS

Ms. W. van Cattenburch
P.O. Box 211, 1000 AE AMSTERDAM,
The Netherlands
Tel: (20) 515.3220/21/22, Telex: 16479 els vi nl
Fax: (20) 683.3041

Chemometrics Tutorials

Collected from Chemometrics and Intelligent Laboratory Systems - An International Journal, Volumes 1-5

edited by **D.L. Massart,** *Brussels,* **R.G. Brereton,** *University of Bristol, Bristol, UK,* **R.E.Dessy,** *Blacksburg, VA,* **P.K. Hopke,** *Potsdam, NY,* **C.H. Spiegelman,** *College Station, TX,* **W. Wegscheider,** *Graz, Austria*

The journal *Chemometrics and Intelligent Laboratory Systems* has a specific policy of publishing tutorial papers, (i.e. articles aiming to discuss and illustrate the application of chemometric and other techniques) solicited from leading experts in the varied disciplines relating to this subject. This book comprises reprints of tutorials from the first 5 volumes of this journal, covering the period from late 1986 to mid 1989. The authors of the papers include analytical, organic and environmental chemists, statisticians, pharmacologists, geologists, geochemists, computer scientists and biologists, which reflects the strong interdisciplinary communication. The papers have been reorganized into major themes, covering most of the main areas of chemometrics. This book is intended both as a personal reference text and as a useful background for courses in chemometrics and laboratory computing.

1990 viii + 428 pages (Paperback)
Price: US$ 66.75 / Dfl. 130.00
ISBN 0-444-88837-3

Elsevier Science Publishers
P.O. Box 211, 1000 AE Amsterdam, The Netherlands
P.O. Box 882, Madison Square Station, New York, NY 10159, USA

An authoritative review... highly recommended...

Optimization of Chromatographic Selectivity

A Guide to Method Development

by **P. Schoenmakers,** *Philips Research Laboratories, Eindhoven, The Netherlands*

(Journal of Chromatography Library, 35)

"The contents of this book have been put together with great expertise and care, and represent an authoritative review of this very timely topic... highly recommended to practising analytical chemists and to advanced students." (Jnl. of Chromatography)

"...an important contribution by a worker who has been in the field almost from its inception and who understands that field as well as anyone. If one is serious about method development, particularly for HPLC, this book will well reward a careful reading and will continue to be useful for reference purposes." (Mag. of Liquid & Gas Chromatography)

This is the first detailed description of method development in chromatography - the overall process of which may be summarized as: method selection, phase selection, selectivity optimization, and system optimization. All four aspects receive attention in this eminently readable book.

The first chapter describes chromatographic theory and nomenclature and outlines the method development process. Guidelines are then given for method selection and quantitative concepts for characterizing and classifying chromatographic phases. Selective separation methods (from both GC and LC) are given - the main parameters of each method are identified and simple, quantitative relations are sought to describe their effects. Criteria by which to judge the quality of separation are discussed with clear recommendations for different situations. The specific problems involved in the optimization of chromatographic selectivity are explained. Optimization procedures, illustrated by examples, are described and compared on the basis of a number of criteria. Suggestions are made both for the application of different procedures and for further research. The optimization of programmed analysis receives special attention, and the last chapter summarizes the optimization of the chromatographic system, including the optimization of the efficiency, sensitivity and instrumentation.

Those developing chromatographic methods or wishing to improve existing methods will value the detailed, structured way in which the subject is presented. Because optimization procedures and criteria are described as elements of a complete optimization package, the book will help the reader to understand, evaluate and select current and future commercial systems.

Contents: 1. Introduction. 2. Selection of Methods. 3. Parameters Affecting Selectivity. 4. Optimization Criteria. 5. Optimization Procedures. 6. Programmed Analysis. 7. System Optimization. Indexes.

1986 1st repr. 1987 xvi + 346 pages
US$ 110.50 / Dfl. 210.00
ISBN 0-444-42681-7

ELSEVIER SCIENCE PUBLISHERS

P.O. Box 211, 1000 AE Amsterdam, The Netherlands
P.O. Box 1663, Grand Central Station, New York, NY 10163, USA

(Data Handling in Science and Technology, 5)

PCs for Chemists

edited by: **J. Zupan**, *University of Ljubljana, Yugoslavia*

PCs for Chemists is a handbook on how, when and with what kind of software a chemist should use a PC. Being a beginners' guide, it does not require any specific knowledge about computers. The book covers word processors, spreadsheets, compilers and databases for chemical applications, and it comprises ten contributions each describing one or two different applications and a suggestion for the best choice. Information on how a PC can be linked to instruments, other computers and data networks is also provided.

PCs for Chemists should prove invaluable for all courses covering computer applications to chemistry, pharmacy, biology, and metallurgy.

1990 xvi + 212 pages
Price: US$ 100.00 / Dfl. 195.00
ISBN 0-444-88623-0

Contents:

ELSEVIER SCIENCE PUBLISHERS

P.O. Box 211, 1000 AE Amsterdam, The Netherlands
P.O. Box 882, Madison Square Station, New York, NY 10159, USA

JOURNAL OF CHROMATOGRAPHY

VOL. 559 (1991)

JOURNAL of CHROMATOGRAPHY

INCLUDING ELECTROPHORESIS AND OTHER SEPARATION METHODS

SYMPOSIUM VOLUMES

ELSEVIER
AMSTERDAM — LONDON — NEW YORK — TOKYO

J. Chromatogr., Vol. 559 (1991)

San Diego Skyline. Nestled between the mountains on the east and the Pacific on the west, San Diego's modern skyline is an imposing contrast to its surroundings. San Diego is the second largest city in California, but still retains its natural beauty. Photo released by San Diego Convention & Visitors Bureau.

0021-9673/91/$03.50

Printed in The Netherlands

SYMPOSIUM VOLUME

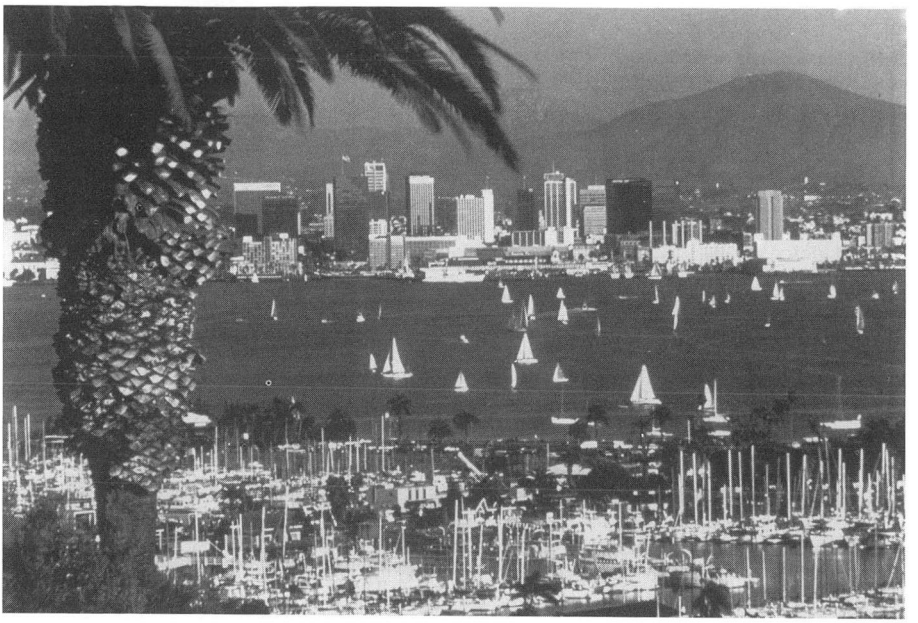

THIRD INTERNATIONAL SYMPOSIUM ON HIGH PERFORMANCE CAPILLARY ELECTROPHORESIS

San Diego, CA (U.S.A.), February 3–6, 1991

Guest Editor

J. W. JORGENSON
(Chapel Hill, NC)

VOL. 559, NOS. 1+2 JOURNAL OF CHROMATOGRAPHY OCTOBER 18, 1991

CONTENTS

3rd INTERNATIONAL SYMPOSIUM ON HIGH PERFORMANCE CAPILLARY ELECTROPHORESIS, SAN DIEGO, CA, FEBRUARY 3–6, 1991

In articles with more than one author, the name of the author to whom correspondence should be addressed is indicated in the article heading by a 6-pointed asterisk (*)

Journal of Chromatography, 559 (1991) 1
Elsevier Science Publishers B.V., Amsterdam

FOREWORD

The *Third International Symposium on High Performance Capillary Electrophoresis (HPCE '91)* was held in San Diego, CA, on February 4–6, 1991. There were approximately 500 participants from around the world, 160 presentations, and exhibits of CE instruments and supplies by 18 companies. Particularly noteworthy were the increases, over the previous two meetings, in the number of papers and exhibitors. Advances continue to be made across the entire spectrum of basic theory, instrumentation and techniques of CE. Research into the application of CE to practical problems was noticeably increased.

Special thanks are due to Shirley Schlessinger, Symposium Manager, for her tireless efforts and sense of humor. These traits proved especially helpful during preparation for a conference held amid a general economic recession and war in the Persian gulf. The assistance of the Scientific Committee of Stellan Hjertén, Shigeru Terabe, Frans Everaerts, and especially Barry Karger (as co-organizer) is gratefully acknowledged. Zdeněk Deyl is thanked for his fine editorial contribution in the production of this volume. Finally, the Bay Area Chromatography Colloquium is to be acknowledged for their assistance in providing travel grants for students to attend this meeting.

Those working in the field of capillary electrophoresis can look forward to HPCE '92 in Amsterdam, February 10–13, 1992. This will be the first meeting in this series outside the USA. The meeting has been lengthened from three days to four days in order to better accommodate the greatly increasing number of presentations appearing in this series of meetings.

Chapel Hill, NC, USA JAMES W. JORGENSON

Journal of Chromatography, 559 (1991) 3–26
Elsevier Science Publishers B.V., Amsterdam

CHROM. 23 416

Mathematical model describing dispersion in free solution capillary electrophoresis under stacking conditions

ANDERS VINTHER*
Department of Fermentation Physiology, Novo Nordisk, Lagergårdsvej 2, DK-2820 Gentofte (Denmark)
and
HENRIK SØEBERG
Department of Chemical Engineering, Technical University of Denmark, Building 229, DK-2800 Lyngby (Denmark)

ABSTRACT

From experiments a mathematical model is derived that quantitatively describes the dispersion processes in free solution capillary electrophoresis (FSCE) under both stacking and non-stacking conditions. The dispersion is subdivided into an axial, a radial and an introduction term. The last term includes an eventual stacking process, extraneous injection and diffusion during sample introduction. Each of the dispersive terms is derived and discussed. Guidelines for improved peak efficiency during FSCE analysis with stacking conditions are presented.

INTRODUCTION

In the past decade, high-performance capillary electrophoresis (HPCE) [1,2] has evolved as a very promising technique well suited for the analysis of, *e.g.*, proteins and peptides [3–14]. With the emergence of commercially available instrumentation, HPCE is on the brink of becoming a major analytical technique in the biotechnological industries.

One of the attractive features of HPCE is high peak efficiencies due to the so-called electroosmotic flow profile. As a measure of peak efficiency, theoretical plate numbers, N of the order of 10^5–10^6 are obtainable with optimized experimental conditions.

There are, however, several factors that can significantly decrease N. As peak resolution is proportional to $\sqrt{N}$ [8], a knowledge of these dispersion factors is of major importance in the efforts to improve the resolution of closely eluting peaks once a buffer system has been chosen.

General HPCE dispersion theory has been discussed by *e.g.*, Hjertén [15], Foret *et al.* [16] and Terabe *et al.* [17]. In some of the earliest papers concerning HPCE dispersion theory, axial diffusion was assumed to be the dominant dispersive term [18–21]. Using Einstein's equation for axial diffusion [18], this leads to a simple

0021-9673/91/$03.50

expression for N which suggests that high voltages should be applied. High power inductions do, however, cause excessive band broadening due to Joule heating of the liquid in the capillary tube [18–27]. Power is induced uniformly across the capillary cross-sectional area but is only removed at the wall (and at the capillary ends). This leads to a parabolic flow profile as the electroosmotic mobility is a function of the temperature [22]. Dispersion caused by Joule heating can be minimized by using capillaries with a high surface-to-volume ratio and low-conductivity buffers.

Among the other band-broadening factors considered in the present work are radial diffusion, diffusion during sample intake, sample plug length, detector length, chromatographic effects caused by analyte–wall electrostatic interactions [15], sample overload [21,28] and extraneous injection [29]. The last factor refers to sample introduced simply by insertion of the capillary into the sample solution.

Huang *et al.* [30] showed that the physical length of the sample plug introduced is often the most significant dispersion factor. Hence, a very powerful technique in the efforts to achieve optimum peak efficiency is to stack the original introduced sample zone plug.

Sample stacking (concentration of the analyte zone) is the process that occurs when a voltage is applied along a capillary tube containing a sample plug with a lower specific conductivity than that of the surrounding running buffer. As the electric field strength is inversely proportional to the specific conductivity of the liquid, the field strength is higher along the sample plug compared with the running buffer. In this way the electrophoretic velocity, which is proportional to the field strength, increases and the ionic analyte zone is narrowed. This "reversed dispersion" is termed sample stacking.

Based on experimental results and with reference to isotachophoresis theory [31], we have developed a mathematical free solution capillary electrophoresis (FSCE) [4,32] dispersion model. The aim of the model is to describe quantitatively the complex dispersion processes taking place during both stacking and non-stacking FSCE analysis in a simplified way. This approach is different from the previous models based on isotachophoresis [15].

All the experiments were carried out with biosynthetic human growth hormone (B-hGH) as the analyte. B-hGH is a 22 125 relative molecular mass protein consisting of 191 amino acids with an isoelectric point of *ca.* pH 5. Analysis was performed at pH 8.0, where B-hGH is a convenient choice of analyte as it has a suitable net mobility and is repelled from the negatively charged capillary surface.

EXPERIMENTAL

Materials

Tricine {N-[tris(hydroxymethyl)methyl]glycine} and sodium chloride were purchased from Fluka (Buchs, Switzerland) and B-hGH from Novo Nordisk (Gentofte, Denmark). Fused-silica capillaries were obtained from Polymicro Technologies (Phoenix, AZ, USA). Peak areas were integrated on a Shimadzu C-R5A integrator (Kyoto, Japan).

Methods

Analysis was performed on an Applied Biosystems Model 270A analytical

capillary electrophoresis system. The fused-silica capillaries had an I.D. of 50 μm, an O.D. of 192 μm, a total length of 100 cm and a length of 75 cm to the detector (effective length). From the introduction end to the detector the capillaries were surrounded by a thermostated air-bath operated at 27°C. The electroosmotic flow was determined by measuring the retention time of the peak of neutral species.

Two series of experiments were carried out. Samples were introduced by applying a 16.8-kPa vacuum at the detector end of the capillary. The applied potential was changed from 5 to 30 kV in steps of 5 kV. Detection was performed at 200 nm. During the experiments three 10 m*M* tricine running buffers of pH 8.0 containing (a) 0 m*M* NaCl (specific conductivity at 21°C, $\kappa_{21°C} = 0.22$ mS cm^{-1}), (b) 25 m*M* NaCl ($\kappa_{21°C} = 2.75$ mS cm^{-1}) or (c) 50 m*M* NaCl ($\kappa_{21°C} = 4.96$ mS cm^{-1}) were employed. In the stacking runs B-hGH was diluted with distilled water to 0.1 mg ml^{-1} ($\kappa_{21°C} = 0.17$ mS cm^{-1}), whereas under non-stacking conditions B-hGH was diluted to the same concentration with the 10 m*M* tricine (pH 8.0)–25 m*M* NaCl running buffer.

Experimental series 1 was subdivided in two series with (1A) stacking and (1B) non-stacking conditions. Samples were introduced for 3.0 s. The running buffer was 10 m*M* tricine (pH 8.0)–25 m*M* NaCl. The purpose of series 1 was to show the effect of stacking on peak efficiency.

Experimental series 2 was subdivided in three series all having stacking conditions, but differing in the NaCl concentration in the 10 m*M* tricine running buffer (pH 8.0): (2A) 0, (2B) 25 and (2C) 50 m*M* NaCl. The sample was B-hGH diluted with distilled water to 0.1 mg ml^{-1} and introduced for 1.0 s. The purpose of series 2 was to show the effect of stacking power (defined as the difference between the sample zone and running buffer field strength, ΔE) on peak efficiency.

THEORY

Fig. 1 depicts the number of theoretical plates, N, *vs.* the applied potential, U, in experimental series 1. B-hGH was diluted either in distilled water (1A, stacking, $\kappa_B > \kappa_S$) or in the running buffer (1B, no stacking, $\kappa_B = \kappa_S$). N was calculated based on experimentally obtained results as

$$N = 5.54\left(\frac{t_R}{w_{\frac{1}{2}}}\right)^2 \quad (1)$$

where t_R is the analyte retention time and $w_{\frac{1}{2}}$ is the peak width at half-height (a measure of dispersion).

The highest N values were obtained at low applied potentials (long analysis time), which means that axial diffusion is not the dominant dispersive factor in these experiments [18–20]. Further, it was concluded that the trend of decreasing N at increasing U was not caused by band broadening due to excessive Joule heating [22].

What puzzled us most in Fig. 1, however, was the greatly improved peak efficiencies at low U when non-stacking conditions were changed for stacking conditions. This is clearly demonstrated in Fig. 2, where the experimentally obtained 5-kV stacking electropherogram is shown below on the corresponding 5-kV non-stacking electropherogram. In an attempt to describe and explain these experimental results, in the following a theoretical approach to the dispersion process is presented.

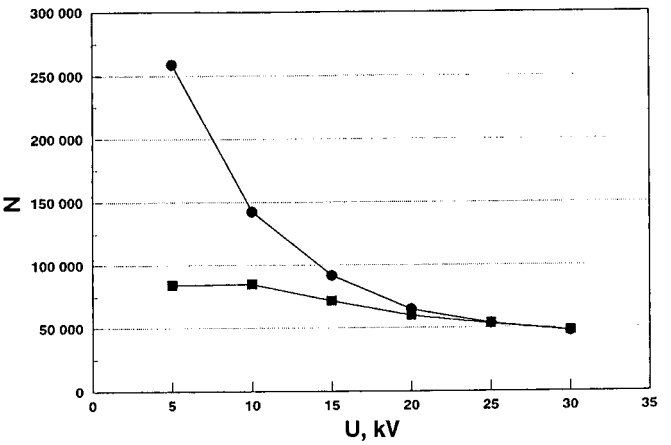

Fig. 1. Experimentally obtained number of theoretical plates (N) *vs.* the applied potential (U, kV) in experimental series 1. The 10 mM tricine running buffer (pH 8.0) contained 25 mM NaCl ($\kappa_{21°C}$ = 2.75 mS cm^{-1}). B-hGH was either diluted with the running buffer [(■) (non-stacking, $\kappa_{21°C}$ = 2.75 mS cm^{-1})] or distilled water [(●) (stacking, $\kappa_{21°C}$ = 0.17 mS cm^{-1}). Sample was introduced for 3.0 s. The total length of the 50 μm I.D. capillary was L_c = 100 cm and the effective length was L_d = 75 cm. The other experimental conditions are given under Experimental. Changing from non-stacking to stacking conditions at low applied potentials greatly improved peak efficiencies.

Eqn. 1 is an easy-to-measure approximation of N applied to experimental data for Gaussian-shaped peaks. N is defined as

$$N = \frac{L_d^2}{\sigma^2} \tag{2}$$

where L_d is the effective length of the capillary and σ^2 is the total analyte zone variance. In the mathematical model we ascribe σ^2 to six terms: axial (σ^2_{axial}) and radial diffusion (σ^2_{radial}), a corrected length of the introduced analyte zone (σ^2_{intro}), detector length (σ^2_{det}), chromatographic effects (σ^2_{chrom}) and sample overload ($\sigma^2_{overload}$):

$$\sigma^2 = \sigma^2_{axial} + \sigma^2_{radial} + \sigma^2_{intro} + \sigma^2_{det} + \sigma^2_{chrom} + \sigma^2_{overload} \tag{3}$$

All six terms are functions of temperature, which has been accounted for in the dispersion model.

With the actual experimental conditions three of the terms were neglected:

$$\sigma^2_{overload} \approx 0 \tag{4}$$

$$\sigma^2_{chrom} \approx 0 \tag{5}$$

(as B-hGH is repelled from the silica surface at pH 8.0) and

$$\sigma^2_{det} = \frac{L^2_{det}}{12} \approx 0 \tag{6}$$

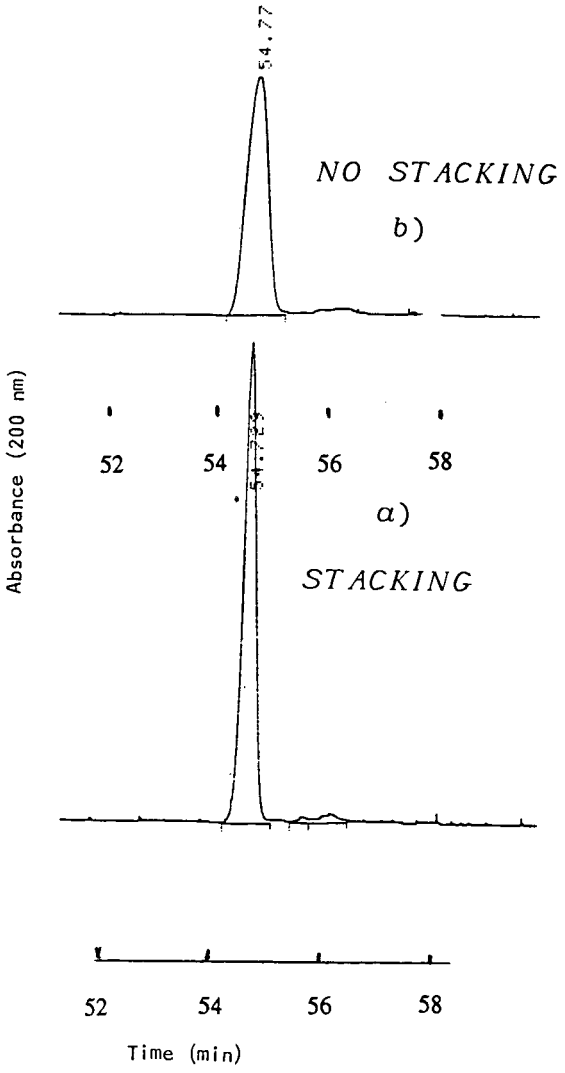

Fig. 2. Experimentally obtained 5-kV electropherograms of the series 1 (a) stacking and (b) non-stacking runs. The abscissa scaling is in minutes. In the stacking run N was *ca.* three times higher than that in the non-stacking run. The improved peak efficiency under stacking conditions is clearly demonstrated.

where L_{det} is the detector length (σ^2_{det} was, however, calculated for all the runs; in general it contributed no more than 1% to the total variance).

Axial dispersion after an eventual stacking process is calculated by the Einstein equation [18]:

$$\sigma^2_{axial} = 2D_B(t_R - t_0) \tag{7}$$

where D_B is the analyte diffusion coefficient when surrounded by running buffer and t_0 is the duration of an eventual stacking process, which we estimate by

$$t_0 = \frac{L_0}{\mu_{EP,S} E_S} \tag{8}$$

$\mu_{EP,S}$ and E_S being the electrophoretic analyte mobility in the sample zone and the field strength along the sample zone, respectively, and L_0 the analyte zone length immediately after sample introduction. Owing to a low ratio of introduction time to hGH diffusional time constant, it can be shown that the concentration profile is elongated into a triangular shape owing to the parabolic velocity profile during introduction [33]. Hence, in order to describe the analyte zone as a rectangular plug in the model, L_0 was multiplied by a factor of 2 (typical t_0 values were in the range 0.5–60 s).

Radial dispersion after an eventual stacking process is calculated as [33,34]

$$\sigma^2_{radial} = \frac{R^2_{inner} v^2}{2D_B} < wh > (t_R - t_0)\left[1 + k_R\left(\frac{\Delta v_{EO} L_0}{v L_c}\right)^2\right] \tag{9}$$

where v is the analyte zone velocity, R_{inner} is the capillary inner radius, k_R is a constant and L_c is the total capillary length. Under non-stacking conditions $1/<wh>$ is a function of the flow profile and the ionic strength ($1/<wh> = 12$ for laminar flow; in FSCE typical values are 1500–4000). Under stacking conditions $1/<wh>$ is a function of the difference between the sample solution and running buffer ionic strength (typical values are 200–1500 during stacking and 1500–6000 after the stacking period). An expression for $<wh>$ during the stacking process is derived in the Appendix. Δv_{EO} is the difference between the two electroosmotic flows that would be measured if the capillary had been filled only with sample solution or running buffer.

The variance due to the introduced analyte zone length is calculated as [30]

$$\sigma^2_{intro} = \frac{L_I^2}{12} \tag{10}$$

where L_I is the analyte zone length corrected for extraneous injection, for diffusional effects during introduction and for an eventual stacking process. Hence, only under non-stacking conditions does $L_0 = L_I$. Obviously, most attention has been drawn towards this term in the mathematical modelling.

Simulation of sampling stacking

Sample stacking is simulated as shown in Fig. 3a and b. The leading edge of the analyte zone migrates with a linear velocity equal to the velocity that would be measured if no stacking took place (sample buffer = running buffer). The terminating edge accounts for the zone stacking as it migrates faster than the leading edge.

The mole flux, j, through the capillary cross-sectional area is calculated relative to the "leading edge velocity":

$$j = C_S \mu_{EP,S} \Delta E \tag{11}$$

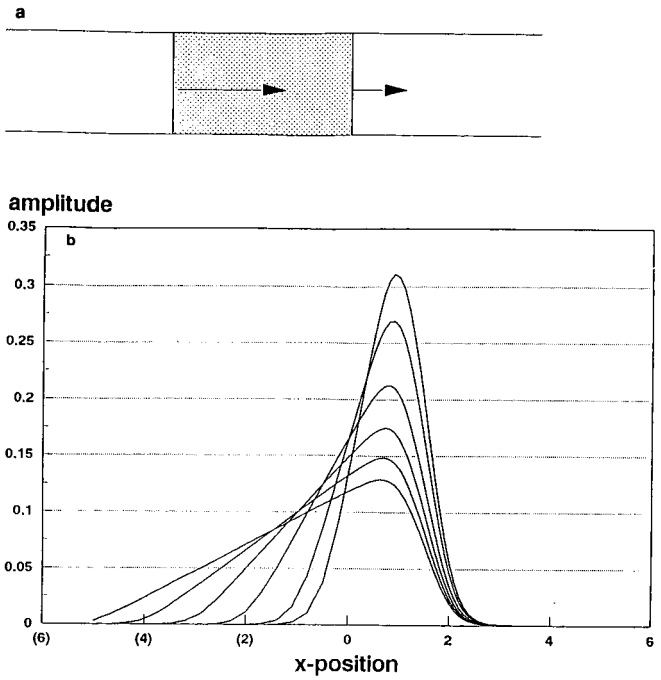

Fig. 3. Computer simulation of sample stacking. (a) One-dimensional; (b) two-dimensional. In the mathematical model it is assumed that the terminating edge of the analyte zone migrates faster than the leading edge, thus reducing the zone length. In (a) this is illustrated by the length of the arrows. In (b) axial position and amplitude are chosen arbitrarily.

where C_S is the analyte concentration in the sample zone. ΔE, which is the "stacking force", is the difference between the field strengths along the sample zone, E_S, and running buffer, E_B:

$$\Delta E = E_S - E_B = \frac{I}{A}\left(\frac{1}{\kappa_S} - \frac{1}{\kappa_B}\right) = \frac{U}{L_S + \frac{\kappa_S}{\kappa_B - \kappa_S} \cdot L_c} \tag{12}$$

where I, A, κ_S, κ_B, L_S and U are the current, the capillary cross-sectional area, the specific conductivities of the sample zone and running buffer, the analyte zone length (which varies during the stacking process) and the applied voltage, respectively.

It is assumed that the total amount of analyte is conserved in the sample zone during the stacking period:

$$C_S L_S = C_0 L_0 \tag{13}$$

where C_S is the analyte concentration when the zone length is L_S and C_0 is the analyte concentration immediately after the sample has been introduced with a corrected plug

length equal to L_0. Dividing eqn. 11 by C_S, combining with eqns. 12 and 13 and introducing the dimensionless length, y,

$$y \equiv \frac{L_S}{L_d} \tag{14}$$

yields

$$\frac{dy}{dt} = -\frac{\mu_{EP,S}U\left(\frac{\kappa_B}{\kappa_S} - 1\right)}{\left[\left(\frac{\kappa_B}{\kappa_S} - 1\right)L_S + L_c\right]L_d} = -\frac{1}{\tau_E}\left(\frac{\kappa_B}{\kappa_S} - 1\right) = -\frac{1}{\tau_B} \tag{15}$$

where τ_E and τ_B have the dimension time. During the stacking period axial and radial diffusion widen the analyte zone with increasing time, while the stacking force as expressed by eqn. 15 has a zone sharpening effect:

$$\frac{d(y^2)}{dt} = \text{axial diffusion} + \text{radial diffusion} - \text{stacking}$$

$$= 2\left(\frac{D_S}{L_d^2} + \frac{R_{inner}^2 \Delta v_{EO}^2 < wh >}{4D_S L_d^2}\right) - 2 \cdot \frac{y}{\tau_B} = 2\left(\frac{1}{\tau_A} - \frac{y}{\tau_B}\right) \tag{16}$$

D_S, which is the analyte diffusion coefficient when surrounded by the sample solution, is calculated as [35]

$$D_S = \frac{\mu_{EP,S}R_{gas}T}{z_{hGH}F} \tag{17}$$

where F is the Faraday constant (96 485 C mol^{-1}), R_{gas} is the gas constant (8.314 J K^{-1} mol^{-1}) and z_{hGH} is the net charge of the hGH molecule (calculated to be *ca.* -7).

If the sample plug was not sandwiched between the running buffer zones, the electroosmotic velocity would be higher in the sample zone compared with the corresponding velocity of the running buffer owing to a higher electroosmotic mobility (higher sample zone zeta potential, wider double layer) and a higher field strength (lower sample zone specific conductivity). The difference between the two velocities is the Δv_{EO} term in eqns. 9 and 16:

$$\Delta v_{EO} = \mu_{EO,S}E_S - \mu_{EO,B}E_B = \left(\mu_{EO,S} \cdot \frac{\kappa_B}{\kappa_S} - \mu_{EO,B}\right)E_B$$

$$= \left(\mu_{EO,S} \cdot \frac{\kappa_B}{\kappa_S} - \mu_{EO,B}\right)\frac{U}{\left(\frac{\kappa_B}{\kappa_S} - 1\right)L_0 + L_c} \tag{18}$$

The tendency for the sample zone to speed up the electroosmotic velocity results in an "electroosmotic pump" pressure on the running buffer. The motive force is in the loosely held part of the double layer close to the capillary wall. Hence, the Δv_{EO} velocity results in an additional dispersive force where the "electroosmotic pump" pressure from the sample zone must be balanced by a backflow.

The so-called electroosmotic flow profile is in general expressed by

$$\frac{v_{EO,S}}{v_{max,EO,S}} = 1 - R^n \tag{19}$$

where $v_{max,EO,S}$ is the maximum electroosmotic velocity of the sample zone (experienced at the tube axis) if the capillary was filled only with sample solution and R is the variable normed inner radius of the capillary tube. The higher the exponent value, n, the more plug-like is the profile. For laminar flow $n = 2$. Martin and co-workers [36,37] proposed the exponent to be 8.54 for electroosmotic flow.

Owing to the backflow we assume the flow profile during stacking conditions to be expressed as

$$\frac{v_{EO,S}}{v_{max,EO,S}} = [(1 - R^S) - k_S(1 - R^B)][1 + f(dT_{inner,S}, dT_{inner,B}, R)]$$

$$\approx (1 - R^S) - k_S(1 - R^B) \tag{20}$$

where k_S indicates the degree of backflow. $f(dT_{inner,S}, dT_{inner,B}, R)$ is a function of R and the sample zone and running buffer temperature elevations in the capillary tube. This function accounts for additional dispersion caused by Joule heating. Under the present experimental conditions it could be neglected [22]. An expression similar to eqn. 20 is derived for the running buffer flow profile.

S and B in eqn. 20 are the exponent n values for the sample zone and running buffer, respectively. They are assumed to be inversely proportional to the Debye layer [35] thickness, δ. Hence,

$$B = k_{DL} \cdot \frac{R_{inner}}{\delta_B} = k_{DL} R_{inner} \sqrt{\frac{F^2 \sum_{B,i} c_i z_i^2}{\varepsilon_0 \varepsilon_r R_{gas} T_B}} \tag{21}$$

$$S = k_{DL} \cdot \frac{R_{inner}}{\delta_S} = k_{DL} R_{inner} \sqrt{\frac{F^2 \sum_{S,i} c_i z_i^2}{\varepsilon_0 \varepsilon_r R_{gas} T_S}} \tag{22}$$

where k_{DL} is a proportionality constant (experimental data fit, $k_{DL} = 0.025$), ε_0 is the permittivity of vacuum ($8.854 \cdot 10^{-14}$ C^2 cm^{-1} J^{-1}), ε_r is the relative permittivity, T_S and T_B are the temperatures of the sample zone and running buffer, respectively, and c_i and z_i are the concentration of and the net number of elementary charges on the ith electrolyte, respectively.

Calculation of k_S in eqn. 20 is based on the demands of a constant mass flow, which means that the difference between the buffer and sample zone mean velocities must equal zero:

$$2\int_{R=0}^{R=1}\left(v_{EO,S} - v_{EO,B}\right)RdR = 0$$

$$\Leftrightarrow$$

$$2\int_{R=0}^{R=1}\{v_{max,EO,S}[1 - R^S - k_S(1 - R^B)] - v_{max,EO,B}[1 - R^B + k_B(1 - R^S)]\}\,RdR = 0 \quad (23)$$

As the electroosmotic pump pressure on the buffer zone is balanced by a back-pressure on the sample zone, k_B can be expressed in terms of k_S:

$$k_B = k_S \cdot \frac{L_0\eta_S}{(L_c - L_0)\eta_B} \quad (24)$$

where η is the viscosity. Eqn. 24 is inserted in eqn. 23, which is solved for k_S:

$$k_S \approx \frac{\Delta v_{EO}}{v_{max,EO,S}} = 1 - \frac{v_{max,EO,B}}{v_{max,EO,S}} \quad (25)$$

In this solution it is assumed that $B \gg 1$, $S \gg 1$ and $L_c \gg L_0$. The equation expresses that the extent of backflow is proportional to Δv_{EO}.

Fig. 4a and b are computer simulations illustrating sample zone profiles as expressed by eqn. 20 during stacking conditions for various $v_{max,EO,S}/v_{max,EO,B}$ values in the range 1–10 (corresponding to the k_S range 0.0–0.9). $v_{max,EO,B}$ was set equal to 1.

At the tube axis the flow profile remains plug-like, but close to the capillary wall the difference between the electroosmotic force in the running buffer and sample zone double layers results in more laminar-like profiles. Very close to the wall the backflow is even stronger than the forward flow resulting in a net negative flow.

As all the parameters in the differential eqn. 16 are now accounted for, it can be solved. Integration from y_0 to y yields

$$\frac{ay_0}{1 - \frac{\tau_E}{\tau_S}} - ay + \ln\left(\frac{ay_0 - 1}{ay - 1}\right) = 0, \qquad a = \frac{\tau_A}{\tau_B} \quad (26a)$$

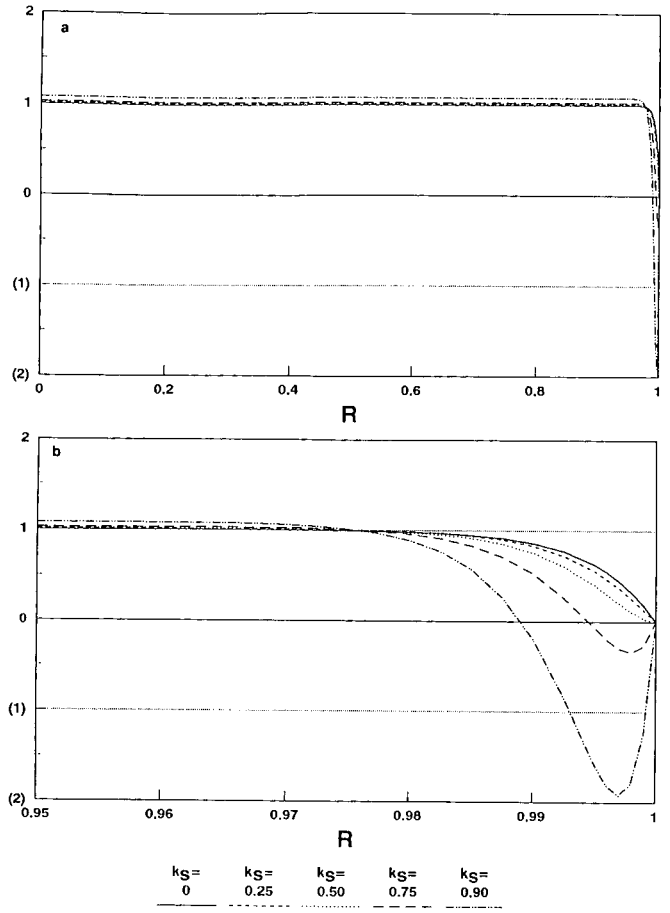

Fig. 4. Computer simulation of the electroosmotic flow profile ($v_{EO,S}$) as a function of the variable normed radial position, R, in the capillary during stacking conditions as calculated by eqn. 20. (a) $0 < R < 1$; (b) $0.95 < R < 1$. The profile is shown for different k_S values in the range 0–0.9. The $v_{max,EO,B}$ value was chosen arbitrarily to be 1.00. Owing to the lower double layer thickness in the running buffer relative to the sample zone, there is a net negative flow very close to the wall. The higher the k_S value (eqn. 25) the more laminar-like is the profile and thereby the larger is the dispersion.

or, expressed by the specific conductivities of the sample zone, κ_S, and running buffer, κ_B:

$$\frac{\kappa_S}{\kappa_B} \cdot ay_0 - ay + \ln\left(\frac{ay_0 - 1}{ay - 1}\right) = 0, \qquad a = \frac{\tau_A}{\tau_B} \tag{26b}$$

Eqn. 26a or 26b is solved iteratively with respect to y.

The ratio of the originally introduced sample zone length to the analyte zone length after the stacking period, $L_0/L_1 = y_0/y$, is a measure of the sample stacking.

Retention time per theoretical plate, t_R/N

Eqns. 7, 9 and 10 represent the contribution of each of the three variance terms (σ^2_{axial}, σ^2_{radial} and σ^2_{intro}) to the total variance (σ^2, cm^2). In the discussion below, the three terms are expressed as contributions to the total retention time per theoretical plate, t_R/N. Hence,

$$\frac{t_R}{N} = \frac{t_R}{L_d^2} \cdot \sigma^2$$

$$= \frac{t_R}{L_d^2}(\sigma^2_{axial} + \sigma^2_{radial} + \sigma^2_{intro})$$

$$= \chi_{axial} + \chi_{radial} + \chi_{intro} = \text{"axial"} + \text{"radial"} + \text{"intro"} \quad (27)$$

In this way the dispersive terms are calculated as

$$\text{"axial"} = \chi_{axial} = 2 \cdot \frac{D_B}{L_d^2} \cdot t_R^2 \left(1 - \frac{t_0}{t_R}\right) \quad (28)$$

$$\text{"radial"} = \chi_{radial} = \frac{R^2_{inner}}{2D_B} < wh > \left(1 - \frac{t_0}{t_R}\right)\left[1 + k_R\left(\frac{\Delta v_{EO} L_0}{v L_c}\right)^2\right] \quad (29)$$

$$\text{"intro"} = \chi_{intro} = \frac{t_R}{12} \cdot y^2 \quad (30)$$

As t_R/N denotes the retention time required to obtain one theoretical plate, the lower the t_R/N value the higher is the peak efficiency at any given t_R value.

RESULTS AND DISCUSSION

The ratio of the originally introduced sample zone length to the analyte zone length after the stacking period, $y_0/y = L_0/L_1$, expresses the sample stacking. For each run the experimentally measured and calculated values are inserted in eqn. 26. The equation is solved iteratively with respect to y. The estimated y_0/y ratios are depicted *vs.* U (Fig. 5) and ay_0 (Fig. 6) for the stacking and non-stacking runs in series 1. The dotted lines in Fig. 6 indicate the solution of eqn. 26 for various theoretical κ_B/κ_S values (given in the caption). The higher the ordinate value the more the analyte zone is reduced in length during the stacking process.

Running under stacking conditions has a dramatic effect on the analyte zone length. Reductions of nearly ten times are obtained for low applied voltages. At higher voltages the dispersive effects caused by the Δv_{EO} and $< wh >$ terms of the radial dispersion during the stacking period (eqn. 16) and the decreasing κ_B/κ_S ratio due to the temperature effects [22] (observed in Fig. 6) become more dominant.

The effect of different stacking powers (defined as ΔE, experimental series 2) is shown in Fig. 7. When there is only a low stacking power the analyte zone is stacked by a factor of *ca.* κ_B/κ_S (the 0 m*M* NaCl running buffer runs, $\kappa_B/\kappa_S \approx 1.3$).

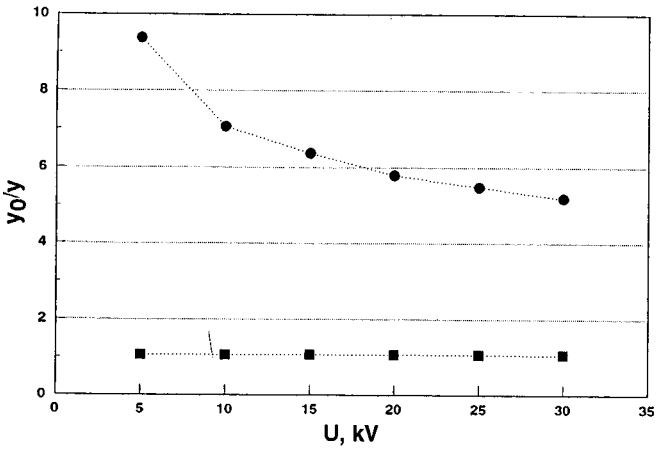

Fig. 5. Mathematical model, $y_0/y = L_0/L_1$ values *vs.* the applied potential (U, kV) in the series 1 experiment. During the stacking process (●) the original introduced analyte zone is reduced in length ($y_0/y > 1$), whereas in the non-stacking runs (■) the zone length is not reduced.

The 50 mM NaCl running buffer runs (Fig. 7) show an example of the increased radial dispersion nearly outbalancing the zone narrowing stacking effect due to the "backflow profile". Hence the analyte zone width is reduced more effectively in the 25 mM NaCl running buffer runs at high applied potentials compared with the 50 mM NaCl running buffer runs even though the specific conductivity ratio of the running buffer to sample zone is larger in the latter.

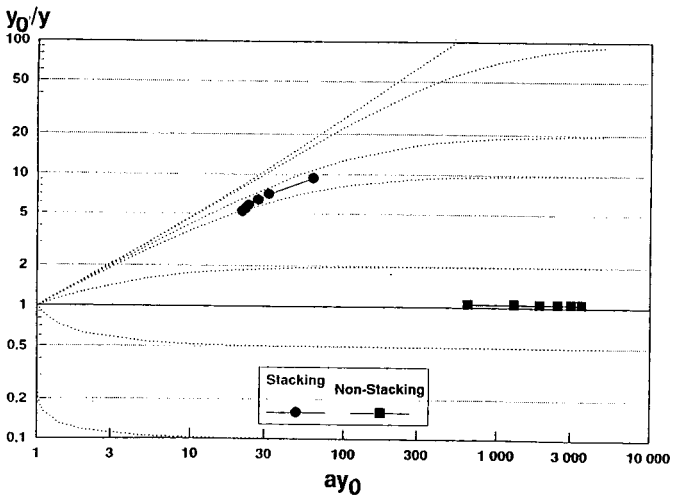

Fig. 6. Mathematical model, $y_0/y = L_0/L_1$ values *vs.* ay_0 in the series 1 experiment. The dotted lines indicate the solution of eqn. 26 for various κ_B/κ_S values. The values from top to bottom are 1000, 100, 20, 10, 2, 1 (horizontal solid line), 0.5 and 0.1. In the stacking runs (●) ay_0 increases with decreasing U. Hence, the figure illustrates that the κ_B/κ_S ratio decreases with increasing U caused by temperature effects [22]. (■) Non-stacking.

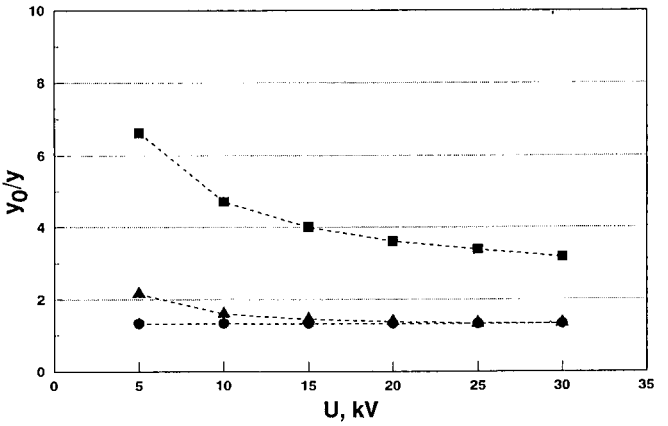

Fig. 7. Mathematical model, $y_0/y = L_0/L_1$ values *vs.* the applied potential (U, kV) in the series 2 experiment. During the stacking process the originally introduced analyte zone is reduced in length ($y_0/y > 1$). Increasing the κ_B/κ_S ratio (increasing NaCl concentration) increases the stacking power (ΔE), but at the same time radial dispersion increases. NaCl concentration: ● = 0; ■ = 25; ▲ = 50 mM.

Comparing mathematical model and experimental results

Series 1, stacking vs. non-stacking. Fig. 8 shows the correlation between the mathematical dispersion model (dashed lines) and the experimentally obtained results (solid lines) in series 1, where the purpose was to show the effect of stacking on peak efficiency. The lower the t_R/N value the higher is the peak efficiency at any given t_R value.

At high applied potentials (20–30 kV), similar and almost constant t_R/N values are obtained for the stacking and non-stacking runs. When U is lowered t_R/N increases

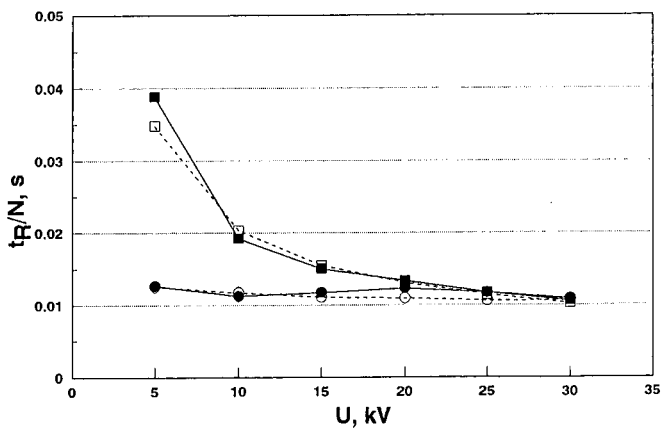

Fig. 8. t_R/N (s) *vs.* the applied potential (U, kV) in the series 1 experiment. The solid lines are experimental curves based on eqn. 1 and the dashed lines are based on the mathematical model (eqn. 27). At low applied potentials, turning from non-stacking (■, □) to stacking conditions (●, ○) greatly improves peak efficiency (decreasing t_R/N). Similar retention times were obtained in the stacking and non-stacking runs at each applied potential.

when the runs are carried out under non-stacking conditions, whereas the value remains almost constant for the stacking runs. The reason for this difference between the non-stacking and stacking runs is revealed by comparing Fig. 9a (stacking) and b (non-stacking), where each of the three additive dispersion terms in eqn. 27 of the mathematical model are plotted. Owing to the narrowed analyte zone length during stacking, the introduction term is much lower in the stacking runs than the non-stacking runs, where it is the largest dispersive contributor at low applied voltages (5–15 kV) owing to its "proportionality" to the analysis time (eqn. 30).

In the non-stacking runs the radial dispersion is lower than in the stacking runs as the $\Delta v_{EO}/v$ term in eqn. 29 is negligible.

Fig. 10 depicts the relative contribution of each of the three additive dispersion terms in each of the runs in stacked-bar form. Radial dispersion is the dominant zone broadener during the stacking runs, contributing 88–98% of the total dispersion.

Axial diffusion is an important quantitative term only when there is a long analysis time, and hence at low applied voltages. One of the explanations for the difference between the experimental and theoretical t_R/N values in the 5-kV runs (Fig. 8) is that the axial dispersion values in general may be estimated too low in the model.

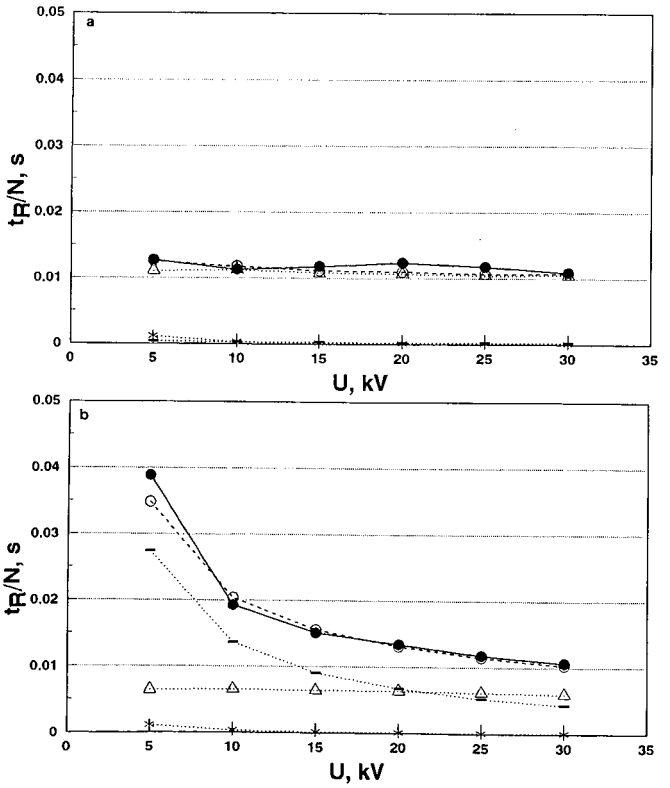

Fig. 9. t_R/N (s) *vs.* the applied potential (U, kV) in the series I experiment when (a) stacking or (b) non-stacking conditions were used. The mathematical model values for each of the three additive dispersive terms in eqn. 27 are shown. ● = Experimental. Models: ○ = total; ✳ = axial; △ = radial; — = introduction.

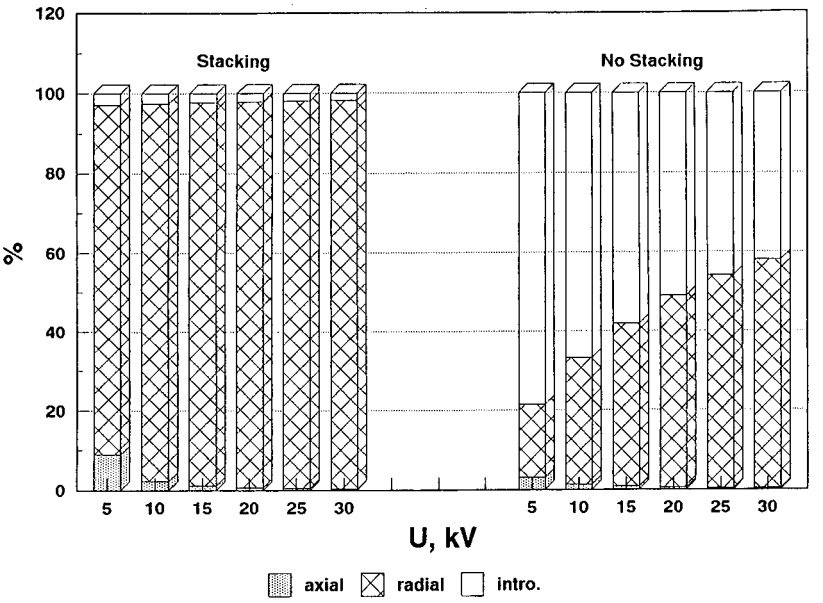

Fig. 10. Experimental series 1. Each of the three dispersive terms in eqn. 27 as a percentage of the total dispersion during analysis is shown in stacked bar form for each of the runs. Left side, stacking; right side, non-stacking. During the stacking runs the introduction term percentage value is much lower than in the corresponding non-stacking runs.

The results of the series 1 experiment suggest a low potential to be applied under stacking conditions as the t_R/N value is almost constant with varying U in the range 5–30 kV. Hence, the longer the analysis time, the higher is the number of theoretical plates is obtained. At very low voltages (5 kV and below) axial diffusion does, however, increase t_R/N, thus creating a lower limit to the applied potential.

Fig. 1 shows the theoretical plate numbers vs. U in the series 1 experiment. McCormick [9] reported similar observations, with low applied voltages giving the highest number of theoretical plates. Separation was improved when the operating voltage was applied as a gradient instead of instantly. McCormick [9] did not discuss the reasons for these observations, but according to the present model the latter phenomenon might be due to a lower radial dispersion when applying the voltage as a gradient.

Prestacking is used to describe the use of low U values during the initial stacking period, t_0, followed by a higher U when the analyte zone has left the original introduced sample plug. Prestacking has proved very useful in our laboratory, serving the purpose of reducing retention times yet giving high peak efficiencies.

Series 2, different stacking powers (ΔE). Fig. 11 shows the correlation between the mathematical dispersion model (dotted lines) and the experimental results (solid lines) in series 2, where the purpose was to show the effect of stacking power, ΔE, on peak efficiency.

The lowest t_R/N values are obtained when there is only a low stacking power (0 mM NaCl running buffer), and hence a low κ_B/κ_S value above unity. Fig. 12a (0 mM

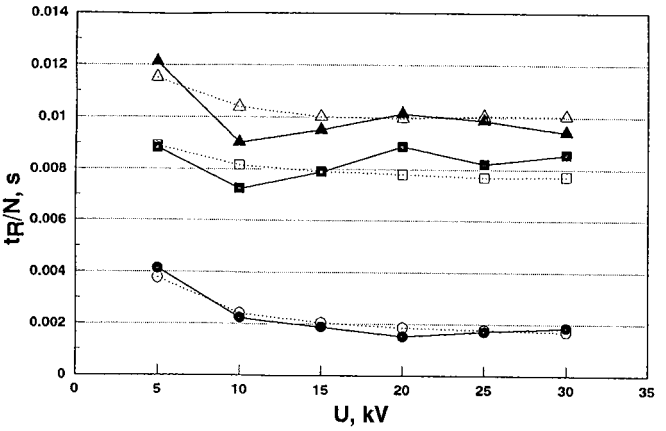

Fig. 11. t_R/N (s) *vs.* the applied potential (U, kV) in the series 2 experiment. The solid lines are experimental curves based on eqn. 1 and the dotted lines are based on the mathematical model (eqn. 27). At each applied potential the retention time order was 50 mM NaCl (▲,△) > 25 mM NaCl (■,□) > 0 mM NaCl (●,○).

NaCl), b (25 mM NaCl) and c (50 mM NaCl), which show each of the three additive dispersive terms of eqn. 27, elaborate this. Increasing the initial κ_B/κ_S value above unity at any given U results in a higher stacking power, thus increasing the narrowing of the original analyte zone length. At the same time, however, radial dispersion increases, thus opposing the narrowing effect of the stacking power.

Increasing the applied potential (and thereby ΔE) has the same general effect: stacking the analyte zone, but at the same time increasing the radial dispersion.

As in the series 1 experiment, it is only at low applied potentials (long analysis time) that the axial term has any quantitative importance with respect to the total dispersion (Fig. 13).

The series 2 experiment is substantial in the discussion of dispersion during FSCE analysis with stacking conditions. Moring *et al.* [38] discussed the importance of sample stacking during FSCE analysis and argued that "much lower ionic strength and conductivity" of the sample solution relative to the running buffer (thus high κ_B/κ_S ratios) should be employed, resulting in very narrow analyte zones. The experimental results as illustrated in Figs. 11 and 14 (N *vs.* U, experimental series 2) oppose this suggestion. Whereas it takes *ca.* 2 ms to obtain one theoretical plate in the 20 kV, 0 mM NaCl run, it takes *ca.* 9 and 10 ms in the 20 kV, 25 mM and 50 mM NaCl runs where the κ_B/κ_S values are higher.

Hence, increasing the κ_B/κ_S ratio has a narrowing effect on the analyte zone, as discussed by Moring *et al.* [38], but at the same time the radial dispersion both during and after the stacking period increases, as observed in Fig. 12a–c where the radial term increases from the 0 to the 25 to the 50 mM NaCl runs.

As in series 1, radial dispersion is the main zone broadener at high applied potentials (Fig. 13) and at high κ_B/κ_S ratios.

An additional experimental series was carried out. Different plug lengths were introduced (0.2–15-s introduction) and the experiments were performed under stacking, no stacking or reversed stacking conditions ($\kappa_B < \kappa_S$) in 10 mM tricine buffer (pH 8.0).

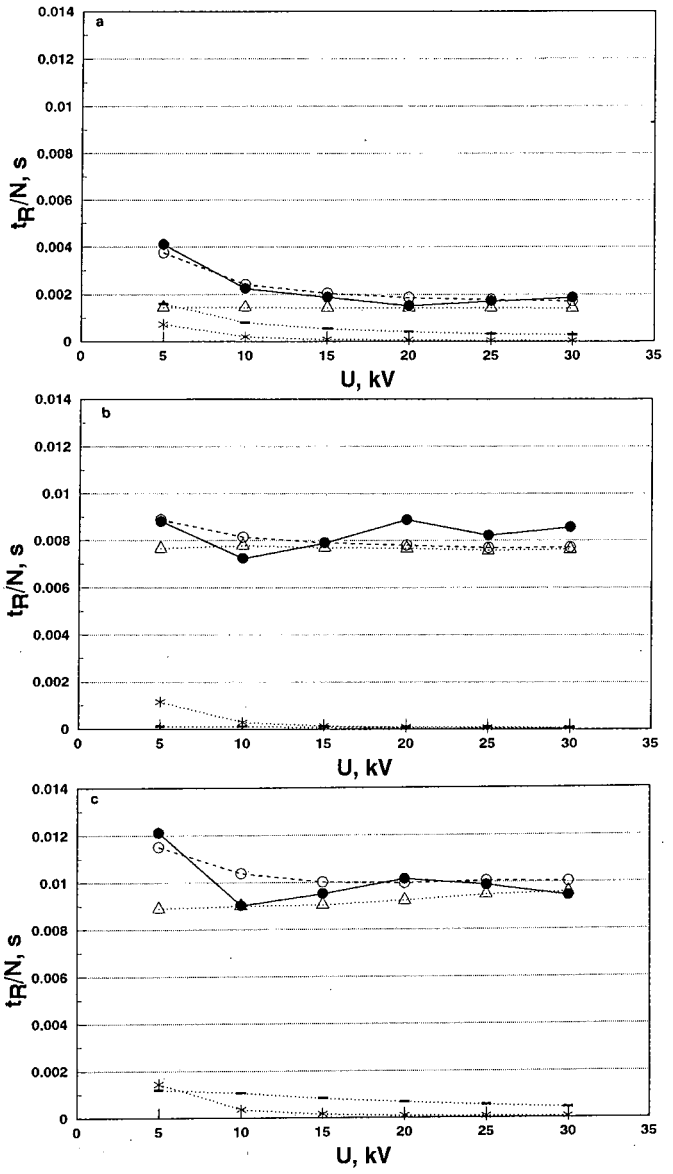

Fig. 12. t_R/N (s) *vs.* the applied potential (U, kV) in the series 2 experiment when the 10 mM tricine running buffer (pH 8.0) contained (a) 0, (b) 25 or (c) 50 mM NaCl. The values for each of the three dispersive terms in eqn. 27 are shown. Increasing the κ_B/κ_S ratio (increasing the NaCl concentration in the running buffer) strongly increases radial dispersion and the t_R/N values. Symbols as in Fig. 9.

Increasing the introduction time, t_{inj}, dramatically decreased the peak efficiency (Fig. 15) as the introduction term of the total dispersion becomes more dominant with longer injection times [30] (eqn. 30). In the 0.2-s non-stacking run the introduction term contributed *ca.* 1% to the total dispersion whereas for a 15-s introduction the

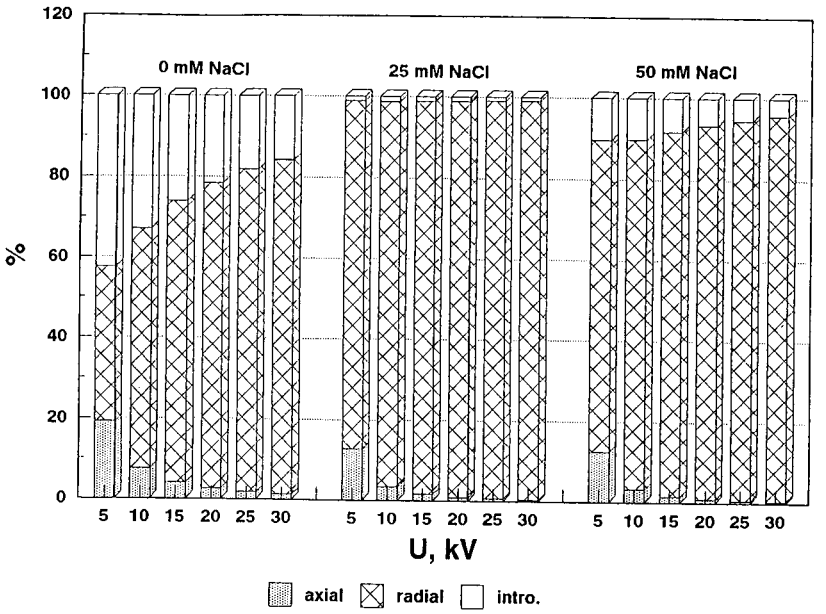

Fig. 13. Experimental series 2. Each of the three dispersive terms in eqn. 27 as a percentage of the total dispersion during analysis is shown in stacked bar form for each of the runs. Left side, 0 m*M* NaCl; middle, 25 m*M* NaCl; right side, 50 m*M* NaCl. Only at low applied potentials and with low stacking power (0 m*M* NaCl) does the introduction term exceeds 20% of the total dispersion.

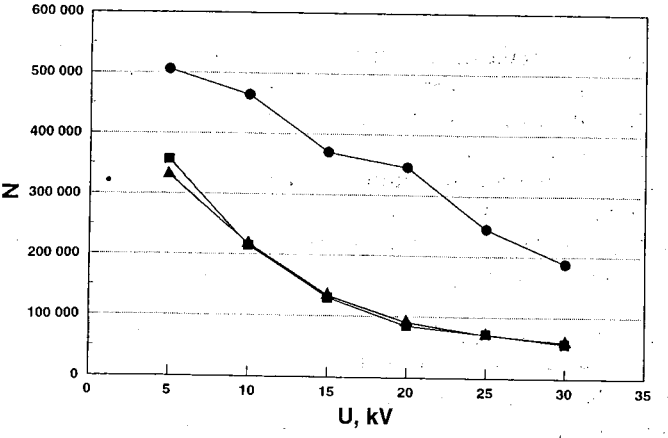

Fig. 14. Number of experimentally obtained theoretical plates (*N*) *vs.* the applied potential (*U*, kV) in the series 2 experiment. The t_R/N values are higher in the 50 m*M* NaCl runs than in the 25 m*M* NaCl runs at each applied potential. As the retention time is longer in the 50 m*M* runs, however, with this combination of t_R/N and t_R almost identical *N* values were obtained in the two buffers. NaCl concentration: (●) 0; (■) 25; (▲) 50 m*M*.

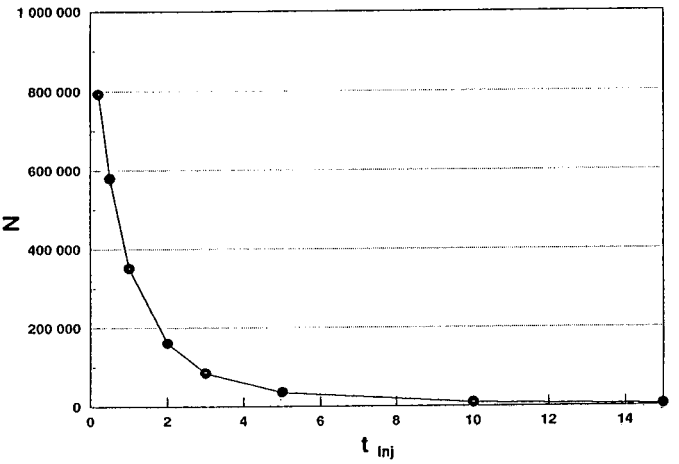

Fig. 15. Number of experimentally obtained theoretical plates (N) *vs.* the introduction time (t_{inj}, s). Increasing t_{inj} dramatically decreases N. Experimental conditions: sample, B-hGH diluted to 0.1 mg ml^{-1} with distilled water ($\kappa_{21°C}$ = 0.17 mS cm^{-1}); running buffer, 10 mM tricine (pH 8.0) ($\kappa_{21°C}$ = 0.22 mS cm^{-1}); samples introduced for 0.2–15 s; applied potential, 15 kV. Other conditions as under Experimental.

value was *ca.* 98%. Hence, with long sample introduction times, where the introduction dispersion term is totally dominant, a stacking process can be very effective in narrowing the analyte zone length. Changing from stacking to non-stacking conditions decreased t_R/N by a factor of 5–10 in the t_{inj} = 15 s runs.

In the reversed stacking runs the original analyte zone was widened relative to the originally introduced sample plug length. If experiments have to be carried out under reversed stacking conditions, short injection times should be used.

CONCLUSIONS

Based on simple assumptions in the development of the mathematical model for dispersion during FSCE analysis, a few general suggestions can be made.

Stacking is a powerful technique in narrowing the analyte zone length, thus increasing the number of theoretical plates.

The specific conductivity of the running buffer should be kept low in order to avoid dispersive effects caused by excessive Joule heating.

Stacking conditions ($\kappa_S/\kappa_B < 1$) should be employed and the specific conductivity of the sample solution should only be slightly lower than that of the buffer solution. We term this "moderate stacking".

Increasing the κ_B/κ_S ratio increases the stacking power (ΔE), reducing the analyte zone length, but at the same time the radial dispersion is increased, thus widening the analyte zone. With increasing κ_B/κ_S ratios and increasing applied potentials the radial dispersion dominates over the "zone stacking". Hence, the applied potential should be kept low during the stacking period, t_0, with a lower limit governed by axial diffusion.

After the stacking period the analyte zone has left the originally introduced sample zone and the applied potential can be increased in order to speed up analysis. It

must be kept in mind, however, that according to the model the originally introduced sample zone exerts an electroosmotic pump pressure on the analyte zone even after the stacking period, resulting in a radial dispersion which increases slightly with increasing potential.

If long introduction times are necessary owing to, *e.g.*, a low analyte concentration in the sample solution and/or a low detector sensitivity, moderate stacking conditions and low applied potentials are very effective in narrowing the analyte zone and superior to non-stacking and reversed stacking experimental conditions.

In accordance with existing FSCE theory, the mathematical model predicts that the number of theoretical plates increases with decreasing introduction time.

If reversed stacking conditions cannot be avoided, the introduction time should be kept as short as possible.

In summary, generally the introduction time should be medium to short depending on the detector performance, moderate stacking conditions and low applied potentials should be employed during the stacking period, the running buffer conductivity should be kept as low as possible and the applied potential should be increased after the stacking period (depending on the κ_B/κ_S and κ_B values) in order to speed up analysis.

APPENDIX

Calculation of $<wh>$ during stacking

The term w is a velocity profile function of the normed radius, R, and defined as [33]

$$w = m \cdot \frac{v_{EO,S}}{v_{max,EO,S}}$$

$$= m[1 - R^S - k_S(1 - R^B)]$$

$$= m[1 - z^n - k_S(1 - z^u)] \qquad \text{(A1)}$$

$$n \equiv \frac{S}{2}; \qquad u \equiv \frac{B}{2}; \qquad z \equiv R^2$$

n, u and z are introduced in order to simplify the mathematical manipulations concerning the mean of the wh product ($= <wh>$).

Here m is a constant which meets the demand that the mean value of $w = 1$:

$$<w> \equiv 1 \qquad \text{(A2a)}$$

$$\Leftrightarrow$$

$$\int_{z=0}^{z=1} m[1 - z^n - k_S(1 - z^u)]\,dz = 1 \qquad \text{(A2b)}$$

$$\Leftrightarrow$$

$$m = \frac{1}{\frac{n}{n+1} - \frac{u}{u+1} \cdot k_S} \tag{A2c}$$

This means that eqn. A1 can be rewritten as

$$w = \frac{1 - z^n - k_S(1 - z^u)}{\frac{n}{n+1} - \frac{u}{u+1} \cdot k_S} \tag{A3}$$

In this equation h is a function of the radial position z and stationary solution to the concentration profile in the Taylor approximation [39] of the solution to the dispersed plug flow model [33,39,40]:

$$-\nabla^2 h = -\frac{\partial}{\partial z}\left(z \cdot \frac{\partial h}{\partial z}\right) = w - 1 \tag{A4}$$

The equation is solved by the use of eqn. A3 and the boundary conditions

$$<h> = 0, \qquad \frac{\partial h(1)}{\partial z} = 0$$

thus yielding

$$h = \frac{-\frac{1}{(n+1)} + \frac{1}{(n+1)^2} \cdot z^{n+1} + k_S \cdot \frac{1}{u+1} \cdot z - k_S \cdot \frac{1}{(u+1)^2} \cdot z^{u+1}}{\frac{n}{n+1} - k_S \cdot \frac{u}{u+1}} + h_0 \tag{A5}$$

After extensive calculations and reductions, the mean value of the product wh is found to be

$$<wh> = \frac{n^2}{\frac{2(n+1)^3(n+2)}{\left(\frac{n}{n+1} - k_S \cdot \frac{u}{u+1}\right)^2}}$$

$$- k_S \cdot \frac{un \cdot \frac{(n+4) + u(n+5) + u^2}{(n+1)(u+1)^2(n+2)(u+2)(n+u+2)}}{\left(\frac{n}{n+1} - k_S \cdot \frac{u}{u+1}\right)^2} + k_S^2 \cdot \frac{\frac{u^2}{2(u+1)^3(u+2)}}{\left(\frac{n}{n+1} - k_S \cdot \frac{u}{u+1}\right)^2} \tag{A6}$$

If there is no backflow (no stacking), $k_S = 0$ and eqn. A6 reduces to

$$<wh> = \frac{1}{2(n+1)(n+2)} \tag{A7}$$

For laminar flow where $n = S/2 = 1$, the value of $<wh>$ is 1/12, as used by, *e.g.*, Golay and Atwood [34]. The higher the value of n, the lower is the value of $<wh>$ and, in accordance with eqn. 16, the lower is the radial dispersion.

As generally $n \gg 1$ and $u \gg 1$, eqn. A6 is simplified to

$$<wh> \approx \frac{1}{2}\left(\frac{\frac{k_S}{u} - \frac{1}{n}}{1 - k_S}\right)^2 \tag{A8}$$

Inserting the expression for k_S as found in eqn. 25 into eqn. A8 yields

$$<wh> \approx \frac{1}{2k_{DL}^2}\left[\frac{v_{max,EO,S}}{v_{max,EO,B}}\left(\frac{\delta_B}{r} - \frac{\delta_S}{r}\right) - \frac{\delta_B}{r}\right]^2 \tag{A9}$$

In practice, the $<wh>$ values change as a function of time [33]. We did, however, simply calculate them as being constant in each separate run by the use of eqn. A9. The constant k_{DL} is estimated based on a trial-and-error best fit for all three experimental series and we chose a value of 0.025. The $<wh>$ term after the stacking process was chosen to fit the experimental data.

REFERENCES

1 B. L. Karger, A. S. Cohen and A. Guttman, *J. Chromatogr.*, 492 (1988) 585.
2 W. G. Kuhr, *Anal. Chem.*, 62 (1990) 403R.
3 H. Lüdi, E. Gassmann, H. Grossenbacher and W. Märki, *Anal. Chim. Acta*, 213 (1988) 215.
4 P. D. Grossman, J. C. Colburn, H. H. Lauer, R. G. Nielsen, R. M. Riggin, G. S. Sittampalam and E. C. Rickard, *Anal. Chem.*, 61 (1989) 1186.
5 J. Frenz, S.-L. Wu and W. S. Hancock, *J. Chromatogr.*, 480 (1989) 379.
6 R. G. Nielsen, R. M. Riggin and E. C. Rickard, *J. Chromatogr.*, 480 (1989) 393.
7 P. D. Grossman, J. C. Colburn and H. H. Lauer, *Anal. Biochem.*, 179 (1989) 28.
8 H. H. Lauer and D. McManigill, *Anal. Chem.*, 58 (1986) 166.
9 R. M. McCormick, *Anal. Chem.*, 60 (1988) 2322.
10 M. V. Novotny, K. A. Cobb and J. Liu, *Electrophoresis*, 11 (1990) 735.
11 A. Vinther, S. E. Bjørn, H. H. Sørensen and H. Søeberg, *J. Chromatogr.*, 516 (1990) 175.
12 A. Vinther, A. M. Jespersen, H. H. Sørensen and H. Søeberg, *Talanta*, (1991) in press.
13 M. M. Bushey and J. W. Jorgenson, *J. Chromatogr.*, 480 (1989) 301.
14 J. S. Green and J. W. Jorgenson, *J. Chromatogr.*, 478 (1989) 63.
15 S. Hjertén, *Electrophoresis*, 11 (1990) 665.
16 F. Foret, M. Deml and P. Bocek, *J. Chromatogr.*, 452 (1988) 601.
17 S. Terabe, K. Otsuka and T. Ando, *Anal. Chem.*, 61 (1989) 251.
18 J. W. Jorgenson and K. D. Lukacs, *Anal. Chem.*, 53 (1981) 1298.
19 J. W. Jorgenson and K. D. Lukacs, *Science*, 222 (1983) 266.
20 H. H. Lauer and D. McManigill, *Trends Anal. Chem.*, 5 (1986) 11.
21 J. W. Jorgenson, *New Directions in Electrophoretic Methods*, American Chemical Society, Washington, DC, 1987, Ch. 13, pp. 182–198.

22 A. Vinther and H. Søeberg, *J. Chromatogr.*, 559 (1991) 27.
23 E. Grushka, R. M. McCormick and J. J. Kirkland, *Anal. Chem.*, 61 (1989) 241.
24 A. E. Jones and E. Grushka, *J. Chromatogr.*, 466 (1989) 219.
25 J. H. Knox, *Chromatographia*, 26 (1988) 329.
26 J. H. Knox and K. A. McCormack, *J. Liq. Chromatogr.*, 12 (1989) 2435.
27 K. D. Lukacs and J. W. Jorgenson, *J. High Resolut. Chromatogr. Chromatogr. Commun.*, 8 (1985) 407.
28 W. Th. Kok, *Zone Broadening in Capillary Zone Electrophoresis*, Amsterdam Summer Course in Capillary Zone Electrophoresis, University of Amsterdam, Amsterdam, 1990.
29 E. Grushka and R. M. McCormick, *J. Chromatogr.*, 471 (1989) 421.
30 X. Huang, W. P. Coleman and R. N. Zare, *J. Chromatogr.*, 480 (1989) 95.
31 F. M. Everaerts, J. L. Beckers and Th. P. E. M. Verheggen, *Isotachophoresis—Theory, Instrumentation and Applications*, Elsevier, Amsterdam, 1976.
32 V. P. Burolla, S. L. Pentoney and R. N. Zare, *Am. Biotechnol. Lab.*, Nov./Dec. (1989) 7:10, 12.
33 H. Søeberg, *Course on Dispersion Models*, Department of Chemical Engineering, Technical University of Denmark, Lyngby, 1989.
34 M. J. E. Golay and J. G. Atwood, *J. Chromatogr.*, 186 (1979) 353.
35 P. W. Atkins, *Physical Chemistry*, Oxford University Press, Oxford, 1982.
36 M. Martin and G. Guiochon, *Anal. Chem.*, 56 (1984) 614.
37 M. Martin, G. Guiochon, Y. Walbroehl and J. W. Jorgenson, *Anal. Chem.*, 57 (1985) 559.
38 S. E. Moring, J. C. Colburn, P. D. Grossman and H. H. Lauer, *LC·GC Int.*, 3 (1989) 46.
39 G. Taylor, *Proc. R. Soc. London, Ser. A*, 219 (1953) 186.
40 O. Levenspiel, *Chemical Reaction Engineering*, Wiley, Toronto, 1972.

Journal of Chromatography, 559 (1991) 27–42
Elsevier Science Publishers B.V., Amsterdam

CHROM. 23 417

Temperature elevations of the sample zone in free solution capillary electrophoresis under stacking conditions

ANDERS VINTHER*
Department of Fermentation Physiology, Novo Nordisk, Lagergårdsvej 2, DK-2820 Gentofte (Denmark)
and
HENRIK SØEBERG
Department of Chemical Engineering, Technical University of Denmark, Building 229, DK-2800 Lyngby (Denmark)

ABSTRACT

The combination of a low specific conductivity ratio of sample solution to surrounding running buffer (under stacking conditions) and high applied potentials can result in high power inductions and high temperatures of the sample zone. Eventually boiling occurs. Calculations of the sample zone and running buffer temperatures are based on changes in viscosity, relative permittivity, zeta potential and specific conductivity of the buffer solutions as a function of temperature. The temperature gradients across the capillary inner radius, the glass wall, the polyimide coating and the "thermo layer" from the capillary outer coating to the surroundings are estimated. Heat-transfer coefficients for liquid- and air-cooled capillaries were obtained.

INTRODUCTION

One of the characteristics of high-performance capillary electrophoresis (HPCE) [1,2] is the high peak efficiences due to the plug-like so-called electroosmotic flow profile [3–5]. With optimized separation conditions, theoretical plate numbers of the order of 10^5–10^6 are obtainable on a routine basis. There are, however, several factors that can cause excessive band broadening and loss of resolution [5–16]. One of these factors is Joule heating.

Most often high voltages are applied in HPCE with typical average field strengths in the range 50–1000 V cm^{-1}. Power is assumed to be uniformly induced across the capillary cross-sectional area, but only removed at the capillary wall (and at the capillary ends). This results in a parabolic temperature profile in the liquid inside the capillary tube with the maximum temperature being at the axis. The combination of highly conductive buffers and/or high field strengths results in high power inductions and the Joule heat produced causes the analyte zone to be excessively dispersed.

The general approach when minimizing dispersion due to Joule heating is to

0021-9673/91/$03.50

remove the heat effectively by the use of capillaries with a high surface-to-volume ratio (narrow-bore tubes) and a thermostated forced convection. Several workers have described how effectively peak efficiencies can be improved by lowering the capillary radius [9,10,13–19]. The drawback of lowering the capillary radius is a decreased path length for UV absorbance detection. Knox [19] and Grushka and co-workers [17,18] showed that most of the temperature gradient from the capillary tube axis to the surroundings was in the "thermo layer" from the capillary outer coating to the surroundings. Nelson *et al.* [20] compared different means of heat removal and found the order of effectiveness to be Peltier device > fan cooling > natural convection.

Estimations of, among others, the sample plug and running buffer temperatures as a function of radial position under various stacking conditions are reported here. A knowledge of the sample zone and running buffer temperatures during capillary electrophoresis analysis is crucial (a) when heat-labile analytes are employed and (b) when describing the dispersion processes by mathematical modelling. This is especially true when stacking conditions prevail.

Sample stacking (concentration of the analyte zone) is the process that occurs when a voltage is applied along a capillary tube containing a sample plug with a lower specific conductivity than that of the surrounding running buffer. As the electric field strength is inversely proportional to the specific conductivity of the liquid, the field strength is higher along the sample plug compared with the running buffer. In this way the electrophoretic velocity, which is proportional to the field strength, increases and the ionic analyte zone is narrowed. This "reversed dispersion" is termed sample stacking.

The HPCE experiments were performed in the free solution capillary electrophoresis [21] (FSCE) mode. When FSCE analysis is performed under stacking conditions with a large difference between the sample plug and running buffer specific conductivities, high temperature elevations of the analyte zone can result when applying a voltage.

All the experiments were carried out with biosynthetic human growth hormone (B-hGH) as the analyte. B-hGH is a 22 125 relative molecular mass protein consisting of 191 amino acids with an isoelectric point of *ca.* pH 5. Analysis was performed at pH 8.0, where B-hGH is a convenient choice of analyte as it has a suitable net mobility and is repelled from the capillary surface.

EXPERIMENTAL

Materials

Tricine {N-[tris(hydroxymethyl)methyl]glycine} and sodium chloride were purchased from Fluka (Buchs, Switzerland) and B-hGH from Novo Nordisk (Gentofte, Denmark). Fused-silica capillaries were obtained from Polymicro Technologies (Phoenix, AZ, USA). Peak areas were integrated on a Shimadzu C-R5A integrator (Kyoto, Japan).

Methods

Analysis was performed on an Applied Biosystems Model 270A analytical capillary electrophoresis system. The fused-silica capillaries had an I.D. of 50 μm, an O.D. of 192 μm, a total length of 100 cm and a length of 75 cm to the detector (effective

length). From the introduction end to the detector the capillaries were surrounded by a thermostated air-bath operated at 27°C. The electroosmotic flow was determined by measuring the retention time of the peak of neutral species.

Unless stated otherwise, the experimental conditions were as follows. Samples were introduced for 3 s by applying a 16.8-kPa vacuum at the detector end of the capillary. A 10 m*M* tricine (pH 8.0)–25 m*M* NaCl running buffer (specific conductivity at 21°C, $\kappa_{21°C} = 2.75$ mS cm^{-1}) was used. The applied potential was changed from 5 to 30 kV in steps of 5 kV. Detection was performed at 200 nm. Two series of experiments were performed: one with stacking and the other with non-stacking conditions. During the stacking runs B-hGH was diluted with distilled water to 0.1 mg ml^{-1} ($\kappa_{21°C} = 0.17$ mS cm^{-1}), whereas under non-stacking conditions B-hGH as diluted to the same concentration with running buffer ($\kappa_{21°C} = 2.75$ mS cm^{-1}).

THEORY

From experiments the electroosmotic mobility, μ_{EO}, can be measured as

$$\mu_{EO} = \frac{v_{EO}}{E} = \frac{L_d L_c}{t_{EO} U} \tag{1}$$

where v_{EO} is the electroosmotic velocity, E is the field strength, U is the applied voltage, t_{EO} is the retention time of the neutral species and L_d and L_c are the effective and total length of the capillary, respectively.

Fig. 1 shows the measured μ_{EO} values from the non-stacking experimental runs.

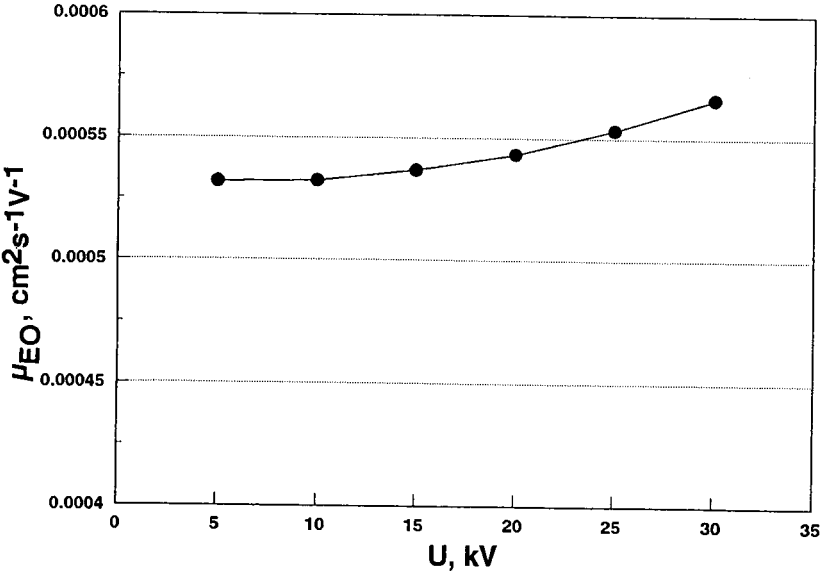

Fig. 1. Experimentally obtained electroosmotic mobility (μ_{EO}, cm^2 V^{-1}s^{-1}) *vs.* the applied potential (U, kV) in the non-stacking experiments. μ_{EO} was calculated by eqn. 1 after measuring the retention time of the peak of neutral species. The running buffer was 10 m*M* tricine (pH 8.0) containing 25 m*M* NaCl. The thermostated air-bath temperature was 27°C and the total capillary length was 100 cm. Other conditions as under Experimental.

As the only parameter changed during the experiment is the applied potential, the increase in μ_{EO} with increasing U must be due to an increased temperature of the running buffer.

In order to estimate the elevated temperature, instead of eqn. 1 μ_{EO} can be written as a function of one constant [the permittivity of vacuum ($\varepsilon_0 = 8.854 \cdot 10^{-14}$ C^2 cm^{-1} J^{-1})] and three temperature-dependent parameters {the relative permittivity (ε_r), the zeta potential [22,23] (ζ) and the viscosity (η)}:

$$\mu_{EO} = \frac{\varepsilon_0 \varepsilon_r \zeta}{\eta} \tag{2}$$

In order to estimate the average temperature change during analysis, a knowledge of how ε_r, ζ and η vary with temperature is crucial. In the HPCE literature most often it is assumed that the variations of ε_r and ζ can be neglected compared with the variations of η with temperature [18,24]. We do, however, use all three variables as functions of the temperature.

Calculation of ε_r

According to ref. 25, the relative permittivity change is related to the temperature change, dT, by

$$-\frac{d\log_{10}\varepsilon_r}{dT} = 0.00200 \tag{3}$$

Integrating ε_r from $\varepsilon_r(298\ K) = 78.54$ to $\varepsilon_r(T)$ yields

$$\varepsilon_r = 309.78 \exp(-0.004605T) = c_{\varepsilon 1} \exp(-c_{\varepsilon 2} T) \tag{4}$$

Calculation of η

In the temperature range 20–100°C the viscosity of water (cP) is related to the temperature (T, °C) by

$$\log\left(\frac{\eta}{\eta_{20}}\right) = \frac{1.3272(20 - T) - 0.001053(T - 20)^2}{T + 105} \tag{5}$$

where η_{20} is the viscosity at 20°C [25]. As an approximation, eqn. 5 is simplified to (T in K)

$$\eta = \frac{1}{800} \exp\left(\frac{1958}{T}\right) = c_{\eta 1} \exp\left(\frac{c_{\eta 2}}{T}\right) \tag{6}$$

Calculation of ζ

The zeta potential is considered to be proportional to temperature [22]:

$$\zeta = c_\zeta T \tag{7}$$

where T is in K and $c_\zeta = 4(k_{Bltz}/ze)$ mV K^{-1}, k_{Bltz}, z and e being the Boltzmann constant ($1.381 \cdot 10^{-23}$ J K^{-1}), the number of charges and the elementary charge ($1.602 \cdot 10^{-19}$ C), respectively.

Calculation of μ_{EO}

When the same running buffer is used throughout a series of experiments, where U is the only parameter changed from run to run, the mean temperature, T, during analysis can be calculated by the use of a reference μ_{EO} value where the temperature is known (T_{ref}):

$$\mu_{EO} \cdot \frac{\eta}{\varepsilon_0 \varepsilon_r \zeta} = \mu_{EO,ref} \cdot \frac{\eta_{ref}}{\varepsilon_0 \varepsilon_{r,ref} \zeta_{ref}} \tag{8}$$

Combining eqns. 4 and 6–8 and solving for μ_{EO} results in

$$\mu_{EO} = \mu_{EO,ref} \exp\left[c_{\eta 2}\left(\frac{1}{T_{ref}} - \frac{1}{T}\right) + c_{\varepsilon 2}(T_{ref} - T) \right] \frac{T}{T_{ref}} \tag{9}$$

Once the temperature T has been estimated, the viscosity and relative permittivity are calculated by the use of eqns. 4 and 6. The zeta potential is estimated relative to that at the reference temperature (eqn. 7), which in turn is estimated by rearranging eqn. 2:

$$\zeta_{ref} = \mu_{EO,ref} \cdot \frac{\eta_{ref}}{\varepsilon_0 \varepsilon_{r,ref}} \tag{10}$$

Power vs. temperature elevation

A linear relationship between dT and P (P is the power induced = UI, where I is the current) is assumed:

$$P = a dT + b \approx a dT \tag{11}$$

where a and b are constants. This is a simplification of reality, but the presumption is acceptable in the experiments (see Results and Discussion) as it does not induce serious errors in the temperature model. The actual dT–P curve deviates slightly from linearity at high dT values. Hence the dT values are not as large as would be expected from eqn. 11.

Radiation of energy

One of the factors that can make the dT–P curve deviate from linearity is the net radiation of energy per unit area from the capillary to the surroundings. In accordance with the Stefan–Boltzmann law, the radiation of energy is

$$Q = Q_{capillary} - Q_{surroundings} = \varepsilon_{capillary} \sigma_{Stf} T^4_{capillary} - \varepsilon_{surroundings} \sigma_{Stf} T^4_{surroundings} \tag{12}$$

where σ_{Stf} is the Stefan–Boltzmann constant ($5.67 \cdot 10^{-8}$ W m^{-2} K^{-4}) and ε_x is the

dimensionless emissivity constant, which is 1 for black bodies and <1 for all other bodies. If $T_{\text{capillary}} = 373.15$ K (100°C) and the 192 μm O.D. capillary is assumed to be a black body, the radiation of power from the 100-cm capillary would be 0.66 W, thus decreasing dT by less than 3°C (eqn. 11; see Results and Discussion). This must be compared with a temperature increase of *ca.* 73°C due to Joule heating of the capillary. As the actual net radiation from the capillary is even lower than 0.66 W at 100°C (emissivity constant <1, and subtraction of the radiation from the surroundings), the radiation of energy is neglected in the model.

Non-uniform electric field

When the conductivity of the sample zone differs from that of the running buffer, so do the field strength and the temperature during analysis [5,26]. In order to estimate the temperature of the buffer and sample zone, a few calculations have to be made.

The power which is induced in the capillary is separated into (a) power induced in the running buffer, P_B:

$$P_B = I^2 R_B = I^2 \cdot \frac{L_B}{A\kappa_B} = I^2 \cdot \frac{L_c - L_0}{A\kappa_B} \tag{13}$$

and (b) power induced in the sample zone, P_S:

$$P_S = I^2 R_S = I^2 \cdot \frac{L_0}{A\kappa_S} \tag{14}$$

Hence,

$$P = P_B + P_S = \frac{I^2}{A}\left(\frac{L_c - L_0}{\kappa_B} + \frac{L_0}{\kappa_S}\right) \tag{15}$$

Subscripts B and S denote buffer and sample solution, respectively; A is the cross-sectional area, R is the resistance, κ is the specific conductivity and L_B and L_0 are the length of the buffer and the originally introduced sample zone, respectively. Combining eqns. 13–15 and solving eqn. 15 with respect to P_B and P_S results in

$$P_B = \frac{P}{1 + X} \tag{16}$$

$$X \equiv \frac{\kappa_B L_0}{\kappa_S (L_c - L_0)} \tag{17}$$

and

$$P_S = P_B X = \frac{P}{\frac{1}{X} + 1} \tag{18}$$

Now the temperature elevations of the running buffer, dT_B, and of the sample zone, dT_S, can be estimated with the use of eqn. 11:

$$dT_B = \frac{P_B L_c}{a(L_c - L_0)} = \frac{PL_c}{a(1 + X)(L_c - L_0)} \tag{19}$$

$$dT_S = \frac{P_S L_c}{aL_0} = \frac{PL_c}{a\left(\frac{1}{X} + 1\right)L_0} \tag{20}$$

Specific conductivity vs. temperature

As the running buffer and sample zone experience different temperature elevations under stacking conditions, it remains to find the specific conductivity as a function of the temperature. From experiments, identical and linear conductivity index (CI) *vs.* T (T in °C) curves were obtained (see Results and Discussion), where CI is defined as

$$CI = 100 \cdot \frac{\kappa_T}{\kappa_{21°C}} = c_{\kappa 1} + c_{\kappa 2} T \tag{21}$$

Eqns. 16–21 are solved iteratively in order to estimate the specific conductivities and temperatures of the running buffer and sample zone during each run in the stacking and non-stacking runs.

Temperature gradient as a function of radial position

Fig. 2 is a schematic diagram of a capillary tube. The total temperature

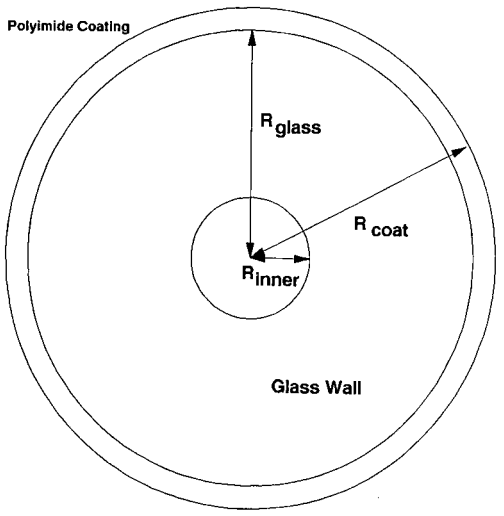

Fig. 2. Schematic diagram of a capillary tube. R_{inner} = distance from capillary axis to inner radius; R_{glass} = distance from capillary axis to the glass wall outer radius; R_{coat} = distance from capillary axis to outer radius.

difference between the centre of the capillary tube and the air-bath is made up of four contributions:

$$dT = dT_{inner} + dT_{glass} + dT_{coat} + dT_{surr} \tag{22}$$

where dT_{inner}, dT_{glass}, dT_{coat} and dT_{surr} are the temperature gradients from the centre of the tube to the capillary inner radius, across the glass wall, across the polyimide coating and from the capillary outer jacket to the surroundings, respectively.

Owing to the temperature-dependent electroosmotic and electrophoretic mobilities, a knowledge of the temperature difference from the centre of the tube to the fused-silica glass wall, dT_{inner}, is of special interest when considering dispersion. By use of eqn. 9 the electroosmotic mobility is calculated to increase by 2–3% per °C in the range 20–100°C.

The temperature difference from the centre of the tube to the capillary inner radius, R_{inner}, is found by solving the heat conduction equation [27]

$$\frac{1}{r}\left(\frac{d}{dr}\right)\left[rk_w\pi R_{inner}^2 L_c \cdot \frac{dT_{inner}(r)}{dr}\right] = -P \tag{23}$$

where r is the variable radius and k_w is the thermal conductivity of the buffer. Integrating eqn. 23 with the appropriate boundary conditions yields

$$dT_{inner} = P \cdot \frac{1}{4\pi k_w L_c} = c_{inner}P \tag{24}$$

at the glass wall where $r = R_{inner}$.

dT_{glass} and dT_{coat} are calculated by solving equations similar to eqn. 23 and integrating from R_{inner} to R_{glass} (radius from the tube axis to the polyimide coating) and from R_{glass} to R_{coat} (radius from the tube axis to the outside of the polyimide coating), respectively. The solutions are

$$dT_{glass} = \frac{\ln\left(\frac{R_{glass}}{R_{inner}}\right)}{2\pi k_{glass} L_c} \cdot P = c_{glass}P \tag{25}$$

and

$$dT_{coat} = \frac{\ln\left(\frac{R_{coat}}{R_{glass}}\right)}{2\pi k_{coat} L_c} \cdot P = c_{coat}P \tag{26}$$

The temperature gradient across the air film from the capillary outer wall to the thermostated air-bath, dT_{surr}, is calculated by subtraction of the three other dT_x terms from the total temperature difference, dT, which was found by eqn. 9. Hence,

$$dT_{surr} = \frac{P}{a} - c_{inner}P - c_{glass}P - c_{coat}P = c_{surr}P \tag{27}$$

The heat-transfer coefficient, h, indicates the effectiveness of the heat removal from the air film on the capillary polyimide coating to the surroundings. h is estimated by combining eqn. 27 with Newton's law of cooling [27]:

$$P = hA\mathrm{d}T_{\mathrm{surr}} \tag{28}$$

thus yielding

$$h = \frac{1}{c_{\mathrm{surr}}A} \tag{29}$$

RESULTS AND DISCUSSION

Estimation of buffer temperature

As the slope of the experimentally obtained μ_{EO} curve from 5 to 10 kV in Fig. 1 is approximately zero, it is reasonable to assume that there is no increase of the buffer temperature relative to the thermostated air-bath surrounding the capillary. Hence, inserting $T_{\mathrm{ref}} = 300$ K (27°C), $\mu_{\mathrm{EO,ref}} = \mu_{\mathrm{EO}}$ (300 K, 5 kV) and the measured μ_{EO} values in eqn. 9 and solving iteratively for T, the temperatures of the running buffer are estimated in the remainder of the runs (10–30 kV).

Fig. 3 shows the calculated temperature elevations. The η, ε_{r} and ζ values (calculated by eqns. 4, 6 and 10) are depicted in Fig. 4 relative to the values at 27°C (300 K), and Table I contains the absolute values. The relative changes of ε_{r} and ζ as a function of U approximately cancel each other out.

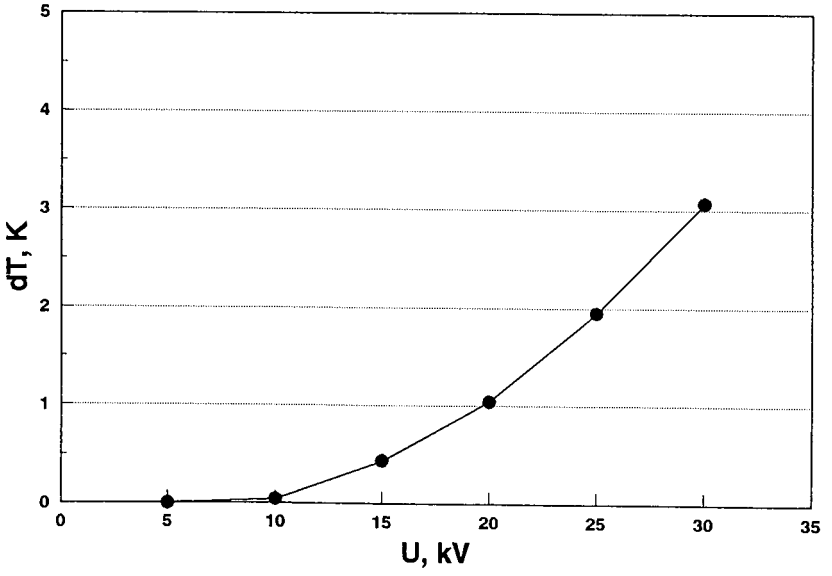

Fig. 3. Calculated temperature elevations (dT, K) of the running buffer *vs.* the applied potential (U, kV) in the non-stacking experiments. The dT values are found by inserting the measured μ_{EO} values in eqn. 9 and solving iteratively with respect to T. Experimental conditions as in Fig. 1.

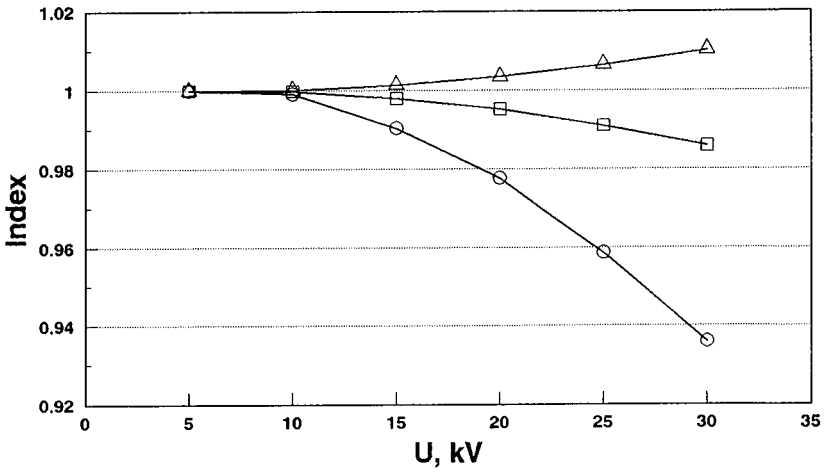

Fig. 4. Calculated (○) relative viscosity (η), (□) relative permittivity (ε_r) and (△) zeta potential (ζ) *vs.* applied potential (U, kV). The η, ε_r and ζ values are shown relative to the values in the 5-kV run. Table I summarizes the absolute values. Experimental conditions as in Fig. 1.

Power vs. temperature elevation

A plot of the measured average power, $P = UI$, *vs.* the estimated temperature changes, dT, results in Fig. 5. As assumed in eqn. 11, omitting the lowest x-value point on the curve a linear dT *vs.* P relationship is observed with slope $a = 0.207$ W K^{-1} and intercept with the ordinate $b = 0.073$ W.

The reason for the non-zero intercept of the power curve and the ordinate, is explained as being due to the $dT = 0$ assumption in the 5-kV experiment. For simplicity b is neglected when estimating dT from the measured P values (error 0.35 K).

Specific conductivity vs. buffer temperature

In order to relate the specific conductivity to the temperature of the running buffers, the specific conductivities of three 10 mM tricine running buffers (pH 8.0) containing (a) 0 mM NaCl ($\kappa_{21°C} = 0.22$ mS cm^{-1}), (b) 25 mM NaCl ($\kappa_{21°C} = 2.75$ mS cm^{-1}) or (c) 50 mM NaCl ($\kappa_{21°C} = 4.96$ mS cm^{-1}) were measured in the temperature range 21–93°C by heating the buffer in a stirred beaker. In Fig. 6 the resultant conductivity index (CI) values are plotted *vs.* the measured temperatures. In

TABLE I

ABSOLUTE VALUES OF THE VISCOSITY (η), RELATIVE PERMITTIVITY (ε_r) AND ZETA POTENTIAL (ζ) FROM EXPERIMENTS AS A FUNCTION OF THE APPLIED POTENTIAL (E_{app}) AND THE TEMPERATURE ELEVATION (dT) IN THE NON-STACKING RUNS

U	dT (K)	η (cP)	ε_r	ζ (mV)
5	0.00	0.851	77.82	65.73
10	0.04	0.850	77.80	65.74
15	0.44	0.843	77.66	65.83
20	1.04	0.832	77.45	65.96
25	1.95	0.816	77.12	66.16
30	3.08	0.797	76.73	66.41

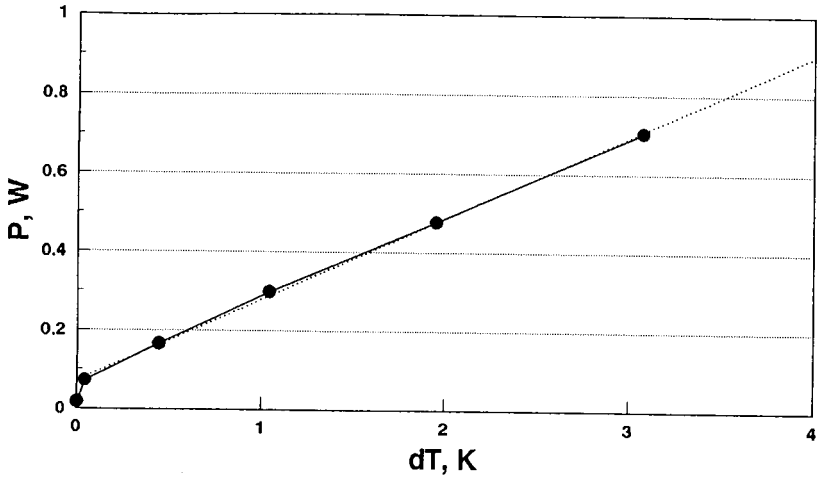

Fig. 5. Measured power inductions ($P = UI$, W) *vs.* the calculated temperature elevations (dT, K) in the non-stacking experiment. Omitting the lowest x-value point, linear regression yields $P = 0.207\,\mathrm{d}T + 0.073$. The correlation factor is 0.9992. See text and Experimental for details. ●—● = Experiments; dotted line = linear regression.

accordance with eqn. 21, linearity is observed. The constants in eqn. 21 were found to be $c_{\kappa 1} = 38.67$ and $c_{\kappa 2} = 2.62°C^{-1}$ by linear regression on all data points.

Sample zone temperature, stacking vs. non-stacking conditions

Solving eqns. 16–21 iteratively with the appropriate experimental values yields the specific conductivities and temperatures of the running buffer and sample zone during each run under stacking and non-stacking conditions. The results are shown in

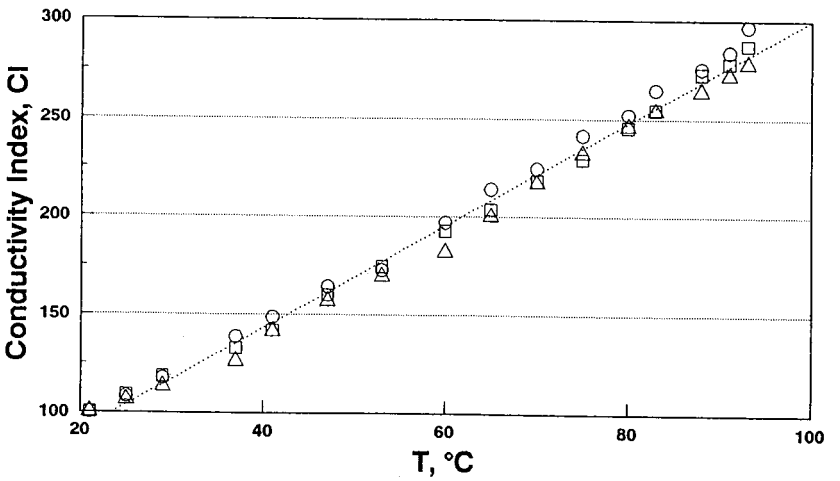

Fig. 6. Conductivity index ($CI = 100\kappa_T/\kappa_{21°C}$) *vs.* the temperature (T, °C) for three 10 mM tricine buffers (pH 8.0) containing (○) 0, (□) 25 or (△) 50 mM NaCl. The buffer was heated in a stirred beaker and the specific conductivity measured in the range 21–93°C. A linear CI–T relationship is observed. Linear regression (dotted line) on all data points gave a correlation factor equal to 0.9961.

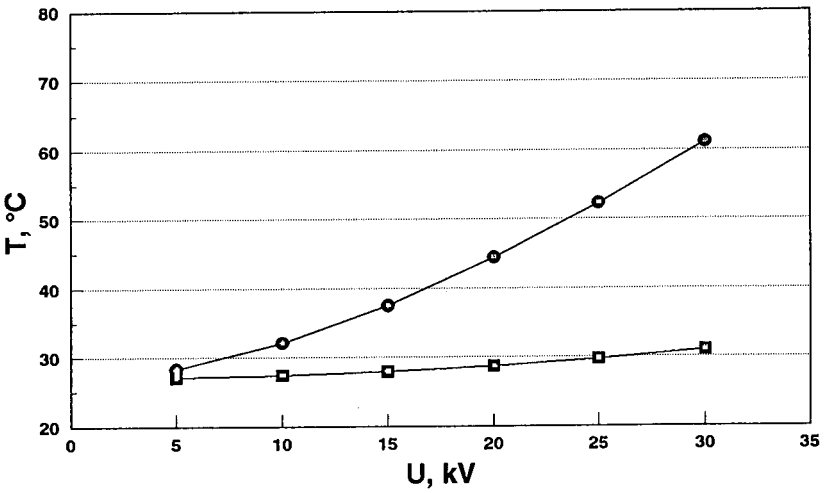

Fig. 7. Estimated sample zone temperature (T, °C) *vs.* the applied potential (U, kV) in the (●) stacking and (■) non-stacking runs. The sample zone experiences higher temperatures when diluted with distilled water (stacking) compared with dilution with running buffer (non-stacking).

Fig. 7 with respect to sample zone temperature. When the analyte is diluted with distilled water, the temperature elevation at any U is higher than that experienced when diluting the analyte with the running buffer. The reason for the higher temperature of the sample zone during stacking conditions is due to the specific conductivity difference between the running buffer and the sample solution, thus resulting in different field strengths.

This is further elaborated in Fig. 8. Three 10 mM tricine buffers (pH 8.0) containing either 0, 25 or 50 mM NaCl were used in three experimental series. The B-hGH analyte was diluted to 0.1 mg ml^{-1} with distilled water ($\kappa_{21°C}$ = 0.17 mS cm^{-1}). As the specific conductivity of the sample was lower than that of any of the three running buffers, stacking conditions prevailed in all three experimental series. The purpose of the three experiments was to show the effect of different "stacking powers" (κ_B/κ_S) on the sample zone temperature elevations.

The highest temperature elevation of the buffer zone was experienced in the 30-kV run with the 50 mM NaCl tricine buffer [T_B (50 mM) *ca.* 6°C], where the induced power was *ca.* 1.4 W. However, when the specific conductivity ratio κ_B/κ_S and the specific conductivity of the buffer solution, κ_B, are both high, the sample zone reaches very high temperatures at high applied potentials. At 30 kV with the 50 mM NaCl tricine buffer as running buffer the sample zone is close to the boiling point [T_S (50 mM)] according to the estimations.

When the temperature of the sample zone increases more than the temperature elevation of the running buffer (owing to the different field strengths), the specific conductivity ratio decreases compared with the ratio which is experienced when the two solutions have the same temperature. This change is taken into consideration in eqn. 21 and shown in Fig. 9 for the three experimental series with running buffers of different NaCl concentration.

One must consider the temperature of the analyte zone when the analysis is

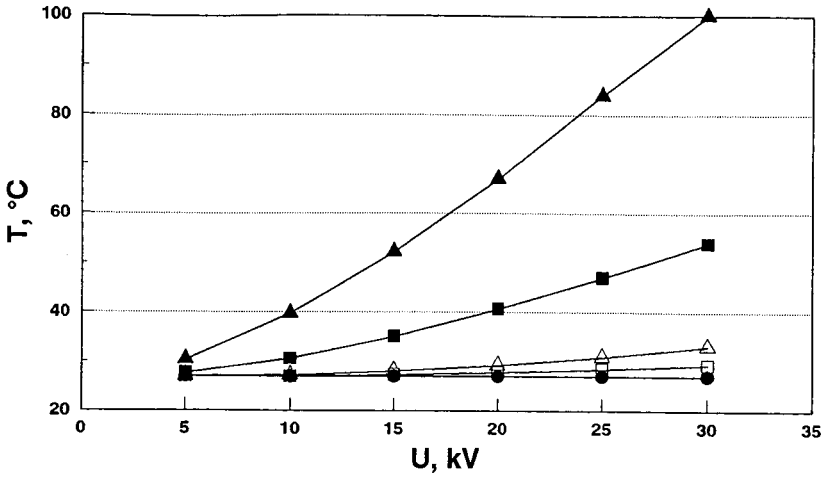

Fig. 8. Estimated temperatures of (open symbols) the running buffer (T_B, °C) and (closed symbols) the sample zone (T_S, °C) *vs.* the applied potential (U, kV). The sample was B-hGH diluted to 0.1 mg ml^{-1} with distilled water ($\kappa_{21°C}$ = 0.17 mS cm^{-1}). Sample was introduced for 1.0 s by means of a 16.8-kPa vacuum. All the runs were performed under stacking conditions. Three experimental series were carried out in 10 m*M* tricine buffers (pH 8.0) containing (○, ●) 0 m*M* NaCl ($\kappa_{21°C}$ = 0.22 mS cm^{-1}), (□, ■) 25 m*M* NaCl ($\kappa_{21°C}$ = 2.75 mS cm^{-1}) or (△, ▲) 50 m*M* NaCl ($\kappa_{21°C}$ = 4.96 mS cm^{-1}). Other conditions as under Experimental.

performed using stacking conditions. As long as the analyte zone is still in the original sample zone, it will experience an elevatad temperature compared with that of the running buffer. The fact that the temperature elevations can even become so dramatic that boiling of the sample zone is possible under certain experimental conditions is

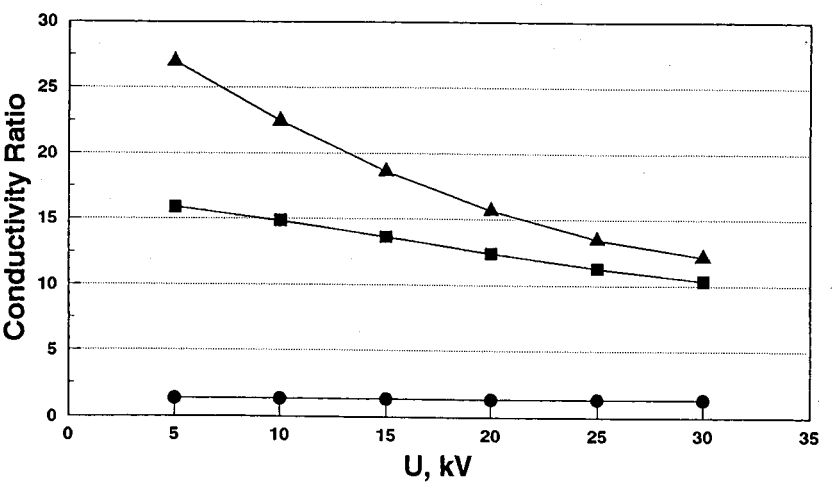

Fig. 9. Specific conductivity ratio (κ_B/κ_S) *vs.* the applied potential (U, kV) in the three experimental series, where the running buffer contained (●) 0, (■) 25 or (▲) 50 m*M* NaCl. Experimental conditions as in Fig. 8. As the difference in temperature between the sample zone and the running buffer increases with higher U, the specific conductivity ratio decreases in accordance with eqn. 21.

interesting. Most important, however, is that knowledge of the temperature elevation can be crucial when the analyte is heat-labile. In that event high temperatures resulting in degradation of the analyte could be misinterpreted as, *e.g.*, impurities in the original sample.

Temperature calculations based on Ohm's law

As an alternative to the electroosmotic mobility-based temperature estimations, which are used in this model, the temperature elevations could be based on eqn. 21 and Ohm's law. The values obtained in this way varies by less than 6% from the already estimated values. Owing to the different specific conductivities along and across the capillary tube, and the current contributions from ions making up the electroosmotic flow, all the temperature calculations shown here are, however, based on changes in the electroosmotic mobilities.

Temperature gradient as a function of radial position

Inserting $R_{inner} = 25$ μm, $R_{glass} = 90$ μm, $R_{coat} = 96$ μm, $k_{glass} = 1.50$ W m^{-1} K^{-1} [18], $k_{coat} = 0.155$ W m^{-1} K^{-1} [18] and $k_w = 0.605$ W m^{-1} K^{-1} [18] in eqns. 24–27 yields the values $c_{inner} = 0.1315$ K W^{-1}, $c_{glass} = 0.1359$ K W^{-1}, $c_{coat} = 0.0663$ K W^{-1} and $c_{surr} = 4.4972$ K W^{-1}. Each of the four temperature difference terms is tabulated as a percentage of the total temperature difference in Table II. More than 90% of the resistance to heat transfer is in the air film on the outer jacket of the capillary. This means that one should focus on this resistance if the heat removal should be more effective.

Inserting $c_{surr} = 4.4972$ K W^{-1} in eqn. 29 results in a heat-transfer coefficient of 369 W m^{-2} K^{-1} for the air-bath-thermostated capillary in the ABI Model 270A HPCE instrument. In the Beckman P/ACE System 2000 HPCE instrument, where the capillary is thermostated with circulating liquid by the use of a Peltier device, similar calculations gave an h value of 501 W m^{-2} K^{-1} when a 75 μm I.D. capillary was employed for the analysis (50 μm I.D. in the ABI Model 270A). It is surprising that the heat-transfer coefficient is only slightly larger for the liquid cooling than the air cooling.

TABLE II

EACH OF THE FOUR TEMPERATURE GRADIENTS IN EQN. 22 WRITTEN AS THEIR PERCENTAGE OF THE TOTAL TEMPERATURE GRADIENT, dT

The values were obtained by solving eqns. 24–27 with the appropriate experimental values. More than 90% of the total heat flux resistance is in the air film on the outer wall of the capillary tube. Hence this air film acts as a "thermo layer".

dT_X	$\frac{dT_X}{dT} \cdot 100$ (%)
dT_{inner}	2.7
dT_{glass}	2.8
dT_{coat}	1.4
dT_{surr}	93.1
Total	100.0

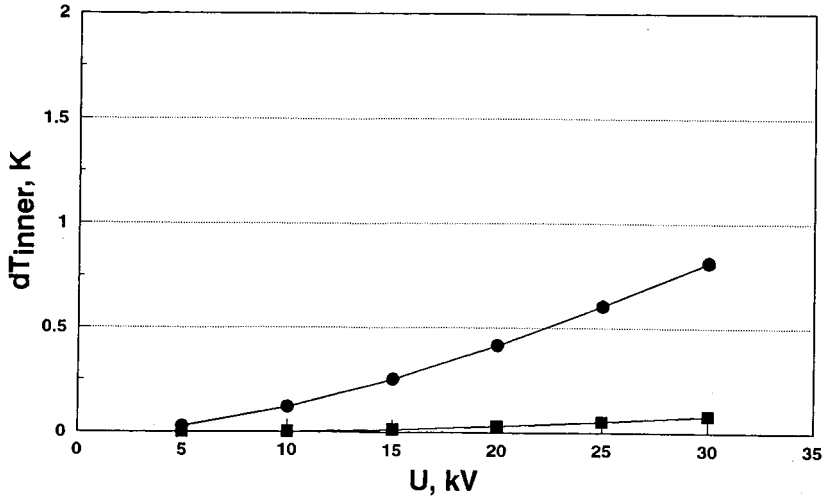

Fig. 10. Sample zone temperature gradient from the capillary tube axis to the inner radius (dT_{inner}, K) *vs.* the applied potential (U, kV) in the (●) stacking and (■) non-stacking runs. Experimental conditions as in Fig. 1.

As only 2.7% of the total temperature difference is from the centre of the capillary tube to the glass wall in the air-bath-thermostated HPCE apparatus (Table II), a dT value of 10°C only results in a dT_{inner} value of 0.27°C. Fig. 10 shows the calculated dT_{inner} values of the sample zone in the stacking and non-stacking experiments. In Fig. 11 the estimated sample zone temperatures when employing the running buffers with three different NaCl concentrations are plotted. The dT_{inner} values are kept within 2°C even at dT_S values of *ca.* 70°C (30 kV, tricine buffer with 50 m*M* NaCl). These results are in accordance with similar calculations reported by Grushka *et al.* [18] and Knox [19].

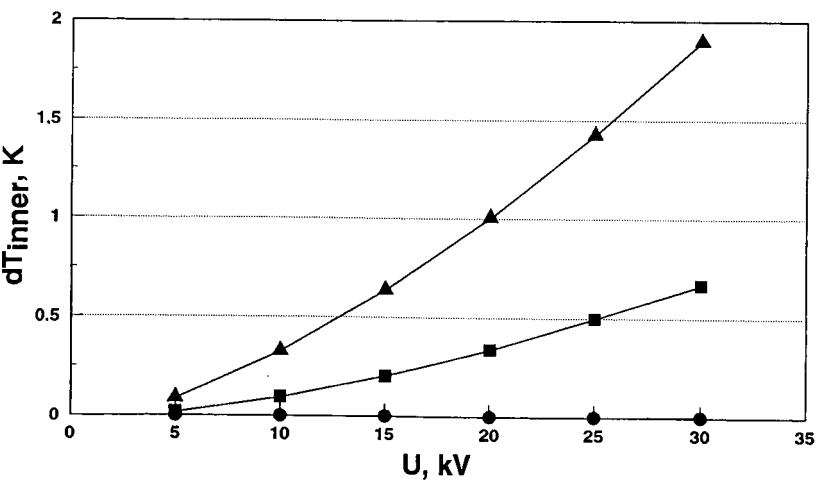

Fig. 11. Sample zone temperature gradient from the capillary tube axis to the inner radius (dT_{inner}, K) *vs.* the applied potential (U, kV) in the three experimental series where the 10 m*M* tricine buffer (pH 8.0) contained (●) 0, (■) 25 or (▲) 50 m*M* NaCl. Experimental conditions as in Fig. 8.

Two approaches can be considered in order to minimize dispersion caused by Joule heating of the analyte zone. Either the heat removal should be very effective, thus minimizing the total temperature gradient, dT, or the dT_{inner}/dT ratio should be kept low. The latter is accomplished either by increasing the surface-to-volume ratio of the capillary tube or by making the glass tube, the polyimide coating and/or the "thermo layer" on the capillary tube act as a heat-transfer resistor, which increases the overall dT, however. A combination of the air film acting as a heat-transfer resistor (by the use of the thermostated air-bath) and a small capillary I.D. and O.D. was used in the actual experiments. While the dT_{inner} to dT percentage ratio for the thermostated air-bath was 2.7%, the corresponding value for the Peltier-based liquid cooling system was 11.7%. When a 75 μm I.D. capillary is used in the Beckman P/ACE System 2000 and a 50 μm I.D. capillary is used in the ABI Model 270A, almost identical temperatures are obtained when identical buffers and field strengths are employed. Hence, with the same temperatures inside the capillaries, the additional analyte zone dispersion caused by Joule heating is largest when liquid cooling is used. The overall dT is, however, lower in the liquid-cooled system when identical I.D. and O.D. capillaries are used in the two instruments.

The relatively low temperature elevations as a function of radial position in the liquid, dT_{inner}, should not be confused with the fact that the buffer/sample zone as a whole experiences an elevated temperature, dT.

REFERENCES

1 B. L. Karger, A. S. Cohen and A. Guttman, *J. Chromatogr.*, 492 (1989) 585.
2 W. G. Kuhr, *Anal. Chem.*, 62 (1990) 403R.
3 C. L. Rice and R. Whitehead, *J. Phys. Chem.*, 69 (1965) 4017.
4 M. Martin, G. Guiochon, Y. Walbroehl and J. W. Jorgenson, *Anal. Chem.*, 57 (1985) 559.
5 A. Vinther and H. Søeberg, *J. Chromatogr.*, 559 (1991) 3.
6 J. W. Jorgenson and K. D. Lukacs, *Science*, 222 (1983) 266.
7 X. Huang, W. F. Coleman and R. N. Zare, *J. Chromatogr.*, 480 (1989) 95.
8 H. H. Lauer and D. McManigill, *Trends Anal. Chem.*, 5 (1986) 11.
9 F. Foret, M. Deml and P. Bocek, *J. Chromatogr.*, 452 (1988) 601.
10 S. Hjertén, *Electrophoresis*, 11 (1990) 665.
11 W. Th. Kok, *Zone Broadening in Capillary Zone Electrophoresis*, Amsterdam Summer Course in Capillary Zone Electrophoresis, University of Amsterdam, Amsterdam, 1990.
12 S. Terabe, K. Otsuka and T. Ando, *Anal. Chem.*, 61 (1989) 251.
13 S. Terabe, paper presented at the *3rd International Symposium on High Performance Capillary Electrophoresis (HPCE '91), San Diego, CA, Feb. 3–6, 1991* paper LW-3.
14 J. H. Knox and K. A. McCormack, *J. Liq. Chromatogr.*, 12 (1989) 2435.
15 K. D. Lukacs and J. W. Jorgenson, *J. High Resolut. Chromatogr. Chromatogr. Commun.*, 8 (1985) 407.
16 S. Terabe, K. Otsuka and T. Ando, *Anal. Chem.*, 57 (1985) 834.
17 A. E. Jones and E. Grushka, *J. Chromatogr.*, 466 (1989) 219.
18 E. Grushka, R. M. McCormick and J. J. Kirkland, *Anal. Chem.*, 61 (1989) 241.
19 J. H. Knox, *Chromatographia*, 26 (1988) 329.
20 R. J. Nelson, A. Paulus, A. S. Cohen, A. Guttman and B. L. Karger *J. Chromatogr.*, 480 (1989) 111.
21 V. P. Burolla, S. L. Pentoney and R. N. Zare, *Am. Biotechnol. Lab.*, Nov./Dec. (1989) 7:10, 12.
22 D. C. Crow, *Principles and Applications of Electrochemistry*, Chapman & Hall, London, 1988.
23 T. S. Stevens and H. J. Cortes, *Anal. Chem.*, 55 (1983) 1365.
24 D. S. Burgi, K. Salomon and R.-L. Chien, presented at the *2nd International Symposium on High Performance Capillary Electrophoresis (HPCE '90), San Francisco, CA, Jan. 29–31, 1990*, poster P-112.
25 R. C. Weast and M. J. Astle (Editors), *CRC Handbook of Chemistry and Physics*, CRC Press, Boca Raton, FL, 62nd ed., 1982, E-51.
26 S. E. Moring, J. C. Colburn, P. D. Grossman and H. H. Lauer, *LC · GC Int.*, 3 (1990) 46.
27 R. B. Bird, W. E. Stewart and E. N. Lightfoot, *Transport Phenomena*, Wiley, New York, 1960.

Journal of Chromatography, 559 (1991) 43–56
Elsevier Science Publishers B.V., Amsterdam

CHROM. 23 455

Factors influencing the resolution and quantitation of oligonucleotides separated by capillary electrophoresis on a gel-filled capillary

DAVID DEMOREST* and ROBERT DUBROW
Applied Biosystems, Inc., 3745 N. First Street, San Jose, CA 95134 (USA)

ABSTRACT

Instrumental and sample matrix factors were examined for their effect on the resolution, sensitivity and detectability of oligodeoxynucleotides separated on 50 μm I.D. gel-filled capillaries. Substantial errors in the calculated percentage purity may result from using peak areas not corrected for peak velocity. Area multiplied times velocity, not area, is used as the quantitative response with units of area counts cm/min. At high oligonucleotide concentrations the response varies linearly with increasing sample oligonucleotide concentration, but at low concentrations the response varies anomalously. This finding indicates the importance of using internal standards for quantitations. Increases in the sample conductivity dramatically decrease the sensitivity, whereas changes in the sample pH have only a minor effect. The mass loading increases linearly with increase in the injection voltage and duration. With injection durations of up to 20 s, the sensitivity is increased in excess of one order of magnitude with only a 15% decrease in resolution. The separation efficiency of larger sized oligonucleotides decreases more readily with increasing on-column mass than smaller species. Increases in the separation field strength and column length increase the resolution consistent with theory only when the detector rise time is reduced. An increase in the column temperature results in a decrease in the migration times by 1.1% per °C with only minor decreases in resolution.

INTRODUCTION

The use of capillary electrophoresis employing gel-filled capillaries for the separation and quantitation of oligodeoxynucleotides is emerging as a powerful tool in molecular biology and biotechnology. This technique, using capillaries of 50–100 μm I.D. and field strengths of 100–450 V/cm, has been used for the single-base resolution of synthetic oligonuclotides of 12–160 bases [1–5] and for the separation of DNA restriction fragments [6], polymerase chain reaction (PCR) amplified products [6] and DNA sequencing products [7–10]. The high resolution achieved on gel-filled capillaries is similar to those of conventional slab-gel separations, but the capillary separations have the additional advantages of short analysis times, low volume–low mass sample requirements and the real-time detection and post-run quantitative data manipulation of traditional chromatographic methods.

As the making of reliable, trouble-free, gel-filled capillaries has been reported to be problematic [4,7], the current availability of consistently performing gel capillaries

0021-9673/91/$03.50

will help dramatically in the acceptance of this technique. With this growth comes the need to understand better the instrumental and chemical factors that influence the performance of gel-filled capillaries for the separation of oligonucleotides. The purpose of this paper is to present, in a quantitative and comprehensive approach, those factors which influence the resolution, detectability and sensitivity of selected synthetic oligonucleotides. With this information, users of gel-filled capillaries should be able to optimize better their separations to suit their individual needs.

EXPERIMENTAL

Materials

Micro-Gel™ 100 capillaries of 50 μm I.D., total length 51 cm and separation length 30 cm, filled with a proprietary gel matrix developed and manufactured by Applied Biosystems (Foster City, CA, USA) were used. The running electrophoresis buffer was 75 m*M* Tris–phosphate (pH 7.6)–methanol (90:10) from Applied Biosystems. Other buffers were made with high-purity Tris (Sigma, St. Louis, MO, USA), phosphoric acid (analytical-reagent grade, J.T. Baker, Phillipsburg, NJ, USA), methanol [high-performance liquid chromatographic (HPLC) grade, Burdick & Jackson, Muskegon, MI, USA], urea (electrophoresis grade, Bio-Rad Labs., Richmond CA, USA), formamide (analytical-reagent grade, Sigma) and ethylene glycol (analytical-reagent grade, Pierce, Rockford, IL, USA). The oligonucleotides $p(dA)_{12,17,18}$ and $d(AGTC)_{3,6,9}$ were synthesized on a Model 380B DNA synthesizer (Applied Biosystems) using standard 5-hydroxyl-protected cyanoethyl phosphoramidite chemistry. The oligonucleotides were purified by HPLC followed by ethanol precipitation. Water purified with a Milli-Q system (Millipore, Bedford, MA, USA) was used to prepare all buffers and to reconstitute oligonucleotide samples, except were indicated.

Methods and apparatus

Separations were performed on a Model 270A capillary electrophoresis system (Applied Biosystems) under the conditions specified later for total capillary length (*L*), effective separation length (*l*), I.D. (*d*), field strength (*E*), current (*i*), temperature (*T*), electrokinetic injection duration (*t*), voltage (*V*) and oligonucleotide concentration (*C*). The gel concentration (about 8.5% polymer) and running buffer were held constant in order to explore fully the effects of changing the other parameters. On-gel UV detection was applied at 260 nm, range 0–10 ma.u.f.s., with a rise time of 0.1–1.0 s as specified later. The detector signal output was processed through either an HP 3396 integrator (Hewlett-Packard, Avondale, PA, USA) or an SP Chromjet integrator (Spectra-Physics, San Jose, CA, USA) or recorded on a strip-chart recorder (Applied Biosystems). Conductivity measurements were made on a Model 1481-60 conductivity meter (Cole-Parmer Instruments, Chicago, IL, USA) using a micro-conductivity electrode (Microelectrodes, Londonderry, NH, USA). pH measurements were made on a Model 701A digital Ionanalyzer (Orion Research, Cambridge, MA, USA) using micro-pH and reference electrodes (Microelectrodes).

RESULTS AND DISCUSSION

Relationship between peak area and peak velocity

In chromatographic separations using post column detection, the separated analytes pass through a detector flow cell at the same velocity. Analytes separated by electrophoretic methods, using on-column detection, move at different velocities through the detection cell during run-time detection. A given analyte mass moving through a detector cell at a slower rate will be integrated for a longer period of time and, thus, produce a larger area count on a standard laboratory integrator. It would be expected that for the same mass moving at a different rate that area times velocity would be constant according to the following equation:

$$m = kAv \tag{1}$$

where m is the mass moving through the detector cell, A is the area counts, v is the mass velocity and k is a constant dependent on the detector optics and integration sensitivity. According to eqn. 1, the on-gel detection of oligonucleotides during separation by capillary electrophoresis would require, for quantitative accuracy, that area times velocity be used as the quantitative response factor with units of area counts cm/min. For practical purposes, with separations being performed on the same system, we can set $k = 1$ and

$$v = l / t \tag{2}$$

where l is the effective separation length (cm) and t is the peak migration time (min). Combining eqns. 1 and 2, we obtain the following relationship between mass and area:

$$m \propto Al / t \tag{3}$$

Eqn. 3 is valid only if the separating analytes have a uniform velocity during transport through the gel capillary and do not speed up or slow down before they enter the detector cell. The validity of eqn. 3 was demonstrated by the results shown in Fig. 1.

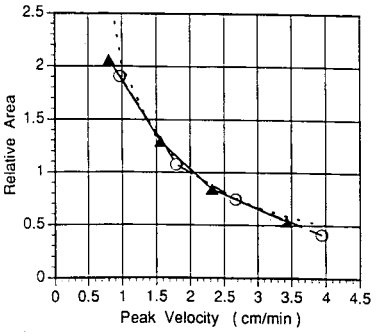

Fig. 1. Effect of oligonucleotide velocity on the area, calculated relative to the area at a velocity of 2.0 cm/min. The data are averages of four separate experiments using gel-filled capillary conditions of L = 39, 43, 44, and 47 cm, l = 20, 24, 25 and 28 cm, T = 50°C, E = 100–400 V/cm, i = 6–24 μA, t = 3 s, V = −5kV and C = 70 ng/ml. ▲———▲ = $p(dA)_{18}$; O----O = $p(dA)_{12}$; ····· = theoretical, based on eqn. 3 using a relative area of 1.0 at 2.0 cm/min. See text for definition of abbreviations.

Holding the injection duration and voltage constant, the same concentrations of polydeoxyadenylic acids [$p(dA)_{12}$ and $p(dA)_{18}$] were separated at different field strengths and different separation lengths. The different velocities were achieved by changing the field strengths and the separation lengths were varied to test for on-column time-dependent changes in mass. The average of all data shows a close fit to that expected from eqn. 3 when normalizing to an area of 1.0 at 2 cm/min.

If area instead of area times velocity units are used to calculate the percentage purity of oligonucleotides, errors in the actual mass% may result if there is a significant amount of a major failure sequence or large numbers of minor failure sequences. To put this fact into perspective, consider that equal area counts are obtained for an n-mer and a $(n-1)$-mer oligonucleotide. The calculated purity of the n-mer would be 50%. The migration time of the $n-1$-mer is about 0.95 times that of the n-mer, so that its relative area times velocity would be 1.05 compared with 1.0 for the n-mer. Using area times velocity units to calculate purity would result in 48.8%, a 1.2% difference in the mass purity calculation. In another example, if the n-mer had an area purity of 90% compared with the $(n-1)$-mer, then the calculated area times velocity purity would be 89.6%, only a 0.4% difference in mass purity. Obviously, as the migration time difference between the n-mer and its n-minus (or -plus) failure sequences increase, the greater will be the difference in purity calculations between area and area times velocity units.

The quantitative response units used in this paper are calculated from eqn. 3 and are labelled as area–velocity (counts cm/min).

Effect of oligonucleotide concentration, sample conductivity, pH and organic modifiers on detectability and sensitivity

The results showing the detector response as a function of sample oligonucleotide concentration in water are plotted in Fig. 2. As shown at lower values of concen-

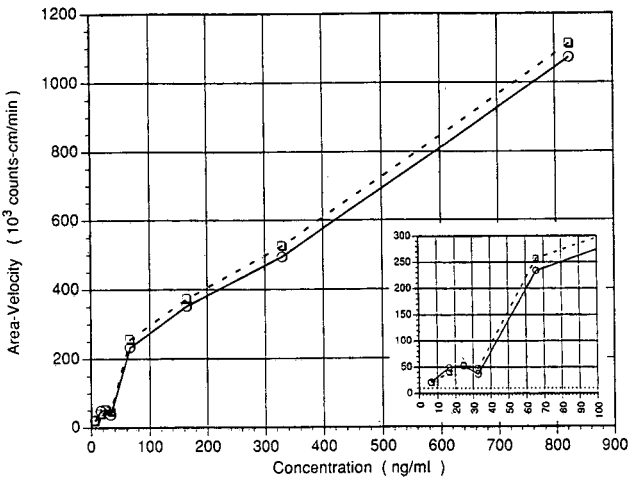

Fig. 2. Effect of sample oligonucleotide concentration on the quantitative response, area times velocity at 260 nm. The gel-filled capillary conditions of analysis were L = 47 cm, l = 28 cm, T = 50°C, E = 298 V/cm, i = 18 μA, t = 10 s and V = −5kV. O———O = $p(dA)_{12}$; □-----□ = $d(AGTC)_6$. The dotted line in the inset represents the lower limit of response for $p(dA)_{12}$.

tration, the lower limit of response (r) is the area times velocity for $p(dA)_{12}$ calculated from the equation

$$r = Al / t \tag{4}$$

where r is area times velocity, l is the separation length, t is the migration time and A is the average area of noise peaks plus three standard deviations of the noise. For $p(dA)_{12}$, $A = 1930 + 3\,(550) = 3580$ counts, $l = 28$ cm and $t = 9.56$ min, then $r = 10\,485$ counts cm/min. Extraprolating the lower curve to zero through this point yields a minimum detectable concentration (MDC) of 3 ng/ml (equivalent to about 0.00009 AU_{260}/ml) for the conditions used. Increases in the injection duration and voltage may be used, as described later, to reduce the MDC further. It should be noted that the MDC will not be a constant for any one system, but according to eqn. 4 will vary with the oligonucleotide velocity. Slower moving oligonucleotides (*i.e.*, larger species with lower mobilities or separations using lower field strengths) will have a lower MDC as the area noise is usually a constant during the run time.

Fig. 2 demonstrates a complex relationship between oligonucleotide concentration and quantitative response. Theoretical factors affecting electrokinetic injections in free solution [11,12] or gels [1] would lead one to expect a linear correlation. A linear correlation is found for relatively high concentrations of the oligonucleotide (>70 ng/ml), but as the concentration falls below 70 ng/ml the response decreases to an unusual plateau region (about 10–40 ng/ml) where the response appears to be independent of concentration. At levels below about 15 ng/ml the response decreases towards the lower limit of response.

It appears that the oligonucleotides are augmenting those factors, such as field strength or possibly electroendosmotic flow at the capillary tip, which influence the rate of migration of the oligonucleotides into the capillary gel during the injection process. The conductivity of the 100 ng/ml sample is equal to the conductivity of the water (5 μS/cm). Therefore, the oligonucleotides do not appear to be affecting the sensitivity by alterations of the sample conductivity. These results stress the importance of using an internal standard for quantification. Fig. 2 demonstrates that equal mass concentrations of $p(dA)_{12}$ and $d(AGTC)_6$ yield similar responses. Over the entire concentration range the ratio of $p(dA)_{12}/d(AGTC)_6$ area times velocity was 0.97 ± 0.13 S.D. This finding indicates that there is no mass discrimination based on size or sequence during the injection cycle. These results demonstrate the feasibility of using a different size and sequence oligonucleotide as an internal standard.

The velocity at which the oligonucleotide migrates from the sample solution into the capillary gel is directly proportional to the field strength between the capillary tip and electrode in the sample solution. It would be expected that if the conductivity of the sample solution is increased (*i.e.*, by the addition of buffer ions), the field strength between the capillary and electrode will decrease, resulting in less oligonucleotide mass migrating into the capillary from solution. The data plotted in Fig. 3 demonstrate exactly this case. The different size and sequence oligonucleotides at different concentrations show a greater than 50% loss in on-column mass at a sample conductivity of 40 μS/cm or greater [equivalent to about a 0.5 m*M* Tris–phosphate (pH 7.2) buffer] when compared with a conductivity of about 15 μS/cm or less. Increasing the conductivity above 500 μS/cm decreases the response to a few percent

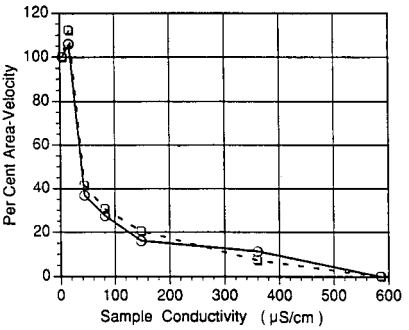

Fig. 3. Effect of sample conductivity on the quantitative response, percentage of area times velocity at 260 nm of the area times velocity at a conductivity of 5 μS/cm. Tris–phosphate buffer (pH 7.2) was used at concentrations from 0 to 10 mM to achieve different sample conductivities at relatively constant pH (7.2–7.5). The gel-filled capillary conditions were L = 47 cm, l = 28 cm, E = 298 V/cm, i = 18 μA, T = 50°C, t = 10 s and V = −5 kV. O———O = $p(dA)_{18}$, C = 48 ng/ml; □-----□ = $d(AGTC)_9$, C = 82 ng/ml.

of the lower conductivity value. This higher conductivity, depending on the oligonucleotide concentration, may result in little or no oligonucleotide being detected.

The data in Fig. 3 shows that in order to obtain a sufficient response for the analysis of low levels of oligonucleotides (less than 40 ng/ml), the conductivity must be kept below about 15 μS/cm.

In order to demonstrate the effect of sample pH on response, the oligonucleotides $p(dA)_{18}$ and $d(AGTC)_3$ in dilute sample buffers of nearly equal conductivity (88–102 μS/cm) were analyzed. In the pH range 6.5–9.1 the area times velocity varied by 12.8% (relative standard deviation), demonstrating relatively little or no effect of pH on the migration of oligonucleotides into the gel column from the sample solution. As increasing the pH increases electroendosmotic flow (EOF) [13], these results

TABLE I

EFFECT OF ADDITION OF ORGANIC MODIFIERS TO THE SAMPLE BUFFER ON MASS LOADING

The oligonucleotides were dissolved in a 1.0 mM Tris–phosphate buffer (pH 7.2) (conductivity = 80 μS/cm) at a concentration of 165 ng/ml containing the organic modifiers at the indictated concentrations. The gel-filled capillary conditions were d = 50 μM, L = 47 cm, l = 28 cm, E = 298 V/cm, i = 17 μA, T = 30°C, t = 10 s and V = −5kV. The data are presented as the percentage of area times velocity of that obtained in the absence of any modifier.

Modifier	Oligonucleotide area times velocity (%)			
	$p(dA)_{12}$	$p(dA)_{18}$	$p(AGTC)_6$	Average
Methanol (20%)	89.1	61.4	79.4	76.6
Formamide (10%)	42.1	40.7	35.0	39.2
Urea (2.5 M)	106.7	102.3	101.4	103.4
Ethylene glycol (10%)	109.9	92.1	93.1	98.4

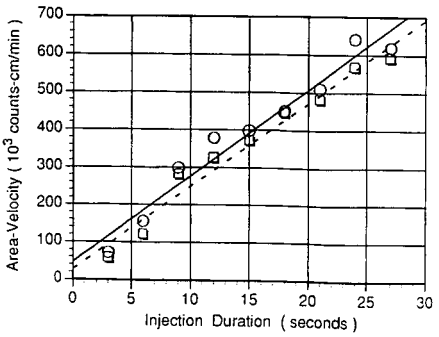

Fig. 4. Effect of injection duration at constant injection voltage on the quantitative response, area times velocity at 260 nm, plotted as linear regressions. The gel-filled capillary conditions were L = 47 cm, l = 27 cm, E = 298 V/cm, i = 17 μA, T = 30°C, V = −5 kV and C = 165 ng/ml. ○———○ = $p(dA)_{12}$ (R^2 = 0.96); □-----□ = $d(AGTC)_6$ (R^2 = 0.97).

suggest that EOF at the capillary tip may not be a factor affecting the migration of oligonucleotides into the gel column.

Various organic compounds were introduced into a sample solution to establish whether or not the decrease in sensitivity due to the increased conductivity of a dilute buffer could be augmented. Samples of $p(dA)_{12}$, $p(dA)_{18}$ and $d(AGTC)_6$ in dilute Tris–phosphate buffer (conductivity *ca.* 80 μS/cm) were analyzed with or without methanol, formamide, urea or ethylene glycol and the results are shown in Table I. Urea and ethylene glycol had no effect on sensitivity, but formamide and, to a lesser extent, methanol caused a reduction in sensitivity.

Effect of injection field strength and duration on resolution and mass loading

The oligonucleotide mass entering the gel capillary from the sample solution would be expected to increase on increasing either or both the injection duration or field strength [1,11,12]. Fig. 4 shows the data from experiments in which the injection voltage is held constant and the injection duration is varied. For the two different oligonucleotides the quantitative response increases linearly with an increase in injection time. The different size and sequence of the oligonucleotides did not appear to influence the amount injected significantly. This lack of discrimination between analytes during injection is in contrast to the discrimination found for electrokinetic injections of differently charged analytes in free solution [12,14]. This lack of discrimination would be expected owing to the equal mobilities of oligonucleotides in the sample solution.

Fig. 4 also shows the feasibility, as discussed previously, of using an internal standard that differs in size and sequence for quantitative analyses. The slopes of the two regression lines differed by only 3.5%. Changing the injection duration will not significantly affect the relative response of different oligonucleotides.

The effect of injection duration on resolution was investigated. Because (as discussed later) the oligonucleotide mass injected affects the resolution, it was necessary to inject from progressively lower concentrations of $p(dA)_{17}$ and $p(dA)_{18}$ as the injection duration was increased in order to maintain the same on-column mass. The

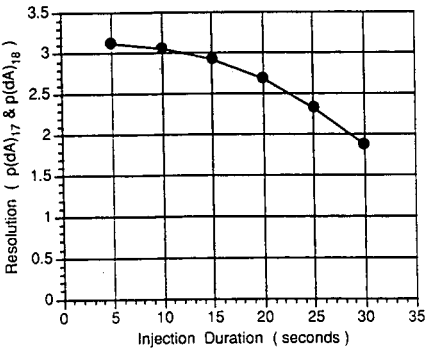

Fig. 5. Effect of injection duration on the resolution of $p(dA)_{17}$ and $p(dA)_{18}$. The gel-filled capillary conditions were L = 45 cm, l = 26 cm, E = 311 V/cm, i = 19 μA, T= 50°C, V = −5 kV and concentration of the oligonucleotides (24–212 ng/ml) adjusted to give a relatively constant on-column mass.

results of this experiment are shown in Fig. 5. The resolution (R_s) was calculated using the equation

$$R_s = \Delta t/w \tag{5}$$

where Δt is the difference in migration times of $p(dA)_{17}$ and $p(dA)_{18}$ and w is the average of the peak widths (as 4σ) of $p(ddA)_{17}$ and $p(dA)_{18}$. Fig. 5 shows that as the injection duration is increased, there is a gradual decrease in resolution. For injection times less than 20s the decrease is less than 15% of the value at 5 s, but above 20 s the resolution decreases more rapidly, approaching a 40% loss at 30 s. For critical separations, it appears necessary to keep the injection time below 20 s in order to maintain resolution.

Increasing the field strength between the capillary tip and electrode is accomplished by increasing the voltage across the entire capillary during the injection cycle. The data in Fig. 6 demonstrate how the quantitative response varies with increasing

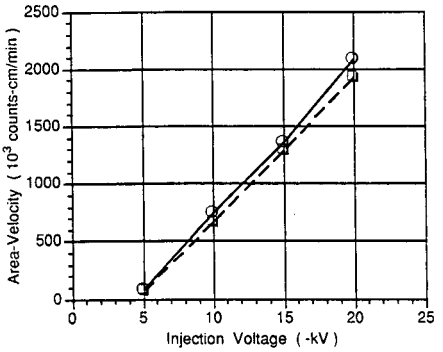

Fig. 6. Effect of injection voltage at constant injection duration on the quantitative response, area times velocity at 260 nm. The gel-filled capillary conditions were L = 48 cm, l = 22 cm, T = 50°C, E = 312 V/cm, i = 19 μA, t = 3 s and C = 20 ng/ml. ○———○ = $p(dA)_{12}$; □-----□ = $p(dA)_{18}$.

injection voltage while the injection duration is held constant. The oligonucleotide mass injected onto the gel capillary increases linearly with increase in injection voltage. There appears to be a slight discrimination such that increasing voltages increase the proportion of mass of the smaller oligonucleotide being injected onto the column. There are other disadvantages to using higher injection voltages: higher injection voltages increase the frequency of column electrical breakdown by the formation of bubbles in the capillary tip, and higher injection voltages have also been observed occasionally to cause severe peak distortion.

The increase in mass loading brought about by the increase in the injection duration and/or injection voltage can exceed one order of magnitude with minimal decrease in resolution. Fig. 7 shows examples of electropherograms that demonstrate the pronounced effect of increasing the injection duration to achieve higher levels of detectability. The electropherogram from the shorter injection duration shows a major $p(dA)_{18}$ peak with marginally detectable minor peaks in a sample from an HPLC-"purified" fraction. When the same sample is analyzed using a longer injection duration, the sensitivity is increased about 17-fold and the electropherogram clearly shows the presence of six or seven minor peaks ranging from 1 to 9% of the total response. This ability of the capillary gels to preconcentrate analytes at the capillary tip during the injections step, referred to as a zone "focusing" [15] or "sharpening" [1] effect, is probably due to the lower mobility of the oligonucleotides in the gel matrix relative to their much higher mobility in the sample solution.

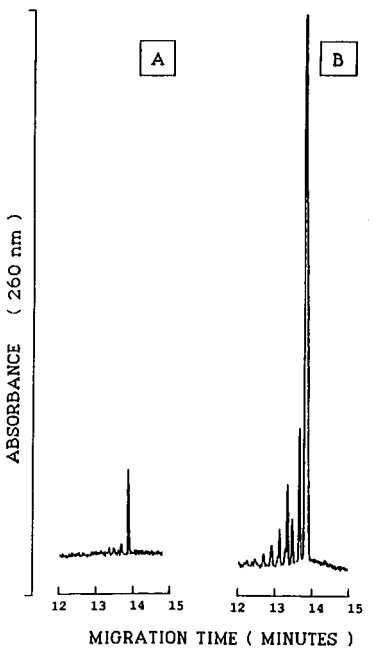

Fig. 7. Effect of sample "focusing"' on quantitative response, absorbance at 260 nm, caused by increasing the injection duration. A sample of HPLC-"purified" $p(dA)_{12}$ was separated on the gel-filled capillary using injection times of (A) 3 s and (B) 15 s with conditions L = 46 cm, l = 28, E = 304 V/cm, i = 19 μA, T = 30°C, V = −5 kV and C = 330 ng/ml.

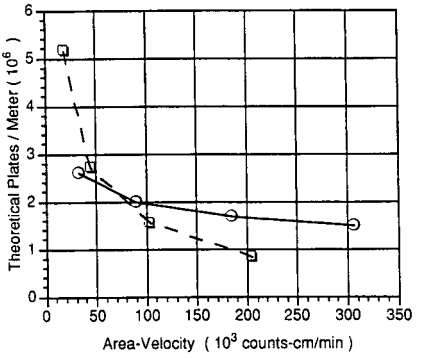

Fig. 8. Effect of on-column mass, as area times velocity at 260 nm, on the separation efficiency of a gel-filled capillary. The analysis conditions were L = 46 cm, l = 24 cm, E = 326 V/cm, i = 19 μA, T = 50°C, t = 3 s, V = −5 kV and C = 20–160 ng/ml. ○———○ = $p(dA)_{12}$; □-----□ = $p(dA)_{18}$.

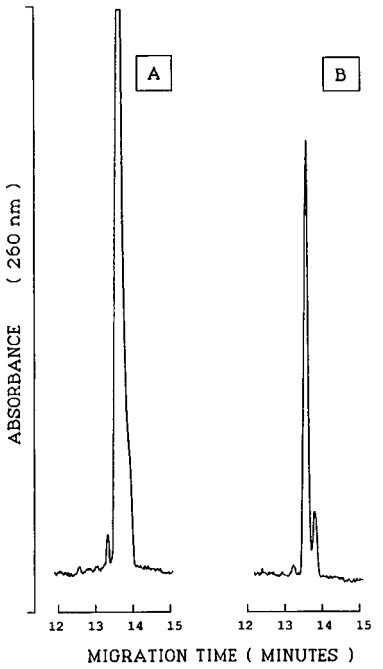

Fig. 9. Effect of on-column mass on the resolution of oligonucleotides of the same size but different sequence. The separation in (A) using a 5-s injection had about a five times greater area times velocity than the separation in (B) using a 2-s injection of the same sample. The large peak at 13.6 min is $p(dA)_{12}$ and the small peak at 13.7 min, resolved in (B) but not (A), is $d(AGTC)_3$. The conditions were L = 47 cm, l = 28 cm, E = 298 V/cm, i = 17 μA, T = 30°C, V = −5 kV and C = 2574 ng/ml for $p(dA)_{12}$ and 396 ng/ml for $d(AGTC)_3$.

Effect of on-column mass on efficiency

It has been shown qualitatively that analyte mass overloading can cause a decrease in resolution and peak distortion in capillary gel separation [1]. Fig. 8 shows the quantitative effect of mass on efficiency in the capillary gel separations of oligonucleotides. The efficiency was calculate using the equation

$$N/L = 5.54\,(t/w)^2/l \tag{6}$$

where N/L is the number of theoretical plates per meter, t is the migration time, w is the peak width at half-height and l is the effective separation length in meters. As the mass injected onto the column increases, there is a corresponding decrease in the efficiency of the separation. The larger oligonucleotide [$p(dA)_{18}$] appears to be more sensitive to decreases in efficiency than the smaller oligonucleotide [$p(dA)_{12}$] on an equivalent mass basis. A five-fold increase in the on-column mass (from $3 \cdot 10^4$ to $15 \cdot 10^4$ counts cm/min) resulted in a 30% efficiency loss for $p(dA)_{12}$ and about a 70% loss for $p(dA)_{18}$. The electropherograms in Fig. 9 illustrate how this increase in on-column mass can significantly compromise the resolution. Fig. 9 shows the separation between $p(dA)_{12}$ and $d(AGTC)_3$ at low and high on-column mass. This critical resolution between oligonucleotides of identical size but different sequence is accomplished in the low-mass but not in the high-mass separation.

It is evident that the needs for resolution may have to be weighed against the needs for detectability in some applications. Separations that require high efficiency, such as sequence dependence, may be limited in their ability to detect trace levels of one component. This problem will be more pronounced in the separation of larger oligonucleotides. For well resolved components, such as single-base size differences, adequate resolution will be maintained over a wider range of on-column mass.

Effect of separation field strength, column length and column temperature on resolution and migration times

In the interests of decreasing analysis times and maintaining resolution, the effects of increasing the separation field strength, decreasing the effective separation length and increasing the column temperature were investigated. Fig. 10 shows the

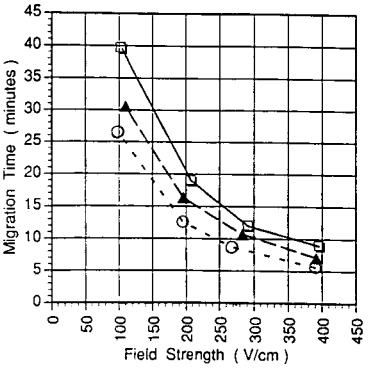

Fig. 10. Effect of separation field strength and effective separation length on the migration time of $p(A)_{18}$. The gel-filled capillary conditions were L = 37, 44 or 47 cm, T = 50°C, i = 6–24 μA, t = 3 s, V = −5 kV and C = 707 ng/ml. Effective separation length: □————□ = 28 cm; ▲-----▲ = 25 cm; ○·····○ = 20 cm.

variation in migration times for $p(dA)_{18}$ as the column field strength and effective separation length are changed. The velocity of charged analytes in capillary electrophoresis are directly proportional to the field strength [15]. It is not suprising to find that the migration time of $p(dA)_{18}$ decreases by about half when the field strength is doubled. Reducing the separation length reduces the distance that the oligonucleotide must be transported from capillary tip to detector. If the oligonucleotide is transported at a uniform velocity, a decrease in this distance would be expected to result in a proportional decrease in the migration time when the field strength is the same. The data show that a proportional decrease does occur. A 29% decrease in the separation length resulted in about a 34% decrease in the migration time of the $p(dA)_{18}$.

The variation in the resolution between $p(dA)_{17}$ and $p(dA)_{18}$ caused by increases in the field strength was examined and the results are plotted in Fig. 11. The data show that the resolution increases by about 40% for every two-fold increase in the field strength, which agrees well with the 41% that would be predicted by theory, *i.e.*, resolution $\propto$ (field strength)$^{1/2}$ [7,15]. The data also demonstrate that if the detector rise time is set to high values, an increase in field strength may actually lead to decreases in resolution. As the difference in migration time, Δt, is inversely proportional to the field strength [7,15], according to eqn. 5 the resolution will decrease if the average peak width, w, does not correspondingly change inversely with the field strength. The detector rise time will add significantly to the peak width if it approaches or exceeds about one third of the peak width at half-height [16]. As the field strength is increased, the peak width decreases and, without any decrease in the detector rise time, may lead to a decrease in resolution. At a field strength of 400 V/cm, the oligonucleotide half-height approaches 1.0 s, necessitating a detector rise time of 0.3 or less to maintain resolution. The signal-to-noise ratio will decrease with decreasing rise time, causing an increase in the MDC. Also, as discussed earlier in relation to eqn. 4, an increased peak velocity caused by increases in the field strength will increase the MDC. Therefore, increasing the field strength as a means of decreasing analysis times is an approach that should weigh in the balance the need for resolution and the needs of detectability.

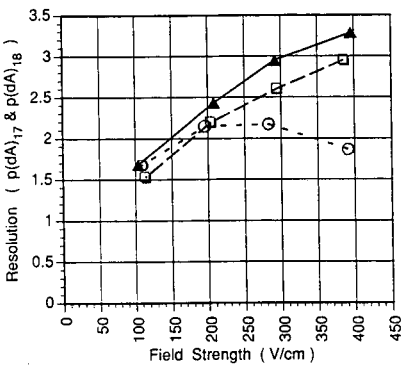

Fig. 11. Effect of separation field strength, effective separation length and detector rise time on the resolution of $p(dA)_{17}$ and $p(dA)_{18}$. The gel-filled capillary conditions were L = 43, 44 or 47 cm, i = 6–24 μA, T = 50°C, t = 3 s, V = −5 kV and C = 707 ng/ml. Separation length and rise time: ▲——▲ = 28 cm, 0.1 s; □-----□ = 24 cm, 0.1 s; ○·····○ = 25 cm, 1.0 s.

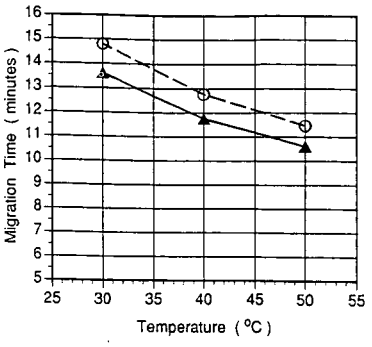

Fig. 12. Effect of separation temperature on the migration time of ▲———▲ = $p(dA)_{12}$ and ○--○ = $p(dA)_{18}$. The gel-filled capillary conditions were L = 48 cm, l = 28 cm, E = 292 V/cm, i = 18 μA, t = 3 s, V = −5 kV and C = 141 ng/ml.

Fig. 11 shows the effect on resolution (R_s) of reducing the effective separation length (l). A 14% reduction in separation length resulted in about a 9% decrease in resolution, which agrees with the 7% that would be predicted from theory, *i.e.*, $R_s \propto l^{1/2}$ [7,15]. Reduction of the separation length is a viable alternative for reducing the analysis time. A 30% reduction in the separation length, with no change in the field strength, should decrease the analysis time by 30% and the resolution by only about 14%. This decrease in resolution will not affect significantly non-critical separations and it avoids the detectability problems associated with increases in field strength. Of course, critical separations may be affected by small reductions in the resolution and necessitate increases in the field strength in order to compensate for the resolution loss.

The variation of migration time and resolution with changes in column temperature were examined. Fig. 12 shows that an increase in column temperature results in corresponding significant decreases in the migration times of $p(dA)_{12}$ and $p(dA)_{18}$. The overall migration time decreases by about 1.1% per °C, which is lower than the 2% quoted in the literature [3]. The migration time of $p(dA)_{18}$ relative to $p(dA)_{12}$ remains the same during temperature changes. Increasing the temperature from 30 to 50°C results in a 22% decrease in the migration times.

The resolution of $p(dA)_{17}$ and $p(dA)_{18}$ was determined at different temperatures. There is about a 15% decrease in resolution when the temperature is increased from 30 to 50°C. Increasing the column temperature is a method that can significantly reduce the analysis time with minimum decreases in resolution. In critical separations, however, this decrease in resolution may have to be offset by a corresponding increase in the field strength.

CONCLUSIONS

The results demonstrate that numerous operating parameters may affect, in a mutually dependent way, the resolution, sensitivity and detectability of oligonucleotides separated on a gel-filled capillary. Analysis times are decreased by increasing the field strength, decreasing the separation length and increasing the column temperature. However; this decrease in migration time may be accompanied by decreases in

detectability (due to increased peak velocity and decreased signal-to-noise ratio) and decreases in resolution (due to shorter separation lengths). A poor response from the injection of an unknown sample may be improved by decreasing the sample conductivity, increasing the injection time or voltage and, in many instances, increasing the oligonucleotide concentration. On the other hand, injection of excessive mass onto the column may decrease the resolution, possibly obscuring the presence of a trace component. Using the information presented, separations may be optimized for particular needs more effectively for speed, resolution and sensitivity.

ACKNOWLEDGEMENTS

We thank Bill Giusti and Tess Adriano, DNA Service Support, Applied Biosystems (Foster City, CA, USA) for the supply of the purified oligonucleotides.

REFERENCES

1 A. Paulus and J. I. Ohms, *J. Chromatogr.*, 507 (1990) 113.
2 A. S. Cohen, D. R. Najarian, A. Paulus, A. Guttman, J. A. Smith and B. L. Karger, *Proc. Natl. Acad. Sci. U.S.A.*, 85 (1988) 9660.
3 A. Guttman, A. S. Cohen, D. N. Heiger and B. L. Karger, *Anal. Chem.*, 62 (1990) 137.
4 H.-F. Yin, J. A. Lux and G. Schomburg, *J. High Resolut. Chromatogr.*, 13 (1990) 624.
5 R. Dubrow, presented at the *2nd International Symposium on High Performance Capillary Electrophoresis, January 29–31, 1990*, paper P-208.
6 D. N. Heiger, A. S. Cohen and B. L. Karger, *J. Chromatogr.*, 516 (1990) 33.
7 H. Swerdlow and R. Gesteland, *Nucleic Acids Res.*, 18 (1990) 1415.
8 H. Drossman, J. A. Luckey, A. J. Kostichka, J. D'Cunha and L. M. Smith, *Anal. Chem.*, 62 (1990) 900.
9 A. S. Cohen, D. R. Najarian and B. L. Karger, *J. Chromatogr.*, 516 (1990) 49.
10 H. Swerdlow, S. Wu, H. Harke and N. J. Dovichi, *J. Chromatogr.*, 516 (1990) 61.
11 X.-H. Huang, M. J. Gordon and R. N. Zare, *Anal. Chem.*, 60 (1988) 377.
12 D. J. Rose, Jr., and J. W. Jorgenson, *Anal. Chem.*, 60 (1988) 642.
13 K. D. Altria and C. F. Simpson, *Chromatographia*, 24 (1987) 527.
14 S. E. Moring, J. C. Colburn, P. D. Grossman and H. H. Lauer, *LC · GC*, 8 (1990) 34.
15 B. L. Karger, A. S. Cohen and A. Guttman, *J. Chromatogr.*, 492 (1989) 585.
16 S. E. Moring, personal communication.

Journal of Chromatography, 559 (1991) 57–68
Elsevier Science Publishers B.V., Amsterdam

CHROM. 23 461

Influence of operating parameters on reproducibility in capillary electrophoresis

SCOTT C. SMITH[a], JOOST K. STRASTERS and MORTEZA G. KHALEDI*
Department of Chemistry, North Carolina State University, Box 8204, Raleigh, NC 27695-8204 (USA)

ABSTRACT

The reproducibility of two migration parameters (retention time and mobility) of a seven-component test mixture was examined under various operating conditions using laboratory-built capillary electrophoresis systems. It was found that the frequency of rinsing the capillary and the solutions used for rinsing had the greatest effect on migration reproducibility. In addition, it was found that the migration behavior of solutes that interact with micelles is not repeatable unless the proper rinse protocol is applied. Inconsistent migration behavior is linked to inconsistent total current of the system. Preliminary investigations indicate that the fluctuation in total current were associated with non-equilibrium conditions between the buffer and the capillary wall.

INTRODUCTION

In order for any analytical technique to be useful, the results obtained must be reproducible. The reproducibility of the results obtained by capillary electrophoresis (CE) has been addressed in the work of several researchers. Some researchers pretreat new columns with caustic rinses before use [1–3]. VanOrman *et al.* [4] investigated the reproducibility of electroosmotic flow over three days and four capillaries. Black [5] presented results on the effects of temperature, ionic strength, pre-run washing and ion depletion in relation to CE system design. Lambert and Middleton [6] compared the effects of acidic and caustic pretreatments on electroosmotic flow.

The migration reproducibility may depend on several operational factors: ionic strength of the buffer, age of the capillary, previous capillary treatments, frequency of capillary treatments, applied voltage and external capillary temperature. The purpose of this study was to observe the influences of these operational factors on the reproducibility of the migration parameters of test solutes. This study was restricted to varying the parameters that did not alter the system hardware; therefore, the type of capillary (*e.g.*, coated *vs.* uncoated) or the capillary diameter, for example, were not altered.

[a] Present address: Magellan Laboratories Inc., P.O. Box 13341, Research Triangle Park, NC 27560, USA.

0021-9673/91/$03.50

The migration reproducibility of any system may also be influenced by the migration parameter used for evaluation. In CE, two parameters are the solute retention times (t_r) and the electrophoretic mobilities (μ). The value for μ is calculated from retention time as follows:

$$\mu = \left(\frac{1}{t_r} - \frac{1}{t_0}\right)\left(\frac{l_t l_d}{V}\right) \quad (1)$$

where t_0 is the retention time of an unretained marker, l_t is the total length of the capillary, l_d is the length from the upstream end of the capillary to the detector window and V is the applied voltage.

EXPERIMENTAL

Apparatus

Experiments were carried out on two laboratory-built CE systems that were patterned after the original system described by Jorgenson and Lucacs [7–9]. Both systems used a 0–30-kV high-voltage power supply (Series EH, Glassman High Voltage, Whitehouse Station, NJ, USA), a variable-wavelength UV detector (Model 200, Linear Instruments, Reno, NV, USA) operating at 210 nm and 50 μm I.D. × 375 μm O.D. fused-silica capillary tubing (Polymicro Technologies, Phoenix, AZ, USA). Electropherograms were recorded with an electronic integrator (Model SP4200, Spectra-Physics, San Jose, CA, USA, or Model QA-1, Waters Assoc., Milford, MA, USA). Total current was recorded on a stripchart recorder by measuring the voltage across a 1-kΩ resistor in series with and downstream of the capillary.

Reagents and chemicals

For all experiments, a seven-component test mixture was used. The test compounds were arterenol (Sigma, St. Louis, MO, USA) (a cationic solute), 2-chlorophenol, 2,3-dichlorophenol, 2,4,5-trichlorophenol, *m*-methylbenzoic acid, *p*-hydroxybenzoic acid and 2,4,6-trimethylbenzoic acid (Aldrich, Milwaukee, WI, USA) (anionic or partially dissociated acidic solutes). In the remainder of this paper, these compounds will be referred to as ART, 2CP, 23CP, 245CP, mMBA, pOHBA and 246BA, respectively. Phosphate buffer (pH 7) was used as the mobile phase with sodium chloride present to adjust the ionic strength. For micellar electrokinetic capillary chromatography (MECC) experiments, sodium dodecyl sulfate (SDS) (Sigma) was used in the mobile phase and Sudan III (Aldrich) was used as the micelle mobility marker in the test mixture. All other chemicals were of analytical-reagent grade.

Procedure

Gravity injection was used for all runs. The test mixture was held 2–5 cm above the level of the downstream buffer for 5–20 s. This technique does not provide the reproducible injection volumes possible with electroinjection techniques; however, our interest was in the reproducibility of migration parameters rather than peak quantification. The capillary was rinsed by applying vacuum from a water aspirator to the sealed downstream buffer flask. When not under vacuum, the flask was open to air.

The time for each rinse was measured in column volumes, which was determined by aspirating an air bubble through the capillary and noting the time required for the bubble to be detected. Typically, one column volume passed through the capillary in 15 s while under aspiration vacuum.

RESULTS AND DISCUSSION

Influence of rinsing solution

As mentioned above, the preconditioning of the silica capillary surface has been described by many researchers; however, with the exception of Lambert and Middleton's recent study of acidic and alkaline preconditioning [6], little attention has been paid in the literature to the effects of various rinsing solutions. For this study, three solutions were chosen: phosphate buffer, pure methanol and 0.1 *M* sodium hydroxide. The buffer was chosen because its means of preconditioning would be mechanical; that is, it has no chemical effect on the capillary wall, but would rinse away any particulate matter and fill the capillary with fresh buffer. Methanol was chosen because it would remove organic solutes that may have attached to the silica capillary wall. Sodium hydroxide was chosen for its ability to remove older silica and expose a fresh surface.

Tests were carried out on two capillaries from the same capillary stock. Comparisons of the rinsing solutions were made by considering the average retention time and mobility for each component in each set and also the 95% confidence intervals (CI) of the means. For this study, *ca.* 1600 runs were made. In order to keep track of this large number of runs, individual runs were grouped into "sets" in which each set contained runs performed under similar conditions. Sets were grouped into "blocks", in which sets varied in one or two operational parameters. The data sets used are presented in Table I. These data are from two blocks (1 and 2); different capillaries were used for each block.

Before examining the influence of particular rinsing solutions, it is interesting to observe the behaviour of retention times over all sets. The retention time for the longest

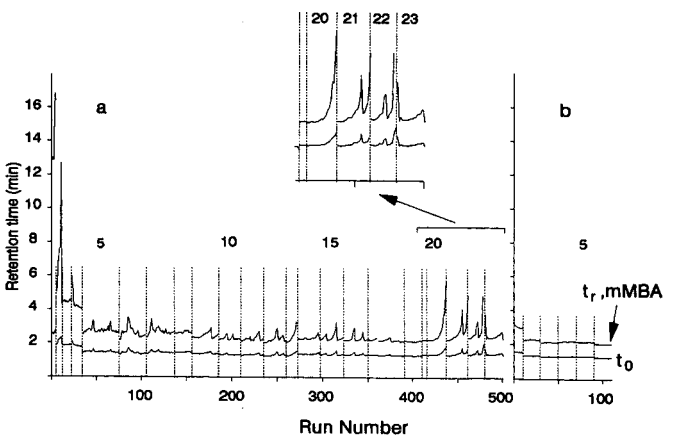

Fig. 1. Retention times of mMBA (top trace) and methanol (t_0; bottom trace) for (a) capillary 1 and (b) capillary 2. Vertical dotted lines delineate sets; numbers indicate the set number.

TABLE I

EXPERIMENTAL CONDITIONS: INFLUENCE OF RINSING SOLUTION

Conditions for all sets: 10 m*M* ionic strength phosphate buffer, no SDS, 15 kV.

Block and set	No. of runs	Rinsing solution	Rinsing protocol[c]
1/1[a]	5	Buffer	60 c.v., start of set
1/2	6	CH_3OH	2 c.v., start of set
1/3	11	CH_3OH	100 c.v., start of set
1/4	12	CH_3OH	20 c.v., start of set
1/5	41	NaOH and CH_3OH	2 c.v. of each, start of set
1/6	30	NaOH and CH_3OH	2 c.v. of each, start of set
1/7	25	NaOH and CH_3OH	30 c.v. NaOH, 2 c.v. CH_3OH, start of set
1/8	20	NaOH and CH_3OH	2 c.v. of each, start of set
1/9	30	Buffer	10 c.v., start of set
1/10	25	Buffer	10 c.v., start of set
1/11	25	Buffer	10 c.v., start of set
1/12	25	CH_3OH	10 c.v., start of set
1/13	12	CH_3OH	10 c.v., start of set
1/14	26	CH_3OH	10 c.v., start of set
1/15	25	Buffer	10 c.v., start of set
1/16	27	NaOH	10 c.v., start of set
1/17	40	Buffer	2 c.v., between each run
1/18	20	Buffer	2 c.v., between each run
1/19	5	Buffer	20 c.v., start of set
1/20	22	NaOH and CH_3OH	2 c.v. of each, start of set
1/21	24	MeOH	10 c.v., start of set
1/22	18	NaOH	10 c.v., start of set
1/23	19	Buffer	2 c.v., between each run
2/1[b]	10	Buffer	60 c.v., start of set
2/2	20	CH_3OH	10 c.v., start of set
2/3	20	CH_3OH	10 c.v., start of set
2/4	20	Buffer	60 c.v., start of set
2/5	20	Buffer	10 c.v., start of set
2/6	20	NaOH	10 c.v., start of set

[a] Block 1: l_t = 40 cm, l_d = 26.5 cm, capillary 1.
[b] Block 2: l_t = 40 cm, l_d = 26.5 cm, capillary 2.
[c] c.v. = Column volumes.

retained compound (mMBA) and t_0 are plotted *versus* the run number in Fig. 1a (capillary 1) and 1b (capillary 2), where vertical dotted lines mark the starting and ending runs for each set. It is apparent that the retention behavior of the two capillaries is different. The number of runs required to obtain consistent retention times was much smaller for capillary 2 (10 runs; set 2/1) compared with capillary 1 (34 runs; sets 1/1–1/4), even though both were from the same stock. This may be due to contamination of the inner surface of capillary 1 occurring during its installation in the system.

The initial runs with capillary 1 show very unstable behavior. As described in Table I, the capillary was rinsed with buffer or methanol for the first four sets. It may be that the inner capillary surface was initially contaminated and the buffer and

methanol did not clean the surface. After treatment with the combined sodium hydroxide–methanol rinse (1/5–1/8), the retention time stabilized. Subsequent rinses with either buffer or methanol (1/9–1/15) showed similar retention times and similar behavior with respect to minor retention time fluctuations.

Sodium hydroxide was again used in 1/16, 1/20 and 1/22. When used by itself (1/16), it has no more effect than buffer or methanol. However, note that in sets 1/20–1/22 the retention time increased exponentially and did not decrease until rinsed again. This was accompanied by a similar increase in current. Flushing the capillary with any rinsing solution returned the retention time (and current) to a reasonable level again, as shown in 1/21, 1/22 and 1/23.

It appears that the combination of a sodium hydroxide rinse followed immediately by a methanol rinse may lead to the anomalous behavior of retention time and current. This may be due to the formation of cavities by the sodium hydroxide in the capillary wall that become filled with methanol. As the methanol diffused from the cavities, the zeta potential near the wall may be reduced, causing the electroosmotic mobility to decrease.

It is important to note that the fluctuations in retention time coincide with those in t_0. Identical observations were made for all compounds in the test mixture; therefore, the fluctuation is due to irregularities in the electroosmotic flow and not to any characteristic of the test compounds. If this is the case, then a figure of merit that compensates for electroosmotic mobility fluctuation (such as mobility) should show greater stability than retention time.

The average and 95% CI for retention time and mobility are presented in Fig. 2a and b, respectively, for the longest retained compound, mMBA, for capillary 1. On initial inspection, it is clear that mobility is more stable and shows less error than retention time for the first four sets. Closer examination also shows that sets which

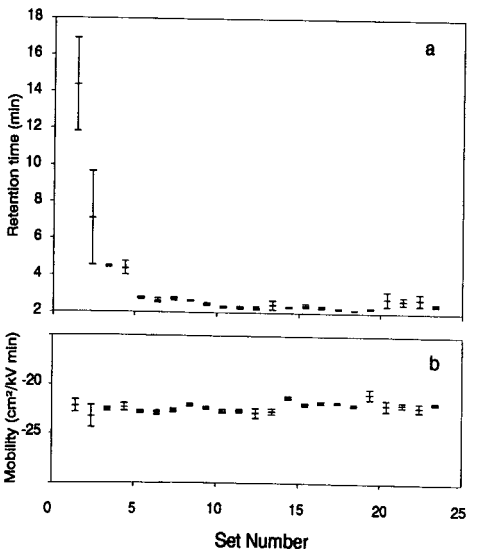

Fig. 2. Average and 95% CI of (a) retention time and (b) mobility of mMBA for the sets of data illustrated in Fig. 1 for capillary 1.

experienced exponential increases in retention time (1/20, 1/21 and 1/22) show no difference in mobility. It may be concluded that the increase in retention time was due to a reduction in electroosmotic flow and that mobility is a much more rugged migration parameter than retention time.

From this information, it appears that the type of rinsing solution to be used depends on the situation. For cases where retention time is initially unstable, a rinse with sodium hydroxide is helpful. After achieving stable retention time, rinses with either sodium hydroxide, methanol or buffer work equally well, but the combination of sodium hydroxide and an organic rinsing solution such as methanol sometimes appears to alter retention time and should be avoided.

Influence of rinsing frequency

As with the question of the type of rinsing solution to use, there is no consensus on how frequently the capillary should be rinsed. This study follows two rinsing protocols: 1, rinse only at the beginning of a set, and 2, rinse between each run in a set. The experimental conditions for this analysis are presented in Table II.

TABLE II

EXPERIMENTAL CONDITIONS: INFLUENCE OF RINSING FREQUENCY

Conditions for all sets: buffer rinse solution, 15 kV.

Block and set	No. of runs	[SDS] (m*M*)	Rinsing protocol[d]
1/9[a,b]	30	0	10 c.v., start of set
1/10	25	0	10 c.v., start of set
1/11	25	0	10 c.v., start of set
1/15	25	0	10 c.v., start of set
1/17	40	0	2 c.v., between each run
1/18	20	0	2 c.v., between each run
3/1[c]	20	10	60 c.v., start of set
3/2	20	10	2 c.v., between each run

[a] Block 1: l_t = 40 cm, l_d = 26.5 cm, capillary 1.
[b] Block 1 data are also listed in Table I and are recompiled here for comparison with Block 3 data.
[c] Block 3: l_t = 40 cm, l_d = 26.5 cm, capillary 2.
[d] c.v. = Column volumes.

In studying the influence of rinsing frequency on reproducibility, three factors were considered: the magnitude of the errors in retention time and mobility, the total current of the system and its correlation with migration behavior and the variation in selectivity. First, the errors in retention time and mobility will be discussed.

To compare errors from several sets of experiments, relative confidence intervals (RCI) were used (confidence intervals have been used throughout this work because they reflect the number of measurements used to determine the average). The RCI was the 95% CI divided by the average retention time or mobility. These RCI are presented in Fig. 3a for retention time and in Fig. 3b for mobility. The averages and 95% CI from which these graphs were generated are presented in Table III for retention time and mobility for five of the compounds.

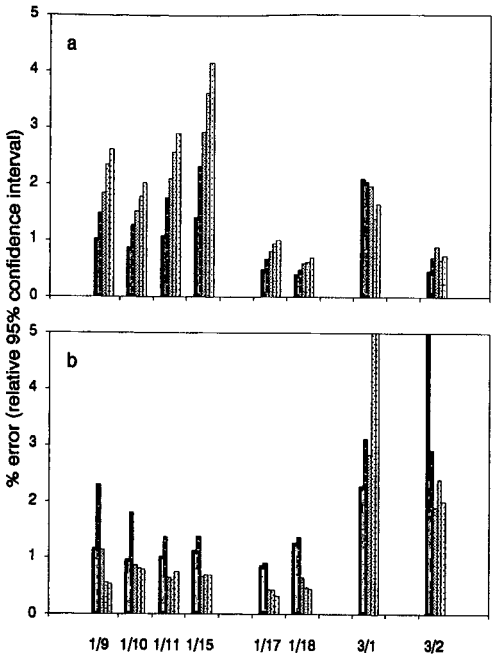

Fig. 3. Relative percentage error based on the 95% CI in (a) retention time and (b) mobility for ART, 23CP, 245CP, 246BA and mMBA under four conditions: no SDS, rinsing before sets (1/9, 1/10, 1/11, 1/15); no SDS, rinsing between runs (1/17, 1/18); SDS, rinsing before sets (3/1); and SDS, rinsing between runs (3/2).

Comparison of the retention time error in sets with rinsing before each set (1/9–1/11, 1/15, 3/1) *versus* sets with rinsing between each run (1/17, 1/18, 3/2) shows that rinsing before each run leads to less error. This was true regardless of the presence of SDS micelles (3/1 *vs.* 3/2). Both the relative error (Fig. 3a) and actual error (Table III) increase with increased retention, characteristic of random error.

The mobility data in Table III show a relatively constant absolute error, which leads to decreasing relative error with increasing retention as shown in Fig. 3b. The calculation of mobility (eqn. 1) reduces the systematic error by removing the influence of the variation of the electroosmotic flow. However, the random error increases because mobility is based on two measurements (t_r and t_0) instead of one (t_r). Without micelles present, the reduction in systematic error is greater than the increase in random error. The presence of micelles makes the measurement of t_0 less certain; therefore, the random error is greater with micelles present.

In CZE, mobility is preferred as the relative error is much less than the error in retention time (1% *vs.* 2–2.5%), especially for sets with rinsing at the beginning of the set. In MECC, retention time appears to be better than mobility as the figure of merit when SDS is present (1–2% *vs.* 2–5%). However, as with runs without SDS, rinsing between runs leads to lower error.

The second factor considered in comparing the rinsing protocols was the fluctuation in total current and its correlation with fluctuations in migration behavior. As shown in Fig. 4a, the current for 1/9–1/11 gradually increases with time and

TABLE III

COMPARISON RUNS WITH DIFFERENT RINSING FREQUENCIES

Block and set	ART	23CP	245CP	246BA	mMBA
Retention times (min) and 95% confidence intervals					
1/9[a]	1.073 ± 0.011	1.563 ± 0.023	1.856 ± 0.034	2.218 ± 0.052	2.451 ± 0.064
1/10[a]	1.041 ± 0.009	1.506 ± 0.019	1.779 ± 0.027	2.088 ± 0.037	2.296 ± 0.046
1/11[a]	1.032 ± 0.011	1.498 ± 0.026	1.771 ± 0.037	2.075 ± 0.053	2.278 ± 0.066
1/15[a]	1.072 ± 0.015	1.564 ± 0.036	1.852 ± 0.054	2.167 ± 0.078	2.387 ± 0.099
1/17[b]	1.045 ± 0.005	1.500 ± 0.010	1.760 ± 0.014	2.027 ± 0.019	2.217 ± 0.022
1/18[b]	1.024 ± 0.004	1.463 ± 0.007	1.711 ± 0.010	1.975 ± 0.012	2.154 ± 0.015
6/3[c]	1.434 ± 0.030	2.304 ± 0.047	3.125 ± 0.061	2.913 ± 0.040	3.348 ± 0.055
6/4[d]	1.542 ± 0.007	2.449 ± 0.017	3.273 ± 0.029	2.747 ± 0.018	3.129 ± 0.023
Mobilities ($cm^2/kV\ cm$) and 95% confidence intervals					
1/9[a]	14.60 ± 0.17	−6.05 ± 0.14	−13.17 ± 0.15	−19.35 ± 0.11	−22.36 ± 0.12
1/10[a]	14.35 ± 0.14	−6.62 ± 0.12	−13.79 ± 0.12	−19.67 ± 0.16	−22.73 ± 0.18
1/11[a]	14.68 ± 0.15	−6.55 ± 0.09	−13.82 ± 0.09	−19.64 ± 0.12	−22.66 ± 0.17
1/15[a]	14.18 ± 0.16	−6.50 ± 0.09	−13.50 ± 0.09	−19.00 ± 0.13	−21.96 ± 0.15
1/17[b]	13.97 ± 0.12	−6.57 ± 0.06	−13.53 ± 0.06	−18.81 ± 0.08	−21.79 ± 0.07
1/18[b]	14.12 ± 0.18	−6.57 ± 0.09	−13.57 ± 0.09	−19.10 ± 0.09	−22.08 ± 0.10
6/3[c]	4.56 ± 0.10	−14.08 ± 0.44	−22.15 ± 0.63	−20.5 ± 1.2	−23.7 ± 1.2
6/4[d]	4.30 ± 0.35	−12.67 ± 0.37	−19.93 ± 0.38	−15.80 ± 0.38	−18.94 ± 0.38

[a] Buffer rinse before each set; no SDS.
[b] Buffer rinse each run; no SDS.
[c] Buffer rinse before each set; 10 m*M* SDS.
[d] Buffer rinse before each run; 10 m*M* SDS.

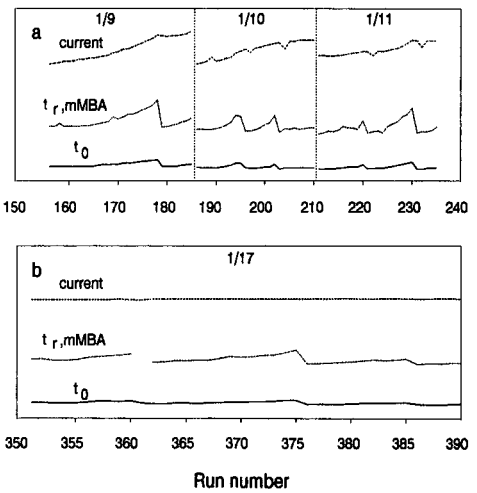

Fig. 4. Relationship between (dashed lines) current, (dotted lines) retention time of a typical solute (mMBA) and (solid lines) the retention time of methanol (t_0) for (a) sets 1/9, 1/10 and 1/11 (rinsing before sets) and (b) set 1/17 (rinsing between runs). Currents and retention times are not to scale.

contains many fluctuations. The cause of this increase may be temperature equilibration or non-steady-state capillary wall interactions; these will be addressed further in a later section. This behavior has been observed to correlate to fluctuations in retention time and t_0, as illustrated in Fig. 4 for mMBA (again, mMBA was representative of the behavior of all solutes).

Rinsing returns the system to "first run" conditions. The current for the first runs of 1/9, 1/10 and 1/11 were all about 6.7 μA. This was also the current of each run in 1/17 (Fig. 4b) and 1/18 (not shown), in which rinsing was done between runs. In addition to keeping the current constant from run to run, rinsing between runs also reduced the fluctuations in retention time and t_0. It was the reduction in these fluctuations by rinsing between runs that led to the lower error shown in Fig. 3 and Table III.

Set 1/23 is another example of the benefit of rinsing between runs. In the inset in Fig. 1, 1/23 follows three consecutive sets that experienced exponential, anomalous increases in retention (and also current). The initial retention time in 1/23 was high, but quickly reduced to normal levels. Later in the set the retention time began to climb, but decreased again before becoming too large. This small rise late in the set can be seen for several sets in Fig. 1 (1/9–1/16), so it is not uncommon. It is noteworthy that rinsing before each run in set 1/23 eventually returned the system to normal operation. Without rinsing between each run, it would seem necessary to replace the column based on the observed behavior in 1/20–1/22.

The third factor considered in comparing the influence of rinsing frequency is the variation in separation selectivity (*i.e.*, relative retention of compounds). Rinsing between runs will maintain the selectivity in an MECC separation as described below.

The mobilities for 3/1 and 3/2 are presented in Fig. 5 for 245CP, 246BA, pOHBA and mMBA. The mobilities of 3/2 (rinsing between runs) show relatively stable behavior, although not as stable as the behavior seen in CZE. The fluctuations were constant for all compounds, so the selectivity did not alter from run to run. On the other hand, the mobilities of 3/1 (rinsing before sets) show a constant increase. (The sign convention dictates that migration toward the positive electrode is in the negative direction; negative mobility would be expected for anionic solutes.) More critical than

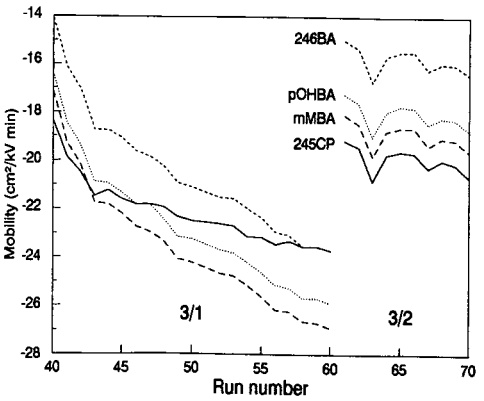

Fig. 5. Dependence of mobility on run number. Runs 40–60 were performed with rinsing before the set; runs 61–70 were performed with rinsing between runs.

the magnitude of the change in mobility is the change in selectivity that occurred. For the initial runs in both protocols, 245CP was the longest retained. As the run number in 3/1 increased, 245CP shifted position and, after twenty runs, co-eluted with 246BA. This is further evidence that rinsing before each run restored the system to the initial conditions and that rinsing should be performed before every run.

Influence of other operating parameters

The influence of ionic strength and the use of Sudan III were also tested. Ionic strength was examined by performing runs with phosphate buffer at three levels of ionic strength: 10, 50 and 100 m*M*. Rinsing was performed at the beginning of the set in order to test the ionic strength contribution under "worst case" conditions. The variance in mobility within a set was compared with the variance between sets in the standard ANOVA format [10,11]. In general, the sets at low ionic strength were most similar to one another, and the similarity between sets decreased with increasing ionic strength.

The presence of Sudan III in MECC was also investigated as a possible source of irreproducible behavior. It was thought that Sudan III, used in the sample as the micelle retention marker, precipitated in the column or interacted with the wall due to its low solubility. Analysis of sets run in a two-day period with and without Sudan III showed that the variation in mobility as a result of Sudan III was less than the day-to-day variation.

Examination of increase in total current

It was shown in Fig. 4 and has been a long-standing observation in this laboratory that the total current increases as the number of runs increases if rinsing is performed between sets, and the current ultimately reaches a plateau after several runs. Two factors were thought to contribute to this behavior. The first factor was slow warming of the capillary to an equilibrium temperature. Since a temperature gradient exists from the center of the capillary to the outer surface, it was thought that the warming of the capillary might contribute to the rise in current. The second factor was slow equilibration of the inner capillary surface. The surface of the capillary may be altered during the rinse and its alteration may result in the depletion of current carriers during the initial runs of a set until a steady-state condition was reestablished.

To study this behavior further, a 15-min delay was introduced between runs. This delay would allow the capillary temperature to re-equilibrate to an initial value before every run within a set. The initial and final current readings for each run are combined and illustrated in Fig. 6.

Examination of Fig. 6 shows that the current increased with increasing run number for all sets, regardless of the presence of the delay period. This shows that temperature equilibration was not the cause of the increase in total current. It is interesting to note two observations regarding the role of SDS micelles with respect to the equilibrium current level. First, with SDS present, the current for sets with delays was less than that for sets without delays. Second, the contribution of SDS to the total curent was not as great as might have been expected. With SDS present, the current increased by 32% on average. This increase can be attributed to the addition of 30 m*M* Na^+ to the buffer, which increased the ionic strength from 50 to 65 m*M*, or by 30%. The contribution of the free dodecyl sulfate would increase the ionic strength to 67

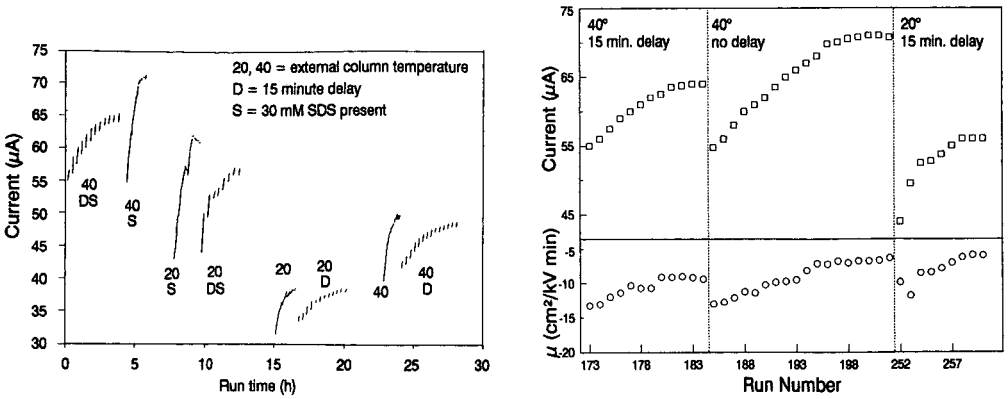

Fig. 6. Comparison of sets with and without 15-min delays between injections. The run time excludes times in which the system was not operating, *i.e.*, nights and weekends. 20, 40 = External column temperature (°C); D = 15-min delay; S = 30 m*M* SDS present.

Fig. 7. Relationship between total current and mobility of ART for sets 4/1, 4/2 and 4/3.

m*M*, assuming that the critical micelle concentration (CMC) is 4 m*M*, raising the increase in ionic strength to 34%.

It appears that the micelles contribute very little to the increase in current. If 50 dodecyl sulfate monomers comprise one micelle [12], the effective concentration of micelles is (30−4)/50, or 0.52 m*M*, and the effective charge of each micelle would be −50, making the contribution of micelles to the ionic strength $(0.5)(0.52)(-50^2)$, or 650 m*M*. If the micelles contributed to the total current, one would expect the current to be much larger than the value observed.

The change in mobility of one of the solutes may shed light on the increase in current. Examination of the behavior of ART in 4/1, 4/2 and 4/3 in Fig. 7 shows a correlation between the behavior of mobility and total current. The increase in current may be due to an increase in charge carriers as the number of runs increases, or may be due to a depletion of charge carriers in the first run and a gradual increase with subsequent runs. It has been shown that phosphate will bind to the silica surface of the capillary with a coverage of *ca.* 23 phosphates per silanol [12]. The presence of the electric field may cause a change in the steady-state coverage of the silica by phosphate. As the phosphate re-establishes a steady-state condition, the solute mobility would level off and the current would rise to an equilibrium value.

From the experiments above, it appears that the increase in current was more likely to be due to interactions of the buffer with the capillary wall than to temperature effects.

CONCLUSIONS

The reproducibility in capillary electrophoresis depends initially on the migration parameter used; the use of mobility is generally, but not universally, better than retention time. When a term such as mobility is used as the basis for comparison, the greatest reproducibility occurred when the capillary was rinsed between each run, when low ionic strength buffers were used and when SDS was not present in the buffer.

The nature of the rinsing solution appears to be of little importance, however, the combination of NaOH and an organic rinsing solution seems to destabilize the migration behaviour. Sodium hydroxide solutions may be required, however, if the new capillary demonstrates poor behavior that may be the result of contamination.

There is evidence that the surface of the capillary undergoes modification until a steady-state condition has been established. At this steady state, the total current and the retention times reach steady values. It may require several runs to reach this condition, however. By rinsing the capillary before each injection, the initial, unmodified conditions can be reproducibly achieved.

ACKNOWLEDGEMENTS

We thank David M. Smith and Chang-yu Quang for their assistance in collecting data and Helen K. Smith for assistance with the manuscript. We also thank Burroughs Wellcome (Research Triangle Park, NC, USA) for the use of the SP4200 integrator. A research grant from the National Institutes of Health (FIRST Award, GM38738) is gratefully acknowledged.

REFERENCES

1 H. H. Lauer and D. McManigill, *Anal. Chem.*, 58 (1986) 166–170.
2 S. Terabe and K. Otsuka, *J. Microcol. Sep.*, 1 (1989) 150–154.
3 J. Liu, K. A. Cobb and M. Novotny, *J. Chromatogr.*, 468 (1988) 55–65.
4 B. B. VanOrman, G. G. Liversidge, G. L. McIntire, T. M. Olefirowicz and A. G. Ewing, *J. Microcol. Sep.*, in press.
5 B. Black, *14th International Symposium on Column Liquid Chromatography, Boston, MA, May 22, 1990*, poster 403.
6 W. J. Lambert and D. L. Middleton, *Anal. Chem.*, 62 (1990) 1585–1587.
7 J. W. Jorgenson and K. D. Lucacs, *Anal. Chem.*, 53 (1981) 1298.
8 J. W. Jorgenson and K. D. Lucacs, *Science*, 222 (1983) 266–272.
9 J. W. Jorgenson and K. D. Lucacs, *J. Chromatogr.*, 218 (1981) 209.
10 J. C. Miller and J. N. Miller, *Statistics for Analytical Chemistry*, Ellis Horwood, Chichester, 2nd ed., 1988.
11 R. L. Scheaffer and J. T. McClave, *Statistics for Engineers*, Duxbury Press, Boston, 1982.
12 R. M. McCormick, *Anal. Chem.*, 60 (1988) 2322–2328.

Journal of Chromatography, 559 (1991) 69–80
Elsevier Science Publishers B.V., Amsterdam

CHROM. 23 431

Evaluation of fundamental properties of a silica capillary used for capillary electrophoresis

KAREN SALOMON*, DEAN S. BURGI and JOHN C. HELMER
Varian Research Center, 3075 Hansen Way, Palo Alto, CA 94304-1025 (USA)

ABSTRACT

A model was developed that accounts for the decrease in the electroosmotic flow in a capillary electrophoresis system when the buffer concentration is increased. Important parameters are: the initial charge per unit area at the silica capillary wall, Q_o; a compact layer of molecules of constant thickness d_o that exists between the capillary wall and the buffer; and the equilibrium constant, K_{wall}, between the cations in the buffer and adsorption sites on the silica capillary. An excellent fit of an equation derived from the model to experimental results was obtained. Values for the above parameters were determined in a number of different buffers and the effect of pH, buffer composition and column coatings on these parameters was evaluated.

INTRODUCTION

Capillary electrophoresis (CE) has a wide range of applications in the separation of charged species. Among the advantageous features of this technique are rapid analysis times and high resolution. Migration times and resolution are governed by the applied voltage, the electrophoretic mobilities (μ_{ep}) of the samples being separated and the electroosmotic flow (μ_{eo}). A reduction in the electroosmotic flow can lead to an improvement in the resolution of components in a sample. However, control of electroosmosis is not straightforward; modifications of the chemical environment of the column are necessary.

There have been several approaches to the control of the electroosmotic flow with particular emphasis on its reduction or elimination. The use of coated capillary columns [1–5] has been employed to reduce greatly the electroosmotic mobility, with the additional benefit of minimizing the adsorption of proteins to the silica capillary wall. The addition of organic modifiers such as methanol or acetonitrile also leads to a reduction in μ_{eo} [6–10], as does an increase in the concentration of the buffer [3,10–15]. The pH of the buffer also has an effect on the electroosmotic mobility [12,13,16–18]. Recently the application of a radial electric field has been shown to increase or decrease the electroosmotic flow [19]. With the exception of the latter instance, all of the above techniques involve altering the chemical properties of the buffer or the capillary wall to reduce the zeta potential, which is proportional to the electroosmotic flow.

0021-9673/91/$03.50

The zeta potential is the potential induced by the negatively charged capillary wall acting on a layer of positive ions next to it. The zeta potential is proportional to the product of the number of charges on the silica surface and the thickness of the counter ion layer. These in turn are affected by the nature of the ions in the counter ion layer, the pH of the buffer and the equilibrium between the cations in the buffer and the silica surface. An exact relationship between the zeta potential and the fundamental properties of the system has not been derived and therefore it has not been possible to obtain values for the thickness of the counter ion layer or the number of charges per unit area at the silica surface. Such values would be useful in the evaluation of various methods used in the reduction of the electroosmotic flow. One method may be more effective than another simply because it controls one key parameter. On the other hand, different methods may have the same effect on the properties of the silica surface, so that there is no advantage of one method over another.

In order to gain some insight into the fundamental properties of the chemistry at the capillary wall, we have developed an equation relating the electroosmotic mobility to the concentration of the buffer. From a fit of the equation to experimental results, it is possible to obtain values of the initial charge at the capillary surface and the equilibrium constant between the silanol groups on the silica surface and the cations in the buffer. The model incorporates a mass-action (Langmuir isotherm) law for neutralization of the wall, and a compact layer of mobile cations, buffer and water molecules in close proximity to the capillary surface. The actual structure of the compact layer is open to speculation. The effect of various strategies used to control the electroosmotic flow such as changing the pH, the addition of organic modifiers and column coatings are discussed in terms of changes induced in the fundamental properties of the silica column.

EXPERIMENTAL

Instrumentation

The research CE instrument used was similar to those described previously [1,20]. A 50 μm I.D. fused-silica capillary (Polymicro Technologies, Phoenix, AZ, USA) 1 m long with a window at 50 cm was suspended between two buffer reservoirs. The applied voltage was supplied by a 30-kV Glassman (Whitehouse Station, NJ, USA) high-voltage power supply. Voltages were adjusted to keep the power below 0.06 W. A 20% solution of acetone was used as a neutral marker. The detector was a modified Jasco UV detector set to 265 nm. Injections were done by raising the sample vial 3 in. above the end reservoir and then dipping the capillary column into the sample vial for 10 s.

The column was etched for 30–60 min with either 0.1 *M* NaOH, KOH, LiOH or RbOH at the start of each day. Distilled water was used to rinse out the column before introducing the buffer. For the phosphate buffer systems, the column was rinsed with 0.015 *M* phosphoric acid before introducing the buffer. When the buffer concentration was changed, the column was re-etched for 5–15 min before introducing the new buffer. The 2-(N-morpholino)ethanesulfonic acid (MES)–histidine (His) buffer was the one exception in that the column was not etched before the introduction of a different concentration to avoid contamination with NaOH. At least two measurements of the electroosmotic flow were conducted for any given buffer.

Chemicals

Several organic and inorganic buffers were used. In the pH 9.55 regime, 3-(cyclohexylamino)-2-hydroxy-1-propanesulphonic acid (CAPSO) was adjusted to the desired pH with NaOH. When methanol was used in the CAPSO–NaOH buffer, the pH was adjusted after the methanol had been added. The CAPSO–NaOH–CH_3OH buffers contained 8 wt.% of methanol. In the pH 6.05 regime, MES was adjusted to the required pH with either NaOH, KOH, LiOH, RbOH or histidine. A phosphate buffer, made from KH_2PO_4 and phosphoric acid, was used at pH 3.8. The organic acids and histidine were purchased from Sigma (St. Louis, MO, USA), RbOH and LiOH from Aldrich (Milwaukee, WI, USA) and methanol, NaOH, KOH, KH_2PO_4 and phosphoric acid from J. T. Baker (Phillipsburg, NJ, USA).

Control of heating

The passage of current through a resistive buffer will cause heating of the buffer in proportion to the applied voltage and the current. If enough heat is generated the buffer viscosity will decrease, which leads to an increase in the measured electroosmotic mobility. Therefore, it is important to work in a regime where very little heat is being generated or to use some method of cooling the column. We chose the former approach.

In Fig. 1, the electroosmotic mobility is plotted as a function of power (applied

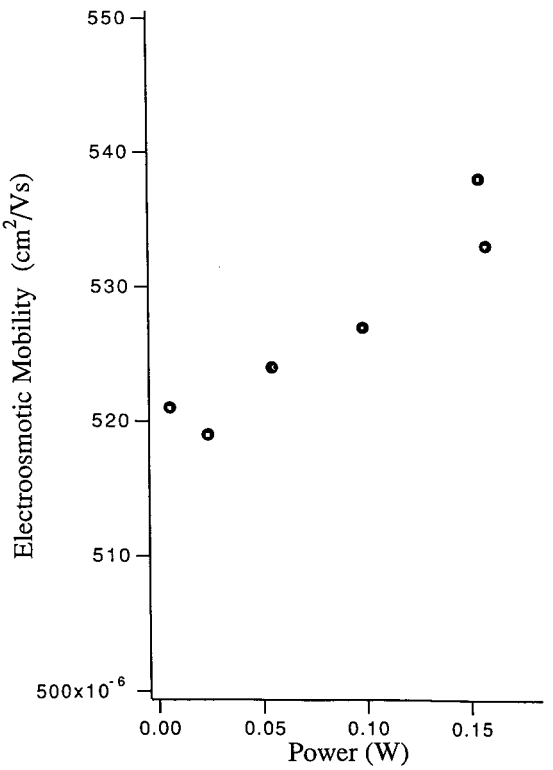

Fig. 1. Measured electroosmotic mobility as a function of power. Buffer is 20 m*M* MES–8 m*M* NaOH (pH 6.05). The applied voltage ranged from 5 to 25 kV.

voltage × measured current) for a 20 m*M* MES–8 m*M* NaOH (pH 6.05) buffer. Above 0.06 W, μ_{eo} begins to increase with increasing power. We limited the studies to powers less than 0.06 W and the applied voltage was adjusted accordingly. At this power, the internal temperature of the column was below 26°C [21].

DERIVATION OF THE ELECTROOSMOTIC FLOW MODEL

We are interested in the formulation of an equation for the electroosmotic mobility in terms of easily measured quantities such as the buffer concentration and the buffer viscosity. In a simple system, where there is no coating on the inside of the column and there are no surfactants in the buffer, the negatively charged capillary wall is balanced by a layer of positive ions in the vicinity of the capillary surface. Some of the positive ions may be adsorbed onto the capillary surface, but the other cations remain in the buffer and are relatively mobile. A potential is induced by the negatively charged capillary surface acting on the positive ions; the magnitude of the potential diminishes as one moves further away from the capillary wall. When an external electric field is applied parallel to the wall, the positive ions in the buffer move toward the negative electrode, thereby setting up the electroosmotic flow. The electroosmotic mobility is proportional to the potential at the interface between the immobile capillary wall (including any adsorbed ions) and the freely moving buffer. This potential is called the zeta potential (ζ). An exact expression for μ_{eo} is [22]

$$\mu_{eo} = \frac{\varepsilon \, \varepsilon_0 \, \zeta}{\eta} \tag{1}$$

where η is the buffer viscosity, ε is the dielectric constant of the buffer and ε_0 is the permittivity of free space. The potential induced by the capillary surface is compensated by positive ions over an effective distance x (perpendicular to the wall), such that the electroosmotic mobility can be rewritten as

$$\mu_{eo} = \frac{Q \, x}{\eta} \tag{2}$$

where Q is the charge per unit area at the interface between the capillary wall and the buffer solution and x is usually referred to as the thickness of the counter-ion layer.

As a first approximation to obtaining a relationship between μ_{eo} and the buffer concentration, we assume that Q is a constant (at a given pH) and that x is dependent on the buffer concentration. If the potential at the capillary surface decreases exponentionally as one moves away from the capillary surface, we can apply the Gouy–Chapman model to our system. In such a case the counter-ion layer thickness would be equal to δ, the Debye–Hückel thickness [11]; the distance δ corresponds to a drop in potential equivalent to a value that is 1/e of the potential at the capillary surface. The Debye–Hückel thickness is inversely proportional to the square root of the ion concentration, $[M^+]$ [23]. For a system in which both the buffer and counter-ion are monovalent the following expression can be derived from eqn. 2:

$$\mu_{eo} = \frac{Q}{\eta \, K' \sqrt{[M^+]}} \tag{3}$$

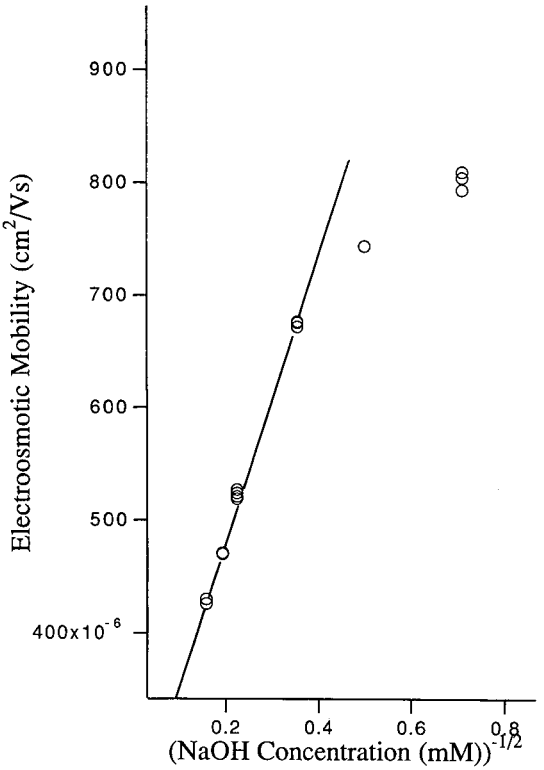

Fig. 2. Measured electroosmotic mobility plotted against the reciprocal of the square root of the NaOH concentration. The line drawn through the points at higher concentrations is there to emphasize the linearity in this regime. Buffer as in Fig. 1; voltages adjusted to keep the power below 0.06 W.

where K' is equal to $3.2 \cdot 10^9$ m^{-1} (mol l^{-1})$^{-1/2}$ for a dilute, aqueous system at 25°C [23]. Although eqn. 3 accounts for the observed decreases in μ_{eo} with increasing buffer concentration at a given pH, it is not exact. As seen in Fig. 2, a plot of μ_{eo} *vs.* [NaOH]$^{-1/2}$ has a non-zero intercept. This offset can be remedied by postulating that the double-layer thickness is the sum of a compact layer of fixed thickness, d_0, and the Debye–Hückel thickness, δ; this modification is analogous to the Stern modification of the Gouy–Chapman model:

$$x = d_0 + \delta = d_0 + \frac{1}{K' \sqrt{[M^+]}} \tag{4}$$

As x is the thickness of a mobile charge layer defined by eqn. 2, the compact layer of thickness d_0 and the diffuse layer thickness, δ, in the above equation are also considered to be mobile. While the above correction takes into account a non-zero intercept when μ_{eo} is plotted against [NaOH]$^{1/2}$, the non-linearity of the plot at low buffer concentrations is still a problem.

It may be argued that the non-linearity in the plot is due to a breakdown in the

assumption that the charge per unit area at the interface (Q) is constant. It seems likely that Q is also a function of buffer concentration; as the buffer concentration is increased, more cations are adsorbed on the capillary wall and the number of exposed silanol groups is proportionately reduced. Cations are known to adsorb to silica surfaces and can be held there by forces in addition to electrostatic attraction; however, the situation is not well understood [24]. We examined a simple adsorption mechanism [15] as shown below:

$$M^+ + SiO^-(H_2O) \rightarrow SiO^-M^+ + H_2O \tag{5}$$

where SiO^- is a silanol group on the surface, M^+ is a monovalent cation other than H^+ and SiO^-M^+ is a silanol group with an adsorbed cation. The equilibrium constant based on this mechanism can be written as follows:

$$K_{wall} = \frac{[SiO^-M^+]}{[M^+][SiO^-]} \tag{6}$$

The charge per unit area at the interface (Q) is simply the concentration of SiO^-. We denote the total number of ionized silanol groups at the capillary surface as Q_0:

$$Q_0 = [SiO^-] + [SiO^-M^+] \tag{7}$$

The following expression for Q can then be derived from eqns. 6 and 7:

$$Q = \frac{Q_0}{1 + K_{wall}[M^+]} \tag{8}$$

According to eqn. 8, $1/Q$ is proportional to $(1 + K_{wall}[M^+])$. If one assumes that the thickness of the counter-ion layer (x) is constant, then based on eqn. 2, $1/\mu_{eo}$ is also proportional to $(1 + K_{wall}[M^+])$. A plot of $1/\mu_{eo}$ *vs.* [NaOH] is shown in Fig. 3. Linear behavior is observed at lower concentrations; however, there is slight curvature at higher concentrations, indicating that the simple adsorption model does not completely describe the concentration dependence of μ_{eo}.

A more accurate description of the chemistry involved at the surface of the capillary column may have both Q and x being dependent on the buffer concentration. Q is affected by the adsorption of cations on the capillary surface and x is affected by the number of cations in the buffer. A schematic diagram is shown in Fig. 4. By substituting eqn. 4 for x and eqn. 8 for Q in eqn. 2, the following expression for the electroosmotic mobility as a function of buffer concentration can be obtained:

$$\mu_{eo} = \frac{Q_0}{\eta\,(1 + K_{wall}[M^+])}\left(d_0 + \frac{1}{K'\sqrt{[M^+]}}\right) \tag{9}$$

Eqn. 9 provides an excellent fit to our data on the dependence of μ_{eo} on cation concentration; a few examples are shown in Fig. 5. χ^2 values are of the order of 10^{-10}.

Parameters determined from a fit of the above equation to the MES–NaOH data

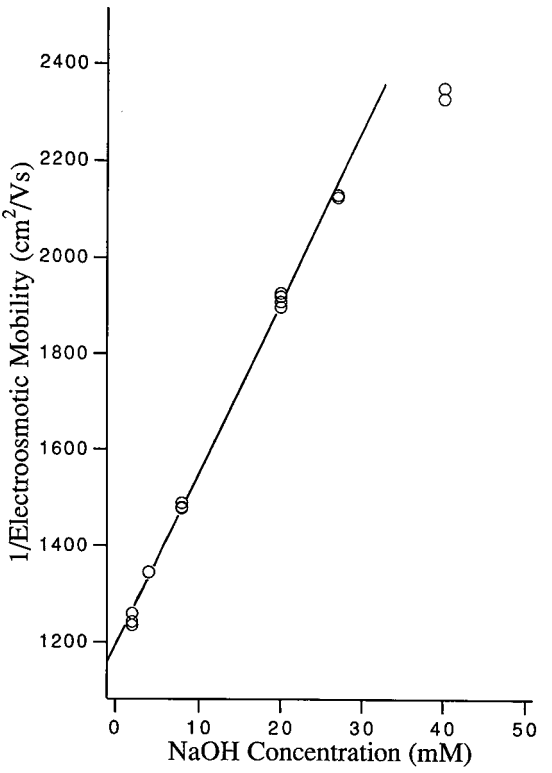

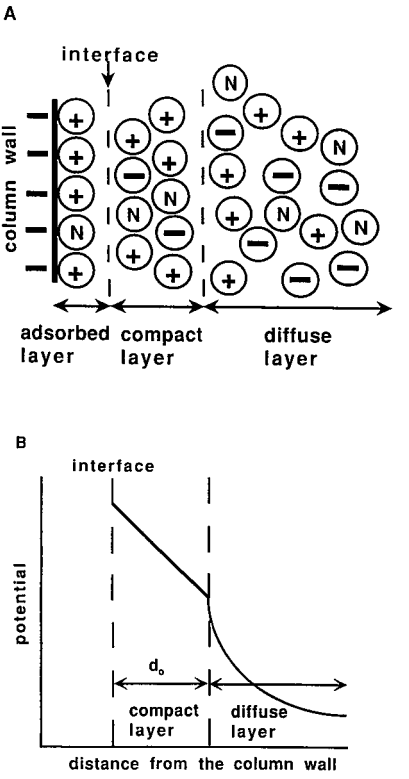

Fig. 3. Reciprocal of the measured electroosmotic flow plotted against NaOH concentration. Conditions as in Fig. 2. The line drawn through the points at lower concentration is used to emphasize the linearity of the data in this regime.

Fig. 4. (A) Representation of our model of the parameters associated with the silica capillary. (B) Potential of the system as a function of the distance away from the wall.

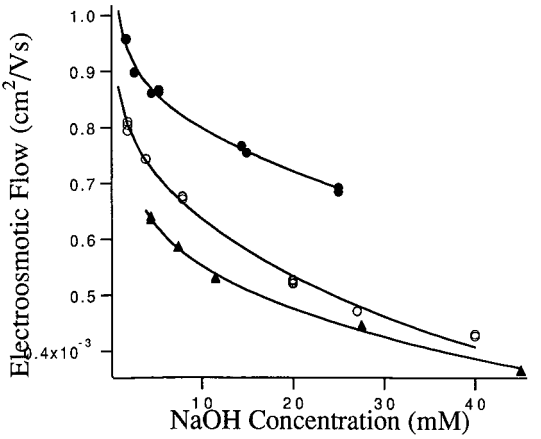

Fig. 5. Electroosmotic flow *vs.* NaOH concentration for three different buffers. ● = CAPSO–NaOH (pH 9.55); ○ = MES–NaOH (pH 6.05); ▲ = CAPSO–NaOH–CH_3OH (pH 9.55). The lines drawn through the points in each data set are the result of a fit of the data to eqn. 9.

TABLE I

CONSTANTS DERIVED FROM A FIT OF EQN. 9 TO THE DATA

System		K_{wall} (l mmol^{-1})	d_0 ($\times 10^{-8}$ m)	Q_0 ($\times 10^{16}$ sites m^{-2})
pH	Components			
9.55	CAPSO–NaOH	0.0093	3.9	1.3
	CAPSO–NaOH–CH_3OH	0.011	1.3	2.9
6.05	MES–LiOH	0.017	1.6	1.4
	MES–NaOH	0.020	3.9	1.1
	MES–KOH	0.034	3.2	0.9
	MES–RbOH	0.023	2.8	1.4
	MES–His	0.034	0.95	2.2
3.8	KH_2PO_4	0.084	2.8	0.50
	KH_2PO_4, coated column[a]	0.083	0.88	1.1

[a] Ref. 3.

are shown in Table I. The compact layer thickness (d_0) was determined to be $3.9 \cdot 10^{-8}$ m. This distance is much larger than the diameter of a hydrated sodium cation, which is of the order of $3 \cdot 10^{-10}$ m [25]. Hence, it appears that the compact layer is more than a single layer of cations. A better description involves several layers of ordered hydrated cations interspersed among buffer molecules and buffer anions. The total number of ionized silanol groups per unit area on the capillary wall is *ca.* 0.3% of the surface SiOH groups, assuming that there are between $4 \cdot 10^{18}$ and $5 \cdot 10^{18}$ SiOH groups per square meter [24]. Because of the good fit to the data, we feel that eqn. 9 will be useful for the elucidation of key parameters relating to the chemistry at the silica capillary surface.

APPLICATIONS OF THE MODEL

In this section we utilize eqn. 9 to evaluate Q_0, d_0 and K_{wall} in a number of different buffer systems by measuring μ_{eo} at several different concentrations of a given buffer. We were interested in elucidating the changes in the above parameters caused by variations in the type of cation present in the buffer, the buffer pH, the addition of organic modifiers to the buffer and the applications of column coatings.

Effect of buffer cation

The choice of the counter-ion used in a given buffer can have a large effect on the electroosmotic flow, as shown in Table II. At a given concentration and pH, μ_{eo} is greatest for MES–NaOH, while decreasing slightly for MES–RbOH. The electroosmotic flows in MES–KOH, MES–LiOH and MES–His were all roughly the same and about 30% less than that for MES–NaOH. The variation in μ_{eo} with buffer cation cannot be accounted for by changes in the hydrated cation radius, which increases from Rb to K to Na to Li (Table II). For all five buffer systems, we measured μ_{eo} at five different concentrations of the buffer and then fitted eqn. 9 to the results to obtain the parameters associated with the capillary wall. Values of Q_0, d_0 and K_{wall} are included in Table I.

TABLE II

PHYSICAL CONSTANTS AND MEASURED ELECTROOSMOTIC FLOW FOR MES BUFFERS WITH DIFFERENT COUNTER-IONS

Cation	Li	Na	K	Rb	His
Conductivity[a] ($cm^2\ \Omega^{-1}\ mol^{-1}$)	38.69	50.11	73.50	–	–
Ion mobility[b] ($\times 10^{-4}\ cm^2\ V^{-1}\ s^{-1}$)	4.01	5.19	7.62	7.92	–
Hydrated cation radius[c] (Å)	2.1	1.6	1.1	1.1	–
Current[d] (μA)	0.78	0.70	1.18	1.6	0.61
Electroosmotic flow[d,e] ($\times 10^{-4}\ cm^2\ V^{-1}\ s^{-1}$)	5.03	8.0	4.98	7.43	5.55

[a] Ref. 23.
[b] Ref. 25.
[c] Calculated from the ion mobility; see ref. 25, p. 827.
[d] Measured at 25 kV in a buffer of 5 m*M* MES and 2 m*M* cation (5 m*M* histidine).
[e] Uncertainties are less than 1% based on day-to-day reproducibility.

The variation in the electroosmotic flow with the type of buffer cation is a complicated combination of factors; however, some trends are apparent. Low values of the compact layer thickness predominate over changes in the other parameters, leading to the observed low values of μ_{eo} for MES–LiOH and MES–His. An anomaly is the MES–KOH system, which has a d_0 value similar to those for the MES–NaOH and MES–RbOH systems but has a much lower electroosmotic flow. Here a greater value of the equilibrium constant appears to be important.

One striking result is that the value of Q_0 is roughly the same for the alkali metal cations in the MES buffers, indicating that the initial number of SiO^- groups does not depend on the type of cation used. However, in the case of the MES–His buffer, the value of Q_0 is twice that of the other MES buffers. It appears that the bulky histidine may act to mediate the charge repulsion between SiO^- groups on the surface and allow for more SiO^- groups to be present in a given area.

Effect of pH

To study how changing the pH affects the condition of the capillary column, we measured μ_{eo} at several concentrations of a CAPSO–NaOH buffer at pH 9.55 and at several concentrations of a potassium phosphate buffer at pH 3.8. Eqn. 9 provided an excellent fit to the data (Fig. 5) and values of Q_0, d_0 and K_{wall} are included in Table I.

A comparison of CAPSO–NaOH values with those for MES–NaOH at pH 6.05 shows that both Q_0 and d_0 were unchanged. It is surprising to find that the initial charge at the capillary wall changed so slightly from pH 6 to 9. From our analysis, the increase in the electroosmotic flow from $7.4 \cdot 10^{-4}\ cm^2\ V^{-1}\ s^{-1}$ at pH 6.05 (4 m*M* NaOH) to $8.7 \cdot 10^{-4}\ cm^2\ V^{-1}\ s^{-1}$ at pH 9.55 (4 m*M* NaOH) is attributable to the reduction in K_{wall} by a factor of two. In our simple adsorption model, pH effects on K_{wall} were not included. However, it is known [26] that equilibrium constants are dependent on the concentration of other ions in the medium. The origin appears to be due to electrostatic attraction between ions in solution for the ions involved in the equilibrium process of interest. In our case, at higher pH values, the equilibrium shifts in the direction of more free cations; the increased OH^- concentration is apparently removing adsorbed cations from the capillary surface.

In the lower pH regime, there are significant changes in Q_0. Q_0 increases from 0.50 in a pH 3.8 KH_2PO_4–H_3PO_4 buffer to 0.9 in a pH 6.05 MES–KOH buffer. The equilibrium constant (K_{wall}) decreases from pH 3.8 to 6.05 as it did in going from pH 6.05 to 9.55; the mechanism may be the same, namely the increased solvation of the cation (K^+ in this case) by the increased OH^- concentration. Finally, the compact layer thickness (d_0) does not appear to be influenced by changes in pH, provided that the type of cation remains the same.

Effect of methanol

The addition of methanol to a buffer is known to lead to a reduction in the electroosmotic mobility [6–10], but the exact mechanism remains unclear. We are able to obtain values of Q_0, d_0 and K_{wall} in a pH 9.55 CAPSO–NaOH–MeOH buffer which are included in Table I. As can be seen, the addition of methanol leaves the equilibrium constant unchanged. However, Q_0 more than doubled; it appears that methanol shields charged sites from each other, thus allowing more to exist in a given area. The same increase in Q_0 was observed in the MES–His buffer at pH 6.05 where histidine is capable of the same kind of shielding. The addition of methanol also leads to a shrinking of the compact layer, which may be the result of improved solvation of the charges in this region. The reduction in the compact layer thickness overrides the increase in Q_0 to result in an overall reduction in the electroosmotic velocity (Fig. 5).

Effect of column coating

Bruin *et al.* [3] used coated capillary columns to improve the separation of proteins in a phosphate buffer. In addition to the elimination of protein adsorption to the capillary wall, a reduction in the electroosmotic mobility was noted. Because μ_{eo} was measured at several concentrations, we were able to fit eqn. 9 to their results and obtain values for the fundamental parameters, which are included in Table I. In addition, we measured the electroosmotic mobility in an uncoated column at several concentrations using the same phosphate buffer. The results of a fit of eqn. 9 to our data are also included in Table I.

A comparison of values for the coated and uncoated columns shows that the application of a coating to the capillary wall had no effect on the equilibrium constant, indicating that the coating does not alter the chemistry between the silica wall and the cations in the buffer. However, the use of a coating reduced the thickness of the compact layer by a factor of three; the origin of this effect is not clear. An increase in Q_0 is observed with the coated column, presumably owing to better shielding of the SiO^- groups by the coating. As seen with the addition of methanol to the buffer, the reduction in the thickness of the compact layer overwhelms the increase in Q_0 to lead to an overall reduction in μ_{eo}.

Summary of individual influences

From the above analyses of various column treatments, several trends are evident. The equilibrium constant between the buffer cations and adsorption sites on the capillary wall is insensitive to column coatings and to the presence of organic modifiers in the buffer. The equilibrium constant decreases as the pH is increased and is sensitive to the type of cation used in the buffer. The effect of adding methanol to the buffer is similar to that of coating the column, namely leading to an increase in Q_0 due

to better shielding of surface SiO^- groups from each other. In both instances the increase in Q_0 is overshadowed by a decrease in d_0 which leads to the observed reduction in the electroosmotic flow. The use of histidine in the MES–His buffer has the same effect as the addition of methanol or the coating of the column. Increasing the pH causes an increase in Q_0 with the greatest effect occurring between pH 3.8 and 6.05, which is in agreement with some recent studies of the electroosmotic flow as a function of pH [17]. The thickness of the compact layer (d_0) is not affected by changes in pH provided that the type of cation in the buffer is kept constant.

CONCLUSIONS

We have developed a model of electroosmotic flow as a function of buffer concentration that is a useful tool for analyzing the surface parameters of a fused-silica capillary column under a variety of conditions. An excellent fit of the model to our own data and to the results of other work was obtained. From our analysis, it appears that both the addition of organic modifiers and the coating of the capillary column lead to a reduction in the electroosmotic flow by the same mechanism, namely the reduction in compact layer thickness which overwhelms the increase in initial charge at the surface. Raising the pH leads to an increase in Q_0 at lower pH, but above pH 6.05 Q_0 increases only slightly. The equilibrium constant between buffer cations and the silica surface decreases as the pH is increased. The type of cation used in the buffer can also lead to a reduction in μ_{eo} through a combination of factors.

ACKNOWLEDGEMENT

The help of Maria Ladle Ristow with the cation studies is gratefully acknowledged.

REFERENCES

1 J. W. Jorgenson and K. D. Lukacs, *Science*, 222 (1983) 266–272.
2 R. M. McCormick, *Anal. Chem.*, 60 (1988) 2322–2328.
3 G. J. M. Bruin, J. P. Chang, R. H. Kuhlman, K. Zegers, J. C. Kraak and H. Poppe, *J. Chromatogr.*, 471 (1989) 429–436.
4 K. Cobb, V. Dolnik and M. Novotny, *Anal. Chem.*, 62 (1990) 2478–2483.
5 J. K. Towns and F. E. Regnier, *J. Chromatogr.*, 516 (1990) 69–78.
6 S. Fujiwara and S. Honda, *Anal. Chem.*, 59 (1987) 487–490.
7 J. Gorse, A. T. Balchunas, D. F. Swaile and M. J. Sepaniak, *J. High Resolut. Chromatogr. Chromatogr. Commun.*, 11 (1988) 554–559.
8 J. Liu, K. Cobb and M. Novotny, *J. Chromatogr.*, 468 (1988) 55–65.
9 M. M. Bushey and J. W. Jorgenson, *J. Microcol. Sep.*, 1 (1989) 125–130.
10 K. Salomon, D. S. Burgi and J. C. Helmer, *J. Chromatogr.*, 549 (1991) 375–385.
11 T. Tsuda, K. Nomura and G. Nakagawa, *J. Chromatogr.*, 248 (1982) 241–247.
12 S. Fujiwara and S. Honda, *Anal. Chem.*, 58 (1986) 1811–1814.
13 V. Dolnick, J. Liu, J. F. Banks, M. Novotny and P. Bocek, *J. Chromatogr.*, 480 (1989) 321–330.
14 B. B. VanOrman, G. G. Liversidge, G. L. McIntire, T. M. Olefirowiczand and A. G. Ewing, *J. Microcol. Sep.*, 2 (1990) 176–180.
15 A. W. Adamson, *Physical Chemistry of Surfaces*, Wiley, New York, 5th ed., 1990, p. 423.
16 K. D. Lukacs, *Ph.D. Thesis*, University of North Carolina, 1983.
17 K. Otsuka and S. Terabe, *J. Microcol. Sep.*, 1 (1989) 150–154.
18 W. J. Lambert and D. L. Middleton, *Anal. Chem.*, 62 (1990) 1585–1587.

19 C. S. Lee, W. C. Blanchard and C.-T. Wu, *Anal. Chem.*, 62 (1990) 1550–1552.
20 S. Pentoney, X. Huang, D. S. Burgi and R. N. Zare, *Anal. Chem.*, 60 (1988) 2625–2629.
21 D. S. Burgi, K. Salomon and R.-L. Chien, *J. Liq. Chromatogr.*, 14 (1991) 847–867.
22 A. S. Cohen, A. Paulus and B. L. Karger, *Chromatographia*, 24 (1987) 15–24.
23 A. J. Bard and L. R. Faulkner, *Electrochemical Methods. Fundamentals and Applications*, Wiley, New York, 1980.
24 R. K. Iler, *The Chemistry of Silica*, Wiley, New York, 1979.
25 P. W. Atkins, *Physical Chemistry*, Freeman, San Francisco, 1978.
26 D. A. Skoog and D. M. West, *Analytical Chemistry. An Introduction*, Holt, Rinehart and Winston, New York, 2nd ed., 1974.

Journal of Chromatography, 559 (1991) 81–93
Elsevier Science Publishers B.V., Amsterdam

CHROM. 23 433

Effect of hydrostatic flow on the efficiency in capillary electrophoresis

ELI GRUSHKA
Department of Inorganic and Analytical Chemistry, The Hebrew University, 91904 Jerusalem (Israel)

ABSTRACT

An expression is derived for the plate height in capillary electrophoresis for cases where hydrostatic flow (HF) is present. HF will occur whenever the buffer levels at both ends of the capillary are not at the same height. Whereas the plate height equation for an HF-free system has only a molecular diffusion term, the plate equation in the presence of HF has an additional term which is a resistance to mass transfer term. The second term is a function of capillary radius, the hydrostatic velocity, the solute diffusion coefficient and the electrophoretic velocity. Unlike in chromatography, the mass transfer term usually does not increase with increasing solute velocity. Nonetheless, the contribution of this additional term to the total plate height can be substantial for wide capillaries and large solute molecules. We calculated maximum allowable buffer height differences, Δh_{max}, for a given loss in plate height. It was found that for large molecules and wide capillaries, Δh_{max} can be less than 1 mm, making severe demands on the instrumental design. With small solutes and narrow capillaries, the requirement for extract buffer levelling at both ends of the capillary is less acute.

INTRODUCTION

The use of capillary electrophoresis, because of its high efficiency and separation power, is growing continuously. In particular, capillary electrophoresis holds the promise of becoming the separation method of choice for biomacromolecules such as proteins and nucleic acids. Frequently, however, the theoretical efficiencies cannot be attained in practice and peaks of retained solutes are much broader than expected.

There are several possible contributors to the excess, or extra-column, zone broadening. Perhaps the most studied contribution is that due to the Joule heating effect. Knox and Grant [1,2] and Grushka *et al.* [3] discussed in detail the effects of temperature gradients on the efficiency in capillary electrophoresis. In general, it is felt that temperature effects are of minor importance provided that the capillary radius is small and that the ionic strength of the running buffer is not too high.

Other contributions to zone broadening have been investigated. For example, Martin and co-workers [4,5] studied the effect of wall distortion of the plug flow in capillary electrophoresis. Lukacs and Jorgenson [6], although they did not consider extra-column effects, examined the dependence of the efficiency on several experimental parameters. Sepaniak and co-workers [7,8] investigated the effects of sample

0021-9673/91/$03.50

injection, applied voltage, buffer concentration and column dimensions on the efficiency of micellar electrokinetic capillary chromatography systems. Jones *et al.* [9] discussed several other contributions to zone broadening.

This paper examines whether the presence of a hydrostatic flow component is a possible source of additional zone broadening. When the buffer levels in the reservoirs at the capillary ends are not equal, pressure-induced flow, known as hydrostatic flow (HF), results. This flow will be superimposed on the electrophoretic flow (EF). HF can be either in the same direction as, or opposite to, EF. The velocity profile associated with HF, as in any pressure-induced flow, is parabolic in nature. Therefore, HF can contribute to zone broadening, making the experimental efficiency less than the theoretical prediction.

THEORY

The velocity profile of HF is given by

$$u_{Hs}(r) = 2u_s\left(1 - \frac{r^2}{a^2}\right) \tag{1}$$

where u_{Hs} is hydrostatic velocity, r is the radial position, a is capillary radius and u_s is the cross-sectional average of the hydrostatic velocity, which is given by

$$u_s = \frac{\Delta h \rho g a^2}{8\eta L} \tag{2}$$

Δh is the height difference between the buffer levels, ρ is the buffer density, g is the gravitational acceleration, η is the buffer viscosity and L is the capillary length (see Appendix for units). The overall velocity of the solute is

$$u(r) = u_{ef} \pm 2u_s\left(1 - \frac{r^2}{a^2}\right) \tag{3}$$

where u_{ef} is the electrophoretic velocity.

Eqn. 3 can be used, in conjunction with the following mass balance equation, in order to obtain the plate-height equation:

$$\frac{\partial C}{\partial t} = D\left[\frac{1}{r}\cdot\frac{\partial}{\partial r}\left(r\frac{\partial C}{\partial r}\right)\right] + D\cdot\frac{\partial^2 C}{\partial x^2} - u(r)\cdot\frac{\partial C}{\partial x} \tag{4}$$

where C is the solute concentration, D is the solute's diffusion coefficient, t is analysis time and x is longitudinal direction. Suitable boundary and initial values, needed to solve eqn. 4, are

$$C(t,\infty,r) = 0$$

$$C(0,0,r) = C_0$$

$$C(0,x,r) = 0$$

$$\partial C(t,x,a)/\partial r = 0$$

$$\partial C(t,x,0)/\partial r = 0$$

$$u(a) = u_{ef}$$

Eqn. 4 was solved in a manner similar to that described previously [3], using the method of Gill (*e.g.*, ref. 10). The solution yields a concentration dispersion expression which, in turn, allows the derivation of the following plate-height (H) equation (Appendix A in ref. 3 gives the details of the derivation):

$$H = \frac{2D}{u_{ef} \pm u_s} + \frac{a^2 u_s^2}{24D(u_{ef} \pm u_s)} \tag{5}$$

This paper assumes that, in addition to hydrostatic flow, molecular diffusion is the major broadening mechanism. Other contributions, such as temperature gradients, wall adsorption or extra-column effects, are not taken into account here. These additional contributions can be added, via their variances, to give a total H expression.

DISCUSSION

Contribution of the hydrostatic flow effect to plate height

In eqn. 5, the hydrostatic velocity is added to or subtracted from the electrophoretic velocity. In the following discussion we shall assume that the hydrostatic velocity is in the same direction as the electrophoretic velocity. The extension of the treatment to cases where the two velocity components are in opposite directions is fairly straightforward.

Eqn. 5 shows that the existence of HF results in an additional term in the plate-height equation which resembles the resistance to mass transfer in the mobile phase term in chromatography. The equivalent term in chromatography is a linear function of the average mobile phase velocity; the contribution of the resistance to mass transfer in the mobile phase to the plate height increases linearly with the average velocity of the mobile phase. In the present case, the velocity dependence is more complicated and it is a function of both u_{ef} and u_s. Assuming that the buffer height difference is constant (*i.e.*, it is equipment dependent), then the HF term in eqn. 5 is an inverse function of the electrophoretic velocity as in the molecular diffusion term. Thus, provided that Δh is constant, the relative importance of the HF term to the plate height is roughly a constant at all EF velocities.

Eqn. 5 has another very important implication. The existence of the HF component introduces an aliasing effect on the H behaviour. The additional flow component changes not only H but also the experiment migration velocity. As a result, the H *vs.* velocity curve can change in some unexpected ways. As will be discussed in a later section, this change in the H curve is particularly troublesome with small solute molecules.

Fig. 1 shows three H plots for a large solute ($D = 1 \cdot 10^{-10}$ m^2/s). The solid line

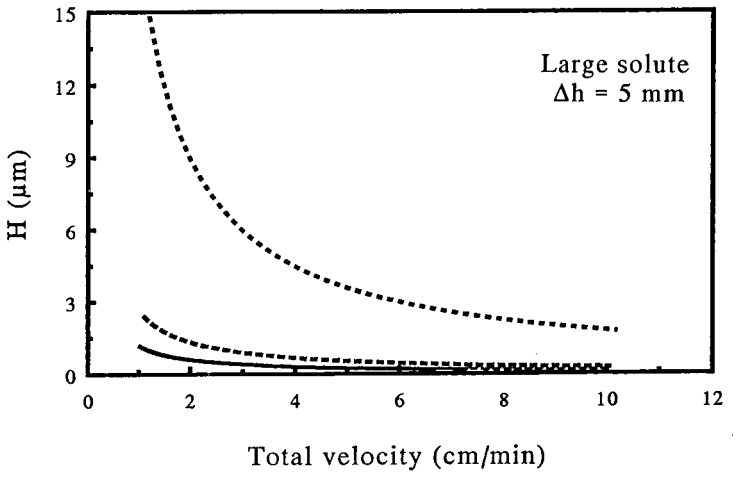

Fig. 1. Effect of capillary radius on H plots for a large solute ($D = 1 \cdot 10^{-10}$ m^2/s) when $\Delta h = 5$ mm. The solid line depicts the theoretical behaviour; the dashed line is for a 50-μm radius capillary; the dotted line is for a 75-μm capillary. The values of other parameters are given in the Appendix.

is the theoretical H behaviour ($H = 2D/u_{ef}$). Each line refers to a different capillary radius. Fig. 1 shows that as the capillary radius decreases, the effect of hydrostatic flow diminishes owing to a decrease in u_s. The velocity of the hydrostatic flow component is 0.207 and 0.0919 for the 75- and 50-μm capillaries, respectively (the relevant data for the calculation of u_s can be found in the caption of Fig. 1 and in the Appendix). It should be pointed out that for a 25-μm radius capillary, the plate-height line is identical with the theoretical line, within 1–2%.

Fig. 2 shows H values for a large solute in a 50-μm radius capillary at three

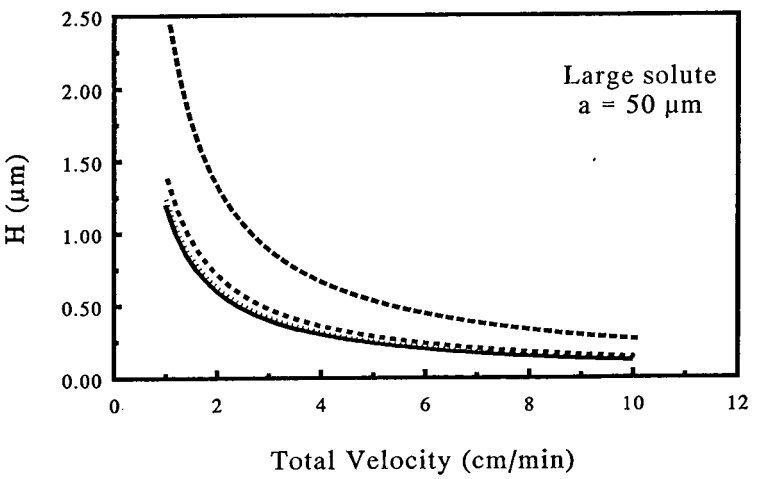

Fig. 2. Effect of Δh on the plate height for a large solute ($D = 1 \cdot 10^{-10}$ m^2/s) in a 50-μm radius capillary. The solid line is for $\Delta h = 0$ (theoretical behaviour); the dotted line is for $\Delta h = 1$ mm; the short dashed line is for $\Delta h = 2$ mm; the dashed line is for $\Delta h = 5$ mm. The values of other parameters are indicated in the Appendix.

different Δh values, 1, 2 and 5 mm. Also shown is the theoretical H behaviour. As expected, the larger is Δh, the greater is the contribution of hydrostatic flow to the plate height.

Figs. 1 and 2 indicate two main points. (a) Assuming that Δh is constant, the hydrostatic flow contribution does not cause the H curve to give a hyperbolic shape as in chromatography. As mentioned previously, the relative effect of HF is independent of the EF velocities. (b) For large solutes, the contribution of HF can be significant. For example, in the case of the 50-μm radius capillary, a 5-mm Δh can double the H values. Even a 2-mm height difference can cause a 15–20% increase in H. With the 75-μm radius capillary the situation is much worse; a 2-mm height difference triples H, whereas a 5-mm height difference increases H by a factor of 10. The HF velocity in this last example is 0.207 cm/min. Thus, at the low u_{ef} values, u_s is about 20% of the total velocity and the H curve at the low velocity is "aliased" toward slightly higher velocities than the theoretical curve. At high velocities, the contribution of u_s to the total velocity is only about 2% and the aliasing is not too noticeable.

With small solute molecules the HF effect is much less pronounced. Fig. 3 shows the H behaviour for a solute whose diffusion coefficient is $1 \cdot 10^{-9}$ m^2/s in a 75-μm radius capillary when Δh is 5 mm. The solid line is the theoretical behaviour and the dashed line is the H behaviour for $\Delta h = 5$ mm. Fig. 3 demonstrates very well the aliasing effect mentioned above: it looks as if the theoretical curve is shifted towards faster velocities and higher plate values. The dashed line is the "experimentally" observed H behaviour in the presence of HF. As the dashed line lies slightly above the theoretical line, the experimental conclusion is that there is a slight loss in efficiency. From a purely formalistic point of view, this conclusion is correct. However, at low u_{ef} velocities, the presence of the HF component actually improves slightly the efficiency *vis-à-vis* the expected value at the given EF velocity. For example, the plate height at $u_{ef} = 1$ cm/min is higher than the plate height at the total velocity of 1.2 cm/min ($u_{ef} =$

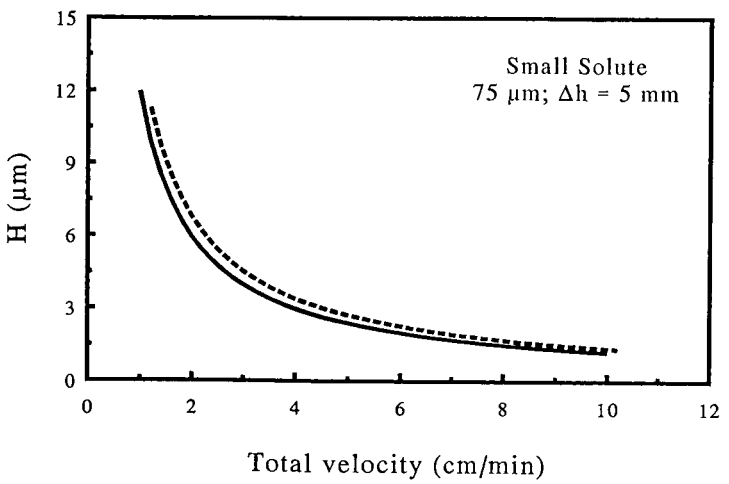

Fig. 3. Plate-height behaviour for small solute ($D = 1 \cdot 10^{-9}$ m^2/s) when $\Delta h = 5$ mm. The solid line is the theoretical curve; the dashed line is for a 75-μm radius capillary. The values of other parameters are indicated in the Appendix.

1 cm/min; u_s = 0.2 cm/min for a 75-μm radius capillary and Δh = 5 mm). The lowering of the plate height can best be demonstrated by plotting both curves in Fig. 3 against the electrophoretic velocity, that is, eliminating the hydrostatic velocity from the dashed line. In such a plot, the dashed line, at u_{ef} velocities of up to about 2 cm/min, would lie below the theoretical line. At high electrophoretic velocities, the dashed line would lie above the solid line.

Figs. 1–3 lead to the following important conclusion: the larger the solute molecule and the wider the capillary, the more critical is the need to balance the buffer reservoirs at the ends of the tubing. Narrow capillaries are advantageous not only because of their excellent heat transfer characteristics, but also owing to the much smaller HF effect.

The existence of an optimum Δh

As discussed above, provided that u_{ef} and u_s have the same sign, the presence of an HF component can yield better H values. The improvement in efficiency occurs because the HF component causes the solute molecules to elute faster, thus lowering the contribution of molecular diffusion. For each u_{ef} there is a unique Δh value which will give the best possible H for the total migration velocity $u_{ef} + u_s$. The optimum Δh can be found as follows: the ratio of eqn. 5 to the theoretical H equation is

$$\frac{H_s}{H} = \frac{u_{ef}}{u_{ef} + u_s} + \frac{a^2 u_s^2 u_{ef}}{48D^2(u_{ef} + u_s)} \tag{6}$$

H_s is the expression in eqn. 5. Eqn. 6 is differentiated with respect to u_s, set equal to zero and solved for $u_{s_{opt}}$:

$$u_{s_{opt}} = -u_{ef} + \frac{1}{a}\sqrt{a^2 u_{ef}^2 + 48D^2} \tag{7}$$

Eqn. 7, together with eqn. 2, allows the calculation of an optimum Δh value. Fig. 4 plots the optimum Δh values *vs.* u_{ef} for large molecules with three capillary radii. As the radius becomes larger, the optimum height difference becomes smaller. Also, the optimum Δh values decrease with increasing electrophoretic velocities. Moreover, with large molecules the optimum Δh values are very small, usually significantly less than 1 mm. As a consequence, for large solutes, the optimum u_s values are very small and the improvement in H is usually negligible.

Fig. 5 plots optimun Δh values *vs.* u_{ef} for small molecules with three capillary radii. As expected, Δh is much higher for small molecules. In fact, at slow EF velocities, the height difference leading to an improved H can be tens of centimetres, especially with the 25-μm radius capillary. Here, the improvement in H can be noticeable. Table I gives some H values with and without the HF component. At very low EF velocities, the improvements in H and the migration time can be substantial. However, owing to the very long migration times at such low EF velocities, the benefit of HF is questionable, except where very low voltages are desired. At more reasonable u_{ef} values, such as 3.5 cm/min, the improvement in H is not as impressive; *e.g.*, with a 25-μm capillary H improves from 3.43 to 3.25, a 5% decrease. With larger capillaries the improvement is even smaller.

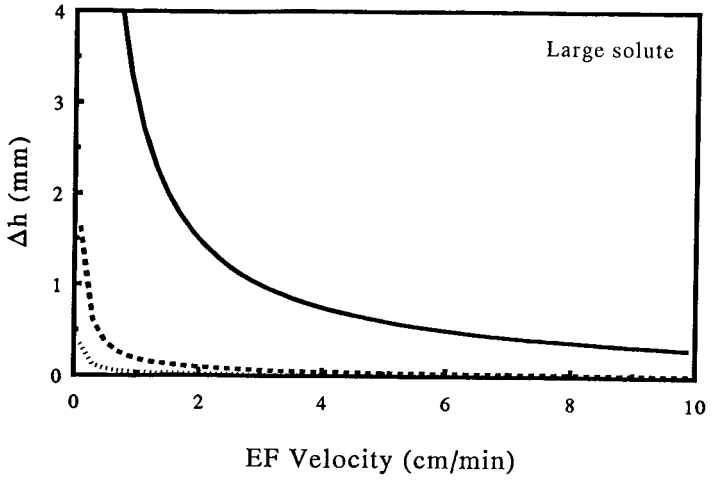

Fig. 4. Height difference which will give the optimum H value at a given u_{ef}. The curves are for large solute ($D = 1 \cdot 10^{-10}$ m^2/s). The solid line is for a 25-μm radius capillary; the dashed line is for a 50-μm capillary; the dotted line is for a 75-μm capillary. The values of other parameters are indicated in the Appendix.

The equivalent increase in efficiency and decrease in migration time can be accomplished by eliminating HF and increasing the applied electric field. If the electric field is increased so that the migration time is equal to that in the system with HF, the efficiency improvement will be better than indicated above. Therefore, from an efficiency point of view, it is always better to increase the electrophoretic velocity. However, when an increase in the applied field is detrimental to the system, then intentionally unlevelled buffer reservoirs may be beneficial.

The above discussion about a decrease in migration time and an increase in efficiency as a result of HF assumes that the added flow component is in the direction

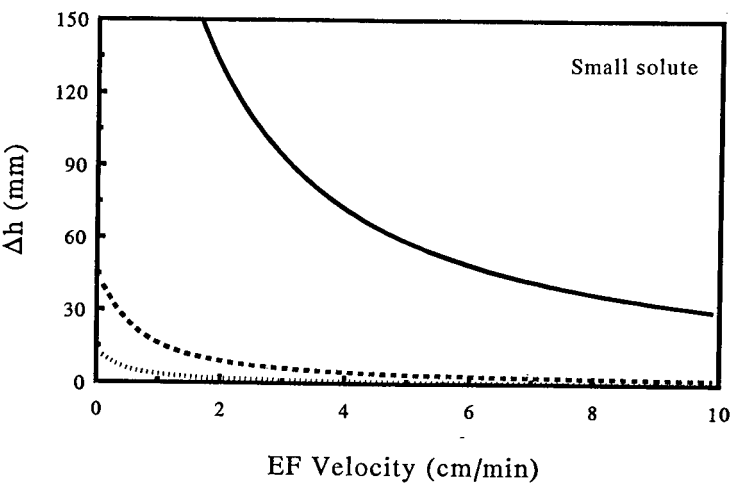

Fig. 5. Height difference which will give the optimum H value at a given u_{ef}. The curves are for small solute ($D = 1 \cdot 10^{-9}$ m^2/s). The solid line is for a 25-μm radius capillary; the dashed line is for a 50-μm capillary; the dotted line is for a 75-μm capillary. The values of other parameters are indicated in the Appendix.

TABLE I

IMPROVEMENT IN EFFICIENCY AS A RESULT OF HYDROSTATIC FLOW

H_s represents H with HF; t_{Rs} represents migration time with HF.

u_{ef} (cm/min)	a (μm)	u_s (cm/min)	Δh (mm)	H (μm)	H_s (μm)	t_R (s)	t_{Rs} (s)
0.1	25	1.56	340	120	13.6	36 000	2156
	50	0.737	40	120	25.6	36 000	4301
	75	0.463	11	120	36.2	36 000	6394
1.1	25	0.811	180	10.9	7.77	3237	1884
	50	0.243	13	10.9	9.7	3237	2680
	75	0.113	2.7	10.9	10.3	3237	2968
3.5	25	0.375	82	3.43	3.25	1029	929
	50	0.097	5.3	3.43	3.38	1029	1001
	75	0.044	1.1	3.43	3.41	1029	1016

of the electrophoretic flow. If HF is in the opposite direction, then the migration times will increase and the efficiency will decrease.

Maximum allowed height difference (Δh_{max}) for a given loss in plate height

It is of practical importance to be able to calculate Δh values for a given loss in H. However, because of the aliasing effect, the calculation of the maximum allowable Δh is not straightforward. An equation for Δh_{max} can be derived in one of two ways. The first approach assumes a given electrophoretic velocity, with its associated theoretical H value, and then proceeds to calculate Δh_{max} based on the assumed u_{ef}. In this approach, the derivation of Δh_{max} is done as follows: if we can tolerate a fraction x loss in H, then

$$\frac{H_s}{H} = 1 + x \tag{8}$$

Eqns. 8, 5 and 2 yield an expression for the Δh which is responsible of the above loss in efficiency:

$$\Delta h_{max} = \frac{(8\eta L)[48D^2 y \pm \sqrt{(48D^2 y)^2 - 192a^2 D^2 u_{ef}^2 (1 - y)}]}{2a^4 u_{ef} \rho g} \tag{9}$$

where $y = 1 + x$. Only the positive root of eqn. 9 is physically significant. The strong inverse dependence on the capillary radius should be noted. Fig. 6 plots the maximum height difference which will result in a 20% loss ($x = 0.2$) in H for large molecules as a function of electrophoretic velocity. Fig. 6 shows that Δh_{max}, which will cause 20% decrease in H, is relatively insensitive to electrophoretic velocity, especially with wide capillaries. It also shows the strong dependence of Δh_{max} on the radius; the narrower the capillary, the larger is the maximum height difference. For example, for a 25-μm radius capillary, the height difference between the buffer levels can be as large as 1.8

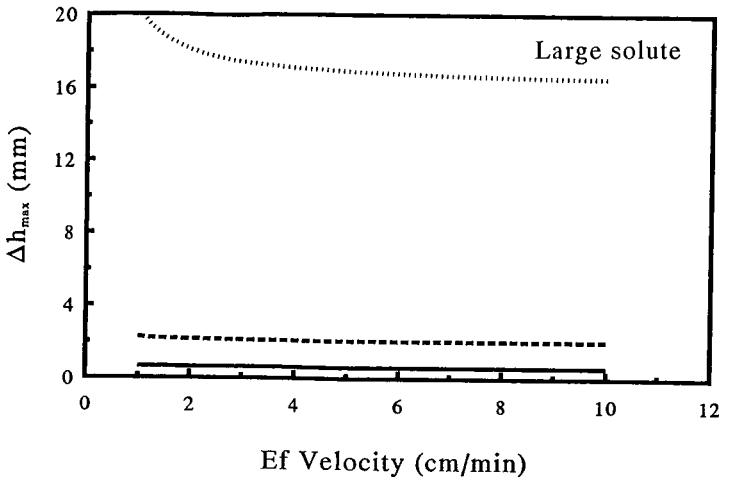

Fig. 6. Maximum allowed height differences which will cause a 20% decrease in plate height. Large solute ($D = 1 \cdot 10^{-10}$ m^2/s). The solid line is for a 25-μm radius capillary; the dashed line is for a 50-μm capillary; the dotted line is for a 75-μm capillary. The values of other parameters are indicated in the Appendix.

cm. In practice, actual height differences between the buffer levels can be easily maintained below that Δh_{max}. However, with 75-μm radius capillary, Δh should be less than about 0.61 mm to ensure a loss in H of less than 20%. Such a Δh is much more difficult to attain in practice. Even if we allow 40% loss in H, Δh_{max} for the 75-μm capillary, as calculated from eqn. 9, should be less than 0.85 mm, which still may be difficult to realize experimentally.

With large molecules, as in the examples in the previous section, Δh_{max} and the associated hydrostatic velocities are small. Therefore, the velocity shift in the H curve is barely noticeable. However, with small molecules, Δh_{max} and u_s can be large. For example, Fig. 7 plots the dependence of Δh_{max} that will cause a 20% loss in H on electrophoretic velocity for a solute with $D = 1 \cdot 10^{-9}$ m^2/s. Some of the characteristics of Fig. 7 are similar to those of Fig. 6, namely, a strong dependence of the allowed height difference on capillary radius and relative independence of Δh_{max} on u_{ef} in wide capillaries. Fig. 7 shows that for a 75-μm capillary, the allowed height difference, for a loss of 20% in H, is about 6.8 mm. However, with narrow capillaries, Δh_{max} can be fairly high, *e.g.*, with a 25-μm radius the allowed Δh is above 200 mm even at high velocities. Therefore, we might conclude that with narrow capillaries and small solutes, exact levelling of the two reservoirs is not essential, and almost any reasonable arrangement of the buffer solutions should yield close to theoretical H values. That conclusion is erroneous because, if Δh is high, the associated u_s is also very high, possibly higher than u_{ef}, causing a severe aliasing effect. The H curve will be very distorted, and the loss in efficiency, at the total velocity of $u_{ef} + u_s$, will be much higher than expected based on the electrophoretic velocity for which the calculations of Δh_{max} were made. Fig. 8 plots the H values associated with Δh_{max} curves in Fig. 7. Particularly noteworthy is the H behaviour for the 25-μm radius capillary. Owing to the very high hydrostatic velocity, the H curve cannot be measured at total velocities below about 4 cm/min. The highest H value for the 25-μm capillary is 14.4 μm. This value was

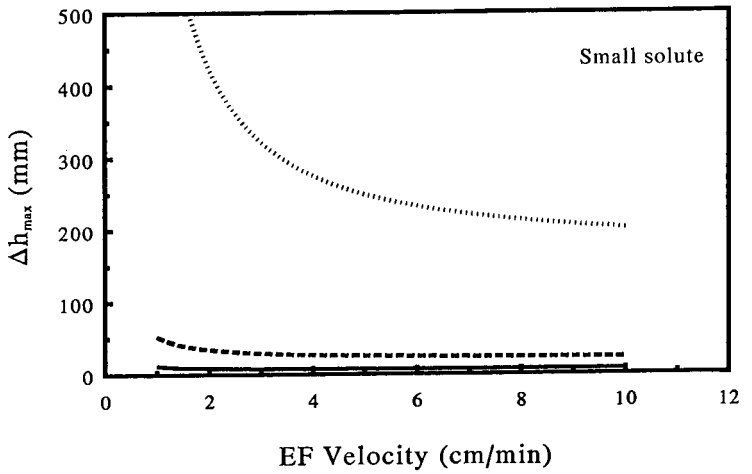

Fig. 7. Maximum allowed height differences which will cause a 20% decrease in plate height. Small solute ($D = 1 \cdot 10^{-9}$ m^2/s). Solid line is for a 25-μm radius capillary; dashed line is for a 50-μm capillary; dotted line for a 75-μm capillary. The values of other parameters are indicated in the Appendix.

calculated using $u_{ef} = 1$ cm/min as the reference electrophoretic velocity. The theoretical H value, at that u_{ef}, is 12 μm. Therefore, the value of 14.4 μm does represent a 20% loss, as was stipulated in the calculation. However, the apparent H curve is at much higher velocities and the *apparent* loss in the efficiency is much greater.

The "hook" shape of the curves for the 25-μm capillary in Fig. 8 is due to the very high u_s at low u_{ef} values. However, it should be stressed that the above discussion centred on the *maximum* allowed Δh for a given loss in H. In practice, it is expected that the actual Δh values will be, at most, a few millimetres. Therefore, the experimental H curves can be higher than expected, but not as high as depicted in Fig. 8.

The second approach to the calculation of Δh_{max} assumes an electrophoretic velocity, which we will indicate by u_{ef1}, and its associated theoretical H value. The next step is to equate a fractional increase in that H to the plate expression in eqn. 5, coupled with the condition that the total velocity, in the modified H expression, equals u_{ef1}. This last conditions ensures that we compare two H values, one theoretical and the other as a result of a buffer height difference, at the same migration velocity. As we have here two unknowns; namely, u_s and a new electrophoretic velocity, u_{ef2}, we need to solve two equations:

$$u_{ef1} = u_{ef2} + u_s \tag{10}$$

and

$$(1 + x)\frac{2D}{u_{ef1}} = \frac{2D}{u_{ef2} + u_s} + \frac{a^2 u_s^2}{24D(u_{ef2} + u_s)} \tag{11}$$

where x is the fractional loss in H. The solution for u_s is

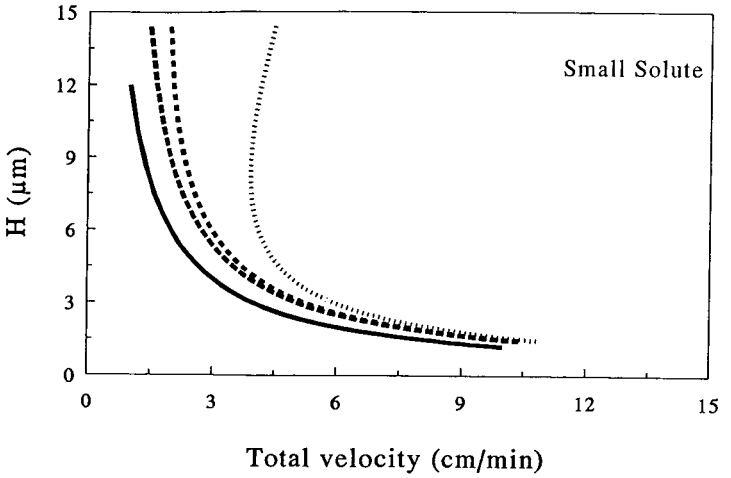

Fig. 8. Plate heights, in the presence of Δh_{max} which will cause a 20% loss in efficiency, as a function of total velocity for a small solute. Eqn. 9 is used to calculate Δh_{max}. The solid line represents theoretical H behaviour; the dashed line is for a 75-μm radius capillary; the short dashed line is for a 50-μm capillary; the dotted line is for a 25-μm capillary. The values of other parameters are indicated in the Appendix.

$$u_s = \frac{\sqrt{48xD}}{a} \tag{12}$$

Eqn. 12, together with eqn. 2, allows us to write an expression for Δh_{max}:

$$\Delta h_{max} = \frac{8\sqrt{48x\eta LD}}{\rho g a^3} \tag{13}$$

Eqn. 13 is much simpler than eqn. 9 although some similarities exist, *e.g.*, the strong inverse dependence of Δh_{max} on the radius of the capillary (see Fig. 9). In the limit of small diffusion coefficients, high u_{ef} and wide capillaries, eqn. 9 reduces to eqn. 13. In the present case, and for a given buffer system, u_s and Δh_{max} depend only on the diffusion coefficient of the solute and on the capillary radius. Hence the H curve for the uneven buffers will be shifted upward, from the theoretical curve, by the fractional efficiency loss, x, but it will not be distorted in the velocity direction; that is, at each velocity, the upper curve will be a fraction x higher than the theoretical curve.

Table II gives typical maximum allowed height differences for several capillary radii, several losses in H and for a large and a small solute. The general trend of the data is similar to those in Figs. 6 and 7. Thus, for large molecules, the requirement for buffer levelling is much greater. The demands for smaller Δh_{max} increase in severity as the capillary radius increases.

For large molecules, Δh_{max} values calculated from eqn. 9 or 13 are nearly identical, especially at high migration velocities. For small solutes, eqn. 13 yields lower allowed Δh values than eqn. 9, for a given loss in H. The results in the Table II indicate again the need to keep the buffer levels at equal heights in order to minimize the effects of hydrostatic flow.

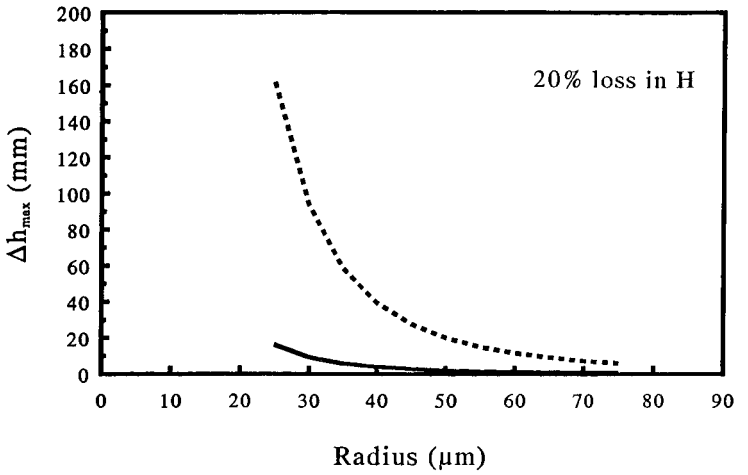

Fig. 9. Δh_{max}, for a 20% loss in H, *versus* capillary radius. Eqn. 13 was used to calculate the height difference. The solid line represents the behaviour for a large solute and the dashed line for a small solute.

CONCLUSIONS

The existence of hydrostatic flow in capillary zone electrophoresis can cause an additional zone broadening, which lowers the expected efficiency of the method. The hydrostatic flow effect is particularly important with large solutes and wide capillaries. In such cases, theory shows that the height levels of the buffer solutions, at both ends of the capillary, should be controlled to better than 1 or 2 mm. The situation is less critical with narrow capillaries, or with small molecules. Thus, narrow capillaries are beneficial not only because they minimize the Joule heating effect, but also because they reduce the influence of hydrostatic flow. Experimental work is now being pursued to validate the theoretical prediction.

TABLE II

MAXIMUM ALLOWED HEIGHT DIFFERENCE FOR SEVERAL CAPILLARY RADII AND SEVERAL ACCEPTABLE LOSSES IN H

Shown are values for large solutes (small diffusion coefficient) and small solutes (larger diffusion coefficient). Values used in the calculations are the same as those in the legend for Fig. 1.

Radius (μm)	D (m^2/s)	Δh_{max} (mm)		
		10% loss in H	20% loss in H	40% loss in H
25	$1 \cdot 10^{-10}$	11.44	16.18	22.88
50		1.43	2.02	2.86
75		0.42	0.60	0.85
25	$1 \cdot 10^{-9}$	114.4	161.8	228.8
50		14.3	20.22	28.6
75		4.24	5.99	8.47

ACKNOWLEDGEMENTS

This research was supported by grant No. 88-00021 from the United States–Israel Binational Science Foundation (BSF), Jerusalem, Israel.

TABLE AI

UNITS USED IN CALCULATIONS

Symbol	Meaning	Units	Value used
a	Capillary radius	m	See text
C	Solute concentration	mol/m^3	None
D	Diffusion coefficient	m^2/s	See text
g	Gravitational acceleration	m/s^2	9.807
H	Plate height	m	See text
L	Capillary length	m	1
r	Radial position	n	None
t	Time	s	None
u_{ef}	Electrophoretic velocity	m/s	See text
u_{hs}	Hydrostatic velocity	m/s	None
u_s	Average hydrostatic velocity	m/s	See text
Δh	Height difference	m	See text
η	Buffer viscosity	kg/m · s	0.001
ρ	Buffer density	kg/m^3	1000

APPENDIX

The calculations in this paper were done using mks units, and these units are listed in Table AI. In the text we use the more familiar units of cm/min for velocity, μm for capillary radius and plate-height values and mm for Δh.

REFERENCES

1 J. H. Knox and I. H. Grant, *Chromatographia*, 24 (1987) 135.
2 J. H. Knox, *Chromatographia*, 26 (1988) 329.
3 E. Grushka, R. M. McCormick and J. J. Kirkland, *Anal. Chem.*, 61 (1989) 241.
4 M. Martin and G. Guiochon, *Anal. Chem.*, 56 (1984) 614.
5 M. Martin, G. Guiochon, Y. Walbroehl and J. W. Jorgenson, *Anal. Chem.*, 57 (1985) 559.
6 K. D. Lukacs and J. W. Jorgenson, *J. High Resolut. Chromatogr. Chromatogr. Commun.*, 8 (1985) 407.
7 D. E. Burton, M. J. Sepaniak and M. P. Maskarinec, *Chromatographia*, 21 (1986) 583.
8 M. J. Sepaniak and R. O. Cole, *Anal. Chem.*, 59 (1987) 472.
9 H. K. Jones, N. T. Nguyen and R. D. Smith, *J. Chromatogr.*, 504 ((1990) 1.
10 N. S. Reejhsinghani, A. J. Barduhn and W. N. Gill, *AIChE J.*, 14 (1968) 100.

Journal of Chromatography, 559 (1991) 95–101
Elsevier Science Publishers B.V., Amsterdam

CHROM. 23 520

Field effect electroosmosis

KIUMARS GHOWSI*
Department of Chemistry and Biochemistry, Texas Tech University, Box 4260, Lubbock, TX 79409-1061 (USA)
and
ROBERT J. GALE
Department of Chemistry, Louisiana State University, Baton Rouge, LA 70803-6100 (USA)

ABSTRACT

A novel effect, called field effect electroosmosis has been postulated. By coating the outside of a silica capillary with a conductive layer and applying a perpendicular voltage, V_G, across its wall, the zeta potential, can be changed by varying V_G. Through flexible control of the zeta potential, the electroosmotic flow can be controlled. This adds a new dimension to capillary electrophoresis (both capillary zone electrophoresis and micellar electrokinetic capillary chromatography). Some of the advantages, including tuneability, are discussed. Based on this effect, the design of the first electrokinetic transistor, called a metal–insulator–electrolyte–electrokinetic field-effect device (MIEEKFED), was proposed. This device could be used for separation-based sensors. It also has great potential for miniaturization, especially because of the advances that have occurred in the micromachining technology of silicon. Recently, an experimental study of the use of an additional electric field outside a capillary to control the zeta potential has been reported. This work provides confirmation of our theoretical predictions.

INTRODUCTION

Capillary electrophoresis (CE), as an instrumental technique, started with the work of Hjertén [1] and continued slowly through the works of Virtanen [2] and Mikkers *et al.* [3]. The first revolution in the field was that of Jorgenson and Lukacs [4]. In their study, plate heights of less than 1 mm were predicted and values of a few micrometers were experimentally obtained by their timely advance to smaller diameter capillaries. This work, which demonstrated the potential of CE as a very powerful instrumental technique for separation, was termed capillary zone electrophoresis (CZE). The second revolution in the field was the work of Terabe and co-workers [5,6]. Before their work, CE was limited to the analysis of charged species. They demonstrated that by adding micelles to the liquid the separation of neutral solutes is also possible. This technique was termed micellar electrokinetic capillary chromatography (MECC). Recently, we proposed the novel technique of field effect electroosmosis [7–9], which has the potential to be a further revolution in the field.

Capillary electrophoresis places a buffer-filled capillary between two buffer

reservoirs and a potential field is applied across the capillary. The electric field creates an electroosmotic flow of buffer solution toward the cathode. The electric field also causes electrophoretic flow of ionic solutes in CZE or micelles in MECC. Separation takes place due to different ion mobilities of the solutes or micelles. The electroosmotic flow and solutes travel toward the cathode, where the latter can be detected.

Electroosmosis, the major component of CE, is flow of a liquid (generally a polar liquid) in contact with a porous solid under the influence of an applied electric field. Electroosmotic flow in a capillary has been attributed to the formation of an electric charged layer at the solid/liquid interface. Under the influence of an electric field parallel to that interface, a portion of the liquid's diffuse layer moves. This migration of cations causes a concomitant migration of fluid through the capillary. The electric potential across the diffuse layer is called ζ, the zeta potential.

THEORY

The linear velocity, υ, of the liquid under the influence of an applied electric field E is approximately

$$\upsilon = \left(\frac{\varepsilon}{4\pi\eta}\right)\zeta E \tag{1}$$

where ε is the dielectric constant of the liquid and η is its viscosity. Thus υ is proportional to the zeta potential. The magnitude of the zeta potential depends on, among other things, the nature of the solid surface, the concentration of ions and the pH of the electrolyte.

One method to control the rate of electroosmosis is to change the voltage applied across the length of the capillary, but such a change also affects the electrophoretic flow of solute and will not affect the overall degree of electrophoretic separation. Other methods of controlling the rate of electroosmosis are to change the concentrations of species in solution or suspension, to change the pH or to change the nature of material forming the inner layer of the capillary. None of these methods is flexible or capable of rapid change and each has disadvantages [4,10].

Field effect electroosmosis is a novel means of controlling the rate of electroosmosis due to a first electric potential across a capillary. In this method, a second electric potential is applied between the electrically insulating walls of a capillary and the liquid. This field changes the charge on the wall of the capillary and thus allows manipulation of the zeta potential within the capillary. Manipulation of the zeta potential in this manner permits flexible and rapid control of the rate of electroosmosis independent of the rate of electrophoresis.

Based on this principle of field effect electroosmosis, we proposed the first field effect electrokinetic transistor called a metal–insulator–electrolyte–electrokinetic field-effect device (MIEEKFED) [7–9]. This device could be considered analogous in some ways to the conventional metal oxide field-effect transistor (MOSFET) in electronics. In a MIEEKFED the electrolyte flow may be controlled, whereas in a MOSFET the electric current flow may be controlled, in either case by means of an electric field applied perpendicular to the respective flow.

A schematic diagram of a MIEEKFED is shown in Fig. 1. This device should

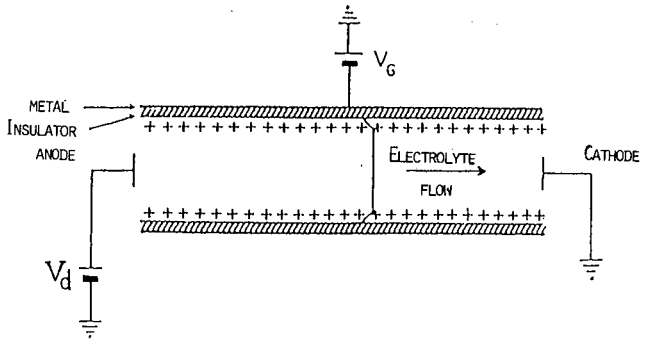

Fig. 1. Cross-section of a MIEEKFED. V_d is the voltage applied between cathode and anode and V_G is the voltage between metal layer and cathode.

allow the control of the flow of an electrolyte by two voltages, V_d, the applied voltage across the capillary, and V_G, the gate voltage. First, it is necessary to show how the zeta potential is a function of V_G. When pyrogenic silica is in contact with an aqueous solution, its surface hydrolyzes to form silanol surface groups. These groups may be positively charged, negatively charged or neutral, depending on the electrolyte pH. For silica, the surface group density is of the order of $5 \cdot 10^{14}$ cm^{-2} and can be described by the following equations:

$$\mathrm{SiOH} \rightleftharpoons \mathrm{SiO^-} + \mathrm{H_s^+} \qquad K_a = \frac{[\mathrm{SiO^-}][\mathrm{H^+}]_s}{[\mathrm{SiOH}]} \tag{2}$$

$$\mathrm{SiOH} + \mathrm{H_s^+} \rightleftharpoons \mathrm{SiOH_2^+} \qquad K_b = \frac{[\mathrm{SiOH_2^+}]}{[\mathrm{SiOH}][\mathrm{H^+}]_s} \tag{3}$$

where $[H^+]_s$ is the concentration of hydrogen ions at the surface and $[SiO^-]$, $[SiOH]$ and $[SiOH_2^+]$ are the surface sites at the oxide.

In addition to the amphoteric dissociation mentioned previously, the supporting electrolyte can also form ion pairs with the charged surface sites. This is illustrated below using potassium chloride as a typical, univalent, supporting electrolyte:

$$\mathrm{SiOH_2^+} + \mathrm{Cl_s^-} \rightleftharpoons \mathrm{SiOH_2Cl} \qquad K' = \frac{[\mathrm{SiOH_2^+}][\mathrm{Cl^-}]_s}{[\mathrm{SiOH_2Cl}]} \tag{4}$$

$$\mathrm{SiO^-} + \mathrm{K^+} \rightleftharpoons \mathrm{SiOK} \qquad K'' = \frac{[\mathrm{SiO^-}][\mathrm{K^+}]_s}{[\mathrm{SiOK}]} \tag{5}$$

where $[SiOH_2Cl]$ and $[SiOK]$ are the surface sites at the oxide. The total number of sites per unit area is given by

$$N_s = [\mathrm{SiOH}] + [\mathrm{SiOH_2^+}] + [\mathrm{SiO^-}] + [\mathrm{SiOH_2Cl}] + [\mathrm{SiOK}] \tag{6}$$

The concentrations of $[Cl^-]_s$, $[K^+]_s$ and $[H^+]_s$ at the surface could be related to the bulk electrolyte by the Boltzmann distribution, given by the following equations [8,9,11]:

$$[H^+]_s = [H^+] \exp(-q\psi_a/kT) \tag{7}$$

where $\psi_a = \psi_0 - V_G$, ψ_0 is the potential at the insulator electrolyte interface, q is electronic charge magnitude, k is the Boltzmann constant and T is temperature.

$$[Cl^-]_s = n_0 \exp\left(\frac{q\psi_b}{kT}\right) \tag{8}$$

$$[K^+]_s = n_0 \exp\left(\frac{-q\psi_b}{kT}\right) \tag{9}$$

where $\psi_b = \psi_\beta - V_G$, ψ_β is the inner Helmholtz layer potential [8,9] and n_0 is the concentration of bulk electrolyte. By solving the above equations, a complex analytical function can be found which relates V_G to ζ [7]:

$$V_G = f(\zeta) \text{ and } \zeta = f^{-1}(V_G); \qquad V_d = 0 \tag{10}$$

Figs. 2 and 3 depict the zeta potential as a function of V_G for different pH values and different concentrations of potassium chloride solution. For these figures, an

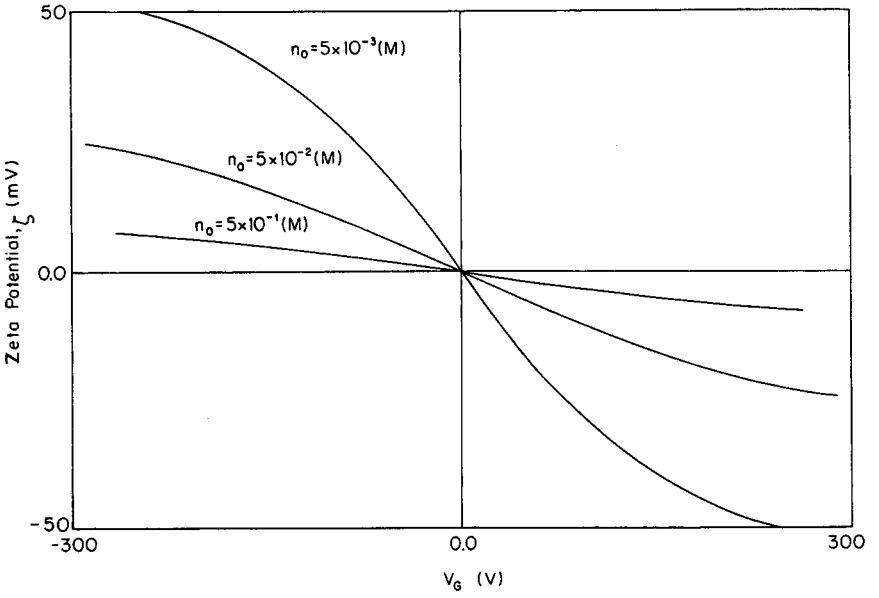

Fig. 2. Change in zeta potential as a function of V_G for potassium chloride solutions of different concentrations, n_0, and a constant pH of 3.0. $C_0 = 35 \cdot 10^{-10}$ F/cm^2; x_{ox} (insulator or capillary wall thickness) = 1 μm.

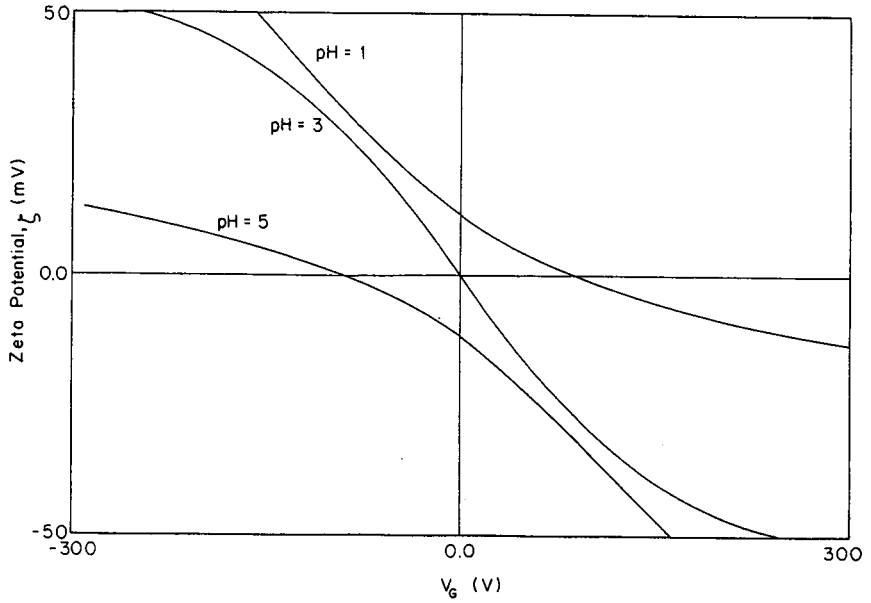

Fig. 3. Change in zeta potential as a function of V_G for potassium chloride solutions of different pH values and a constant concentration of $5 \cdot 10^{-3}$ *M*. $C_0 = 35 \cdot 10^{-10}$ F/cm^2; $x_{ox} = 1$ μm.

insulator thickness of 1 μm was chosen. For silica as an insulator, the capacitance, C_0, per cm^2 and with a 1-μm thickness would be $35 \cdot 10^{-10}$ F/cm^2. The applied voltage, V_G, in Figs. 2 and 3 ranges from -500 to $+500$ V and these voltages can create a maximum electric field of $5 \cdot 10^6$ V/cm, which is below the dielectric strength of silica of $1 \cdot 10^7$ V/cm. In order to manipulate the voltage distribution in the double layer, one needs to apply an electric field within the same order of magnitude as the electric field in the double layer. That is why an insulator with high dielectric breakdown such as silica is required. For higher oxide thicknesses, V_G must be increased in order to generate a high enough electric field for the manipulation of the zeta potential. A suitable electric field would be ± 500 V/μm. For instance, for 10 and 100 μm the proper ranges of V_G would be ± 5 kV and 50 kV, respectively.

Physical modeling of the first field-effect electrokinetic transistor for electroosmosis has been proposed by us [7].

In a MIEEKFED, a second voltage V_d is applied across the length of a capillary of length L, then the voltage perpendicular to the capillary wall is not constant or equal to V_G. The new voltage at any point across the capillary, at a distance X from the cathode, is

$$V_G - \left(V_d \cdot \frac{X}{L}\right) \tag{11}$$

where L is the length of the capillary. Now the zeta potential as a function of X is

$$\zeta(x) = f^{-1}\left[V_G - \left(V_d \cdot \frac{X}{L}\right)\right] \tag{12}$$

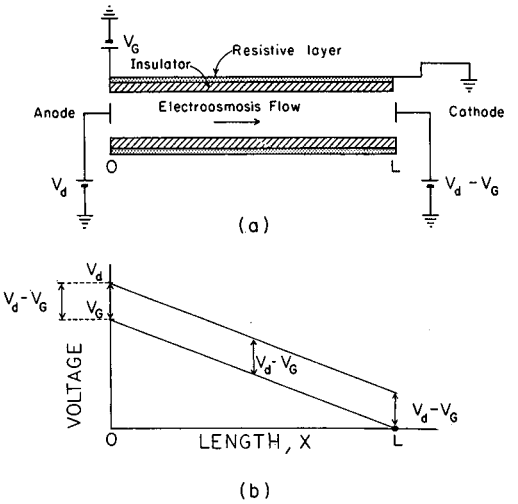

Fig. 4. (a) Schematic diagram of a MIEEKFED with constant zeta potential across the capillary. (b) Voltage perpendicular to the wall of the capillary *versus* length, X.

The design shown in Fig. 4a is proposed for constant zeta potential across the capillary. As illustrated in Fig. 4b, this circuit topology creates a constant voltage $(V_d - V_G)$ between the resistive layer and the electrolyte. The zeta potential across the capillary is

$$\zeta = f^{-1}(V_d - V_G) \tag{13}$$

Substituting eqn. 12 into eqn. 11 gives the field-effect electroosmosis velocity:

$$\zeta = f^{-1}(V_d - V_G) \tag{14}$$

and the electroosmosis mobility, μ_{EO}, is proportional to the zeta potential:

$$\mu_{EO} = \left(\frac{\varepsilon}{4\pi\eta}\right)\zeta \tag{15}$$

POTENTIAL APPLICATIONS

The major advantage of a MIEEKFED is its tuneability. If the rate of electroosmosis is adjusted to be equal and opposite to the electrophoretic mobility of a certain component of the analyte, that component will become essentially immobile within the capillary, *i.e.*, it is trapped. Maintaining this trapping position for a while causes the separation of that particular component. In the next step, the electroosmotic mobility could be increased such that the component is drifted toward the cathode and it is detected there. This application of MIEEKFED could be categorized as the use of a separation-based sensor.

Using MIEEKFED in a capillary electrophoresis apparatus results in a number

of advantages. The zeta potential, and therefore the rate of electroosmosis, may be flexibly controlled without unwanted restrictions on pH, electrolyte concentration or the inner layer of the capillary. The MIEEKFED could also be used to reduce the degree of "tailing" commonly observed in the capillary electrophoresis of macromolecules. The tailing can be reduced by creating a low zeta potential and a low charged layer at the solid electrolyte interface.

The MIEEKFED has great potential for miniaturization, particularly in the light of recent advances in the technology of micromachining silicon [12]. Thus, in conclusion, although our work and predictions [7–9] have been based on theory and model computer simulations, Lee *et al.* [13] have recently demonstrated field-effect electroosmosis experimentally. These experimental data unequivocably support our first prediction of this effect.

REFERENCES

1 S. Hjertén, *Chromatogr. Rev.*, 9 (1967) 122.
2 R. Virtanen, *Acta Polytech. Scand.*, 123 (1974) 1.
3 F. Mikkers, F. Everaerts and T. Verheggen, *J. Chromatogr.*, 169 (1979) 1.
4 J. W. Jorgenson and K. D. Lukacs, *Anal. Chem.*, 53 (1981) 1298.
5 S. Terabe, K. Otsuka, K. Ichikawa, A. Tsuchiya and T. Ando, *Anal. Chem.*, 56 (1984) 111.
6 S. Terabe, K. Otsuka and T. Ando, *Anal. Chem.*, 57 (1985) 834.
7 K. Ghowsi and R. J. Gale, in R. P. Buck, W. E. Hatfield, M. Umana and E. F. Bowden (Editors), *Biosensor Technology (Proceedings of the International Symposium on Biosensors, University of North Carolina, Chapel Hill, NC, September 7–9, 1989)*, Marcel Dekker, New York, 1990, p. 55.
8 K. Ghowsi and R. J. Gale, *J. Electrochem. Soc.*, submitted for publication.
9 K. Ghowsi, *Ph.D. Dissertation*, Louisiana State University, Baton Rouge, LA, 1990.
10 R. McCormic, *Anal. Chem.*, 60 (1989) 2322.
11 D. E. Yates, S. Levine and T. W. Healy, *J. Chem. Soc., Faraday Trans. 1*, 70 (1974) 1807.
12 K. E. Peterson, *Proc. IEEE*, 70 (1982) 420.
13 C. S. Lee, W. C. Blanchard and C. T. Wu, *Anal. Chem.*, 62 (1990) 1550.

Journal of Chromatography, 559 (1991) 103–110
Elsevier Science Publishers B.V., Amsterdam

CHROM. 23 419

Split injector for capillary zone electrophoresis

TAKAO TSUDA[a] and RICHARD N. ZARE*
Department of Chemistry, Stanford University, Stanford, CA 94305 (USA)

ABSTRACT

A split injector is described for capillary zone electrophoresis. It consists of a pump for delivery of the medium, a rotary injector, an interface, and a fused-silica capillary connected between the interface and the rotary injector. Several factors affecting split injection are examined, such as geometrical configuration of the interface and sample loop volume. The use of this split injector is demonstrated for both rectangular capillaries with large cross-sectional areas and the more conventional circular capillaries. The present injection method requires no interruption of the applied voltage.

INTRODUCTION

Although the initial development of capillary zone electrophoresis (CZE) was rather slow [1–5], CZE has become one of the best high-performance separation techniques for the analysis of complex mixtures because of its high resolution [6–8]. Compared with ordinary liquid chromatography (LC), the sample amount used in CZE (with a circular capillary column of 50 μm I.D.) is very small. To avoid band broadening, the amount of sample injected is limited to a few nl. The development of an improved injection method is a key factor in encouraging further acceptance of CZE.

Several injection methods are currently in use: gravity [2–4], electrokinetic injection [2,3,9], hydrostatic force [9–12], rotary valve [13], partial electric sampling [14], side flow caused by an electric field [15,16], and split-flow sample introduction [17]. Split-flow sample introduction, developed by Tehrani *et al.* [17], interrupts the applied voltage: the procedure is a stepwise method that has the same scheme as gravity injection.

These injection methods are not applicable to capillaries with large cross sections. A rectangular capillary has several advantages in CZE [18], but injecting a sample is difficult because of its low flow resistance. Most of these injection methods require interruption of the applied voltage during injection. This voltage interruption

[a] On sabbatical leave; permanent address: Department of Applied Chemistry, Nagoya Institute of Technology, Gokiso, Showa, Nagoya 466, Japan.

0021-9673/91/$03.50

may recondition the double layer on the capillary walls, thus potentially reducing reproducibility.

In the present paper, we describe a split-injection method for CZE. This method is done under continuous flow using a pump and a rotary valve. The sample is introduced into the capillary by electrokinetic injection. The injection procedure does not interrupt the applied voltage. Although the present method is developed for rectangular capillaries with large cross-sectional area, it is also applicable to circular capillaries. We describe the construction of this injector and characterize its operation.

EXPERIMENTAL

Schematic diagrams of the CZE system, the split-injection system, and the CZE interface are shown in Figs. 1 and 2. The present system uses either a circular or a rectangular capillary. The latter has a large cross section, is fragile, and is not flexible. The rectangular capillary terminates inside a reservoir (7 in Fig. 1). The space between the end of the reservoir and the rectangular capillary is sealed with epoxy. Care should be taken to ensure that the epoxy does not extend into the end of the rectangular capillary column.

The capillary column is washed and filled with buffer as follows. Electrode 5 is removed and the mouth of the reservoir is capped; liquid is then supplied from syringe

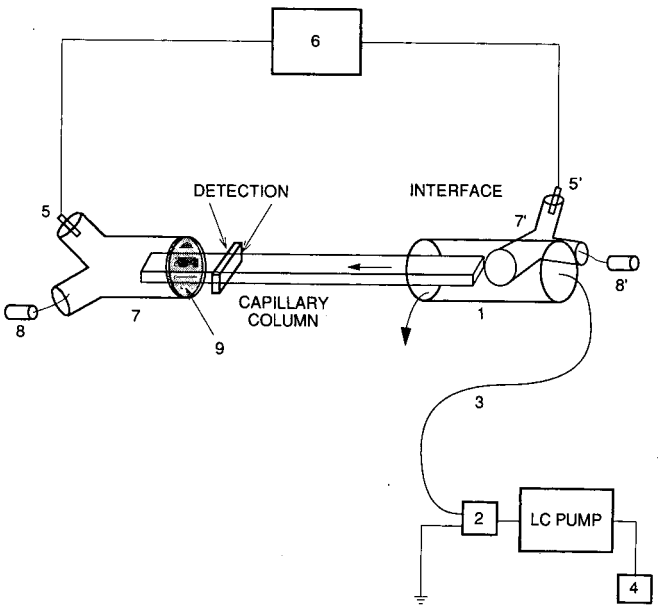

Fig. 1. Schematic diagram of capillary electrophoretic system with split injector. 1 = Interface; 2 = injection valve; 3 = delivery tube of fused-silica capillary, 50 or 100 μm I.D. and 1.5–2 m in length; 4 = reservoir for LC pump; 5 and 5′ = electrodes; 6 = high-voltage supply; 7 and 7′ = reservoirs using 3-way PTFE connectors; 8 and 8′ = syringes for filling reservoirs; 9 = epoxy seal.

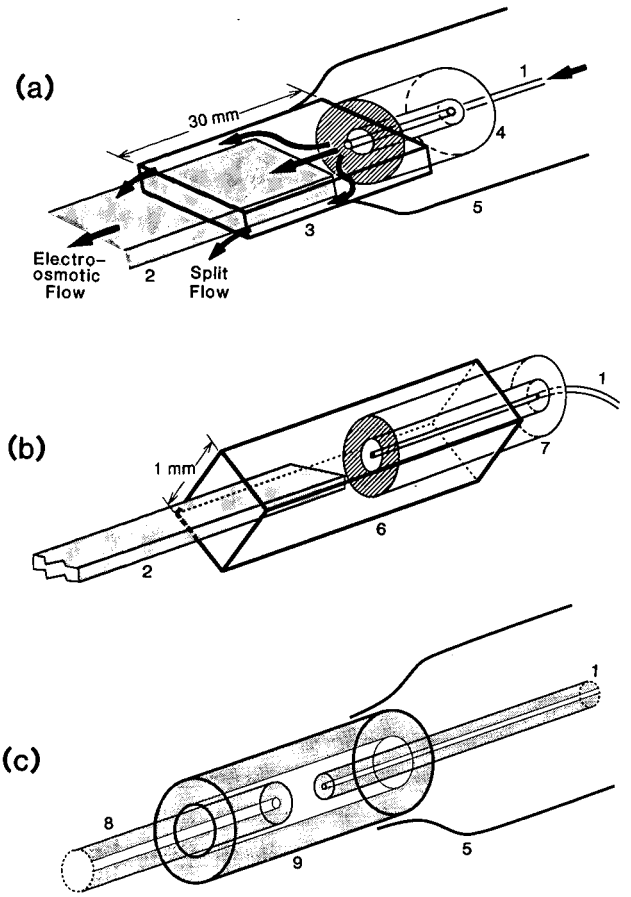

Fig. 2. Interface for split injector having (a) "rectangular" interface for rectangular capillary (50 × 1000 μm); (b) "square" interface for rectangular capillary (50 × 1000 μm); (c) "circular" interface for circular capillary (50–100 μm I.D.). Arrows show directions of sample and solvent flow. 1 = Fused-silica capillary from injection valve (2 in Fig. 1); 2 = rectangular capillary; 3 = rectangular 200 × 2000 μm capillary; 4 = PTFE tubing, 0.5 mm I.D. , 2.0 mm O.D., and 10 mm in length; 5 = cover; 6 = square tubing (side 1 mm long); 7 = PTFE tubing, 0.5 mm I.D. and 1 mm O.D.; 8 = circular capillary; 9 = circular capillary tubing, 0.5 mm I.D. × 0.8 mm O.D.

8 by pressing the cylinder by hand. Syringe 8′ is also used for filling reservoir 7′ and interface 1. The latter also serves as a reservoir.

Another possible procedure is to use suction. Here one end of the rectangular or circular capillary is inserted into the reservoir, and the other end is inserted a few millimeters into a larger capillary, which is connected by vacuum tubing to a pump.

When voltage is applied, the nature of the media in the reservoirs changes continuously due to the gain and loss of specific ions and possible electrochemical reactions at the electrodes. Although the reservoir (7 in Fig. 1) has a volume of only 0.2 ml, no effect is observed for the first hour of continuous operation. After 1 h, we observe a variation in the elution time of a solute. Therefore, the buffer must be

changed in the reservoir every hour. This problem can also be overcome by supplying a fresh buffer from another reservoir with gravity flow via a small PTFE tube.

The sample is introduced with a pressurized flow using split injection. This device is similar in principle to that used for microcapillary liquid chromatography [19]. The transfer line consists of an LC pump (Beckman solvent delivery module 112), an injection valve (Model 7030 for 1-μl and 5-μl loops; Model 7410 for 10-μl loop; Rheodyne, Cotati, CA, USA), a long delivery tube (fused-silica capillary, 50 or 100 μm I.D. and 1.5–2.0 m or 41 cm long), and an interface. A large electric voltage drop occurs between the interface and the injection valve because the injection valve is grounded and high voltage is applied at electrode 5′. The delivery tube (3 in Fig. 1) acts as an insulator. The parasitic current is less than one-third the current of the round (50 μm I.D.) analytical column and one-fifteenth the current of the rectangular (50 × 100 μm) analytical column. Although the parasitic current is relatively small compared to that of the analytical column, the injection valve should be grounded. If not, the voltage at the injection valve will approach that of the interface.

A metal-free automatic injector (Model 8126 with 4- or 5-μl loop, operated by a compressed-gas controller Model 7163, Rheodyne) was also tried. It is located close to the interface. The automatic injector is connected to the interface with a short fused-silica capillary, 11.5 cm in length. Because the automatic injector is at high voltage, the supply of sample to the injection loop is via a long fused-silica tubing (*ca.* 1 m), the end of which was connected to a microsyringe and grounded.

Three interfaces are shown in Fig. 2, which will be termed (a) "rectangular", (b) "square", and (c) "circular". The sample to be separated is placed inside the injection valve. The LC pump provides pressure to the supply buffer and forces the sample through the delivery tube and into the interface. At the interface some portion of the sample is injected into the capillary.

A delivery tube (3 in Fig. 1) of variable length (11.5, 41, and 150 cm) connects the interface with the injection valve and acts as an insulator as well as a transfer tube for the sample. For a delivery tube 50 μm I.D. and 1.5 m long, the sample remains in the capillary for 0.2–0.6 s (flow velocity is estimated to be 7.5–2.5 m/s), and the flow-rate of the medium is between 0.3 and 0.7 ml/min. At the interface, the flow velocity of the sample decreases because the inner diameter is larger than the delivery tube. The sample zone is opposite to the inlet of the capillary column.

The inlet of the capillary must be carefully aligned with the outlet of the delivery tube. Both the capillary and the delivery tube must be centered in the tubing of the interface. In the square interface, centering of the rectangular capillary is easily accomplished. In the rectangular interface, however, the end of the analytical capillary is frequently off axis. Therefore, the square interface is more reliable than the rectangular one. The length between the inlet of the capillary and the outlet of the delivery tube was varied from 0 to 10 mm; the optimum length was approximately 2 mm. Glass, PTFE, and polyethylene have been tested as possible materials for the interface. Glass is the superior material because the inner surface of the interface should be smooth and have good wettability.

The split flow leaves the interface, shown by the arrows in Fig. 2a. In some cases the split flow generates a back pressure because of the narrow path between the interface and the inserted portion of the capillary. For these situations, the surface level of the buffer at the position of electrode 5′ in Fig. 1 should be sufficiently high

compared to the level in the interface to maintain the flow in the forward direction. The concentration of the sample at the inlet of the analytical capillary column is crudely estimated to be one-seventh or one-fifth of its original concentration, depending on whether the 1.5-m or the 41-cm delivery tube is used. These values are obtained with the square interface, using the same experimental conditions as in Fig. 4. The dilution factor is very dependent on the experimental setup; it could be reduced in the future. The equipment and reagents used, experimental setup, and conditions are similar to those described previously [18], except as noted above.

RESULTS AND DISCUSSION

After the solute passes from the rotary value through a delivery tube, it travels a short distance between the end of the delivery tube and the inlet of the capillary in the interface, as shown in Figs. 1 and 2. Then a small part of the solute is transferred into the capillary by electrokinetic injection. The remainder exits the interface and is removed. The amount injected depends on the electroosmotic flow velocity, v_{osm}, the electrophoretic velocity of the solute, v_{el}, the cross-sectional area of the capillary, A_{column}, and the rate of flow (volume per unit time) pumped through the delivery tube, V. The split ratio, R_{split}, for a solute is given by

$$R_{split} = V/[(v_{osm} + v_{el}) A_{column}]$$

Of course, when the solute is uncharged, v_{el} vanishes in the above expression. Split injection introduces a bias in quantitation, as previously discussed [20]. The split ratio for a neutral compound is calculated from the pressurized flow volume divided by the estimated electroosmotic flow volume. The electroosmotic flow is determined by measuring the elution time of a neutral compound, such as benzene or water. Values of the split ratio used in the present experiment range from 25 to 500.

Band broadening caused by the split injector degrades the quality of the electropherogram. Solute and buffer mix in both the delivery tube and the interface. Shortening the delivery tube minimizes the band broadening caused by mixing. Tube lengths of 150, 41 and 11.5 cm gave $1.0 \cdot 10^5$, $1.2 \cdot 10^5$ and $1.4 \cdot 10^5$ theoretical plates,

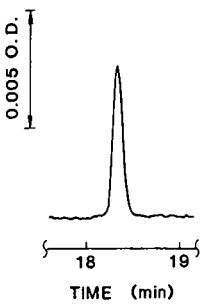

Fig. 3. Electropherogram with a short delivery tube. Delivery tube = 11.5 cm; interface is for a rectangular capillary (200 × 2000 μm); split flow = 0.4 ml/min; split ratio = 133; rectangular capillary = 50 μm × 100 μm × 75 cm (length between column inlet and detector = 55 cm); sample = 5 μl of dansyl-L-serine ($4.7 \cdot 10^{-4}$ *M*); medium = 5 m*M* phosphate buffer (pH 6.55) with 5% ethylene glycol; applied voltage = 9 kV; and current = 71 μA. The theoretical plate number is $1.4 \cdot 10^5$.

respectively, for the separation of dansyl-L-serine. Fig. 3 shows a typical peak obtained using a short delivery tube and the rectangular interface. Note the symmetry of this peak.

Assessing the band broadening in the interface is difficult, but an estimation can be made by comparing the separation efficiency obtained by gravity to that by split injection. With gravity injection, $1.6 \cdot 10^5$ and $2.1 \cdot 10^5$ theoretical plates are obtained using rectangular capillaries with small cross-sectional areas of 16 × 195 μm and 27 × 340 μm, respectively [18]. With a circular capillary (51 μm I.D.), $2.1 \cdot 10^5$ theoretical plates are obtained by gravity injection [18]. Using split injection, $1.4 \cdot 10^5$ theoretical plates are obtained using a rectangular capillary with a large cross-sectional area (50 × 1000 μm). Although these capillary geometries differ, we can compare their theoretical plate numbers to judge the band broadening caused by the split injector. We conclude that split injection causes 1.2–1.5 times more band broadening than gravity injection.

Fig. 4 shows electropherograms obtained with three injector loops of different volumes using a rectangular capillary and a rectangular interface. The peak height is proportional to the volume of the sample loop. The relation is given as $y = ax + b$, where x and y are the injection volume (μl) and the peak height (mm), respectively. The constants a and b are estimated to be 7.89 and 7.0, respectively.

For dansyl-L-serine, the peak height is recorded as a function of sample concentration. The plot is a straight line with a correlation coefficient of 0.990 in the range 10^{-4}–10^{-6} M of sample solution. Application of the split injector to a 50 × 1000 μm rectangular capillary using a square interface is shown in Fig. 5. The long optical path length (1000 μm) provides about 7 times higher sensitivity than obtained in the electropherogram shown in Fig. 4b. Fig. 6 shows a typical electropherogram using a circular capillary with a circular interface.

Table I lists the run-to-tun reproducibilities of 8 injections of dansyl-L-serine and 3 injections of dansyl-L-cysteic acid and pyridoxamine. A square interface is more

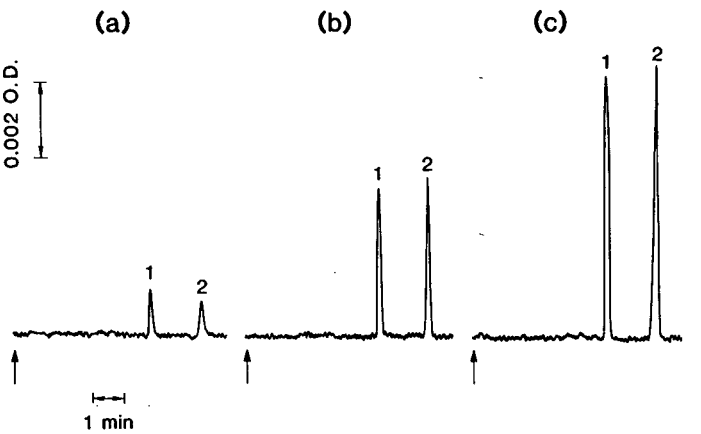

Fig. 4. Effect of loop volume: (a) 1 μl, (b) 5 μl and (c) 10 μl. Conditions are: rectangular capillary, 57 cm long, 50 × 1000 μm; rectangular interface; split flow = 0.5 ml/min; split ratio = 70; sample = (1) pyridoxamine ($1.6 \cdot 10^{-3}$ M), (2) dansyl-L- serine ($1.8 \cdot 10^{-3}$ M); medium = 5 mM phosphate buffer (pH 6.8) with 5% ethylene glycol; applied voltage = 7.8 kV; current = 76 μA; detection wavelength = 310 nm; and cell path length = 50 μm.

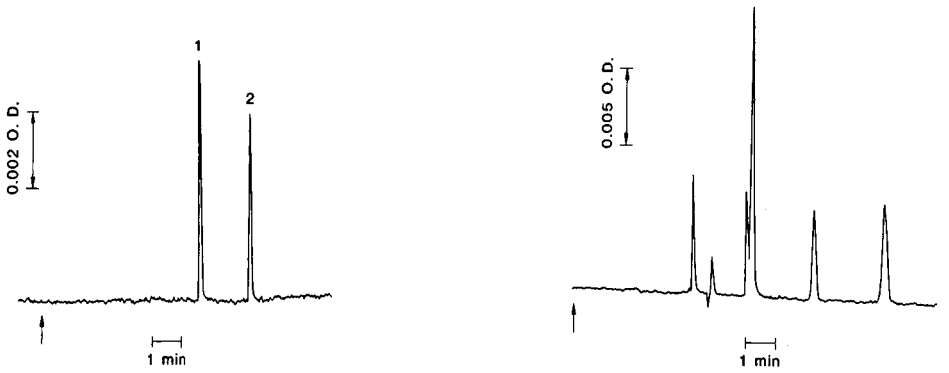

Fig. 5. Typical electropherogram using square interface. Conditions are: loop = 5 μl; split flow = 0.7 ml/min; split ratio = 70; applied voltage = 9.8 kV; current = 77 μA; detector wavelength = 310 nm; and cell path length = 1000 μm. Other experimental conditions are the same as in Fig. 3. Sample = (1) pyridoxamine ($1.6 \cdot 10^{-4}$ *M*), (2) dansyl-L-serine ($2.9 \cdot 10^{-4}$ *M*); split flow = 0.7 ml/min; applied voltage = 9.8 kV; current = 77 μA; detector wavelength = 310 nm; path length = 50 μm. Capillary and medium are the same as in Fig. 3.

Fig. 6. Typical electropherogram using circular interface. Conditions are: loop = 5 μl; capillary column = circular fused-silica tubing, 100 μm I.D. and 65 cm long; split flow = 0.5 ml/min; split ratio = 550; sample = quinine, guanosine, 5-bromouracil, dansyl-L-serine, dansyl-L-cysteic acid and flavianic acid, eluted in order, each of $1–2 \cdot 10^{-3}$ *M* except quinine ($3 \cdot 10^{-4}$ *M*); medium = 20 m*M* phosphate buffer (pH 6.45) with 5% ethylene glycol; applied voltage = 12 kV; current = 54 μA; and detection wavelength = 310 nm.

TABLE I

REPRODUCIBILITY OF PEAK HEIGHTS

	Interface		
	Rectangular	Square	Square
Flow-rate (ml/min)	0.2	0.5	0.3
Sample	Dansyl-L-serine, 10^{-3} *M*	Dansyl-L-cysteic acid, $6 \cdot 10^{-4}$ *M*	Pyridoxamine, $2 \cdot 10^{-4}$ *M*
Peak height	23.0 23.1 23.0 23.2 21.3 21.1 22.3 21.4	43.0 42.0 45.0	37 37.5 40.0
Mean peak height	22.0	43.3	38.2
R.S.D. (%)	6.07	3.52	4.2

reliable than a rectangular one. Relative standard deviations (R.S.D.) are 3–4% for dansyl-L-cysteic acid and pyridoxamine using the square interface. Fluctuations of the pressurized flow affect the reproducibility. In this experiment we used a syringe-type pump. If we had used a pulseless pump, the R.S.D. values would have been smaller.

Compared with other injection methods for CZE separations, the split injector described here has definite advantages and disadvantages. By their nature, split injectors are wasteful of sample. Moreover, the concentration of the sample is diluted by this injection method. Consequently, the split injection method is not the method of choice in ultra-trace analysis or when the sample volume is extremely limited.

The advantage of the present split injector is that it offers convenient sample introduction without the need to interrupt the applied voltage during the injection step. Using the split injector, the separation efficiency ranges from 20 000 to 150 000 theoretical plates, which is more than adequate for most separations. Additionally, this injection method can be interfaced easily to an autosampler. Note that the analytical capillary is held stationary during injection. This feature allows large cross-sectional capillaries to be used, unlike other injection methods. In particular, it enables use of rectangular capillaries of large cross-sectional area.

ACKNOWLEDGEMENTS

Useful discussions with Harry G. Rennagel, Jonathan V. Sweedler, and Xiaohua Huang are greatly appreciated. T. T. thanks the Ministry of Education, Japan, for support during this sabbatical leave. Support from Beckman Instruments, Inc. is gratefully acknowledged.

REFERENCES

1 F. E. P. Mikkers, F. M. Everaerts and Th. P. E. M. Verheggen, *J. Chromatogr.*, 169 (1979) 11.
2 J. W. Jorgenson and K. D. Lukacs, *Anal. Chem.*, 53 (1981) 1298.
3 J. W. Jorgenson and K. D. Lukacs, *Science (Washington, DC)*, 222 (1983) 266.
4 T. Tsuda, K. Nomura and G. Nakagawa, *J. Chromatogr.*, 264 (1983) 385.
5 W. G. Kuhr, *Anal. Chem.*, 62 (1990) 403R.
6 M. J. Gordon, X. Huang, S. L. Pentoney, Jr. and R. N. Zare, *Science (Washington, DC)*, 242 (1988) 224.
7 A. G. Ewing, R. A. Wallingford and T. M. Olefirowicz, *Anal. Chem.*, 61 (1989) 292A.
8 B. L. Karger, A. S. Cohen and A. Guttman, *J. Chromatogr.*, 492 (1989) 585.
9 S. Honda, S. Iwase and S. Fuijwara, *J. Chromatogr.*, 404 (1987) 313.
10 T. Tsuda, G. Nakagawa, M. Sato and K. Yagi, *J. Appl. Biochem.*, 5 (1983) 330.
11 H. E. Schwartz, M. Melera and R. G. Brownlee, *J. Chromatogr.*, 480 (1989) 129.
12 D. J. Rose and J. W. Jorgenson, *Anal. Chem.*, 60 (1988) 642.
13 T. Tsuda, T. Mizuno and J. Akiyama, *Anal. Chem.*, 59 (1987) 799.
14 M. Deml, F. Foret and P. Boček, *J. Chromatogr.*, 320 (1985) 159.
15 R. A. Wallingford and A. G. Ewing, *Anal. Chem.*, 59 (1987) 678.
16 R. A. Wallingford and A. G. Ewing, *Anal. Chem.*, 60 (1988) 1972.
17 J. Tehrani, L. Day and R. Macomber, *Proceedings of 11th Int. Symposium on Capillary Chromatogr., 14–17 May, 1990*, Huethig, Heidelberg, 1990, p. 899.
18 T. Tsuda, J. V. Sweedler and R. N. Zare, *Anal. Chem.*, 62 (1990) 2149.
19 T. Tsuda and M. Novotny, *Anal. Chem.*, 50 (1978) 271.
20 X. Huang, M. J. Gordon and R. N. Zare, *Anal. Chem.*, 60 (1988) 1837.

Journal of Chromatography, 559 (1991) 111–118
Elsevier Science Publishers B.V., Amsterdam

CHROM. 23 421

Moving boundary capillary electrophoresis with concentration gradient detection

JANUSZ PAWLISZYN* and JIAQI WU
Department of Chemistry, University of Waterloo, Waterloo, Ontario N2L 3G1 (Canada)

ABSTRACT

A rugged and inexpensive Schlieren optics detection system consisting of a laser, focusing lens and light beam position sensor was combined with moving boundary electrophoresis performed in a 10 cm × 20 μm I.D. capillary. This system facilitated rapid analysis and universal detection of sample components. The laser beam, which is focused directly into the separation capillary, probes the refractive index gradients produced by the arrival of new boundaries. The frontal injection method used in this approach introduces samples into the capillaries without discrimination and provides higher sensitivities because of the lack of dilution during the separation process compared with the zone technique. A specially designed cartridge accommodates a short piece of the separation capillary and reservoirs for buffer and sample. The separation in this method is completed usually within 30 s. During this short separation time only a small dispersion associated with diffusion of analytes along the flow direction occurs, which ensures that high gradients are generated in the detection volume. The detection limits in this approach are sub-micromolar concentrations of analyte injected for low-molecular-weight compounds such as sucrose. This system has been applied to the separation of amino acids and carbohydrates.

INTRODUCTION

Recent advances in electrophoretic methods have produced dramatic improvements in the efficiency of these techniques. For example, capillary zone electrophoresis achieves efficiencies of close to 10^6 theoretical plates [1–3]. This technique holds promise for increasing the speed of analysis, not only for ions, but also for neutral species. Electroosmotic flow which is present in electrophoretic separations is uniform across the diameter of the capillary, unlike the hydrodynamic flow associated with chromatographic methods characterized by parabolic velocity profiles [4]. Therefore, the dispersion process in capillary electrophoretic techniques is governed primarily by diffusion along the flow direction [5,6]. This results in sharp peaks and high efficiencies of the electrophoretic methods.

The narrow peaks produced in capillary electrophoretic separations generate high concentration gradients in the detection volume which can be effectively monitored by using the concentration gradient detector based on Schlieren optics [7–9]. The low detection volume, derivative response and universal nature of the technique make it very attractive for this application. In this method a laser beam is

0021-9673/91/$03.50

focused directly into the separation capillary. The refractive index gradients (dn/dx) associated with high concentration gradients (dC/dx) of eluting analytes deflect the beam towards higher refractive indexes [9]:

$$\theta = \frac{l}{n} \cdot \frac{dn}{dx} = \frac{l}{n} \cdot \frac{dn}{dC} \cdot \frac{dC}{dx} \quad (1)$$

where θ is the deflection angle in rad and l is the separation capillary diameter. This deflection is monitored using a silicon position sensor [10]. This detection method is most effective in rapid short-column separations [9], as under the conditions used the dispersion is small.

Investigations of capillary electrophoretic methods are focused on zone electrophoretic separations [9]. In this method, in the injection step, a narrow sample plug is introduced at the front of the capillary. This task is usually accomplished by the electromigration technique, which is slow and discriminates between analytes [3]. In addition, it is very difficult to introduce sub-millimetre plugs which are required to perform successful short-time separations.

In this paper we discuss the use of another technique, moving boundary capillary electrophoresis, to facilitate rapid analysis. In this method a sample mixture is introduced continuously throughout the separation [2]. The injection in this technique is very rapid and convenient as the separation begins as soon as the contact is made between the buffer in the capillary and the sample. We describe the application of moving boundary capillary electrophoresis with concentration gradient detection for the rapid separation of amino acids and sugars. The method is in principle similar to the early experiments reported by Tiselius *et al.* [11] almost a half century ago, but the performance of the system has increased significantly with the use of modern optical components to design the detector, and by using capillaries for electrophoresis.

EXPERIMENTAL

Instrumental

A 20 μm I.D. $\times$ 0.35 mm O.D. fused-silica capillary (Polymicro Technologies, Tucson, AZ, USA) was used for separations. The total length of the capillary was 12.5 cm and the effective separation length, from the anodic end to the detection point, was about 10 cm. Fig. 1 shows the separation cell used in the experiments. The capillary was fixed on a Plexiglas plate using epoxy glue, and its two ends were connected to small buffer reservoirs made of polyethylene. First, both reservoirs were filled with buffer. The injection of the sample was performed by emptying and then filling the reservoir at the anodic end with sample mixture. This step was accomplished by using a syringe and a small-diameter tube made of a copolymer of tetrafluoroethylene and hexafluoropropylene (Cole Parmer, Chicago, IL, USA). The separation was driven by a high-voltage d.c. power supply (Spellman, Plainview, NY, USA). The current passing through the capillary was monitored at the cathodic end of the capillary. After each run the capillary was rinsed with 0.1 *M* sodium hydroxide solution for 30 s, with water for 30 s and finally with buffer for 2 min. The capillary electrophoresis separation cell and detection system are also shown in Fig. 1. The whole system was mounted on a vibration isolation table.

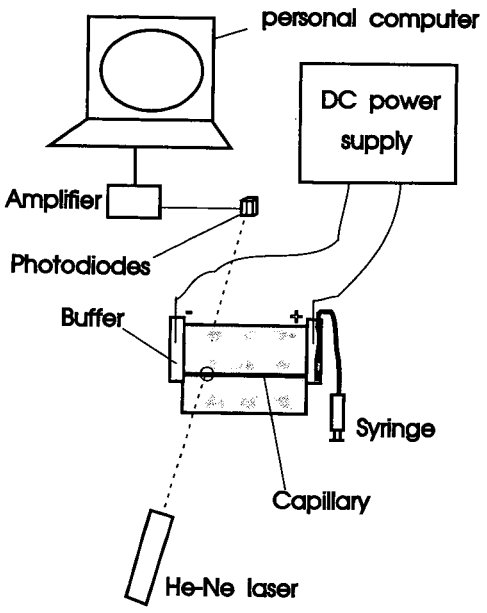

Fig. 1. Experimental arrangement.

A beam from a helium–neon laser (Uniphase, San Jose, CA, USA) or a laser diode (MWK Industries, Pomona, CA, USA) was focused by a 30-mm focal length lens directly into the capillary. The beam deflection was monitored by a position sensor consisting of a dual silicon detector (United Detector Technologies) with appropriate electronics. The probe beam is arranged so that the far-field intensity profile points to the centre between two photodiodes placed close together in the bicell configuration. When irradiated uniformly, the photodiodes generate equal amounts of photocurrent. On encountering a concentration gradient the laser probe baem is deflected and the amount of light reaching the diode is not equal. The difference in photocurrent associated with the two diodes corresponds to the magnitude of deflection of the laser beam. The difference in photocurrent genrrated by the diodes is converted to a voltage. The data is collected by an IBM DACA board, in a PC-AT compatible personal computer, using the software ASYST (Asyst Software Technology, Rochester, NY, USA).

Reagents

All chemicals were of analytical-reagent grade, and solutions were prepared using deionized water. Borate or phosphate buffers were used to perform separations. All samples were dissolved in buffers before use. All solutions were filtered through 200-nm pore size filters and degassed by purging with helium.

RESULTS AND DISCUSSION

Rapid moving boundary capillary electrophoretic separations were conveniently performed in the separation cell shown in Fig. 1. First, both reservoirs and the capillary

were filled with buffer, and the high d.c. voltage was turned on. Then buffer in the reservoir of the anodic end was removed with a syringe and filled with sample. In our experiments the separation begins to occur immediately after the sample solution reaches the separation capillary. Various sample components migrate with different velocities related to their mobilities and applied electric field gradient. The analytes are never fully separated from one another as in zone electrophoresis, but rather they form boundaries which move with characteristic velocities. Fig. 2a illustrates the situation in the capillary after the boundaries have reached the detector volume. The migration direction of ions is from right to left. The electrolyte composition varies along the separation capillary because the analytes have different velocities. The first boundary is formed when the front associated with the fastest ion, alanine, has reached the detector. Immediately afterwards histidine arrives, which produces a zone consisting of buffer constituents, alanine and histidine. Finally, the tryptophan, with the slowest migration velocity, begins to elute and forms the third boundary.

The composition of the electrolyte varies along the separation capillary. Along with the composition change, properties such as refractive index will also vary. For example, a refractive index detector could be applied to the separation shown in Fig. 2a to yield a hypothetical trace as given in Fig. 2b. The moving boundary electropherogram would consist of "steps" indicating the position of the boundary. The height of the step will be proportional to the analyte concentration corresponding to the given boundary. The exact concentration profile of the boundary (Fig. 3a) can be described as [12]

$$C = \frac{1}{2} C^0 \left[\operatorname{erf}\left(\frac{x - x_r}{2\sqrt{Dt_r}} \right) + 1 \right] \tag{2}$$

where C^0 is the concentration of analyte in the sample, D is the diffusion coefficient of the analyte in the electrolyte, x_r is the position of the centre of the boundary and t_r is the retention time. In this expression we assume that the longitudinal diffusion is the primary cause of the boundary broadening. In that situation the width of the boundary can be defined by the parameter σ_x (Fig. 3):

$$\sigma_x = \sqrt{2Dt_r} \tag{3}$$

Eqn. 3 indicates that, assuming "ideal" injection, the width of the zone depends on the separation time, t_r. For rapid separations using very short capillaries as discussed in this paper, the concentration "steps" are expected to be very sharp. Under these conditions high concentration gradients (dC/dx) are produced at the boundaries (Fig. 3b):

$$\frac{\partial C}{\partial x} = \frac{1}{2} C^0 \exp\left[- \frac{(x - x_r)^2}{4Dt_r} \right] \Big/ \sqrt{\pi Dt_r} \tag{4}$$

Fig. 3b and eqn. 4 show that the gradient signal consists of a single Gaussian peak per boundary with height proportional to the concentration of the analyte in the

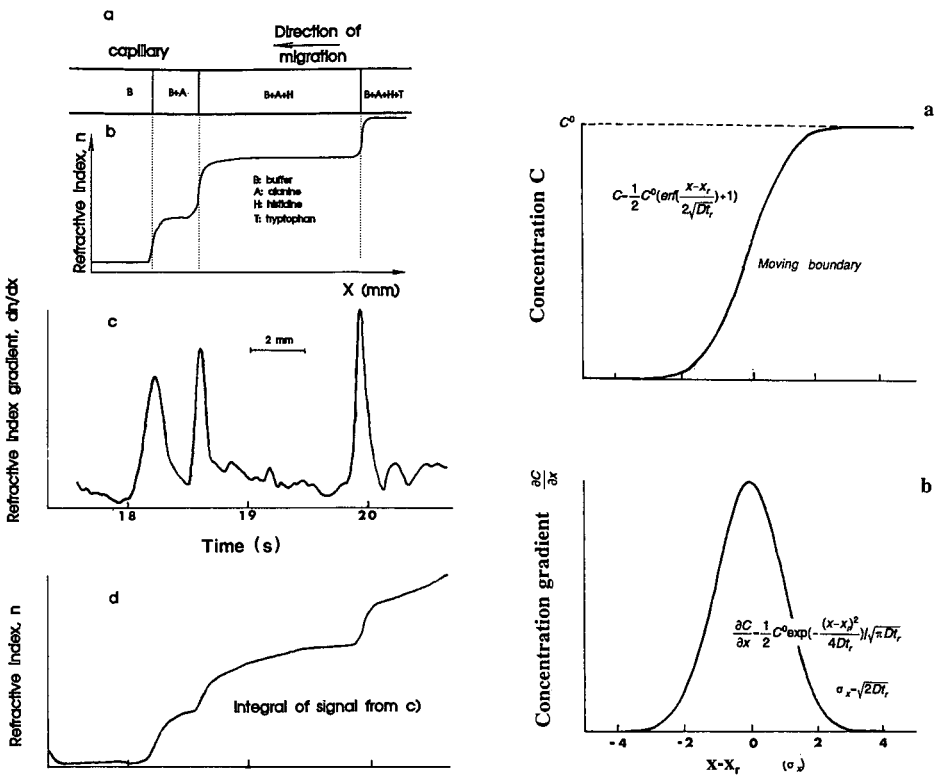

Fig. 2. (a) The moving boundaries inside a capillary; the three boundaries are generated by alanine, histidine and tryptophan; (b) the refractive index steps corresponding to these boundaries; (c) the deflection signals of the probe beam generated by the refractive index steps; (d) integral of signal from (c).

Fig. 3. (a) Moving boundary in capillary; (b) its first derivative.

sample. Indeed, as shown in Fig. 2c, three peaks corresponding to the boundaries associated with alanine, histidine and tryptophan are present in the moving boundary capillary electropherogram detected by the concentration gradient detector.

The clearly visible peaks produced by the gradient detector are in direct contrast to the small "steps", difficult to recognize from drifts, which would be produced by the refractive index detector as illustrated in Fig. 2d. Fig. 2d is generated by integrating the refractive index gradient trace from Fig. 2c. In contrast to the hypothetical trace in Fig. 2b, actual refractive index detection is subject to drifts most likely associated with temperature fluctuations.

The peak corresponding to tryptophan from Fig. 2c is about 200 ms wide. Therefore, the dimension of the corresponding boundary is about 1 mm as the total length of the capillary is 10 cm and the separation time is about 20 s. The standard deviation (σ_x) of the Gaussian is therefore about 0.2 mm. This value is in agreement with the calculated value obtained from eqn. 3 assuming a diffusion coefficient of 10^{-5} cm^2/s [13]. Diffusion of the analytes along the capillary determines the dispersion in this separation.

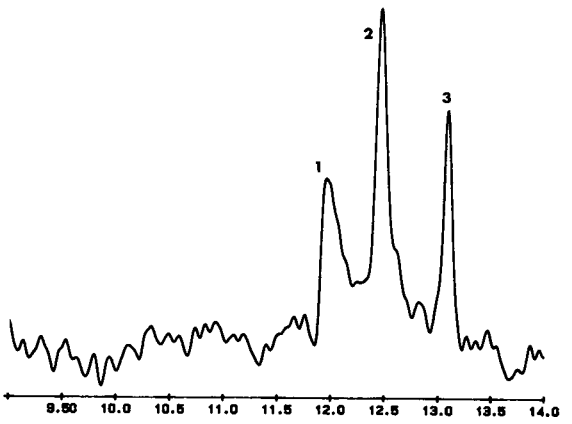

Fig. 4. Rapid separation and detection of amino acids. Buffer, 50 m*M* borate (pH 10); applied voltage, 12 kV. 1 = 2.5 m*M* alanine; 2 = 1 m*M* histidine; 3 = 1 m*M* tryptophan.

The number of theoretical plates generated in the separation illustrated in Fig. 2c is about 25 000 for the 11-cm separation capillary. This short capillary is sufficient to separate the three amino acids completely. In fact, the capillary can be shortened by about 20% and still produce a successful separation, as shown in Fig. 4. Now the total analysis time is reduced to 13 s because of the shorter capillary length and higher electric field gradients. Also, the sensitivity of detection is improved since the boundaries are narrower. The limit of detection estimated from Fig. 4 is in the sub-millimolar range and is similar to the theoretical limits that can be calculated using eqns. 1 and 4 [9].

The unique feature of the Schlieren optics detection is its universal nature. Therefore, all eluted analytes are detected and derivatization procedures are unnecessary. This is particularly beneficial in the case of sugars which are difficult to tag. It has been shown that sugars can be successfully separated by electrophoresis using borate

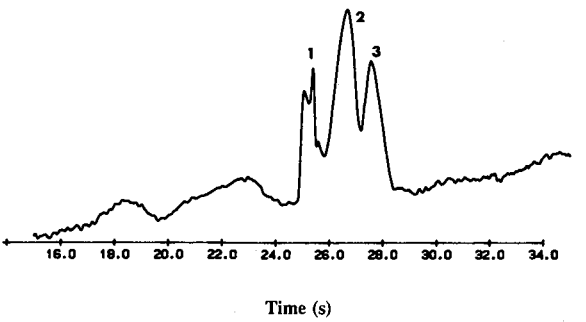

Fig. 5. Separation and detection of sugars as the borate complexes. Buffer, 50 m*M* borare (pH 10); applied voltage, 9 kV. 1 = 5 m*M* glucose; 2 = 5 m*M* sucrose; 3 = 2 m*M* raffinose.

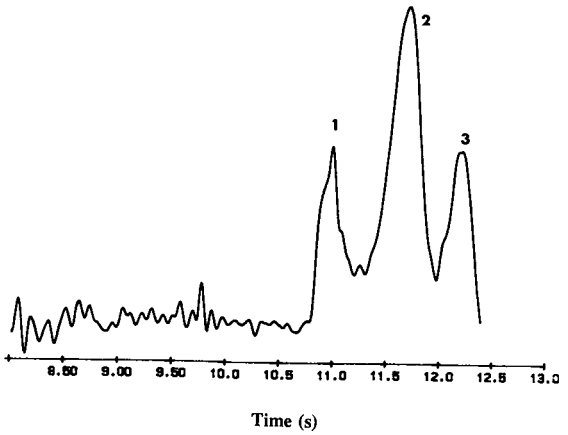

Fig. 6. Separation and detection of sugars as the borate complexes. Buffers, 50 m*M* borate (pH 10); applied voltage, 15 kV. 1 = 5 m*M* glucose; 2 = 5 m*M* sucrose; 3 = 2 m*M* raffinose.

buffer as these molecules form charged borate complexes [14,15]. Figs. 5 and 6 show the separation of underivatized glucose, sucrose and raffinose. The total time of the analysis is about 30 s. This time can be substantially decreased by increasing the separation voltage (Fig. 6). The detection limit is estimated to be in the sub-millimolar range from the signal-noise ratio in Figs. 5 and 6. This sensitivity is of the same order of magnitude as that of the indirect fluorescence method [16], which needs an expensive helium–cadmium laser, a photomultiplier and carefully selected buffer systems. The detection of glucose and sucrose by the direct spectrophotometric method is impossible because of the lack of a chromophore in their structure. It can be noted that the width of the peaks is similar in both instances, about 3 mm, much higher than expected when assuming the diffusion model discussed above. It appears that the heterogeneity of the complexes formed plays an important role in the contribution to peak broadening. This mechanism was discussed extensively when considering

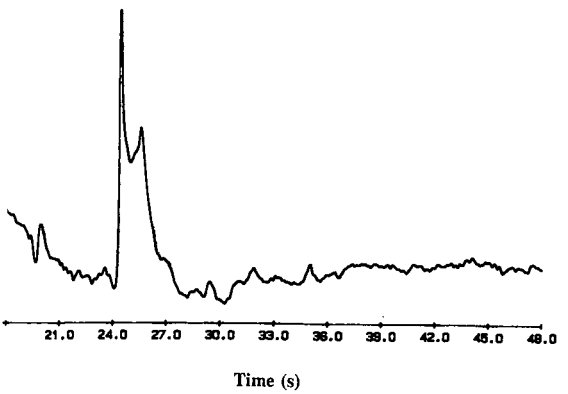

Fig. 7. Rapid separation and detection of sugars in a sample of corn syrup. Buffer, 50 m*M* borate (pH 10); applied voltage, 9 kV; sample concentration. 4 mg/ml.

micellar capillary electrophoresis [17]. The efficiency of the separation process is still over 10 000 theoretical plates. Fig. 7 shows the rapid separation of sugars in a sample of corn syrup. The individual components are not fully resolved because of the many components present. However, such a separation has application in rapid quality control by examining the electrophoretic trace as is commonly done in polymer analysis with size-exclusion chromatography. To improve separations for complicated samples, the length of the capillary needs to be substantially increased. This, however, will result in longer separation times and lower sensitivities of the concentration gradient detection method.

ACKNOWLEDGEMENTS

This work was supported by the Natural Sciences and Engineering Research Council of Canada, Eward Bioengineering and Beckman Instruments.

REFERENCES

1 F. Mikkers, F. Everaerts and Th. Verheggen, *J. Chromatogr.*, 169 (1979) 11.
2 J. Jorgenson and M. Phillips, *New Directions in Electrophoretic Methods (ACS Symposium Series*, Vol. 335), American Chemical Society, Washington, DC, 1987.
3 R. Wallingford and A. Ewing, *Adv. Chromatogr.*, 29 (1989) 1.
4 G. Taylor, *Proc. R. Soc. London, Ser. A*, 219 (1953) 186.
5 M. Martin, G. Guiochon, Y. Walbroehl and J. Jorgenson, *Anal. Chem.*, 57 (1985) 561.
6 G. Roberts, P. Rhodes and R. Snyder, *J. Chromatogr.*, 480 (1989) 35.
7 J. Pawliszyn, *J. Liq. Chromatogr.*, 10 (1987) 3377.
8 J. Pawliszyn, *Anal. Chem.*, 60 (1988) 2796.
9 J. Pawliszyn, *Spectrochim. Acta Rev.*, 13 (1990) 311.
10 J. Pawliszyn, *Rev. Sci. Instrum.*, 58 (1987) 245.
11 A. Tiselius, K. Pedersen and I. Eriksson-Quensel, *Nature (London)*, 139 (1937) 546.
12 J. Crank, *The Mathematics of Diffusion*, Oxford Science Publications, Oxford, 1989, p. 14.
13 D. R. Lide (Editor), *CRC Handbook of Chemistry and Physics*, CRC Press, Boca Raton, FL, 72nd ed., 1991, p. 6-165.
14 B. Bettler, R. Amado and H. Neukom, *J. Chromatogr.*, 498 (1990) 213.
15 S. Honda, S. Iwase, A. Makino and S. Fujiwara, *Anal. Biochem.*, 141 (1984) 366.
16 T. W. Garner and E. S. Yeung, *J. Chromatogr.*, 515 (1990) 639.
17 S. Terabe, K. Otsuka and T. Ando, *Anal. Chem.*, 61 (1989) 251.

Journal of Chromatography, 559 (1991) 119–131
Elsevier Science Publishers B.V., Amsterdam

CHROM. 23 490

Capillary zone electrophoresis analysis of acrylamido buffers for isoelectric focusing in immobilized pH gradients

MARCELLA CHIARI, CLAUDIA ETTORI and PIER GIORGIO RIGHETTI*
Chair of Biochemistry and Department of Biomedical Sciences and Technologies, University of Milan, Via Celoria 2, Milan 20133 (Italy)

ABSTRACT

Studies are described using fourteen weak acrylamido acids and bases (Immobilines) as buffers and titrants for isoelectric focusing in immobilized pH gradients (IPG), plus one strongly acidic (pK 1.0) and one strongly basic (pK > 12) titrants, utilized in general to reach pH extremes in extended IPG ranges. Three fundamental properties of these buffers were evaluated: (a) resistance to alkaline hydrolysis of the amido bond; (b) hydrophilicity (so as to avoid hydrophobic interactions with the matrix during electrophoretic migration); and (c) resistance to oxidation by peroxodisulphate during the polymerization step. Capillary zone electrophoresis (CZE) was used to evaluate these properties. The acidic compounds were resolved in 100 mM acetate (pH 4) whereas the alkaline species were separated in 50 mM phosphate buffer (pH 7.7) (or pH 7.2 for the weaker compounds). All the acrylamido derivatives were detected underivatized by their absorption at 214 or 254 nm. The degradation kinetics of all compounds were monitored, after hydrolysis in 0.1 M NaOH at 70°C (up to 6 h), by CZE in 0.1 M borate buffer (pH 9). The decrease in the Immobiline peak and the appearance of its hydrolytic products (acrylic acid and a diamine in the case of the acrylamido bases) could easily be monitored and quantified in CZE by using the Gold integration system. A hydrophobicity scale was constructed by measuring the partition coefficients of the basic acrylamido derivatives in 1-octanol–water. General guidelines are given for the proper use of these chemicals and for the synthesis of additional compounds.

INTRODUCTION

In contrast to conventional isoelectric focusing (IEF), which utilizes a vast number of soluble, amphoteric buffers having isoelectric points (pI) fairly evenly distributed along the pH scale [1] (carrier ampholytes, or Ampholines), immobilized pH gradients (IPG) exploit a set of a few, well defined non-amphoteric chemicals having pK values covering the pH range 3.1–10.3 [2]. Six such chemicals (acrylamido weak acids and bases) are commercially available through Pharmacia-LKB (Bromma, Sweden) as Immobilines. They are in fact "immobilized" into the polyacrylamide matrix by covalent bonding through the acrylic double bond. There are several advantages of the Immobilines over the "carrier ampholyte" buffers; most striking, however, is the fact that whereas the latter produce an interpenetrating, quasi-Gaussian steady-state profile (with a system of $n-1$ boundaries for n species), the former generate an evenly changing chemical field along the migration path. The absence of

0021-9673/91/$03.50

such boundaries in the gel bed is most beneficial to protein migration and to the focusing process. In addition, the Immobiline chemicals contain a single protolytic group, whereas Ampholines are oligoamino-oligocarboxylic acids; it turns out that oligoprotic species have a tendency to "stick" to proteinaceous surfaces, giving spurious bands [1,2].

We have recently decoded the structure and given the formulae of the acidic [3] and basic [4] Immobiline chemicals. In addition, we have proposed over the years a number of additional compounds for expanding the fractionation ability of IPGs: both more acidic [5,6] and more alkaline [7] compounds have been produced in our laboratory. We have also synthesized analogues of the weakest Immobiline bases (the morpholino derivatives, with pK values of 6.2 and 7.0); by introducing a thiomorpholino ring, the pK values of these compounds have been increased to 6.6 and 7.4, respectively, thus offering additional species buffering around neutrality, *i.e.*, in a region which normally lacks suitable buffering groups and where the bulk water conductivity reaches a minimum [8]. A new, hydrophilic Immobiline with pK 8.05 has also recently been synthesized, in order to close the gap in the pH 7.0–8.5 region [9]. We have also reported a pK 6.85 compound (1-acryloyl-4-methylpiperazine; AMPip) [10] and another pK 7.0 species [2-(4-imidazolyl)ethylamine-2-acrylamide or -acryloylhistamine, pK 7_{AH}] [11]. Thus, the family of acrylamido buffers is expanding: we have now described a total of sixteen monoprotic compounds and there is a report on a biprotic species, itaconic acid [12]. The formulae names, pK values and relative molecular masses (M_r) values of all the species produced so far are listed in Tables I–III.

In recent years, we have focused our attention on three most desirable properties of the Immobiline chemicals: (a) resistance to alkaline hydrolysis (particularly pronounced with the basic species, which autocatalyse the lysis of the amido bond [15]; (b) hydrophilicity (when grafted into the polyacrylamide matrix, any hydrophobic property of Immobilines will be amplified); and (c) resistance to oxidation, during the polymerization step, caused by peroxodisulphate [16]. Whereas conventional gel electrophoresis techniques are excellent for the analysis of macromolecules, they are not so readily amenable to the characterization of small molecules. Capillary zone electrophoresis (CZE) has been useful in analysing all these properties and for checking the purity of the new synthetic products.

EXPERIMENTAL

Commercial Immobilines, Repel- and Bind-silane, Gel Bond PAG, the Multiphor II chamber, Multitemp thermostat, the Macrodrive power supply and Pharmalyte carrier ampholytes (pH 7–9) were purchased from Pharmacia-LKB. Noncommercial acrylamido weak acids and bases were synthesized in our laboratory as reported [3–11]. Acrylamide, N,N′-methylenebisacrylamide (Bis), N,N,N′,N′-tetramethylethylenediamine (TEMED), ammonium peroxodisulphate and Coomassie Brilliant Blue were obtained from Bio-Rad Labs. (Richmond, CA, USA). Acrylic acid was purchased from Fluka (Buchs, Switzerland) and was distilled just prior to use. Horse heart myoglobin was purchased from Sigma (St. Louis, MO, USA) and haemoglobin mutants were a gift from Dr. A. Mosca (University of Milan). Mandelic acid, used as an internal standard in capillary zone electrophoresis (CZE) runs, was purchased from Aldrich (Steinheim, Germany).

TABLE I

ACIDIC ACRYLAMIDO BUFFERS

pK^a	Formula	Name	M_r	Source[b]
1.0	$CH_2=CHCONH-C(CH_3)(CH_2SO_3H)-CH_3$	2-Acrylamido-2-methylpropanesulphonic acid	207	A
3.1	$CH_2=CHCONHCH(OH)COOH$	2-Acrylamidoglycolic acid	145	B
3.6	$CH_2=CHCONHCH_2COOH$	N-Acryloylglycine	129	C
4.4	$CH_2=CHCONH(CH_2)_2COOH$	3-Acrylamidopropanoic acid	143	C
4.6	$CH_2=CHCONH(CH_2)_3COOH$	4-Acrylamidobutyric acid	157	C

[a] The pK values for the three Immobilines and for 2-acrylamidoglycolic acid are given at 25°C; for AMPS (pK 1.0) the temperature of pK measurement was not reported.
[b] A, Polysciences, Warrington, PA, USA; B, ref. 6; C, Pharmacia–LKB.

Alkaline hydrolysis

All acrylamido derivatives and Immobiline buffers were dissolved (20 mM each) in 0.1 M NaOH and incubated at 70°C, under a nitrogen atmosphere, for up to 6 h. At hourly intervals aliquots were collected and diluted in 0.1 M borate buffer (pH 9.0) to 2.5 mM. Mandelic acid (2.50 mM) was then added and the mixtures were analysed by CZE.

Capillary zone electrophoresis

CZE was performed in a Beckman (Palo Alto, CA, USA) P/ACE System 2000 instrument equipped with a 50 cm × 75 μm I.D. capillary. All runs were performed at 25°C in a thermostated environment. Analysis of acidic acrylamido compounds was

TABLE II

BASIC ACRYLAMIDO BUFFERS

pK^a	Formula	Name	M_r	Source[b]
6.2	$CH_2=CHCONH(CH_2)_2-N$ 	2-Morpholinoethylacrylamide	184	A
7.0	$CH_2=CHCONH(CH_2)_3-N$ 	3-Morpholinopropylacrylamide	198	A
8.5	$CH_2=CHCONH(CH_2)_2N(CH_3)_2$	N,N-Dimethylaminoethylacrylamide	142	A
9.3	$CH_2=CHCONH(CH_2)_3N(CH_3)_2$	N,N-Dimethylaminopropylacrylamide	156	A
10.3	$CH_2=CHCONH(CH_2)_3N(C_2H_5)_2$	N,N-Diethylaminopropylacrylamide	184	B
>12	$CH_2=CHCONH(CH_2)_2-\overset{+}{N}(C_2H_5)_3$	N,N,N-Triethylaminoethylacrylamide	198	C

[a] All pK values (except for pK 10.3) measured at 25°C. The value of pK 10.3 refers to 10°C.
[b] A, Pharmacia–LKB. B, Ref. 13. C, IBF, Villeneuve La Garenne, France.

TABLE III

NEW BASIC ACRYLAMIDO BUFFERS

pK^a	Formula	Name	M_r	Ref.
6.6	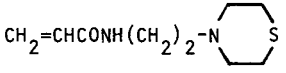	2-Thiomorpholinoethylacrylamide	200	8
6.85	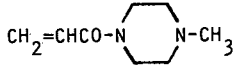	1-Acryloyl-4-methylpiperazine	154	10
7.0	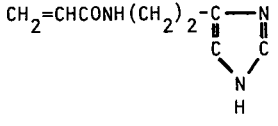	2-(4-Imidazolyl)ethylamine-2-acrylamide	165	11
7.4	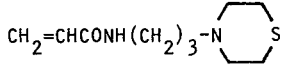	3-Thiomorpholinopropylacrylamide	214	8
8.05	$CH_2=CHCONH(CH_2)_3N(CH_2CH_2OH)_2$	N,N-Bis(2-hydroxyethyl)-N′-acryloyl-1,3-diaminopropane	200	9

[a] All pK values measured at 25°C.

performed in 100 m*M* acetate (pH 4.0) at 20 kV and 23 μA, of the commercial basic Immobilines in 50 m*M* phosphate buffer (pH 7.7) at 13 kV and 80 μA, of the weakly basic acrylamido buffers in 50 m*M* phosphate buffer (pH 7.0) at 20 kV and 100 μA and for checking the hydrolytic products in 0.1 *M* borate (pH 9.0) at 15 kV and 55 μA. In all instances the migration direction was toward the negative electrode, which means that the acidic species (acrylic and mandelic acid) are transported there by electroosmosis, as they migrate electrophoretically toward the positive electrode. The sample was injected into the capillary by pressure from a nitrogen tank (*ca.* 0.8 MPa), usually for 10 s. The calibration graph for each acrylamido derivative analysed was constructed with the Beckman Gold integration system, with concentration points of 0.25, 0.50, 1.00, 1.25, 2.00, 2.50 and 3.50 m*M*. In each run mandelic acid (2.50 m*M*) was used as an internal standard [17].

Partition coefficient

In order to establish a hydrophobicity scale, the available alkaline Immobilines (p*K* 6.2, 7.0, 7_{AH}, 7.4, 8.05, 8.5, 9.3 and 10.3) were subjected to partitioning in 1-octanol–water as described by Purcell *et al.* [18]. The partition coefficient *P* is defined as the ratio of the molarities of a given compound in the organic and the aqueous phase. Partitioning is performed under conditions in which the alkaline Immobilines are fully deprotonated. For the p*K* 10.3 compound, as partitioning was executed at pH 11.6 (borate buffer, under nitrogen), a correction factor was applied to account for the small degree of protonation at this pH [18]. After partitioning, both the water and 1-octanol phases were monitored at 254 nm to measure the concentration in each phase. As an independent assessment, the water phase was also analyzed by CZE and the peak area measured with the Beckman Gold integration system. The two sets of data agreed within a relative standard deviation of 5% ($n = 8$).

RESULTS

CZE analysis of acrylamide weak acids and bases

Fig. 1a shows the separation of five acidic Immobilines (p*K* 4.6, 4,4, 3.6, 3.1 and 1.0) and of a contaminant, acrylic acid, added to the mixture. It is seen that the conditions used are able to separate these species completely, and are clearly optimum for the weaker acids (p*K* 4.6, 4.4 and 3.6 and acrylic acid). Owing to its high mobility, the p*K* 1.0 (2-acrylamido-2-methylpropanesulphonic acid) peak is highly skewed, as its anodic transport competes strongly with the cathodic electroosmotic flow. To a lesser extent, this is also true for the p*K* 3.1 peak. In fact, these two compounds show fronting, as opposed to very slight tailing of the other peaks.

Fig. 1b shows an interesting application of the CZE technique: by plotting the p*K* values of the four Immobiline weak acids (p*K* 4.6, 4.4, 3.6 and 3.1) *versus* their respective migration times, a straight line is obtained. This can be used as a calibration graph for measuring unknown p*K* values of compounds with intermediate mobilities. Thus, by entering the calibration graph with the mobility of acrylic acid (vertical arrow), a p*K* value of 4.2 (horizontal arrow) is obtained, which compares well with literature data (p*K* 4.25) [14].

Fig. 2a shows the separation of the four commercially available basic Immobilines (p*K* 6.2, 7.0, 8.5 and 9.3) in phosphate buffer (pH 7.7). In this instance, both the

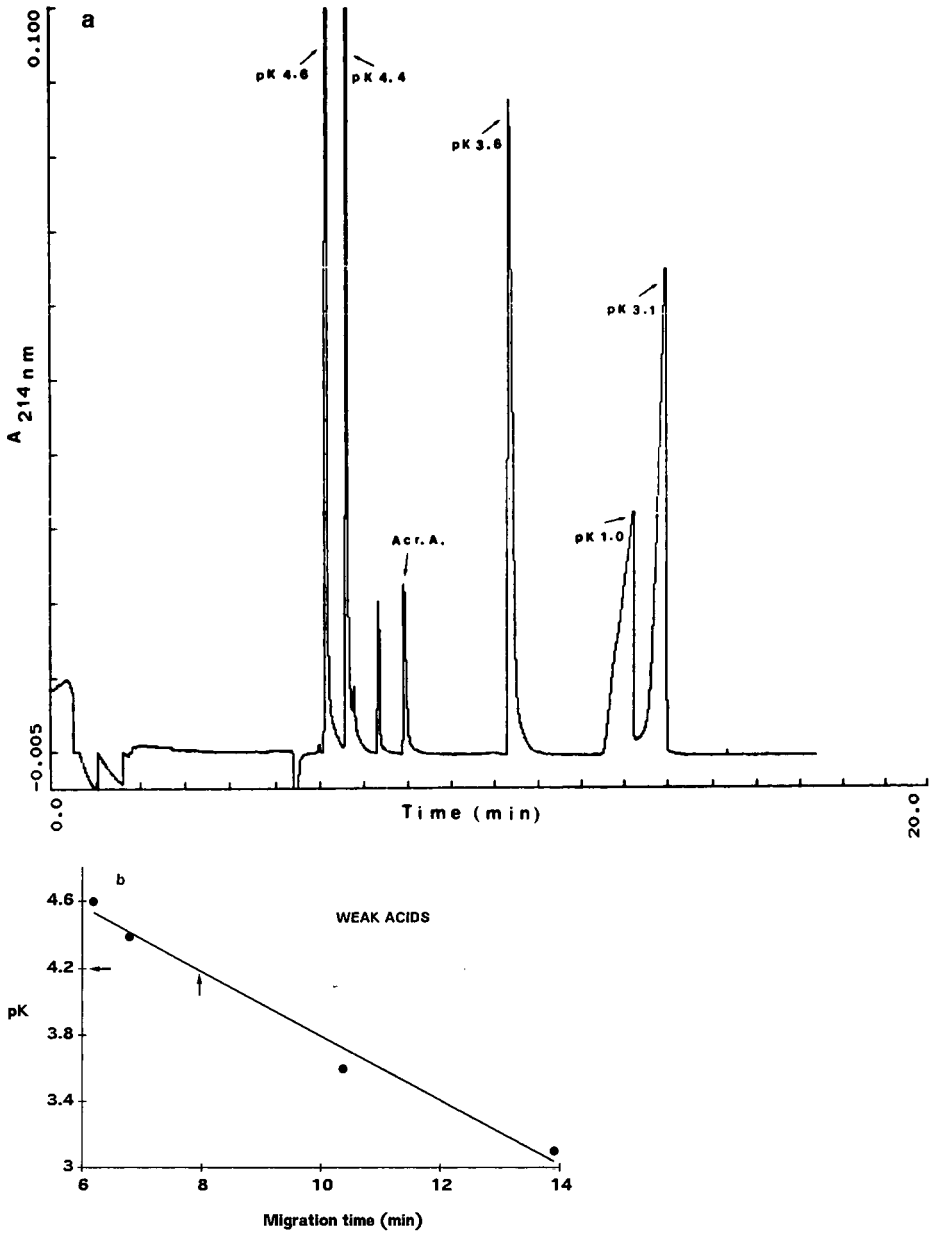

Fig. 1. Analysis of acidic Immobilines by CZE. A mixture of 2.5 m*M* each of Immobilines of p*K* 4.6, 4.4, 3.6, 3.1 and 1.0 was introduced by pressure (10 s) into a 50 cm × 50 μm I.D. capillary in the Beckman P/ACE System 2000. The run was at 25°C in 100 m*M* acetate buffer (pH 4.0) at 20 kV and 23 μA. Detection was by UV absorption at 214 nm. The sample was contaminated with 2.5 m*M* acrylic acid (Acr. A.). Migration toward the cathode by electroosmosis. (a) CZE profile; (b) correlation between p*K* values and migration times. The vertical arrow indicates the migration time of acrylic acid and the horizonal arrow its corresponding p*K* value as derived from the plot.

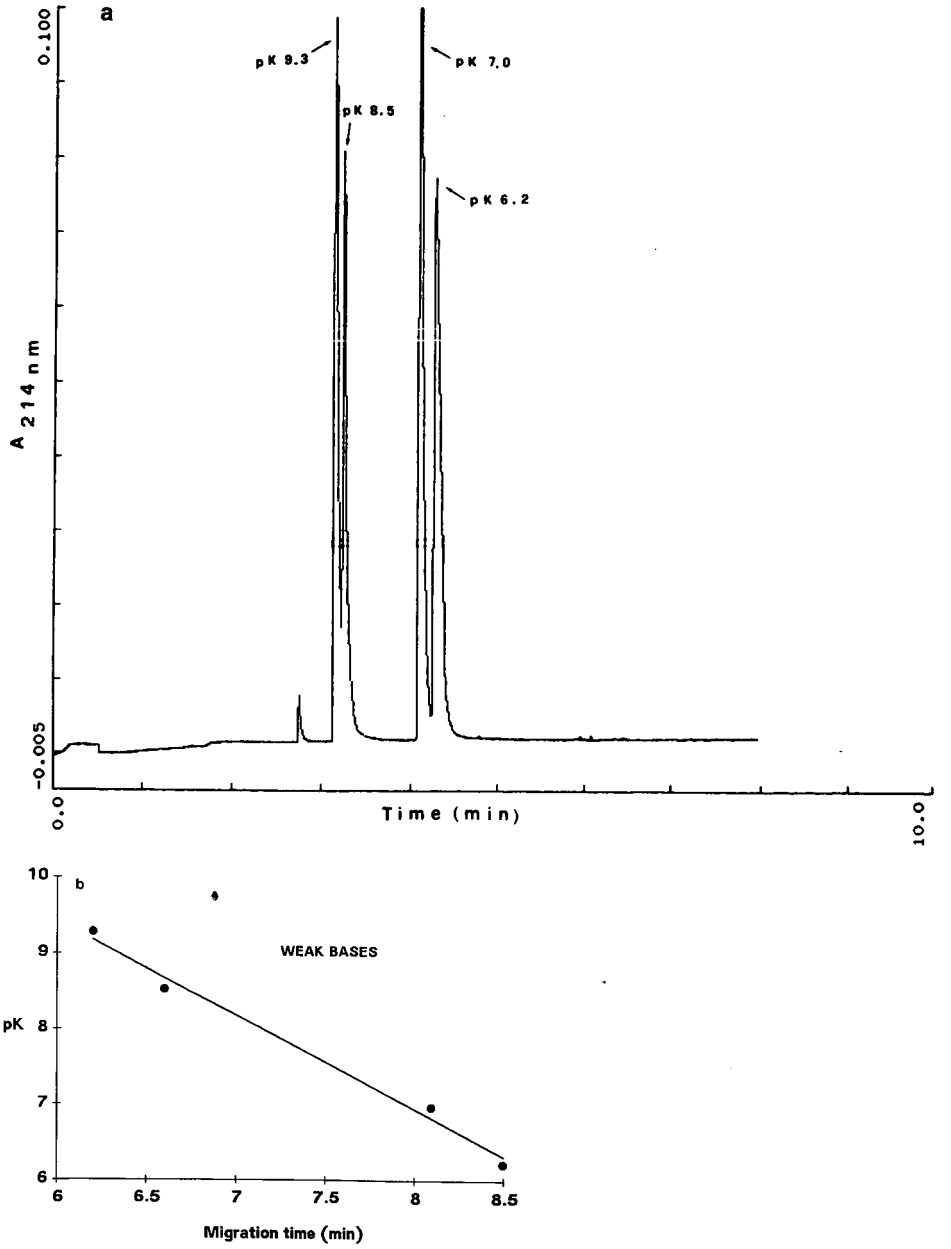

Fig. 2. Separation of alkaline Immobilines by CZE. A mixture of 2.5 m*M* each of Immobilines of p*K* 9.3, 8.5, 7.0 and 6.2 was run in the P/ACE System 2000 in 50 m*M* phosphate buffer (pH 7.7) at 13 kV and 80 μA. All other conditions as in Fig. 1. Cathodic migration. (a) CZE profile; (b) correlation between p*K* values and migration times.

electrophoretic migration and electroosmotic flow are in the same direction, and the peaks are sharp, with a much reduced separation time (less than 5 min, as opposed to 15 min in Fig. 1). Here too, a plot of pK values *vs.* migration time gives a straight regression line, suggesting that this also can be used as a calibration graph for measuring the pK values of unknown compounds (Fig. 2b).

As we have recently synthesized two analogues of the weak bases of pK 6.2 and 7.0 (with a thiomorpholino substituting the morpholino ring), it was of interest to examine the separation of these compounds. By decreasing the operating pH, this analysis is easily accomplished (Fig. 3a). Note that as the pK values are regularly spaced at 0.4 pH unit intervals, so is the peak distance in the electropherogram. In fact, a plot of pK *vs.* migration time (Fig. 3b) gives a straight regression line with all the points on the line.

Hydrolytic stability of the basic acrylamido buffers

It is known that the alkaline acrylamido buffers are the species most prone to hydrolytic degradation, as the high pH of these solutions (supplied as free bases) auto-catalyse the lysis of the amido bond. Thus, structures which stabilize these chemicals against degradation are highly desirable. We subjected all the alkaline Immobilines to hydrolysis in 0.1 *M* NaOH at 70°C for up to 6 h and analysed the degradation products by CZE. A summary of these data is presented as a bar graph in Fig. 4, which gives the percentage of undegraded material left at the end of the 6-h period. Curiously, it is seen that the stability, contrary to expectations, is in order of pK values: the higher the pK, the more stable is the chemical. This order is, however, merely accidental, as the stability is not so much a function of the pK value but rather of the type of substituents on the nitrogen of the amido group (see Discussion).

Hydrophobicity of the basic acrylamido buffers

Owing to the types of substituents on the nitrogen of the amido bond, the alkaline Immobilines have a much greater chance of presenting a hydrophobic surface than the acidic species, as the latter are in general less substituted and contain a carboxyl group, which is decidedly more hydrophilic than an amino group. Therefore, our efforts to construct a hydrophobicity scale were concentrated solely on the alkaline compounds. Partitioning of the deprotonated species was performed in 1-octanol–water mixtures and the concentration in each phase read at 254 nm. The data in the water phase were double checked by CZE and peak integration. A summary of these data is presented as a bar graph in Fig. 5, which gives the partition coefficients (P) of the alkaline Immobilines studied (the maximum P value being 6). It is seen that most species are fairly hydrophilic, having P values below 1. However, in the morpholino ring, when the oxygen is substituted with a sulphur atom, for synthesizing the thiomorpholino analogues (pK 6.6 and 7.4) the hydrophobicity greatly increases. The same applies to the pK 10.3 compound, which contains two N-ethyl groups as opposed to the two N-methyl groups in the pK 9.3 buffer.

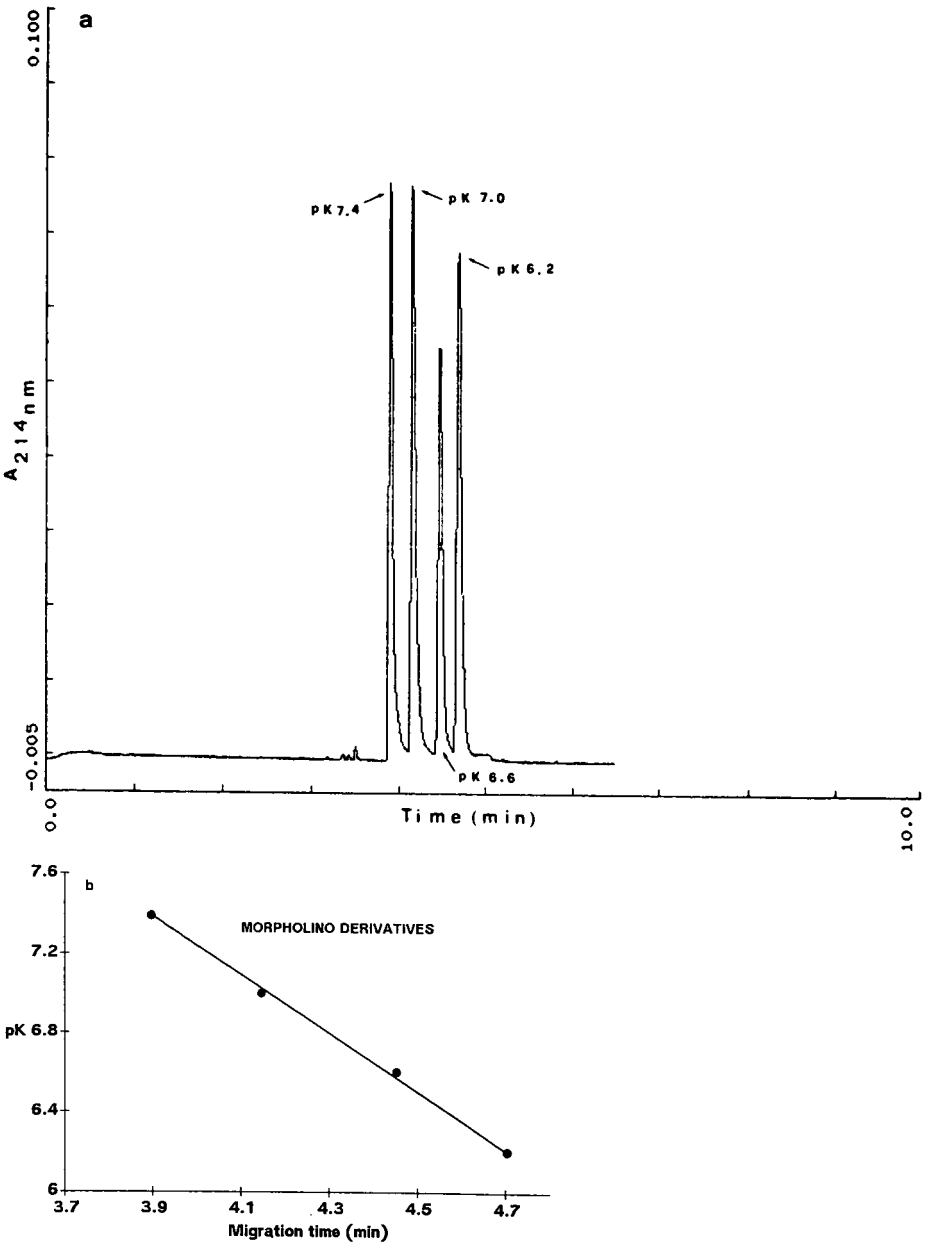

Fig. 3. Separation of weakly basic Immobilines by CZE. A mixture of 2.5 m*M* each of Immobilines of p*K* 7.4, 7.0, 6.6 and 6.2 was run in the P/ACE System 2000 in 50 m*M* phosphate buffer (pH 7.0) at 20 kV and 100 μA. The p*K* 7.4 and 6.6 buffers are the thiomorpholino derivatives of the commercial morpholino species (p*K* 7.0 and 6.2, respectively). All other conditions as in Fig. 1. (a) CZE profile; (b) correlation between p*K* values and migration times.

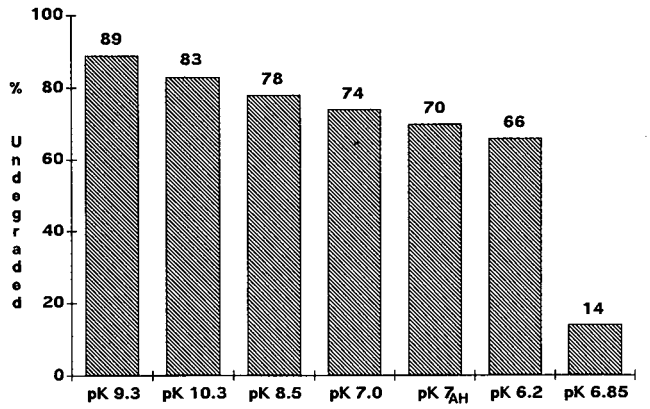

Fig. 4. Summary of the degradation kinetics of the seven acrylamido bases studied. The vertical bars represent the amounts of undegraded product remaining after 6 h of hydrolysis at 70°C in 0.1 *M* NaOH. p*K* 6.85 = 1-acryloyl-4-methylpiperazine; p$K\,7_{AH}$ = acryloylhistamine (p*K* 7.0). All data obtained by CZE in a Beckmann P/ACE 2000 with a 50 cm × 75 μm I.D. capillary. Run at 15 kV and 25°C in 0.1 *M* borate buffer (pH 9). All migrations toward the cathode. Detection at 214 nm. Mandelic acid (2.5 m*M*) was used as an internal standard in all runs. Peak integrations were done with the Beckman system Gold. The numbers on each bar give the reading on the ordinate (% intact compound).

DISCUSSION

Determination of pK values

Although our data would appear to be limited to the analysis of acrylamido buffers, some results could have wider implications. Noteworthy is the fact that there appears to be a linear relationship between p*K* values (of both weak acids and bases) and the migration (or transit) times. This could lead to a simple and rapid method for

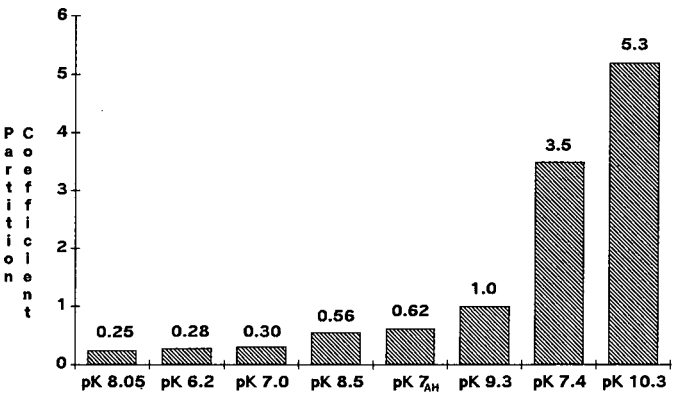

Fig. 5. Partition coefficients (*P*) of different alkaline Immobilines in 1-octanol–water. The *P* values were assessed by partitioning the different bases in the fully deprotonated form. The molarity ratios in the two phases were measured by absorbance readings at 214 nm in a spectrophotometer. For the water-phase values, all data were double checked by CZE under the same conditions as in Fig. 4. The data presented are the averages of the spectrophotometric readings and the CZE peak integrations. The number on top of each bar is the *P* value.

the determination of the pK values of unknown compounds. The Immobiline weak acids and bases (well characterized compounds) could be used to construct calibration graphs in certain pH regions for the rapid assessment of unknown pK values. The problem of determining ionic mobilities and dissociation constants of weak acids and bases has been extensively studied in capillary isotachophoresis [19–21]. Most workers have elaborated methods that combine computer simulations with experimental measurements of conductivities of the isotachophoretic zones in the steady state: if agreement between simulated and experimental data for pK and mobility was achieved, such data were considered to be valid [19–21]. More recently, Pospichal *et al.* [22] built a micropreparative isotachophoresis unit in which, in addition to an on-line measurement (relative effective mobility), an off-line determination (pH) could be performed in the collected zone. In a linear plot of 1/mobility *vs.* $[H^+]$, the K (and thus pK) value could then be accurately assessed. In a different approach, Beckers *et al.* [23] proposed a double detector system in zone electrophoresis for measuring absolute mobilities of cation and anions. In the latter instance, the experimental and literature data agreed to within 1%.

What we propose here is a simple approach by which a pK value can be determined by interpolation on a calibration graph, which is obtained in a run simultaneously with the unknown sample. Constructing a plot of pK *vs.* migration time is thus similar to a plot of log M_r *vs.* K_{av} used for M_r determination in gel filtration [24]. The rule in gel permeation is that a solute must have a K_{av} between V_e (totally excluded) and V_t (totally included), preferably in fact K_{av} should be on the linear portion of the curve (between 0.2 and 0.8). Thus, for a correct assessement of pK values from our proposed calibration graph, the unknown sample should be dissolved at a pH encompassing the interval p$K \pm 0.5$. In a similar approach, Nishi and Terabe [25] proposed the concept of t_o and t_{mc} for measuring the partition coefficient of a solute in micellar electrokinetic chromatography.

This is a simple approach to the problem of assessing a true thermodynamic dissociation constant, which represents a complex system of equilibria, involving first a K_i, *i.e.*, a thermodynamic constant of the true ionization process of an ionogenic molecule, followed by a K_d, *i.e.*, the constant of the dissociation process on the basis of which the solvated ion pairs are finally separated into solvated ionic species by action of the solvent molecules [26]. Nevertheless, CZE could prove useful not only as a simple tool for practical pK determinations, but also for discriminating substances with very small ΔpK values. In fact, Terabe *et al.* [27] have demonstrated, in the separation of oxygen-isotopic benzoic acids (BA), that three isotopes ($^{16}O_2$[BA]; $^{16}O^{18}O$[BA] and $^{18}O_2$[BA]) differing in pK values by only 1% could still be effectively separated.

Hydrolytic stability of alkaline Immobilines

All Immobilines analysed here are monosubstituted amides, except for the pK 6.85 (AMPip) species, which is disubstituted.Although we agree with the general knowledge on the greater stability of such compounds in comparison with unsubstituted amides, it is clear from our results that there are other, more subtle, mechanisms governing such stability. On the basis of our data, and of the known structures of these acrylamido derivatives (see Tables II and III), we can thus derive the following rules.

(a) To afford protection of the amido bond, the most important parameter is not the degree of substitution in the nitrogen engaged in the amido plane (mono- or disubstituted) but the type of substituent.

(b) In particular, rigid ring structures (as in AMPip) are completely inefficient in protecting the adjacent amido bond, as their rigidity prevents them from oscillating in the surrounding space and thus shielding the amido plane.

(c) Flexible chains bound to the nitrogen of the amido bond are efficient in protecting the amido plane, as they can oscillate in the surrounding space and shield the amido group.

(d) If rigid structures are present in the nitrogen substituents, there should be some distance from the plane of the amido bond. This is why the pK 7.0 (3-morpholinopropylacrylamide) degrades substantially less than the pK 6.2 (2-morpholinoethylacrylamide) derivative.

(e) If a simple, flexible chain is present as a substituent on the nitrogen of the amido bond, greater protection of the latter is afforded by a longer chain. This is why the pK 9.3 (N,N-dimethylaminopropylacrylamide) is more resistant than the pK 8.5 (N,N-dimethylaminoethylacrylamide) derivative.

Hydrophobicity scale

Generally, most of the Immobilines that we have analysed are fairly hydrophilic, as they have a P value below 1(on a scale of up to 6). There is a trend of increasing hydrophobicity with increasing pK value, no doubt due to the increasing complexity of the molecules and the longer aliphatic chains as substituents on the nitrogen of the amido bond (in a homologous series). Some small exceptions can be found, *e.g.*, the pK 7_{AH} species, which in the hydrophobicity scale of Fig. 5 is located between the pK 8.5 and 9.3 derivatives, with a partition coefficient of $P = 0.62$. It was surprising that the P value should be higher than that of the commercial analogue pK 7.0 ($P = 0.3$), considering that the substituent chain on the amido group is two carbon atoms shorter than that in the pK 7.0 compound. Conversely, a huge hydrophobicity increment is noted when the oxygen in the morpholino ring of the pK 7.0 Immobiline is replaced with a sulphur atom (pK 7.4 compound, 3-thiomorpholinopropylacrylamide). The highest hydrophobicity jump in the scale is, however, exhibited by the pK 10.3 buffer (an analogue of the pK 9.3 species with two ethyl, instead of methyl, substituents on the tertiary nitrogen); in the deprotonated form, *ca.* 95% of it is extracted into the 1-octanol phase ($P = 5.3$). Hence, the addition of only two carbon atoms (compared with the pK 9.3 compound) has the effect of increasing the partition coefficient by a factor of > 5 (see Fig. 5). In the light of these data, it appears worthwhile to search for new, basic Immobilines with more hydrophilic substituents able to lower the P value. In fact, IPG in very alkaline ranges has often been plagued by the adsorption of protein on the gel matrix [28]. A balance will have to be obtained between he hydrophobicity and hydrophilicity of such alkaline compounds, because the addition of two terminal OH groups (see the formula of the pK 8.05 species) lowers the pK value of the pK 10.3 species by more than 2 pH units.

ACKNOWLEDGEMENTS

This work was supported in part by grants from Progetto Finalizzato Biotec-

nologia e Biostrumentazione, CNR (Rome) and Agenzia Spaziale Italiana (ASI, Rome). We are greatly indebted to Drs. R. Montini and S. Di Biase of Beckman Italia for the kind loan of the instrument and for their patient teaching of all the secrets of CZE. We thank Dr. M. Giacomini and Miss C. Micheletti for help with part of the work on the synthesis of the new Immobilines.

REFERENCES

1 P. G. Righetti, *Isoelectric Focusing: Theory, Methodology and Applications*, Elsevier, Amsterdam, 1983.
2 P. G. Righetti, *Immobilized pH Gradients: Theory and Methodology*, Elsevier, Amsterdam, 1990.
3 M. Chiari, E. Casale, E. Santaniello and P. G. Righetti, *Appl. Theor. Electrophoresis*, 1 (1989) 99–102.
4 M. Chiari, E. Casale, E. Santaniello and P. G. Righetti, *Appl. Theor. Electrophoresis*, 1 (1989) 103–107.
5 E. Gianazza, F. Celentano, G. Dossi, B. Bjellqvist and P. G. Righetti, *Electrophoresis*, 5 (1984) 88–97.
6 P. G. Righetti, M. Chiari, P. K. Sinha and E. Santaniello, *J. Biochem. Biophys. Methods*, 16 (1988) 185–192.
7 C. Gelfi, M. L. Bossi, B. Bjellqvist and P. G. Righetti, *J. Biochem. Biophys. Methods*, 15 (1987) 41–48.
8 M. Chiari, P. G. Righetti, P. Ferraboschi, T. Jain and R.Shorr, *Electrophoresis*, 11 (1990) 617–620.
9 M. Chiari, L. Pagani, P.G. Righetti, T. Jain, R. Shorr and T. Rabilloud, *J. Biochem. Biophys. Methods*, 21 (1990) 165–172.
10 M. Chiari, C. Ettori, A. Manzocchi and P. G. Righetti, *J. Chromatogr.*, 548 (1991) 381–392.
11 M. Chiari, M. Giacomini, C. Micheletti and P. G. Righetti, *J. Chromatogr.*, 558 (1991) 285–295.
12 R. Charlionet, R. Sesboüé and C. Davrinche, *Electrophoresis*, 5 (1984) 176–178.
13 P. K. Sinha and P. G. Righetti, *J. Biochem. Biophys. Methods*, 15 (1987) 199–206.
14 R. C. Weast (Editor), *CRC Handbook of Chemistry and Physics*, CRC Press, Boca Raton, FL, 1987, p. D-161.
15 B. M. Gåveby, P. Petterson, J. Andrasko, L. Ineva-Flygare, U. Johannesson, A. Görg, W. Postel, A. Domscheit, P. L. Mauri, P. Pietta, E. Gianazza and P. G. Righetti, *J. Biochem. Biophys. Methods*, 16 (1988) 141–164.
16 P. G. Righetti, M. Chiari, E. Casale and C. Chiesa, *Appl. Theor. Electrophoresis*, 1 (1989) 115–121.
17 P. G. Righetti, C. Ettori and M. Chiari, *Electrophoresis*, 12 (1990) 55–58.
18 W. P. Purcell, G. E. Bass and J. M. Clayton (Editors), *Strategy of Drug Design: a Guide to Biological Activity*, Wiley-Interscience, New York, 1973, pp. 126–143.
19 T. Hirokawa, M. Nishino and Y. Kiso, *J. Chromatogr.*, 252 (1982) 49–56.
20 T. Hirokawa, S. Kobayashi and Y. Kiso, *J. Chromatogr.*, 318 (1985) 195–201.
21 J. L. Beckers, *J. Chromatogr.*, 320 (1985) 147–155.
22 J. Pospichal, M. Deml and P. Bocek, *J. Chromatogr.*, 390 (1987) 17–26.
23 J. L. Beckers, T. P. E. M. Verheggen and F. M. Everaerts, *J. Chromatogr.*, 452 (1988) 591–600.
24 R. P. Bywater and N. V. B. Marsden, in E. Heftmann (Editor), *Chromatography, Part A*, Elsevier, Amsterdam, 1983, pp. 257–330.
25 H. Nishi and S. Terabe, *Electrophoresis*, 11 (1990) 691–701.
26 G. Franchini, A. Marchetti, L. Tassi and G. Tosi, *Anal. Chem.*, 62 (1990) 1004–1010.
27 S. Terabe, T. Yashima, N. Tanaka and M. Araki, *Anal. Chem.*, 60 (1988) 1673–1677.
28 C. Gelfi, M. L. Bossi, B. Bjellqvist and P. G. Righetti, *J. Biochem. Biophys. Methods*, 14 (1987) 139–147.

Journal of Chromatography, 559 (1991) 133–140
Elsevier Science Publishers B.V., Amsterdam

CHROM. 23 491

Analysis of separation efficiency in capillary electrophoresis with direct control of electroosmosis by using an external electric field

CHENG S. LEE*, CHIN-TIAO WU, TERESA LOPES and BHISMA PATEL
Department of Chemical and Biochemical Engineering, University of Maryland Baltimore County Campus, Baltimore, MD 21228 (USA)

ABSTRACT

Direct control of electroosmosis in capillary electrophoresis with the application of an external electric field is demonstrated by the UV marker method. When the zeta potential at the capillary/aqueous solution interface is small, the capacitor model qualitatively and quantitatively predicts the effectiveness of the external electric field for controlling electroosmosis at different electrolyte concentrations and capillary dimensions. To investigate the separation efficiency of capillary electrophoresis with the direct control of electroosmosis, frontal analysis of dimethyl sulfoxide as a UV marker are examined. There is no measurable additional band broadening induced by the application of an external electric field.

INTRODUCTION

With the application of the current monitoring method [1], we have recently demonstrated the direct control of electroosmosis in capillary electrophoresis by using an additional electric field applied from outside the capillary [2,3]. This technique vectorally couples the externally applied electric potential with the internal electric potential across the buffer solution inside the capillary. This electric potential gradient across the capillary between the external and internal electric potential is uniform and constant along the length of the capillary. This newly created electric field is therefore perpendicular across the capillary and controls the polarity and magnitude of the zeta potential on the interior surface of the capillary wall. Because the direction and flow-rate of electroosmosis are dependent on the polarity and magnitude of the zeta potential [4], the electroosmotic flow can therefore be directly manipulated by simply varying the external electric potential.

To investigate the fundamentals of the use of an external electric potential for controlling the electroosmotic flow, a capacitor model as shown in Fig. 1 was proposed [3]. The capacitance of the electrostatic diffuse layer at the inner capillary/inner aqueous interface, C_{ei} in faraday at 25°C, was given by

$$C_{ei} = 228.5 \cdot 10^{-6} C^{1/2} \cosh(19.46\,\zeta)\,\pi\, D_{id} l \qquad (1)$$

0021-9673/91/$03.50

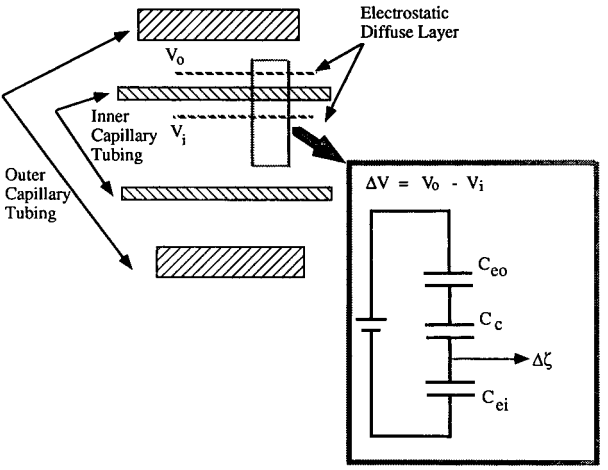

Fig. 1. The proposed capacitor model for predicting the change in the zeta potential due to the application of an external electric field.

where C is the concentration of ions in the solution in mol/l, ζ is the zeta potential at the capillary/aqueous interface in volts, D_{id} is the inner diameter of inner capillary tubing in cm and l is the length of capillary tubing in cm [4]. The capacitance of the inner capillary tubing, C_c, was given by

$$C_c = \varepsilon_c 2\pi l/[\ln (D_{od}/D_{id})] \tag{2}$$

where ε_c is the electrical permittivity of silica surface and D_{od} is the outer diameter of inner capillary tubing [5]. The capacitance of the electrostatic diffuse layer at the inner capillary/outer aqueous interface (in the annular space between the outer and inner capillaries), C_{eo} in faraday at 25°C, was given by

$$C_{eo} = 228.5 \cdot 10^{-6} C^{1/2} \cosh(19.46\,\zeta)\, \pi D_{od} l \tag{3}$$

where D_{od} is the outer diameter of inner capillary tubing in cm [4]. The total capacitance of three capacitors in series, C_T, was given as [5]

$$(C_T)^{-1} = (C_{eo})^{-1} + (C_c)^{-1} + (C_{ei})^{-1} \tag{4}$$

Because the capacitance of the electrostatic layer was much greater than that of the capillary tubing for the accumulation of mobile ions in the electrostatic layer, the total capacitance, C_T, was simplified to

$$C_T = C_c \tag{5}$$

The change in the zeta potential at the inner capillary/inner aqueous interface, $\Delta\zeta$, due to the applied potential gradient across the inner capillary wall, ΔV, was given by [5]

$$\Delta\zeta = \Delta V/[(C_{ei})/(C_T)] = \Delta V/[(C_{ei})/(C_c)] \quad (6)$$

The change in the zeta potential was then converted to the change in the electroosmotic mobility for the comparison with the experimental results [3].

Direct control of electroosmosis with the application of an external electric field under various operating conditions including different solution pHs, electrolyte concentrations and capillary dimensions were examined [3]. The experimental results were then compared with the predictions obtained from the capacitor model. In a previous study [3], the capacitor model only predicted the trend of experimental results at various operating conditions, and failed as a quantitative model for predicting the effectiveness of the applied external electric field for controlling the electroosmotic flow.

One problem was encountered in the comparison of experimental results with the predictions from the capacitor model. Owing to the nature of the current monitoring method employed in the experiment for measuring the change in the electroosmotic flow [2,3], the electrolyte concentration inside the inner capillary tubing was varied during the measurement. Thus, an average electrolyte concentration was used for the calculation of the capacitance of the electrostatic diffuse layer as shown in eqn. 1 in the capacitor model. The use of an average electrolyte concentration in the calculation may affect the ability of the capacitor model to predict the experimental results quantitatively. To examine this issue, the UV marker method [6] was used in this study for measuring the changes in the direction and rate of the electroosmotic flow on application of an external electric field. In contrast to the current monitoring method, the electrolyte concentration in the capillary tubing was kept constant during the experiment with the use of UV marker method. Further, frontal analyses of the UV marker were examined for investigating the separation efficiency of capillary electrophoresis with the direct control of electroosmosis.

EXPERIMENTAL

A complete capillary electrophoresis system with a UV detector as shown in Fig. 2 was installed in our laboratory for delivering electric fields both externally through the annulus between the inner and outer capillaries and internally across the buffer solution in the inner capillary. A 23-cm fused-silica capillary with 25 μm I.D. (150 μm O.D.) or 50 μm I.D. (150 μm O.D.) was placed inside a larger capillary (250 μm I.D., 375 μm O.D.) which was 20 cm long. The smaller (inner) capillary was attached between reservoirs 1 and 4 while the larger (outer) capillary was attached between reservoirs 2 and 3. The inner capillary tubing without the external polyimide coating was obtained from Polymicro Technologies (Phoenix, AZ, USA). A 1-mm section of the polyimide coating on the exterior surface of the outer capillary tubing was removed by using concentrated sulfuric acid solution to create a window for the UV radiation.

Two high-voltage power supplies were obtained from Spellman High-Voltage Electronics (Plainview, NY, USA). One high-voltage power supply was connected to reservoirs 2 and 3 so that an outer electric field was applied to the annular space between the two capillaries. The annular space was filled with a 1 m*M* phosphate buffer solution (pH 6) as the conductive medium for applying the outer electric field.

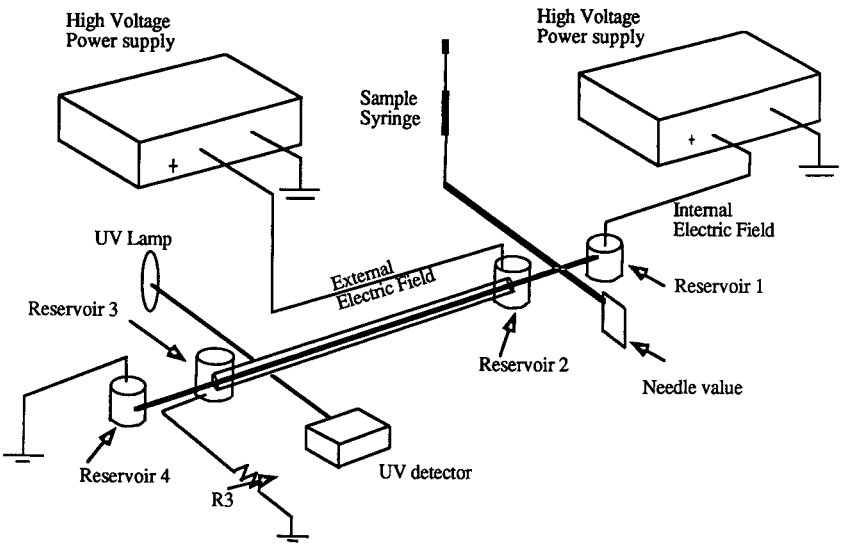

Fig. 2. A complete capillary electrophoresis system with a UV detector delivers the electric fields both externally through the annulus between the inner and outer capillaries and internally across the buffer solution in the inner capillary.

A circulation pump was used to accelerate a fluid flow in the annulus between the inner and outer capillaries. This fluid flow was to enhance the heat transfer in the annulus for removing the additional heat generated by the application of external electric field. Another high-voltage power supply connecting reservoir 1 with reservoir 4 applied a constant inner electric potential of 5.5 kV inside the inner capillary. The inner electric field strength was therefore equal to 5.5 kV/23 cm = 239 V/cm. With adjustable resistor R3, we were able to establish a constant electric potential gradient between the inner and outer electric potential along the 20-cm long annulus between reservoirs 2 and 3. This newly created electric field was perpendicular across the wall of the inner capillary and controlled the zeta potential at the inner capillary/inner aqueous interface. By varying the outer electric field and the resistance of R3, various electric fields (potential gradients) across the inner capillary were generated.

A UV detector from Linear Instruments (Reno, NV, USA) was used for monitoring the change in the direction and rate of the electroosmotic flow on application of an external electric field in the UV marker method [6]. The distance between reservoir 1 and the UV detector was 14.5 cm. An uncharged marker solute (no electrophoretic mobility) such as dimethyl sulfoxide with UV absorbance was selected for this study. Dimethyl sulfoxide was carried through the capillary under the action of only the electroosmotic flow inside the capillary. The changes in the elution time of the front of a 0.1% dimethyl sulfoxide solution from reservoir 1 to the UV detector were recorded as the externally electric field was changed. With this set-up and procedure, we were able to monitor the direction and rate of electroosmotic flow with or without an additional external electric field during the experiment. In addition, the number of theoretical plates, N, with the direct control of electroosmosis was measured from the shape of the front [7].

Sodium phosphate buffer, dimethyl sulfoxide and hydrochloric acid were purchased from Sigma (St. Louis, MO, USA). The pH of the buffer solution was adjusted with 0.1 *M* hydrochloric acid.

RESULTS AND DISCUSSION

The experimental results for the control of electroosmosis inside a 50 μm I.D. × 150 μm O.D. inner capillary tubing with 1 m*M* phosphate buffer (pH 6) were used for comparisons with the predictions obtained from the capacitor model. Details of the calculation of the capacitor model were discussed previously [3]. As shown in Fig. 3, the capacitor mode still failed to predict quantitatively the observed changes in the electroosmotic mobility even with the application of the UV marker method. The positive value of the electroosmotic mobility indicated that the direction of flow was from reservoir 1 to reservoir 4 when the cathode end of inner electric field was at reservoir 4. The experimental error in measuring the change in the electroosmotic flow was about 1–3% for various potential gradients for over five runs.

The zeta potential at the aqueous/inner capillary interface was calculated by using the measured electroosmotic mobility [4]. The zeta potential in the presence of a zero potential gradient (between the outer and inner electric potential) was decreased from −49 to −4 mV by changing the solution conditions from a 1 m*M* phosphate buffer of pH 6 to a 10 m*M* phosphate buffer of pH 2.7. The decrease in the zeta potential was due to the application of a higher ionic strength and a lower pH at the inner capillary/inner aqueous interface [4]. As shown in eqn. 1, the capacitance of the electrostatic diffuse layer decreased with decrease in the zeta potential. However, the use of a higher buffer concentration (10 m*M*) increased the capacitance of the electrostatic diffuse layer. The effect of the buffer concentration was greater than the effect of the zeta potential on the capacitance of the electrostatic diffuse layer, as shown in eqn. 1. Thus, the capacitance of the electrostatic diffuse layer was greater with 10 m*M* phosphate buffer of pH 2.7 than with 1 m*M* phosphate buffer of pH 6. As shown in

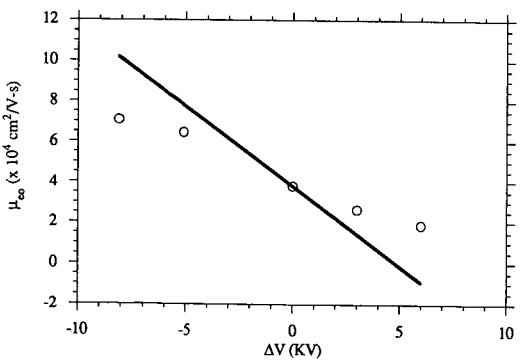

Fig. 3. Plot of electroosmotic mobility, μ_{eo}, against applied potential gradient, ΔV. (○) Experimental data for 1 m*M* phosphate buffer (pH 6) with the use of a 50 μm I.D. × 150 μm O.D. inner capillary tubing in the UV marker method. Solid line, predictions obtained from the capacitor theory. The positive value of electroosmotic mobility indicates that the direction of flow is from reservoir 1 to reservoir 4 when the cathode end of inner electric field is at reservoir 4.

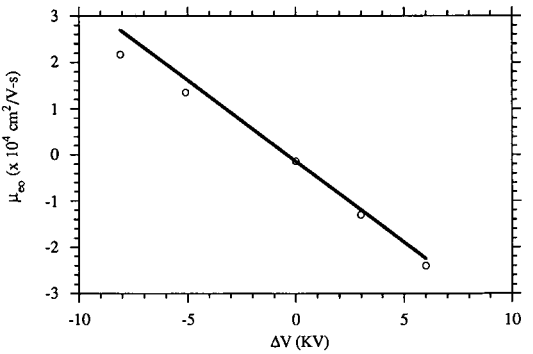

Fig. 4. Plot of electroosmotic mobility, μ_{eo}, against applied potential gradient, ΔV. Details as in Fig. 3 except that 10 m*M* phosphate buffer (pH 2.7) was used.

eqn. 6, the larger capacitance of the electrostatic diffuse layer in the solution of 10 m*M* phosphate buffer at pH 2.7 would result in less control of the electroosmotic flow. This theoretical analysis qualitatively explained why the range of controlled electroosmotic mobility as shown in Fig. 4, between $-2 \cdot 10^{-4}$ and $+2 \cdot 10^{-4}$ $cm^2/V \cdot s$, was less than that as shown in Fig. 3, between $+7 \cdot 10^{-4}$ and $+2 \cdot 10^{-4}$ $cm^2/V \cdot s$. Further, the capacitor model quantitatively predicted the observed changes in the electroosmotic mobility with the application of various potential gradients as shown in Fig. 4. The experimental error in measuring the change in the electroosmotic flow was about 1% for various potential gradients for over five runs. The only significant difference in the solution conditions between the previous study [3] and the experimental results shown in Fig. 4 was the solution pH. At solution pH 2.7, the zeta potential in the presence of a zero potential gradient was -4 mV, close to zero. Was this the reason for achieving relatively good agreement between the experimental results shown in Fig. 4 and the predictions from the capacitor model? To answer this question, the direct control of electroosmosis inside a 25 μm I.D. × 150 μm O.D. inner capillary was investigated under solution conditions of pH 2.7 with 1 and 10 m*M* phosphate buffers.

The experimental results for the control of electroosmosis inside a 25 μm I.D.

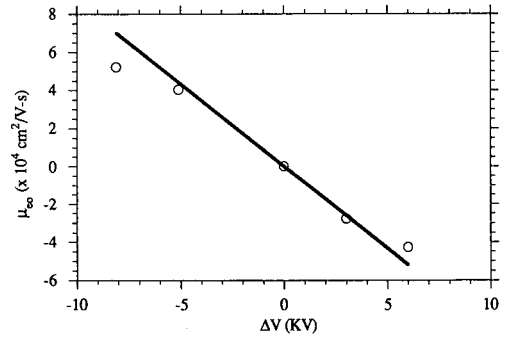

Fig. 5. Plot of electroosmotic mobility, μ_{eo}, against applied potential gradient, ΔV. Details as in Fig. 3 except that the buffer pH was 2.7 and 25 μm I.D. × 150 μm O.D. inner capillary tubing was used.

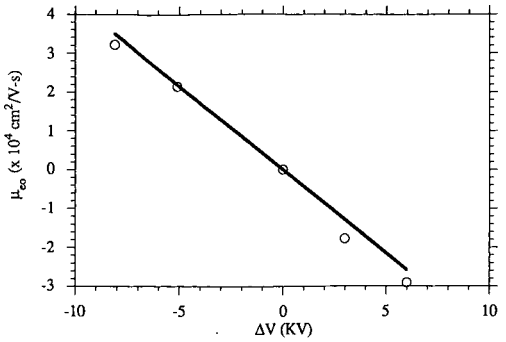

Fig. 6. Plot of electroosmotic mobility, μ_{eo}, against applied potential gradient, ΔV. Details as in Fig. 5. except that the phosphate buffer concentration was 10 mM.

× 150 μm O.D. inner capillary tubing at pH 2.7 with 1 and 10 mM phosphate buffer were used to compare with the predictions obtained from the capacitor model. As shown in Figs. 5 and 6, the capacitor model quantitatively predicted the effectiveness of the applied potential gradient for controlling the electroosmotic flow. The experimental error in measuring the change in the electroosmotic flow was about 1% for various potential gradients for over five runs. The experimental results shown in Figs. 5 and 6 further supported the proposed hypothesis: the use of a lower solution pH for obtaining a smaller zeta potential was essential for achieving relatively good agreement between the experimental results and the predictions from the capacitor model. This conclusion is currently used in efforts to improve the capacitor model as a quantitative model for predicting the effectiveness of the applied external electric field in the direct control of electroosmosis.

The external electric field was applied to the 20-cm long annular space between the inner and outer capillaries filled with the phosphate buffer solution. Only 20 cm of the 23-cm long inner capillary tubing was affected by the external electric field for controlling the electroosmotic flow inside the inner capillary. In this current configuration, the flow disturbance and mixing at the interface between the controlled and

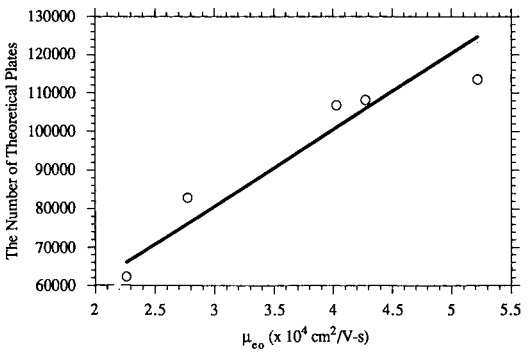

Fig. 7. Plot of number of theoretical plates against the absolute value of the electroosmotic mobility, μ_{eo}, measured from the experiment. (○) Number of theoretical plates measured with 1 mM phosphate buffer (pH 2.7) with the use of a 25 μm I.D. × 150 μm O.D. inner capillary tubing. Solid line, number of theoretical plates calculated from the molecular diffusion.

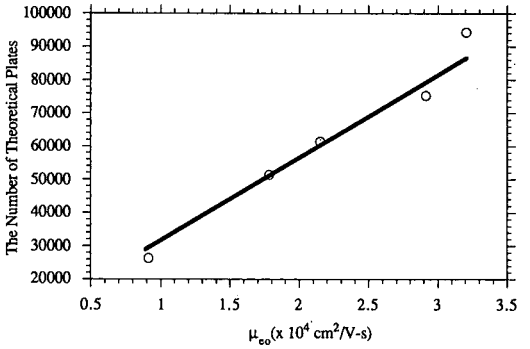

Fig. 8. Plot of number of theoretical plates against the absolute value of the electroosmotic mobility, μ_{eo}, measured from the experiment. Details as in Fig. 7 except that the phosphate buffer concentration was 10 m*M*.

uncontrolled regions in the inner capillary could possibly cause the additional dispersion and band broadening. To investigate this potential problem, frontal analyses of a 0.1% dimethyl sulfoxide in a 25 μm I.D. × 150 μm O.D. inner capillary tubing at pH 2.7 with 1 and 10 m*M* phosphate buffer solutions were studied. As shown in Figs. 7 and 8, the number of theoretical plates measured from the experiment was plotted against the absolute value of the corresponding electroosmotic mobility measured from the experiment. The experimental error in measuring the number of theoretical plates was about 5–10% for various electroosmotic mobilities for over five runs. By assuming that molecular diffusion alone was responsible for zone broadening, the number of theoretical plates was also calculated [8]. A value of 5×10^{-6} cm^2/s was used as the diffusion coefficient of dimethyl sulfoxide in the calculation. The number of theoretical plates obtained from the calculation was then compared with the number of theoretical plates measured from the experiment. As shown in Figs. 7 and 8, the comparisons clearly indicated that there was no measurable additional dispersion and band broadening induced by the direct control of electroosmosis.

ACKNOWLEDGEMENTS

Support for this work by Engineering Research Center of the University of Maryland and Petroleum Research Grant administered by the American Chemical Society is gratefully acknowledged.

REFERENCES

1 X. Huang, M. J. Gordon and R. N. Zare, *Anal. Chem.*, 60 (1988) 1837.
2 C. S. Lee, W. C. Blanchard and C. T. Wu, *Anal. Chem.*, 62 (1990) 1550.
3 C. S. Lee, D. McManigill, C. T. Wu and B. Patel, *Anal. Chem.*, 63 (1991) 1519.
4 R. J. Hunter, *Zeta Potential in Colloid Science: Principles and Applications*, Academic Press, New York, 1981.
5 F. W. Sears, H. D. Zemasky and H. D. Young, *University Physics*, Addison-Wesley, Readings, MA, 1979.
6 T. Tsuda, K. Nomura and G. Nakagawa, *J. Chromatogr.*, 248 (1982) 241.
7 D. McManigill, personal communication, 1990.
8 J. W. Jorgenson and K. D. Lukacs, *Anal. Chem.*, 53 (1981) 1298.

Journal of Chromatography, 559 (1991) 141–152
Elsevier Science Publishers B.V., Amsterdam

CHROM. 23 415

Field amplified sample injection in high-performance capillary electrophoresis

RING-LING CHIEN* and DEAN S. BURGI
Varian Research Center, Varian Associates, Inc., 3075 Hansen Way, Palo Alto, CA 94304 (USA)

ABSTRACT

A simple on-column concentration technique in high-performance capillary electrophoresis (HPCE) is reported. In conventional electro-injection in HPCE, samples are prepared in a buffer solution which has the same concentration as that inside the capillary column. The amount of ions injected into the column under this condition is limited. By preparing samples in a low-conductivity solution, *e.g.*, water, and injecting the sample solution electroosmotically into the column, one can achieve a field enhancement at the injection point. The amount of ions injected will then be proportional to this enhancement factor. However, if one samples by switching the column directly from the high-conductivity buffer reservoir to the low-conductivity sample solution, the buffer boundary at the end of the column is disturbed and the electric field at the injection point might not be amplified properly. By injecting a short plug of water before sample introduction, one can provide a high electric field strength from the beginning of the injection. Several hundred-fold enhancements in the amount of injection were confirmed experimentally.

INTRODUCTION

High-performance capillary electrophoresis (HPCE) has become a major analytical tool for separating charged compounds because of its high resolution capability [1–3]. To preserve the high resolution, samples must be introduced into the capillary column with the minimum volume in a very short time. The small volume of material introduced into the column makes it difficult to detect low concentrations of the material. Therefore, one of the major challenges in HPCE is to improve the injection technique to achieve high sensitivity of detection without sacrificing resolution.

There are a number of methods for injecting a small volume of sample into the column. The two principle techniques are electrokinetic and hydrostatic injection. The electrokinetic injection is performed through pumping activity from the combination of electroosmosis and electrophoresis. A bias towards more positive ions is seen because of the faster ion mobility of the species [4]. The hydrostatic injection is characterized by physically introducing samples into the capillary column and might be referred to as suction, pressure or gravity injection. The hydrostatic injection will increase zone broadening due to laminar flows generated during the injection which can degrade the separation efficiency in HPCE. Comparison of electrokinetic and

0021-9673/91/$03.50

hydrostatic injection shows that each technique has its advantages and disadvantages [5,6]. Nevertheless, the short optical path length demands a high sample concentration in all injection methods.

Several techniques have been reported for performing on-column concentration to enhance the detectability in HPCE. The sample stacking technique, which is well known in electrophoresis [7–9], was first introduced in HPCE by Mikkers *et al.* [2]. In sample stacking, a large plug of sample dissolved in water is introduced hydrostatically into the capillary. The sample ions will form into a narrow band when they migrate into the region with more concentrated background electrolyte. Moring *et al.* [10] reported an increase of a factor of 10 in detectability in HPCE with sample stacking. We have recently studied the optimization of peak variance in sample stacking in an uncoated column. We found that the peak broadening process due to the laminar flow generated by the mismatch of electroosmotic flows between different concentrations is the limiting factor in sample stacking [11].

The second on-column concentration technique is to apply isotachophoresis before HPCE. In an isotachophoretic process, the concentrations of species in their migrating zones will be adjusted to the concentration of the leading electrolyte. Several groups have combined isotachophoresis with zone electrophoresis to achieve an enhancement in signal detectability [12–15]. However, a careful choice of leading, terminating and background electrolytes is required in order to perform this isotachophoretic preconcentration step.

An alternative and simpler method for enhancement of signals is to use electro-injection with samples prepared in a highly diluted buffer or water [4,16–18]. In conventional electro-injection for HPCE, samples are prepared in a buffer solution which has the same concentration as that used in the separation. The amount of ions injected into the column under this condition is limited. However, if the sample is prepared in a diluted buffer, which has the same composition as the background buffer inside the column, an enhanced electric field strength at the injection point will exist as the high voltage is applied. This field amplified sample injection, first used in zone electrophoresis in a glass powder column by Haglund and Tiselius [16], can yield a large enhancement in the amount of ions injected into the column.

However, manipulation of the column during the injection process can produce a physical disturbance at the end of the capillary which causes improper field amplification at the injection point. In this paper, we propose the injection of a short plug of water into the column prior to sample introduction to insure proper field amplification. This field amplified sample injection with water plug can give a 100-fold enhancement in the amount of ions injected without losing the high resolution feature of HPCE. In addition to this enhancement, we also show that the peak narrowing effect due to sample stacking allows one to inject samples using a higher voltage or a longer injection time. Therefore, another order of signal enhancement compared with conventional electro-injection can be obtained.

THEORY

All of the common phenomenon in electrophoresis are based on the Kohlraush equation [19]. A complete theory of the effect of electrophoretic migration of ions on the concentration distributions in free zone electrophoresis has also been developed by

Mikkers *et al.* [20]. In this paper, we present a simplified model for electro-injection of samples prepared in a low-concentration buffer into a column filled with the same buffer of higher concentration. Our model is based on the electric field strength distributions across a pseudo-stationary boundary resulting from different buffer concentrations [21], the contribution from the sample ions being assumed to be very small.

According to Ohm's law, the local field strengths at the injection end $E^{(i)}$ and the remainder of the column $E^{(c)}$ are given by

$$E^{(i,c)} = \frac{\rho^{(i,c)}E_0}{\rho^{(i)}x + \rho^{(c)}(1-x)} \tag{1}$$

where $E_0 = V/L$ is the field strength of a uniform system with voltage V applied across the column length L, x is the ratio of the length of the low ionic strength region inside the capillary column with respect to L and $\rho^{(i)}$ and $\rho^{(c)}$ are the resistivities in their respective regions.

In general, if different buffers have the same composition and the sample concentration is very low, the resistivity is simply inversely proportional to the buffer concentration as

$$\frac{\rho^{(i)}}{\rho^{(c)}} = \frac{C_b^{(c)}}{C_b^{(i)}} \equiv r \tag{2}$$

where $C_b^{(i)}$ and $C_b^{(c)}$ are the buffer concentrations at the injection point and in the column, respectively. For a sample prepared in water or highly diluted buffer, the effect of impurities and sample ions on the total resistivity also has to be considered.

Substituting eqn. 2 into eqn. 1, we obtain

$$E^{(i)} = \frac{rE_0}{rx + (1-x)} \tag{3}$$

and

$$E^{(c)} = \frac{E_0}{rx + (1-x)} \tag{4}$$

For a short injection time such that $x \ll 1$ and $rx \ll 1$, the electric field in the column changes very little from the original uniform field and the electric field at the injection point is enhanced by the factor r, thus, $E^{(c)} = E_0$ and $E^{(i)} = rE_0$. In the case of very large r such that $x \ll 1$ but $rx \gg 1$, eqns. 3 and 4 give $E^{(c)} = 0$ and $E^{(i)} = (1/x)E_0$. The field enhancement at the injection end is inversely proportional to the plug length of the low-concentration buffer.

The total amount of ion species i injected into the column is given by

$$N_i = \int_0^t AC_i^{(i)}[v_{eo}(t) + v_{epi}(t)]dt \tag{5}$$

where $C_i^{(i)}$ is the concentration of ion species i in the sample reservoir, A is the cross-sectional area of the capillary, t is the length of injection time, v_{epi} is the electrophoretic velocity for ion species i and v_{eo} is the electroosmotic velocity of the bulk solution. The electrophoretic velocity for ion species i at the injection point is the product of its electrophoretic mobility and the local electric field at that point, *i.e.*, $v_{epi} = \mu_{epi}E^{(i)}$. On the other hand, the velocity of the bulk solution during injection changes by only a small amount from the electroosmotic velocity of the pure buffer system, *i.e.*, $v_{eo} = \mu_{eo}E_0$, where μ_{eo} is the electroosmotic mobility of the high-concentration buffer inside the column [21]. Thus, for $E^{(i)} > E_0$, the ions will probably be injected more rapidly into the colunn than the neutral solution.

To calculate the total ions and the plug length injected into the column using eqn. 5, a complete knowledge of the concentration distribution and the dependence of v_{eo}, $E^{(i)}$ and $E^{(c)}$ with respect to the injection time t is required. For a short injection time and very low sample concentration, those parameters could be assumed to be constant, as mentioned earlier. Hence, we can rewrite eqn. 5 as

$$N_i = C_i^{(i)}A(v_{eo} + v_{epi})t$$

$$= C_i^{(i)}A(\mu_{eo} + r\mu_{epi})E_0t \tag{6}$$

where we use the approximation $v_{epi} = r\mu_{epi}E_0$.

If the electrophoretic velocity is much faster than the electroosmotic velocity at the injection point, some of the sample ions will soon pass the buffer concentration boundary and move into the low-field region. Once the sample ions pass the concentration boundary, they will slow down and stack together to a higher concentration. Inside the capillary column, the injected sample ions themselves will now distribute into two different concentrations in the two regions separated by the buffer concentration boundary. In the region limited by the electroosmotic flow, the sample ions have the same concentration as in the original solution $C_i^{(i)}$. In the region past the concentration boundary, the sample ion concentration $C_i^{(c)}$ is enhanced by the same factor r, thus, $C_i^{(c)} = rC_i^{(i)}$ [22]. Eqn. 6 can now be written as

$$N_i = C_i^{(i)}AX_i^{(i)} + C_i^{(c)}AX_i^{(c)} \tag{7}$$

where $X_i^{(i)} = \mu_{eo}E_0t$ and $X_i^{(c)} = \mu_{epi}E_0t$ are the plug lengths of sample ions in low and high buffer concentration regions, respectively.

After sample injection, the end of the column is returned to the buffer reservoir and a high voltage is applied to perform separation. The electric field distribution inside the column follows eqn. 1. The ion species i in the plug of low-concentration region will eventually all migrate into the high-concentration region and stack together into a single zone with concentration $C_i^{(c)}$. Accordingly, eqn. 7 changes to

$$N_i = C_i^{(c)}AX_i \tag{8}$$

Neglecting the diffusion, the effective plug length, or the width of the sample zone during separation, for ion species i can be obtained from eqns. 6 and 8 as

$$X_i = (\mu_{eo}/r + \mu_{epi})E_0t \tag{9}$$

For large r, the contribution from the electroosmotic flow can be neglected and the effective plug length is simply proportional to the electrophoretic mobility.

On the other hand, the plug length using conventional electro-injection is

$$X_i = (\mu_{eo} + \mu_{epi})E_0 t \tag{10}$$

If μ_{eo} is larger than μ_{epi}, the plug length will then be dominated by the electroosmotic flow in conventional HPCE.

Comparing eqns. 9 and 10, we can see that the effective sample plug length using field amplified sample injection is narrower than the plug length using conventional electro-injection because of the stacking effect. Consequently, one can further enhance the sample introduction under the enhanced field by injecting much longer in time or at a higher voltage without much peak broadening from the longer plug length.

We have assumed that the effect of sample ions on the conductivity of the water plug and the column buffer is negligible. This is usually true for sample concentrations less than 10^{-5} M; however, for higher sample concentrations, the field enhancement factor is reduced and the assumption is no longer valid. In addition, we have assumed that the conductivities of the water plug and the sample buffer are constant during sample injection. This is obviously not true as the migration of co-ions and counter ions causes a change in either the conductivity and/or pH, which further complicates our model. A full-scale computer simulation will be necessary to perform an accurate calculation [20,23–25]. However, the simple model allows us to made several predications which are supported by experimental data.

EXPERIMENTAL

Instrumentation

Experiments were performed using an in-house constructed CE system similar to that reported by Jorgenson and Lukacs [3]. Electrophoresis was carried out in a 100 cm × 75 μm I.D. × 365 μm O.D. fused-silica capillary column (Polymicro Technologies, Phoenix, AZ, USA). A high-concentration electrolyte was supplied to the capillary column from a reservoir at the inlet end. A reservoir at the outlet end of the column collects the leaving electrolyte. Two more reservoirs were used for sample introduction, one filled with low-concentration electrolyte or water and the other with the sample solution prepared in the low-concentration electrolyte or water.

A laboratory-made electronic box was connected to the back of a high-voltage power supply (Glassman, Whitehouse Station, NJ, USA) to control the voltage between injection (−5kV) and separation (−30 kV). The high-voltage end of the power supply was connected to a platinum wire dipped into the reservoir filled with a high-conductivity buffer at the outlet end of the column. The ground end of the power supply was connected to a platinum wire at the inlet end of the column and dipped into the reservoir filled with a low-concentration electrolyte or the reservoir filled with the sample solution during injection. After sample introduction, this ground electrode end and the inlet end of the column were both dipped into the reservoir with a high-concentration buffer. The high voltage was then switched to −30 kV and the separation began.

Detection was accomplished by on-column absorption using a high-perfor-

mance liquid chromatographic UV detector (Varian, Palo Alto, CA, USA). The distance from the injection point to the detector was held at 75 cm. In addition to the optical signal, we also monitored the electrophoresis current by measuring the voltage drop across a 10-kΩ resistor in series with the capillary column. Both the optical and electrical signals were then sent to a two-channel analog-to-digital converter board in a Compaq 386 computer. Data were collected and analyzed first by the Varian LC/STAR system and converted later to ASCII files for further processing by computer programs written in-house.

Chemical and electrolytes

To reduce heating effects, a buffer of 2-N-(morpholino)ethanesulfonic acid (MES) and histidine (HIS) at pH 6.2 was chosen for our study. A stock solution of 100 m*M* with respect to both MES and HIS was prepared. A stock solution containing 2.1 mg PTH-arginine and 2.0 mg PTH-histidine in 10 ml of water was prepared. The sample solution was further diluted to about 10^{-4}, 10^{-5} or 10^{-6} *M*, respectively, in both water and MES–HIS buffer. All reagents were purchased from Sigma (St. Louis, MO, USA).

RESULTS AND DISCUSSION

According to eqn. 2, the enhancement factor could easily be several hundred if one injects the sample ions prepared in water, which has very high resistivity, into the column filled with 100 m*M* MES–HIS buffer. However, a much smaller than prediced signal enhancement is usually found when one switches the column directly between the high-conductivity buffer reservoir and the low-conductivity aqueous sample solution. It is possible that during sampling the buffer boundary at the end of the column is disturbed and the electric field at the injection point may not be amplified properly. By injecting a short plug of low-concentration buffer or water before sample introduction, one definitely establishes a high electric field at the injection point from the very beginning of injection.

Fig. 1 compares electropherograms obtained using three different injection methods: (a) conventional electro-injection with $5 \cdot 10^{-5}$ *M* sample dissolved in 100 m*M* MES–HIS buffer; (b) field amplified injection with sample dissolved in water; (c) field amplified injection with a water plug in front of the sample–water. All three injections were done at −5 kV for 10 s. Peaks A and B in Fig. 1 are the two positive ions, PTH-arginine and PTH-histidine, respectively. Peak C is the neutral species and water signal. It is evident from our electropherograms that we achieved a large field enhancement at the injection point. Table I lists the peak heights of these two ions using various injection techniques; the results are normalized to the gravity injection. A two orders of magnitude signal enhancement is obtained for positive ions using field amplified sample injection with a water plug compared with the use of conventional electro-injection.

It is well known that electro-injection will introduce bias in the amount injected. As a reference, Fig. 2 shows the resulting electropherogram using gravity injection. Comparison of Figs. 1 and 2 clearly shows the bias in the amount of PTH-arginine ions relative to PTH-histidine ions. Table II lists the ratio of peak heights normalized to gravity injection of PTH-arginine to PTH-histidine ions using various electro-injections. The expected bias factor is also listed in Table II.

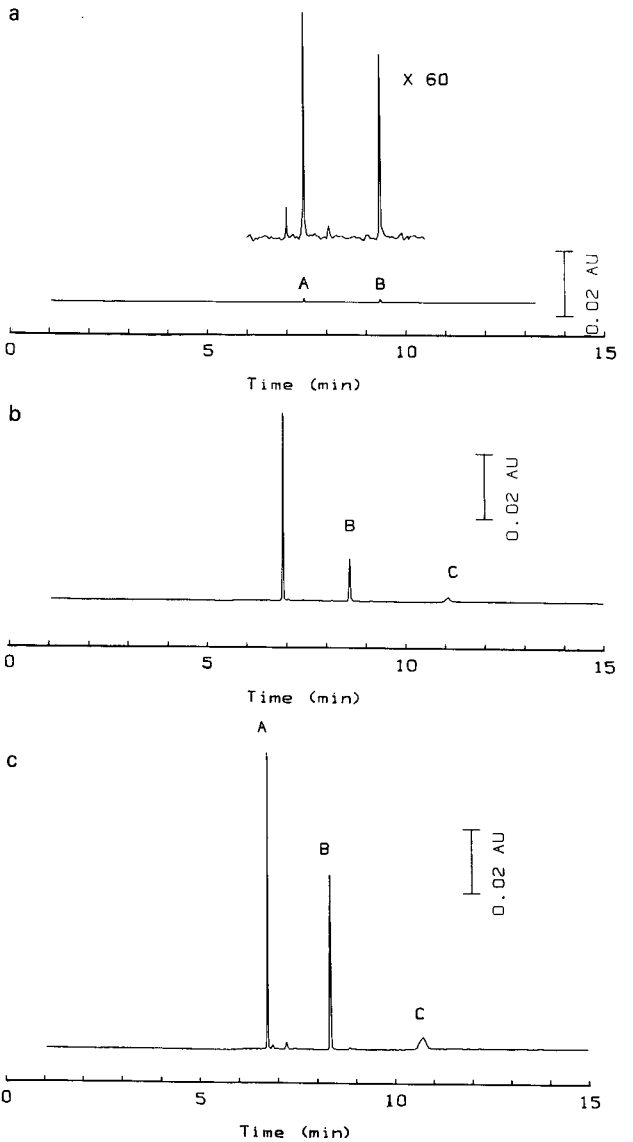

Fig. 1. (a) Electropherogram using conventional electro-injection. The column was filled with 100 m*M* MES–HIS buffer and the sample prepared in 100 m*M* MES–HIS buffer was injected into the column at −5 kV for 10 s. (b) Electropherogram using electro-injection as (a) except the sample was prepared in water. (c) Electropherogram using field amplified sample injection: a short plug of water was injected into the column first by gravity and the sample prepared in water was then injected into the column at −5 kV for 10 s. All experiments were operated with a −30-kV separation voltage. Peaks A, B and C correspond to PTH-arginine, PTH-histidine and neutral marker, respectively.

In conventional electro-injection, this bias factor is proportional to the inverse of the retention time [4]. In field amplified sample injection, as the electroosmotic velocity is much smaller than the electrophoretic velocity during injection, the bias factor is

TABLE I

COMPARISON OF PEAK HEIGHTS FOR PTH-ARGININE AND PTH-HISTIDINE IONS USING VARIOUS INJECTION METHODS

All peaks are normalized with respect to the gravity injection.

Method	PTH-arginine	PTH-histidine
Gravity injection	1	1
Conventional electro-injection sample in 100 m*M* MES–HIS	0.311	0.225
Field amplified sample injection without a water plug in front of the sample	16.96	3.38
Field amplified sample injection with a water plug in front of the sample	28.04	13.44

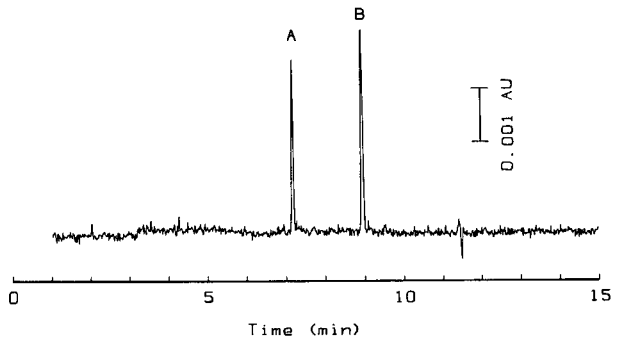

Fig. 2. Electropherogram using gravity injection. The sample prepared in 100 m*M* MES–HIS buffer was injected into the column by raising the sample reservoir to 7.6 cm high for 10 s.

directly proportional to the electrophoretic mobility, which can be calculated from the difference in retention times of sample ions and the neutral marker. Comparison of columns 2 and 3 shows good agreement between theoretical and experimental bias factors for conventional electro-injection and for field amplified sample injection with

TABLE II

COMPARISON OF BIAS FACTORS BETWEEN PTH-ARGININE AND PTH-HISTIDINE IONS USING VARIOUS INJECTION METHODS

Method	Peak A/peak B[a]	Calculated bias factor
Conventional electro-injection sample in 100 m*M* MES–HIS	1.37	1.26[b]
Field amplified sample injection without a water plug in front of the sample	5.02	2.06[c]
Field amplified sample injection with a water plug in front of the sample	2.09	2.06[c]

[a] Ratio of peak heights is normalized with respect to the gravity injection results.
[b] Calculated from the ratio of retention times.
[c] Calculated from the electrophoretic mobilities.

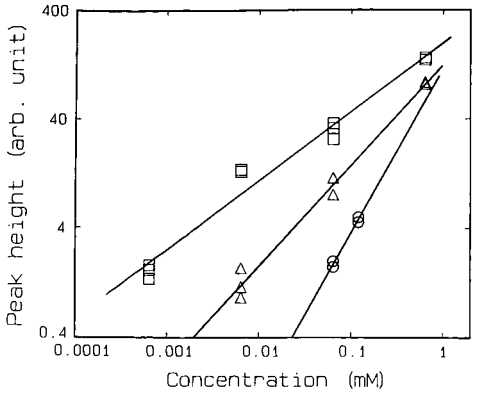

Fig. 3. Peak height of PTH-arginine ions as a function of sample ion concentration. ○ = Results from conventional electro-injection; △ = results from electro-injection with samples prepared in water; □ = results from field amplified sample injection with a short plug of water ahead of the sample.

a water plug. However, a large discrepancy exists in the bias factor for field amplified sample injection without a water plug. An obvious reason is that a large amount of arginine ions, which has an higher mobility, stacks up at the concentration boundary at the inlet of the column when there is no water plug. This high concentration of injected arginine ions will decrease the local electric field at the injection point. Consequently, the amount of injected histidine ions which has a smaller mobility will be reduced. By introducing a water plug before sample injection, we provide not only a high field strength at the injection point, but also a void region for injecting the sample.

Similarly, the sample ion concentration also has an effect on the signal enhancement. Fig. 3 shows the peak height of PTH-arginine ions at various concentrations with three different injection methods. At high concentration, the conductivity of the sample will decrease the effective electric field strength and reduce the signal enhancement. By lowering the sample concentration, an order of magnitude improvement in detection limit is obtained between field amplified sample injection without a water plug and conventional electro-injection. Another order of magnitude improvement in detection limit is obtained between field amplified sample injection with and without a water plug. Instead of $1 \cdot 10^{-5}$ M for conventional electro-injection, the detection limit for PTH-arginine is now less than $1 \cdot 10^{-7}$ M using electro-injection with a water plug.

Field amplified sample injection not only introduces a large amount of ions into the capillary column, it will also perform on-column concentration at the same time. Eqns. 9 and 10 predict that the effective injected plug length of sample ions will be even shorter than using conventional electro-injection. For a rectangular injection profile, the peak variance, σ_i, due to the effective plug length from injection, is equal to $X_i^2/12$. The total variance of a peak is then given by

$$\sigma_t^2 = \sigma_d^2 + \sigma_i^2 \tag{11}$$

where σ_d^2 is the variance due to diffusion, $2Dt$. If the final observed peak shape is

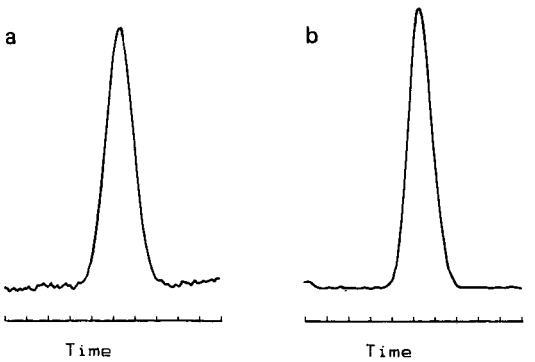

Fig. 4. Comparison of peak shape of PTH-arginine signals between using (a) conventional electro-injection and (b) field amplified sample injection, both at 5 kV for 10 s.

Gaussian, the $X_{1/2}$ (full width at half-maximum) of the peak is equal to $(5.545)^{1/2}\sigma_t$. Substituting $X_{1/2}$ and eqn. 9 or 10 into eqn. 11, we obtain

$$X_{1/2}^2 = 5.545[\sigma_d^2 + (\mu' E_0 t)^2/12] \tag{12}$$

where $\mu' = (\mu_{eo}/r + \mu_{epi})$ in field amplified sample injection and $\mu' = (\mu_{eo} + \mu_{epi})$ in conventional injection. The spatial width of a peak can also be converted to the temporal width by using

$$t_{1/2} = X_{1/2}(t_m/L_d) \tag{13}$$

where t_m is the retention time of the peak and L_d is the column length to the detector.

Eqn. 12 shows that in the case of a short injection time, the peak width in both field amplified sample injection and conventional injection will approach the diffusion limited value. As the injection time increases, the peak width in conventional injection will increase much faster than in field amplified injection. Fig. 4 is a comparison of peak shape of PTH-arginine signals between using conventional electro-injection and field amplified sample injection, both at -5 kV for 10 s. As the ratio of the absolute

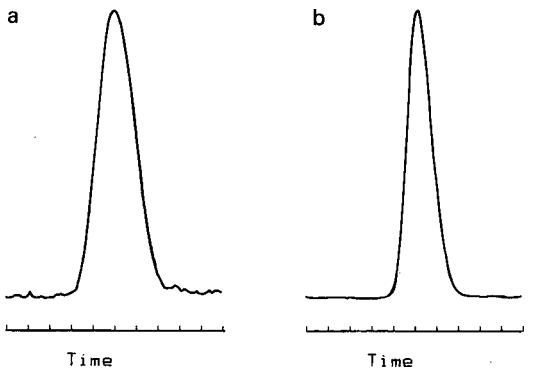

Fig. 5. Comparison of peak shape of PTH-arginine signals between using (a) conventional electro-injection and (b) field amplified sample injection, both at -5 kV for 30 s.

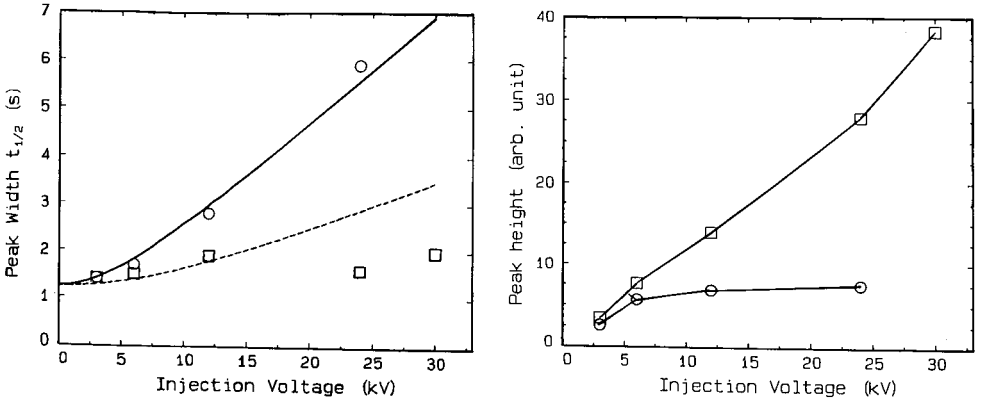

Fig. 6. Full width at half-maximum of PTH-arginine peaks as a function of the injection voltage for (○) conventional electro-injection and (□) field amplified sample injection. The solid and dashed lines were calculated using eqn. 12.

Fig. 7. Peak height of PTH-arginine peaks as a function of the injection voltage for (○) conventional electro-injection and (□) field amplified sample injection. The sample concentration in field amplified sample injection experiments is an order of magnitude lower than that in conventional electro-injection so that the peak heights are of the same order of magnitude at low voltage.

signal differs by two orders of magnitude, both peaks are normalized to their respective peak maxima. The result shows that the $t_{1/2}$ of the peak drops from 1.5 s in conventional injection to the diffusion limited peak width of 1.3 s in field amplified sample injection. As the injection time is increased to 30 s, the $t_{1/2}$ in conventional injection increases rapidly to 2.0 s as expected, while the $t_{1/2}$ in field amplified sample injection remains at 1.3 s as shown in Fig. 5. Figs. 4 and 5 clearly show that one can achieve an even larger enhancement in signal detectability while preserving high resolution just by using a longer injection time.

In addition to a longer injection time, we can also use a higher injection voltage. Fig. 6 shows the plot of $t_{1/2}$ of PTH-arginine signal peaks *vs.* the injection voltage for both conventional injection and field amplified sample injection. The solid and dashed lines are the results for conventional injection and field amplified sample injection, respectively, obtained from eqn. 12 with the mobilities calculated from the retention times. Once again, the $t_{1/2}$ in conventional injection increases rapidly from 1.4 s at 3 kV to 5.9 s at 24 kV. The $t_{1/2}$ in field amplified sample injection, on the other hand, increases very slowly at first from the diffusion-limited value of 1.3 s at 3 kV to 1.8 s at 12 kV. Then, surprisingly, the peak width decreases to 1.5 s as injection voltage increases to 24 kV. We believe that this extra narrowing effect, which is similar to isotachophoresis, is probably due to changes in buffer conductivity at high sample concentration. In field amplified sample injection at high voltage, a tremendous amount of sample ions moves into the running buffer and tries to stack up in front of the water boundary. As the sample concentration becomes higher, the local conductivity of the stacking region will increase, which causes a further decrease in the electric field strength. Consequently, the leading edge of the sample region will slow down more and further enhance the stacking effect.

As the peak width remains very narrow, the peak height will increase accordingly

as one injects more samples into the column. Fig. 7 shows the peak height *vs.* the injection voltage for PTH-arginine ions using both conventional injection and field amplified sample injection. The sample concentration in field amplified experiments is an order of magnitude lower than that in conventional electro-injection so the peak heights are of the same order of magnitude at low voltage. While the conventional injection shows a saturation in peak height beginning around 5 kV, field amplified sample injection shows a continuous increase in the peak height. Another order of magnitude increase in signal enhancement is obtained by using an injection voltage of 30 kV compared with the normal 3-kV injection.

In conclusion, simple on-column concentration in HPCE is achieved using field amplified sample injection. Large amounts of sample ions can be injected into the capillary column while the high resolution feature of HPCE is retained. In addition, only a small amount of neutral plug is introduced into the column, which means that the peak broadening caused by the laminar flow originated from the mismatch of electroosmotic velocities is minimized. By injecting a short plug of water before sample introduction, the minimum detectable concentration of sample injected is of the order of 10^{-8} *M*. This sensitivity is now comparable to the best results obtained from high-performance liquid chromatography.

REFERENCES

1 S. Hjertén, *Chromatogr. Rev.*, 9 (1967) 122.
2 F. E. P. Mikkers, F. M. Everaerts and Th. P. E. M. Verheggen, *J. Chromatogr.*, 169 (1979) 11.
3 J. W. Jorgenson and K. D. Lukacs, *Anal. Chem.*, 53 (1981) 1298.
4 X. Huang, M. J. Gordon and R. N. Zare, *Anal. Chem.*, 60 (1988) 375.
5 E. Grushka and R. M. McCormick, *J. Chromatogr.*, 471 (1989) 421.
6 D. J. Rose and J. W. Jorgenson, *Anal. Chem.*, 60 (1988) 642.
7 S. Hjertén, S. Jerstedt and A. Tiselius, *Anal. Biochem.*, 11 (1965) 219.
8 L. Ornstein, *Ann. N.Y. Acad. Sci.*, 121 (1964) 321.
9 R. J. Wieme, in E. Heftmann (Editor), *Chromatography*, Reinhold, New York, 1967, p. 210.
10 S. E. Moring, J. Colburn, P. D. Grossman and H. H. Lauer, *LC·GC*, 8 (1989) 34.
11 D. S. Burgi and R.-L. Chien, *Anal. Chem.*, 63 (1991) in press.
12 F. M. Everaerts, Th. P. E. M. Verheggen and F. E. P. Mikkers, *J. Chromatogr.*, 169 (1979) 21.
13 S. Hjertén, K. Elenbring, F. Kilar, J. Liao, A. J. C. Chen, C. J. Siebert and M. Zhu, *J. Chromatogr.*, 403 (1979) 47.
14 F. Foret, V. Sustacek and P. Bocek, *J. Microcolumn Sep.*, 2 (1990) 229.
15 V. Dolnik, K. A. Cobb and M. Novotny, *J. Microcolumn Sep.*, 2 (1990) 127.
16 H. Haglund and A. Tiselius, *Acta Chem. Scand.*, 4 (1950) 957.
17 L. Gross and E. S. Yeung, *J. Chromatogr.*, 480 (1989) 169.
18 B. M. Michov, *Electrophoresis*, 10 (1989) 686.
19 F. Kohlrausch, *Ann. Phys. Chem.*, 62 (1897) 209.
20 F. E. P. Mikkers, F. M. Everaerts and Th. P. E. M. Verheggen, *J. Chromatogr.*, 169 (1979) 1.
21 R.-L. Chien and J. C. Helmer, *Anal. Chem.*, 63 (1991) 1354.
22 R.-L. Chien and D. S. Burgi, *J. Chromatogr.*, 559 (1991) 153.
23 M. Bier, O. A. Palusinski, R. A. Mosher and D. A. Saville, *Science (Washington, D.C.)*, 219 (1983) 1281.
24 R. A. Mosher, D. Dewey, W. Thormann, D. A. Saville and M. Bier, *Anal. Chem.*, 61 (1989) 362.
25 G. O. Roberts, P. H. Rhodes and R. S. Snyder, *J. Chromatogr.*, 480 (1989) 35.

Journal of Chromatography, 559 (1991) 153–161
Elsevier Science Publishers B.V., Amsterdam

CHROM. 23 430

Field-amplified polarity-switching sample injection in high-performance capillary electrophoresis

RING-LING CHIEN* and DEAN S. BURGI
Varian Research Center, Varian Associates, Inc., 3075 Hansen Way, Palo Alto, CA 94304 (USA)

ABSTRACT

In conventional electro-injection in high-performance capillary electrophoresis, although one is able to inject both positive and negative ions into the column, the number of negative ions injected is rather limited because of their movement against the electric field, assuming the column wall is negatively charged. If one simply reverses the polarity of the field, the electroosmotic flow will deter all positive and most of negative ions from injecting into the column. In the case of field-amplified sample injection, where samples are prepared in a low-conductivity buffer and injected electrically into the column, the number of positive ions injected is porportional to the field enhancement factor at the injection point. The negative ions will not be enhanced, but will be pushed away from the column by this high field strength. However, since the electroosmotic velocity of the bulk solution is much slower than the electrophoretic velocity of sample ions under the enhanced field, one can inject and concentrate both positive and negative ions into the column by switching the polarity of the electrodes at the proper time. Furthermore, one can also achieve selected charge discrimination.

INTRODUCTION

High-performance capillary electrophoresis (HPCE) has become a major analytical technique for separating charged compounds [1–3]. In HPCE, a high voltage is applied across a fused-silica capillary column filled with an electrolytic buffer. Charged species introduced at one end of the column migrate under the influence of the electric field to the other end of the column. The migration velocity of a particular ion species is a combination of the electrophoretic velocity of that species and the bulk electroosmotic velocity of the buffer. In many cases, depending on the column properties and the buffer conditions, the electrophoretic velocity is much less than the electroosmotic velocity. The net movement of the ions is in the same direction as the electroosmotic flow; generally positive ions migrate ahead of the neutral compounds followed by the negative ions.

One of the most interesting properties of HPCE is the electroomotic flow. The electroomotic force in a capillary column is produced by an electric field and transmitted by the drag of ions acting in a thin sheath of charged fluid adjacent to the silica wall of the column. The origin of the charge in the sheath is an unbalance between

0021-9673/91/$03.50

positive and negative ions in the bulk solution which balances a fixed charge on the silica wall thus generating a zeta potential ζ.

While the electrophoretic velocity of ionic species is simply the product of their electrophoretic mobilities and the electric field strength acting on them, the analysis of the electroosmotic velocity of the bulk solution is rather complicated. In columns where the electric field strength E and the zeta potential are constant throughout the whole column, the bulk electroosmotic velocity, v_{eo} can be expressed as $\mu_{oe}E$, where $\mu_{oe} = \varepsilon\zeta/4\pi\eta$ is called the electroosmotic mobility and ε is the dielectric constant and η is the viscosity of the buffer. However, in the case where there is a non-constant distribution in either field strength or zeta potential, the bulk electroosmotic velocity has to be averaged over all different local electroosmotic velocities weighted by the distribution factor [4–6]. This special property of electroosmotic flow in the averaging process turns out to be very useful in sample introduction, especially in field-amplified sample injection.

For conventional electro-injection in HPCE, samples are prepared in a buffer solution which has the same concentration as that used in separation. The number of ions, both positive and negative, injected into the column under this condition is rather limited. To increase the number of ions introduced into the column, the sample can be prepared in a highly diluted buffer or water, and then injected by electro-injection into the column. Because of the high resistivity of the sample solution, an enhancement in the electric field strength is set up at the injection point [7,8]. This field-amplified sample injection, first used in zone electrophoresis in a glass powder column by Haglund and Tiselius [9], can yield several hundred fold enhancement in the number of ions injected in HPCE [10–12]. In addition, the difference in the field strength distributions will casue injected sample ions stack into a narrow band once they migrate into the region of high-concentration buffer.

In the absence of electroosmotic flow, one can achieve sample enhancement for either positive or negatieve ions by simply choosing the proper polarity of electrodes. However, field-amplified sample injection only works for one type of ions if there is an electroosmotic flow. Under normal polarity, where the electroosmotic flow is toward the outlet of the column, the high field strength at the injection point will push away ions which have a negative mobility with respect to the electroosmotic flow. With reversed polarity, although the high field strength will pull the negative ions into the column, they will be carried out immediately from the injection end by the electroosmotic flow during sample injection.

Nevertheless, the electroosmotic velocity of the solution is a bulk property and has to be averaged over the whole column. As a result, it changes insignificantly from the pure buffer system during sample injection and is much slower than the electrophoretic velocity of sample ions under the enhanced field [6]. Therefore, by introducing a short plug of water prior to sample injection and selecting the proper polarity of the electrodes, one can inject and concentrate either positive or negative ions into the capillary column using field-amplified sample injection. Furthermore, if one switches polarities *during* the injection procedure at the proper time, an enhanced sample injection of both negative and positive ions under amplified conditions can be accomplished. This report will describe and present the experimental results of both charge discrimination sample enhancement injection and field-amplified polarity-switching injection.

EXPERIMENTAL

The experimental apparatus is very similar to the one described by Jorgenson and Lukacs [3]. Electrophoresis was carried out in a 100 cm × 365 μm O.D. × 75 μm I.D. fused-silica capillary column (Polymicro Technologies, Phoenix, AZ, USA). We used two power supplies in the system: one for injection, ±5 kV (Tennelec, Oak Ridge, TN, USA), the other for separation, −30 kV voltage (Glassman, Whitehouse Station, NJ, USA). The high-voltage end of the injection power supply, which can be switched between ±5 kV, was connected to a platinum wire dipped into the reservoir filled with low-concentration electrolyte or the reservoir filled with the sample solution. This power supply was connected to the system only during sample injection.

After sample injection, the ground end of the power supply for separation was connected to a platinum wire dipped into the reservoir filled with high conductivity at the inlet end of the column. The high-voltage end of the power supply, which was set at −30 kV, was connected to a platinum wire dipped into the reservoir at the outlet end of the column.

Chemical and electrolytes

To minimize Joule heating effects, a buffer of 2-N-(morpholine)ethanesulfonic acid (MES) and histidine (HIS) at pH 6.2 was chosen for our study. A stock solution of 100 m*M* with respect to both MES and HIS was prepared. Four amino acids, two positive ions: phenylthiohydantion (PTH)-arginine, PTH-histidine, and two negative ions: PTH-aspartic acid, PTH-glutamic acid, were chosen to illustrate our technique. A stock solution contained 2.1 mg PTH-arginine, 2.0 mg PTH-histidine, 2.8 mg PTH-aspartic acid and 3.2 mg PTH-glutamic acid in 10 ml of water was made. The sample was then diluted down to about $5 \cdot 10^{-5}$ *M* in both water and 100 m*M* MES–HIS. All reagents were purchased from Sigma (St. Louis, MO, USA).

RESULTS AND DISCUSSION

Charge discrimination enhanced injection

It is well known in electrophoresis that one can achieve sample enhancement by preparing the sample in a highly dilute buffer or water. Fig. 1 is a schematic diagram showing our experimental procedures for positive ion injection. A short plug of water is introduced into the capillary column before sample injection to establish enhanced electric field. The sample, which is dissolved in water, is then injected electro-kinetically into the column under this enhanced field. Once the positive ions reach the concentration boundary, they slow down and stack into a narrow band. Two to three orders of signal enchancement have been achieved using field amplified sample injection [12]. Fig. 2a and b compare the electropherograms of our sample solution using conventional electro-injection and field amplified sample injection. The absorbance unit in Fig. 2b is 100 times the unit in Fig. 2a. Peaks A and B in Fig. 2 are the two positive ions, PTH-arginine and PTH-histidine, respectively. Peak C is the neutral and water signal. Peaks D and E in Fig. 2a are the two negative ions, PTH-aspartic acid and PTH-glutamic acid, respectively.

In the conventional electro-injection, although there is a large bias against negative ions, they still can migrate into the column as long as the absolute value of their

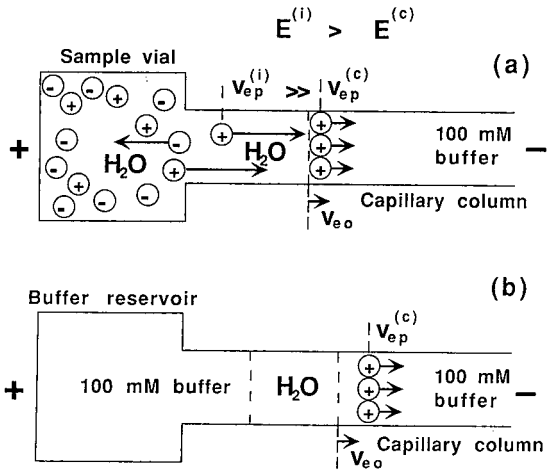

Fig. 1. A schematic diagram showing field-amplified sample injection for positive ions only: A short plug of water is introduced into the column before sample injection to set up the high field strength. (a) The sample prepared in water is then injected into the column using a positive voltage with respect to the other end of the column. (b) After sample injection, the inlet end of the column is switched into the high concentration buffer to start the separation process. $E^{(i)}$ is the electric field strength and $v_{ep}^{(i)}$ is the electrophoretic velocity of the ions at the injection end. $E^{(c)}$ and $v_{ep}^{(c)}$ are the field strength and electrophoretic velocity in the rest of column. v_{eo} is the averaged electroosmotic velocity of the bulk solution.

mobility is smaller than the electroosmotic mobility [10]. Fig. 2a shows that a small number of negative ions are detected using conventional electro-injection. When the sample is prepared in water, there is an enhanced electric field strength at the injection point. The negative ions in the sample solution are now pushed away from the column by this high field strength. Fig. 2b shows no detection of negative ions in field-amplified sample injection. For comparison, a electropherogram without sample bias using gravity injection is shown in Fig. 3.

To inject only negative ions into the uncoated column under the enchanced field strength, a plug of water is introduced into the column first by raising the water reservoir up to 15 cm for 30 s. After the water plug is injected, the inlet end of the column is then switched from the water reservoir to the fourth reservoir containing the sample dissolved in the water. A -5 kV with respect to the outlet end of the column is applied for 10 s at the inlet causing negative ions to electro-migrate into the column. A subtle difference in injecting the negative ions is that the water (or low concentration buffer) plug is now moving out of the column from the injection end. Consequenlty, the length of this water plug should be long enough such that some of it remains inside the column at the end of the sample injection time. A schematic diagram showing the negative ion injection is displayed in Fig. 4. The positive ions will be pushed away from the column during injection under the reversed polarity. A very effective charge discrimination signal-enhanced injection is achieved.

After sample injection, the column is then switched back to high-concentration buffer and the separation voltage with the normal polarity is applied to the column. The bulk solution and the sample plug now migrate toward the detector and the negative ions migrate back toward the injection end as shown in Fig. 4b. Once the

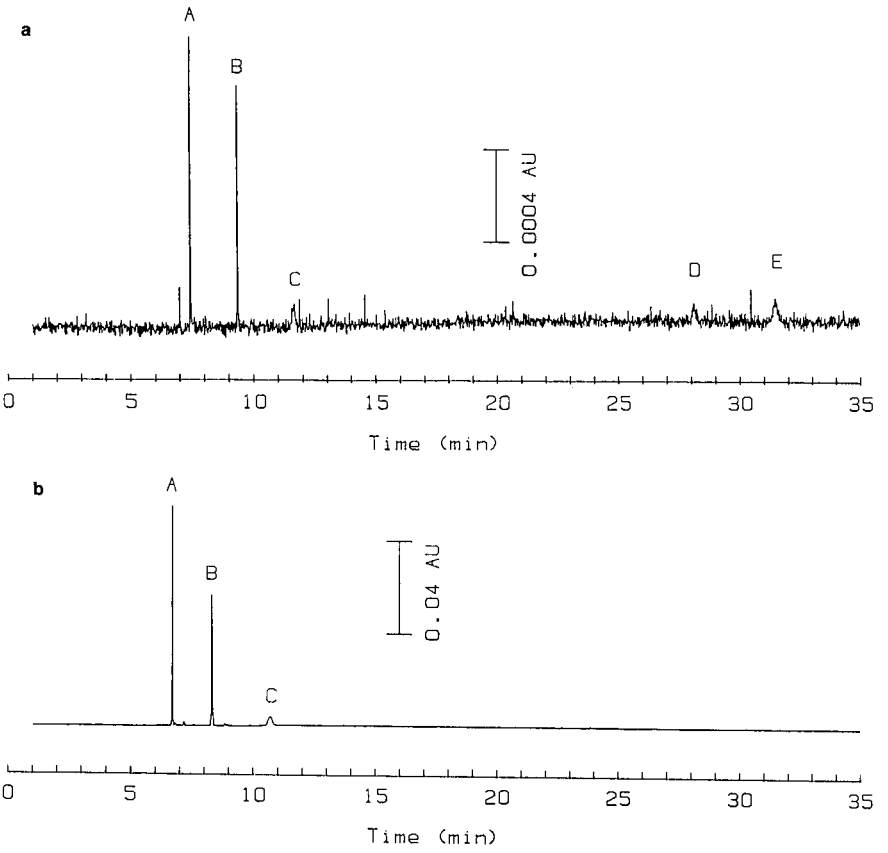

Fig. 2. (a) Electropherogram using conventional electro-injection: column was filled with 100 m*M* MES–HIS buffer, sample was also prepared in 100 m*M* MES–HIS buffer, −5 kV injection voltage for 10 s, −30 kV separation voltage; (b) electropherogram using field-amplified sample injection: experimental conditions are the same as in (a) except the sample was prepared in water. Peaks A, B, C, D and E correspond to PTH-arginine, PTH-histidine, neutral marker, PTH-aspartic acid and PTH-glutamic acid, respectively.

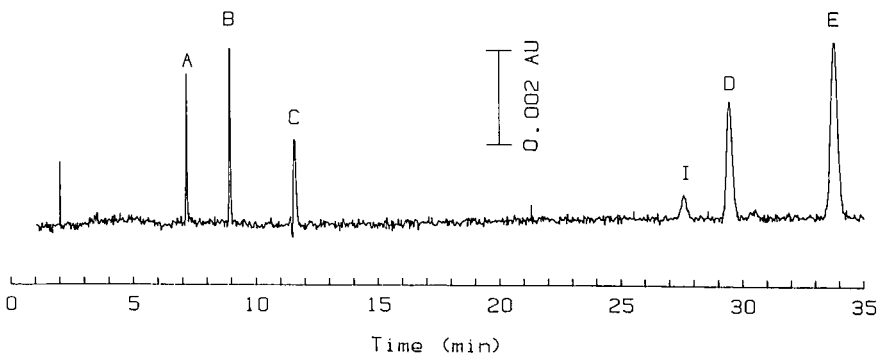

Fig. 3. Electropherogram using gravity injection. The experimental conditions are the same as described in Fig. 1. Peak I is the impurity.

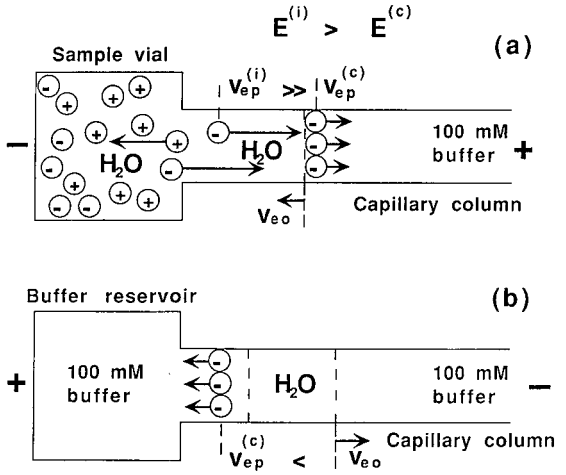

Fig. 4. A schematic diagram showing field-amplified sample injection for negative ions only. (a) A short plug of water is introduced into the column before sample injection, the sample prepared in water is then injected into the column using a negative voltage with respect to the other end of the column. (b) After sample injection, the inlet end of the column is transferred into the high concentration buffer and the polarity of the electrodes is switched back to normal setting to start the separation process.

negative ions reach the high-concentration region, they will experience the normal field strength and slow down into a narrow band. If the absolute value of their electrophoretic mobility is smaller than the value of the bulk electroosmotic mobility, the negative ions in the low electric field region will change direction again and be pushed passed the detector at the outlet end of the column.

Fig. 5 shows the electropherograms resulting from the charge discrimination injection of our sample solution. It shows large enhanced negative ion signals, peaks D and E, with no detection of positive ions. Compared with conventional electro-injection shown in Fig. 2a, a factor of 500 in signal enhancement for negative ions is observed. Also note that the impurities, peaks I in Fig. 5, are concentrated so they are now detectable whereas in conventional electro-injection, Fig. 2a, these compounds are not seen.

Field-amplified polarity-switching injection

Field-amplified sample injection described above only works for one type of ion, either positive or negative ions depend on the electrode configuration. By switching the polarity of the electrodes at proper times during injection, one can manage to inject and concentrate both positive and negative ions into the column. This process is shown schematically in Fig. 6.

In field-amplified polarity-switching injection, samples of both positive and negative ions are prepared in the low-conductivity buffer. We first inject, either by gravity or by electro-injection, a plug of low-conductivity buffer of water into the column before sample introduction. Then, a large number of positive ions can be injected into the column under a positive high voltage with respect to the outlet end of the column for a time period t_1 as described earlier. We then switch the voltage to the

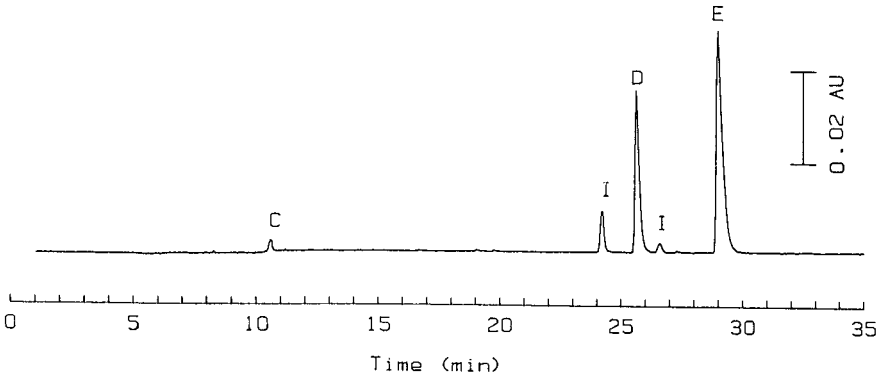

Fig. 5. Electropherogram using field-amplified sample injection with reversed polarity. The experimental conditions are the same as described in Fig. 1. A small amount of neutral molecules (C) and large negative ion peaks (D en E) were detected, no detection of positive ions. Two small peaks (I) are the impurities inside the sample solution which are barely detectable in gravity injection.

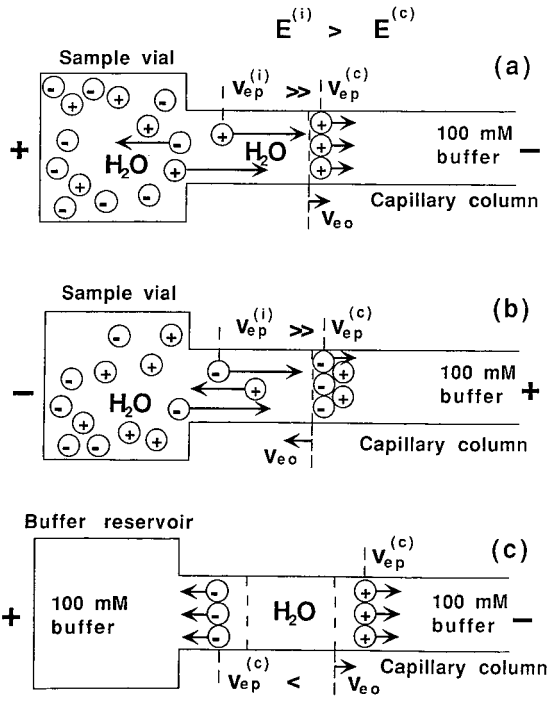

Fig. 6. A schematic diagram showing field-amplified polarity-switching injection. (a) A short plug of water is introduced into the column before sample injection. The positive ions are injected into the column first using a positive voltage with respect to the other end of the column. (b) The negative ions are then injected using reversed polarity. (c) After sample injection, the inlet end of the column is transferred into the high concentration buffer and the polarity of the electrodes is switched back to normal setting to start the separation process.

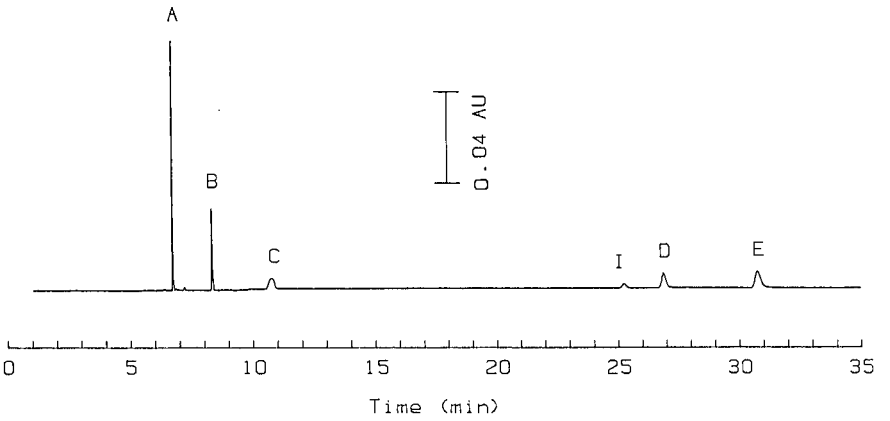

Fig. 7. Electropherogram using field-amplified polarity-switching injection. Both positive and negative ions were detected.

opposite polarity and cause the electroosmotic flow to migrate in the opposite direction and cause some of the positive ions to flow out of the column. However, since the electric field at the injection end of the column is very high, the negative ions which now have a very high electrophoretic velocity will overcome the electroosmotic flow and migrate into the column as we decribed earlier in charge discrimination injection. This reversed polarity can last for a shorter period of time t_2 such that part of the positive ions will remain inside the column.

After injection of both positive and negative ions, the inlet end of the column is switched back into the high conductivity buffer reservoir. The polarity of the high voltage is also switched back to the normal setting and the separation process begins. Both positive and negative sample ions will now migrate rapidly into the high-concentration regions, at opposite ends of the water plug and stack into narrow bands.

TABLE I

COMPARISON OF PEAK HEIGHTS FOR BOTH POSITIVE AND NEGATIVE IONS USING VARIOUS INJECTION METHODS

All peaks are normalized with respect to the gravity injection.

	PTH-Arginine	PTH-Histidine	PTH-Aspartic acid	PTH-Glumatic acid
Gravity injection	1	1	1	1
Conventional electro-injection sample in 100 m*M* MES–HIS	0.311	0.225	0.025	0.022
Field-amplified sample injection: positive ions only	28.04	13.44	0	0
Field-amplified sample injection: negative ions only	0	0	13.66	12.58
Field-amplified polarity-switching injection: both positive and negative ions	32.03	9.28	2.58	1.96

Different time programming schemes could be used to inject both positive and negative ions. One could also reverse the procedure, inject negative ions first then positive ions later.

Fig. 7 shows an electropherogram of the $5 \cdot 10^{-5}$ *M* sample mixture using 20 s -5 kV injection followed by 10 s $+5$ kV injection. A short water plug is also introduced into the column by raising the water reservoir up to 15 cm for 30 s prior to sample injection. All four ion peaks, two positive and two negative, are observed. Although one can also obtain signals of both positive and the negative ions using conventional electro-injection, the number of ions injected, especially negative ions, is greatly enhanced in field-amplified polarity-switching injection. Table I shows the comparison between peak heights normalized to the gravity injection for various electro-injection methods.

In conclusion, we have shown a rather simple electro-injection technique to concentrate *both* positive and negative ions into an uncoated column while retaining the high resolution in HPCE. Several orders of magnitude in signal enhancement was confirmed. In addition, selected charge discrimination was demonstrated, which might be very useful in real-life samples.

REFERENCES

1 S. Hjertén, *J. Chromatogr. Rev.*, 9 (1967) 122.
2 F. E. P. Mikkers, F. M. Everaerts and Th. P. E. M. Verheggen, *J. Chromatogr.*, 169 (1979) 11.
3 J. W. Jorgenson and K. D. Lukacs, *Anal. Chem.*, 53 (1981) 1298.
4 R. J. Wieme, in E. Heftmann (Editor), *Chromatography*, Reinhold, New York, 1967, p. 210.
5 S. Hjertén, *J. Chromatogr.*, 347 (1985) 191.
6 R.-L. Chien and J. C. Helmer, *Anal. Chem.*, 63 (1991) 1354
7 S. Hjertén, S. Jerstedt and A. Tiselius, *Anal. Biochem.*, 11 (1965) 219.
8 F. E. P. Mikkers, F. M. Everaerts and Th. P. E. M. Verheggen, *J. Chromatogr.*, 169 (1979) 1.
9 H. Haglund and A. Tiselius, *Acta Chem. Scand.*, 4 (1950) 957.
10 X. Huang, M. J. Gordon and R. N. Zare, *Anal. Chem.*, 60 (1988) 375.
11 L. Gross and E. S. Yeung, *J. Chromatogr.*, 480 (1989) 169.
12 R.-L. Chien and D. S. Burgi, *J. Chromatogr.*, 559 (1991) 141.

Journal of Chromatography, 559 (1991) 163–181
Elsevier Science Publishers B.V., Amsterdam

CHROM. 23 458

Optimization and evaluation of the performance of arrangements for UV detection in high-resolution separations using fused-silica capillaries

G. J. M. BRUIN, G. STEGEMAN, A. C. VAN ASTEN, X. XU, J. C. KRAAK and H. POPPE*
Laboratory for Analytical Chemistry, Nieuwe Achtergracht 166, 1018 WV Amsterdam (Netherlands)

ABSTRACT

The evaluation of arrangements for UV measurements in fused-silica capillaries as applied in, *e.g.*, high-performance capillary electrophoresis, capillary liquid chromatography and hydrodynamic chromatography is described. The various designs are characterized with respect to sensitivity, noise, linearity, contribution to the peak width and sensitivity to refractive index effects. Some guidelines are formulated, based on theoretical and experimental observations, in order to maximize the performance. A cell with a focusing lens in front of the capillary resulted in a higher sensitivity and linear range than a cell with an adjustable aperture width. With the U-cell, having a design which is comparable to Z-shaped cells and having a longer longitudinal light path, a substantial increase in signal-to-noise ratio was achieved. Some applications of the UV cells are shown.

INTRODUCTION

Detectors for capillary electrophoresis and other miniaturized techniques have been given much attention in recent years as a direct consequence of the demand for sufficient sensitivity in high-resolution separation techniques such as high-performance capillary electrophoresis (HPCE) [1], capillary liquid chromatography [2,3] and hydrodynamic chromatography (HDC) in packed columns [4] or open capillaries [5].

The most important requirements for designs of detection cell suitable for capillary separation methods are well known, *i.e.*, a small contribution to the peak width and a sufficiently low detection limit. UV detection has remained the most popular detection principle, although the sensitivity is low compared with other detection modes developed for capillary separation systems, such as electrochemical [6], mass spectrometric [7] and fluorimetric [8] detection. The latter methods are only available in research institutes so far.

In HPCE, UV detection is mostly applied in the "on-column" mode and the detection limits are in the 10^{-5}–10^{-6} mol l^{-1} range [9,10] as a result of the short available light path, the inside diameter of the capillary. In HPCE, this value usually does not exceed 100 μm. One of the first reports dealing with the evaluation of UV detectors was from Wahlbroehl and Jorgenson [9]. In their experimental set-up, the

0021-9673/91/$03.50

reference and sample light beams passed through 100-μm pinholes. They found concentration detection limits of $8.6 \cdot 10^{-7}$ mol l^{-1} for isoquinoline and $2.8 \cdot 10^{-7}$ mol l^{-1} for lysozyme. Further, an increase in noise was observed after applying a high voltage, probably caused by vibrations of the capillary. A UV cell with an adjustable aperture width was described by Wang *et al.* [10]. Determination of the linear range resulted in an upper limit of about $3 \cdot 10^{-3}$ mol l^{-1} and a concentration detection limit of $3 \cdot 10^{-5}$ mol l^{-1} for acetophenone in acetonitrile at 240 nm.

Grant and Steuer [11] presented a novel way to extend the path length for UV absorbance into the millimetre range by illuminating along the column axis. By adding a fluorescent marker to the background electrolyte, the indirect measurement of the incident light beam can be monitored a few millimetres from the outlet of the column.

Theoretical optimization of cell designs was done by Bruno *et al.* [12]. They used a three-dimensional ray tracing algorithm, which simulates the optical phenomena at the air–glass and glass–liquid interfaces. This enabled them to choose optical fibre dimensions for a given choice of capillary inside and outside diameters. The experimental use of optical fibres in capillary zone electrophoresis (CZE) with UV detection was also demonstrated by the same group [13] and by Foret *et al.* [14].

Chervet *et al.* [15] have shown the usefulness of a Z-shaped longitudinal capillary flow cell for capillary liquid chromatography (LC) and HPCE. The Z-cell is constructed as part of the capillary by bending a small section into a Z-shape. The path length of the cell is dependent on the length of the chosen template and that of the detector configuration. Recently, they demonstrated the use of this type of cell with a light path of 2–3 mm for the CZE separation of some nucleosides and peptides [16]. They found a sixfold improvement in signal-to-noise ratio and a loss in plate number ranging from 11 to 33% compared with on-column detection.

In this work, a comparison has been made between different UV flow cells for HPCE, *i.e.*, a cell with an adjustable aperture width, a cell with a focusing sapphire lens just in front of the capillary and a U-cell with a light path of 8 mm. Also, a comparison was made between two commercially available UV detectors with focusing lenses.

The following aspects of the performance of the cells were studied: sensitivity, upper limit of the linear range, concentration detection limit and linear range; sensitivity for refraction index changes; and contribution to peak broadening.

THEORY

UV absorption in cylindrical cells

The transmission of light through a cylindrical cell can be calculated as described by Hjertén [17] in 1967. He used the calculations to check the performance of UV detection in wide-bore capillaries (3 mm I.D., 7.8 mm O.D.). The following assumptions were made: no refraction and reflection of the light; monochromatic UV light; uniform intensity of the incident light beam; and 100% collection of transmitted light by the photocell.

Considering the Lambert–Beer law for every infinitely small liquid element (see Fig. 1) with path length $l (= 2\sqrt{r^2 - x^2})$ and integration of the intensity to x leads to the following expression for the transmission in the cell:

$$T = \frac{N}{N_0} = \frac{1}{2s} \int_{-s}^{s} \exp(-2\,\varepsilon'\, c\, \sqrt{r^2 - x^2})\, dx \qquad (1)$$

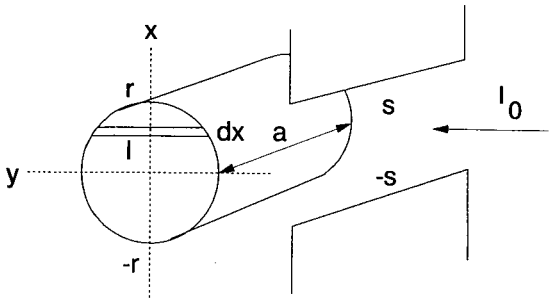

Fig. 1. Schematic representation of an on-column cell with adjustable aperture width. r = Radius of the capillary; s = half the aperture width.

where T is the transmission, N_0 is the number of photons per second that leave the cell in the case of no absorption, N is the number of photons when absorption takes place, r is the capillary radius, ε' is ln 10 times the molar absorptivity, s is half the slit width, c is the concentration and x is the position relative to the capillary centre. When $2\varepsilon' c \sqrt{r^2 - x^2} \ll 1$, eqn. 1 can be approximated as

$$T = \frac{1}{2s} \int_{-s}^{s} (1 - 2\,\varepsilon'\,c \sqrt{r^2 - x^2})\,\mathrm{d}x \tag{2}$$

This integral can be found:

$$\begin{aligned} T &= 1 - \varepsilon'\,c \left[\sqrt{r^2 - s^2} + \frac{r^2}{s} \cdot \arcsin\left(\frac{s}{r}\right) \right] \\ &\approx \exp\left\{ -\varepsilon'\,c \left[\sqrt{r^2 - s^2} + \frac{r^2}{s} \cdot \arcsin\left(\frac{s}{r}\right) \right] \right\} \end{aligned} \tag{3}$$

Eqn. 3 is a good approximation when the absorbance is <0.1. In that case, the effective absorbance, being equal to $-\log T$, can be written as

$$A = \varepsilon\,c \left[\sqrt{r^2 - s^2} + \frac{r^2}{s} \cdot \arcsin\left(\frac{s}{r}\right) \right] \tag{4}$$

When the aperture width is adjusted to the inside diameter of the capillary ($s = r$), the effective light path is

$$l_{\mathrm{eff}} = \frac{1}{2}\,\pi\,r \tag{5}$$

For absorbances >0.1, eqn. 1 cannot be rewritten as eqn. 2, but the integral can be obtained numerically using a computer program, such as Mathcad (version 2.5; Mathsoft). An example of this exercise is shown in Fig. 2. The theoretical calibration graphs for uracil ($\varepsilon = 6980$ l mol^{-1} cm^{-1}, $\lambda = 234$ nm) in a 50 μm I.D. capillary are

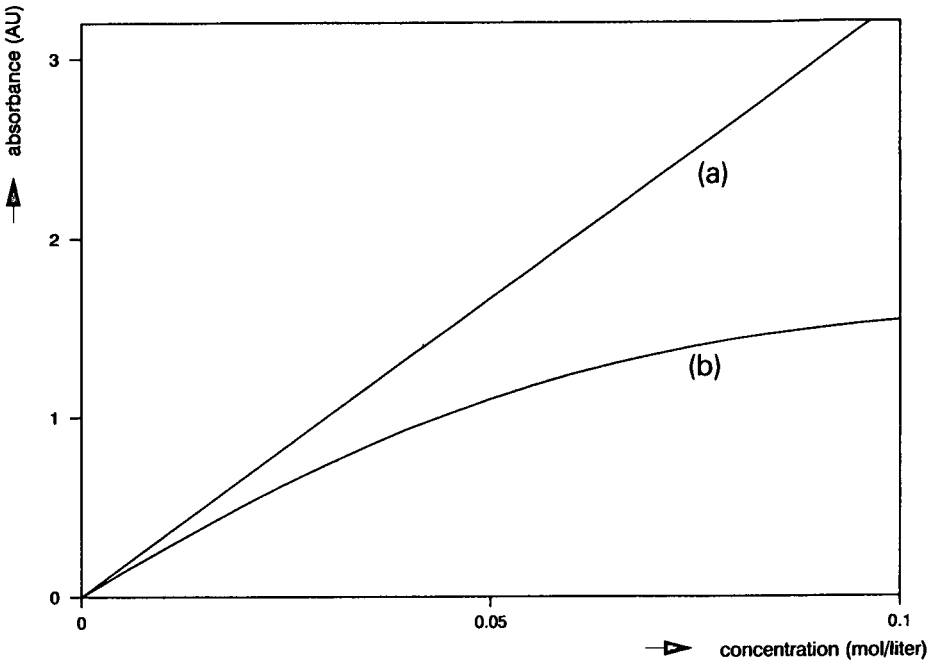

Fig. 2. Theoretical calibration graphs at different aperture widths. Capillary I.D., 50 μm. ε (uracil, 254 nm) = 6980 l mol^{-1} cm^{-1}. (a) Aperture width = 25 μm; (b) aperture width = 50 μm.

plotted against the concentration for two aperture widths, (a) 25 and (b) 50 μm. For an aperture width of 25 μm the sensitivity is higher as a result of the longer effective light path compared with an aperture width of 50 μm. The linearity of the calibration graph is also better because the shape of the cell approximates a rectangle. Further analysis of these results indicates that eqn. 2 can be used instead of eqn. 1 for absorbances <0.3.

When the aperture width has a value between the outside and inside diameters of the capillary, a fraction of the incident light beam does not take part in the absorption process at all. This light also reaches the photocell and degrades the sensitivity. Now, the total number of photons reaching the photocell per second can be expressed as

$$N = I_0\, a \int_{-r}^{r} \exp(-2\,\varepsilon'\, c\, \sqrt{r^2 - x^2})\, dx + 2\, I_0\, a \int_{r}^{s} dx \tag{6}$$

The transmission T can be written as

$$T = \frac{N}{N_0} = \frac{s - r}{s} + \frac{1}{2s} \int_{-r}^{r} \exp(-2\,\varepsilon'\, c\, \sqrt{r^2 - x^2})\, dx \tag{7}$$

In Fig. 3 the theoretical absorbance as a function of the aperture width is given. An increase in the absorbance with decreasing aperture width can be observed. At a width larger than the inside diameter of the capillary, the increase can be explained by

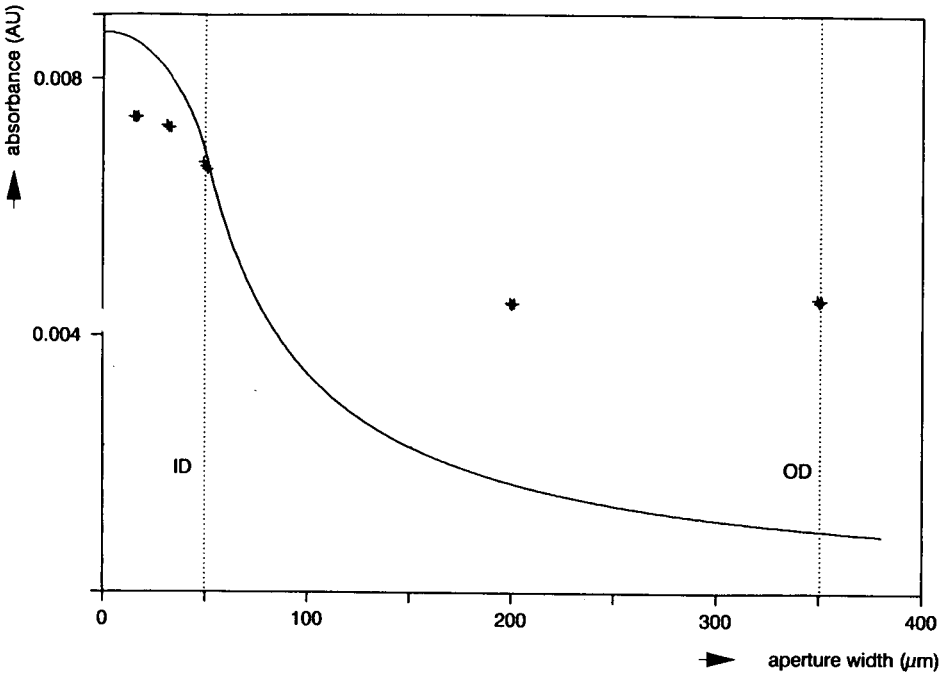

Fig. 3. Measured absorbance at various aperture widths (+) compared with the theoretical values (solid line). Capillary: 50 μm I.D., 350 μm O.D. Uracil concentration = $2.5 \cdot 10^{-4}$ *M*.

the fact that a larger fraction of the light is affected by the absorption process. The experimental values (+) will be discussed later.

Calculation of fraction of light that passes the detection window

Eqn. 7 can be rewritten as

$$T = \alpha + (1 - \alpha)\frac{1}{2r}\int_{-r}^{r} \exp(-2\,\varepsilon'\,c\,\sqrt{r^2 - x^2})\,dx \tag{8}$$

where α is the fraction of light that does not strike the liquid. α can be written as

$$\alpha = \frac{2s - 2r}{2s} \tag{9}$$

For small absorbances (*e.g.*, <0.3), this can be simplified to

$$T = \alpha + (1 - \alpha)T^* \tag{10}$$

where T^* is described by eqn. 3. Eqn. 10 would also be a good approximation for non-uniform light distributions.

We can express α as

$$\alpha = \frac{10^{-A} - 10^{-A^*}}{1 - 10^{-A^*}} \tag{11}$$

where A^* is the absorbance when all the light strikes the liquid and A the measured absorbance. If $10^{-A^*} \ll 10^{-A}$, or in other words when the absorbance of a compound is high, α can be calculated using

$$\alpha = 10^{-A} \tag{12}$$

This means that the value of α can be determined with a simple experiment.

Noise

For a good description of the performance of a detector, the signal-to-noise ratio is an important aspect to consider. Baumann [18] presented a theoretical treatment of signal, noise and signal-to-noise ratio for various types of detectors. He concluded that if the aperture width is decreased (or in other words the number of photons per second reaching the photocell becomes smaller), the relative noise level becomes higher as a result of shot noise.

Light refraction and reflection in cylindrical cells

In the theoretical treatment as described above, changes in the light intensity caused by reflection and refraction are neglected. Hjertén [17] pointed out that reflection losses are very small. Only at the outer edge of the capillary, where the angle of incidence is high, significant light reflection can occur.

Refraction can have a more significant impact. Light rays entering the detection window between the centre and the inside diameter of the capillary will not undergo much refraction. For light entering the capillary between the inside and outside diameters, the capillary glass wall works as a converging lens. Refraction and probably reflection can have a strong influence on the absorbance signal. To study these phenomena, a computer simulation can be a valuable tool. In the program developed in our laboratory, different parameters can be varied to optimize a certain cell configuration, *e.g.*, the distance from the focusing lens to the capillary, the inside and outside diameters of the capillary, the aperture width and the refraction index of the medium.

Some results of simulation are given in Fig. 4A–E for a cell with an adjustable aperture width and a cell with a focusing lens. It can be observed easily, on comparing Fig. 4A, B and C, that only at small aperture widths refraction and reflection can be neglected in the absorption calculations. This indicates that the assumptions made in the theoretical treatment of UV absorption in cylindrical cells are not always valid, *e.g.*, in the situation depicted in Fig. 4C.

When a sapphire lens is used to focus the light in the liquid flow, the performance of this type of cell depends strongly on the outside diameter of the capillary and the distance between the lens and the capillary (see Fig. 4D and E).

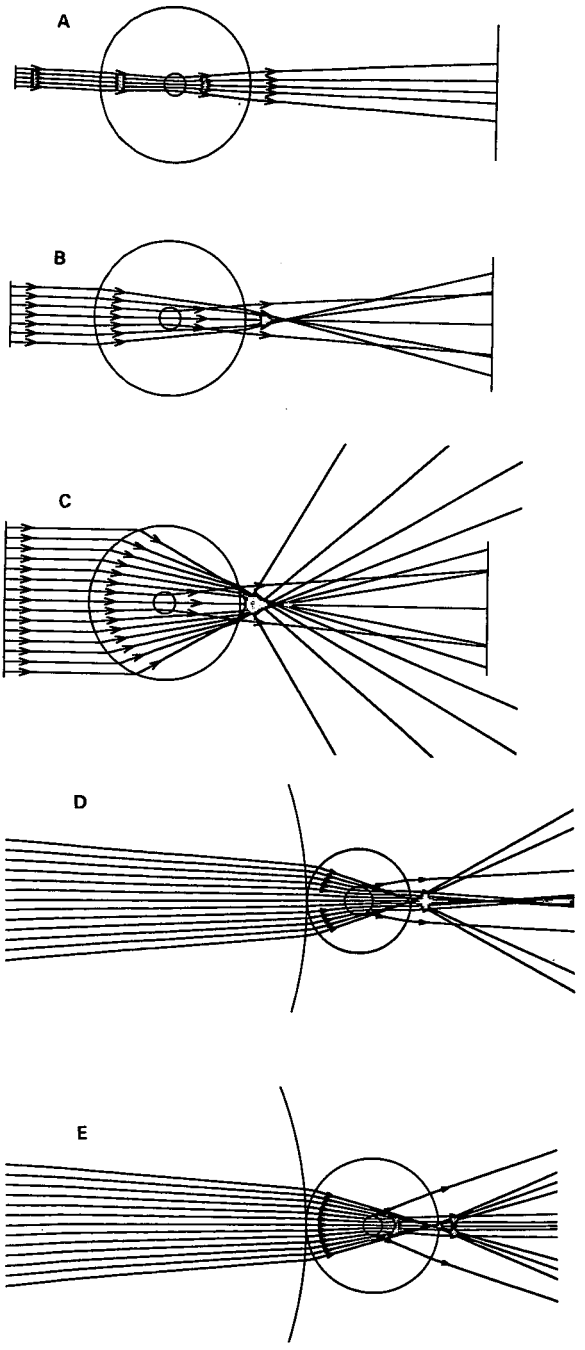

Fig. 4. Light refraction through cylindrical UV detection cells. Capillary: 50 μm I.D., 350 μm O.D. Cell A: (A) aperture width = 50 μm; (B) aperture width = 145 μm; (C) aperture width = 350 μm. Cell B: (D) capillary 75 μm I.D., 275 μm O.D.; (E) capillary 50 μm I.D., 350 μm O.D.

EXPERIMENTAL

Schematic diagrams of the four cells tested are depicted in Fig. 5A–D. Cell A is laboratory made and has an adjustable aperture width. The polyimide coating is burned off the capillary to provide an optical window by using an electrically heated wire. The window is cleaned with methanol. The capillary is fixed by sandwiching it between two pieces of metal covered with PTFE. One of the two metal pieces has a groove that retains the capillary in the correct position. Next, the body with the adjustable blades is placed on the connected metal pieces. The adjustment of the aperture width to the desired width can be performed by turning the small screws, which are connected with the blades. This has to be done while the entire cell is placed under a microscope. The length of the aperture along the capillary is 1 mm and the distance from the centre of the capillary to the photocell is 5 mm. The photocell itself has a square shape with an area of 36 mm^2.

Cell B is commercially available (Applied Biosystems, Foster City, CA, USA). It contains a focusing lens with a diameter of 2 mm, which is placed just in front of the optical window of the capillary (Fig. 5B).

Cell C closely resembles the design of cell B holder and is also commercially available (Linear Instruments, Reno, NV, USA). An advantage of this design is that the optical system (including the photocell) is placed outside the main cabinet of the detector, which facilitates thermostating the capillary over nearly the whole length (Fig. 5C).

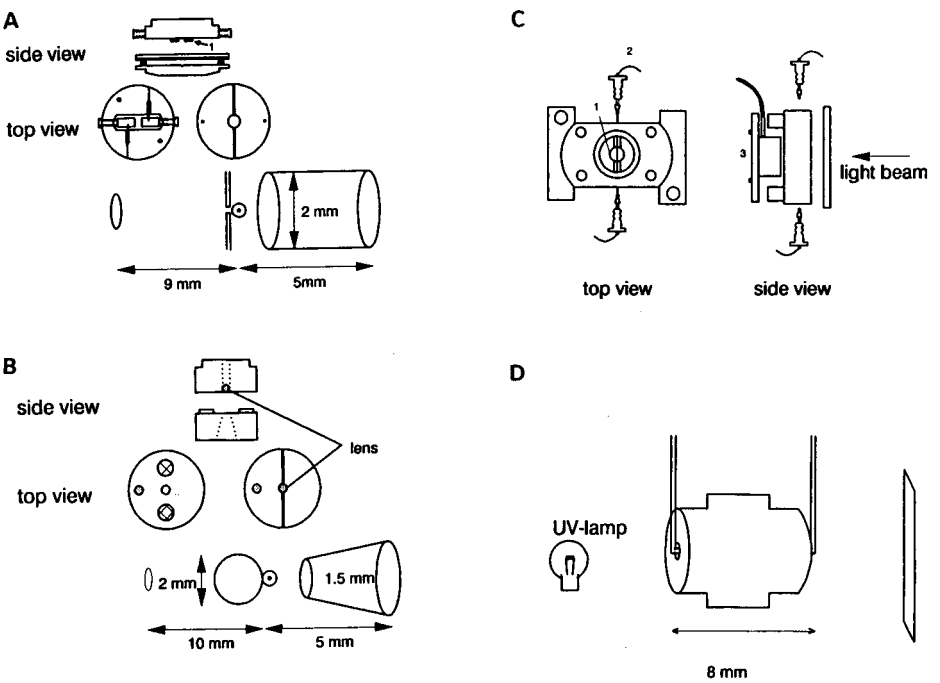

Fig. 5. (A) Scheme of cell A with adjustable aperture width (1). (B) Cell B with focusing lens. (C) Cell C with focusing lens. 1 = Lens; 2 = capillary; 3 = photocell. (D) Cell D (U-cell).

Cell D is the U-cell, custom-designed for use in a commercial detector (Applied Biosystems, Model 747) in cooperation with LC Packings (Amsterdam, Netherlands). It consists of a metal body with a hole along the central axis. The flow cell holder, which has the same outer dimensions as cell B, served as a template to align the capillary flow cell with the optical axis. The diameter of the hole matches the outside diameter of the inserted capillary, which is bent into a U-configuration. The bending of fused-silica tubing has been described elsewhere [19]. This design results in much longer path lengths, being 8 mm for the cells tested (Fig. 5D).

Two commercial UV detectors were used (Applied Biosystems, Model 757, and Linear Instruments, Model 203). The filter rise time of the UV detectors was 1 s in all the experiments.

All capillaries were supplied by Polymicro Technologies (Phoenix, AZ, USA). The calibration graphs for the different cell designs were constructed for uracil as test compound. Uracil was chosen because it has a broad absorption band in the vicinity of the wavelength chosen for the test (254 nm). The molar absorptivity was found to be 6980 l mol^{-1} cm^{-1}.

Calibration was carried out as follows. By injecting a large sample plug of known concentration (20–100 μl, depending on the inside diameter of the capillary), a constant signal is created for 2–3 min on the recorder. The plug is flushed through the capillary by using helium to pressurize a solvent reservoir filled with water.

The sensitivity S is defined as the ratio of the absorbance read out at the detector and the concentration. Noise is reported as peak-to-peak noise (four times the standard deviation of the noise, σ) over a period of 3 min. The concentration detection limit at the detector is defined as $c_{det} = 3\sigma/S$ (S = sensitivity).

The experimental set-up for the electrophoretic separations has been described in detail elsewhere [20]. When the influence of high voltage on the noise levels was studied, use was made of a phosphate buffer (0.05 M, pH 7.0).

Separation of oligonucleotide samples was performed in 100 μm I.D. gel-filled capillaries which were prepared according to the method described by Paulus and Ohms [21]. The temperature during the electrophoretic separations was kept at 25.0°C.

Cells B and D were applied for the separation of proteins in packed-column hydrodynamic chromatography (HDC). For this application, the fused-silica capillaries were directly coupled to the column outlet. The HDC column was a 150 × 4.6 mm I.D. stainless-steel column, filled with 1 μm non-porous silica particles. The particles were coated with polyethylene glycol (PEG 1000) according to Chang *et al.* [22].

Chemicals

Methanol (obtained from Merck, Darmstadt, Germany) was of high-performance liquid chromatographic grade. Methanol was checked for impurities by taking a UV spectrum of a 1% (v/v) solution in water. Oligodeoxyadenylic acid samples were purchased from Pharmacia (Woerden, Netherlands) and Isogen Biosciences (Amsterdam, Netherlands). Uracil, cytosine and thymine were supplied by Merck. Thyroglobulin (porcine) and albumin (chicken egg) were obtained from Sigma (St. Louis, MO, USA) and L-tyrosine from Merck.

RESULTS AND DISCUSSION

Cell with adjustable aperture width (cell A)

First, the results from cell A are discussed. The use of a fused-silica capillary of I.D. 50 μm and O.D. 350 μm resulted in calibration graphs as shown in Fig. 6. Each data point in the plot corresponds to the average of three measurements. Summarized data are given in Table I. It can be concluded from Fig. 6 and Table I that adjusting the slit width to the inside diameter results in the lowest concentration detection limit and the highest linear range. The higher sensitivity for a 20 μm aperture width is accompanied by higher noise. As predicted in the theoretical part, the highest sensitivity at the smallest aperture width is a result of the increased effective light path.

To obtain a better insight into these aperture width effects on sensitivity, the absorption at constant uracil concentration was measured at various aperture widths and compared with the theoretically predicted values, calculated from eqn. 7. The results are shown in Fig. 3. The value of the absorbance for an aperture width equal to the inside diameter is predicted with high accuracy. Also the trend towards higher absorbances at smaller aperture widths agrees with theory. However, at an aperture width larger than the inside diameter of the capillary, the recorded signal is much higher than theoretically expected. This deviation is caused by the assumption that refractive effects are negligible in the theoretical treatment used. This assumption cannot be justified, as can be seen in Fig. 4C. The fraction of light that enters the

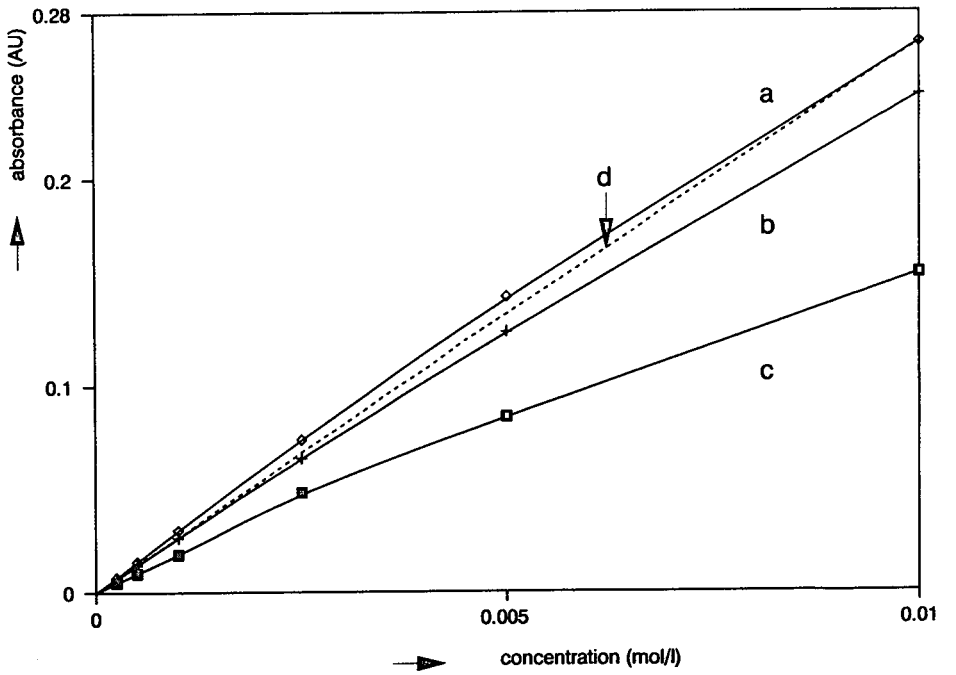

Fig. 6. Calibration graphs for cell A at various aperture widths. Capillary: 50 μm I.D., 350 μm O.D. Test compound: uracil. The data points are the average of three measurements. Aperture width: (a) 20; (b) 50; (c) 350 μm. The dashed line d represents the theoretical line for case b, calculated by using eqn. 4.

TABLE I

SENSITIVITY, NOISE, CONCENTRATION DETECTION LIMIT, UPPER LIMIT AND LINEAR RANGE AT THREE DIFFERENT APERTURE WIDTHS FOR CELL A

Aperture width (μm)	Sensitivity in linear range (absorbance l mol^{-1})	Peak-to-peak noise (absorbance)	c_{det} (l mol^{-1})	c_{upp} (l mol^{-1})	Linear range
20	29.5	$1.2 \cdot 10^{-4}$	$3.1 \cdot 10^{-6}$	$3.5 \cdot 10^{-3}$	1129
50	26.2	$5.0 \cdot 10^{-5}$	$1.4 \cdot 10^{-6}$	$3.5 \cdot 10^{-3}$	2500
350	18.6	$5.0 \cdot 10^{-5}$	$2.0 \cdot 10^{-6}$	$2.0 \cdot 10^{-4}$	100

capillary between the inside and outside diameter at the glass wall converges to the centre of the capillary. These refracted light rays partly do not reach the photocell, resulting in absorbance values higher than theoretically predicted. This also means that shielding these light rays with the adjustable aperture has no influence on the measured intensity, because they do not contribute to the intensity anyway. The absorbances for aperture widths smaller than the inside diameter are lower than theoretically predicted. This is probably caused by some experimental complications. Although it is not very difficult to adjust a certain aperture, it appears difficult to position the aperture completely symmetrically around the centre of the capillary. Slight misalignment can lead to significant deviations from the calculated effective light path.

A more detailed study on noise levels is shown in Fig. 7. In agreement with theory, there is an increase in the noise for a decreasing aperture width, no matter whether the capillary is installed or not. It can be seen that the noise is constant when the aperture is larger than the inside diameter with an installed capillary in the cell. This means that the intensity measured by the photocell is constant. It can be assumed, as discussed earlier, that a fraction of the incident light rays striking the optical window between the inside and outside diameters do not reach the photocell.

These experiments show that a decreased aperture width results in higher noise levels and higher sensitivities. There is an optimum aperture width where the highest signal-to-noise ratio can be found. As can be seen in Fig. 8, the highest signal-to-noise ratio and the resulting lowest concentration detection limit were found for an aperture width equal to the inside diameter of the capillary. This result has the additional advantage that adjustment of the aperture width to the inside diameter is easy to do, because the inner wall is clearly visible under the microscope.

A comparison between theoretical (line d) and experimental (line b) calibration graphs is given in Fig. 6 for a 50-μm aperture. The experimental data points for low concentrations agree very well with theory. There is a negative deviation from linearity at higher concentrations, starting at a lower concentration than theoretically expected. Accepting a 5% deviation, $3.5 \cdot 10^{-3}$ mol l^{-1} was found to be the upper limit. This value agrees well with upper limits from other test compounds and on-column cells as reported by others, *e.g.*, Wang *et al.* [10]. Theoretically, according to eqn. 7, a much larger upper limit, up to $2 \cdot 10^{-2}$ mol l^{-1}, is expected. It is difficult to find an explanation for this deviation.

The same calibration graph was obtained for a 75 μm I.D., 275 μm O.D.

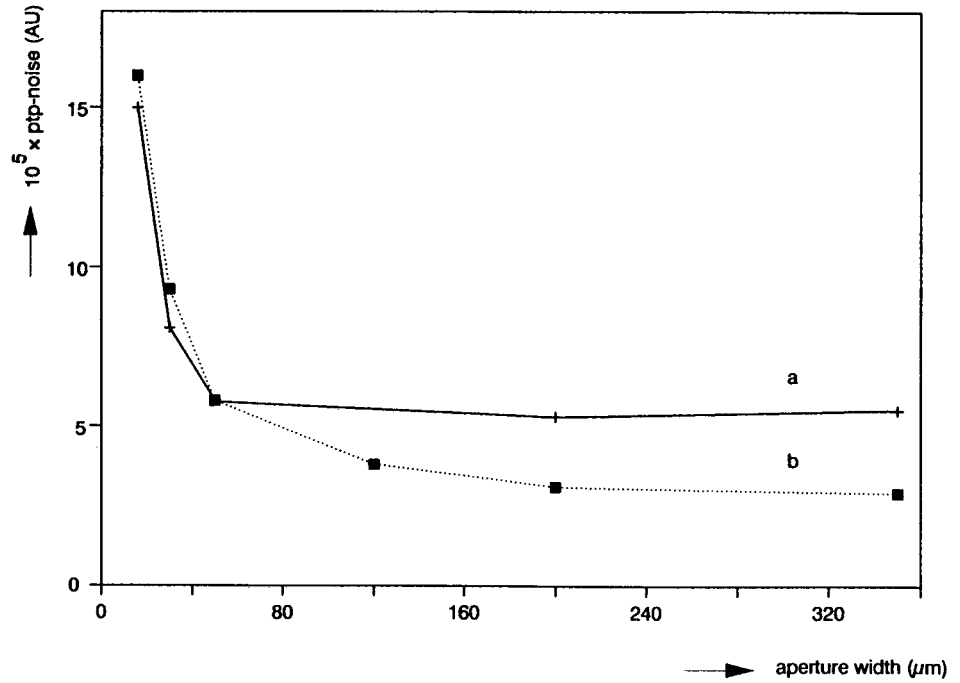

Fig. 7. Noise at various aperture widths, (a) with and (b) without an installed capillary (50 μm I.D., 350 μm O.D.) in the cell.

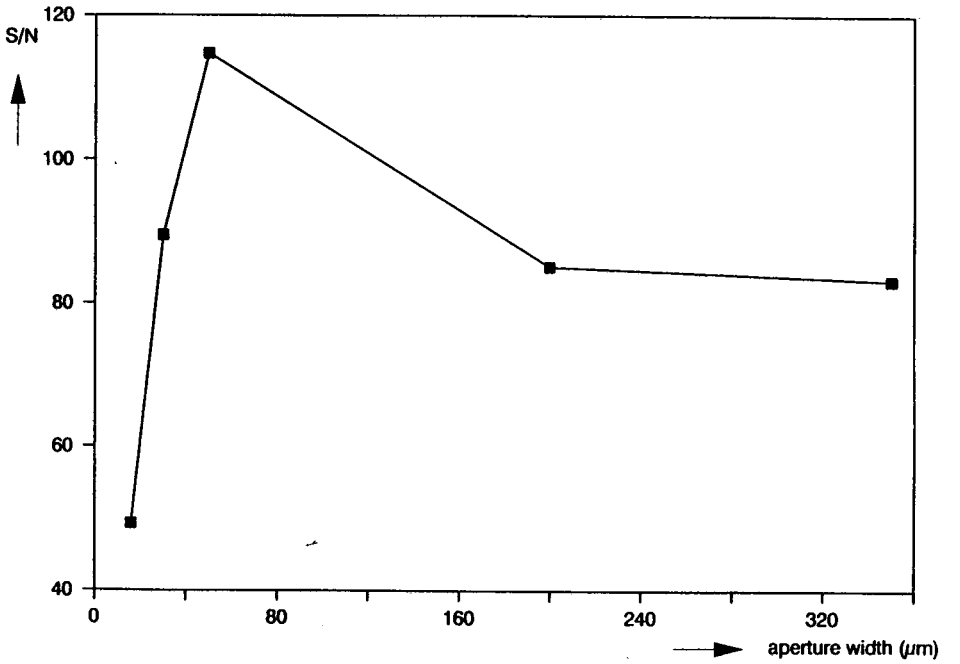

Fig. 8. Signal-to-noise ratio (S/N) at various aperture widths. Capillary: 50 μm I.D., 350 μm O.D. Compound: uracil, $c = 2.5 \cdot 10^{-4}$ mol l^{-1}.

capillary. This was done to make a fair comparison with the U-cell, which was supplied with a standard 75 μm I.D. capillary. The ratio of the sensitivities found for a 75 and a 50 μm I.D. capillary is 1.57, which agrees fairly well with the ratio of the inside diameters. The concentration detection limit and upper limit are $1.5 \cdot 10^{-6}$ and $2.5 \cdot 10^{-3}$ mol l^{-1}, respectively.

Wahlbroehl and Jorgenson [9] reported an increase in the noise when a high voltage was applied compared with the static measurements. This was possibly caused by vibrations of the capillary in the cell holder. In this work, no difference in noise level was found, which is an indication of good fixation of the capillary in the cell.

Cell with focusing lens (B)

The relevant results are summarized in Table II. Comparing the results for a 50 μm I.D. capillary with those obtained with cell A, it can be seen that the detection limits are nearly the same, whereas the linear range is nearly twice as large.

Changing the diameter from 50 to 75 μm results in a peculiar effect on the linear range, which becomes smaller, caused by the smaller upper limit. Apparently, the performance of this kind of cell depends strongly on the diameters of the capillaries used, as illustrated in Fig. 4D and E. Use of other than the optimum dimensions of the capillary will result in some misalignment. Also for this cell there was no increase in the noise levels when a high voltage was applied.

Cell with focusing lens (C)

Fig. 9 shows calibration graphs for four different inside diameters, from 25 to 100 μm I.D. Compared with cell B, the sensitivity is 2.5 and 2.0 times lower for a 50 and a 75 μm I.D. capillary, respectively, with cell C. Also, the noise is roughly five times lower than for cell B, which results in slightly improved detection limits for cell C. Because of the lower sensitivity and the non-linearity of the calibration graphs, it was suspected that in this device a substantial part of the light does not strike the liquid. The factor α describing this (see Theoretical) was determined by measuring the absorbance of a saturated solution ($c > 0.25$ *M*) of potassium dichromate and using eqn. 12. The results are summarized in Table III. In Table III, also the calculated width of the light beam, $2s$, is given by substituting the α values for the four diameters in eqn. 9. The average light beam width is 139 μm. This means that capillaries having an I.D. $\gtrsim 140$ μm, should not give a sensitivity loss caused by by-passing effects.

TABLE II

SENSITIVITY, NOISE, CONCENTRATION DETECTION LIMIT AND UPPER LIMIT FOR CELL B

I.D. (μm)	Sensitivity in linear range (absorbance l mol^{-1})	Peak-to-peak noise (absorbance)	c_{det} (l mol^{-1})	c_{upp} (l mol^{-1})	Linear range
50	30.8	$5.5 \cdot 10^{-5}$	$1.3 \cdot 10^{-6}$	$5.8 \cdot 10^{-3}$	4142
75	48.5	$8.5 \cdot 10^{-5}$	$1.3 \cdot 10^{-6}$	$4.5 \cdot 10^{-3}$	3461

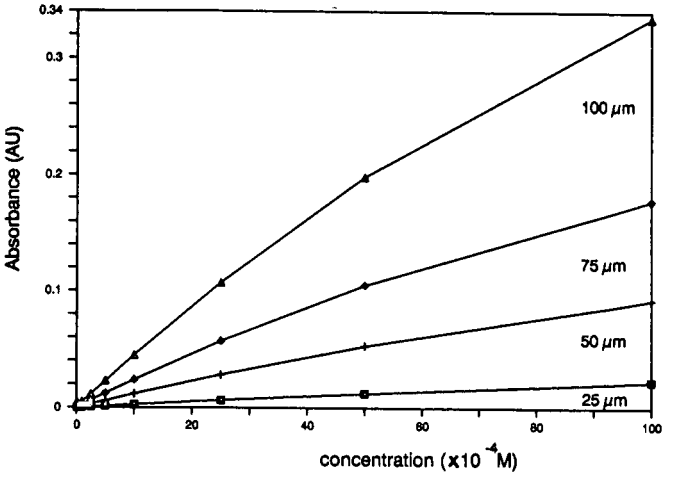

Fig. 9. Calibration graphs for cell C with four different I.D. capillaries (100, 75, 50 and 25 μm I.D.) as indicated. Test compound: uracil.

U-cell (D)

Two U-cells, made according to the same procedure [18], were evaluated and some of the results obtained are summarized in Table IV. The calibration graphs show strong non-linearity, which complicates the determination of the upper limit and the linear range. The sensitivities and the related concentration detection limits are rough estimates from measurements in the low concentration range. The non-linear character can be explained by complicated refraction and reflection patterns at the position where the light beam enters the capillary. Here the capillary is sharply bent, almost at right-angles. Although the non-linearity is a problem, it can be circumvented by calibration of the detection system.

The sensitivity of U-cells 1 and 2 is roughly 30 times higher than those found for cells A–C. It is remarkable that the two cells, although nominally the same, have different characteristics; cell 1 has a lower sensitivity and a lower noise level than cell 2, which results in comparably low detection limits ($9.8 \cdot 10^{-8}$ and $1.2 \cdot 10^{-7}$ mol l^{-1}, respectively). These detection limits are about fifteen times lower than those for cells A and B. On going to higher concentrations, the gain in signal-to-noise ratio decreases

TABLE III

CALCULATED α AND LIGHT BEAM WIDTH AT FOUR INNER DIAMETERS FOR CELL C

I.D. (μm)	A^* (absorbance)[a]	$A_{measured}$ (absorbance)	α	w_{beam} (μm)
25	2.7	0.08237	0.827	144
50	5.4	0.2072	0.620	131
75	8.1	0.3263	0.472	142
100	11	0.5512	0.281	139

[a] A^* is calculated using $A^* = \varepsilon cl$; $\varepsilon = 4037$ l mol^{-1} cm^{-1}.

TABLE IV

SENSITIVITY, NOISE AND CONCENTRATION DETECTION LIMIT FOR THE U-CELLS

Cell No.	Sensitivity in linear range (absorbance 1 mol^{-1})	Peak-to-peak noise (absorbance)	c_{det} (mol l^{-1})
1	950	$1.3 \cdot 10^{-4}$	$9.8 \cdot 10^{-8}$
2	1400	$2.2 \cdot 10^{-4}$	$1.2 \cdot 10^{-7}$

because of the non-linearity. This effect is clearly demonstrated in Fig. 10, where the signal-to-noise ratio for the three cell types is plotted against concentration.

Sensitivity for changes in the refractive index

A plug of a 1% (v/v) solution of methanol in water was injected to evaluate the response to a small change in refractive index of the streaming liquid flow. A plug of water was injected as a reference. As can be seen in Fig. 11A and B, the signal is nearly negligible for cell A and very small for cell B. Cell D is very sensitive to changes in the refractive index. The large signal as shown in Fig. 11C, injection 2, corresponds to a UV absorbance resulting from injection of $2 \cdot 10^{-6}$ *M* uracil.

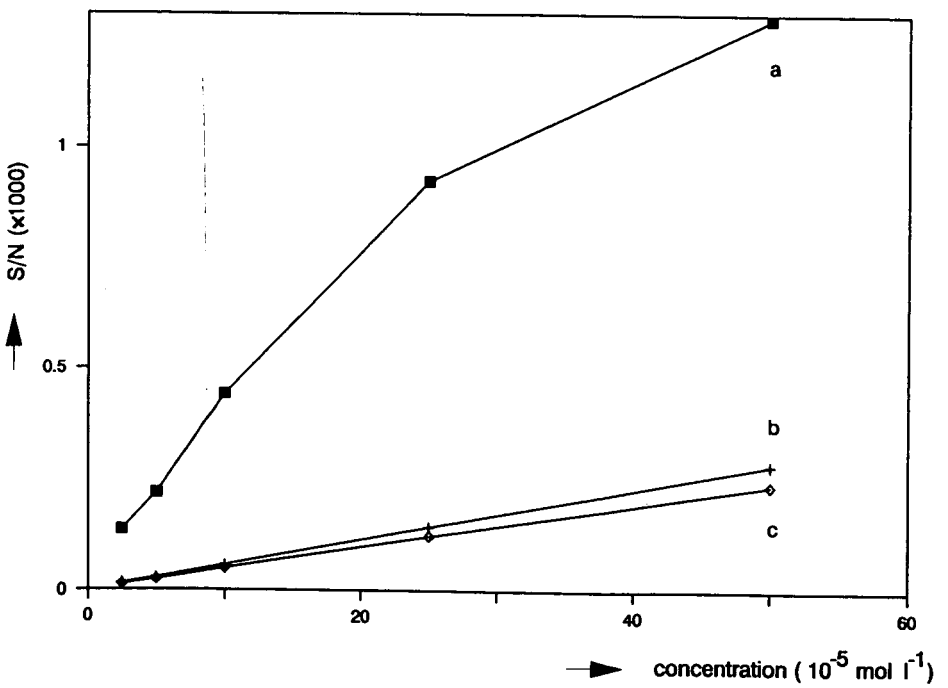

Fig. 10. Signal-to-noise ratio (S/N) for (a) cell D, (b) cell B and (c) cell A *versus* uracil concentration.

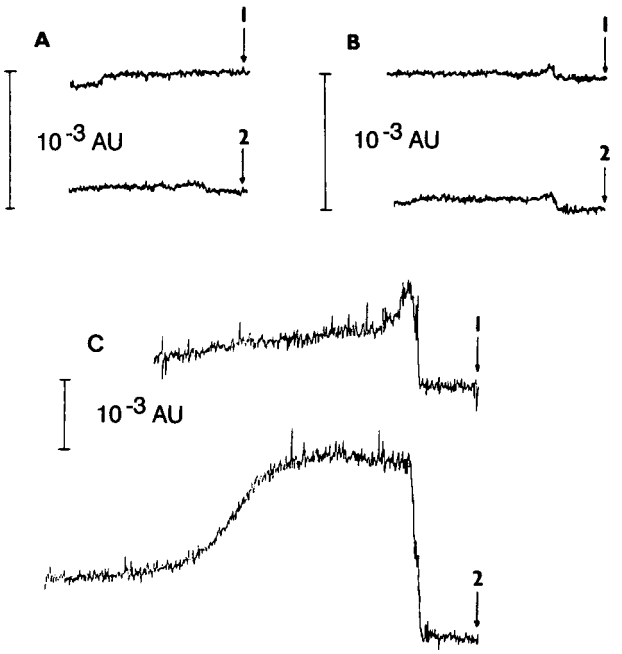

Fig. 11. Signal caused by changes in the refractive index after injection of 1% (v/v) aqueous methanol solution. Capillary: 75 μm I.D., 275 μm O.D. (A) Cell A; (B) cell B; (C) cell D; (1) injection of water and (2) injection of 1% (v/v) aqueous methanol in each instance. Arrows indicate injection points.

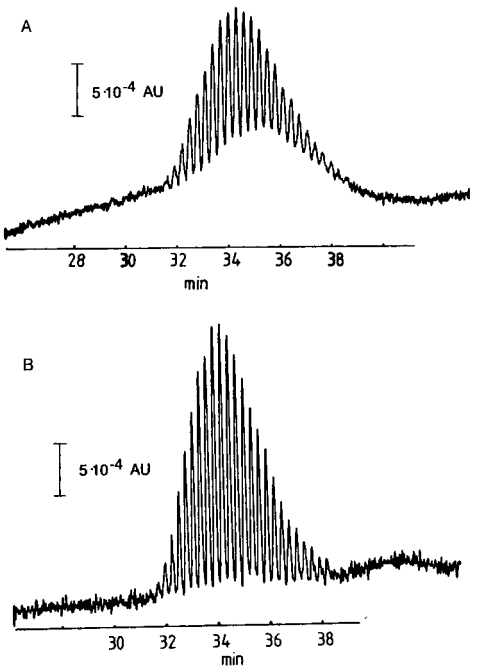

Fig. 12. CGE separation of a sample of oligonucleotides $p(dA)_{40-60}$. Buffer composition: 100 m*M* Tris, 100 m*M* boric acid, 2 m*M* EDTA, 7 *M* urea (pH 8.85). Capillary: 100 μm I.D., 220 μm O.D. Gel composition: 7.5% T, 3.3% C. UV detection at 260 nm. (A) Cell A; (B) cell B; aperture width 100 μm.

Contribution to peak width

This aspect will not be treated theoretically in detail here because it has been reported already by others [23,24]. Only some examples of efficient capillary electrophoretic and hydrodynamic chromatographic separations will be presented.

Fig. 12A and B show high-efficiency separations performed in gel-filled capillaries for a sample of oligonucleotides $pd(A)_{40-60}$ obtained with cells A and B, respectively. When cell B is used, all the peaks are baseline resolved. This good resolution is impaired when cell A is used. The influence of the detection cell length is very pronounced here. The length standard deviation of the separation (estimated from Fig. 12B, where external effects seem to be small) is 0.3 mm. The theoretical contribution to the peak width from a detection cell with an aperture length of 1.0 mm

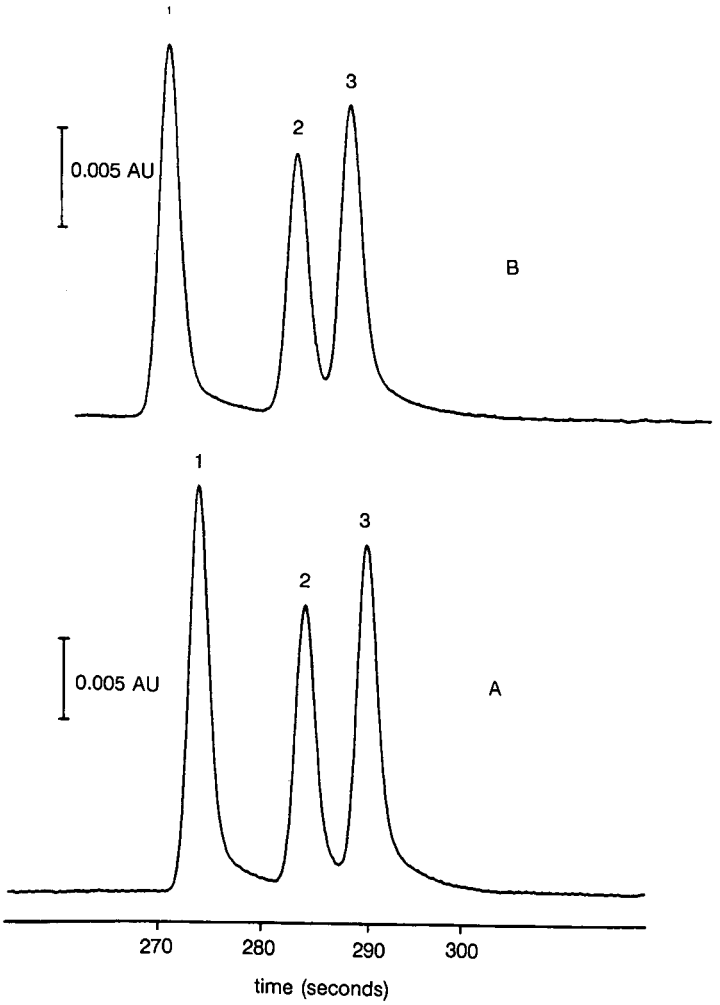

Fig. 13. MECC separation of (1) uracil, (2) cytosine and (3) thymine. Capillary: 50 μm I.D., 350 μm O.D. UV detection at 260 nm. (A) Cell A; (B) cell B.

along the capillary axis is $\sigma_{z,det} = 1.0/\sqrt{12} = 0.29$ mm. If a contribution of 5% from the detection cell to the total peak broadening is accepted, then it follows that

$$\sigma_{det} \leqslant 0.3\sigma_{sep} \tag{13}$$

A loss in resolution of about $\sqrt{2}$ can be expected in this particular separation. Hence, in case of capillary gel electrophoretic (CGE) separations, where plate numbers in the range of several millions can be achieved, it is preferable to use cells with a small aperture length along the capillary (< 100 μm).

Another comparison of this type, a micellar electrokinetic capillary chromatographic (MECC) separation of uracil, cytosine and thymine, is shown in Fig. 13A and B. There is a small decrease in efficiency of *ca.* 5% (from $N = 84\,000$ to 80 000 for peak 2) when cell A is used instead of cell B. The standard deviations in length units, $\sigma_{z,tot}$, are 1.26 and 1.23 mm for cells A and B, respectively. The theoretical contribution to the peak width from cell A, being 0.29 mm, is smaller than $0.3\sigma_{z,sep}$. This means that for this separation a cell with a length of 1 mm along the capillary is acceptable.

For the U-cell, the value of $\sigma_{z,det}$, calculated in the same way, is 2.3 mm. Although the U-cell has the highest sensitivity, its use in the above-mentioned separations was not considered. Unacceptable contributions to the peak width can be expected.

Full advantage of the high sensitivity of the U-cell can be achieved for less efficient separations or for separations on a larger volume scale. An example is given

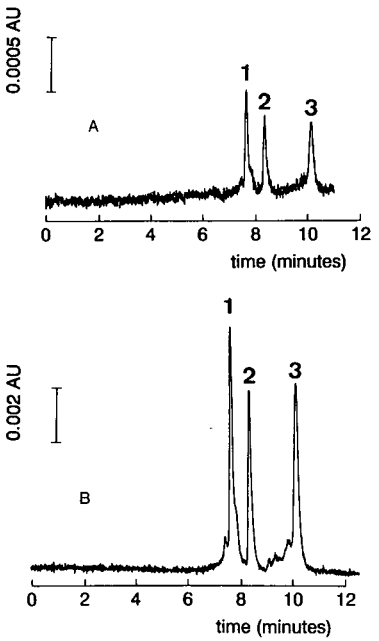

Fig. 14. HDC separation of some proteins. Mobile phase: 0.001 mol l^{-1} Tris–HNO_3 (pH 7.0) containing $5 \cdot 10^{-4}$ mol l^{-1} sodium azide. Wavelength, 230 nm; filter rise time, 0.2 s. (1) Thyroglobulin; (2) albumin; (3) L-tyrosine (1 mg ml^{-1} each). (A) Cell B; (B) cell D.

by packed column HDC. In earlier experiments with HDC [4,25] it was found necessary to perform detection in a fused-silica capillary fitted in the column outlet in order to avoid unacceptable peak broadening. This resulted in a serious loss of sensitivity. Cell D combines high sensitivity with acceptable peak broadening. HDC separations of proteins using cells B and D are shown in Fig. 14. The volume standard deviation of the separated compounds is so large ($\sigma_v \approx 5.5$ μl) that none of the cells contribute to the peak width. Cell D gives a much better detection limit. At the selected wavelength of 230 nm, it shows that cell D yields a four times better signal-to-noise ratio than cell B. However, this gain is smaller than the factor of *ca.* 20 reported at 254 nm and it decreases even further at lower wavelengths. This phenomenon can be explained by either mobile phase absorption at lower wavelengths or by the different refraction and reflection patterns at shorter wavelengths.

REFERENCES

1 J. W. Jorgenson and K. D. Lukacs, *Anal. Chem.*, 53 (1981) 1298.
2 J. Vindevogel, G. Schuddinck, C. Dewaele and M. Verzele, *J. High Resolut. Chromatogr. Chromatogr. Commun.*, 11 (1988) 317.
3 X. Xi and E. S. Yeung, *Anal. Chem.*, 62 (1990) 1580.
4 G. Stegeman, R. Oostervink, J. C. Kraak and H. Poppe, *J. Chromatogr.*, 506 (1990) 547.
5 R. Tijssen, J. P. A. Bleumer and M. E. van Kreveld, *J. Chromatogr.*, 260 (1983) 297.
6 R. A. Wallingford and A. G. Ewing, *Anal. Chem.*, 61 (1989) 98.
7 R. D. Smith, J. A. Loo, C. G. Edmonds, C. J. Barinaga and H. R. Udseth, *J. Chromatogr.*, 516 (1990) 157.
8 S. Wu and N. J. Dovichi, *J. Chromatogr.*, 480 (1989) 145.
9 Y. Wahlbroehl and J. W. Jorgenson, *J. Chromatogr.*, 315 (1984) 135.
10 T. Wang, R. H. Hartwick and P. B. Champlin, *J. Chromatogr.*, 462 (1989) 147.
11 I. H. Grant and W. Steuer, *J. Microcolumn Sep.*, 2 (1990) 74.
12 A. E. Bruno, E. Gassmann, N. Pericles and K. Anton, *Anal. Chem.*, 61 (1989) 876.
13 H. Lüdi, E. Gassmann, H. Grassenbach and W. Märki, *Anal. Chim. Acta*, 213 (1988) 215.
14 F. Foret, M. Deml, V. Kahle and P. Boček, *Electrophoresis*, 7 (1986) 430.
15 J. P. Chervet, M. Ursem, J. P. Salzmann and R. W. Vannoort, *J. High Resolut. Chromatogr.*, 12 (1989) 278.
16 J. P. Chervet, personal communication.
17 S. Hjertén, *Chromatogr. Rev.*, 9 (1967) 122.
18 W. Baumann, *Fresenius' Z. Anal. Chem.*, 284 (1977) 31.
19 J. P. Chervet, LC Packings, *Eur. Pat.*, No. 89106700, 1990.
20 G. J. M. Bruin, R. H. Huisden, J. C. Kraak and H. Poppe, *J. Chromatogr.*, 480 (1989) 339.
21 A. Paulus and J. I. Ohms, *J. Chromatogr.*, 507 (1990) 113.
22 J. P. Chang, Z. H. Rassi and Cs. Horváth, *J. Chromatogr.*, 319 (1985) 396.
23 K. Otsuka and S. Terabe, *J. Chromatogr.*, 480 (1989) 91.
24 X. Huang, W. F. Coleman and R. N. Zare, *J. Chromatogr.*, 480 (1989) 95.
25 J. C. Kraak, R. Oostervink, H. Poppe, H. Esser and K. K. Unger, *Chromatographia*, 27 (1989) 585.

Journal of Chromatography, 559 (1991) 183–196
Elsevier Science Publishers B.V., Amsterdam

CHROM. 23 632

Laser-induced fluorescence and fluorescence microscopy for capillary electrophoresis zone detection[a]

LUIS HERNANDEZ*,[b] and JOSE ESCALONA
Laboratory of Behavioral Physiology, School of Medicine, Los Andes University, Merida 5101-A (Venezuela)
NARAHARI JOSHI
Center for Advanced Optic Studies, Physics Department, Los Andes University, Merida 5101-A (Venezuela)
and
NORBERTO GUZMAN[c]
Princeton Biochemicals Inc., Princeton, NJ 08543 (USA)

ABSTRACT

A procedure to improve on-column fluorescence detection for capillary zone electrophoresis is reported. A fluorescence detector was built using an epillumination fluorescence microscope and an argon-ion air-cooled laser. The 488-nm line was isolated with a band pass filter to eliminate the ultraviolet line. A dichroic mirror which reflected wavelengths under 510 nm and a 0.75 numerical aperture (NA), 0.3 mm working distance objective of the microscope condensed the laser beam on a fused-silica capillary and a cross-shaped fluorescence spot was observed. The emitted light was collected with the same objective, filtered with a 520-nm high pass filter, a spatial filter and a notch filter, and focused on a photodetector. The photodetector was either a gallium–arsenide or a multialkali photomultiplier tube. The signal generated was fed to a current-to-voltage converter and registered on a strip chart recorder. The detector was tested with fluorescein-derivatized amino acids. For the fluorescein thiocarbamyl (FTC)-amino acids the limit of concentration detection varied according to the amino acid. Taking FTC-arginine as the best example, the limit of concentration detection (LOCD) was $3.75 \cdot 10^{-12}$ *M*. Assuming that 1 nl was injcted, the limit of mass detection (LOMD) was $3.75 \cdot 10^{-3}$ amol or about 2250 molecules. This represents an improvement of about three orders of magnitude with respect to previous laser induced fluorescence on-column detection. The potential and advantages when using an epillumination fluorescence microscope with laser induced fluorescence as a detection system for capillary electrophoresis are discussed.

INTRODUCTION

Since Gassman *et al.* [1] introduced laser induced fluorescence detection (LIFD) for capillary electrophoresis (CE), LIFD has gradually become the most sensitive technique for analyte detection in narrow bore capillaries. With the 325-nm line of the

[a] Part of this work was presented at the *2nd International Symposium on High Performance Capillary Electrophoresis, San Francisco, CA, January 29–31, 1990.*

[b] Address for correspondence: Europhor SA, Parc Technologique du Canal, 10 Avenue de l'Europe, 31520 Ramonville, Toulouse, France.

[c] Present address: Pharmaceutical Research and Development, Hoffmann-La Roche Inc., 340 Kingsland Street, Nutley, NJ 07110-1199, USA.

0021-9673/91/$03.50

He–Cd laser, dansylated derivatives of amino acids, vitamins, and drugs have been detected on-column [1–5]. The limit of concentration detection (LOCD) for some dansylated amino acids was about 10^{-9} *M* and the limit of mass detection (LOMD) was about 10 amol. For some drugs such as metrotexate the LOCD was 10^{-10} *M*. The same type of laser has been used for indirect fluorescence detection to analyze non-fluorescent and non-derivatizable compounds, in the same on-column detection mode [6–9]. When applying the indirect fluorescence detection system the LOCD was about 10^{-6} *M* and the LOMD was approximately 1 fmol, using 50 μm I.D. capillaries.

When using the 442-nm line of the He–Cd laser and fluorescein isothiocyanate (FITC) as derivatizing agent, the LOCD for phenylalanine was close to 10^{-10} *M* and the LOMD about 1 amol. For other derivatized amino acids such as glutamic acid, the LOCD was 10^{-7} *M* [10]. In these experiments an excess of amino acids with respect to FITC was used. The LOCD was calculated on the basis of the fluorescein thiocarbamyl (FTC)-amino acid concentration assuming full reaction of the FITC. In the same report, with the 325-nm line and the 420-nm line of the He–Cd laser, and for ortho-phthalaldehyde (OPA) and naphthalenedialdehyde (NDA) derivatized amino acids, the LOCD was 10^{-8} *M* and 10^{-9} *M*, respectively. These values represent the highest sensitivities for amino acids in the on-column detection mode. The He–Cd laser has also been used to detect rapidly separated dansylated or OPA-derivatized amino acids in 10 μm I.D. capillaries [11]. In these experiments a mixture of eight amino acids was resolved in less than 90 s, but the LOCD was reduced by one order of magnitude due to the smaller diameter of the capillary. Other laser-based detection methods such as fluorescence detected circular dichroism [12], thermooptical absorbance detection [13], refractive index detection [14], and refractive index and absorbance detection [15] have been used, but the sensitivity values reported were lower than for LIFD.

A recent breakthrough was the use of the 488-nm wavelength line of an argon-ion laser for the detection of fluorescein isothiocyanate-derivatized amino acids separated by CE in 50 μm I.D. capillaries with a post-column detection mode [16]. Detection was carried out on a quartz sheath-flow cuvette at the cathodic end of the capillary. Again, the concentration of tagged amino acid was calculated assuming full reaction of FITC with an excess of amino acid. Subattomole amounts of FTC-amino acids were measured; in the case of arginine, the LOCD was 10^{-12} *M* [17]. This concentration value represents the highest sensitivity ever reached for CE. Therefore, 10^{-9} *M* seems to be the best LOCD for on-column detection, and 10^{-12} *M* for post-column detection.

There are many applications in which post-column detection is used. However, on-column detection may be required in many other applications of CE, such as in the case of DNA sequencing. In this application CE and LIFD have proved to be an excellent method for rapid separation and detection of fluorescein-derivatized fragments of DNA using gel-filled capillaries [18–20]. The LOCD for a fluorescein primer was about 10^{-11} *M* in 50 μm I.D. and 75 μm I.D. capillaries. In these experiments, the fluorescein primer was not electrophoretically migrated through the capillary. A vacuum pump was used to flush the capillary continuously with the fluorescein solution. Under these circumstances, photobleaching is minimized and the LOCD is better than in electromigration. When the primer was injected in a gel-filled capillary [20], the LOCD was $1.5 \cdot 10^{-10}$ *M*. Recently, a successful attempt to put together the sheath-flow cuvette method and DNA separation in gel-filed capillaries

was conducted [21]. Subattomole amounts of FITC-labelled DNA fragments were measured. But it seems that the procedure does not allow detection from several capillaries in a single run. This represents a disadvantage because to make CE DNA sequencing competitive with slab gel DNA sequencing, multiple capillaries will have to be used simultaneously. This technical problem may be solved in the near future, but in any event improvement in sensitivity for on-column LIFD in capillaries of 50 μm I.D. or less remains a necessity for both DNA sequencing and amino acid analysis by CE-LIFD.

In all these instruments the direction of the excitation radiation is orthogonal with the emitted radiation. Glass or quartz lenses or fiber optics have been used to focus the laser on the capillary and to focus the emitted radiation on the light sensitive element. However, the orthogonal design makes it hard to use lenses of very small working distance and, as a consequence, limits the numerical aperture (NA) of the lenses to about 0.45. Fiber optics solve the alignment difficulties inherent to the lenses and the fiber can collect very close to the capillary. However, the feeble fluorescent signals are attenuated by internal scattering in the fiber.

In a previous report [22] we examined the advantages of the collinear arrangement when using an epillumination fluorescence microscope as an alternative to the orthogonal arrangement for the on-column detection in CE. Using a mercury lamp as the excitation source, a quadratic relationship was found between the numerical aperture or magnification of the microscope lenses and the intensity of the fluorescence. Maximum signals were obtained with high magnification, high numerical aperture lenses that had a working distance of less than 1 mm. At the present time, the collinear arrangement has not been used in LIFD for CE, and therefore the advantages of lenses of high numerical aperture have not been fully exploited. The combination of an epillumination fluorescence microscope and a coherent source of excitation radiation may improve LIFD in several ways. (1) Focusing the laser on the capillary could be easy because the microscope already has a highly precise XYZ displacement device, and the alignment of the capillary can be guided visually. (2) The excitation of the sample and the detection of the emitted light would be done on the same side of the capillary (collinear arrangement). For the majority of phonon symmetries, Raman scattering efficiencies are nearly maximum perpendicular to the plane of symmetry and therefore the directions of incident and scattered light are generally at right angles to each other [23,24]. Then, the orientation of the sample is adjusted relative to the incident beam to achieve maximum response (this angle very often lies between 37 and 42°). Contribution of Raman scattering originating from prominent vibrational modes is avoided completely in the back scattering geometry. (3) The emitted light could be collected with lenses of less than 1 mm working distance and higher numerical aperture than the lenses that have been used so far in the orthogonal arrangement for the purpose of enhancing the fluorescent signal. (4) The emitted light could easily be focused on the photodetector because the microscope already has the optics for that task.

We now report this application and an improvement of at least 3 orders of magnitude in LOCD for the on-column detection of FTC-amino acids.

EXPERIMENTAL

Instrumentation

A diagram of the instrument is shown in Fig. 1. The microscope as a Model Standard 14 IFD Zeiss epillumination fluorescence microscope. It was equipped with heat suppression and interference filters. The laser was a Model 161-C Spectraphysics, 488-nm, argon-ion, air-cooled laser, kindly donated by Europhor SA (Toulouse, France). This laser was placed behind the microscope on a jack. The beam of coherent light was filtered through a 450–490 nm filter band pass (Model BP 450-490, Carl Zeiss, Oberkochen, Germany), reflected by a 510-nm chromatic beam splitter (Model FT-510, Carl Zeiss) and condensed on the capillary by means of a fluorite objective (Model Neofluar, Carl Zeiss). The emitted light was collected by the same objective. After crossing the chromatic beam splitter, it was filtered through a 520-nm long wave pass filter (Model LP-520, Carl Zeiss), a home made spatial filter, and a custom made notch filter centered at 492 nm, with a bandwidth of 33 nm and 90% transmittance at 530 nm (kindly donated by Andover Corp., Salem, NH, USA). This last one sup-

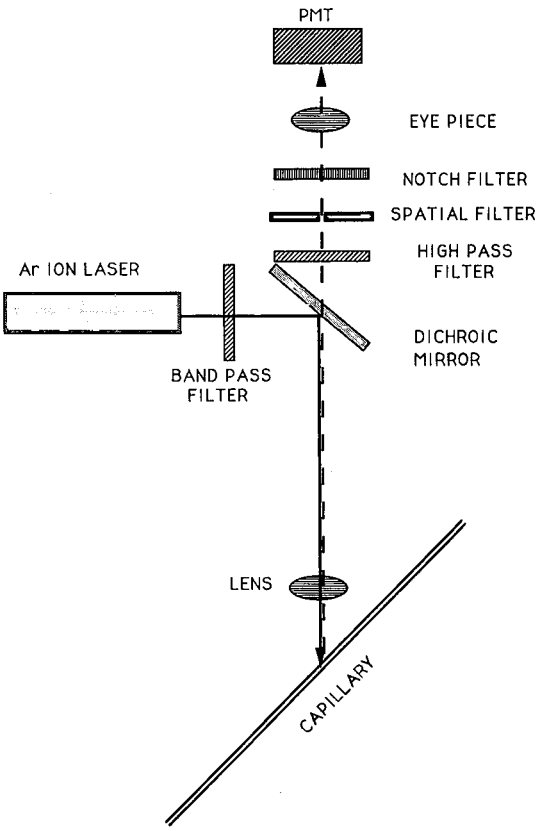

Fig. 1. Diagram of a collinear laser-induced fluorescence detection system. The data of the objectives are tabulated in Table I. The main axis of the capillary is at a 90° angle with the laser beam and with the optical axis of the microscope. The ocular is a 10× glass lens, the spatial filter either 2 or 3 mm diameter.

pressed the 488-nm line that the capillary reflected toward the photodetector; even though specular reflection was high, it was well suppressed by the notch filter. A glass 10× ocular was placed between the notch filter and the detector to focus the fluorescence on one of the following components. For one experiment the fluorescence was focused on the monochromator of a SPEX spectral analyzer equipped with a water-cooled cathode, galium–arsenide Model 60-ER Hamamatsu tube operated at 2000 V (SPEX Industries, Edison, NJ, USA). For the other experiments the signal was focused on the quartz window of a multialkali Model R928 Hamamatsu photomultiplier tube (PMT) (Hamamatsu, Bridgewater, NJ, USA), operated at 750 V with a Model 215 Bertan high-voltage power supply (Bertan, Hicksville, NY, USA). The output of the Ga–As PMT was connected to a photon counting module and to a dedicated computer for statistical processing. The output of the multialkali PMT was connected to a Model 485 Keithley picoammeter (Keithley, Cleveland, OH, USA) operated at 200 nA for weak signals. Photographs were made with an automatic camera (Model M-63, Carl Zeiss), and the signal was recorded on a strip chart recorder (Model L-6512, Linseis, Princeton Junction, NJ, USA). A special capillary carrier described elsewhere was used [22]. To diminish light scattering and reduce background noise a hole was drilled in the capillary carrier. The laser went through the hole and was absorbed by a black cylinder underneath the hole. The capillaries used were fused-silica, 90 cm long (Polymicro Technologies, Phoenix, AZ, USA). The I.D. of the capillaries varied between 5 and 75 μm and the O.D. between 140 and 144 μm. The polyimide cover of the capillary was burned away on a 0.5-cm segment at 60 cm from the injection end, and the capillary was positioned in the capillary carrier and set on the stage of the microscope. The two ends of the capillary were immersed in a 40 mM carbonate buffer solution at pH 10.0. The capillary was primed by means of a vacuum pump. The driving force to load and run the samples was provided by a Model prime vision V Europhor high-voltage power supply (Europhor) in the constant voltage mode.

Laser and capillary alignment. The laser was easily aligned with the capillary because the microscope has a feature to simplify this operation. A reticule on one ocular indicated where the center of the visual field was. With the leveled jack the laser could be raised and lowered. The lateral movements were done by hand. Since the microscope is equipped with binoculars to watch the object, it was an entirely visually guided operation. The capillary was filled with a fluorescent solution (for example 10^{-10} M derivatized glycine) to facilitate alignment. The capillary was displaced with the XY displacement mechanism of the stage. The capillary and the laser were displaced until they coincide with the reticule. The entire operation lasted about two minutes. Once the laser and the capillary were centered, the Z displacement was used to produce a sharp image of the capillary. When the PMT is properly set, the image of the fluorescent spot is focused on the light sensitive window.

Reagents

Sodium carbonate, sodium bicarbonate, arginine, glycine, cysteine, isoleucine, leucine, methionine, alanine and fluorescein isothiocyanate isomer I were purchased from Sigma (St. Louis, MO, USA). Acetone was obtained from Aldrich (Strasbourg, France).

Procedure

A $2.1 \cdot 10^{-4}$ *M* solution of fluorescein isothiocyanate (FITC) isomer I (Sigma) in acetone was prepared by dissolving 0.5 mg of FITC in 6 ml of acetone. Then, 2 mg of each amino acid were dissolved in 2 ml of 0.2 *M* carbonate buffer at pH 9.0. Of each amino acid solution 1 ml was allowed to react with 1 ml of the FITC solution for 4 h in the dark. At the same time, 1 ml of a $2.1 \cdot 10^{-4}$ *M* solution of FITC in acetone was mixed with 1 ml of 0.2 *M* carbonate buffer to obtain a blank and kept in darkness fo 4 h. Then, both the FITC solution and the amino acid plus FITC solution were diluted 10^8 times by steps of 10 in 0.05 *M* carbonate buffer at pH 10. The samples were electrokinetically loaded by immersing one end of the capillary and the positive electrode into the sample and applying 10 kV during 7.5 s. According to previous calculations of electroosmotic flow the injection volume is about 1 nl for 25 μm I.D. capillaries [22]. Then the end of the capillary and the positive electrode were transferred to a buffer reservoir and run at 20 kV. After each run the capillary was washed by sequential hydrodynamic injections of 1 *M* NaOH (2 min), 0.1 *M* NaOH (2 min), water (3 min) and buffer (4 min).

Several experiments were conducted to determine the optimum combination of numerical aperture, capillary diameter, and laser power in order to achieve the highest sensitivity. Then measurements of derivatized amino acids were performed.

In the first experiment 10^{-10} *M* FTC-leucine was injected into several capillaries and the signal was magnified with three different fluorite objectives. The data for the objectives are shown in Table I.

The fluorescent material was continually introduced by a vacuum pump. The laser power was 4 mW and the spatial filter was 2 mm diameter. The I.D.s of the capillaries were 5, 12, 15, 21, 29, 50 and 75 μm, and the O.D. varied between 140 and 144 μm. The best fitting curves for each NA were obtained from polynomial equations or from the linearized form of exponential equations [25]. The correlation coefficients were calculated for each curve. Pictures of the fluorescent spot were taken for the three objectives and without spatial filter on the 50 μm I.D. capillary. Then, with the 0.75 NA objective and the 10× ocular, three pictures were made of the image of the capillary, without spatial filter, with the 3-mm spatial filter and with the 2-mm spatial filter.

In the second experiment, the FTC-leucine solution signal and the background light of the capillary and the buffer were measured at ten different laser powers with 0.20, 0.40 and 0.75 NA objectives. In this experiment, the sample was continually introduced by vacuum in a 50 μm I.D., 140–144 μm O.D. capillary. No spatial filter was used and the ocular was 10×. The laser power was attenuated by regulating the

TABLE I

DATA OF THE OBJECTIVES USED IN EXPERIMENT I

Magnification (×)	Numerical aperture	Working distance (mm)	Focal length (mm)
6.3	0.20	10.8	23.6
16.0	0.40	0.9	10.8
40.0	0.75	0.33	4.5

current. The laser power at the exit of the laser was read on the remote control unit of the laser. Regression analysis was used to calculate the slopes of the best-fitting curves. In this experiment samples of the PMT current fluctuations due to the capillary and the buffer were measured 20 times at each laser power during bouts of 5 s. The standard deviation of this fluctuations was calculated and the noise estimated as three times the standard deviation. A comparison with the root mean square of the peak-to-peak measurements of the noise gave the same noise level as the 3σ method.

In the third experiment a spectral analysis of 10^{-11} *M* fluorescein-labelled isoleucin was performed. A 25 μm I.D. capillary and a 40 ×, 0.75 NA fluorite objective combined with a 10 × ocular and a 2-mm spatial filter were used. The capillary was continually flushed with the fluorescent solution by means of a vacuum pump. The fluorescence spot was fed into a spectrum analyzer (SPEX) and processed by a computer driven monochromator. Because of the low intensity of radiation, the largest slit widths (1.2-mm entrance and 0.8-mm exit) were used. In this way, radiation detection capability was increased at the expense of spectral resolution. The 60-ER has a flat response in the entire range and, therefore, detector correction was not needed.

In the fourth experiment the tagged amino acids (10^{-6}, 10^{-7}, 10^{-8}, 10^{-9}, 10^{-10} and 10^{-11} *M* solutions) were loaded in a 25-μm capillary and analyzed to determine the LOCD, the LOMD and the linearity of the analysis. The laser power was kept at 4 mW and a spatial filter of 2 mm diameter was used. Each amino acid was run individually at the above-mentioned concentrations. The PMT current produced by the peak of the FTC-amino acid was recorded and the baseline subtracted from the fluorescent signal. Then the log of the FTC-amino acid concentration *vs.* the log of the PMT current were plotted. A linear regression analysis was carried out to establish the dynamic range of the instrument. Then a mixture of six amino acids was prepared and run under the same conditions as for the individual FTC-amino acids.

RESULTS

The results of the first experiment are shown in Figs. 2, 3, 4 and 5. The three curves in Fig. 2 correspond to the three fluorite objectives. For the 0.20 NA objective, an increase of signal of 50 nA was observed between the 50 μm I.D. and the 75 μm I.D. capillaries. For the 0.40 NA objective, the largest increase of signal (86 nA) was observed between the 15 μm I.D. and 20 μm I.D. capillaries. The best signals were obtained with the 0.75 NA objective. The largest increase of signal (178 nA) was observed between the 5 μm I.D. and the 12 μm I.D. capillaries.

The pictures of the fluorescent spot are shown in Figs. 3 and 4. First of all, the size of the fluorescent spot increases as the numerical aperture of the objective increases. Comparing the surface of the spots in Fig. 3, the sizes for the three spots are: 0.20 NA, 24 mm^2; 0.40 NA, 96 mm^2; and 0.75 NA, 380 mm^2. In other words: the size of the fluorescent spot for the 0.75 NA objective is four times and fifteen times larger than the size of the fluorescent spots for the 0.40 NA and 0.20 NA objectives, respectively. When the surface of the spots were normalized to the surface of the spot seen with the 0.20 NA lens, the relative surface of the spot (1, 4 and 15) for the three objectives increased linearly with the collection efficiency of the objectives (1, 4 and 18%). Second, the three spots also differed in shape. For the 0.20 NA objective the spot is rectangular with the largest arista oriented in the same direction as the main axis of the

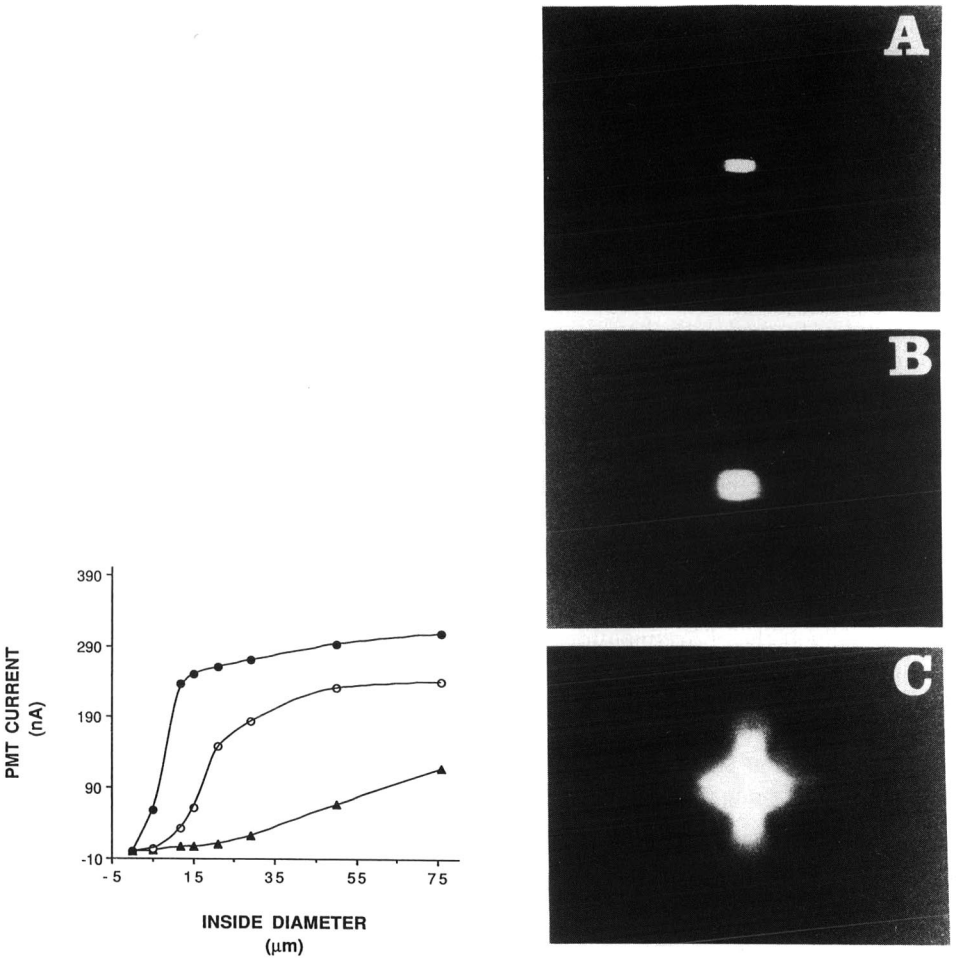

Fig. 2. Magnitude of a fluorescent signal as a function of the I.D. of the capillary and the numerical aperture of the objective. ● = 0.75 NA; ○ = 0.40 NA; ▲ = 0.20 NA. Notice the sharp rise of the intensity of the signal between the 5-μm and the 12-μm capillaries in the 0.75 NA curve.

Fig. 3. Microphotographs of the fluorescence with three objectives of different numerical aperture. (A) 0.20 NA, (B) 0.40 NA, (C) 0.75 NA. The size of th spot increases and the shape changes as the numerical aperture of the objectives increases. The 0.75 NA objective captures fluorescence emitted orthogonal as well as parallel to the main axis of the capillary. By contrast, the 0.20 NA and the 0.40 NA objectives capture only the fluorescence emitted parallel to the main axis of the capillary.

capillary. This shape is preserved by the 0.40 NA objective, but for the 0.75 NA objective the spot looks like a cross. Although it cannot be appreciated in these black-and-white reproductions, the cross is surrounded by a yellow halo that is produced by the walls of the capillary. The insertion of a spatial filter between the long wave pass filter and the notch filter reduces the size of the spot and suppresses the yellow halo (Fig. 4). At the same time there is a reduction of fluorescent intensity that can be compensated by raising the power of the laser.

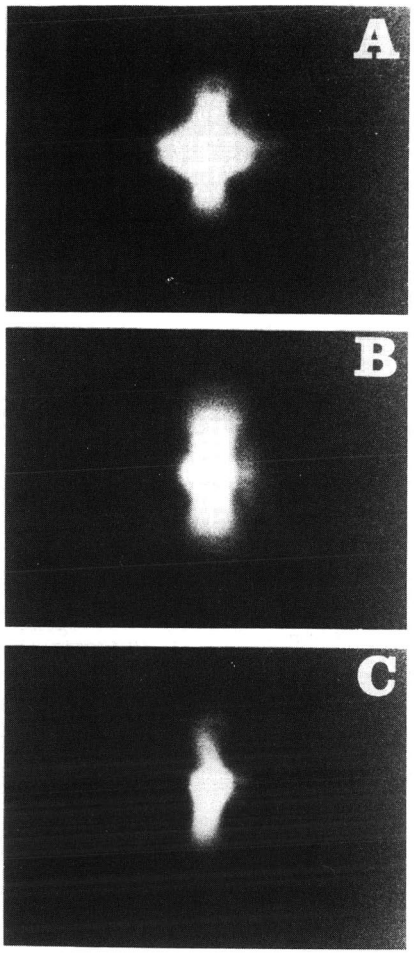

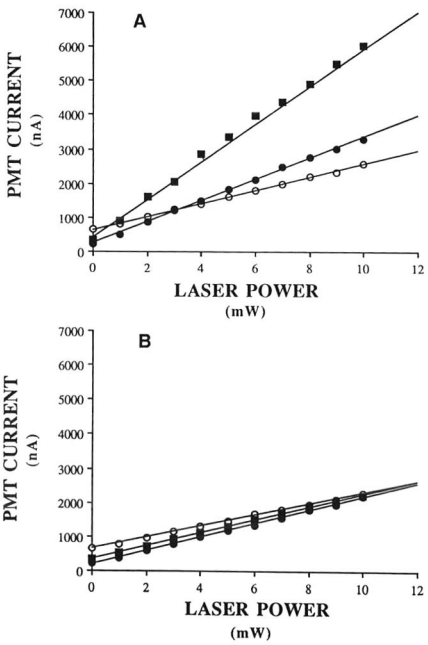

Fig. 4. Microphotographs showing the effects of spatial filters. (A) Unfiltered signal; (B) filtered through a 3 mm diameter spatial filter; (C) filtered through a 2 mm diameter spatial filter.

Fig. 5. Relationship between the laser power, the fluorescence and the numerical aperture of the objective. (A) Shows the fluorescence (in terms of PMT current) of a 10^{-10} *M* FTC-leucine solution *vs.* the laser power. Three objectives were tested: ■ = 0.75 NA, ● = 0.40 NA, ○ = 0.20 NA. The slope of the curves increases as a function of numerical aperture. (B) Shows the same relation but for a buffer filled capillary. No change of slope was observed as the numerical aperture of the objectives increased.

The increase of the laser power between 0 and 10 mW also increases the background light due to the capillary and the buffer, as shown in Fig. 5. However, the increase of numerical aperture increases the slope of the laser power *vs.* fluorescence curve only when a fluorescent solution is present into the capillary. As can be observed in Fig. 5, the slope of the curve generated by the 0.75 NA lens was 570, for the 0.40 NA the slope was 313.5 and for the 0.20 NA it was 193.7. This increase of signal due to the increase of numerical aperture is not observed when the buffer is filling the capillary. The bottom of Fig. 5 shows that the slopes of the equations for buffer-filled capillaries were 192, 198.5 and 166.5 for the 0.75, 0.40 and 0.20 NA objectives, respectively. The

fluctuations of the PMT current for the buffer were 1.76 ± 0.05 nA at any of the tested laser powers.

The result of the third experiment is shown in Fig. 6. The curve of fluorescent intensity rises from 515 nm and reaches a peak at 533 nm. Then it falls gradually to 585 nm. No peak is observed between 570 and 585 nm where the major Raman bands for water are located and detected in an orthogonal configuration.

Fig. 7 shows the electropherograms of six FTC-arginine solutions ranging from $2.1 \cdot 10^{-11}$ to $2.1 \cdot 10^{-6}$ *M* in steps of one order of magnitude. The top of the figure (electropherogram a) corresponds to the electropherogram of a $2.1 \cdot 10^{-11}$ *M* solution. The signal-to-noise ratio for this amount of FTC-arginine was 17:1. On this basis the LOCD was calculated to be a $3.75 \cdot 10^{-12}$ *M*. Since the signal was generated by an injection volume of 1 nl, the LOMD was $3.7 \cdot 10^{-3}$ amol or 2250 molecules. Fig. 7 also shows the log–log plot of concentration *vs.* signal intensity. This relationship was linear as demonstrated by the high correlation coefficient. The insets of Fig. 7 show the small margin of variation of the actual electropherograms, particularly between $2.1 \cdot 10^{-11}$ and $2.1 \cdot 10^{-7}$ *M* FTC-arginine concentrations. A large decrease of signal is observed at $2.1 \cdot 10^{-6}$ *M* (electropherogram f). However, the linearity of the measurements had a high correlation coefficient even when the data of the $2.1 \cdot 10^{-6}$ *M* solution were included in the analysis. For the detailed description of Fig. 7, please see the figure legend.

The result of the analysis of a mixture of six amino acids is shown in Fig. 8. The order of elution was arginine, leucine, methionine, cysteine, alanine and glycine. The concentration of FTC-amino acid was $2.1 \cdot 10^{-9}$ *M* for each. The peaks correspond to 2 amol in column. Arginine and glycine showed off-scale fluorescence, and cysteine showed the smallest signal. In addition, three blank peaks were observed. The largest

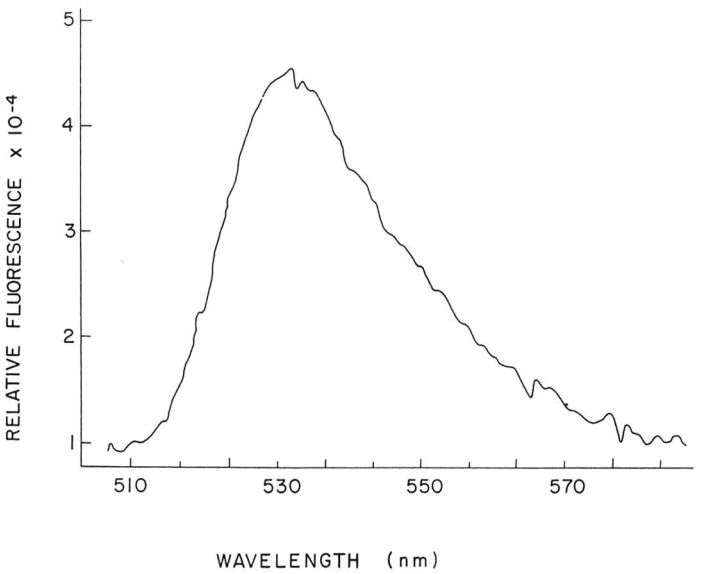

Fig. 6. Spectral analysis of a FTC-leucine solution. A peak is observed at 533 nm. No emission is observed between 560 and 580 nm.

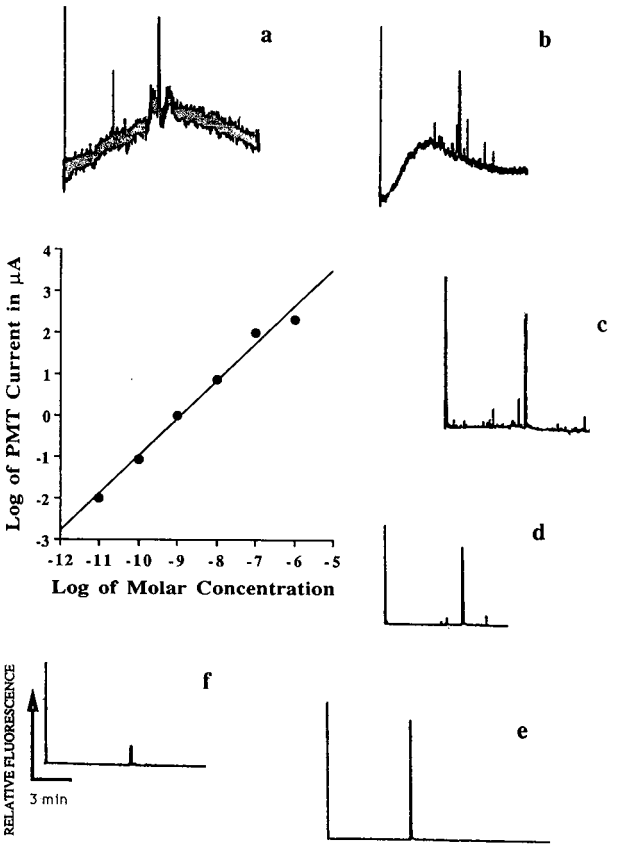

Fig. 7. Electropherograms of FTC-arginine solutions. The concentrations increased clockwise from a ($2.1 \cdot 10^{-11}$ *M*) to f ($2.1 \cdot 10^{-6}$ *M*) in steps of 10. The sensitivity of the instrument was decreased by steps of 10 from a to f. For example, the electropherogram c was generated at a sensitivity 1000 times lower than the electropherogram a. Between a and e the signals kept roughly the same height. Between e and f there is a decrease in signal height. The linearity of the instrument was analyzed by plotting the log of molar concentration *vs.* the log of the PMT current generated by the signal minus the baseline. Only between $2.1 \cdot 10^{-7}$ *M* and $2.1 \cdot 10^{-6}$ *M* was a deviation from linearity observed. The equation for this line was $y = 8.0 + 0.91x$ and the regression coefficient was $r = 0.98$.

one (peak 2) corresponds to unreacted fluorescein. Arginine and alanine had the trend to react fully with FITC. In their individual electropherograms no blank peaks were observed. By contrast, cysteine and glycine showed large peaks of unreacted FITC.

DISCUSSION

LIFD in a collinear arrangement allows on-column measurement of picomolar concentrations of FTC-amino acids in 25 μm I.D. capillaries. This represents an improvement of three orders of magnitude for laser-induced fluorescence on-column detection for CE. Several factors contribute to this sensitivity improvement. First, there is less Raman scattering due to the low volume of water in the detection cell, and

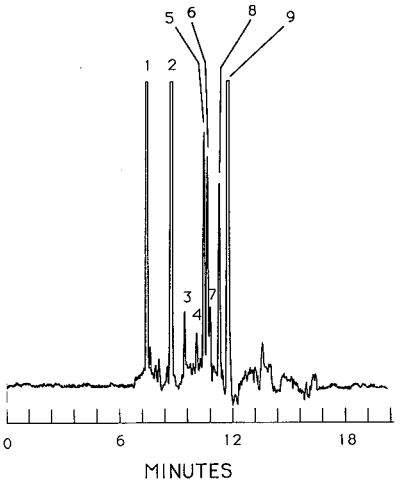

Fig. 8. Electropherogram of a mixture of six FTC-amino acids. The laser power was 4 mW, the spatial filter 2 mm diameter and the objective was the 0.75 NA one. The ocular was 10 ×. The analyte concentration was $2.1 \cdot 10^{-9}$ *M*, and the injection volume was 1 nl. The amount injected was 2.1 amol. Peaks: 1 = arginine; 2 = blank (probably unreacted FITC); 3 = blank; 4 = impurity of reagent; 5 = leucine; 6 = methionine; 7 = cysteine; 8 = alanine; 9 = glycine. FTC-arginine and FTC-glycine peaks were clipped.

due to the collinear collection of the fluorescence. The spectral analysis showed only the FITC emission band. No Raman bands were observed. Therefore, the background light was reduced and that allowed an increase in the current-to-voltage converter gain. Second, the collinear arrangement permits the use of higher numerical aperture lenses than those used in previous orthogonal instruments. This is an advantage because more fluorescence can be collected with large numerical aperture lenses. Fig. 3 shows that the largest numerical aperture gives the largest signal. In addition, Fig. 5 shows that the numerical aperture of the lenses is directly correlated with fluorescence collection but not with background radiation collection. In other words, the larger the numerical aperture of the lens, the larger the fluorescence, but this is not true for the background light produced by the capillary and the buffer. Therefore, the major source of noise in the instrument is scattered laser radiation, and not fluorescence of the capillary wall or the buffer. Third, the use of a notch filter to remove stray laser radiation decreases the background noise without significant decrease of the signal.

A 0.75 NA also allows work with narrow capillaries (between 12 and 15 μm I.D. capillaries) without a significant degradation of the LOCD due to smaller signal. Fig. 2 shows that there is a sharp drop in signal magnitude for the 0.40 NA lens when we pass from capillaries of 29 μm I.D. to 12 μm I.D. Such a drop was not observed with the 0.75 NA lens. This indicates that the instrument described here should perform with 12 μm I.D. capillaries nearly as well as with 25 μm I.D. capillaries. This feature can make it very useful for quick separation of amino acids by using the technique described by Nickerson and Jorgenson [10,11], with the advantage that the dynamic range will be extended to at least 10^{-11} *M* LOCD.

The collinear arrangement adds simplicity to the design of a laser-induced fluorescence detector. In fact, it eliminates the need for an optic bench. The instrument

of the present paper was assembled on a regular laboratory bench on a 40 × 50 cm area. This area is smaller than the one required to assemble orthogonal instruments. The alignment operation is also greatly simplified by the fact that it is visually guided with the microscope eyepieces and by means of a high quality *XY* displacer. Only one *XYZ* displacer is required in contrast with the orthogonal instruments in which at least two *XYZ* displacers are required. Moreover, orthogonal instruments require two optical systems, one for excitation and another for fluorescence collection. The present collinear instrument uses one optical system for both tasks. This helps to simplify the collinear instrument even further.

The linearity of the measurements extended over five orders of magnitude. Only at a very high concentration, $2.1 \cdot 10^{-6}$ *M* in the case of FTC-arginine, was deviation of linearity observed. Since this instrument is designed to work with rather small concentrations, the range of linearity of the instrument is satisfactory.

The sensitivity of this instrument still has considerable room for improvement. The dark current of the PMT operating in a dark room and with a shutter blocking all access of light to the tube, was about 200 pA with fluctuations of about 20 pA. The current generated by a picomolar solution was calculated to be about 6000 pA. It means that a picomolar solution can generate a signal 300 times larger than the dark current fluctuations of the PMT. However, the noise due to laser fluctuations was 1.76 nA, and the background current under our best conditions was about 90 nA. So the actual limiting factor for better sensitivity are the laser fluctuations. Nevertheless, the frequency of the laser fluctuations was about 1 Hz, and the minimal frequency of the unfilterad signal was 0.16 Hz. Therefore, with better electronic filtering, a noise reduction of at least one order of magnitude should be possible. This speculation indicates that, even though the sheath-flow cuvette technique still has the highest sensitivity for LIFD (the LOMD of the sheath-flow cuvette instrument is a few hundred molecules), in the near future, on-column detection with collinear arrangement could reach the sensitivity of post-column detection with the sheath-flow cuvette and orthogonal arrangement.

Another advantage of the collinear arrangement is that it simplifies the operation with multiple capillaries. Just by adding a motor-driven *XY* displacer it should be possible to change the excited capillary precisely. The technique of displacing an object by precise steps in the *XY* plane under the objective of a microscope is very well known in the field of microfluorometry. So it can be readily adapted to collinear LIFD with multiple capillaries. Currently, research is going on in this direction in our laboratories.

REFERENCES

1 E. Gassman, J. E. Kuo and R. Zare, *Science (Washington, D.C.)*, 230 (1985) 813.
2 D. Burton, M. J. Sepaniak and M. P. Maskarenik, *J. Chromatogr. Sci.*, 24 (1986) 347.
3 P. Gozel, E. Gassman, H. Michelsen and R. Zare, *Anal. Chem.*, 59 (1987) 44.
4 A. T. Balchunas and M. J. Sepaniak, *Anal. Chem.*, 59 (1987) 1466.
5 M. C. Roach, P. Gozel and R. Zare, *J. Chromatogr.*, 426 (1988) 129.
6 W. Kuhr and E. Yeung, *Anal. Chem.*, 60 (1988) 1832.
7 W. Kuhr and E. Yeung, *Anal. Chem.*, 60 (1988) 2642.
8 E. Yeung, *LC · GC*, 7 (1989) 118.
9 L. Gross and E. S. Yeung, *Anal. Chem.*, 62 (1990) 427.

10 B. Nickerson and J. W. Jorgenson, *J. High Resolut. Chromatogr.*, 11 (1988) 878.
11 B. Nickerson and J. W. Jorgenson, *J. High Resolut. Chromatogr.*, 11 (1988) 533.
12 P. L. Christensen and E. S. Yeung, *Anal. Chem.*, 61 (1989) 1344.
13 M. Yu and N. J. Dovichi, *Anal. Chem.*, 61 (1989) 37.
14 C.-Y. Chen, T. Demana, S. D. Huang and M. D. Morris, *Anal. Chem.*, 61 (1989) 1590.
15 D. J. Bornhop and N. J. Dovichi, *Anal. Chem.*, 59 (1987) 1632.
16 Y. F. Cheng and N. J. Dovichi, *Science (Washington, D.C.)*, 242 (1988) 562.
17 S. Wu and N. J. Dovichi, *J. Chromatogr.*, 480 (1989) 141.
18 H. Drossman, J. A. Luckey, A. J. Kostichka, J. D'Cunha and L. M. Smith, *Anal. Chem.*, 62 (1990) 900.
19 H. Swerdlow and R. Gesteland, *Nucleic Acid Res.*, 18 (1990) 1415.
20 A. S. Cohen, D. R. Najarian and B. L. Karger, *J. Chromatogr.*, 516 (1990) 49.
21 H. Swerdlow, S. Wu, H. Hake and N. J. Dovichi, *J. Chromatogr.*, 502 (1990) 61.
22 L. Hernandez, R. Marquina, J. Escalona and N. A. Guzman, *J. Chromatogr.*, 502 (1990) 247.
23 R. London, *Advanc. Phys.*, 13 (1960) 423.
24 D. A. Long, *Raman Spectroscopy*, McGraw-Hill, New York, 1977, pp. 46–75.
25 C. Daniel and F. S. Wood, *Fitting Equations to Data*, Wiley-Interscience, New York, 1971.

Journal of Chromatography, 559 (1991) 197–208
Elsevier Science Publishers B.V., Amsterdam

CHROM. 23 465

Instrumentation for high-performance capillary electrophoresis–mass spectrometry

RICHARD D. SMITH*, HAROLD R. UDSETH, CHARLES J. BARINAGA and CHARLES G. EDMONDS

Chemical Methods and Separations Group, Chemical Sciences Department, Pacific Northwest Laboratory, Richland, WA 99352 (USA)

ABSTRACT

An automated, commercially available capillary electrophoresis (CE) instrument was modified for interfacing with electrospray ionization mass spectrometry (ESI-MS). A Beckman P/ACE 2000 CE instrument with both electrokinetic and hydrostatic sample injection capabilities and efficient temperature control of the separation conditions was selected on the basis of these characteristics for this project. Modifications to it included extension of the fluid circulation path in an interface block extension and electrical modifications due to changes in electrophoresis current measurement capabilities. The capabilities for complete computer automation, capillary temperature control and on-line UV detection were retained. The minimum capillary length was increased by 35 cm due to the extension to the electrospray ionization–mass spectrometer interface. Initial results employing a laboratory-designed liquid sheath electrospray source are presented which show that very high separation efficiencies can be routinely obtained using the modified instrumentation. Capabilities for combined CE–MS are demonstrated for peptide and protein mixtures.

INTRODUCTION

The applications of capillary electrophoresis (CE) are expanding rapidly and a number of commercial instruments are now available. As applications have developed, the advantages of CE combined with mass spectrometry (MS) have been increasingly recognized and a number of laboratories are now pursuing instrumentation and method development for CE–MS. The first CE–MS was based on an electrospray ionization (ESI) interface developed in our laboratory [1,2]. Following this initial work with capillary zone electrophoresis–MS we reported an improved interface using a flowing sheath liquid electrode [3], the combination of capillary isotachophoresis with MS [4,5] and CE–MS–MS [5,6]. More recently, other researchers have reported on similar interfaces, including Hail *et al.* [7], Moseley *et al.* [8,9] and Lee *et al.* [10]. Alternative CE–MS interface designs have also been reported based on continuous-flow fast atom bombardment (CF-FAB) mass spectrometry [11–14]. However, the ESI methods appear to offer clear advantages in most instances owing to better sensitivity, reduced background and interface designs which do not require long transfer lines or incur a pressure drop across the capillary [15–17]. Per-

0021-9673/91/$03.50

haps the most significant advantage of the ESI interface to CE is the applicability to higher molecular weight compounds which are impractical by CF-FAB methods [18–20].

To date, none of the CE–MS instrumentation developed has effectively utilized the full capabilities of the automated CE instruments now commercially available. Such capabilities include precise electrokinetic or hydrostatic injection, on-column spectrophotometric detection and temperature control of nearly the entire capillary. The advantages of computer-controlled injection are significant for both accuracy and precision, as well as freedom from the frequent artifacts that arise from unreliable manual injection methods [21]. Temperature control has been recognized as important in obtaining good reproducibility for separations. Additionally we have noted the need to cool the ESI source under some operating conditions [17]. This arises from the fact that bubbles generated in either the CE capillary or the ESI sheath electrode (which consists largely of more volatile organic solvent) can create a region of high resistance and effectively terminate a separation. Hence our aim has been to exploit all the advantages of automated CE instrumentation, and particularly provisions for capillary temperature control.

In this paper, we describe the modifications made to a commercially available instrument, a Beckman (Palo Alto, CA, USA) P/ACE 2000 system. This instrument was selected on the basis of its advanced capabilities rather than ease of MS interfacing. Therefore, several hardware modifications were made which reflect the design of this particular CE instrument, as well as the physical constraints imposed by the design of the mass spectrometer used. We describe details of interface and hardware modifications, and report initial results which clearly show that the capabilities for high-performance CE separations are maintained in this CE–MS instrument.

EXPERIMENTAL

P/ACE 2000 system modifications

Physical constraints dictated some modifications. The Beckman P/ACE 2000 system as marketed is too large to be mounted directly in front of our mass spectrometers and still maintain the solution vials at the same height as the capillary outlet and inlet to the mass spectrometer. Height differences between the inlet and outlet lead to pressure driven flow (siphoning), which disturbs the flat flow profile of electrophoresis and degrades the separation efficiency. We opted to separate the P/ACE 2000 system into two subunits according to their practical and logical functions.

The autosampler, interface block, optics module and detector were removed from the mainframe and mounted in a box as a separate "experimental module". The system power supplies (high and low voltage), controller, keyboard, temperature and pressure controls were left on the mainframe as a "control module" (Fig. 1). All connecting electrical leads and cooling fluid and pressure lines were lengthened. The system was tested before and after modification to assure that no degradation of CE separation performance resulted from these changes.

One of the attractive features of the Beckman P/ACE 2000 system is the capability for temperature regulation of the capillary by means of fluid (a mixture of C_5–C_{18} perfluoro compounds containing sodium) circulation around the capillary. Our aim was to retain and enhance this feature when the system was adapted to use

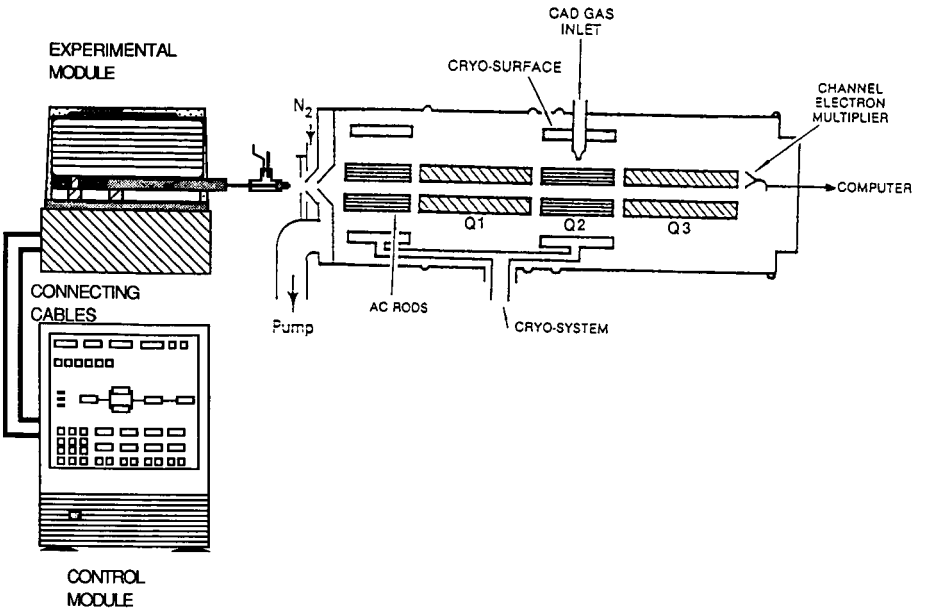

Fig. 1. Overall schematic illustration of the instrumentation for combined CE–MS showing the separated experimental and control modules of the Beckman P/ACE 2000 system.

on a mass spectrometer so as to retain temperature control over as much of the capillary as possible. In order to accomplish this, the interface block of the instrument (which holds the capillary cartridge) was modified by the addition of an extension. This extension attaches to the existing block and houses most of the added capillary. The extension is sealed by septa at each end, has separate inlet and outlet lines for the temperature regulation fluid and bolts onto the block immediately below the normal capillary exit. With the downstream septa removed the capillary can be threaded through the extension without removing it from the instrument. In this manner only 1 cm of the capillary between the cartridge and the extension housing is not temperature regulated by the fluid. Fluid is circulated in series through the capillary cartridge and the extension to the electrospray interface.

Relatively few changes to the instrument electronics were needed. The interlock to the high-voltage access panel of the mainframe was disabled. The instrument also checks to see that the current entering the capillary is the same as that leaving the capillary. When an electrospray source is coupled to the end of the column this condition could not be effectively fulfilled as the electrospray removes *ca.* 0.1 μA. This feature was disabled and the system no longer reported the column current. However, the output current of the high-voltage supply can be externally monitored, and this was done in our experiments.

With this arrangement, a capillary of *ca.* 35 cm additional length is required. A portion of this length remains in the air in order to facilitate connection to the current ESI source. However, this length can be reduced in future modifications by direct incorporation of the electrospray interface at the end of the extension.

Electrospray interface

The electrospray interface used is similar to that reported previously [3–6, 15–21] and is shown in Fig. 2. It incorporates a flowing sheath of liquid which allows the composition and flow-rate of the electrosprayed solution to be different than those of the electrophoresis system, a desirable feature when working with aqueous solutions. The electrical contact at the terminus of the capillary is also established through the liquid sheath (typically composed of methanol, acetonitrile, acetone or isopropanol with the addition of acetic acid and in some instances a small percentage of water). The electrical contact is made remotely to eliminate metal parts near the end of the capillary. In this interface design the sheath liquid and the electrospray/terminating electrode are introduced through on the same arm of a tee (see Fig. 2).

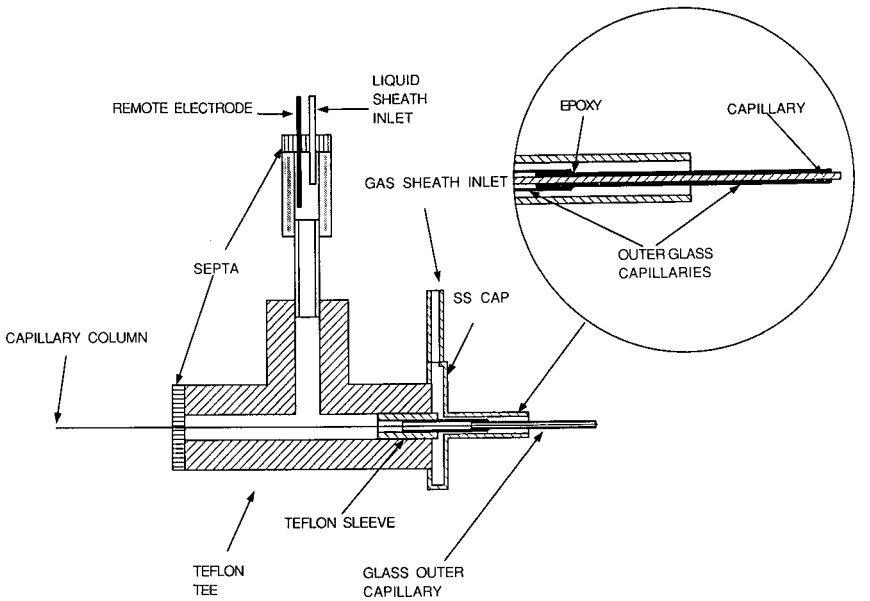

Fig. 2. Detailed schematic illustration of the electrospray ionization interface for combined CE–MS. The inset shows details of the ESI source "tip" region.

The ESI source consists of a 50 μm I.D. uncoated fused-silica capillary used for CE that protrudes 0.2–0.4 mm from a concentric fused-silica capillary. The continuously flowing liquid sheath provides a conducting path to the terminating electrode. This electrode is mounted in the adjacent arm of a 1/16-in. PTFE tee. High voltage, generally +4 to +6 kV for positive ions or −5 kV for negative ions, is applied to this electrode. The ESI source (CE capillary) tip is mounted *ca.* 1.5 cm from the ion sampling nozzle of the sampling orifice (nozzle) inlet to the quadrupole mass spectrometer. The mass spectrometer used for all reported results was a Sciex TAGA 6000E triple quadrupole mass spectrometer modified in our laboratory by the addition of a stage of differential pumping to improve sensitivity (Fig. 1).

A 3–6 l/min counter-current flow of nitrogen is introduced between the nozzle and ESI source to aid desolvation of the highly charged electrospray droplets and to minimize any solvent cluster formation during expansion into the vacuum chamber.

Analyte clustering of charged species is precluded by the mutual repulsion of highly charged ions and droplets. Clustering of any remaining solvent with analyte ions, and removal of residual solvent association, is effected by collisional activation in the interface [22]. A lens placed in front of the sampling nozzle is used to help focus the ions (or electrosprayed droplets) to the sampling orifice. Ions enter through a 1-mm diamter orifice and are focused efficiently into a 2-mm diameter skimmer orifice directly in front of the radiofrequency focusing quadrupole lens.

Materials

Biochemical samples were purchased from Sigma (St. Louis, MO, USA) and were used without further purification. Tryptic digests utilized an enzyme-to-substrate ratio of 1:25 in 50 m*M* ammonium hydrogen carbonate solution (pH 8.3) at 37°C for 18 h. The capillaries used in these studies are 50 μm I.D. × 185 μm O.D. uncoated fused silica with a polyimide sheath. It was purchased in bulk from Polymicro Technologies (Phoenix, AZ, USA) and cut to length. The acetonitrile was of UV grade from Burdick & Jackson Labs. (Muskegon, MI, USA). The water used was distilled and then processed in a Barnstead (Boston, MA, USA) Nanopure II reverse osmosis and ion-exchange system. As a final step before use, the water was filtered to remove particulates larger than 0.2 μm.

RESULTS AND DISCUSSION

Instrumental design considerations

In addition to maintaining the desired capabilities of the commercial CE instrumentation, *i.e.*, automation, precision injection, ancillary on-column UV detection and capillary temperature regulation, part of our efforts were dictated by a set of dimensional constraints. We wished to minimize any increase in the capillary length and minimize height differences between capillary termini. It was also desired that this could be accomplished with any of three ESI-MS instruments used in our laboratory. We decided to modify the CE instrument by separating the instrument into two modules consisting of the CE experimental module (automation, injection and detection hardware) and control module (power supplies, programming interface and ancillary equipment). Although physical separation of these modules was necessarily limited, these modifications removed the major constraints on obtaining the desired proximity to the ESI source.

Figure 1 gives a schematic illustration of the arrangement, showing the separated CE experimental and control modules of the Beckman P/ACE 2000 and the triple quadrupole mass spectrometer, a Sciex 6000 E modified as described previously. The separated modules allow the height of the experimental module to be adjusted for the separate demands of various mass spectrometers. The separation capillary extends *ca.* 10 cm beyond the temperature-regulated region of the interface block extension and forms the central capillary of the ESI source region (shown in detail in Fig. 2). In this region, the temperature is separately controlled by temperature control of the sheath liquid and surrounding gas flow (air). In these studies all experiments were conducted at 25°C, close to ambient temperature, and no additional temperature regulation of the ESI source was needed. Thus uniform temperature was well maintained over most of the capillary length. The minimum column length for the Beckman P/ACE 2000

with the conventional cartridge design was increased by *ca.* 35 cm, increasing the minimum column length to *ca.* 60 cm. Incorporation of the ESI interface on the end of the interface block extension, and minimizing the size of this extension, would reduce this length by *ca.* 10 cm.

CE–MS operation

Prior to and between each experiment, the capillary column was flushed and rinsed on a fixed schedule. Approximately four column volumes of 0.1 *M* sodium hydroxide solution were used to flush the column. This was followed by *ca.* eight column volumes of doubly distilled water and finally by 24 column volumes of the running buffer solution. Samples were injected for 10 s in the low-pressure injection mode. UV detection was monitored at 214 nm and on-line with the mass spectrometry in all instances. The UV detection window was approximately in the middle of the capillary column and thus analyte signals in the UV trace could be directly compared with the MS signals by approximately doubling the time of detection.

The effect of siphoning on the performance of the system was investigated in a series of experiments in which the height difference between the inlet reservoir and the electrospray tip was changed from 0 to 2.5 cm. This resulted in a 4% decrease in the elution time and no significant change in the widths of the peaks or the resolution of the separation. It was found, however, that the reliability of the ESI source was improved with the 2.5-cm height difference. The background noise in the spectra was reduced and the signal levels were improved. Therefore, in these preliminary studies a 2.5-cm height difference was maintained.

The mass spectrometer was tuned by injecting a standard solution through the electrophoresis capillary by using the high-pressure rinse mode of the P/ACE system to force the sample through the column. Hence neither the physical layout of the system components nor the operating parameters are changed when switching from MS tuning to CE–MS operation. The full specificity in mass spectrometric analysis in combination with analytical separations is obtained in general by the acquisition of the full m/z range over the time course of the separation. With the present quadrupole instrumentation, the time required for acquisition of the full mass spectrum at useful ratios signal-to-noise ratios for large molecules exceeds the typical peak width in capillary electrophoresis. These limitations could be largely removed by the development of more efficient ion transport methods from the ESI source, or the use of an ion trap mass spectrometer. In our experiments we have monitored selected m/z values specific to the known constituents of our samples determined by prior injection of the unseparated sample. For the present experiments this multiple ion monitoring method permits the evaluation of our interface development. Additionally, practical applications based on the analysis of known targeted compounds is well suited to current capabilities. However, the full realization of the specificity for scanning mass spectrometry in combination with capillary electrophoresis for the classes of analyte chosen here (particularly proteins) will benefit significantly from further advances in the sampling, analysis and detection of electrospray ions.

Peptide and protein CE–MS separations

The performance of the combined CE–MS system was evaluated in these preliminary studies with a mixture of myoglobin proteins ($M_r \approx 17$ kilodalton). The

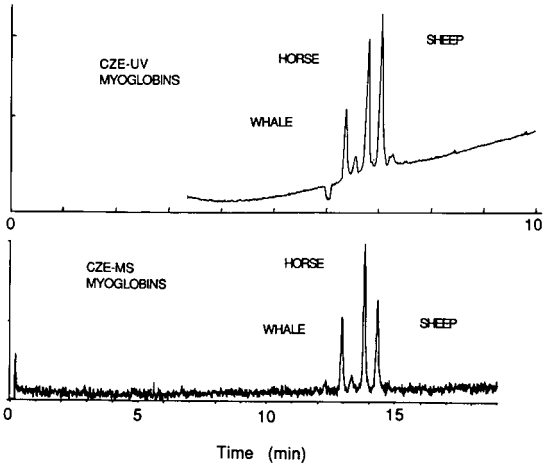

Fig. 3. CE–MS separation of a mixture of whale (M_r 17 199.1), horse (M_r 16 950.7) and sheep (M_r 16 923.3) myoglobins. The on-line UV response and later MS reconstructed ion signal have been superimposed with adjusted time scales. The separation was done in 10 m*M* Tris (pH 8.3) at 120 V/m. Approximately 100 fmol per component were injected.

separation was done in 10 m*M* Tris buffer (pH 8.3) with an electric field strength of 120 V/cm. Approximately 100 fmol per component were injected onto the capillary column. The results are shown in Fig. 3. The top half of the figure shows the UV trace for the separation and the bottom half is the reconstructed ion electropherogram (RIE) from MS detection for the same separation. MS detection is accomplished at about twice the separation time for the on-column UV detection. It is clear that the ESI–MS interface has not degraded the separation by broadening of the peaks in the electrospray source. We estimate that the additional volume of mixing at our interface is less than 10 nl (composed primarily of sheath liquid) and therefore one would not expect significant peak broadening. Measurements of the peak widths in this experiment show that peaks in the UV trace are 3.5 s wide at half-height and those in the RIE are 4.5 s wide. These measurements show that the combined electrophoretic and detector contributions to broadening are modest and the major source of peak broadening in this experiment results from the injection step. More efficient injection methods designed to concentrate the analyte at the head of the column would reduce the peak width in these separations to *ca.* 1 s at the UV detector. As the widths of the peaks decrease, the effect of the width of the detector window becomes more important. Finite width windows in optical systems will inevitably broaden very narrow peaks. The mass spectrometer with this ESI interface offers a detector where the only possible peak broadening is mixing in the small volume at the ESI source [2,4], which is negligible for conventional CE separation times. In fact, these peak widths are sufficiently narrow to exceed current capabilities when signal intensities are low and slower scan speed required. For targeted compound analysis, where a single ion could be monitored continuously, detecting peaks of 0.1 s in width could be done without detector broadening.

The specificity of mass spectrometric detection can provide useful additional information even when only a few ions are monitored, as in this example. Three ions

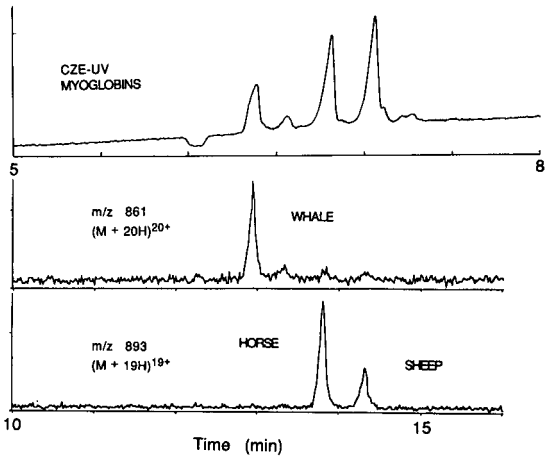

Fig. 4. Expanded view and single-ion electropherograms for the separation shown in Fig. 3. The molecular ion at m/z 861 is characteristic of whale myoglobin and shows that this molecule elutes first. The ions from horse and sheep myoglobin could not be resolved in these experiments, and a common response is seen at m/z 893. The excellent reproducibility of the electropherograms allowed retention time indices from the injection of pure compounds to determine the order of elution.

were monitored at m/z 893, 861 and 617. The resolution setting of the mass spectrometer was too low to distinguish the 19^+ molecular ion of horse myoglobin (M_r 16 950.7) from the same ion of sheep myoglobin (M_r 16 923.3) and both species were detected at m/z 893. Whale myoglobin (M_r 17 199.1) was detected at m/z 861 and carried 20^+ charges. The ion at m/z 617 is due to the heme group of the myoglobins. Fig. 4 gives an expanded view of the UV and selected m/z electropherogram for the molecular ions. As the heme is not covalently bound to these proteins it is labile under typical ESI conditions (*i.e.*, with organic solvents and/or acidic pH). In these experi-

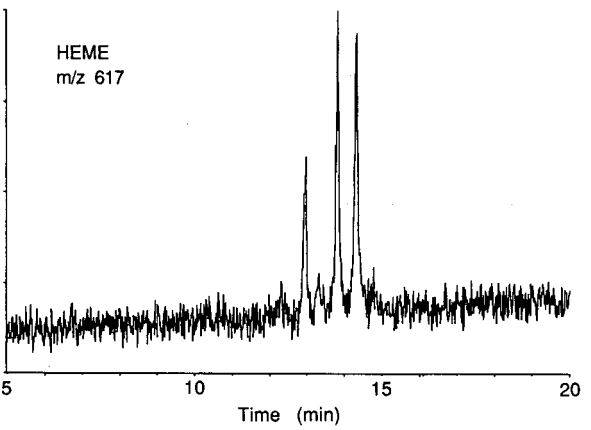

Fig. 5. Single-ion electropherogram of the ion of m/z 617 from the separation shown in Fig. 3. This signal derives from the non-covalently bonded heme group, which is labile (detached) under the ESI source conditions. The peak between the whale and horse myoglobins indicates that the heme moiety is also present in the contaminant and detached during ESI-MS analysis.

ments it accounts for approximately half the signal in each of the large peaks. Two other peaks are clearly evident in the UV trace. The peak eluting after the three myoglobins does not appear in the RIE and is not closely related to the myoblobins. The peak appearing between the whale and horse myoglobins does respond to the mass spectrometer. An examination of the single-ion plot for m/z 617 (Fig. 5) shows a corresponding response indicating that the peak is in response to an ion containing the heme moiety. As the heme appears in the mass spectrum at its characteristic m/z value, it is bound by hydrogen bonds to the protein during electrophoretic separation in the column. This is consistent with the known structure of myoglobin under the separation conditions. A response at m/z 861 but not at m/z 893 allows us to conclude that the polypeptide is similar in molecular weight to the whale myoglobin, and therefore that the small peak is probably due to a variant of whale myoglobin with a non-covalenly bound heme group. These results were obtained from the injection of 100 fmol per component.

With the ability of ESI to produce molecular ions with more than one charge, the idenfication of a compound from its response at a single m/z in the spectrum is risky. Multiple ion detection of two or more of these allows for more positive identification. The analysis of a sample of B-chain insulin provides an example. Fig. 6 shows the single-ion electropherograms for two molecular ions found in the ESI mass spectra of B-chain insulin. The separation was done in 10 m*M* Tris (pH 8.3) at an electric field strength of 150 V/cm on 0.7 pmol of sample. UV detection showed a second peak eluting after the main peak. The simultaneous MS detection of a corresponding peak in both single-ion plots suggests that the contaminant is probably a dimer, or possibly a variant of the peptide differing only slightly in mass. The dimer is indeed a significant contributor to the ESI mass spectra of this species, supporting this origin.

As an example of a separation of a more complex mixture, a tryptic digest of tuna cytochrome *c* was also examined. A sample of the digest was initially infused into the mass spectrometer and an ESI mass spectrum recorded. The most prominent

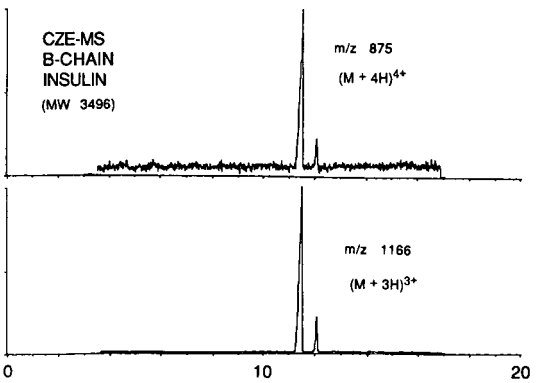

Fig. 6. Multiple-ion detection of the two ions characteristic of B-chain insulin in ESI. The electrophoresis was done in 10 m*M* Tris (pH 8.3) at 150 V/m. The response at both values of m/z suggests that the second peak is likely a dimer, or alternatively is a digopeptide variant of similar molecular weight to B-chain insulin.

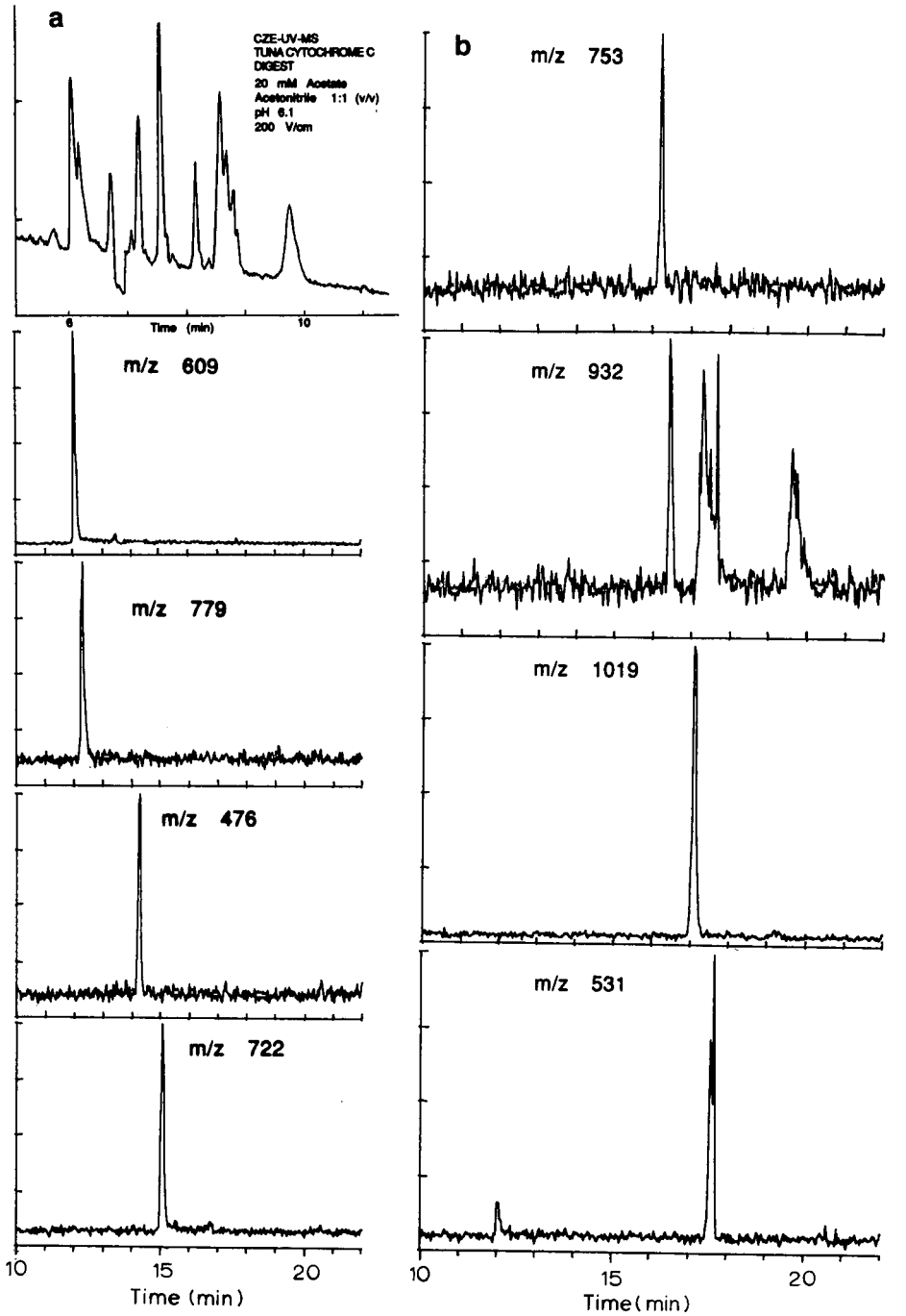

Fig. 7. CE–MS separation with on-line UV detection of a tryptic digest of tuna cytochrome *c*. The UV trace and several selected ion electropherograms are given in (a), superimposed as in Fig. 3. In (b) four later eluting ions are shown. Most of the peaks in the UV signal correlate with strong signals in mass spectrometry. Approximately 0.6 pmol per component was injected.

ions in the spectra were identified and these were monitored in a multiple-ion detection CE–MS experiment. The separation was carried out in 20 m*M* acetate buffer (pH 6.1) mixed with an equal volume of acetonitrile. The field strength used for the separation was raised to 200 V/cm to compensate for the reduced electroosmosis and the resulting longer analysis times. The results are shown in Fig. 7. Again, the time to the mass spectrometer is approximately twice the time of detection at the UV monitor. Most of the major features of the UV trace are reproduced by the ions monitored. These ions correlate with expected tryptic fragments. It is again apparent that the ESI interface has not degraded the separation.

CONCLUSION

A commercially available, automated electrophoresis instrument can be successfully adapted to ESI-MS. The interface provides a very low dead volume detector that does not compromise the performance of the system. This low dead volume is of interest in the detection of very narrow peaks, where detector broadening is intolerable, and optimum separation efficiency is desired.

ACKNOWLEDGEMENTS

We thank Beckman Instruments for support of this work and Howard Whitted of Beckman Instruments for advice and extensive assistance in the modification of the CE instrumentation.

REFERENCES

1 J. A. Olivares, N. T. Nguyen, C. R. Yonker and R. D. Smith, *Anal. Chem.*, 59 (1987) 1230.
2 R. D. Smith, J. A. Olivares, N. T. Nguyen and H. R. Udseth, *Anal. Chem.*, 60 (1988) 436.
3 R. D. Smith, C. J. Barinaga and H. R. Udseth, *Anal. Chem.*, 60 (1988) 1948.
4 H. R. Udseth, J. A. Loo and R. D. Smith, *Anal. Chem.*, 61 (1989) 228.
5 R. D. Smith, S. M. Fields, J. A. Loo, C. J. Barinaga, H. R. Udseth and C. G. Edmonds, *Electrophoresis*, 11 (1990) 709.
6 C. G. Edmonds, J. A. Loo, S. M. Fields, C. J. Barinaga, H. R. Udseth and R. D. Smith, in A. L. Burlingama and J. A. McCloskey (Editors), *Biological Mass Spectrometry*, Elsevier, Amsterdam, 1990, p. 77.
7 M. Hail, J. Schwartz, I. Mylchreest, K. Seta, S. Lewis, J. Zhou, I. Jardine, J. Liu and M. Novotny, in *Proceedings of the 38th ASMS Conference on Mass Spectrometry and Allied Topics, Tucson, AZ, June 3–8, 1990*, p. 353.
8 M. A. Moseley, L. J. Deterding, K. B. Tomer and J. W. Jorgenson, *J. Chromatogr.*, 516 (1990) 167.
9 M. A. Moseley, L. J. Deterding, K. B. Tomer and J. W. Jorgenson, *Anal. Chem.*, 63 (1991) 109.
10 E. D. Lee, W. Mück, J. D. Henion and T. R. Covey, *Biomed. Environ. Mass Spectrom.*, 18 (1989) 844.
11 M. A. Moseley, L. J. Deterding, K. B. Tomer and J. W. Jorgenson, *J. Chromatogr.*, 480 (1989) 197.
12 R. M. Caprioli, W. T. Moore, M. Martin, B. B. DaGue, K. Wilson and S. Moring, *J. Chromatogr.*, 480 (1989) 247.
13 N. J. Reinhoud, E. Schroder, U. R. Tjaden, W. M. A. Niessen, M. C. ten Noever de Brauw and J. van der Greef, *J. Chromatogr.*, 516 (1990) 147.
14 M. A. Moseley, L. J. Deterding, K. B. Tomer and J. W. Jorgenson, *J. Chromatogr.*, 516 (1990) 167.
15 R. D. Smith, J. A. Loo, C. J. Barinaga, C. G. Edmonds and H. R. Udseth, *J. Chromatogr.*, 480 (1989) 211.
16 C. G. Edmonds, J. A. Loo, C. J. Barinaga, H. R. Udseth and R. D. Smith, *J. Chromatogr.*, 474 (1989) 21.

17 R. D. Smith, J. A. Loo, C. G. Edmonds, C. J. Barinaga and H. R. Udseth, *J. Chromatogr.*, 516 (1990) 157.
18 R. D. Smith, J. A. Loo, C. G. Edmonds, C. J. Barinaga and H. R. Udseth, *Anal. Chem.*, 62 (1990) 882.
19 J. A. Loo, C. G. Edmonds, H. R. Udseth and R. D. Smith, *Anal. Biochem.*, 179 (1989) 404.
20 J. A. Loo, H. K. Jones, C. G. Edmonds, H. R. Udseth and R. D. Smith, *J. Microcol. Sep.*, 1 (1989) 223.
21 R. D. Smith, H. R. Udseth, J. A. Loo, B. W. Wright and G. A. Ross, *Talanta*, 36 (1989) 161.
22 R. D. Smith, J. A. Loo, C. J. Barinaga, C. G. Edmonds and H. R. Udseth, *J. Am. Soc. Mass Spectrom.*, 1 (1990) 53.

Journal of Chromatography, 559 (1991) 209–214
Elsevier Science Publishers B.V., Amsterdam

CHROM. 23 466

Chiral separations by micellar electrokinetic chromatography with sodium N-dodecanoyl-L-valinate

KOJI OTSUKA*, JUNKO KAWAHARA and KAORU TATEKAWA
Department of Industrial Chemistry, Osaka Prefectural College of Technology, Saiwai-cho, Neyagawa, Osaka 572 (Japan)
and
SHIGERU TERABE
Department of Material Science, Faculty of Science, Himeji Institute of Technology, Harima Science Park City, Kamigori, Hyogo 678–12 (Japan)

ABSTRACT

Chiral separations by micellar electrokinetic chromatography with sodium N-dodecanoyl-L-valinate (SDVal) were investigated. Addition of sodium dodecyl sulphate (SDS), urea and methanol to SDVal micellar solutions improved the peak shapes and resolution and also changed the selectivity. Phenylthiohydantoin (PTH) derivatives of six DL-amino acids (serine, α-aminobutyric acid, norvaline, valine, tryptophan and norleucine) were separated from each other and each pair of enantiomers was optically resolved with a 50 m*M* SDVal–30 m*M* SDS–0.5 *M* urea (pH 9.0)–10% (v/v) methanol solution. Some other enantiomers were also resolved.

INTRODUCTION

Recently, high-performance capillary electrophoresis (HPCE) [1–3], an instrumental version of electrophoresis, has been widely used in various fields because of its high efficiency. Most commercial HPCE instruments are operated automatically with microcomputer systems so that they can be used for routine work. Electrokinetic chromatography (EKC) [4], which is one branch of HPCE and based on chromatographic principles using homogeneous solutions, has also become a well known high-resolution separation technique. One of the unique characteristics of EKC is that it can separate both neutral analytes and charged solutes electrophoretically. Among various modes of EKC, micellar EKC (MEKC) [5,6], also called micellar electrokinetic capillary chromatography (MECC) [7], has become the most popular method for separating small neutral compounds. MEKC uses an ionic micelle as a "carrier" in EKC [4].

Chiral separations will be one of the major applications of both HPCE and EKC. Zare and co-workers [8,9] first reported optical resolution by EKC using copper(II) complexes. In MEKC, optical resolution of racemic compounds can be

0021-9673/91/$03.50

achieved by using chiral surfactants. Recently, some papers have appeared on chiral separations by MEKC without any additives such as metal ions or complexation reagents. As chiral surfactants L-amino acid derivatives, *e.g.*, sodium N-dodecanoyl-L-valinate (SDVal) [10,11], or bile salts [12–14] were used. We have reported the enantiomeric resolution of some phenylthiohydantoin-DL-amino acids (PTH-DL-AA) by MEKC with chiral surfactants, digitonin and SDVal [15]. Some PTH-DL-AA were optically resolved with SDVal alone, although seriously tailed peaks were observed. By adding methanol and urea to SDVal solutions, the worst peak shapes could be improved and the selectivity changed, but sufficient resolution was not attained because of the small capacity factors of the solutes and/or narrow migration-time window [16].

In this investigation, we used SDVal–sodium dodecyl sulphate (SDS) co-micellar solutions containing methanol and urea to improve resolution through increased capacity factors and extended migration-time windows. Changes in the selectivity were also observed. Some PTH-DL-AA were successfully optically resolved and separated from each other. Some other enantiomers were also resolved.

EXPERIMENTAL

SDVal was obtained from Ajinomoto (Tokyo, Japan), SDS and methanol from Nacalai Tesque (Kyoto, Japan), urea and PTH-DL-AA from Wako (Osaka, Japan), benzoin from Tokyo Kasei (Tokyo, Japan) and warfarin from Tanabe Seiyaku (Osaka, Japan). All chemicals were used as received.

Micellar solutions were prepared by dissolving SDVal, SDS and urea in 50 m*M* borate buffers (pH 9.0) or 50 m*M* phosphate buffers (pH 7.0) and then mixed with appropriate amounts of methanol. PTH-DL-AA were injected as acetonitrile solutions and benzoin and warfarin as methanol solutions.

An untreated fused-silica capillary tube (Scientific Glass Engineering, Ringwood, Australia), 650 mm × 0.05 mm I.D., was used as a separation column, and on-column UV detection was carried out at a position 500 mm from the injection end with an SPD-6A spectrophotometric detector (Shimadzu, Kyoto, Japan). A Chromatopac C-R6A (Shimadzu) was used for data processing. Samples were injected manually by siphoning [5]. An HepLL-30P0.08-LS (Matsusada, Kusatsu, Shiga, Japan) was used for a regulated high-voltage power supply operated in the constant-voltage mode. All experiments were carried out at ambient temperature.

RESULTS AND DISCUSSION

Optical resolution of PTH-DL-AA

As reported previously [16], the addition of 5 *M* urea to a 25 m*M* SDVal solution (pH 7.0) containing 10% (v/v) methanol led to a significant improvement in peak shapes. PTH derivatives of three DL-amino acids, norvaline, tryptophan and norleucine, were separated from each other and each pair of enantiomers was resolved. However, reduced capacity factors ($\tilde{k}'$) of the solutes compared with those in the absence of urea were observed and sufficient resolution was not attained although the migration-time window was not narrower. The effects of urea addition will be reported elsewhere [17]: $\log \tilde{k}'$ decreases with increasing concentration of urea (C_{urea}).

The value of t_0/t_{mc}, which is related to the migration-time window [6], also decreases with increasing C_{urea}, where t_0 and t_{mc} are the migration times of an insolubilized solute and of the micelle, respectively, that is, the migration-time window increases with increasing C_{urea}. Although the reason for the improvement in peak shapes on addition of urea is not clear, the adsorption of urea on the inside wall of the fused-silica capillary might prevent the irreversible adsorption of solutes, hence improving the peak shapes.

The capacity factor is related to the concentration of the surfactant (C_{sf}) by [6]

$$\tilde{k}' = K\bar{v}(C_{sf} - \text{CMC}) \quad (1)$$

where K, $\bar{v}$ and CMC are the distribution coefficient, partial specific volume of the micelle and critical micelle concentration, respectively. The term $C_{sf} - \text{CMC}$ represents the net concentration of the micelle. Therefore, larger $\tilde{k}'$ can be obtained with higher C_{sf}. To increase the capacity factors and improve the resolution, we tried to use a higher SDVal concentration, 50 mM, and a lower concentration of urea, 0.5 M, keeping the amount of methanol constant. Here, the pH of micellar solutions was selected as 9.0 to increase the solubility of SDVal. In the pH range 7–9, both the electroosmotic velocity and electrophoretic velocity of the micelle were found to be almost constant [18,19]. With the SDVal–urea–methanol solution, however, improvements in both resolution and separation were not achieved.

We then examined the addition of SDS to the SDVal–urea–methanol solutions. In this instance, negatively charged SDVal–SDS mixed micelles were formed in the solution [10,11] and the selectivity was expected to be changed. By using 50 mM SDVal–30 mM SDS–0.5 M urea (pH 9.0)–10% (v/v) methanol, PTH derivatives of six DL-amino acids, serine (Ser), α-aminobutyric acid (Aba), norvaline (Nva), valine (Val), tryptophan (Trp) and norleucine (Nle), were separated from each other and each DL-pair was optically resolved as shown in Fig. 1. Although PTH-DL-Ser was partially resolved, this pair of enantiomers could not be resolved with SDVal alone, SDVal–methanol or SDVal–methanol–urea solutions. For another PTH derivative, methionine (Met) was successfuly resolved as shown in Fig. 2, but it could no be separated from above six PTH-DL-AA in Fig. 1.

For each pair of the six PTH-DL-AA in Fig. 1, $\tilde{k}'$, the separation factor (α) and resolution (R_s) were calculated using the equations reported previously [6]. The results are given in Table I. Here, t_o and t_{mc} were obtained from the migration times of acetonitrile and Sudan IV, respectively. Note that Sudan IV was assumed not to exist even in the aqueous phase containing methanol. In this instance, $t_0/t_{mc} = 0.16$ and this value is smaller than that in 20 mM SDVal alone (0.20) [15], that is, an extended migration-time window was achieved. All the values of $\tilde{k}'$ for each solute in Table I are 3–4 times larger than those observed with 20 mM SDVal [15]. As the $\tilde{k}'$ values for Ser and Aba are smaller than the optimum value of 2–3, the resolution between each pair of enantiomers might be improved when these $\tilde{k}'$ are increased to the optimum value.

To examine the effect of urea addition, we used the same micellar solution as in Fig. 1 without urea, *i.e.*, 50 mM SDVal–30 mM SDS–10% (v/v) methanol, for separating the same PTH-DL-AA. In this instance, Nva and Val co-migrated and Ser was still only partially resolved although the migration order was the same as in Fig. 1.

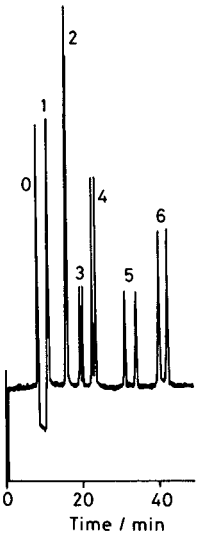

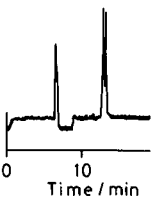

Fig. 1. Chiral separation of six PTH-DL-AA by MEKC. Corresponding amino acids: 1 = Ser; 2 = Aba; 3 = Nva; 4 = Val; 5 = Trp; 6 = Nle. 0 = acetonitrile. Micellar solution, 50 m*M* SDVal–30 m*M* SDS–0.5 *M* urea (pH 9.0) containing 10% (v/v) methanol; separation column, 650 mm × 0.05 mm I.D.; length of the tube used for separation, 500 mm; total applied voltage, 20 kV; current, 17 μA; detection wavelength, 260 nm; temperature, ambient.

Fig. 2. Chiral separation of PTH-DL-Met by MEKC. current, 19 μA; other conditions as in Fig. 1.

Resolution of other chiral compounds

The optical resolution of various chiral compounds was investigated with the same SDVal–SDS–urea–methanol solution as in Fig. 1. As a result, 2-hydroxy-1,2-diphenylethanone (benzoin) and 4-hydroxy-3-(3-oxo-1-phenylbutyl)-2H-1-benzopyran-2-one (warfarin) were successfully resolved, as shown in Fig. 3. These two compounds were not optically resolved with SDVal alone, SDVal–methanol or SDVal–methanol–urea solutions. Moreover, they could not be resolved with digitonin–SDS solutions.

TABLE I

CAPACITY FACTORS ($\tilde{k}'$), SEPARATION FACTORS (α) AND RESOLUTION (R_s) OF SOME PTH DERIVATIVES OF DL-AMINO ACIDS

Conditions as in Fig. 1.

Solute	$\tilde{k}'_1$	$\tilde{k}'_2$	α	R_s
Ser	0.5	0.5	1.00	
Aba	1.4	1.4	1.04	0.7
Nva	2.2	2.4	1.10	1.7
Val	3.2	3.4	1.09	1.8
Trp	7.0	9.2	1.32	3.6
Nle	16.8	22.2	1.32	3.0

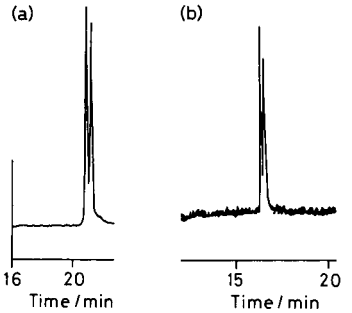

Fig. 3. Optical resolution of (a) benzoin and (b) warfarin by MEKC. current, (a) 20 μA and (b) 19 μA; other conditions as in Fig. 1.

CONCLUSIONS

The addition of SDS to SDVal–urea–methanol solutions caused a change in selectivity and provided a good enantiomeric resolution of PTH-DL-AA and some other enantiomers. The addition of urea to the micellar solution was also effective in improving the peak shapes and resolution. There remain many chiral compounds that cannot be resolved with the same SDVal–SDS–urea–methanol solution. At present, the possibilities for chiral separations of various kinds of enantiomers by MEKC are limited as long as only one type of chiral surfactant is used. Further applications to chiral separations of other compounds are being investigated with some other surfactants and additives.

ACKNOWLEDGEMENTS

The authors are grateful to Dr. Akio Ishiwata of Ajinomoto for kindly providing SDVal. This work was supported in part by a Grant-in-Aid for Scientific Research (No. 02750564) from the Ministry of Education, Science and Culture, Japan.

REFERENCES

1 F. E. P. Mikkers, F. M. Everaerts and Th. P. E. M. Verheggen, *J. Chromatogr.*, 169 (1979) 11–20.
2 J. W. Jorgenson and K. D. Lukacs, *Anal. Chem.*, 53 (1981) 1298–1302.
3 S. Hjertén, *J. Chromatogr.*, 270 (1983) 1–6.
4 S. Terabe, *Trends Anal. Chem.*, 8 (1989) 129–134.
5 S. Terabe, K. Otsuka, K. Ichikawa, A. Tsuchiya and T. Ando, *Anal. Chem.*, 56 (1984) 111–113.
6 S. Terabe, K. Otsuka and T. Ando, *Anal. Chem.*, 57 (1985) 834–841.
7 D. E. Burton, M. J. Sepaniak and M. P. Maskarinec, *J. Chromatogr. Sci.*, 24 (1986) 347–351.
8 E. Gassmann, J. E. Kuo and R. N. Zare, *Science (Washington, D.C.)*, 230 (1985) 813–814.
9 P. Gozel, E. Gassmann, H. Michelsen and R. N. Zare, *Anal. Chem.*, 59 (1987) 44–49.
10 A. Dobashi, T. Ono, S. Hara and J. Yamaguchi, *Anal. Chem.*, 61 (1989) 1984–1986.
11 A. Dobashi, T. Ono, S. Hara and J. Yamaguchi, *J. Chromatogr.*, 480 (1989) 413–420.
12 S. Terabe, M. Shibata and Y. Miyashita, *J. Chromatogr.*, 480 (1989) 403–411.
13 H. Nishi, T. Fukuyama, M. Matsuo and S. Terabe, *J. Microcolumn Sep.*, 1 (1989) 234–241.
14 H. Nishi, T. Fukuyama, M. Matsuo and S. Terabe, *J. Chromatogr.*, 515 (1990) 233–243.
15 K. Otsuka and S. Terabe, *J. Chromatogr.*, 515 (1990) 221–226.

16 K. Otsuka and S. Terabe, *Electrophoresis*, 11 (1990) 982–984.
17 S. Terabe, Y. Ishihama, H. Nishi, T. Fukuyama and K. Otsuka, *J. Chromatogr.*, 545 (1991) 359–368.
18 S. Terabe, H. Utsumi, K. Otsuka, T. Ando, T. Inomata, S. Kuze and Y. Hanaoka, *J. High Resolut. Chromatogr. Chromatogr. Commun.*, 9 (1986) 666–670.
19 K. Otsuka and S. Terabe, *J. Microcolumn Sep.*, 1 (1989) 150–154.

Journal of Chromatography, 559 (1991) 215–222
Elsevier Science Publishers B.V., Amsterdam

CHROM. 23 494

Selected applications of cyclodextrin selectors in capillary electrophoresis

JIRI SNOPEK[a], HELENA SOINI[b] and MILOS NOVOTNY*
Department of Chemistry, Indiana University, Bloomington, IN 47405 (USA)
and
EVA SMOLKOVA-KEULEMANSOVA and IVAN JELINEK
Department of Analytical Chemistry, Charles University, Albertov 2030, CS 128 40 Prague 2 (Czechoslovakia)

ABSTRACT

Through the use of α-, β-, γ- and heptakis(2,6-di-O-methyl)-β-cyclodextrin as stereospecific selectors or electrolyte modifiers, both in capillary zone electrophoresis and isotachophoresis, selected model isomeric compounds (including optical isomers) were resolved. Soluble alkylhydroxyalkylcellulose derivatives were further added to the cyclodextrin-modified background electrolytes under study. Their presence was found to be essential, as demonstrated by improvements in both enantioselectivity and separation efficiency. The results obtained in both electrophoretic modes, under optimized conditions, are compared and discussed.

INTRODUCTION

Cyclodextrin-based complexation phenomena have recently received considerable attention in chromatography and electrophoresis. Through their use, both migration rates and the separation efficiency for various isomeric and structurally related compounds are known to be affected. The corresponding gains in resolution of isomers translate directly to both qualitative and quantitative aspects of such separations. These beneficial phenomena are due to the remarkable capacity of cyclodextrins (CDs) to include selectively, under appropriate experimental conditions, a wide variety of guest neutral molecules or ions within their hydrophobic cavity. Alternatively, additional stereospecific conditions can often be created. During the last decade, most known properties of CDs have been generally explored in analytical electromigration methods.

[a] On leave from the Institute of Biotechnology, Charles University, Albertov 2030, CS-128 40 Prague 2, Czechoslovakia.
[b] On leave from Analytical Department, Orion Pharmaceutica, P.O. Box 65, 02101 Espoo, Finland.

0021-9673/91/$03.50

The first successful uses of CDs and/or their derivatives were reported in isotachophoresis (ITP) of anionic species [1], positional isomers [2] and enantiomeric pairs [3], while other forms of capillary electrophoresis (CE) have also been explored for similar purposes [4–7]. The applications of cyclodextrins in CE have recently been reviewed [8,9].

The purpose of this paper is to demonstrate and compare the merits of ITP and other CE-based procedures with certain selected positional isomers (benzene- and naphthalene-based structures) and the enantiomers of chloramphenicol, thioridazine and ketotifen drugs. The roles of a modifier type and its concentration in the separation effect are emphasized.

EXPERIMENTAL

Distilled water, deionized with a Laboratory Water System XLDRO 1002 apparatus (Liquipure Europe, UK), was used for the preparation of the electrolyte solutions. All chemicals were of the highest quality commercially available: sodium acetate (NaAc), acetic acid (HAc), citric acid (CAc), hydrochloric acid and phosphoric acid (Merck, Darmstadt, Germany); β-alanine (β-Ala), methylhydroxyethylcellulose 3000 or 30 000 (MHEC), methylhydroxypropylcellulose 15 000 (HPMC) and hydroxyethylcellulose (HEC) (Serva, Heidelberg, Germany); 2-(N-morpholino)ethanesulfonic acid (MES), tris(hydroxymethyl)aminomethane (Tris), N-tris(hydroxymethyl)methylglycine (Tricine), α-cyclodextrin (α-CD), β-cyclodextrin (β-CD), γ-cyclodextrin (γ-CD), heptakis(2,6-di-O-methyl)-β-cyclodextrin (DM-β-CD), methanol and Amberlite MB-3 (Sigma, St. Louis, MO, USA); and 6-aminocaproic acid (EACA), benzoic acid (B), the positional isomers of iodobenzoic acid, the isomers of methoxyphenylacetic acid and naphthyl phosphate (Aldrich, Milwaukee, WI, USA). The samples of all drugs and their structurally related enantiomers and/or racemates were obtained from the Research Institute for Pharmacy and Biochemistry (Prague, Czechoslovakia).

Cyclodextrins and hydroxyalkylcellulose solutions were purified using Amberlite MB-3 mixed-bed ion-exchange resin. Stock solutions of analytes were prepared by dissolving each substance in methanol (*ca.* 1 mg ml^{-1}) and were stored in the dark under refrigeration. The structural formulae, names and abbreviations used for the analytes are given in Fig. 1 and Table I.

Methods

The isotachophoretic experiments were performed with a Tachophor 2127 (LKB, Bromma, Sweden) equipped with a conductivity detector and a poly(tetrafluoroethylene) capillary of 0.5 mm I.D. Samples were injected with a 10-μl microsyringe (Hamilton, Bonaduz, Switzerland). Additional operating conditions are given in the captions.

The experiments performed in the capillary zone electrophoretic (CZE) mode were made with a laboratory-made system similar to that described by Jorgenson and Lukacs [10]. The high-voltage power supply (0–30 kV) was a product of Spellman High Voltage Electronics (Plainview, NY, USA). Each end of the fused-silica capillary was placed in a small glass reservoir containing the appropriate platinum electrode connected to the power supply. A Jasco UVIDEC-100-IV detector from Japan

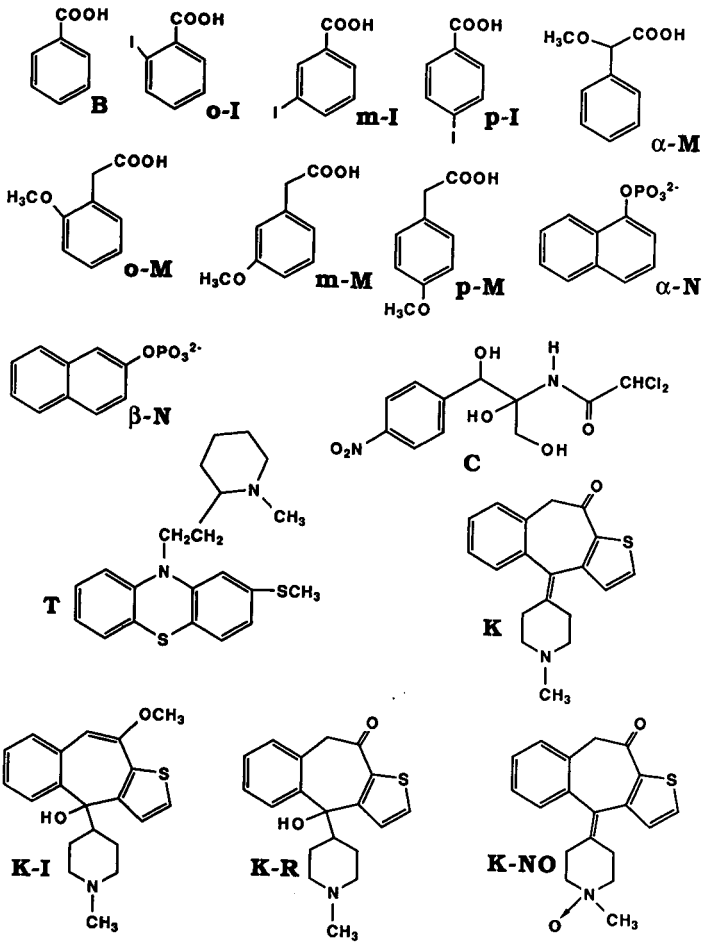

Fig. 1. Analyte structures. For abbreviations, see Table I.

Spectroscopic (Tokyo, Japan) operated at 254 nm was used throughout. An on-line optical detection cell was prepared by removing the polyimide coating from a short segment of the fused-silica capillary. Finally, the system, excluding the detector, was enclosed in a Plexiglas box with an interlock system to protect the operator.

Capillaries (49 μm I.D. × 186 μm O.D.) were purchased from Polymicro Technologies (Phoenix, AZ, USA). The capillary lengths ranged from 50 to 65 cm. The columns were pretreated overnight with 85% phosphoric acid diluted (1:1) with water. The capillary was further rinsed with water (5 min), followed by equilibration with a running buffer (5 min) by means of a vacuum procedure and then electroosmotic pumping for *ca.* 30–45 min at the beginning of each working day. The capillary was rinsed with a running buffer each time (before a run) for 1–2 min. Hydrodynamic sample introduction was utilized in all experiments.

TABLE I

ANALYTE NAMES AND ABBREVIATIONS

Abbreviation	Name
B	Benzoic acid
C	Chloramphenicol; *threo*-2,2-dichloro-N-[β-hydroxy-α-(hydroxymethyl)-β-(4-nitrophenyl)-ethyl]acetamide
o-I	*o*-Iodobenzoic acid; 2-iodobenzoic acid
m-I	*m*-Iodobenzoic acid; 3-iodobenzoic acid
p-I	*p*-Iodobenzoic acid; 4-iodobenzoic acid
K	Ketotifen; 4-(1-methylpiperidylidene)-4H-benzo[4,5]cyclohepta[1,2-*b*]thiophen-10(9H)-one
K-I	A synthesis intermediate of K; 10-methoxy-4-(1-methyl-4-piperidyl)-4H-benzo[4,5]cyclohepta[1,2-*b*]thiophen-4-ol
K-NO	N-Oxide of K; 4-(1-methylpiperidylidene-N-Oxide)-4H-benzo[4,5]cyclohepta[1,2-*b*]-thiophen-10(9H)-one
K-R	A compound structurally related to K; 4-(1-methyl-4-piperidyl)-4H-benzo[4,5]-cyclohepta[1,2-*b*]thiophen-10(9H)-one
α-M	α-Methoxyphenylacetic acid; O-methylmandelic acid
o-M	*o*-Methoxyphenylacetic acid; 2-methoxyphenylacetic acid
m-M	*m*-Methoxyphenylacetic acid; 3-methoxyphenylacetic acid
p-M	*p*-Methoxyphenylacetic acid; 4-methoxyphenylacetic acid
α-N	α-Naphthyl phosphate; 1-naphthyl phosphate
β-N	β-Naphthyl phosphate; 2-naphthyl phosphate
T	Thioridazine; 10-[2-(1-methyl-2-piperidyl)ethyl]-2-(methylthio)phenothiazine

RESULTS AND DISCUSSION

Separation of positional isomers

Owing to varying interactions with their hydrophobic cavities, cyclodextrins possess the remarkable capability of separating certain types of aromatic positional isomers. The overall molecular shape, determined by different substitutions on the aromatic ring structure, is a major factor affecting the migration order of these solutes.

As a model system, positional isomers of iodobenzoic acids were chosen to be separated by ITP. The objective was to compare separations of a mixture of *o*-I, *m*-I, *p*-I and B (Table I) carried out in conventional electrolyte systems with the separations accomplished in the CD-modified systems. Resolution was observed as a function of a CD concentration for a given sample mixture. Fig. 2 shows the correlation between the relative step-height, $(h_i)_r$, of the analytes and the concentration of α-CD in the leading electrolyte (LE). The $(h_i)_r$ value is used here as a solute migration characteristic and is defined by

$$(h_i)_r = h_i - h_L/h_T - h_L \quad (1)$$

where h_i, h_L and h_T are the step-heights of sample, leading electrolyte (LE) and terminator (TE) ions, respectively. Resolution of isomers could not be achieved in a slightly acidic non-modified LE [see ITP record (b) in Fig. 2]. Addition of α-CD resulted in a significant resolution improvement, as illustrated in ITP record (a). With an in-

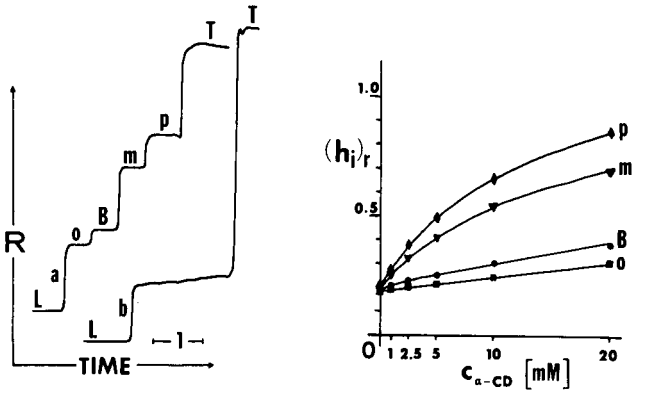

Fig. 2. Effect of α-CD on the ITP separation and $(h_i)_r$ values of (o) *o*-, (m) *m*- and (p) *p*-iodobenzoate and benzoate (B) anions. Concentration of α-CD in LE: record (a) 10 m*M*; (b) 0 m*M*. LE, 5 m*M* HCl + EACA to pH 4.70 + 0.2% HPMC; TE, 5 m*M* MES (pH 5.50); capillary, 400 cm; current, 100 μA (9 min), for detection 50 μA. *R* = conductivity response; L = leading zone; T = terminating zone; $c_{\alpha\text{-CD}}$ = concentration of α-CD in LE; 1 = 1 min.

creased α-CD concentration in LE (in the range 0–20 m*M* α-CD), the separation further improved.

Further separation possibilities with positional isomers are demonstrated under CZE conditions with methoxyphenyl acetates (Fig. 3) and naphthyl phosphates (Fig. 4). In both instances, overlapping peaks of these isomers are shown while using unmodified background electrolytes (BE) in Fig. 3a and Fig. 4 (record 0). Two additives, α-CD and β-CD, proved to be effective and suitable for resolution of both isomeric types: methoxyphenylacetate ions were successfully separated by a β-CD-modified BE (Fig. 3b), while naphthyl phosphates migrated apart owing to α-CD. By increasing the CD concentration, it was possible to achieve a better separation of each isomer type, as seen from the comparison of electropherograms 10 and 20 in Fig. 4.

The remaining questions concern the type of interaction between the model

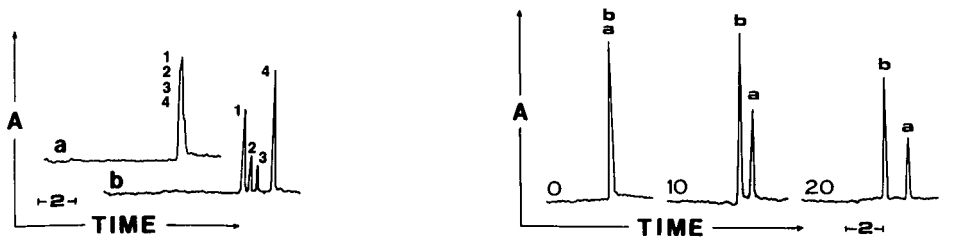

Fig. 3. CD-based CZE separation of (1) *o*-, (3) m-, (4) *p*- and (2) α-methoxyphenylacetates. Record (a) without CD; (b) with 10 m*M* β-CD. BE, 50 m*M* Tris + 50 m*M* Tricine (pH 8.06) + 0.1% MHEC; voltage, 16 kV; current, 7 μA; capillary, 50 cm (35 cm to the detector). *A* = response of UV detector (254 nm); 2 = 2 min.

Fig. 4. CD-based CZE separation of (a) α- and (b) β-naphthylphosphate anions. Record 0, without CD, 10 and 20 with 10 and 20 m*M* α-CD, respectively. BE, 50 m*M* Tris + Tricine to pH 8.50 + 0.1% MHEC; capillary, 50 cm (35 cm to the detector); voltage, 20 kV; current, 9 μA. *A* = response of UV detector (254 nm); 2 = 2 min.

solutes and the CDs. Generally proposed separation mechanisms based on the differences between the stabilities of equatorial and axial CD inclusion complexes for 1- and 2-naphthyl derivatives [11,12] do not seem applicable in this case, as the molecular dimensions of α-CD and the solutes under study are not compatible.

Chiral separations

Separation of enantiomers has traditionally been viewed as one of the more difficult problems in separation science. Such isomeric pairs are not easily separated from each other by any separation method, as their Gibbs free energy differences (ΔG) are zero. In order to enhance the ΔG values between enantiomers, the formation of diastereomers, or at least diastereomeric complexes, has often been advocated. Cyclodextrins (chiral compounds themselves) have been proposed in various separation techniques to cover a reasonable range of optical isomers.

Our ITP and CZE experiments with CD-modified electrolytes confirm the general importance of the cyclodextrin cavity size [8]. In addition, chemical modification of the hydroxyl groups on the cavity collar and the pH value of the buffer system used for the chiral separation may also play significant roles.

In certain instances, enantioselectivity and the separation efficiency can also be influenced by adding soluble alkylhydroxyalkylcellulose derivatives to the CD-modified electrolytes. The effect of MHEC on the CD-based chiral separation of the isomers of chloramphenicol is shown in Fig. 5. In this instance, complete baseline resolution of the enantiomers was achieved only in the electrolytes containing MHEC (Fig. 5a *vs.* b). In various applications of pharmaceutical interest, a complete sep-

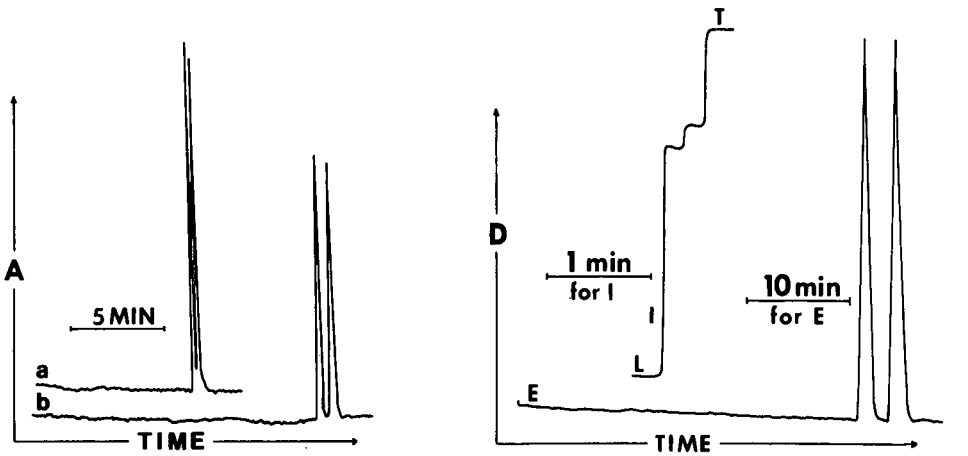

Fig. 5. Influence of MHEC on the chiral separation of chloramphenicol drug enantiomers with cyclodextrins. Record (a) without MHEC; (b) with 0.1% MHEC. BE, 20 m*M* Tris + CAc to pH 3.50 + 10 m*M* DM-β-CD; capillary, 65 cm (45 cm to the detector); voltage 18 kV; current, 6 μA. *A* = response of UV detector (254 nm).

Fig. 6. (I) ITP and (E) CZE separations of thioridazine enantiomers. ITP conditions: capillary, 22 cm; LE, 10 m*M* NaAc + HAc to pH 5.47 + 0.08% HEC + 5 m*M* γ-CD; TE, 10 m*M* β-Ala; current, 100 μA (13 min), 50 μA for detection. L = leading zone; T = terminating zone. CZE conditions: capillary, 65 cm (45 cm to the detector); BE, 20 m*M* Tris + H_3PO_4 to pH 2.50 + 5 m*M* γ-CD; voltage, 18 kV; current, 14 μA. D = response of the conductivity detector (for I) and UV detector (254 nm) (for E).

aration is often necessary for micropreparative recovery and characterization of the chiral metabolites.

Another class of optical isomers resolvable by both CZE and ITP are compounds with a tricyclic (aromatic and heterocyclic) structure. The ITP and CZE separations of a chiral phenothiazine drug, thioridazine, with the aid of γ-CD, are shown in Fig. 6. Both methods appear to offer a very good separation of enantiomers, but the advantage of ITP separation is that the separation time is at least three times shorter.

Separation of the optical isomers of ketotifene (K) and the enantiomers of structurally related compounds (K-I, K-R and K-NO) is illustrated in Figs. 7 and 8. Fig. 7 shows the effectiveness of ITP and CZE for the resolution of K enantiomers by β-CD-modified buffers. No optimum conditions were found for the ITP separation of K and K-I from each other in one analytical run. This separation is important from the standpoint of monitoring the chiral metabolism and the synthesis of ketotifen. Only under CZE conditions with a γ-CD-modified BE (Fig. 8a) did such a complete separation become feasible.

A well-known limitation of ITP is the requirement to find an appropriate terminating electrolyte. For example, the separation of components with relatively low net electrophoretic mobilities appears tedious. We experienced difficulties in finding appropriate conditions for optimum ITP migration of K-NO for this reason. While K-R had a suitable electrophoretic mobility, no chiral resolution was obtained with ITP. This was probably due to excessive and ineffective complexation with γ-CD in the ITP measurements. However, in CZE with the buffers containing small amounts of γ- or β-CD, all analyte enantiomers were easily separable (Fig. 8).

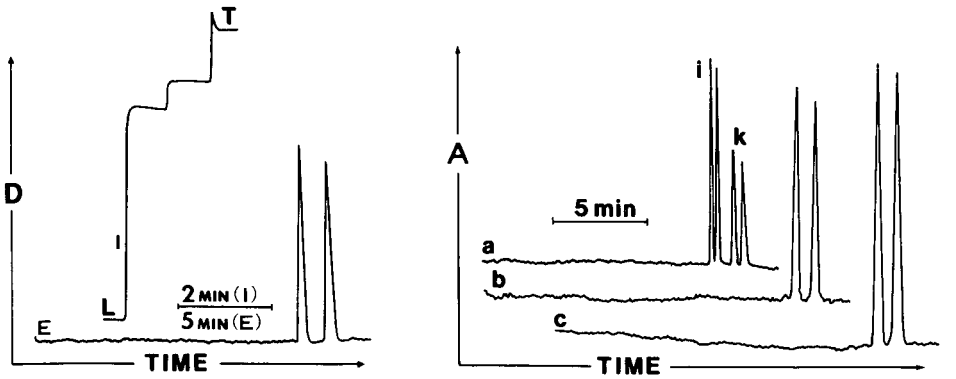

Fig. 7. (I) ITP and (E) CZE separations of ketotifen enantiomers. ITP conditions: capillary, 37 cm; LE, 5 m*M* NaAc + HAc to pH 5.50 + 4 m*M* β-CD + 0.2% HEC; TE, 10 m*M* β-Ala; current, 150 μA (9 min), 50 μA for detection. L = leading zone and T = terminating zone. CZE conditions: capillary, 65 cm (45 cm to the detector); BE, 20 m*M* Tris + CAc to pH 3.50 + 10 m*M* β-CD + 0.05% MHEC; voltage, 24 kV; current, 9 μA. D = response of the conductivity detector (for I) and UV detector (254 nm) (for E).

Fig. 8. CZE chiral separation of ketotifen (K) and its synthesic intermediate, K-I (i) [record (a)] and structurally related compounds, K-R [record (b)] and N-oxide, K-NO [record (c)]. Capillary, 65 cm [50 cm (a) and 45 cm (b and c) to the detector] (a) BE, 20 m*M* Tris + CAc to pH 3.75 + 10 m*M* γ-CD; voltage, 24 kV; current, 7.5 μA. (b) BE, 20 m*M* Tris + CAc to pH 3.50 + 20 m*M* γ-CD; voltage, 24 kV; current, 7 μA. (c) BE, 20 m*M* Tris + H_3PO_4 to pH 2.50 + 10 m*M* β-CD; voltage, 18 kV; current, 12.5 μA. *A* = response of UV detector (254 nm).

CONCLUSIONS

It appears that the complexation of various solutes with CDs may occur by slightly different mechanisms. Minor changes in the molecular shape of the solutes as determined by different substitutions, or even a variable space orientation of a substituent group, may give rise to different solute–CD complex stabilities and net electrophoretic mobilities. While much remains to be elucidated about such interactions, CD additives in both ITP and CZE have become useful in the separation of close isomers.

Both electromigration techniques employed here have distinct advantages and disadvantages. For example, ITP appears more suitable than CZE for the determination, or at least preconcentration, of minute components in a large excess of other mixture components. Unlike in CZE, it is feasible to work with larger sampling volumes in ITP. However, CZE is definitely preferable wherever high separation efficiencies are required. In addition, this mode of operation is also advantageous when working within a wide range of operating conditions, *e.g.*, in micellar electrokinetic chromatography.

Whereas the use of CD additives in electrophoresis is relatively recent, the results obtained for isomeric compounds in this laboratory and others rival the best separations reported using other separation methods.

ACKNOWLEDGEMENTS

This work was supported by Grant No. GM24349 from the Institute of General Medical Sciences, US Department of Health and Human Services, and a grant-in-aid from Dow Chemical.

REFERENCES

1 M. Tazaki, M. Takagi and K. Ueno, *Chem. Lett.*, (1982) 639.
2 M. Tazaki, T. Hayashita, T. Y. Fujino and M. Takagi, *Bull. Chem. Soc. Jpn.*, 59 (1986) 3469.
3 J. Snopek, I. Jelinek and E. Smolkova-Keulemansova, *J. Chromatogr.*, 438 (1988) 211.
4 S. Terabe, H. Ozaki, K. Otsuka and T. Ando, *J. Chromatogr.*, 322 (1985) 211.
5 A. Guttman, A. Paulus, A. S. Cohen, N. Grinberg and B. L. Karger, *J. Chromatogr.*, 448 (1988) 41.
6 S. Fanali, *J. Chromatogr.*, 474 (1989) 441.
7 J. Liu, K. A. Cobb and M. Novotny, *J. Chromatogr.*, 519 (1990) 189.
8 J. Snopek, I. Jelinek, and E. Smolkova-Keulemansova, *J. Chromatogr.*, 452 (1988) 571.
9 J. Snopek and E. Smolkova-Keulemansova, in D. Duchene (Editor), *New Trends in Cyclodextrins and Derivatives*, De Sante, Paris, 1991, in press.
10 J. W. Jorgenson and K. Lukacs, *Anal. Chem.*, 58 (1981) 1928.
11 J. Szejtli, *Cyclodextrins and Their Inclusion Complexes*, Akadémiai Kiadó, Budapest, 1982.
12 K. Harata and H. Uedaira, *Bull. Chem. Soc. Jpn.* 48 (1975) 375.

Journal of Chromatography, 559 (1991) 223–235
Elsevier Science Publishers B.V., Amsterdam

CHROM. 23 429

Separation of fluorescent oligosaccharide derivatives by microcolumn techniques based on electrophoresis and liquid chromatography

JINPING LIU, OSAMU SHIROTA and MILOS NOVOTNY*
Department of Chemistry, Indiana University, Bloomington, IN 47405 (USA)

ABSTRACT

Various aldose oligosaccharides can be quantitatively derivatized into primary amines for subsequent reaction with fluorogenic reagents, such as 3-(4-carboxybenzoyl)-2-quinolinecarboxaldehyde or 3-benzoyl-2-naphthaldehyde. Capillary electrophoresis (CE) and microcolumn liquid chromatography (LC), coupled with laser-induced fluorescence detection, were evaluated as a means of separating complex oligosaccharide mixtures. Whereas microcolumn LC and open-tubular CE appear confined in their utility to relatively small oligosaccharides, unprecedented results were obtained with polyacrylamide gel-filled capillaries on hydrolyzed malto-oligosaccharides and enzymatically degraded samples of chondroitin sulfate and hyaluronic acid.

INTRODUCTION

The characterization of complex oligosaccharide mixtures is among the most challenging problems in biochemical analysis. Structural studies of complex sugar molecules, originating from glycoproteins or other biological sources, have been complicated by the natural polydispersity and heterogeneity (sequence variability) within such biomacromolecules. Although various fragments can be generated from the polysaccharides by specific enzymatic and/or chemical cleavages, effective separation techniques are required to resolve the mixture constituents. Ideally, these should cover the molecular weight range from the monosaccharide units to the size of their original native structures.

Gel filtration chromatography [1,2], ion-exchange chromatography [3,4] and slab gel electrophoresis [5–7] are often employed in the separation and analysis of oligosaccharides such as those of glycosaminoglycan nature. The most obvious current needs in the analysis of complex oligosaccharide mixtures pertain to a lack of both adequate resolving power and a suitable detection principle. For smaller oligosaccharides, the general problems have led to the significant use of the gas-phase analytical techniques [8,9] and, more recently, capillary supercritical fluid chromatography [10,11].

Capillary electrophoresis (CE), in its different separation modes, has recently

0021-9673/91/$03.50

emerged as an advantageous method for certain naturally charged biopolymers. Whereas open-tubular systems appear promising in the separation of proteins [12–14], gel-filled capillaries have been particularly successful in dealing with mixtures of oligo- and polynucleotides [15–17]. The unfavorable mass-to-charge ratios of the latter polyions appear to be a problem for the open-tubular systems [18], but the sizing effect of gels together with extremely high separation efficiencies [15] have been demonstrated as beneficial for regularly shaped and negatively charged oligonucleotides. In order to extend the general benefits of CE to oligosaccharides, the solutes of interest must first be made to possess charged moieties in their structures. In addition, introducing a detectable moiety (a chromophore) into such molecules appears essential.

We have recently succeeded in attaching certain fluorogenic labels to amino sugars [19] and neutral saccharides following their conversion to primary amines [20]. Optimization studies on the reductive amination of selected aldoses are further reported here, while two fluorogenic reagents utilized previously in high-sensitivity amino acid and peptide analysis [21,22] are employed. CE runs in open tubes and gel-filled capillaries are compared in terms of the migration behavior of oligosaccharides. The capabilities of microcolumn liquid chromatography (LC) in packed fused-silica capillaries are also compared with CE. Finally, a preliminary application of gel-filled capillaries to complex mixtures of fragments from acidic polysaccharides is reported.

EXPERIMENTAL

Equipment

The capillary electrophoresis system used for work with both open-tubular and gel-filled capillaries was a laboratory-made instrument described previously [21]. Various lengths of fused-silica capillaries (Polymicro Technologies, Phoenix, AZ, USA) of 50 μm I.D. (187 μm O.D.) were used for all variants of electrophoresis. A high-voltage power supply (Spellman High Voltage Electronics, Plainview, NY, USA), capable of delivering 0–30 kV, was utilized. Different polarity modes had to be selected for open-tubular and gel electrophoresis. The reservoir connected with the positive high-voltage end served for injection, while the reservoir at the detector end was at the ground potential for open-tubular electrophoresis; reversal was needed for gel electrophoresis. On-column fluorescence detection was facilitated by a Model 543 argon ion laser (Omnichrom, Chino, CA, USA) operated at 457 nm. A detailed description of the instrumental set-up and optical alignment can be found in previous papers [19–21].

The microcolumn LC system consisted of a micropump (Brownlee Labs., Santa Clara, CA, USA), a 100-nl sample loop (Valco, Houston, TX, USA) a 90 cm × 250 μm I.D. fused-silica capillary (Polymicro Technologies) slurry-packed with Capcell C_{18} 5-μm silica particles (Shiseido, Tokyo, Japan) and a fluorescence detector. The detector used was a Schoeffel Model FS970 spectrofluorimeter. Gradient elution runs were done with a 10:1 flow splitter connected immediately after the mixing tee of the Brownlee pump. The flow-rate was adjusted to *ca.* 3 μl/min.

Fluorescence measurements under various reaction optimization conditions were carried out with a Perkin-Elmer (Norwalk, CT, USA) Model 650 spectrofluo-

rimeter equipped with a xenon arc lamp, powered by a Perkin-Elmer Model 150 power supply.

Chemicals

Chondroitin sulfate A (from bovine trachea), hyaluronidase (Type I-S, from bovine testes), all maltooligosaccharides and mannose and galactose were purchased from Sigma (St. Louis, MO, USA). Dextrin 15 (maltodextrin) and hyaluronic acid were obtained from Fluka (Ronkonkoma, NY, USA). The fluorogenic reagents, 3-(4-carboxybenzoyl)-2-quinolinecarboxaldehyde (CBQCA) and 3-benzoyl-2-naphthaldehyde (BNA), were synthesized in our laboratory [21,22]. Additional chemicals used for capillary coating and the preparation of gel-filled capillaries were acrylamide, N,N′-methylenebisacrylamide, triethanolamine (TEA), triethanolamine chloride (TEA · HCl), ammonium persulfate and γ-methacryloxypropyltrimethoxysilane (all purchased from Sigma). Sodium cyanoborohydride ($NaBH_3CN$) was obtained from Aldrich (Milwaukee, WI, USA). Potassium cyanide and sodium borate were of analytical-reagent grade from Mallinckrodt (Paris, KY, USA).

Capillary coating and gel preparation

For capillary polyacrylamide gel electrophoresis, surface pretreatment is necessary prior to gel preparation [23]. A stock solution of acrylamide and N,N′-methylenebisacrylamide with concentration of 20% T and 30% C[a] was prepared for the subsequent variations of concentration. Preparation of the polyacrylamide gel was performed by a progressive polymerization (isotachophoretic method) developed in this laboratory [23].

Enzymatic digestion of glycosaminoglycans

Hyaluronidase (30 mg/ml in 0.15 *M* NaCl–0.1 *M* sodium acetate, pH 5.0, corresponding to 9000 units/ml) was prepared in cold solution prior to use. A 100-mg amount of chondroitin sulfate A was dissolved in 0.5 ml of 0.15 *M* NaCl–0.1 *M* sodium acetate (pH 5.0). Chondroitin samples were preincubated at 37°C for about 10 min before adding the hyaluronidase solution. To a preincubated sample vial containing 20 mg of chondroitin sulphate A, 400 μl of hyaluronidase solution was added. The mixture was kept at 37°C for 0.5 h. After digestion, 0.8 ml of solution was withdrawn and put immediately into a boiling water-bath for 10 min for enzyme deactivation. The solution was subsequently centrifuged and kept in a freezer for further treatment.

Approximately 8.0 mg of hyaluronic acid were dissolved in 1.5 ml of dionized water to obtain a clear solution, then 0.2 ml of this solution was mixed with 0.1 ml of hyaluronidase solution and incubated at 37°C for 30 min. The procedures for enzymatic treatment were the same as above.

Preparation of fluorescent carbohydrate derivatives

Before derivatization, all the mono- and oligosaccharides studied were dissolved in water and placed in screw-capped vials or polypropylene plastic sample

[a] C = g N,N′-methylenebisacrylamide (Bis)/% T; T = g acrylamide + g Bis per 100 ml of solution.

vials. Excess of 2.0 *M* ammonium sulfate or 4.0 *M* ammonium chloride and 0.4 *M* sodium cyanoborohydride were added to the vials and mixed. The tightly sealed vials were placed in a heating block and kept at 100°C for 100–120 min. After completion of this reaction, the solutions were immediately cooled by putting the vials in an ice-bath. Such mixtures can either be used directly for derivatization by a fluorogenic reagent, or dried and later redissolved.

The identity of the reductive amination product was verified by ^{13}C NMR spectrometry with a Model Am500 instrument (Bruker, Karlsruhe, Germany). As seen in Fig. 1, the chemical shift of the carbon at the reducing end becomes $\delta = 42$ ppm after introduction of the primary amine group, compared with the original value of $\delta = 98$ ppm. No signal was observed around $\delta = 98$–102 ppm, where the 1′-carbon of the pyranose structure would appear if the reaction were incomplete. The side-reaction of forming a dimer imine usually occurs only with relatively high-concentration sample solutions as observed in the present NMR experiments. With the use of very low sample concentrations for reductive amination, this phenomenon can be neglected. In addition, the dimer imine formed cannot be reacted with our fluorogenic reagent, CBQCA, which reacts only with primary amines.

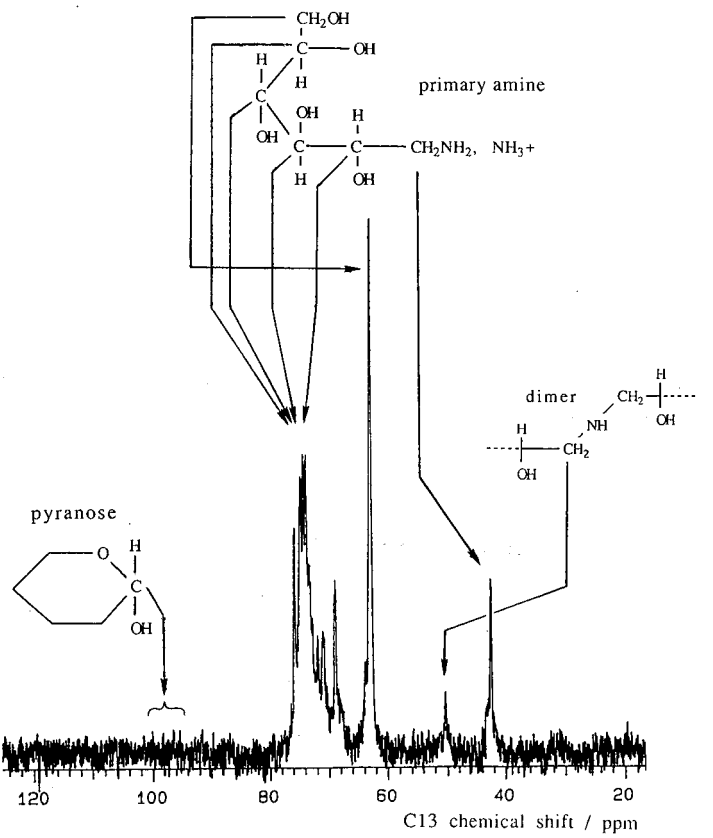

Fig. 1. ^{13}C NMR spectrum of glucose after reductive amination.

Optimization of this derivatization procedure was pursued with respect to temperature, reaction time and the molar ratio of reagents to the model sugars (glucose and galactose).

Oligosaccharides obtained from the enzymatic digestion experiments were treated similarly. A 200-μl volume of digested chondroitin sulfate solution or 300 μl of digested hyaluronic acid was mixed with 200 and 100 μl of a reducing agent [0.2 *M* $NaBH_3CN$ and 1 *M* $(NH_4)_2SO_4$], respectively. The solutions were kept at 100°C for 2–3 h, then cooled and stored in a freezer prior to the next derivatization step.

Derivatization by CBQCA for electrophoresis (or by BNA for microcolumn LC) were carried out as described previously [19–22]. Typically, 20-μl aliquots of the final sample solution were mixed with 20 μl of 20 m*M* KCN and 10 μl of 10 m*M* CBQCA (or BNA) in methanol. The mixtures were allowed to stand at room temperature for at least 1 h prior to injection. Sample introduction was carried out by the hydrodynamic (gravity) method for open-tubular CE and by the electromigration method for gel-filled capillaries.

RESULTS AND DISCUSSION

A lack of detectable features in carbohydrate molecules has been a major hindrance to high-sensitivity measurements within this important class of compounds. The use of reductive amination, followed by the attachment of a fluorophore to the reducing end of mono- and oligosaccharides [20], has enabled us to extend the detection possibilities down to the attomole level. It was further necessary to optimize the reduction amination conditions with respect to reaction temperature and time, and also the molar ratios of the reducing agent and ammonium ion to sugars. Mannose and galactose, two of the most common monosaccharides found in glycoproteins, were chosen as model compounds for these experiments. The fluorescence intensity was measured at least three times, while the entire procedures were repeated several times to ensure adequate precision.

Our studies show that the rate of reductive amination increases with temperature. The maximum fluorescence intensity was reached in about 100 min at 95°C; accordingly, we set 100°C as a standard for all subsequent experiments. Stable fluorescence was observed when the molar ratio of $NaBH_3CN$ to substrate was at least 2:1, while no adverse effects were seen at significantly larger ratios. However, a large excess of ammonium ion [from $(NH_4)_2SO_4$, NH_4Cl or another ammonium salt] was needed to ensure a good reaction yield. Owing to concern that the large excess of ammonium salt needed might yield a side-product with a fluorogenic reagent, it was deemed necessary to check for possible background fluorescence in the absence of sugar; a negligible blank response was observed. In practical measurements by CE–laser-induced fluorescence, a very small peak can be found that has no adverse effects on the analytical results. The results of optimization studies are summarized in Fig. 2.

In exploiting the separation potential of CE together with the extremely high sensitivity of laser-induced fluorescence detection for carbohydrates, we have incorporated both a potent fluorophore and a charged moiety into the molecules of interest by their reaction with CBQCA. Addition of borate to the buffer is also believed to contribute to the overall electrophoretic mobility of oligosaccharides. As seen in Fig. 3A, the maltodextrin oligosaccharides, ranging from one glucose unit to *ca.* the 15-

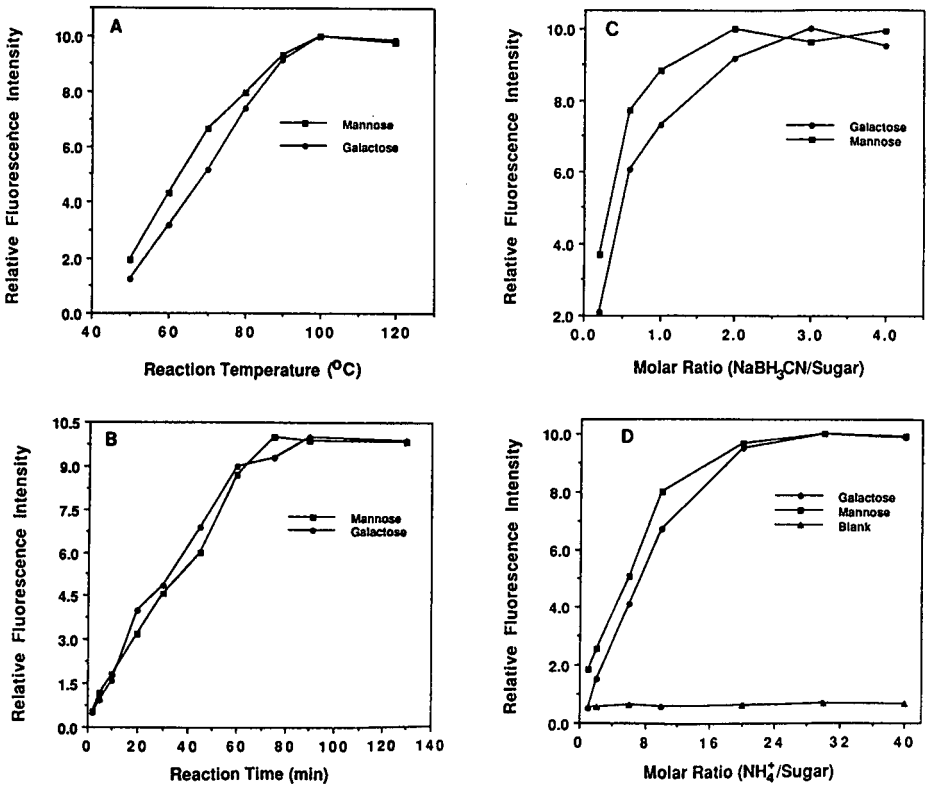

Fig. 2. Dependence of the relative fluorescence intensity of CBQCA-derivatized carbohydrates on the reaction conditions for reductive amination. Monosaccharides were reductively aminated (A) at various temperatures for 120 min and (B) at 95°C for different time periods. Experiments in (C) and (D) were performed by keeping the concentrations of ammonium ion (C) and reducing agent ($NaBH_3CN$) (D), constant, with a reaction temperature of 100°C and a reaction time of 120 min.

mer, can be distinguished by CE in the open-tubular format. Fig. 3B shows the relationship between CE migration times and the degree of polymerization (correlation coefficient 0.996), which corresponds to the peaks detected in Fig. 3A. Obviously, the resolution between the peaks decreases with increasing number of glucose units. The situation is reminiscent of the problems encountered in our previous studies with oligonucleotides [18] possessing an unfavorable mass-to-charge ratio. Our attempts to improve the resolution of large oligosaccharides through the use of mobile phase additives, such as cyclodextrins or detergents, have so far not been successful.

Similar results were achieved with microcolumn LC in the reversed-phase mode. In order to enhance the hydrophobicity of the oligosaccharide solutes, BNA [22] rather than CBQCA [21] was used for derivatization following the reductive amination step. While the lower oligosaccharides are separated efficiently on a C_{18} stationary phase, resolution difficulties arise at approximately ten monosaccharide units, as seen in Fig. 4. Attempts to optimize gradient elution at this point have not been successful.

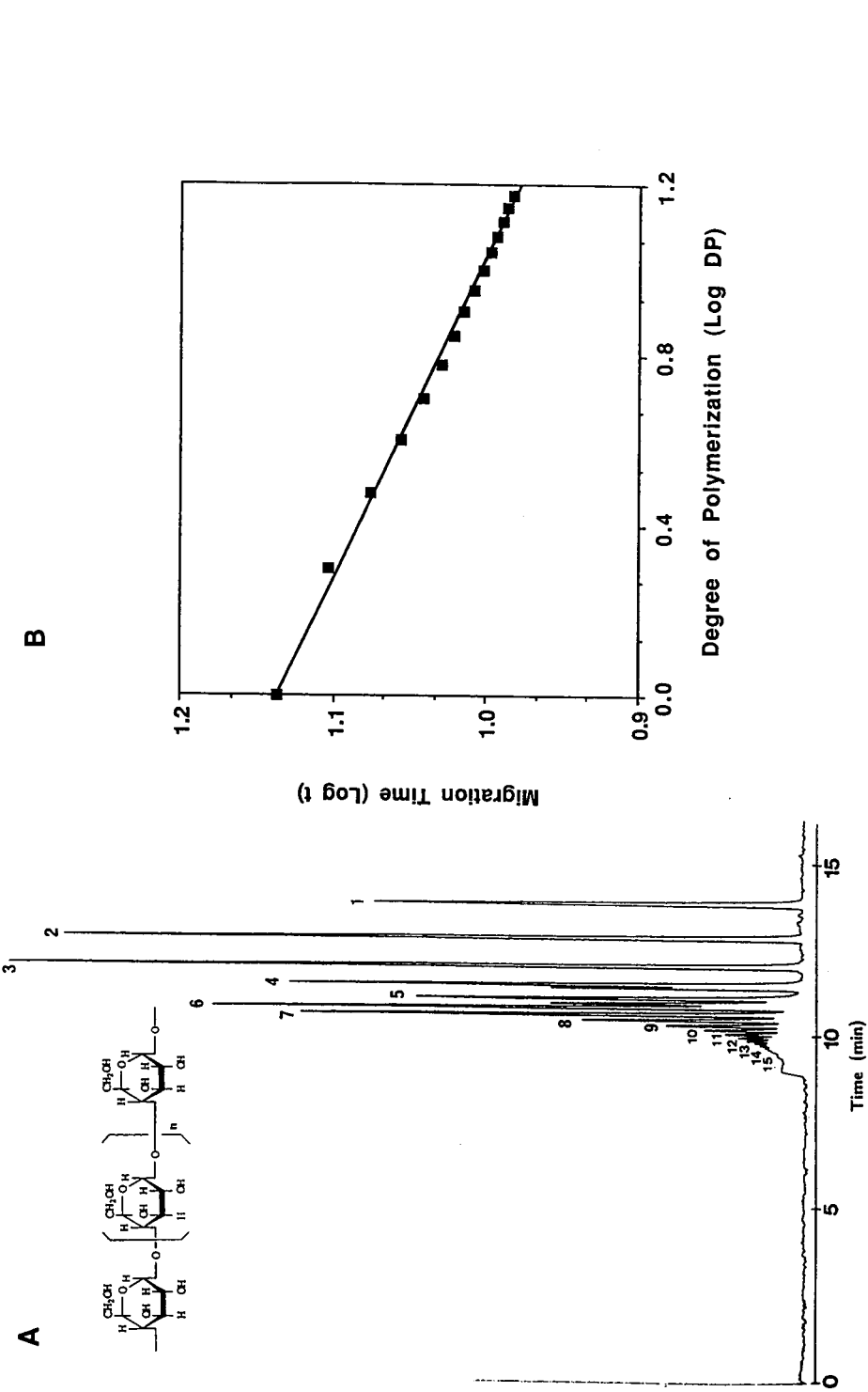

Fig. 3. (A) Electrophoretic separation of a partially hydrolyzed polysaccharide (Dextrin 15) in the open-tubular system. (B) Correlation (log–log) between molecular weight and migration time. Capillary 88 cm [58 cm effective length × 50 μm I.D.; buffer, 10 m*M* Na_2HPO_4–10 m*M* $Na_2B_4O_7 \cdot 10H_2O$ (pH 9.40)]; applied voltage, 20 kV (12 μA).

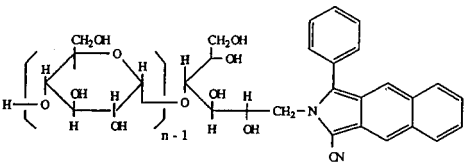

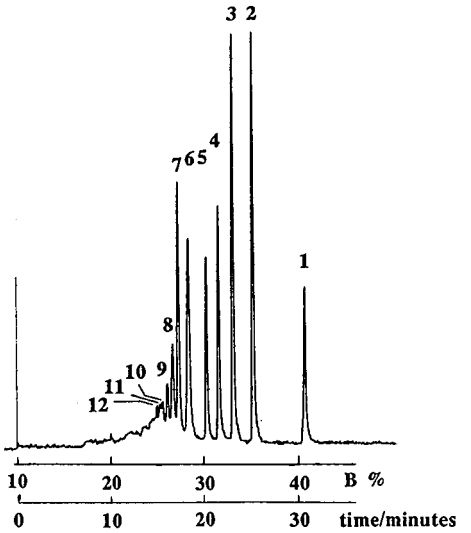

Fig. 4. Chromatogram of the individual BNA-derivatized components of Dextrin 15. Microcolumn: 90 cm × 250 μm I.D. packed with Capcell-C_{18}. Gradient elution: solvent A, water; solvent B, acetonitrile; linear gradient at a flow-rate of 3 μl/min.

Similarly to the success in separating polynucleotides [15], polyacrylamide gel-filled capillaries could be an alternative approach to separating larger oligosaccharides. Initial uses of a relatively low gel concentration (6% T and 3% C) were not satisfactory. However, the utilization of more concentrated gel matrices improved the resolution of oligosaccharides dramatically. Employing 10% T/3% C polyacrylamide gels and Tris–borate–urea buffers led to good separations of higher oligosaccharides (Fig. 5A). Their separation is now based strictly on the molecular size of the separated solutes, as seen in Fig. 5B. The relationship between migration times and the degree of polymerization is linear (correlation coefficient 0.997). Although there is some sacrifice in the speed of analysis compared with the open-tubular approach, the benefits for larger oligosaccharides are obvious when using the gel-filled capillaries. It is commonly thought that the most useful range of oligosaccharide fragments, originating from glycoprotein cleavages, should cover up to about 25 monosaccharide units. However, requirements in other biochemical and pharmaceutical problems may go well beyond that range.

The separation of acidic oligosaccharides such as the glycosaminoglycan-derived entities is yet another important task in purification and analysis for biosynthetic and structural studies. Enzymatic digestion of glycosaminoglycans, such as hyaluronic acid, chondroitin sulfate and heparin, is frequently used to produce smaller

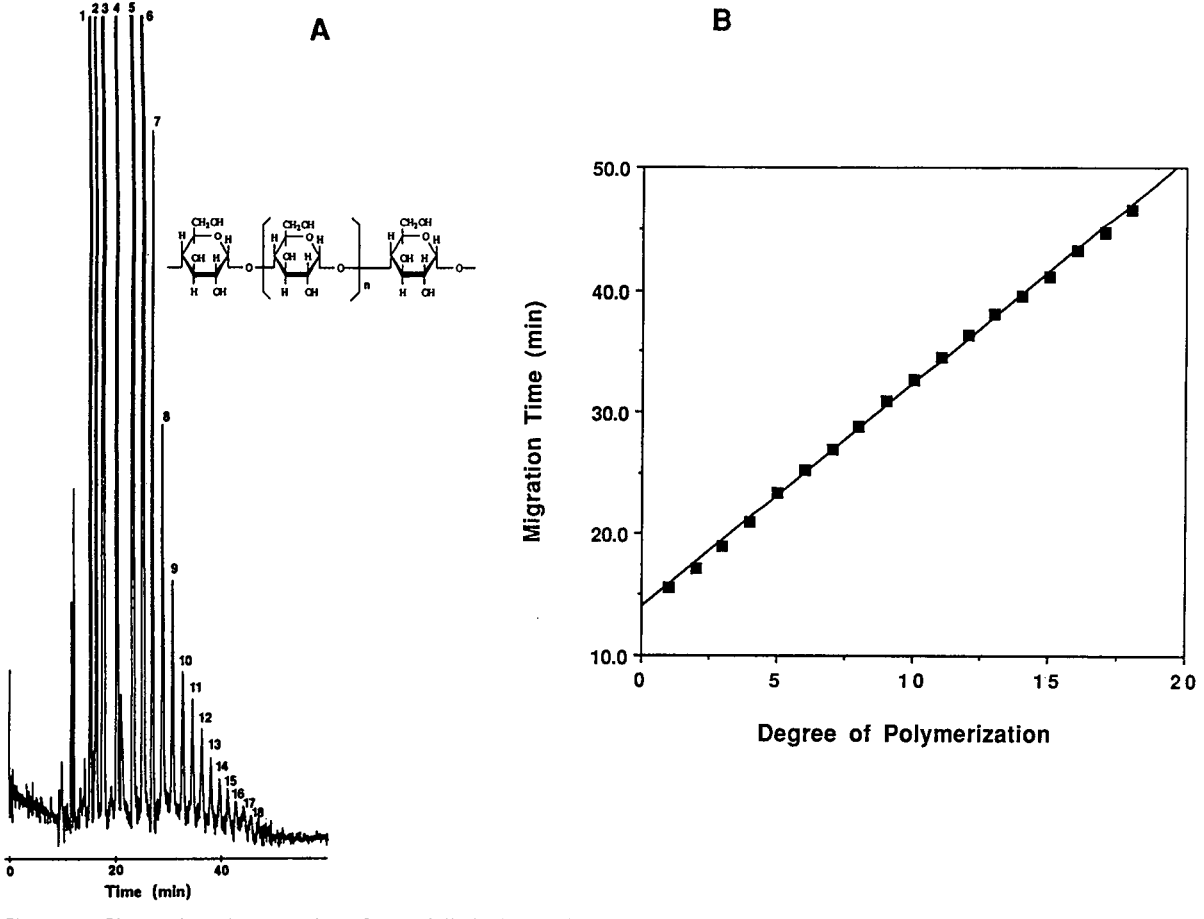

Fig. 5. (A) Electrophoretic separation of a partially hydrolyzed Dextrin 15 in a polyacrylamide gel-filled column. (B) Correlation between molecular masses of the oligomers from maltodextrin and their corresponding migration times. Gel concentration, 10% T, 3% C; capillary, 26 cm (19 cm effective length) × 50 μm I.D.; buffer, 0.1 *M* Tris–0.25 *M* borate–7 *M* urea (pH 8.33); applied field, 269 V/cm (20 μA).

fragments for subsequent separation. Testicular hyaluronidase has been the most common enzyme used extensively for the preparation of oligosaccharidic fragments. In general, chondroitin sulfate and hyaluronic acid can be converted by hyaluronidase into oligosaccharides with N-acetyl-D-hexosamine residues at their reducing terminals, which could further be utilized for chemical modification, and D-glucuronic acid residues with non-reducing terminals. A scheme for depolymerization involving a tetrasaccharide from chondroitin sulphate may proceed as follows:

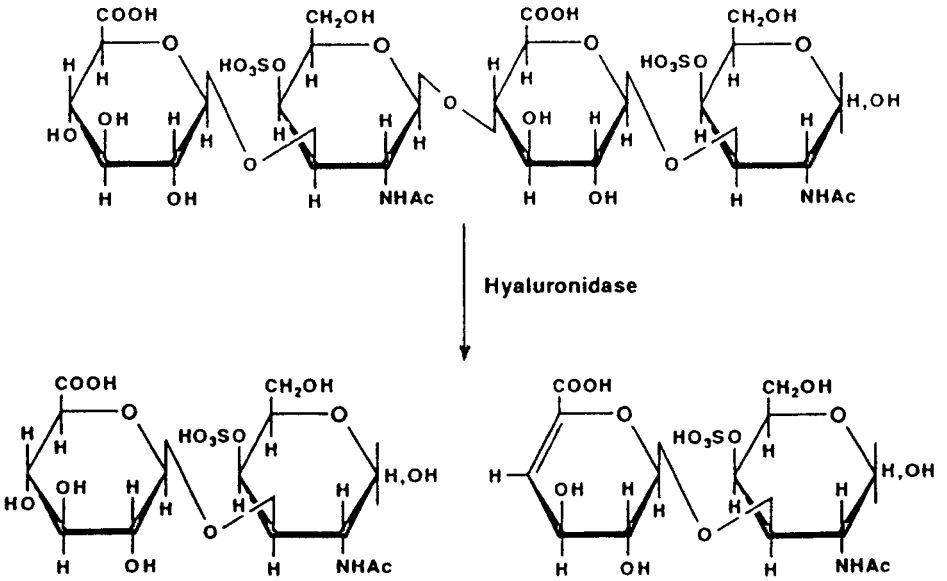

Enzymatic cleavages of such glycans should yield a final mixture of repeatable oligosaccharides with sizes ranging from a disaccharide to oligosaccharides with various chain lengths, depending on the exposure of the starting material to the enzyme. In our initial experiments, CE of chondroitin sulfate A-derived oligosaccharides with low-concentration gels (6% T and 3%) failed to provide adequate component resolution. However, significant improvements were achieved with more concentrated gel matrices (18% T and 3% C) and buffers containing Tris–borate–EDTA or Tris–borate–urea. Fig. 6 demonstrates a representative separation of chondroitin sulfate-derived oligosaccharides with the use of Tris–borate–EDTA buffer; however, further optimization of the buffer composition and gel concentration appears desirable. Technical problems associated with high-concentration gels and their reproducible preparation inside the fused-silica capillaries must still be overcome.

Problems of separating glycosaminoglycan-derived oligosaccharides may also be caused by their general structural features. Normally, glycosaminoglycans are negatively charged, linear polysaccharides built up from disaccharide repeating units. However, structural diversity may be conferred on the macromolecule by variations in both the degree and position of sulfated groups. For example, chontroitin-4- and -6-sulfate are often associated with each other biochemically and during isolation steps. Consequently, oligosaccharides derived from chondroitin sulfate could be a

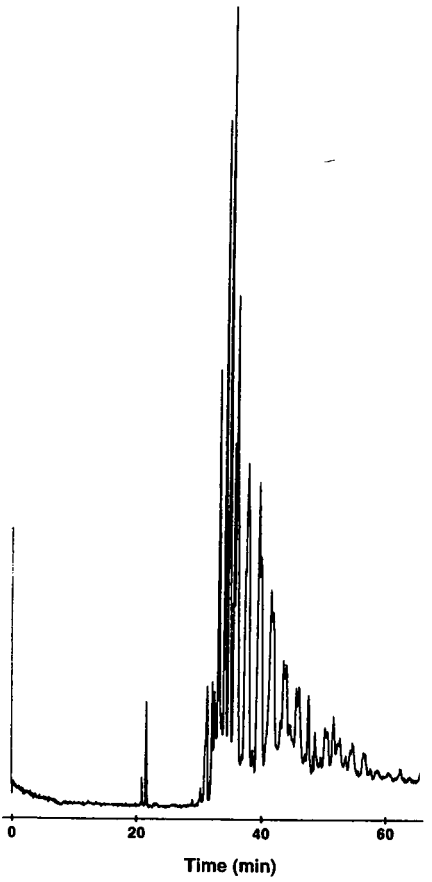

Fig. 6. Electrophoretic separation of the enzymatically digested chondroitin sulfate A in a polyacrylamide gel-filled capillary. Gel concentration, 18% T, 3% C; capillary, 32 cm (23 cm effective length) × 50 μm I.D.; buffer, 0.1 *M* Tris–0.25 *M* borate–2 m*M* EDTA (pH 8.48); applied field, 178 V/cm (7 μA).

mixture of hybrid structures containing both 4- and 6-sulfated disaccharide units. As indicated in Fig. 6, the splitting of each peak may be associated with the difference in positions of the sulfated groups, which could not be distinguished by open-tubular electrophoresis and a relatively low-concentration gel column. Small differences in the migration rates of hybrid oligosaccharides are expected particularly for solutes with a greater number of repeating units. It is also possible that the oligosaccharide peaks reflect conformational differences. It has been speculated that different mobilities of chondroitin-4- and -6-sulfate fragments with identical molecular weights may be related to a subtle difference in chain conformation [5], making the analysis of glycosaminoglycan-derived oligosaccharides a far more complex problem when compared with the separation of polynucleotide fragments.

Fig. 7 shows an additional example of the separation of acidic oligosaccharides in a polyacrylamide gel-filled column (15% T and 3% C). Hyaluronic acid has a similar structure to chondroitin sulfate, except for a lack of sulfation in the former.

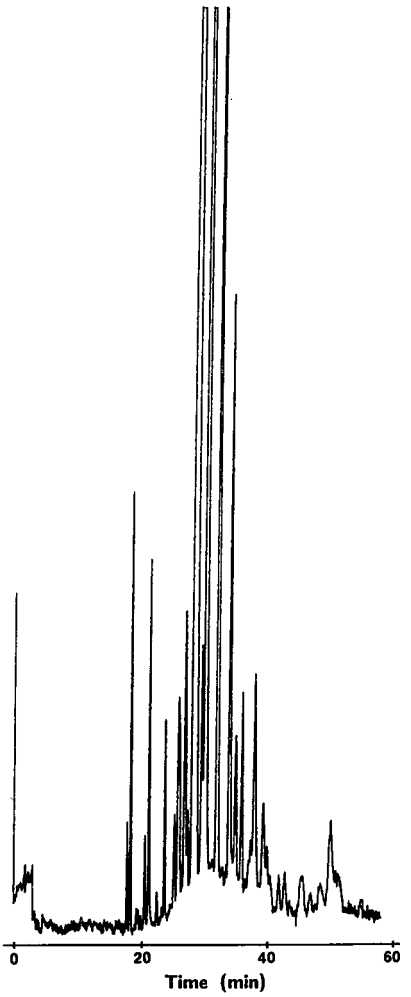

Fig. 7. Electrophoretic separation of enzymatically digested hyaluronic acid in a polyacrylamide gel-filled capillary. Gel concentration, 15% T, 3% C. Capillary, 39 cm (25 cm effective length) × 50 μm I.D.; buffer as in Fig. 6; applied field, 282 V/cm (10 μA).

Disaccharides from hyaluronic acid cleaved by hyaluronidase contain just a singly charged group (a carboxyl group), while two charged moieties are associated with chondroitin sulfate. Better resolution of the oligosaccharide bands (compared with the results for chondroitin sulfate) was achieved with hyaluronic acid. It has been indicated [24] that hyaluronidase catalyzes transglycosylation in addition to hydrolysis and may thus generate oligosaccharides having sequences that were not present in the original substrate. This is likely to make the separation patterns even more complex. Direct measurement of the rate of enzymatically catalyzed transglycosylation relative to that of the hydrolysis in depolymerization of glycans has so far not been feasible.

Although the present studies on the separation of oligosaccharides in gel-filled capillaries must be viewed as preliminary, they clearly show potential for applications to biochemical problems hitherto unsolvable by other analytical techniques. We feel that capillary electrophoresis with laser-induced fluorescence detection is eminently suited to deal with the unique and difficult problems in carbohydrate research.

ACKNOWLEDGEMENTS

This work was supported by grant No. GM 24349 from the National Institute of General Medical Sciences, US Department of Human Health and Services, and a grant-in-aid from Dow Chemical Co.

REFERENCES

1 M. K. Cowman, E. A. Balazs, C. W. Bergmann and K. Meyer, *Biochemistry*, 20 (1981) 1379.
2 J. E. Christner, M. L. Brown and D. D. Dziewiatkowski, *J. Biol. Chem.*, 254 (1979) 4624.
3 M. Hook, U. Lindahl and P.-H. Iverisus, *Biochem. J.*, 137 (1974) 33.
4 A. Malmstrom and L. A. Fransson, *Eur. J. Biochem.*, 18 (1971) 431.
5 M. K. Cowman, M. F. Slahetka, D. M. Hittner, J. Kim, M. Forino and G. Gadelrab, *Biochem. J.*, 22 (1984) 707.
6 I. N. Hampson and J. T. Gallagher, *Biochem. J.*, 221 (1984) 697.
7 K. G. Rice, M. K. Rottink and R. J. Linhardt, *Biochem. J.*, 244 (1987) 515.
8 N. B. Beaty and R. J. Mello, *J. Chromatogr.*, 418 (1987) 187.
9 H. Traitler, S. Del Vedovo and T. F. Schweizer, *J. High Resolut. Chromatogr. Chromatogr. Commun.*, 7 (1984) 558.
10 T. L. Chester and D. D. Innis, *J. High Resolut. Chromatogr. Chromatogr. Commun.*, 9 (1986) 209.
11 V. N. Reinhold, D. M. Sheeley, J. Kuei and G. R. Her, *Anal. Chem.*, 60 2719.
12 H. H. Lauer and D. McManigill, *Anal. Chem.*, 58 (1986) 166.
13 K. A. Cobb and M. V. Novotny, *Anal. Chem.*, 61 (1989) 2226.
14 M. V. Novotny, K. A. Cobb and J. Liu, *Electrophoresis*, 11 (1990) 735.
15 A. S. Cohen, D. R. Najarian, A. Paulus, A. Guttman, J. A. Smith and B. L. Karger, *Proc. Natl. Acad. Sci. U.S.A.*, 85 (1988) 9660.
16 H. Drossman, J. A. Luckey, A. J. Kostichka, J. D'Cunha and L. M. Smith, *Anal. Chem.*, 62 (1990) 900.
17 A. Paulus, E. Gassman and M. J. Field, *Electrophoresis*, 11 (1990) 702.
18 V. Dolnik, J. Liu, J. F. Banks and M. V. Novotny, *J. Chromatogr.*, 480 (1989) 321.
19 J. Liu, O. Shirota and M. V. Novotny, *Anal. Chem.*, 63 (1991) 413.
20 J. Liu, O. Shirota, D. Wiesler and M. V. Novotny, *Proc. Natl. Acad. Sci. U.S.A.*, 88 (1991) 2302.
21 J. Liu, Y.-Z. Hsieh, D. Wiesler and M. V. Novotny, *Anal. Chem.*, 63 (1991) 408.
22 Y.-Z. Hsieh, S. C. Beale, D. Wiesler and M. Novotny, *J. Microcolumn Sep.*, 1 (1989) 96.
23 V. Dolnik, K. A. Cobb and M. V. Novotny, *J. Microcolumn Sep.*, 3(2) (1991) 155–159.
24 W. Knudson, M. W. Gundlach, T. M. Schmid and H. E. Conrad, *Biochemistry*, 23 (1984) 368.

Journal of Chromatography, 559 (1991) 237–246
Elsevier Science Publishers B.V., Amsterdam

CHROM. 23 519

Low-cost, high-sensitivity laser-induced fluorescence detection for DNA sequencing by capillary gel electrophoresis

DA YONG CHEN, HAROLD P. SWERDLOW[a], HEATHER R. HARKE, JIAN ZHONG ZHANG and NORMAN J. DOVICHI*

Department of Chemistry, University of Alberta, Edmonton, Alberta T6G 2G2 (Canada)

ABSTRACT

A low cost, 0.75-mW helium neon laser, operating in the green region at 534.5 nm, is used to excite fluorescence from tetramethylrhodamine isothiocyanate-labelled DNA fragments that have been separated by capillary gel electrophoresis. The detection limit (3σ) for the dye is 500 ymol [1 yoctomole (1 ymol) = 10^{-24} mol] or 300 analyte molecules in capillary zone electrophoresis; the detection limit for labeled primer separated by capillary gel electrophoresis is 2 zmol [1 zeptomole (1 zmol) = 10^{-21} mol]. The Richardson–Tabor peak-height encoded sequencing technique is used to prepare DNA sequencing samples. In 6% T, 5% C acrylamide, 7 *M* urea gels, sequencing rates of 300 bases/hour are produced at an electric field strength of 200 V/cm; unfortunately, the data are plagued by compressions. These compressions are eliminated with addition of 20% formamide to the sequencing gel; the gel runs slowly and sequencing data are generated at a rate of about 70 bases/hour.

INTRODUCTION

In 1977, Sanger *et al.* [1] reported a powerful technique for DNA sequencing based on the dideoxynucleotide chain-terminating reaction. A set of radioactively labeled DNA fragments is generated in four reactions and separated in adjacent lanes of a high-resolution polyacrylamide gel. Detection is by use of autoradiography. The sequence is interpreted from a series of alternating bands in the lanes corresponding to the terminal base.

An advance in sequencing technology occurred in 1986–87 when Smith *et al.* [2], Ansorge *et al.* [3] and Prober *et al.* [4] reported DNA sequencers that replaced the radioactive labels and autoradiography in Sanger *et al.*'s method with fluorescent labels and laser-based detection. In Smith *et al.*'s and Prober *et al.*'s automated sequencers, one of four fluorophores is associated with the terminating dideoxynucleotide either through the use of four separate dideoxynucleotide reactions with four

[a] Visiting scholar from the Department of Human Genetics, University of Utah, Salt Lake City, UT 84132, USA.

0021-9673/91/$03.50

labeled primers that are pooled before use [2] or through the use of fluorescently labeled dideoxynucleotides in a single reaction mixture [4]. In the method of Ansorge *et al.* [3], a single fluorescent label is used with each dideoxynucleotide chain terminating reaction and the products are run on separate lanes of a slab gel. These automated fluorescence sequencers have been commercialized by Applied Biosystems, Pharmacia, and DuPont; as an example, the Applied Biosystems instrument runs sixteen lanes simultaneously on a slab gel to produce sequencing rates of 75 bases/h per lane or 1200 bases/h per slab. Similar sequencing rates are produced by the other instruments. Sequence may be determined, by use of computer algorithms, to about 450 bases, and is limited by the resolution of the gel.

In 1990, Tabor and Richardson [5], and independently Ansorge *et al.* [6] reported a sequencing technique based on a single fluorophore; by varying the amount of dideoxynucleotide in a single reaction mixture, the terminal base is identified with a particular fluorescence peak height during separation in a single lane of an acrylamide gel. This technique relies on uniform labeling of the reaction product through the use of the manganese–T7 polymerase reaction. In the work that has been published, separation is by slab-gel electrophoresis, a fluorescein-labeled primer is excited with an argon ion laser at 488 nm and emission is detected in a single spectral band.

Gel-filled capillaries have attracted interest for DNA sequencing because their high surface-to-volume ratio provides excellent heat transport properties, allowing the use of very high electric field strengths. Early work with capillary-dimension electrophoresis media was performed by Edström [7,8], who described the use of very fine cellulose fibers (5 μm diameter) for the electrophoresis of nucleic acids from single cells at an electric field strength of 125 V/cm. In 1965, Matioli and Niewisch [9] studied hemoglobin from single cells on fine polyacrylamide fibers of 50 μm diameter. Grossbach [10] reported in 1974 the use of 50-μm diameter gel-filled glass capillaries. Larger scale capillary polyacrylamide gel electrophoresis was reported by Neuhoff *et al.* [11] in 1970, who used 5-μl capillaries for the study of ribonucleic acid polymerase. In 1983, Hjerten [12] reported the use of a 150-μm I.D. capillary polyacrylamide electrophoresis separation of several samples, including monomers through pentamers of bovine serum albumin. More recently, Karger and co-workers [13–16] have reported capillary polyacrylamide gel electrophoresis for the separation of proteins, chiral amino acids, polyadenisoic acid fragments and fluorescently labeled products of a single DNA sequencing reaction. Several patents have been issued that describe the use of a bifunctional reagent to bind polyacrylamide chemically to the capillary surface [17–19]. Swerdlow and Gesteland [20] described DNA sequence analysis by use of capillary polyacrylamide gel electrophoresis with on-column fluorescence detection. The separation of a single reaction mixture in gel-filled capillaries was reported by Drossman *et al.* [21]. When operating at 400 V/cm, the system produced sequencing rates of 1000 bases/hour after elution of the primer, a *ca.* 25 times higher sequencing rate per lane than that produced by conventional slab gel electrophoresis. Luckey *et al.* [22] reported a four-color sequencing system based on the reaction products in the ABI sequencing system.

Laser-induced fluorescence detection in slab-gel electrophoresis requires low detection limits, typically in the order of 1–100 amol of each fragment [2,3]. This detection performance is complicated for both Smith *et al.*'s [2] and Prober *et al.*'s [4] techniques because the fluorescence signal must be measured in several spectral chan-

nels. However, the detection requirement in capillary gel electrophoresis is more severe. Based on a comparison of the cross-section of a capillary with the cross-section of a loading well in a slab gel, Drossman *et al.* [21] estimated that the sample loading in capillary gel electrophoresis will be in the order of 1–10 amol. Detection limits in the zeptomole range (1 zeptomole = 10^{-21} mol = 600 molecules)[a] are necessary for DNA sequencing by capillary gel electrophoresis. This task is complicated further by the requirement that the detection volume be less than 10^{-10} l to preserve the separation efficiency of the nano-scale electrophoresis technique. Swerdlow and Gesteland's [20] system used an on-column laser-induced fluorescence detection with detection limits of 200 zmol of fluorescently labeled product. Smith and co-workers [21,22] described the use of one- and four-channel on-column fluorescence detectors; both the single-and four-channel detector produced detection limits of about 100 zmol of labeled fragment. We have reported [24] the use of a post-column fluorescence detector in the gel electrophoresis separation of the products of a single chain-terminating reaction; the detection limit was 10 zmol.

This research group has developed three DNA sequencers based on capillary gel electrophoresis [25]. The first of these sequencers is based on the Applied Biosystems set of four fluorescently labeled sequencing primers. An on-column detector produced a detection limit of 200 zmol for each primer. Sequencing rates of 300 bases/h are produced at an electric field strength of 150 V/cm for samples up to 550 bases in length. The second detector is based on the DuPont set of four fluorescently labeled dideoxynucleotides. A sheath-flow cuvette post-column detector produced a detection limit of 20 zmol for labeled dideoxynucleotide triphosphate. Sequencing rates of 1000 bases/h are produced at an electric field of 465 V/cm. The third of these sequencers is based on the Richardson–Tabor–Ansorge sequencing method.

This paper describes our detector for the single color sequencer based on the Richardson–Tabor–Ansorge sequencing method. Details are also given on the separation of fluorescently labeled DNA fragments in acrylamide–urea gels and acrylamide–urea–formamide gels.

EXPERIMENTAL

Zone electrophoresis

A 48 cm × 10 μm I.D. capillary (Polymicro Technologies, Phoenix, AZ, USA) was used for the separation. The buffer was 5 m*M* borate (pH 9.0)–10 m*M* sodium dodecyl sulfate (SDS); the SDS was added to eliminate peak tailing in the electropherogram. Samples were injected electrokinetically for 5 s at 1 kV, corresponding to 30 pl of sample. The electropherogram proceeded at a potential of 30 000 V. The photomultiplier was operated at 1200 V and a 0.1-s time constant electronic filter was used to condition the data. The sheath stream flow-rate was 0.24 ml/h. The data were displayed on a strip-chart recorder. The standard deviation of the background signal was obtained by recording 100 data points at 1-s intervals; the order of magnitude

[a] Zepto (2) = 10^{-21} and yocto (4) = 10^{-24} were accepted as prefixes by the Comité International des Poids et Mesures in October 1990 to be put forward to the Conférence Générale des Poids et Mesures for adoption in October 1991 [23].

difference between the sampling rate and the electronic time constant ensures that there is minimal correlation between successive data points.

DNA sample

A nested set of fluorescently labeled DNA fragments was kindly provided by C. Fuller of the United States Biochemical Corporation. The sequencing reaction was carried out in 40 m*M* 3-(N-morpholino)propanesulfonic acid (MOPS) buffer (pH 7.5)–50 m*M* NaCl–10 m*M* $MnCl_2$–15 m*M* sodium isocitrate. Dye-labeled primer (Applied Biosystems 21M13 TAMRA, 1.6 p*M*) was annealed to 1 μg of M13mp18 single-stranded DNA at 65°C for 2 min followed by slow cooling. A mixture of deoxy- and dideoxynucleotide triphosphates was added to give an average nucleotide ratio (dNTP/ddNTP) of 1200:1 with 7-deaza-2′-deoxyguanosine-5′-triphosphate used in place of dGTP. The ratios of nucleotides were adjusted to yield a nominal peak-height ratio of 8:4:2:1 for T, G, C and A, respectively. The mixture was warmed to 37°C and 6 units of Sequenase Version 2.0 and 0.006 units of pyrophosphatase were added. Incubation was continued at 37°C for 30 min, after which the DNA was precipitated with ethanol. The sample was resuspended in 2 μl of formamide containing trace EDTA and injected at 150 V/cm for 30 s. After injection, the sample was replaced with a fresh vial of 1 × TBE [1.08% tromethamine (Tris), 0.55% boric acid, 0.07% EDTA in 100 ml water]. The separation proceeded at 150 V/cm. The sheath stream was 1 × TBE at a flow-rate of 0.16 ml/h.

Gel electrophoresis

When the gel-filled capillary was operated at high electric field strength, the gel migrated about 100 μm from the detection (positive electrode) end of the capillary. This migration is different from the well known migration of the gel from the injection (negative electrode) end of the capillary caused by electroosmosis. The migration from the detection end, presumably due to electrostriction, is undesirable because the gel can block the laser beam which is positioned a few micrometers beyond the tip of the capillary. To eliminate this migration, the gel was covalently bound to the wall of the detection tip of the capillary; the last 5 mm of the detection end of the capillary was dipped for a few seconds into a 0.5% (v/v) solution of γ-methacryloxypropyltrimethoxysilane in a water–acetic acid solvent (1:1). The gel was poured within 15 min of treatment of the capillary tip.

Two gels were used in this study. A 6%T, 5%C[a] polyacrylamide–7 *M* urea gel was covalently cross-linked to the last 5 mm of the detection end of the capillary of the 31 cm × 50 μm I.D. × 190 μm O.D. capillary; this gel was operated at 200 V/cm. A highly denaturing 6%T, 5%C polyacrylamide–7 *M* urea–20% formamide gel was covalently cross-linked to the last 5 mm of the 31 cm × 50 μm I.D. × 190 μm O.D. capillary; this gel was operated at 150 V/cm.

Detector

A 0.75-mW helium–neon laser beam (543.5 nm) (Melles Griot, Ontario, Canada) was focused with a 5× microscope objective about 200 μm below the exit of the

[a] %T = g acrylamide + g Bis per 100 ml of solution; %C = %Bis in T.

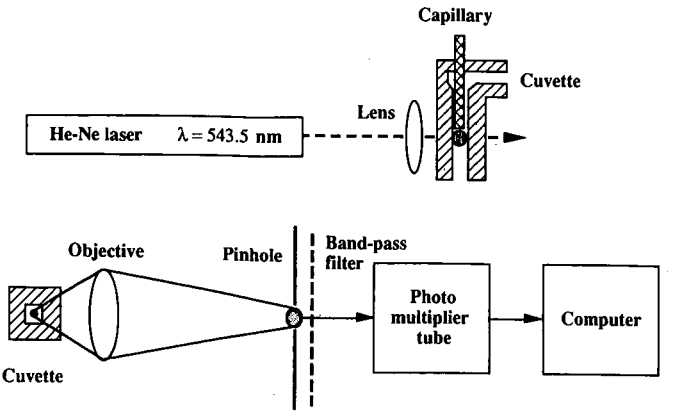

Fig. 1. Optical diagram. See text for description of the instrument.

capillary with a 200-μm square flow chamber and 2-mm thick windows (Fig. 1). Fluorescence was collected at right-angles with an 18×, 0.45 numerical aperture objective (Melles Griot) and imaged onto a 0.8-mm diameter pinhole. A single interference filter (590 nm center, 40 nm band pass, Model 590DF35; Omega Optical, VT, USA) was used to block scattered laser light. Fluorescence was detected with a Hamamatsu (CA, USA) R1477 photomultiplier tube, operated at 1000 V and cooled to −25°C with a Products for Research (MA, USA) photomultiplier (PMT) cooler. The PMT tube output was passed through a 1-s RC low-pass filter, digitized by a computer and treated with a 21-point quadratic–cubic polynomial filter before display. A similar optical system was used for an on-column fluorescence detector, except that an OG-570 colored glass filter (Melles Griot) was added to the collection optics to decrease the background signal. Data were recorded at 0.4-s intervals for conventional gel data and 0.5-s intervals for formamide data.

RESULTS AND DISCUSSION

Detection

The high-sensitivity capillary gel electrophoresis detector is based on a post-column sheath flow cuvette. In this detector, similar to that used in flow cytometry, the sample flows as a narrow stream in the center of a 200-μm square flow chamber, surrounded by a sheath stream consisting of conducting buffer. The high optical quality windows of the cuvette produce at least two orders of magnitude less light scatter than does an on-column detector. Also, by transferring the analyte to the moving sheath stream, the linear velocity, and hence the illumination time of the analyte, is independent of fragment length. The extent of photobleaching, which depends on illumination time, is constant for all analytes. We have reported the use of a single spectral channel fluorescence detector based on the sheath flow cuvette for capillary zone electrophoresis separation of zeptomole amounts of fluorescently labeled amino acids and for capillary gel electrophoresis separation of zeptomole amounts of the products of sequencing reactions [24–28]; Keller and co-workers

[29,30] have reported high-sensitivity detection for neat solutions of highly fluorescent dyes. Recently, Keller's group [31] reported, and Mathies' group [32] confirmed, detection of single phycoerythrin molecules in neat solution with a single spectral channel fluorescence detector.

The argon ion laser (488, 514.5 nm) is used by most investigators for excitation of fluorescence in capillary electrophoresis. However, the laser is rather expensive (*ca.* US$ 10 000) and requires forced air cooling. An interesting alternative excitation source for fluorescence excitation is the helium–neon laser (the so-called Gre–Ne laser) operating in the green region at 543.5 nm. The laser is inexpensive (*ca.* US$ 1000) and features the same construction as the conventional red helium–neon laser. Six conventional red helium–neon lasers have been in operation in this laboratory for 6–8 years with no tube failures; the green helium–neon laser should have a similar lifetime. The laser produces a low output power (0.75 mW) with excellent spatial coherence and good noise characteristics. Finally, the beam is easily focused to a 10-μm radius spot for fluorescence applications.

Tetramethylrhodamine isothiocyanate (TRITC) is well suited for application in laser-induced fluorescence detection. The molecule has a molar absorptivity of about 85 000 l mol^{-1} cm^{-1} at the green helium–neon laser wavelength. Keller [33] reported that the molecule has a fluorescence quantum yield of 15% and a photodestruction yield of 5×10^{-6}; under conditions of complete photobleaching, the molecule is expected to produce about 30 000 fluorescent photons, a factor of four greater signal than produced by fluorescein [34].

A sheath flow cuvette is used as a post-column fluorescence detector to minimize background light scatter. Further reduction in the background signal comes from the relatively long excitation wavelength and low-power excitation beam (750 μW). With this detector, the major contribution to the background signal was dark current produced by the photomultiplier tube. This contribution to the background signal is minimized by cooling the photomultiplier tube to -25°C.

The detection limit of this detector for TRITC was determined in a zone electrophoresis system. The relative standard deviation ($n = 5$) in peak height of a 1.28×10^{-10} *M* TRITC solution was 10%. Fig. 2 shows a zone electropherogram of a 4-zmol injection of analyte corresponding to 2300 analyte molecules. A linear calibration curve ($r = 0.986$) was constructed from $6.4 \cdot 10^{-11}$ to $2.56 \cdot 10^{-10}$ *M* TRITC. The detection limit, three standard deviations above the background signal, was 300 analyte molecules or 500 ymol (1 yoctomole = 1 ymol = 10^{-24} mol) [23]. Note that the data were not conditioned beyond that provided by the 0.1-s time-constant filter,

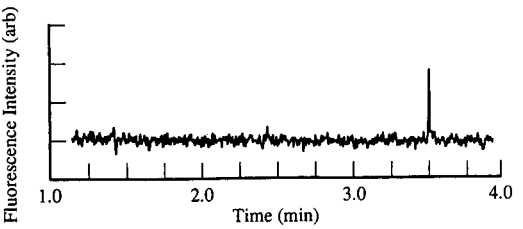

Fig. 2. Capillary zone electropherogram of 4 zmol (2300 molecules) of tetramethylrhodamine isothiocyanate.

appropriate digital filtering would undoubtedly improve the detection performance. Also, the use of a higher power laser would undoubtedly improve the detection limits further.

The major components used in the experiment (laser, high-voltage power supply, optical breadboard, sheath flow cuvette, photomultiplier tube power supply, and PMT cooler) have a total cost of about US$ 8000. It is possible to construct a simple, modest cost instrument with excellent analytical performance.

In our one-color DNA sequencer, a tetramethylrhodamine-labeled primer is excited by a green helium–neon laser (543.5 nm). The standard deviation in the background signal for this system corresponds to 700 ymol of labeled primer introduced onto the capillary; detection limits are, by definition, a factor of three higher (1200 molecules). The difference between these detection limits and the zone electrophoresis system probably reflects the low sample migration rate produced in the gel electrophoresis system; detection limits are degraded by dilution of the sample in the cuvette during the transit time from the capillary exit to the illumination volume. Detection limits improve for higher molecular weight fragments that undergo less diffusion in the cuvette and are more concentrated in the illumination volume. As a result, the detection limit for the system improves for larger DNA fragments that are typically produced in lower concentration compared with early eluting fragments. These detection limits, produced by a very low power laser, are associated with the excellent spectral properties of the tetramethylrhodamine fluorophore and reflect the simple detector design required by the single-color sequencing technique.

An on-column fluorescence detector was constructed for gel electrophoresis; a window was produced by removing a portion of the polyimide coating of the capillary before the capillary was filled with gel. We noticed that a fan of scattered light was generated in the plane perpendicular to the capillary axis. This fan was attenuated significantly if the capillary was tilted by more than *ca.* 15° with respect to the laser beam. The attenuation in scatter intensity does not appear to be associated with Brewster's angle; only one component of the unpolarized laser beam would be extinguished at Brewster's angle. Also, the scattered light remained attenuated if the capillary was tilted by more than 15°, again inconsistent with Brewster's angle. Instead, reflection and refraction at the curved surface of the capillary dominate the background signal; tilting the capillary presumably directs the scattered light out of the field of view of the collection optics. The background light scatter signal does not appear to originate in the gel; similar background signals were observed for a buffer-filled and gel-filled capillary. Instead, the light scatter appears to originate from the walls of the capillary.

The detection limit for the on-column detector was an order of magnitude poorer that the sheath flow cuvette results. The two detectors used identical lasers, focusing optics, collection optics, electrophoresis potential, and PMT tube. Because of the high background signal produced by the capillary, it was necessary to use additional spectral filtering and a different spatial mask in the collection optics for the on-column detector. The additional OG-570 filter produces a three orders of magnitude decrease in background signal at the laser excitation wavelength; assuming that autofluorescence of the filter did not contribute significantly to the background signal, and realizing that the standard deviation of a shot-noise limited background signal increases with the square root of the signal intensity, it appears that the back-

ground signal due to the on-column detector is at least five orders of magnitude higher than that of the post-column detector based on the sheath flow cuvette.

Separation

By varying the ratio of dideoxynucleotides used in the chain extention reaction, the identity of the terminal dideoxynucleotide is encoded in peak height (Fig. 3). In any local neighbourhood, peaks associated with T will be higher than peaks associated with G, which in turn are larger than those for C and A. Unfortunately, in our standard sequencing gel, significant compressions are produced with this fluorescently labeled primer. A sequence of GGGTACCG, corresponding to fragments 59–66 nucleotides in length, is severely compressed. This compression appears to be associated with the low temperature at which the separation proceeds; data generated on a commercial slab gel sequencer showed no compression.

A sequencing gel was modified by addition of 20% (v/v) of formamide; the data generated on this gel show only a slight sequencing error for fragments 63–65 nucleotides in length (Fig. 4). However, this modified gel produces a very low sequencing rate of 70 bases/h at an electric field strength of 150 V/cm. We assume that operation of conventional gels at a temperature above ambient will eliminate the compressions, providing higher sequencing rates.

To obtain accurate base determination with this sequencing method, it is necessary to employ very careful enzymology; minor variations in peak amplitude can lead to poor discrimination in base determination. Pauses in the sequencing reaction can produce ghost peaks that contaminate the peak amplitude. Ghost peaks add the greatest proportional error to the lowest amplitude peaks. It seems that a carefully

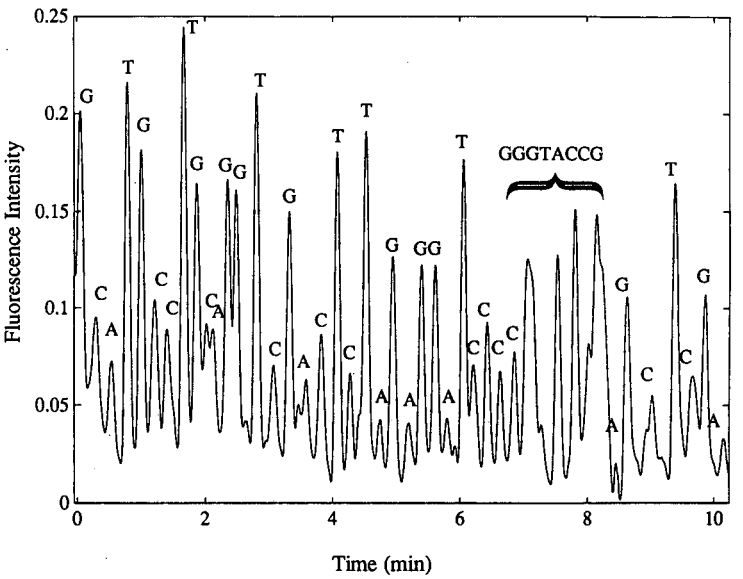

Fig. 3. Capillary gel electropherogram of M13mp18 reaction fragments: 6% T, 5% C–7 *M* urea acrylamide gel; fragments 28–73 nucleotides in length are shown. Time is arbitrarily set to zero for the fragment 27 nucleotides in length.

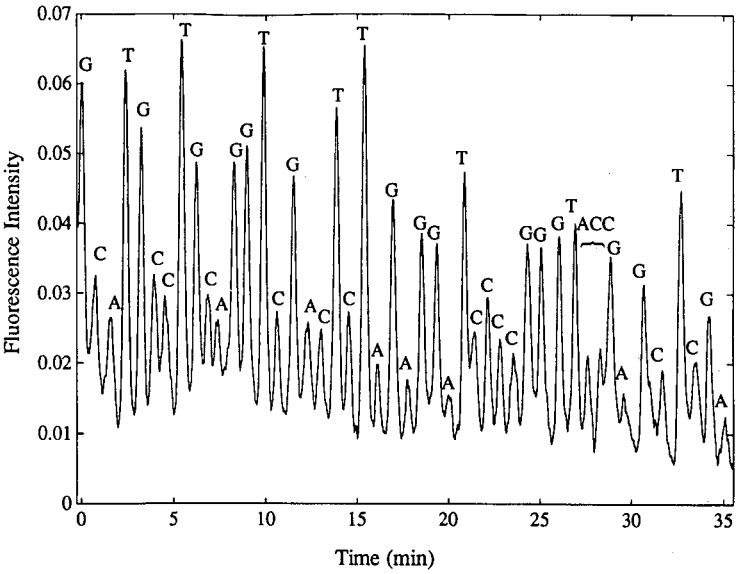

Fig. 4. Capillary gel electropherogram of M13mp18 reaction fragments: 6% T, 5% C–7 *M* urea–20% formamide acrylamide gel; fragments 28–73 nucleotides in length are shown. Time is arbitrarily set to zero for the fragment 27 nucleotides in length.

designed sequencing kit, optimized for a particular sequencing template, must be used to obtain accurate sequencing data from this amplitude modulated sequencing protocol.

ACKNOWLEDGEMENTS

This work was funded by the US Department of Energy–Human Genome Initiative (grant DE-FG02-91E R61123), Natural Sciences and Engineering Research Council of Canada, Department of Chemistry of the University of Alberta, Pharmacia/LKB, Waters Division of Millipore, and Beckman. Support by D.O.E. does not constitute an endorsement of the views expressed in this article. The DNA sample was kindly provided by C. Fuller of United States Biochemical Corporation. H.P.S. acknowledges a predoctoral fellowship from the National Science Foundation and H.R.H. acknowledges a fellowship from the Alberta Heritage Fund for Medical Research. J.E. Bertie of the University of Alberta kindly loaned the photomultiplier cooler.

REFERENCES

1 F. Sanger, S. Nicklen and A. R. Coulson, *Proc. Natl. Acad. Sci. U.S.A.*, 74 (1977) 5463.
2 L. M. Smith, J. Z. Sanders, R. J. Kaiser, P. Hughes, C. Dodd, C. R. Connell, C. Heiner, S. B. H. Kent and L. E. Hood, *Nature (London)*, 321 (1986) 674.
3 W. Ansorge, B. S. Sproat, J. Stegemann and C. Schwager, *J. Biochem. Biophys. Methods*, 13 (1986) 315.
4 J. M. Prober, G. L. Trainor, R. J. Dam, F. W. Hobbs, C. W. Robertson, R. J. Zagursky, A. J. Cocuzza, M. A. Jensen and K. Baumeister, *Science (Washington, D.C.)*, 238 (1987) 336.

5 S. Tabor and C. C. Richardson, *J. Biol. Chem.*, 265 (1990) 8322.
6 W. Ansorge, J. Zimmermann, C. Schwager, J. Stegemann, H. Erfle and H. Voss, *Nucleic Acids Res.*, 18 (1990) 3419.
7 J. E. Edström, *Nature (London)*, 172 (1953)) 809.
8 J. E. Edström, *Biochim. Biophys. Acta*, 22 (1956) 378.
9 G. T. Matioli and H. B. Niewisch, *Science (Washington, D.C.)*, 150 (1965) 1824.
10 U. Grossbach, in R. C. Allen and H. R. Maurer (Editors) *Electrophoresis and Isoelectric Focusing in Polyacrylamide Gel*, Walter de Gruyter, Berlin, 1974, p. 207.
11 V. Neuhoff, W. B. Schill and H. Sternbach, *Biochem. J.*, 117 (1970) 623.
12 S. Hjerten, *J. Chromatogr.*, 270 (1983) 1.
13 A. S. Cohen and B. L. Karger, *J. Chromatogr.*, 397 (1987) 409.
14 A. Guttman, A. Paulus, A. S. Cohen, N. Grinberg and B. L. Karger, *J. Chromatogr.*, 488 (1988) 41.
15 A. S. Cohen, D. R. Najarian, A. Paulus, A. Guttman, J. A. Smith and B. L. Karger, *Proc. Natl. Acad. Sci. U.S.A.*, 85 (1988) 9660.
16 A. S. Cohen, D. R. Najarian and B. L. Karger, *J. Chromatogr.*, 516 (1990) 49.
17 B. L. Karger and A. S. Cohen, *US Pat.*, 4 865 706, 1989.
18 B. L. Karger and A. S. Cohen, *US Pat.*, 4 865 707, 1989.
19 P. F. Bente and J. Myerson, *US Pat.*, 4 810 456, 1989.
20 H. Swerdlow and R. Gesteland, *Nucleic Acids Res.*, 18 (1990) 1415.
21 H. Drossman, J. A. Luckey, A. J. Kostichka, J. D'Cunha and L. M. Smith, *Anal. Chem.*, 62 (1990) 900.
22 J. A. Luckey, H. Drossman, A. J. Kostichka, D. A. Mead, J. D'Cunha, T. B. Norris and L. M. Smith, *Nucleic Acids Res.*, 18 (1990) 4417.
23 G. R. Freeman, personal communication.
24 H. Swerdlow, S. Wu, H. Harke and N. J. Dovichi, *J. Chromatogr.*, 516 (1990) 61.
25 H. Swerdlow, J. Z. Zhang, D. Y. Chen, H. R. Harke, R. Grey, S. Wu, C. Fuller and N. J. Dovichi, *Anal. Chem.*, submitted for publication.
26 Y. F. Cheng and N. J. Dovichi, *Science (Washington, D.C.)*, 242 (1988) 562.
27 S. Wu and N. J. Dovichi, *J. Chromatogr.*, 480 (1989) 141.
28 Y. F. Cheng, S. Wu, D. Y. Chen and N. J. Dovichi, *Anal. Chem.*, 62 (1990) 496.
29 N. J. Dovichi, J. C. Martin, J. C. Jett and R. A. Keller, *Science (Washington, D.C.)*, 219 (1983) 845.
30 N. J. Dovichi, J. C. Martin, J. C. Jett, M. Trkula and R. A. Keller, *Anal. Chem.*, 56 (1984) 348.
31 D. C. Nguyen, R. A. Keller, J. H. Jett and J. C. Martin, *Anal. Chem.*, 59 (1987) 2158.
32 K. Peck, L. Stryer, A. N. Glazer and R. A. Mathies, *Proc. Natl. Acad. Sci. U.S.A.* 86 (1989) 4087.
33 R. Keller, paper presented at *OE-LASE '91, 23 January, 1991*, paper 1435-27.
34 T. Hirshfeld, *Appl. Opt.*, 15 (1976) 3135.

Journal of Chromatography, 559 (1991) 247–256
Elsevier Science Publishers B.V., Amsterdam

CHROM. 23 456

Reproducibility and quantitation of separation for ribonucleoside triphosphates and deoxyribonucleoside triphosphates by capillary zone electrophoresis

RAY TAKIGIKU* and R. E. SCHNEIDER
The Procter and Gamble Co., Miami Valley Laboratories, P.O. Box 398707, Cincinnati, OH 45239-8707 (USA)

ABSTRACT

Capillary zone electrophoresis has been evaluated for the separation and quantitation of ribonucleoside and deoxyribonucleoside triphosphates. For adequate resolution, capillaries were treated to reduce electroosmotic flow and capillary zone electrophoresis was performed with negative high voltage. Results from both a fully automated and a manual instrument are found to have comparable performance characteristiscs. The described method is linear with a minimum concentration detection limit of approximately 0.001 mg/ml per nucleotide.

INTRODUCTION

Capillary electrophoresis has been used to analyze a diverse array of molecules, including proteins and peptides [1–4], nucleosides, nucleotides and oligonucleotides [5–11] and drugs and drug metabolites [12–15]. The most commonly used mode of capillary electrophoresis is performed with open tubes and is termed capillary zone electrophoresis (CZE). When surfactants are added to the buffer at concentrations exceeding their critical micellar concentration, both neutral and charged analytes can be resolved. This mode of capillary electrophoresis is termed micellar electrokinetic capillary chromatography (MECC, or MEKC). Both CZE and MECC have been previously described for the analysis of various nucleotide species [5–10,16]. This paper describes our efforts at resolving and quantitating ribonucleoside triphosphates (NTPs) and deoxyribonucleoside triphosphates (dNTPs) by CZE.

Measurements of NTP and dNTP pools in mammalian cells are of importance in studying aspects of DNA and RNA synthesis and regulation [17,18]. Several methods exist for the measurement of NTP and/or dNTP precursor pools, including enzymatic assays [19,20], gas chromatography [21], and HPLC [22]. Of these, only HPLC has been described to measure the common 8 NTPs and dNTPs (ATP, dATP, CTP, dCTP, GTP, dGTP, dTTP and UTP) simultaneously, but requires *ca.* 60 min to elute all components [22].

0021-9673/91/$03.50

Because CZE offers ease, rapid analysis times and impressive resolving power, we sought to develop a CZE method for the separation and quantitation of NTPs and dNTPs. In CZE, selectivity is a function of the relative differences in the electrophoretic mobilities of the analytes. Mobility is related to molecular charge, size, shape and solution viscosity. Additionally, in uncoated fused-silica capillaries, an electric-field-induced solvent flow occurs within the capillary. This flow is termed electroosmosis. Normally, electroosmotic flow is toward the cathode (CZE with positive high voltage, or "normal polarity"). Hence, while anions would normally migrate towards the anode, electroosmosis is often of sufficient magnitude to force them towards the cathode. Therefore, both cations and anions can be analyzed simultaneously. However, because we were interested in rapidly resolving only strongly anionic compounds, we describe a method for nucleotide separation in the absence of electroosmotic flow, wherein anion migration is permitted to proceed from the cathode to the anode (CZE with negative high voltage, or "reverse polarity"). This CZE method is capable of resolving the common 8 NTPs and dNTPs with UV detection (254 nm) within an 18 min separation time. Reproducibility and quantitation are assessed.

Although the absolute amount of detectable nucleotide in CZE can be very small in comparison to HPLC, the minimum detectable concentration is only comparable, being on the order of 0.001 mg/ml (*ca.* 10^{-6} *M*).

EXPERIMENTAL

Reagents

All ribonucleoside triphosphates, deoxyribonucleoside triphosphates, EDTA and γ-methacryloxypropyltrimethoxysilane were obtained from Sigma (St. Louis, MO, USA), and were used without further purification. All buffer components, N,N,N′N′-tetramethylethylenediamine (TEMED), and electrophoresis-grade acrylamide were obtained from Bio-Rad (Richmond, CA, USA). Methanol was obtained from J. T. Baker, Inc. (Phillipsburg, NJ, USA). Sample solutions were prepared by dissolving (deoxy)nucleotides in 0.1 *M* phosphate buffer at pH 2.5, and stored frozen. The operating buffer was composed of 0.05 *M* phosphate at pH 2.7 with 0.002 *M* EDTA, and was made fresh daily.

Instrumental

CZE was performed with a Beckman P/ACE System 2000 controlled with an IBM PS/2 Model 55SX with Beckman P/ACE v1.1 software; and a Bio-Rad HPE 100. In both instruments, the inlet was held at negative high voltage with respect to the grounded outlet. Both units were used with fused-silica capillaries treated to reduce electroosmosis. The polymer-coated capillary (20 cm total length × 25 μm I.D.; P/N 148-3011) used in the Bio-Rad instrument was obtained from Bio-Rad and was used without further modification.

The fused-silica capillary used in the Beckman was obtained from Polymicro Technologies (75 μm I.D. × 260 μm O.D.; Phoenix, AZ, USA) and was fitted into a Beckman capillary cartridge (P/N 338463). Total capillary length was 69.5 cm. The capillary was treated by the method described by Hjertén [23] with the following modifications (all reactions were performed with the capillary held at 50°C). Capillaries were first rinsed with 0.1 *M* NaOH for 10 min, followed by methanol for 10

min, followed by distilled water for 10 min. Capillaries were then silylated with γ-methacryloxypropyltrimethoxysilane by aspirating a 0.5% solution in distilled water (pH was adjusted to 3.5 with glacial acetic acid) for 30 min. Silylated capillaries were rinsed with distilled water for 10 min, followed by dry nitrogen gas. A polyacrylamide coating was then applied by aspirating a 20 ml deaerated 3% (w/v) acrylamide solution containing 8 μl of TEMED and 10 mg ammonium persulfate for 30 min. Finally, capillaries were rinsed with distilled water for 10 min, followed by dry nitrogen gas.

Two different injection methods were used. Electrokinetic injection was used exclusively with the Bio-Rad and all samples were injected under the same conditions, *i.e.*, 2 kV for 10 s (unless otherwise indicated). Pressure injection was used with the Beckman. Briefly, an inlet pressure of 3.45 mPa pressure was applied for a specified time interval (5 s, unless otherwise indicated) to introduce sample into the capillary.

At least 5 column volumes of operating buffer was used to rinse the capillaries between runs. All other operating conditions are as described in Results and Discussion.

Data collection and processing were accomplished on a IBM PS/2 Model 70 with Turbochrome II software (v. 2.0) and PE Nelson Series 900 Interface units (Cupertino, CA, USA).

RESULTS AND DISCUSSION

Fig. 1 shows an electropherogram of a standard solution of ATP, dATP, CTP, dCTP, GTP, dGTP, dTTP, UTP and ITP (0.6 ng each; ITP at 1.25 ng). The rare

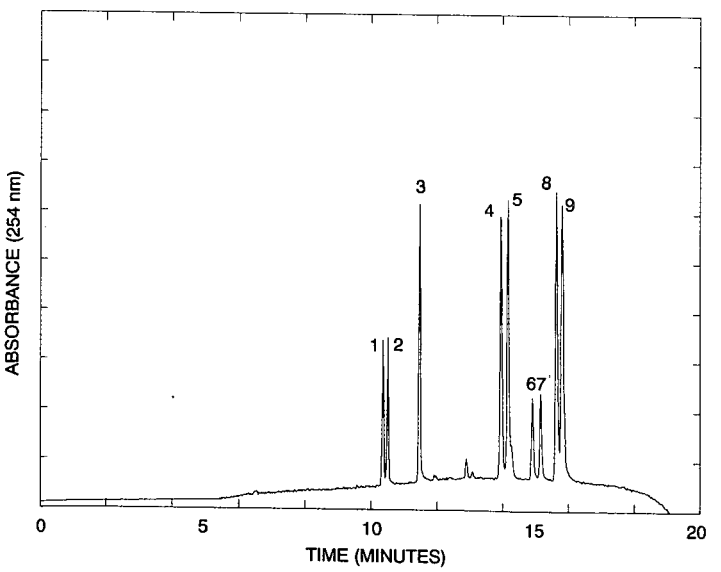

Fig. 1. Electropherogram of NTP and dNTP mixture. Concentration of original mixture was 0.031 mg/ml per nucleotide, ITP was 0.063 mg/ml. All other details are as described in Table I for the Beckman instrument. Peaks: 1 = UTP; 2 = dTTP; 3 = ITP; 4 = GTP; 5 = dGTP; 6 = dCTP; 7 = CTP; 8 = dATP; 9 = ATP.

nucleotide, ITP, was used as an internal standard. All components are clearly separated with the total separation time under 18 min. Interestingly, the elution order for the NTPs corresponds with that reported by Silver *et al.* [24] for an electrophoretic separation on paper as well as a previous CZE separation demonstrating indirect fluorescence detection [25]. CZE separations of the dNTPs have not previously been reported.

For the compounds studied here, the overall net charge of each nucleotide probably primarily affects its respective migration rate. In the pH range of the buffers used (<3), the uracil, thymine and inosine moieties are essentially neutral, while guanine is predominantly positive, and cytosine and adenine are virtually completely positive [26]. Under these experimental conditions, we would expect that the most anionic components would exhibit the largest migration rate, and indeed that is what is observed. Interestingly, the migration rates of the deoxyribonucleotides closely paralled those of their ribonucleotide analogues, which probably further indicates that the overall net charge of the molecules predominantly influences their migration rates. Additionally, size may also play an important role as evidenced by the migration order of the least anionic components (cytidine and adenine nucleotides), where the larger purines, ATP and dATP, exhibited the lowest migration rates.

Reproducibility of the electropherograms

Reproducibility of migration time. Average migration times and relative standard deviations (R.S.D.) for the nucleotides are listed in Table I. Because we used coated capillaries, migration times were not influenced by electroosmotic flow. Hence,

TABLE I

REPRODUCIBILITY OF MIGRATION TIME AND MOBILITY

Conditions: operating buffer, 0.05 *M* phosphate (pH 2.7) with 0.002 *M* EDTA. Beckman instrument capillary 69.5 cm × 75 μm I.D., derivatized; length to detector 62.8 cm; pressure injection for 5 s; 20 kV applied voltage. Bio-Rad instrument capillary 20 cm × 25 μm I.D., derivatized; length to detector 17 cm; electrokinetic injection for 10 s at 2 kV; 2 kV applied voltage.

Instrument	Component	Migration time (n = 5, min)		Mobility
		Mean	R.S.D. (%)	
Beckman	UTP	10.55	0.039	20.69
	dTTP	10.70	0.417	20.40
	ITP	11.65	0.013	18.74
	GTP	14.11	0.088	15.46
	dGTP	14.33	0.013	15.23
	dCTP	15.08	0.017	14.48
	CTP	15.33	0.131	14.24
	dATP	15.74	0.575	13.86
	ATP	16.02	0.601	13.62
Bio-Rad	dTTP	8.35	1.43	20.37
	dGTP	11.01	1.49	15.45
	dCTP	11.58	1.50	14.68
	dATP	12.08	1.47	14.07

electrophoretic mobilities (μ) could be directly calculated by eqn. 1 and are included in Table I.

$$\mu = \frac{L_d L_t}{tV} \tag{1}$$

Here L_d is the length of the capillary from the injection end to the detector, L_t is the total length of the capillary, t is the migration time and V is the applied voltage.

The observed migration order is a direct function of each nucleotide's electrophoretic mobility. Mobility is primarily influenced by analyte size and charge (characteristics which can be influenced by solvent properties such as pH and viscosity), but hydrophobicity [27] and molecular conformation [28] can also affect mobility. Notably, the electrophoretic mobilities as determined from the two instruments used in this study are very similar, indicating comparable performance despite differing capillary lengths, diameters and coating chemistries. However, there are important experimental differences between the two systems. We required the longer (69.5 cm total length) capillary to resolve adequately all 9 nucleotides. The shorter capillary (20 cm total length) used on the Bio-Rad permitted only resolution of a smaller number of components (for these experiments we chose the 4 dNTPs as model compounds). It is reasonable to expect that a longer capillary would perform in an analogous manner to the (longer) capillary we used with the Beckman instrument. Indeed, an application note from Bio-Rad (P/N 1575-14) illustrates a separation of the 8 common NTPs and dNTPs on a 50 cm $\times$ 50 μm I.D. coated capillary, using a 0.1 *M* phosphate buffer at pH 2.5 with 0.002 *M* EDTA.

Mobilities are also influenced by temperature fluctuations [29–32]. Good reproducibility can only be achieved by rigorous temperature control. We would expect better heat dissipation from the 25 μm I.D. column used in the Bio-Rad (relative to the 75 μm I.D. column used in the Beckman), but the Beckman instrument provides temperature regulation via a thermostatted heat transfer fluid. Based on migration time reproducibilities obtained for both instruments (Table I), both mechanisms appear effective. However, optimum temperature control is dependent on the combination of both factors, *i.e.*, efficient radial heat transfer through the capillary and precise thermostatting of the capillary itself.

Quantitation

Both detector linearity and reproducibility of sample introduction primarily affect quantitation. Detection of nucleotides was accomplished by on-column UV absorbance detection at 254 nm. For this study, we chose to measure peak areas (normalized to migration time), instead of peak heights. Other studies have noted the advantages of measuring peak areas [33,34].

Sample introduction. Pressure injection was used exclusively with the Beckman PACE instrument. The volume introduced into the capillary (V_{inj}) by this method can be calculated by the Poiseuille equation:

$$V_{inj} = \frac{\Delta P \pi t^4 t_{ap}}{128 \eta L_t} \tag{2}$$

where ΔP is the pressure difference across a capillary of length L_t and diameter d, t_{ap} is the total duration of applied pressure and η is the buffer viscosity. Although we did not verify calculated values, we determined linearity and reproducibility for a series of different injection times. A good linear correlation was found between peak area and injection time for these nucleotides. A representative plot of UTP peak area *vs.* injection time is shown in Fig. 2A. Each injection was performed in triplicate. The R.S.D. of the mean peak areas for each injection time were between 1 and 8% (represented as error bars in Fig. 2A). Electrokinetic injection was used exclusively with the Bio-Rad CE instrument. The amount of solute introduced into the capillary by this method is dependent on its electrophoretic mobility and on the ionic strengths of the sample solution and running buffer. Again, we determined linearity and reproducibility for a series of different injection times. Good linear correlations were found between peak area and injection time. A representative plot of UTP peak area *vs.* injection time is shown in Fig. 2B. The R.S.D. of the mean peak areas for each injection time was comparable, though somewhat higher (*ca.* 9%), to that observed for pressure injection.

In general, the linearity and reproducibility of peak area *vs.* injection time for pressure injection was slightly better than for electrokinetic injection. In particular, the longest electrokinetic injection time (20 s) seems to have resulted in a lower sample load than what might be expected based on smaller injection times (Fig. 2B). These results are analogous to those reported by Moring *et al.* [33] for similar experiments. Previous comparisons of injection methods [33,35] have generally shown hydrodynamic injections to be more linear than electrokinetic injection. This is primarily because of

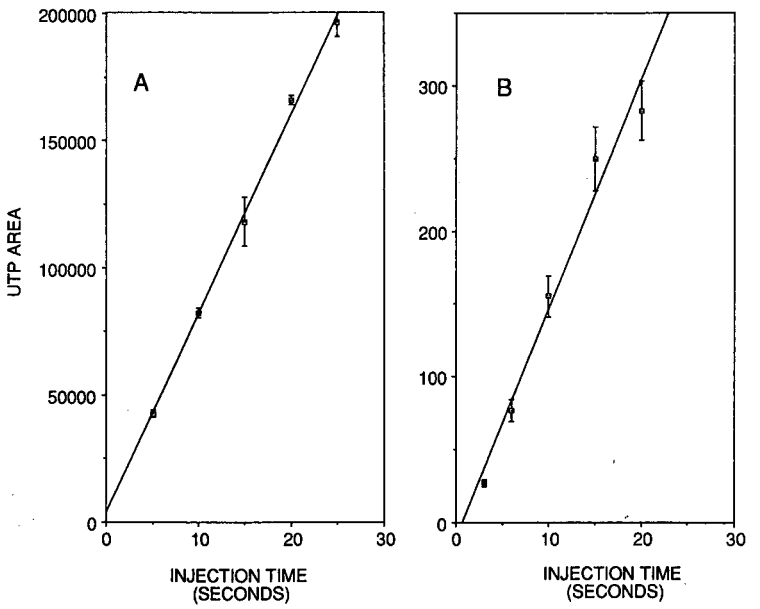

Fig. 2. Linearity of sample introduction as a function of injection duration: (A) represents pressure injection on the Beckman instrument and (B) represents electrokinetic injection on the Bio-Rad. All other details are as described in Table I. (A) $y = 3587.4 + 7836.2x$; $r^2 = 0.997$. (B) $y = -11.756 + 15.772x$; $r^2 = 0.974$.

fluctuating local electric fields at the capillary inlet during electrokinetic injection. This effect can be minimized by dissolving samples in a higher conductivity buffer (relative to the operating buffer) [33], as we have done here.

Peak area–concentration relationships

Nucleotide peak area–concentration relationships were determined for both instruments and the results are summarized in Table II. Table II also summarizes nucleotide peak area–concentration relationships when calculated using ITP (0.0625 mg/ml) as an internal standard. Fig. 3A (CTP sample concentration *vs.* normalized peak area) and B (CTP/ITP concentration ratio *vs.* CTP/ITP response ratio) contain representative plots demonstrating the linearity of the measurements on the Beckman instrument. The relationship between nucleotide peak areas and concentration was found to be linear through nearly three orders of magnitude for both instruments. Interestingly, use of the internal standard did not significantly improve this linearity. Of course, use of an internal standard would be most valuable in a multi-stage sample preparation and extraction process, which was not attempted for this report. The minimum detectable concentration (based on a 3:1 signal-to-noise ratio on the electropherograms) are given in Table III. These figures would change under differing injection conditions. For example, sample stacking during electrokinetic injection would improve the minimum detectable concentration [36,37].

TABLE II

LINEARITY OF PEAK AREA *VS.* SAMPLE CONCENTRATION

Conditions: operating buffer, 0.05 *M* phosphate (pH 2.7) with 0.002 *M* EDTA. Beckman instrument capillary 69.5 cm × 75 μm I.D., derivatized; length to detector 62.8 cm; pressure injection for 5 s; 20 kV applied voltage; individual nucleotide concentrations: 0.0078 mg/ml, 0.0156 mg/ml, 0.0312 mg/ml, 0.0625 mg/ml, 0.125 mg/ml and 0.25 mg/ml; ITP at 0.0625 mg/ml. Bio-Rad instrument capillary 20 cm × 25 μm I.D., derivatized; length to detector 17 cm; electrokinetic injection for 10 seconds at 2 kV; 2 kV applied voltage; individual nucleotide concentrations at 0.0156 mg/ml, 0.0313 mg/ml, 0.0625 mg/ml, 0.125 mg/ml and 0.25 mg/ml. All samples run in triplicate.

Instrument	Component	Equation of the line (concentration *vs.* peak area)			Conc. *vs.* peak area normalized to ITP
		r^2	slope	*y*-intercept	r^2
Beckman	UTP	0.985	$2.2 \cdot 10^5$	−322	0.960
	dTTP	0.996	$1.9 \cdot 10^5$	−286	0.973
	GTP	0.993	$3.9 \cdot 10^5$	−2238	0.990
	dGTP	0.989	$4.1 \cdot 10^5$	−3863	0.995
	dCTP	0.995	$1.1 \cdot 10^5$	−482	0.983
	CTP	0.994	$1.2 \cdot 10^5$	−559	0.986
	dATP	0.998	$4.0 \cdot 10^5$	−856	0.967
	ATP	0.989	$4.9 \cdot 10^5$	−2900	0.990
Bio-Rad	dTTP	0.994	$2.1 \cdot 10^4$	233.9	
	dGTP	0.999	$2.5 \cdot 10^4$	45.5	
	dCTP	0.995	$8.8 \cdot 10^3$	91.7	
	dATP	0.998	$3.0 \cdot 10^4$	303	

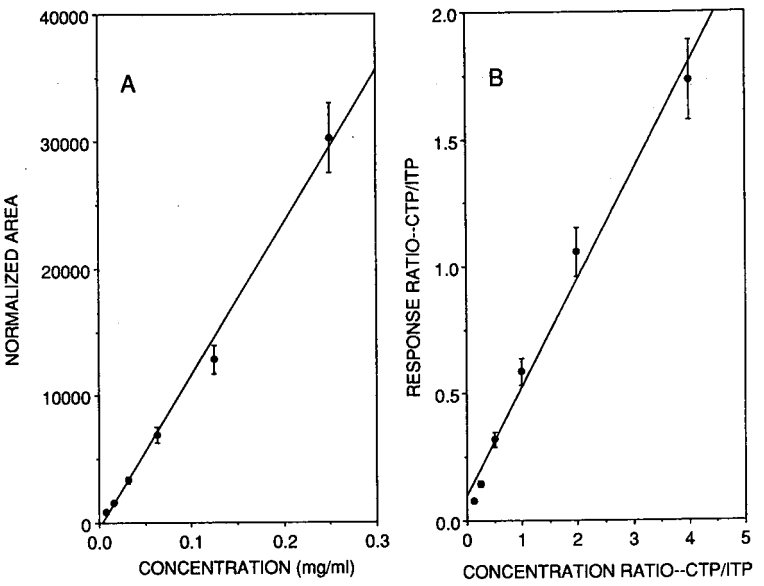

Fig. 3. Linearity of peak area as a function of sample concentration. (A) represents CTP sample concentration *vs.* normalized peak area and (B) represents those same values normalized against the internal standard, ITP (0.063 mg/ml). All other details are as described in Table II. (A) $y = -559 + 1.2 \cdot 10^5 x$; $r^2 = 0.994$. (B) $y = 9.4 \cdot 10^{-2} + 0.43x$; $r^2 = 0.986$.

TABLE III

MINIMUM DETECTABLE CONCENTRATION AT 254 nm

Conditions: operating buffer, 0.05 *M* phosphate (pH 2.7) with 0.002 *M* EDTA. Beckman instrument capillary 69.5 cm × 75 μm I.D., derivatized; length to detector 62.8 cm; pressure injection for 5 s; 20 kV applied voltage. Bio-Rad instrument capillary 20 cm × 25 μm I.D., derivatized; length to detector 17 cm; electrokinetic injection for 10 s at 2 kV; 2 kV applied voltage. Minumum detectable concentration determined where signal-to-noise ratio = 3 (0.01 a.u.f.s., rise time 0.1 s).

Instrument	Component	Minimum detectable concentration	
		pmol/ml	mg/ml
Beckman	UTP	7500	0.0036
	dTTP	6400	0.0031
	ITP	3200	0.0053
	GTP	3000	0.0015
	dGTP	850	0.0004
	dCTP	800	0.0004
	CTP	650	0.0003
	dATP	230	0.0001
	ATP	120	0.0001
Bio-Rad	dTTP	18200	0.0136
	dGTP	3700	0.0019
	dCTP	3500	0.0016
	dATP	1000	0.0005

These experiments indicate that efficient, sensitive and quantitative measurements of nucleotide triphosphates are possible by CZE. We believe this technique is a viable alternative to more traditional high-performance liquid chromatographic [22,38] and enzymatic [19,20] methods and capitalizes on many CZE strengths, including small sample size, simplicity and speed. To assess the quantitative potential of the technique further we are currently conducting a series of comparative experiments with cultured mammalian cell extracts.

ACKNOWLEDGEMENT

We thank Lisa Kalish, Dave Hansen and Tim Wehr for method development efforts and many useful discussions.

REFERENCES

1 J. W. Jorgenson and K. D. Lukacs, *Science (Washington, D.C.)*, 222 (1984) 266.
2 H. H. Lauer and D. McManigill, *Anal. Chem.*, 58 (1986) 166.
3 B. L. Karger, A. S. Cohen and A. Guttman, *J. Chromatogr.*, 492 (1988) 585.
4 R. McCormick, *Anal. Chem.*, 60 (1989) 2322.
5 T. Tsuda, G. Nakagawa, M. Sato and K. Yagi, *J. Appl. Biochem.*, 5 (1983) 330.
6 T. Tsuda, K. Takagi, T. Watanabe and T. Satake, *J. High Resolut. Chromatogr. Chromatogr. Commun.*, 11 (1988) 721.
7 A. Nguyen, J. H. T. Luong and C. Masson, *Anal. Chem.*, 62 (1989) 2490.
8 H. Yamamoto, T. Manabe and T. Okuyama, *J. Chromatogr.*, 480 (1989) 331.
9 K. H. Row and J. I. Raw, *Sep. Sci. Technol.*, 25 (1990) 323.
10 A. Guttman, A. S. Cohen, D. N. Heiger and B. L. Karger, *Anal. Chem.*, 62 (1990) 137.
11 X. Huang, J. B. Shear and R. N. Zare, *Anal. Chem.*, 62 (1990) 2051.
12 S. Fujiwara and S. Honda, *Anal. Chem.*, 59 (1987) 2773.
13 H. Nishi, N. Tsumagari and S. Terabe, *Anal. Chem.*, 61 (1989) 2434.
14 H. Nishi, N. Tsumagari, T. Kakimoto and S. Terabe, *J. Chromatogr.*, 477 (1989) 259.
15 A. Wainright, *J. Microcol. Sep.*, 2 (1990) 166.
16 J. Liu, J. F. Banks, Jr. and M. Novotny, *J. Microcol. Sep.*, 1 (1989) 136.
17 B. A. Kunz, *Environ. Mutagen.*, 4 (1982) 695.
18 R. D. Snyder, *Biochem. Pharmac.*, 33 (1984) 1515.
19 A. W. Solter and R. E. Handschumacher, *Biochem. Biophys. Acta*, 174 (1969) 585.
20 D. Hunting and J. F. Henderson, *Can. J. Biochem.*, 59 (1981) 723.
21 L. S. Ettre, in L. S. Ettre and A. Zlatkis (Editors), *The Practice of Gas Chromatography*, Interscience, New York, 1967, p. 373.
22 F. Arrezo, *Anal. Biochem.*, 160 (1987) 57.
23 S. Hjertén, *J. Chromatogr.*, 347 (1985) 191.
24 M. J. Silver, I. Rodalewicz, Y. Duglas and D. Park, *Anal. Biochem.*, 36 (1970) 525.
25 L. Gross and E. S. Yeung, *J. Chromatogr.*, 480 (1989) 169.
26 E. Harbers, G. F. Domagk and W. Muller, *Introduction to Nucleic Acids*, Reinhold, New York, 1968, p. 25.
27 P. D. Grossman, K. J. Wilson, G. Petrie and H. H. Lauer, *Anal. Biochem.*, 173 (1988) 265.
28 P. D. Grossman, J. C. Colburn, H. H. Lauer, R. G. Nielson, R. M. Riggin, G. S. Sittampalam and E. C. Rickard, *Anal. Chem.*, 61 (1989) 1186.
29 S. Hjertén, *Chromatogr. Rev.*, 9 (1967) 122.
30 J. W. Jorgenson and K. De Arman Lukacs, *Science (Washington, D.C.)*, 222 (1983) 266.
31 A. S. Cohen, S. Terabe, J. A. Smith and B. L. Karger, *Anal. Chem.*, 59 (1987) 1021.
32 E. Grushka, R. M. McCormick and J. J. Kirkland, *Anal. Chem.*, 66 (1989) 241.
33 S. E. Moring, J. C. Colburn, P. D. Grossman and H. H. Lauer, *LC·GC*, 8 (1990) 34.
34 L. R. Snyder and J. J. Kirkland, *Introduction to Modern Liquid Chromatography*, Wiley, New York, 1974, p. 434.

35 D. J. Rose and J. W. Jorgenson, *Anal. Chem.*, 60 (1988) 642.
36 L. Ornstein, *Ann. N.Y. Acad. Sci.*, 121 (1964) 321.
37 H. R. Udseth, J. A. Loo and R. D. Smith, *Anal. Chem.*, 61 (1989) 228.
38 J. Harmenberg, S. Cox and A. Åkesson-Johansson, *J. Chromatogr.*, 508 (1990) 75.

Journal of Chromatography, 559 (1991) 257–266
Elsevier Science Publishers B.V., Amsterdam

CHROM. 23 459

Capillary electrophoresis of DNA in entangled polymer solutions

PAUL D. GROSSMAN* and DAVID S. SOANE
Department of Chemical Engineering, University of California at Berkeley, Berkeley, CA 94720 (USA)

ABSTRACT

Electrophoretic separations of DNA restriction fragments were performed in solutions of hydroxyethylcellulose (HEC) using capillary electrophoresis. Rheological studies confirmed that the entanglement threshold (Φ^*) for the solution is *ca.* 0.003 g/ml, in good agreement with theoretical predictions. A mesh size an order of magnitude smaller than that found in agarose gels was calculated using polymer-entanglement theory and was confirmed by electrophoretic measurements. Electrophoretic migration was shown to follow the Ogston regime under most conditions. An approach for obtaining smaller mesh sizes is presented.

INTRODUCTION

It is well known that the electrophoretic mobility of double-stranded DNA (dsDNA) in free solution is not a strong function of molecular size [1,2]. Therefore, in order to effect an electrophoretic separation of dsDNA mixtures, one has had to perform the separation in a cross-linked rigid gel matrix which alters the frictional characteristics of DNA in such a way as to introduce a molecular weight dependence to its electrophoretic mobility.

However, with the advent of capillary electrophoresis (CE), superior separations of dsDNA mixtures have been demonstrated without the use of a rigid cross-linked gel matrix [3,4]. These studies demonstrate that, by using a semi-dilute, low-viscosity polymer solution as the separation medium, high-resolution separations of dsDNA mixtures can be achieved. Although electrophoresis in non-cross-linked polymer solutions has been previously demonstrated [5,6], never before has such high resolution been achieved in low-viscosity solutions. This technique promises to combine the advantages of free-solution capillary electrophoresis (system automation, speed, reproducibility and accurate quantification) with the range of application and resolving power of gel-based systems.

This paper represents an attempt to interpret these recent results using polymer entanglement concepts and traditional theories of gel electrophoresis. We also report the effect of fragment length and polymer concentration on the electrophoretic mobility of DNA fragments ranging from 118 to 1353 base pairs (bp) in solutions of

0021-9673/91/$03.50

hydroxyethylcellulose (HEC). These data are then compared with theoretical predictions.

EXPERIMENTAL

The capillary electrophoresis system used in this work closely resembles that described elsewhere [7,8]. A straight length of polyimide-coated fused-silica capillary (Polymicro Technologies, Phoenix, AZ, USA), 50 cm long (35 cm to the detector), with I.D. 50 μm and O.D. 375 μm, connects the anodic reservoir with the electrically grounded cathodic reservoir. A high-voltage power supply capable of producing up to 30 000 V (Gamma High Voltage Research, Ormand Beach, FL, USA) was used to drive the electrophoretic process. Current through the capillary was measured over a 1-kΩ resistor in the return circuit of the power supply using a digital multimeter (Model 3465B, Hewlett-Packard, Palo Alto, CA, USA). On-column UV detection at 260 nm was carried out using a modified variable-wavelength detector (Model 783, Applied Biosystems, Foster City, CA, USA). The electrophoresis system was enclosed in an insulated compartment having safety interlocks in order to prevent electric shock. Data were collected using an integrator (Model 3390A, Hewlett-Packard). Samples were introduced into the capillary by applying a vacuum of 5 inchHg (16884 Pa) to the cathodic electrode reservoir for 2–3 s while the anodic end of the capillary was immersed in the sample solution. After the sample slug had been introduced into the capillary, the anodic end of the capillary was placed back in the electrophoresis buffer together with the anodic electrode, and the electrophoretic voltage was then applied. The temperature of the agitated air surrounding the capillary was maintained at 30.0 $\pm$ 0.1°C in all experiments. A description of the methods used to calculate electrophoretic mobilities is provided elsewhere [9].

Viscosity measurements were performed using an Ostwald viscometer [10] thermostated in a water-bath at 30.0 $\pm$ 0.5°C.

The DNA mixture used was a commercially prepared restriction digest of the ΦX174 plasmid (Bethesda Research Labs., Bethesda, MD, USA). The buffer used in all experiments was 89 m*M* tris(hydroxymethyl)aminomethane (Tris)–89 m*M* boric acid–5 m*M* ethylenediaminetetraacetic acid (EDTA) with varying amounts of added hydroxyethylcellulose (HEC).

RESULTS AND DISCUSSION

Polymer entanglement

An important difference exists between polymer solutions which are dilute, where the polymer chains are hydrodynamically isolated from one another, and more concentrated solutions, where the chains overlap and interact. The polymer volume fraction at which the polymer chains begin to interact with one another, Φ^*, is the over-lap threshold. Above this concentration, the solution is said to be entangled (Fig. 1). The over-lap threshold can be estimated using a relationship derived by De Gennes [11]:

$$\Phi^* \approx N^{-\frac{4}{5}} \tag{1}$$

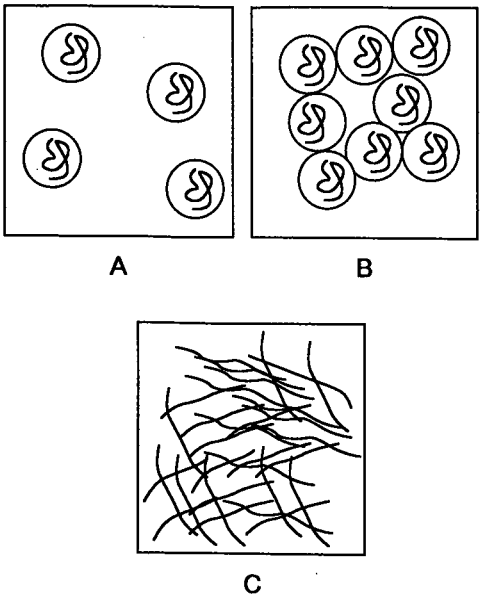

Fig. 1. Representation of the entanglement process. (A) Dilute solution where $\Phi < \Phi^*$; (B) solution at entanglement threshold where $\Phi \approx \Phi^*$; (C) fully entangled solution where $\Phi > \Phi^*$.

where N is the number of segments in the polymer chain. This expression is derived by assuming that at the over-lap threshold, Φ is the same as the local concentration inside a single coil. Eqn. 1 further assumes that the polymer is in an athermal solvent. Note that if N is large, Φ^* can be very small. For example, if $N = 10^4$, Φ^* is of the order of 10^{-3}.

Experimentally, the point at which a polymer solution becomes entangled can be determined by plotting the logarithm of the specific viscosity as a function of polymer volume fraction [12]. For independent, non-interacting polymer molecules, *i.e.*, $\Phi < \Phi^*$, dilute solution theories predict that the slope of such a curve would be *ca.* 1.0 [13]. As the polymer coils begin to interact, the slope is expected to increase. Our experimental results are presented in Fig. 2 for solutions of HEC dissolved in the electrophoresis buffer, giving $\Phi^* \approx 0.29\%$.

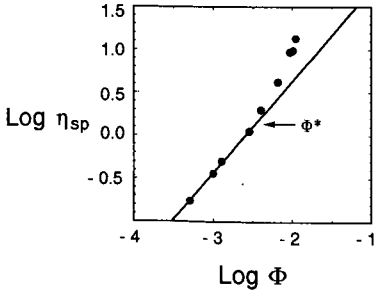

Fig. 2. Dependence of specific viscosity, η_{sp}, of HEC buffer solution on HEC volume fraction. The slope of the line passing through the first four points is 1.07, in good agreement with the value of 1.0 expected from dilute solution theories. Deviation from this line occurs at HEC concentrations between 0.0029 and 0.0040 g/ml, indicating the onset of entanglement effects in this concentration range.

To check the agreement between the experimental value of Φ^* and that predicted by eqn. 1, we must determine an approximate value for N for the HEC. This was done by the application of the Mark–Houwink–Sakurada equation using intrinsic viscosity measurements performed on aqueous solutions of HEC [14]. The measured value of the intrinsic viscosity of HEC in water, $[\eta]$, was found to be 376 ml/g. The resulting value of N is 1025, assuming a monomer molecular weight of 187. With this value of N, eqn. 1 predicts Φ^* to be 0.39%. Given the approximate nature of these scaling laws, this is in good agreement with the experimental value.

Characteristic mesh size

An entangled solution is characterized by an average mesh size for the network, ξ. The expression relating ξ to the polymer concentration is [11]

$$\xi(\Phi) \approx a\,\Phi^{-\frac{3}{4}} \tag{2}$$

where a is the length of one repeat unit along the polymer chain and $\Phi^* < \Phi < 1$. Again, eqn. 2 assumes an athermal solvent.

In order to apply eqn. 2 to calculate mesh size, we must first estimate a value for the statistical segment length, a, for HEC. The value of a can be estimated using intrinsic viscosity measurements. For a random-coil polymer [15],

$$[\eta] = \frac{\Phi_c \langle r^2 \rangle^{\frac{3}{2}}}{\mathrm{MW}} \tag{3}$$

where Φ_c is a universal constant having a value of $2.1 \cdot 10^{23}$ if $[\eta]$ has the units of ml/g and $\langle r^2 \rangle$ is the root-mean-squared end-to-end distance between the ends of the polymer chain. Further, for an unperturbed chain,

$$\langle R_g^2 \rangle = \frac{\langle r^2 \rangle}{6} \tag{4}$$

where R_g is the radius of gyration of the coil. Based on a measured value of 317 ml/g for $[\eta]$ in the electrophoresis buffer (data not shown), eqns. 3 and 4 give a value of 270 Å for R_g. Next, given the relationship between the segment length, a, and R_g for an unperturbed coil,

$$R_g = aN^{0.6} \tag{5}$$

and given that $N = 1025$, we can see that $a = 4.21$ Å. This is close to the 4.25 Å monomer segment length for HEC [14].

Using a value of 4.21 Å for a in eqn. 2 we obtain a mesh size of *ca.* 265 Å at $\Phi = 0.40\%$. Quantitative investigations of the actual mesh sizes in these solutions are in progress. Because an entangled mesh requires no specific cross-linking or gelation, a wide range of polymers may be easily adapted for these applications. Candidate polymers simply need to be water soluble and preferably uncharged. Further, in contrast to gels, polymer solutions are highly homogeneous structures.

Next we compare the mesh sizes of these polymer solutions with those of

traditional gels. Righetti *et al.* [16] developed an empirical relationship to correlate pore sizes in agarose gels with agarose concentration, yielding a relationship of the form

$$p = 140.7\ C^{-0.7} \tag{6}$$

where p is the pore size (in nm) and C is the concentration of agarose (in wt.%). Note that this empirical expression has the same form as eqn. 2. However, at a given concentration, the entangled solution produces a smaller mesh size, consistent with the fact that in a gel the polymer fibers exist as bundles, therefore leaving larger voids. Slater *et al.* [17] also arrived at a similar expression using electrophoresis data, and found an exponent of -0.75, in exact agreement with the form of eqn. 2.

Electrophoresis in a polymer network

Once the network structure of the polymer solution is understood, we address the effects of the polymer solution on electrophoresis. Two main theories describe the migration of a flexible macromolecule through a polymer network: the Ogston sieving model and the reptation model. The applicability of each depends on the size of the migrating molecule relative to the mesh size of the network.

The Ogston model [18,19] treats the polymer network as a molecular sieve. It assumes that the gel consists of a random network of interconnected pores having an average pore size ξ, and that the migrating solute behaves as an undeformable spherical particle of radius R_g. According to this model, smaller molecules migrate faster because they have access to a larger fraction of the available pores. The expression describing the migration of a solute through a polymer network according to the Ogston mechanism is

$$\mu = \mu_0 \exp[-Cb(R_g + r)^2] \tag{7}$$

or

$$\mu = \mu_0 \exp\left[-\frac{1}{4}\pi\left(\frac{R_g + r}{\xi}\right)^2\right] \tag{8}$$

where μ_0 is the free solution electrophoretic mobility, C the concentration of polymer, b a constant dependent on the concentration units chosen for C, R_g the radius of gyration of the migrating solute and r the radius of the mesh-forming polymer chain. Because they do not take into account the effects of the electric field on R_g, eqns. 7 and 8 only hold strictly for $\mu(E \rightarrow 0)$. Therefore, all mobility data presented here are extrapolated to zero field using five field strengths ranging from 400 to 40 V/cm. In eqn. 7 the term $b(r + R_g)^2$ is called the retardation coefficient, K_r.

When a long, flexible molecule travels through a polymer network where $R_g \gg \xi$, the assumption of an undeformed particle breaks down. Instead, the long molecule "snakes" through the polymer network "head first". The migrating solute is assumed to move through "tubes" formed by the gel matrix. In the limit of low electric field, the migrating DNA can still be considered an unperturbed random coil. In this

case, the reptation theory of De Gennes [20] can be used to derive the relationship between electrophoretic mobility and DNA size [21]:

$$\mu \sim \frac{1}{N_{\mathrm{DNA}}} \tag{9}$$

where N_{DNA} is the number of statistical segments in the DNA chain and $\sim$ indicates proportionality. In the case of high electric fields, one must take into account the deformation of the DNA coil caused by the electric field. In this case, the biased reptation model [22] applies, giving

$$\mu = \frac{Q}{3f}\left(\frac{1}{N_{\mathrm{DNA}}} + \frac{E'^2}{3}\right) \tag{10}$$

where Q is the charge on a DNA segment, f is the translational frictional coefficient of a DNA segment along the tube and E' is a dimensionless field strength given by

$$E' = \frac{\xi q E}{2kT} \tag{11}$$

where q is the effective charge on the portion of DNA contained in the pore, k the Boltzmann constant, E the actual field strength and T the absolute temperature (eqn. 10 is only valid when $E' < 1$). Note that eqn. 10 suggests that as N or E' becomes large, μ becomes independent of N.

According to Slater and Noolandi [19], based on both experimentation and numerical simulation, the transition from the Ogston to the reptation regime takes place when $R_g \approx 1.4\xi$.

Fig. 3 shows a representative electropherogram. Note that this separation is

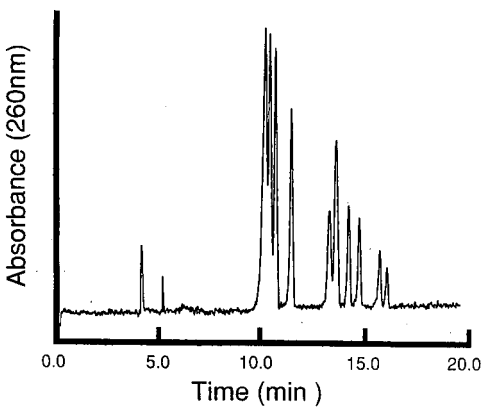

Fig. 3. Representative electropherogram showing the separation of eleven DNA restriction fragments ranging in size from 72 to 1353 bp. Reading from left to right (not including the first two peaks, which are markers) the species are 1353, 1078, 872, 603, 310, 281 + 271, 234, 194, 118 and 72 bp in length, respectively. Conditions: buffer, 0.25% HEC in 89 m*M* Tris–89 m*M* boric acid–5 m*M* EDTA; field strength, 301.3 V/cm; UV detection at 260 nm; capillary dimensions, 50 cm total length (35 cm to detector) × 50 μm I.D.; temperature, 30 ± 0.1°C.

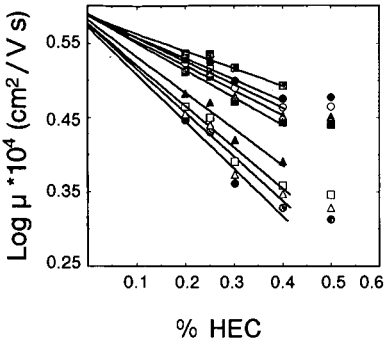

Fig. 4. Ferguson plot for sample DNA fragments. Hatched squares = 118 bp; closed circles = 194 bp; open circles = 234 bp; hatched triangles = 281 bp; closed squares = 310 bp; closed triangles = 603 bp; open squares = 872 bp; open triangles = 1078 bp; hatched circles = 1353 p. All mobility data have been extrapolated to $E = 0$.

performed slightly below Φ^*. The fact that a mesh exists at $\Phi < \Phi^*$ is probably due to the broad molecular weight distribution of the HEC, allowing larger coils to overlap below Φ^*.

According to the Ogston model, a plot of log μ *vs.* % HEC (a Ferguson plot) should give a linear relationship with a slope equal to K_r and an intercept on the ordinate equal to log μ_0. For fragments 118, 194, 234, 281 and 310 bp in solutions up to 0.4% HEC, this behavior is indeed observed (Fig. 4). The intercept for these five lines, 0.588 [relative standard deviation (R.S.D.) = 0.15%], implies a value for μ_0 of $3.87 \cdot 10^{-4}$ cm^2/V · s, in complete agreement with the measured electrophoretic mobility of these fragments at 0% HEC of $3.86 \cdot 10^{-4}$ cm^2/V · s (R.S.D. = 1.2%, $n = 16$). For fragments larger than 310 bp, the agreement degrades. This is probably due to the gradual transition to the reptation regime for these larger fragments. This transition has also been observed in agarose gels [23]. According to the Ogston model, a plot of $K_r^{0.5}$ *vs.* R_g should yield a linear relationship. As seen in Fig. 5, for the smaller fragments, agreement with the prediction of the Ogston model is close, whereas the larger fragments deviate significantly. Assuming that the Ogston–reptation transition

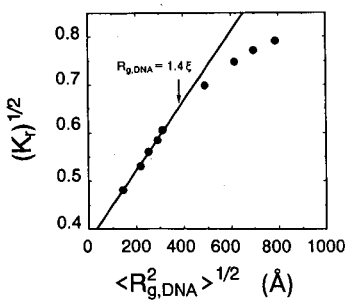

Fig. 5. Square root of the retardation coefficient K_r *vs.* the root-mean-square radius of gyration $\langle R_g^2 \rangle^{1/2}$ of the DNA fragments. $\langle R_g^2 \rangle^{1/2}$ is calculated for DNA using the Porod–Kratky stiff-chain model assuming a persistence length of 450 Å and a contour length of 3.4 Å per base pair [24]. All mobility data have been extrapolated to $E = 0$.

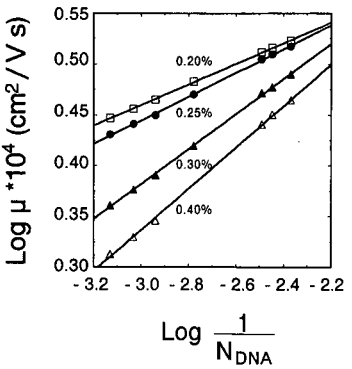

Fig. 6. Logarithm of the electrophoretic mobility *vs.* logarithm of inverse molecular size (in base pairs) for different HEC concentrations. A slope of 1 would be expected if migration exactly followed the reptation mechanism. (□) 0.20% HEC, slope = 0.091; (●) 0.25% HEC, slope = 0.107; (▲) 0.30% HEC, slope = 0.158; (△) 0.50% HEC, slope = 0.201. All mobility data have been extrapolated to $E = 0$.

occurs when $R_g \approx 1.4\xi$, Fig. 5 implies that for HEC at 0.4% in this buffer, 223 Å < ξ < 350 Å. This value for ξ agrees with the mesh size predicted from eqn. 2 (ξ = 265 Å at 0.40% HEC).

Fig. 6 shows log μ as a function of $1/N_{DNA}$. According to eqn. 10, these curves should be linear with slopes of 1.0 if the fragments migrate by the reptation mechanism. As expected from the previous analysis, for the conditions used in these experiments none of the curves adheres to the reptation behavior. However, as the HEC concentration is increased, the slopes of the curves appear to increase towards 1, indicating a transition regime. Again, this behavior has been observed for low-concentration agarose gels using small DNA fragments [23].

It is likely that once $R_g \gg \xi$, *i.e.*, when reptation becomes important, the separation performance of these systems will decrease rapidly. This is because at the high electrical fields typically employed in capillary electrophoresis, the value of E' in eqn. 10 is greater than 1, resulting in a saturated, size-independent mobility [19]. Although this limitation is not unique to the polymer solution system, it does represent a restriction on the ability to exploit the high electric fields and thus enjoy the consequent rapid analysis using CE. In order to overcome this limitation, high-voltage pulsed-field techniques will need to be investigated, a topic currently under investigation.

For some applications, smaller mesh sizes that those used here may be required. Ideally, one would like to maintain the advantages of a low-viscosity solution when going to a smaller mesh. The above relationships give an indication of how this might be accomplished. As can be seen from Fig. 2, in order to minimize the viscosity of the polymer solution, one wants to operate near Φ^*. However, eqn. 2 predicts that, in order to achieve a small mesh, one needs a large Φ. To satisfy both constraints, one must use a short polymer to form the mesh. This can be demonstrated by combining eqns. 1 and 2 to give the expression

$$\xi(\Phi^*) \approx aN^{0.6} \tag{12}$$

Therefore, in order to create larger pores one wants to use a longer polymer and in order to create smaller pores one wants to use a shorter polymer.

The application of entangled polymer solutions as a "sieving" medium has also been exploited by Langevin and Rondelez [25] in the context of centrifugation. This work is a direct analogue to electrophoresis in entangled solutions.

CONCLUSIONS

It appears that low-viscosity polymer solutions provide a good matrix for electrophoretic separations. By performing polymer solution electrophoresis in a capillary, one has in effect decoupled the two roles of a traditional electrophoresis gel: that of a sieving matrix and that of an anti-convective stabilizing medium. Separations of short DNA fragments appear to follow the Ogston model in a manner similar to that found in agarose gel systems. At present, using high electrical fields, separations will be limited to the Ogston regime until pulsed-field techniques are invoked. Also, simple relationships from entangled polymer network theories can be used to guide the further development of these systems.

ACKNOWLEDGEMENTS

The financial support of the University of California at Berkeley BRSG Fund and a generous research grant from Applied Biosystems are greatly appreciated. We thank A. M. Chin, D. S. Nelson and J. C. Colbum for helpful comments and discussions and S. V. Patel for invaluable assistance in performing the experimental work.

REFERENCES

1 B. M. Olivera, P. Baine and N. Davidson, *Biopolymers*, 2 (1964) 245.
2 J. J. Hermans, *J. Polym. Sci.*, 18 (1953) 257.
3 A. M. Chin and J. C. Colburn, *Am. Biotech. Lab. News Ed.*, 7 (1989) 10A.
4 M. Zhu, D. L. Hansen, S. Burd and F. Gannon, *J. Chromatogr.*, 480 (1989) 311.
5 D. Tietz, M. H. Gottlieb, J. S. Fawcett and A. Chrambach, *Electrophoresis*, 7 (1986) 217.
6 D. N. Heiger, A. S. Cohen and B. L. Karger, *J. Chromatogr.*, 516 (1990) 33.
7 J. N. Jorgenson and K. D. Lukacs, *Science*, 222 (1983) 266.
8 H. H. Lauer and D. McManigill, *Anal. Chem.*, 58 (1986) 166.
9 P. D. Grossman, J. C. Colburn and H. H. Lauer, *Anal. Biochem.*, 179 (1989) 28.
10 F. Rodriguez, *Principles of Polymer Systems*, McGraw Hill, New York, 1982, Ch. 7.
11 P. G. De Gennes, *Scaling Concepts in Polymer Physics*, Cornell University Press, Ithaca, NY, 1979, Ch. 3.
12 D. A. Hill and D. S. Soane, *J. Polym. Sci. Polym. Phys. Ed.*, B27 (1989) 2295.
13 H. R. Allcock and F. W. Lampe, *Contemporary Polymer Chemistry*, Prentice-Hall, Englewood Cliffs, NJ, 1981, Ch. 15.
14 J. Brandrup and E. H. Immerut (Editors), *Polymer Handbook*, Wiley, New York, 3rd ed., 1989, Ch. 7.
15 P. J. Flory, *Principles of Polymer Chemistry*, Cornell University Press, Ithaca, NY, 1953.
16 P. G. Righetti, B. C. W. Brost and R. S. Snyder, *J. Biochem. Biophys. Methods*, 4 (1981) 347.
17 G. W. Slater, J. Rousseau, J. Noolandi, C. Turmel and M. Lalande, *Biopolymers*, 27 (1988) 509.
18 A. G. Ogston, *Trans. Faraday Soc.*, 54 (1958) 1754.
19 G. W. Slater and J. Noolandi, *Biopolymers*, 28 (1989) 1781.
20 P. G. De Gennes, *J. Chem. Phys.*, 55 (1971) 572.
21 L. S. Lerman and H. L. Frisch, *Biopolymers*, 21 (1982) 995.

22 O. J. Lumpkin, P. Dejardin and B. H. Zimm, *Biopolymers*, 21 (1985) 1573.
23 H. Hervet and C. P. Bean, *Biopolymers*, 26 (1987) 727.
24 C. R. Cantor and P. R. Schimmel, *Biophysical Chemistry*, Freeman, New York, 1980, Ch. 19.
25 D. Langevin and F. Rondelez, *Polymer*, 19 (1978) 875.

Journal of Chromatography, 559 (1991) 267–283
Elsevier Science Publishers B.V., Amsterdam

CHROM. 23 467

Analysis of DNA restriction fragments and polymerase chain reaction products towards detection of the AIDS (HIV-1) virus in blood[a]

HERBERT E. SCHWARTZ* and KATHI ULFELDER
Beckman Instruments, Inc., Palo Alto, CA 94304 (USA)
and
FRANKLIN J. SUNZERI, MICHAEL P. BUSCH and ROBERT G. BROWNLEE
Irwin Memorial Blood Bank, San Francisco, CA 94118 (USA)

ABSTRACT

A high-performance capillary electrophoresis system with a polysiloxane-coated capillary and polymeric buffer additives was investigated for the analysis of DNA restriction fragments and polymerase chain reaction (PCR) products. Mobility data and Ferguson plots of the DNA fragments at different polymer (hydroxypropylmethylcellulose) concentrations indicated that effective molecular sieving was obtained consistent with existing data of conventional gel electrophoresis and with recent HPCE data. The precision and peak efficiency were excellent and the system was applied to the analysis of specific co-amplified DNA sequences (HIV-1 and HLA-DQ-alpha). After PCR, ultrafiltration was used in the sample preparation step to desalt the sample and to remove superfluous PCR reaction products. Electrokinetic injection was used for sample introduction into the capillary. The addition of ethidium bromide to the buffer resulted in longer migration times of DNA fragments and better peak resolution. During HPCE, an artifact associated with dilute DNA solutions leading to the appearance of extra peaks in the electropherogram was found.

INTRODUCTION

Understanding of diseases caused by viruses has continued apace with advances in molecular virology. As this understanding has increased, it has become obvious that more sensitive techniques are necessary to detect the pathogens, especially in latent infections. Without the ability to identify and measure accurately the amount of pathogen, it is very difficult to design an effective disease treatment. Further, to treat quickly an individual once specific therapy is known and to prevent the spread of the virus to other hosts, it is important to be able to detect that virus rapidly. The human immunodeficiency virus (HIV) is a good case in point.

In clinical settings, viruses are usually detected indirectly by identification of

[a] The authors would like to dedicate this paper to the memory of Bob Brownlee who passed away in February, 1991.

0021-9673/91/$03.50

antibodies to the virus in a host or by cytopathic effects *in vitro*. In latent infections, however, antibodies are often undetectable and *in vitro* assays are problematic. Until recently, it was impractical to look for the virus itself. At present, the polymerase chain reaction (PCR) technique allows detection of actual nucleic acids that are part of the HIV-1 virus [1]. PCR may generate millions of copies of specific DNA or RNA [usually 100–1000 base pairs (bp)], and multiple virus-specific sequences can be searched for and amplified in one reaction mixture.

The process of PCR can be entirely automated [2]. However, detection and quantification of the final amplified product remains a stumbling block to a rapid fully automated system of HIV detection. Conventional means of detection involving hybridization with [^{32}P]ATP labeled probes followed by polyacrylamide gel electrophoresis (PAGE) and autoradiography is time consuming, potentially hazardous and not readily amenable to automation. Chromogenic assays [3] have shown increased rapidity and potential for quantification. Unfortunately, only one pathogen can be detected at a time. Recent work with high-performance liquid chromatography has also shown promise for PCR fragment analysis [2,4].

To overcome the above problems in the analysis of PCR products, we have explored the use of high-performance capillary electrophoresis (HPCE). Our early results have shown promise to achieve one of our objectives, *viz.*, a fully automated analyzer for PCR fragments associated with HIV-1 [5–7]. The HPCE method, which involved a buffer system containing the cationic surfactant cetyltrimethylammonium bromide (CTAB), was used to detect simultaneously multiple retroviral DNA sequences [6]. However, a lack of understanding of the separation mechanism and poor precision were drawbacks leading us to pursue other alternatives.

With HPCE, Hjertén *et al.* [8] and Zhu *et al.* [9] showed that linear hydrophilic polymers can be used as buffer additives to achieve a "molecular sieving" effect to separate proteins and DNA fragments. Similar results, under conditions of electroosmotic flow, were obtained with a commercially available buffer system [10]. Recent work by Heiger *et al.* [11] involving polymerization of linear acrylamide within the capillary permitted high-efficiency separations of DNA fragments up to 12 000 base pairs. The viscous character of these 0%C or low %C media varied from a liquid, at 3% T[a], to a gel, at 12–14% T. Recent presentations by Heiger *et al.* [12] and Guttman and Cooke [13] showed further progress in this area. The term "physical" gels [14] has been used to describe these media for HPCE. Earlier, with classical gel electrophoresis, Bode [15–18] and Tietz *et al.* [19] demonstrated that linear polyacrylamide at low concentrations provided a molecular sieving medium for proteins and nucleic acids. The theoretical foundation for the molecular sieving mechanism was provided by Ogston [20] and Ornstein [21]. Polymers other than polyacrylamide, *e.g.*, polyethylene glycol [9,18], can also be used to achieve sieving in electrophoresis.

As a continuation of our previous work [5–7] dealing with the detection of PCR derived HIV-1 by HPCE, the focus of this paper is on optimization of the sample preparation and on the HPCE methodology. Ultrafiltration was used to remove salt and superfluous reaction components from the PCR samples and was instrumental in achieving better resolution and detectability. An OV-17-coated capillary in conjunc-

[a] C = g N,N'-methylenebisacrylamide (Bis)/%T; T = g acrylamide + g Bis per 100 ml of solution.

tion with a buffer containing a polymeric additive was shown to yield excellent precision and efficiency. Selected polymers were compared in terms of sieving efficiency and the HPCE system was applied to the analysis of PCR-derived HIV-1 sequences. Finally, factors affecting precision and quantification are discussed.

EXPERIMENTAL

Apparatus

A P/ACE System 2000 (Beckman, Palo Alto, CA, USA) automated capillary electrophoresis instrument was used in the reversed polarity mode (negative potential at the injection end of the capillary) for all DNA separations. Detection was accomplished on-line by UV absorption at 260 nm. Data were acquired at 2–20 Hz and stored to disk; post-run analysis of data was performed using Beckman System Gold software (Beckman, San Ramon, CA, USA).

Materials

Most analyses were performed using a surface-modified fused-silica OV-17 capillary (J & W Scientific, Folsom, CA, USA), although OV-1, OV-225 and Carbowax coatings were also evaluated. The coating thickness was 0.1 μm as provided by the manufacturer. The capillary dimensions were 27 or 57 cm × 100 μm I.D. A 2–4-mm segment of polyimide coating was carefully removed from the tubing about 6.9 cm from the end before installation in a capillary cartridge (Beckman) for on-column detection.

HPLC-grade water prepared with a Milli-Q water system (Millipore, Bedford, MA, USA) was used for all water-containing reagents. All salts and other chemicals were either of molecular biology grade or of the highest purity available (Sigma, St. Louis, MO, USA). The basic running buffer system was 89 m*M* Tris borate–2 m*M* EDTA (pH 8.5) (TBE). To this basic buffer were added selected polymers at various concentrations: (1) hydroxypropylmethylcellulose, 4000 cP at 25°C (HPMC-4000), at 0.1–0.7% (w/w); (2) hydroxypropylmethylcellulose, 100 cP at 25°C (HPMC-100), at 0.5–1.0% (w/w); (3) polyethylene glycol (PEG), molecular mass 35 000, at 5.0% (w/w). Ethidium bromide (EB) was added to the buffer in some runs to a concentration of 10 μM. In addition, 0.1 *M* sodium borate (pH 8.35) (Beckman) was used for electroosmotic flow experiments. All buffers were filtered to remove particulates and degassed by sonication.

A Hae III digest of ϕX 174 RF DNA was purchased from New England Biolabs (Beverly, MA, USA). Low-molecular-mass DNA size standards were purchased from Bio-Rad Labs. (Hercules, CA, USA). Oligonucleotides for PCR and detection were synthesized by the Biomolecular Resource Center, University of California (San Francisco, CA, USA).

DNA sample preparation and PCR

DNA was extracted from the positive HIV-1 control cell line, U1.1, which harbors one copy of the HIV-1 provirus per cell, as well as two copies of HLA DQ-α [5,6]. The negative control was the promonocyte U937, the cell line from which U1.1 was derived. Following extraction, DNA was serially diluted and PCR amplified for both HIV-1 (115 bp of the gag gene) and HLA DQ-α (242 bp), as described previously

[6]. The 100-μl PCR amplified samples were divided into two 50-μl aliquots. One aliquot was analyzed by hybridization with ^{32}P-labeled probes, gel electrophoresis and autoradiography [5,6]. The second aliquot was subjected to ultrafiltration: Centricon-30 or Centricon-100 filters (W.R. Grace, Amicon Division, Beverly, MA, USA) were used to desalt and concentrate PCR-amplified samples. Typically, a 50-μl volume was diluted with 2 ml of distilled water, and centrifuged for 30 min at 5000 *g* in a Model GP or GPR centrifuge (Beckman). This procedure was repeated one to three times for most experiments. Following ultrafiltration, the DNA was analyzed by capillary electrophoresis.

The DNA molecular mass markers were not desalted; instead, they were diluted with water prior to injection. The concentration of total DNA ranged from 0.38 to 25.0 μg/ml.

Capillary electrophoresis

The capillary cartridge was inserted into the P/ACE instrument and subsequently filled with the running buffer and allowed to equilibrate to a preset temperature. The temperature was set at 25°C for most experiments; HPCE runs at 20, 35 and 45°C were also investigated. Samples were loaded onto the autosampler to await automatic injection.

Both positive-pressure and electrokinetic sample injections were used. Pressure injections were performed at 3.44 MPa (0.5 psi) for 15–99 s. Electrokinetic injections at negative polarity setting of the HPCE instrument were performed at 35–175 V/cm for 1–40 s. Separations within the coated capillaries were performed at negative polarity under constant voltage for each run, ranging from 175 up to 350 V/cm. Typically, runs lasted from 15 to 45 min.

The coated capillary was rinsed with two capillary volumes of running buffer after each run, and was then ready for the next injection. The capillary was stored dry overnight in the P/ACE 2000 system, after initiating a programmed sequence which involved rinsing with water and drying with nitrogen.

Electroosmotic flow in untreated and coated capillaries was measured by introducing (via pressure injection) a neutral marker, benzyl alcohol, into the capillary. The zone velocity was determined from the migration time of the neutral marker and the length of the capillary.

RESULTS AND DISCUSSION

Role of capillary coating

In previous work [5] we used polyethylene glycol (Carbowax)-coated capillaries and a CTAB buffer to separate DNA restriction fragments. With this separation system, larger DNA fragments showed greater mobilities than smaller fragments. As a consequence of the high separation efficiency, this method appeared to offer very good sensitivity. This is an important consideration for clinical samples where low viral loads often are encountered. However, as we pointed out [5], the mechanism of separation is complex and not completely understood and the precision was relatively poor. In view of this, we decided to investigate an HPCE system similar to that of Zhu *et al.* [9], involving the use of linear polymers added to the buffer.

While the capillary used by Zhu *et al.* [9] involved a proprietary polyacrylamide

coating, we explored the use of various commercially available polysiloxane-coated capillaries. These 100 μm I.D. capillary columns were originally designed for use with supercritical fluid chromatography but have recently found use in HPCE also [5, 22, 23]. Encouraging preliminary results with a relatively polar phase, DB-WAX (polyethylene glycol) and a commercially available buffer system were recently published by our group [5,6]. Recently, we have found other non-polar and intermediate polarity polysiloxane coatings (*i.e.*, OV-17, OV-1, OV-225) to be preferable as these phases yielded better precision and efficiency. The OV-17 coating in conjunction with various polymeric buffer additives was used for all the experiments in this paper.

It is important to note that, in addition to its sieving effect, the polymer additive causes an additional dynamic coating on the capillary wall and, consequently, suppression of the electroosmotic flow (EOF). Using the OV-17-coated capillary and a 0.100 *M* borate buffer (without the polymeric additive), the mobility of the EOF was appreciable, *i.e.*, $5.6 \cdot 10^{-4}$ cm^2/V s. However, replacing the borate buffer with a buffer containing a cellulose derivative resulted in a 98.5% reduction in the EOF mobility. Returning to a borate buffer without the polymer additive, again a negligible EOF was determined. Evidently, the cellulose derivative had dynamically modified the wall of the capillary. This result is consistent with the work of Hjertén *et al.* [8] and Zhu *et al.* [9] on coated capillaries. Earlier, in work with isotachophoresis, Reijenga *et al.* [24] found that various polymeric additives (*e.g.*, cellulose derivatives) were very effective in reducing the EOF in untreated fused-silica capillaries. It seems therefore, that in our case the polysiloxane coating on the fused-silica wall compounds this effect, thereby providing an extra guard against EOF.

HPCE of DNA restriction fragments

An example of a separation of DNA restriction fragments (25 μg/ml) using an OV-17-coated capillary and 0.5% HPMC-4000 as buffer additive is shown in Fig. 1. The Hae III restriction fragments of ϕX 174 DNA provide a good reference for PCR samples because it covers the range of 72–1353 base pairs. Electrokinetic injection was used for the separation in Fig. 1A. Pressure injection was used in Fig. 1B. DNA fragments migrated with mobilities that decreased with increasing base pair number. This is an advantage in terms of analysis speed. If the reverse were the case, then the elution of the larger DNA fragments would occur before the peaks of interest (*i.e.*, in our case the 100–300 bp range) could be detected. In addition, the early peaks generally yield higher plate counts because their residence times in the column are shorter [25].

Note that the electrokinetic injection yields a more efficient separation than the pressure injection. The inset shows *ca.* $1.8 \cdot 10^6$ plates/m for the 118 bp fragment. With electrokinetic injection from a low ionic strength solution, predominantly sample components (*i.e.*, DNA fragments) migrate into the capillary where they are effectively stacked against the higher viscosity run buffer [21]. No sample bias, commonly found with electrokinetic injection [26] should take place as the DNA fragments have equal mobilities in free solution (*i.e.*, same mass-to-charge ratio). With the pressure injection on the other hand, a water plug, in addition to the DNA, is introduced into the capillary, causing less effective stacking and apparent peak broadening. Pressure injection is also limited in HPCE for highly viscous run buffers as the sample injection volume is inversely proportional to the viscosity of the buffer [27].

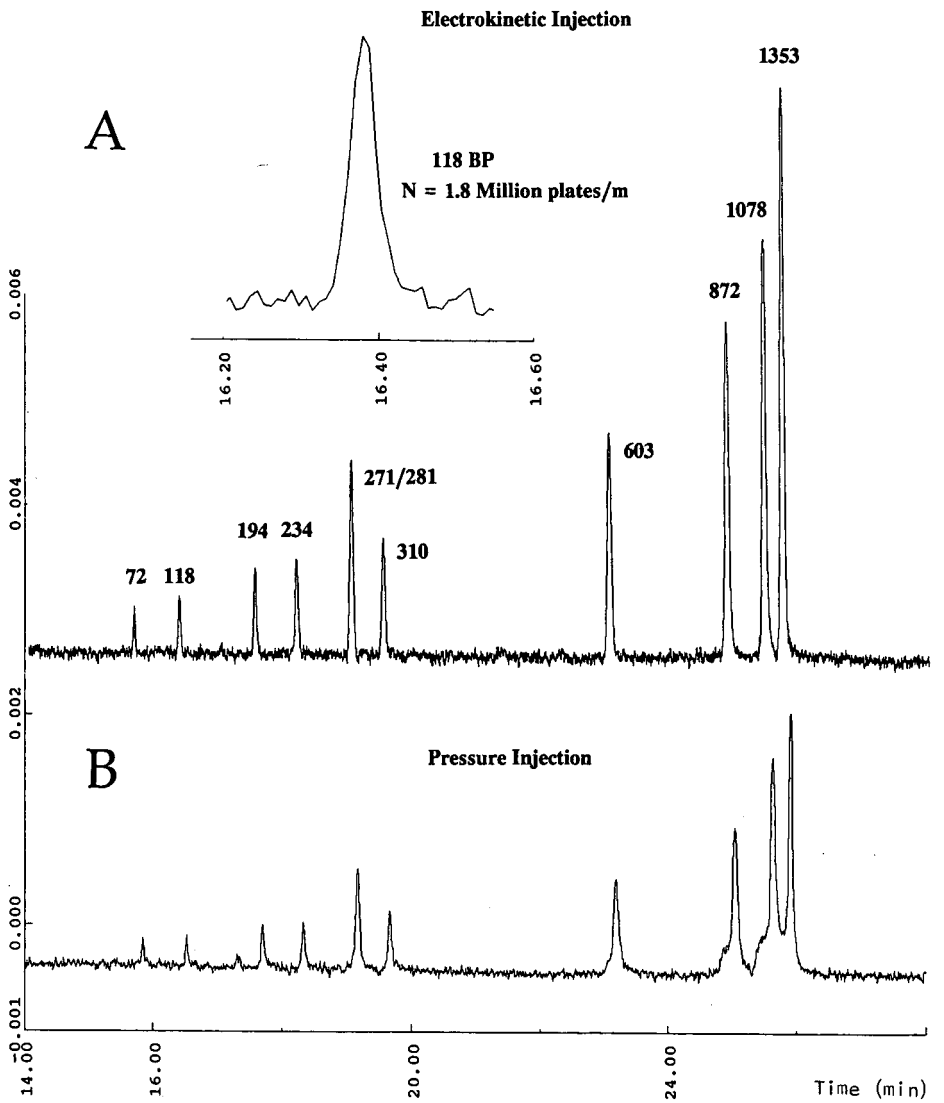

Fig. 1. Separation of a Hae III restriction digest of ϕX 174 DNA using (A) electrokinetic injection (5 s at 2 kV) and (B) positive pressure injection (60 s at 3.44 MPa). The inset shows an enlargement of the peak representing the 118 bp DNA fragment from (A) with a peak efficiency of $N = 1.8 \cdot 10^6$ plates/m. Buffer, 89 m*M* Tris borate–2 m*M* EDTA (pH 8.5)–0.5% HPMC-4000; column, OV-17-coated capillary, 57 cm × 100 μm I.D., 50 cm effective length; applied voltage, 10 kV; UV detection at 260 nm; temperature, 25°C; sample concentration, 25 μg/ml.

It also can be seen in Fig. 1 that, in spite of the high resolution, no separation between the 271 and 281 bp fragments was obtained. This was also the case with other HPMC formulations (*i.e.*, different concentrations and polymer molecular mass). However, baseline separation of this pair was recently achieved by Heiger *et al.* [11]

and Guttman and Cooke [13] with linear polyacrylamide-filled capillaries. Interactions between the DNA fragments and the HPMC polymer may account for the difference with the polyacrylamide system. In this regard, it is interesting that co-elution or even reversal of migration times between specific closely spaced DNA fragments was demonstrated in HPCE with linear polyacrylamide capillaries [11–14]. Electric field strength [11] or temperature-related effects [28] on the tertiary structure of DNA may be responsible for these phenomena. In our case, separations at capillary temperature settings other than 25°C (up to 45°C and down to 15°C) did not resolve the 271 and 281 bp fragments.

Role of intercalating agents

Intercalating agents such as ethidium bromide (EB) bind to DNA by inserting themselves between the base pairs of the double helix and have been used routinely in gel staining [29]. Fig. 2 shows the effect of adding 10 μM ethidium bromide (EB) to the buffer on the separation of ϕX 174 (note: EB was not added to the sample). It can

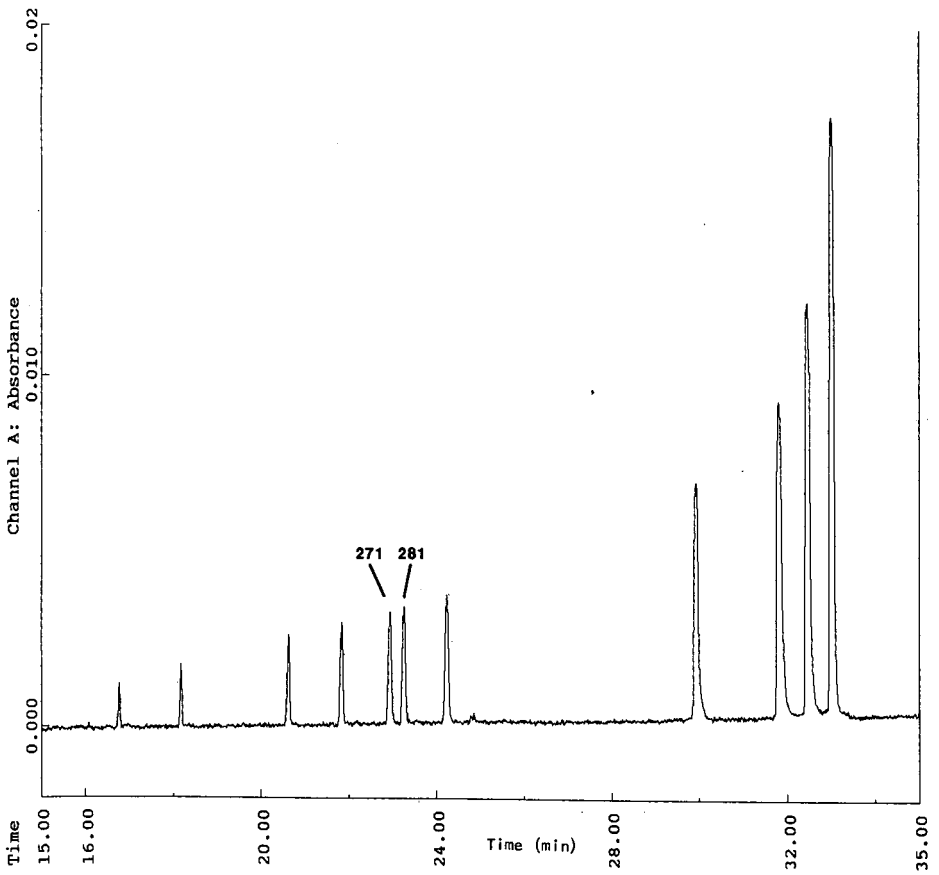

Fig. 2. Effect of ethidium bromide on DNA separation. Run buffer as in Fig. 1 with addition of 10 μM ethidium bromide. Sample concentration, 10 μg/ml. Electrokinetic injection at 2 kV for 10 s. All other conditions as in Fig. 1A. Note the separation of the 271 and 281 bp DNA fragments.

be seen that now, compared with Fig. 1, the 271 and 281 bp pair is completely baseline resolved while the migration times are longer. In addition, on average *ca.* 35% higher peak heights are obtained. The peak capacity is also greater with the EB separation: between the window of 118 and 194 bp, DNA fragments with a 3.0 bp difference are baseline resolved, as opposed to 5.3 bp in the separation without EB.

It is well known that EB alters the structure of DNA: the spacing of succesive base pairs is increased, the sugar phosphate backbone is distorted and the pitch of the double helix is decreased [29]. In addition, EB may alter the charge on the DNA during electrophoresis. These structure and charge-related effects may therefore alter the sieving behaviour of DNA fragments in a "physical" gel, as is evident in the longer migration times in Fig. 2 compared with Fig. 1. The structural changes in the DNA cause an apparent higher UV absorbance of the intercalated DNA. While these preliminary results with EB look promising, more work is necessary to determine its utility in PCR fragment analysis by HPCE. In particular, questions regarding quantification need to be addressed. For example, with HPCE, Kasper *et al.* [30] found the linear response range with UV detection to be dependent on the the EB concentration.

Detection limits

The HPCE system in Fig. 1 was used to determine the detection limits for specific DNA sequences by means of a dilution series. Electrokinetic injection was used. Successive dilutions with water were made from a stock solution containing 100 μg/ml total DNA, 10 m*M* Tris and 2 m*M* EDTA. Fig. 3 shows linear calibration

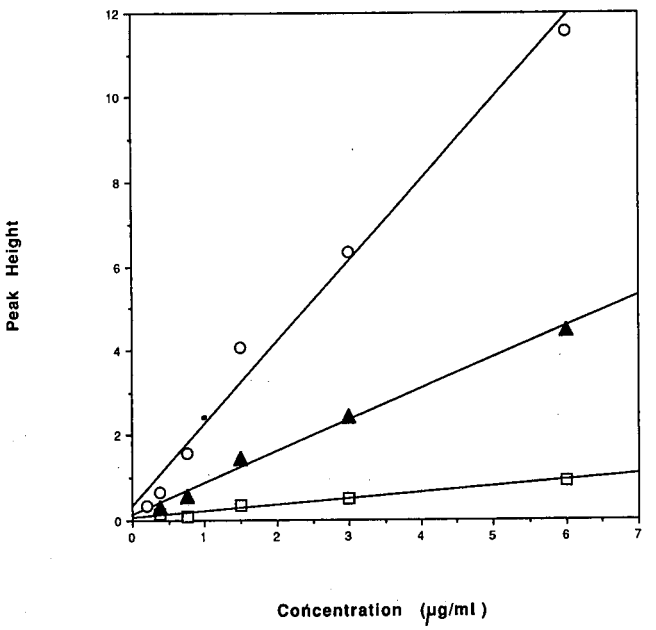

Fig. 3. Calibration graph (peak height *vs.* DNA concentration) for a dilution series in the relevant clinical range. Data were generated using the conditions in Fig. 1A. □ = 1353 bp; ▲ = 271/281 bp; ○ = 118 bp. The minimum detectable concentration for the 118 bp fragment is *ca.* 8 ng/ml.

graphs (peak height *vs.* concentration) for three selected peaks in the clinically relevant, low concentration range. At higher concentrations, the plots become non-linear owing to the increasing Tris salt concentration in the ϕX 174 sample, which, in turn, affects the amount of sample introduced into the capillary with electrokinetic injection [31]. Under optimum conditions, the minimum detectable concentration for the 118 bp restriction fragment is *ca.* 8 ng/ml at a 2:1 signal-to-noise ratio.

Molecular sieving

Next, the sieving efficacy of selected polymers was studied for the separation of DNA restriction fragments. Two cellulose-based polymers, HPMC-100 and HPMC-4000, were examined, in addition to polyethylene glycol (PEG) with an average molecular mass of 35 000. According to the manufacturer, the two hydroxypropylmethylcelluloses have average molecular masses of 26 000 and 90 000, respectively (the viscosities of 2% solutions at 25°C are 100 and 4000 cP, respectively). In addition, for comparison, data based on HPCE of DNA restriction fragments with low cross-linked polyacrylamide (3% T, 0.5% C) were included (data courtesy of Dr. Guttman, Beckman Instruments). In the latter instance, the polymerization was performed *in situ* (*i.e.*, within the capillary), as opposed to adding the polymer to the run buffer.

Molecular sieving with linear polyacrylamide was studied by Bode [15–18] and Tietz *et al.* [19]. It is now generally accepted that cross-linking, *per se*, is not required in order to achieve molecular sieving. The extent of sieving depends on the viscosity of the medium (through Stoke's law, when the viscosity is caused by a low-molecular-mass compound, *e.g.*, glycerol) and on the chain length of the polymer. The mechanism is thought to involve a random association of flexible, inert fibers in which molecules can migrate through dynamic pores. Similar molecular sieving may take place in HPCE with polyacrylamide, cellulose derivatives, PEGs and other polymers, as our data and those of others [9–14] indicate.

With cross-linked polyacrylamide gels, a plot of mobility *vs.* logarithm of molecular mass (or bp number) for nucleic acids should yield a straight line [15,16]. For HPMC-4000 and HPMC-100, mobility *vs.* bp plots (on a semi-logarithmic scale) are shown in Fig. 4A and B at different polymer concentrations. It can be seen that S-shaped curves, with a linear middle portion, are obtained. The shallowness of the slope of the curve is a measure of the molecular sieving power of the medium [16]. The steeper the slope of the curve, the less effective is the sieving. For example, it can be seen in Fig. 4A that at low concentration, *i.e.*, 0.1% (w/w), HPMC-4000 is not an effective sieving agent. The higher the polymer concentration, the better is the sieving, as found by others for linear and weakly cross-linked polyacrylamide [11,16,19]. The apparent deviation from linearity with the larger DNA fragments has also been observed by other workers [11,28]. The mobilities of these fragments are higher than expected and reportedly due to electric field effects [32]. As Heiger *et al.* [11] pointed out, field effects on mobility may occur in HPCE at much smaller fragment sizes than found in conventional gel electrophoresis because the field strength in HPCE is generally much higher.

It is interesting to compare the sieving of the DNA fragments with the HPMC-4000 and the HPMC-100. From Fig. 4A and B it can be seen that at the same polymer concentration [0.5% (w/w)] , greater mobilities are obtained with the low-

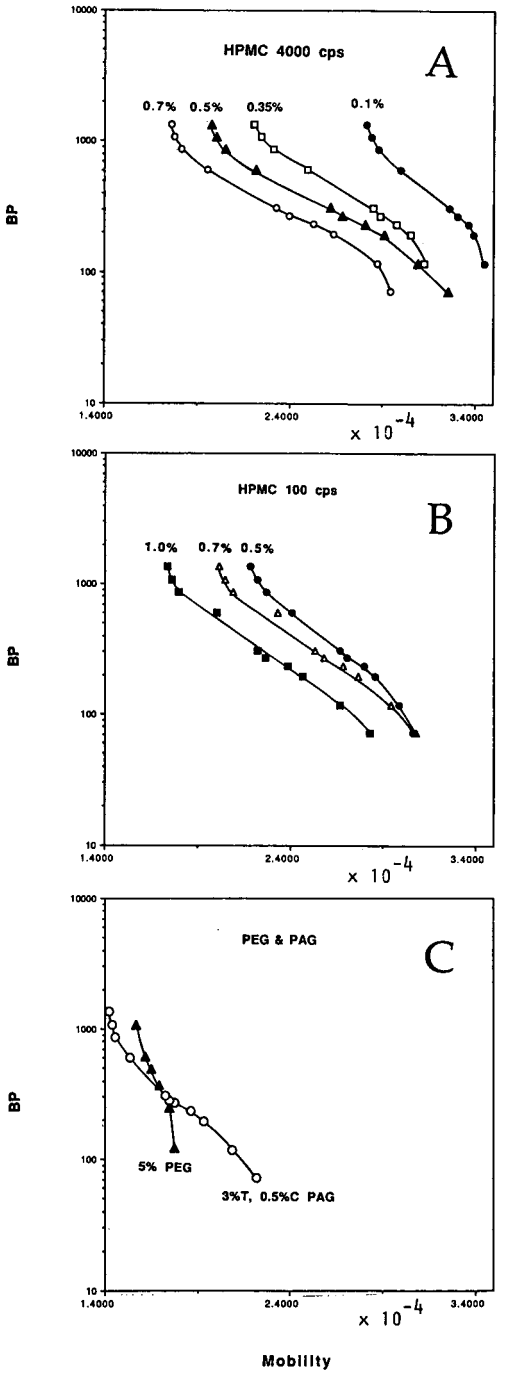

Fig. 4. Effect of different additives on molecular sieving. The plots (semi-logarithmic scale) show the dependence of mobility on the base pair number. DNA fragments from the Hae III restriction digest of ϕX were used as base pair markers. Polymeric additives are (A) HPMC-4000 at 0.1, 0.35, 0.5 and 0.7%; (B) HPMC-100 at 0.5, 0.7 and 1.0% (C) 5% PEG and polyacrylamide (3% T, 0.5% C).

molecular-mass HPMC. This is in agreement with the findings of Bode [16], who determined higher mobilities for nucleic acids in short-chain linear polyacrylamide compared with long-chain polyacrylamide. In another paper, Bode [18] demonstrated a similar chain length dependence for molecular sieving with PEG solutions.

Fig. 4C shows the data obtained with PEG (average molecular mass 35 000) and low-cross-linked polyacrylamide. Compared with the S-shaped polyacrylamide curve, the PEG plot is relatively steep. Hence the selected PEG is not an effective sieving agent for HPCE of DNA restriction fragments. It is not expected that other, lower molecular mass PEGs would provide an improvement in this respect [18]. Examination of Fig. 4A and C reveals that mobilities are lower with the polyacrylamide system than the HPMC-100 and HPMC-4000 systems. This is due to specific differences in the pore structure of these media under the specified conditions. It should also be noted that excellent peak efficiency was obtained with the polyacrylamide capillary [13]. As noted by Heiger *et al.* [11], *in situ* polymerization may have an advantage over a system where the polymer is dissolved in the buffer beforehand in that much higher polymer concentrations (and therefore higher viscosities) can be obtained in the capillary. For example, single-stranded oligonucleotides were separated with a 9% T, 0% C polyacrylamide and capillaries with up to 14% T were used [11]. Our approach of adding the polymer to the run buffer, although simple and reproducible, is limited in that it is more difficult to fill the capillary with viscous buffers. Therefore, only relatively non-viscous buffers can be used in our procedure.

Next, to characterize the sieving effect further, a plot of log mobility *vs.* HPMC-4000 concentration was made. Similar Ferguson plots (log mobility *vs.* %T) are routinely generated in PAGE. They are used to determine the size selectivity of migrating species and to calculate "free" mobilities. Fig. 5 shows the data obtained

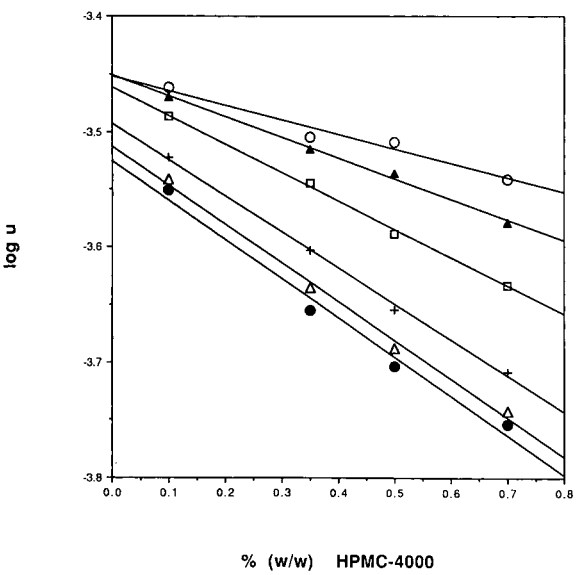

Fig. 5. Ferguson plot [log mobility *vs.* % (w/w) polymeric additive] for a buffer containing HPMC-4000 as the sieving component. Mobilities of selected ϕX 174 Hae III digest fragments were used to generate the plot. ○ = 118 bp; ▲ = 194 bp; □ = 310 bp; + = 603 bp; △ = 872 bp; ● = 1353 bp.

with linear regression analysis for selected DNA fragments. A similar plot was obtained for the data with the HPMC-100 (not shown). It can be seen that better sieving is obtained at higher polymer concentrations as the plots converge at low polymer concentrations. Better linearity, as evident from the correlation coefficients (0.995–0.998), is obtained for the 194, 310 and 603 bp fragments. Poorer linearity is obtained with either very small or larger DNA fragments (correlation coefficients 0.961 and 0.984, respectively).

Using a 0.089 *M* TBE buffer without a polymer additive, we determined the free solution mobility of all DNA fragments to be $3.87 \cdot 10^{-4}$ cm^2/V s ($\log u = -3.41$). This value is substantially higher than the free solution mobilities found from the intercepts of the Ferguson plots. Non-linearity of Ferguson plots at low polymer concentration has been observed with linear polyacrylamide by Tietz *et al.* [19] in a moving boundary electrophoresis system and recently by Heiger *et al.* [11] in HPCE.

Factors affecting precision

The precision results [expressed as relative standard deviation (R.S.D.) in migration time, peak area and peak height] obtained with DNA restriction fragments and an HPMC-4000 containing buffer system are summarized in Table I. Electrokinetic injection and the conditions in Fig. 1A were used. Two cases are distinguished. In the first, consecutive runs were performed while sampling each time from a different vial. In the second, runs were carried out by sampling from the same sample vial. It can be seen from Table I that in both cases excellent precision in migration times can be obtained (R.S.D. < 0.2%). Clearly, this is an improvement over our previous HPCE system involving CTAB buffers [5,6]. Moreover, the described HPCE system is very stable from day to day and we have used the capillary with the HPMC buffer on a daily basis for months without problems.

TABLE I

R.S.D. VALUES FOR FRAGMENTS OF DIFFERENT SIZE (BASE PAIR NUMBER)

Conditions as in Fig. 1A except for sample concentration, as indicated. MT = Migration time.

Base pairs	R.S.D. (%)								
	Vial-to-vial (10 μg/ml, $n=7$)			Vial-to-vial (5 μg/ml, $n=11$)			Within-vial (25 μg/ml, $n=9$)		
	MT	Height	Area	MT	Height	Area	MT	Height	Area
72	0.16	5.71	8.43	0.24	18.98	18.59	0.16	5.46	8.75
118	0.15	7.63	6.04	0.23	17.03	15.19	0.16	6.00	7.38
194	0.09	2.73	3.82	0.21	14.18	18.00	0.19	5.94	6.34
234	0.09	2.91	3.27	0.21	14.09	15.09	0.19	5.28	3.49
271/281	0.09	2.18	3.97	0.22	12.81	13.80	0.20	4.92	6.65
310	0.09	3.26	3.08	0.22	13.85	14.66	0.19	5.70	5.73
603	0.07	2.04	3.87	0.24	27.15	27.98	0.21	4.79	5.96
872	0.08	1.37	2.96	0.22	12.83	14.55	0.22	5.44	6.50
1078	0.08	1.06	1.91	0.22	12.22	13.79	0.22	5.22	5.32
1353	0.09	2.39	5.18	0.23	15.08	14.28	0.22	5.32	9.16

Peak-area precision was found to be concentration dependent. The results in Table I were obtained with a relatively low DNA concentration (10 μg/ml). Better peak-area precision for specific fragments was found at higher DNA concentrations. However, the lower concentration range is of more interest for our clinical application. It was also found that a relatively low injection voltage (*e.g.*, 2 kV) is preferable for the early-eluting 72 and 118 bp fragments, as at high injection voltages distorted peak shapes were obtained which, consequently, affected the precision (note that in Table I the peak-area precision for the 72 and 118 bp fragments is worse than for the other fragments). Possibly this may be due to localized (Joule) heating during the electrokinetic injection from a low-conductivity solution, which, in turn, could lead to (partial) denaturation of specific DNA fragments.

During the course of this work, we found that better peak-area precision was obtained by sampling from different vials (aliquoted samples). When sampling was done from the same vial, peak areas and heights for the first run were significantly larger than those obtained for subsequent runs. Consequently, the R.S.D. will be affected, as indeed is shown in Table I. This phenomenon has also been observed in our laboratory for oligonucleotide analysis with 3% T, 5% C gel-filled capillaries. In this instance electrokinetic injection is a requirement. Further work is in progress to elucidate fully the reason for the decreasing peak area with consecutive injections from the same vial.

Artifacts with HPCE

Another factor occasionally affecting peak-area and peak-height precision is an artifact related to low concentrations of total DNA in the sample. We have repeatedly found that certain DNA restriction fragments in the ϕX 174 sample, *e.g.*, the 603 bp fragment, at low total DNA concentration (*i.e.* <10 μg/ml), yield proportionally lower peak areas when compared with other fragments. The effect is demonstrated in Fig. 6A for a sample with a 3 μg/ml total DNA concentration. The salt concentration in the sample was 0.03 *M* Tris. It can be seen that two "ghost" peaks (indicated by arrows) appear after elution of the last 1353 bp DNA fragment. At the same time, the peak height of the 603 bp fragment is considerably lower than expected, and peak shapes for the 72 and 118 bp fragments have deteriorated. When buffer salt (12.5 m*M* TBE) was added to the sample (Fig. 6B), less sample was injected and the peak efficiency decreased, as expected. However, the ghost peaks disappeared.

The ghost peaks were not present when samples at higher total DNA concentrations (*e.g.*, 25 μg/ml) were injected (results not shown). Conceivably, during the HPCE procedure, partial or complete denaturation of double-stranded DNA into single strands may have taken place, resulting in the ghost peaks in Fig. 6. As the mobility of single-stranded DNA is lower than that of corresponding double-stranded DNA, the peaks marked by arrows in Fig. 6 may represent denatured DNA originating from the 603 bp fragment. Other DNA restriction fragments samples (*e.g.*, a Bio-Rad Labs. DNA size standard) showed similar abnormalities when injected at low concentrations. However, it should be noted that the above phenomena were not always repeatable. The irreproducibility greatly affected the peak-area precision measurements at low concentrations. Hence it appears to be an artifact, possibly related to the presence of endonucleases, which denature DNA, or to the absence of certain double-helix-stabilizing cations.

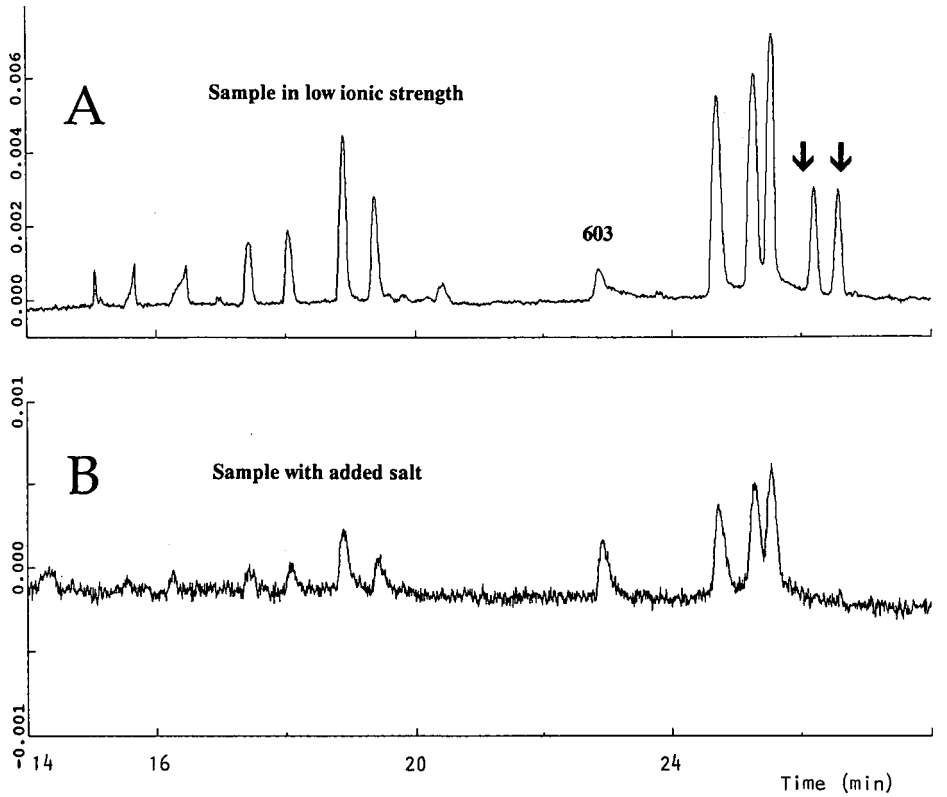

Fig. 6. Artifacts related to DNA and/or salt concentration. (A) Two "ghost" peaks (arrows) appear, while the 72 and 118 bp peaks are broadened. Sample concentration, 3 μg/ml with 0.03 m*M* Tris present. (B) Same sample with added buffer salt (12.5 m*M* TBE). Note the disappearance of the extra peaks. However, the other peak shapes have deteriorated owing to less efficient zone focusing. Conditions as in Fig. 1A.

Application to PCR amplified HIV-1

After establishing optimum separation conditions and good precision, the HPCE system was used to analyze PCR-amplified products. An HIV-1 positive control cell line, U1.1, was used for DNA extraction. This cell line harbors one copy of the HIV-1 provirus per cell in addition to two copies of HLA-DQ-α. HLA-DQ-α is present in all healthy cells and may therefore serve as an internal standard in clinical assays. Using specific primers [5], a 115 bp portion of the gag region of HIV-1 and a 242 bp sequence of HLA-DQ-α were co-amplified by means of 35 cycles of the PCR. Unfortunately, in our case, PCR reaction mixture components (*e.g.*, primers, primer–dimers, dNTPs), when electrophoresed with HPCE, co-migrate with the PCR products of interest. In addition, the PCR product sample has an appreciable ionic strength, which, as pointed out in the discussion in Fig. 6B, renders the electrokinetic injection less efficient with regard to peak shape.

To solve the above problem, we used ultrafiltration with the Centricon system (see Experimental and ref. 33) to concentrate and de-salt the sample. This resulted in removal of low-molecular-mass material and peak sharpening. Salt is removed by

dilution of the 50-μl volume PCR sample with 2 ml of glass-distilled water. After centrifugation with the Centricon system, the sample is reconstituted to its original volume of 50 μl, resulting in a theoretical 97.5% reduction in salt. An identical second Centricon procedure results in a 99.94% reduction in salt, a third procedure in a 99.99% reduction, etc. The effect of ultrafiltration with the Centricon system is shown in Fig. 7. The separations in Fig. 7 were obtained at 20 kV, resulting in less efficient separations but faster analysis times than for the 10-kV runs in Fig. 1. Faster analysis

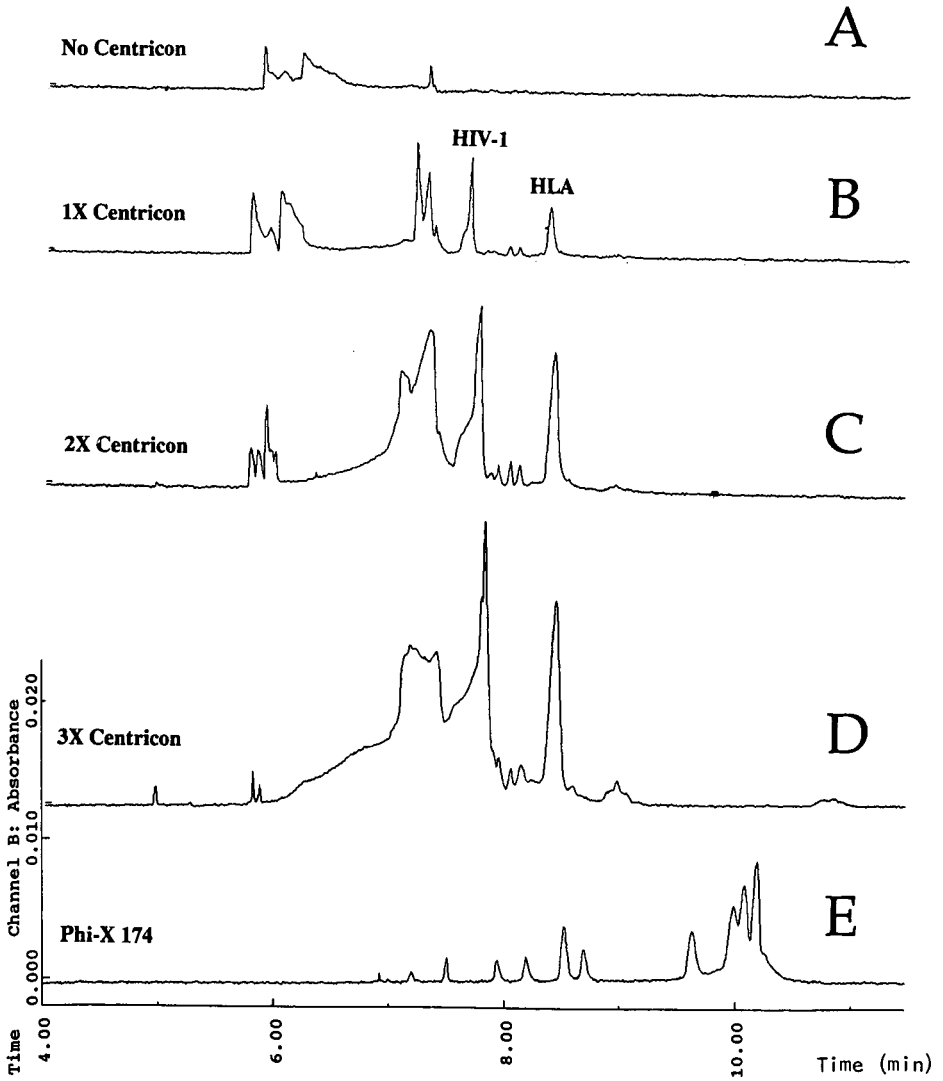

Fig. 7. Effect of ultrafiltration on the PCR-amplified DNA peaks. (A) Untreated sample (no ultrafiltration), a co-amplified HIV-1, HLA (115 and 242 bp, respectively) positive control. Concentration is achieved by increasing the number of desalting steps from (B) 1 × to (D) 3 × . (E) ϕX 174 DNA standard. Run voltage, 20 kV. Sample was injected electrokinetically at 10 kV for 10 s. All other conditions as in Fig. 1A.

times again at the expense of efficiency, can also be obtained by using shorter capillaries.

Fig. 7A shows the electropherogram of the PCR sample when no ultrafiltration was used. Fig. 7E shows the ϕX 174 DNA standard as reference. The peaks of interest are marked as HIV-1 and HLA. By ultrafiltration through the Centricon filters, primers and dNTPs are selectively removed, yielding prominent HIV-1 and HLA peaks (Fig. 7B). As pointed out above, the ultrafiltration procedure can be repeated to allow further concentration and desalting. This effect is shown in Fig. 7C and D. The nominal molecular mass cut-off of the membranes is the point at which more than 90% of the single- or double-stranded pieces of DNA will be retained [33]. For the Centricon-30 and Centricon-100 microconcentrators, the single-stranded DNA cut-off is 60 and 100 bases, respectively. For double-stranded DNA the cut-off is 50 and 125 bp, respectively. Consequently, for our application (HIV-1 sequence, 115 bp) the Centricon-30 is most suitable. The application of the above method to clinical samples is currently in progress.

CONCLUSIONS

We have achieved excellent separation efficiency and precision with sieving buffers for DNA restriction fragments. The HPCE system using a polysiloxane-coated capillary and polymeric buffer additives is relatively simple and straightforward. For clinical assays, precision is a key requirement and the current system, although less efficient in terms of plate count, is preferable compared to our previous HPCE system [5,6]. Our data indicate that certain linear polymers (*e.g.*, HPMC), when added to the buffer, provide effective molecular sieving of DNA fragments. The data are consistent with recent work in HPCE on polyacrylamide capillaries by Karger's group [11,12] and Ogston's model of molecular sieving [20]. Other polymers may work as well or better for different applications, *i.e.*, protein separations [9]. While our separation system offers the benefit of simplicity, the *in situ* polymerization system desribed by Heiger *et al.* [11] and Guttman and Cooke [13] offers interesting possibilities for a wide range of nucleic acids. In these systems, viscosity (%T) can be easily manipulated to optimize for a particular DNA analysis and, as in our case, a high separation efficiency is possible. Further work is necessary to study the role of ethidium bromide (and possibly other intercalating agents) in HPCE separations of DNA, in particular with regard to the quantification of real samples. Our ultimate goal is to achieve a sensitivity level that would enable us to detect a single copy of the target HIV-1 sequence in a blood sample.

ACKNOWLEDGEMENTS

The authors thank Daniel Siu for help with preparation of the figures and Drs. Andras Guttman, Ken Anderson and Barry L. Karger for reviewing the manuscript before submission and for helpful discussions.

REFERENCES

1 H. A. Erlich (Editor), *PCR Technology, Principles and Applications*, Stockton Press, New York, 1989.
2 L. Haff, J. G. Atwood, J. DiCesare, E. Katz, E. Picozza, J. F. Williams and T. Woudenberg, *BioTechniques*, 10 (1991) 102.
3 C. Y. Ou, S. H. McDonough, D. Cabanas, T. B. Ryder, M. Harper, G. Moore and G. Schocketman, *AIDS Res. Hum. Retroviruses*, 6 (1990) 1323.
4 E. D. Katz and M. W. Dong, *BioTechniques*, 8 (1990) 546.
5 R. G. Brownlee, F. J. Sunzeri and M. Busch, *J. Chromatogr.*, 533 (1990) 87.
6 F. Sunzeri, T. H. Lee, R. G. Brownlee and M. Busch, *Blood*, 77 (1991) 879.
7 F. J. Sunzeri, R. G. Brownlee, T. H. Lee and M. P. Busch, *Sixth International Conference on AIDS, San Francisco, CA, 1990*, poster FA-335.
8 S. Hjertén, L. Valtcheva, K. Elenbring and D. Eaker, *J. Liq. Chromatogr.*, 12 (1989) 2471.
9 M. Zhu, D. L. Hansen, S. Burd and F. Gannon, *J. Chromatogr.*, 480 (1989) 311.
10 *Biosystems Rep.*, No. 6, *Applied Biosystems Newsl.*, October 1989.
11 D. N. Heiger, A. S. Cohen and B. L. Karger, *J. Chromatogr.*, 516 (1990) 33.
12 D. N. Heiger, M. Vilenchik, A. S. Cohen and B. L. Karger, presented at the *3rd International Symposium on High-Performance Capillary Electrophoresis, San Diego, CA, 1991*, abstract PT-8.
13 A. Guttman and N. Cooke, *J. Chromatogr.*, 559 (1991) 285.
14 B. L. Karger, A. S. Cohen, D. N. Heiger and K. Ganzler, presented at the *3rd International Symposium on High-Performance Capillary Electrophoresis, San Diego, CA, 1991*, abstract LM-4.
15 H. J. Bode, *Anal. Biochem*, 83 (1977) 204.
16 H. J. Bode, *Anal. Biochem*, 83 (1977) 364.
17 H. J. Bode, in B. J. Radola (Editor), *Electrophoresis '79, Proceedings of the 2nd International Conference on Electrophoresis, Munich, 1979*, Walter de Gruyter, Berlin, 1980, pp. 39–52.
18 H. J. Bode, *FEBS Lett.*, 65 (1976) 56.
19 D. Tietz, M. H. Gottlieb, J. S. Fawcett and A. Chrambach, *Electrophoresis*, 7 (1986) 217.
20 A. G. Ogston, *Trans. Faraday Soc.*, 54 (1958) 1754.
21 L. Ornstein, *Ann. N. Y. Acad. Sci.*, 121 (1964) 321.
22 G. J. M. Bruin, R. Huisden, J. C. Kraak and H. Poppe, *J. Chromatogr.*, 480 (1989) 339.
23 J. A. Lux, H. Yin and G. Schomburg, *J. High Resolut. Chromatogr.*, 13 (1990) 145.
24 J. C. Reijenga, G. V. A. Aben, Th. P. E. M. Verheggen and F. M. Everaerts, *J. Chromatogr.*, 260 (1983) 241.
25 J. W. Jorgenson and K. D. Lukacs, *Science (Washington, D.C.)*, 222 (1983) 266.
26 X. Huang, M. J. Gordon and R. N. Zare, *Anal. Chem.*, 60 (1988) 375.
27 J. Harbaugh, M. Collette and H. E. Schwartz, *Tech. Bull. TIBC-103*, Beckman Instruments, Palo Alto, CA, 1990.
28 N. Stellwagen, *Biochemistry*, 22 (1983) 6186.
29 J. D. Watson, N. H. Hopkins, J. W. Roberts, J. A. Steitz and A. M. Weiner, *Molecular Biology of the Gene*, Benjamin/Cummings, Menlo Park, CA, 4th ed., 1987.
30 T. J. Kasper, M. Melera, P. Gozel and R. G. Brownlee, *J. Chromatogr.*, 458 (1988) 303.
31 R. A. Wallingford and A. G. Ewing, *Adv. Chromatogr.*, 29 (1989) 1.
32 C. R. Cantor, C. L. Smith and M. K. Mathew, *Annu. Rev. Biophys. Chem.*, 17 (1988) 287.
33 *Publication No. 1-259G*, Centricon Microconcentrators, Amicon Division, W. R. Grace & Co., Beverly MA, 1990.

Journal of Chromatography, 559 (1991) 285–294
Elsevier Science Publishers B.V., Amsterdam

CHROM. 23 472

Effect of temperature on the separation of DNA restriction fragments in capillary gel electrophoresis

ANDRAS GUTTMAN* and NELSON COOKE
Beckman Instruments, Inc., Palo Alto, CA 94304 (USA)

ABSTRACT

Two different separation modes were used in high-performance capillary gel electrophoresis to study the effect of temperature on the separation of DNA restriction fragments, isoelectrostatic (use of constant applied electric field) and isorheic (use of constant current). In both instances, the migration properties and resolution of the DNA molecules were studied as a function of column temperature between 20 and 50°C. In the isoelectrostatic separation mode, the migration time and resolution decrease as temperature increases. In the isorheic separation mode, increasing the column temperature results in a maximum migration time for all of the DNA fragments and shows a maximum resolution for the lower molecular weight fragments (<200 kilodalton).

INTRODUCTION

High-performance capillary electrophoresis (HPCE), as an instrumental approach to electrophoresis, is emerging as a powerful bioanalytical method and an effective tool for the characterization and isolation of biologically important macromolecules [1–5]. The use of narrow-bore polyacrylamide gel-filled capillaries allows extremely high efficiency separations for single- and double-stranded deoxyribonucleic acids [6–8].

Uncontrolled variations of temperature in gel electrophoresis can cause severe practical problems with respect to reproducibility, band broadening and migration properties [9–11]. For example, non-uniform column temperatures across the diameter or length of the column, caused by Joule heating, can decrease efficiency and resolution [2,12,13]. Gel-filled capillaries present an additional challenge in this regard because of the possible changes in the gel structure, such as pore size, due to high temperature [14]. In the separation of some biopolymers, such as DNA fragments, conformation changes can occur at elevated temperatures, leading to unexpected changes in migration time [15,16]. All of these problems can be avoided in HPCE by the use of column temperature control, making this technique much more efficient than conventional slab or rod gel systems. High-resolution separations can thus be achieved using constant temperature (isothermal), constant applied electric field (isoelectrostatic), constant current (isorheic), constant power (isoergic) and the use of gradients with each of those modes.

0021-9673/91/$03.50

The objective of this research was first to achieve high-resolution separations of the ϕX-174 DNA-Hae III digest restriction fragment test mixture by HPCE using gel-filled columns and then to study the effect of temperature on the electrophoretic migration properties under both constant-voltage and constant-current separation conditions.

THEORY

If a uniform electric field (E) is applied to a polyion with a net charge Q, the electrical force (F_e) is given by

$$F_e = QE \tag{1}$$

In free solution and in highly viscous media such as a gel, when a polyion is set in motion by the applied electric field, a frictional force (F_f) will act in the opposite direction:

$$F_f = f(dx/dt) \tag{2}$$

where f is the translational friction coefficient and dx and dt are the distance and time increments, respectively.

Differences in sample properties, such as shape, size or net charge, lead to differences in electrophoretic mobility and provide the basis of the electrophoretic separation. The motion of a polyion under an applied electric field can be expressed according to Newton's second law as

$$m(d^2x/dt^2) = QE - f(dx/dt) \tag{3}$$

which states that the product of the mass (m) and acceleration is equal to the difference of the electrical and frictional forces.

When the force from the applied electric field on the polyion is exactly counterbalanced by the frictional force, the particle will move with a steady-state velocity (v):

$$v = l/t_m = QE/f = \mu_e E \tag{4}$$

where l is the effective length of the capillary up to the detection point, t_m is the migration time of the solute and μ_e is the electrophoretic mobility of the polyion, which is defined as the steady-state velocity per unit field strength.

The translational friction coefficient (f) is a function of the viscosity of the surrounding media, *i.e.*, the gel, which is influenced by the temperature. For a spherical particle, when the Reynolds number is less then 0.1, the friction coefficient is given by Stokes law [17]:

$$f = 6\pi\eta r \tag{5}$$

where η is the viscosity of the surrounding medium and r is the root mean square radius of the polyion. From eqns. 4 and 5, we have

$$\mu_e = Q/f = Q/6\pi r\eta \tag{6}$$

which shows an inverse relationship between the mobility (μ_e) of the solute and the viscosity (η) of the surrounding gel–buffer medium. From eqn. 6, it is evident that the ion mobility is highly dependent on solvent viscosity, which is a function of temper-

ature. The viscosity of the gel–buffer system decreases exponentially with temperature [18] according to

$$\eta = C_1 \cdot \exp(E_a/RT) \tag{7}$$

where C_1 is a constant, E_a is the activation energy for the viscous flow, R is the universal gas constant and T is the absolute temperature. By combining eqns. 4–7, the temperature dependence on the migration time of a polyion can be expressed as:

$$t_m = (l/EQ) \cdot \text{constant} \cdot \exp(E_a/RT) \tag{8}$$

Taking the logarithm of eqn. 8 gives a convenient linear relationship between the migration time of the solute and the reciprocal absolute temperature:

$$\ln t_m = \ln(l \cdot \text{constant}/EQ) + E_a/RT \tag{9}$$

where the first term on the right-hand side depends on the length of the capillary, the applied electric field and the charge of the solute [19]. It should be noted that the charge (Q) may be weakly dependent on temperature owing to possible conformational changes of the polyion [15]. The term E_a/RT in eqn. 9 is a function only of the temperature. As a first approximation, in the isoelectrostatic mode, only this last term is temperature dependent. In the isorheic mode when the current is kept constant, the electric field changes with temperature, and therefore both terms on the right-hand side of eqn. 9 vary with temperature.

EXPERIMENTAL

Chemicals

ϕX-174 DNA-Hae III digest (New England Biolabs, Beverly, MA, USA) was diluted with water to 50 μg/ml before injection, and was stored at -20°C when not in use. The molecular weights of the DNA fragments in this mixture range from 47 to 879 kilodalton [72–1353 base pairs (bp)]. Electrophoretic-grade acrylamide, Tris, boric acid, EDTA, ammonium peroxydisulfate and tetramethylethylenediamine (TEMED) were employed (Schwarz/Mann Biotech, Cambridge, MA, USA). All buffer and acrylamide solutions were filtered through a 0.2-μm pore size filter (Schleicher & Schüll, Keene, NH, USA) and carefully vacuum degassed.

Apparatus

The P/ACE System 2000 capillary electrophoresis apparatus (Beckman, Palo Alto, CA, USA) was used. The separations were monitored on-column at 254 nm. The temperature of the gel-filled columns was controlled to ± 0.5°C by the liquid cooling system of the P/ACE instrument.

Procedures

Polymerization of the polyacrylamide was initiated by ammonium peroxydisulfate, catalyzed by TEMED and accomplished within a 0.1 mm I.D. DB-17-coated capillary (J&W, Sacramento, CA, USA) in 100 mM Tris–boric acid–2 mM EDTA (pH 8.5) (20°C) (TBE). The total length of the capillary column was 270 mm, with 200 mm to the detector. The pH of the buffer at different temperatures was determined with a Beckman ϕ-21 pH meter.

RESULTS AND DISCUSSION

Before performing these experiments, it was first important to understand the effect of temperature on the buffer pH and the resistance of the gel. The change in pH of the 100 m*M* Tris–borate–EDTA buffer employed in the range 20–50°C was determined to be only 0.4 pH unit. This did not lead to any significant difference in migration time for the large polyion molecules used in the experiments [20].

As the conductivity of the gel increases with temperature, when a constant voltage is applied to a gel-filled capillary the resistance of the column decreases as shown in Fig. 1. Therefore, in accordance with Ohm's law, the current will increase with temperature in the isoelectrostatic mode and the voltage will decrease with temperature in the isorheic mode.

Effect of temperature in the isoelectrostatic separation mode

Fig. 2 compares the separations of the ϕX-174 DNA restriction fragment mixture by capillary gel electrophoresis at different temperatures using the isoelectrostatic separation mode. It can be seen that the migration time of the DNA fragments decreases as temperature increases in accordance with the inverse relationship between the viscosity of the gel–buffer system and temperature (eqn. 9) [21,22]. Of particular interest is the relative change and reversal in peak height of the last two peaks (1078 and 1353 bp) as temperature is increased. This effect is explained by the data in Table I, where it can be seen that the column efficiency (*i.e.*, the number of theoretical plates) decreases as temperature increases. The higher molecular weight range appears to be particularly susceptible to this effect, which might be due to excessive band broadening caused by conformational changes at elevated temperature [22].

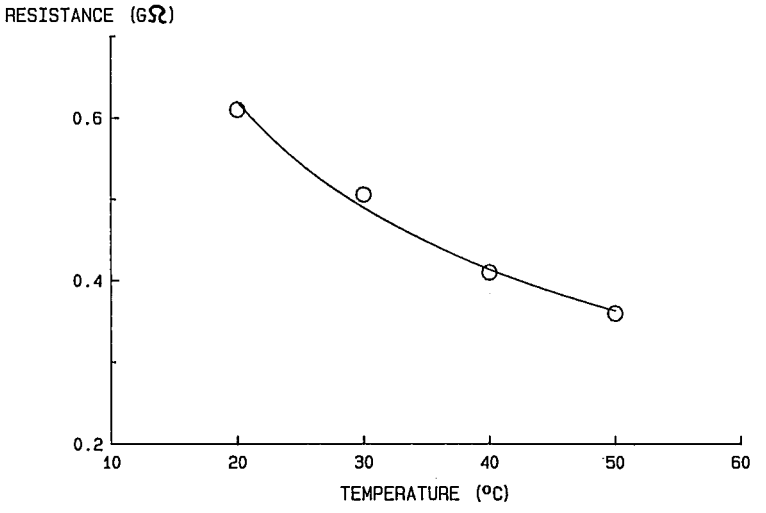

Fig. 1. Relationship between the temperature and the resistance of the gel-filled capillary column under a constant applied electric field. Conditions: isoelectrostatic mode, 400 V/cm; polyacrylamide gel column, effective length 20 cm, total length 27 cm; buffer, 0.1 *M* Tris–boric acid–2 m*M* EDTA (pH 8.5).

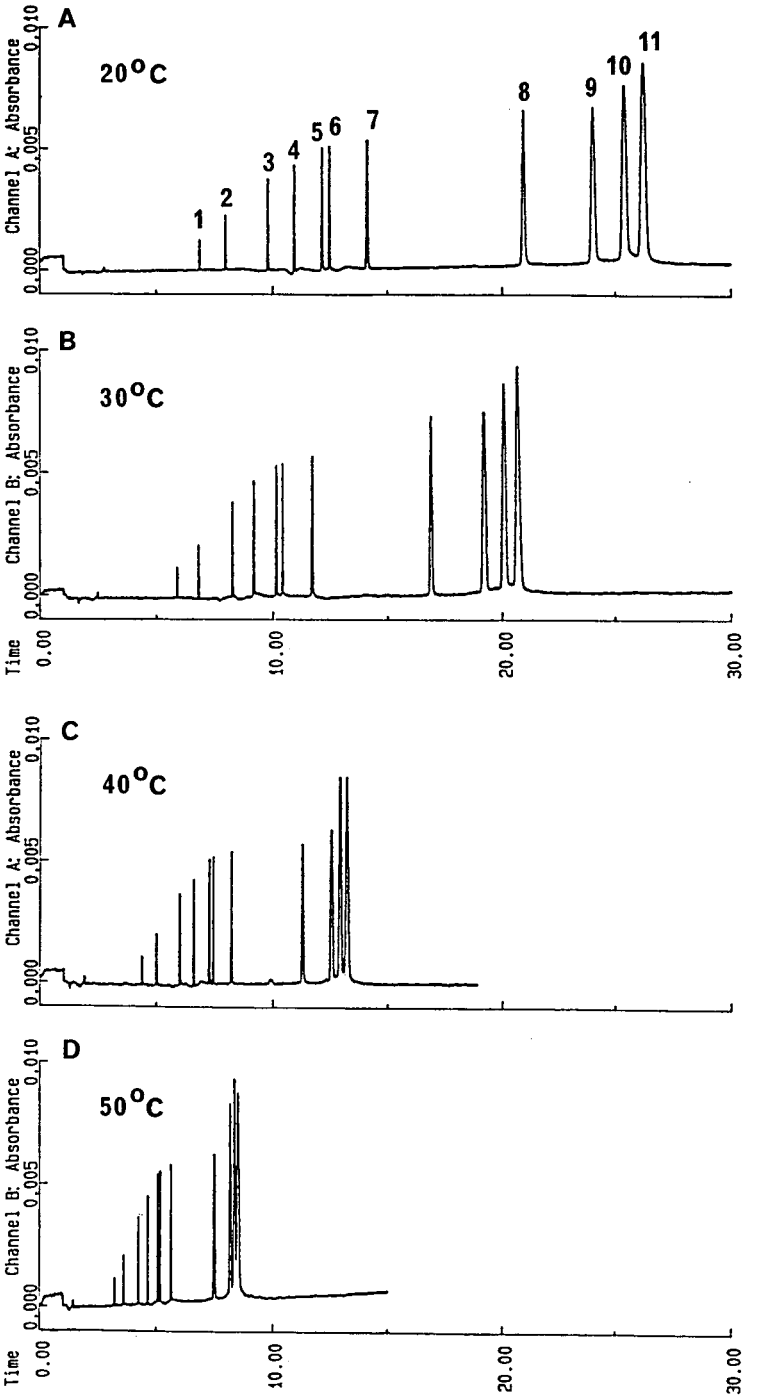

Fig. 2. Separation of the ϕX-174 DNA restriction fragment mixture by capillary gel electrophoresis at different temperatures in the isoelectrostatic separation mode: (A) 20; (B) 30; (C) 40; (D) 50°C. Peaks: 1 = 72; 2 = 118; 3 = 194; 4 = 234; 5 = 271; 6 = 281; 7 = 310; 8 = 603; 9 = 872; 10 = 1078; 11 = 1353 base pairs. Conditions as in Fig. 1. Injection, 2 s, 45 mW. Sample, 50 μg/ml of ϕX-174 DNA-Hae III digest.

TABLE I

PEAK-HEIGHT RATIOS (NORMALIZED TO PEAK AREA) AND THEORETICAL PLATE NUMBERS OF THE 1078 AND 1353 BASE PAIR FRAGMENTS OF ϕX-174 DNA-Hae III DIGEST USING THE ISOELECTROSTATIC AND ISORHEIC MODES

Conditions as in Figs. 2 and 4.

Temperature (°C)	Normalized peak-height ratio (1353/1078 bp)		Theoretical plates × 10^3 (1353 bp)	
	Constant voltage	Constant current	Constant voltage	Constant current
20	1.07	1.12	75	61
30	1.03	0.92	68	39
40	1.00	0.79	60	25
50	0.95	0.72	48	18

The logarithm of migration time for different DNA fragments is plotted in Fig. 3 as a function of reciprocal temperature and shows a linear relationship. These data agree well with eqn. 9, where the first term on the right-hand side is assumed to be constant and therefore the term E_a/RT describes the migration properties of the DNA.

Effect of temperature in the isorheic separation mode

According to Ohm's law, the voltage is directly proportional to the resistance when the current is kept constant. As the resistance is a function of temperature (Fig. 1), the apparent electric field will be determined to a large extent by the temperature of the column. Further, as the viscosity of the gel–buffer system decreases with tem-

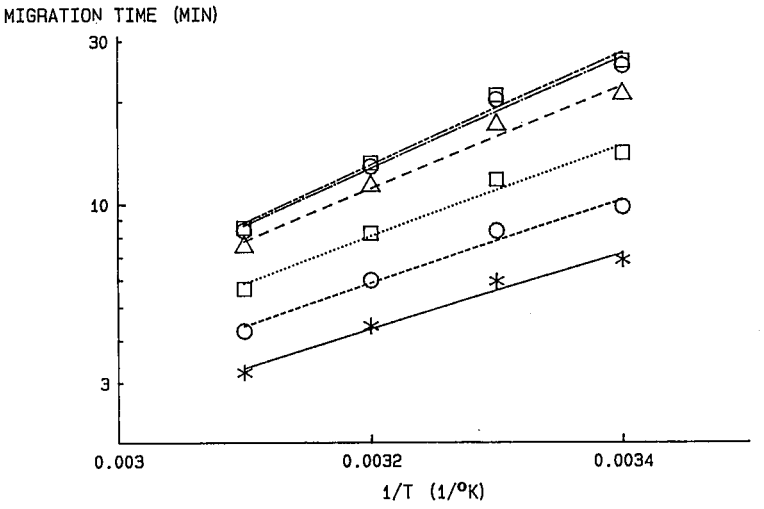

Fig. 3. Semi-logarithmic plot of the electrophoretic migration times of DNA restriction fragments as a function of the separation temperature in the isoelectrostatic mode. Conditions as in Fig. 2. Lines correspond to different sized DNA fragments: from top to bottom, 1353, 1078, 603, 310, 194 and 72 base pairs.

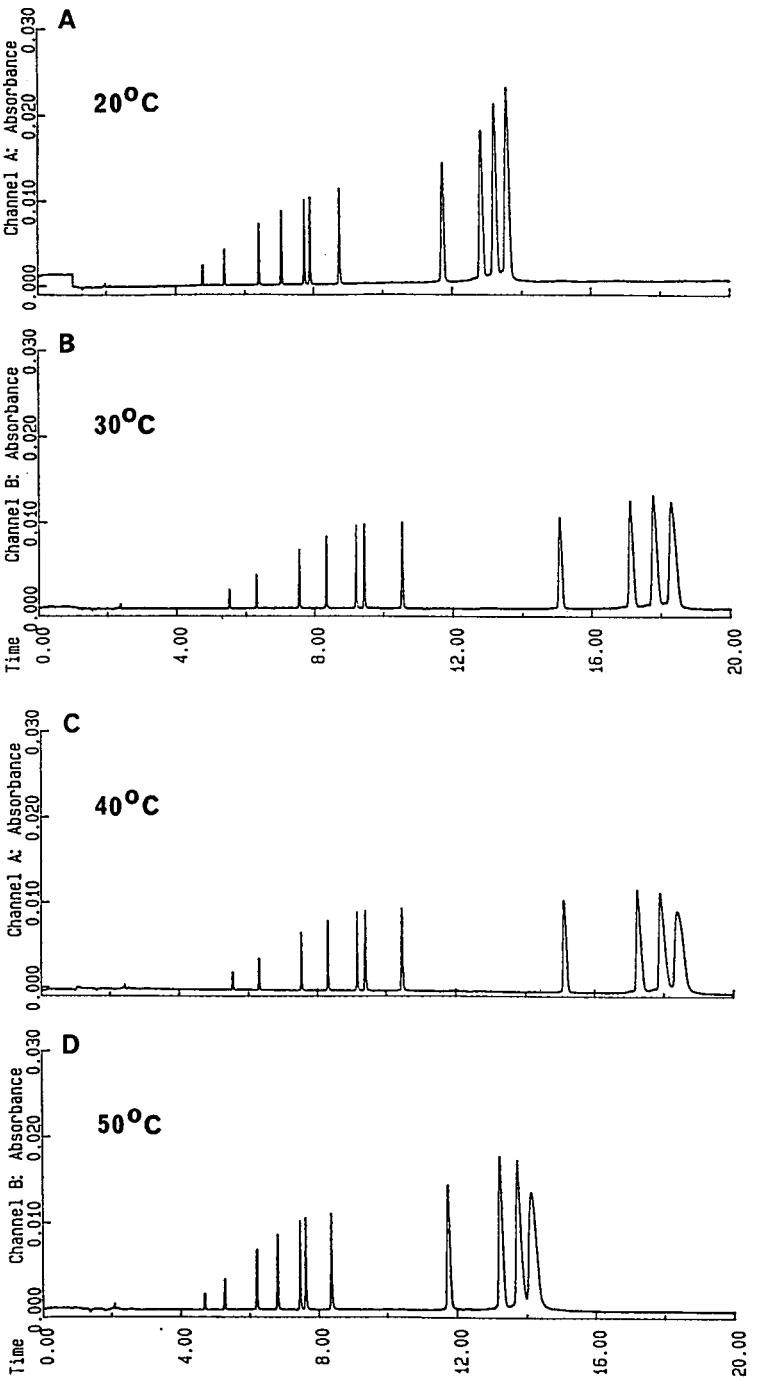

Fig. 4. Separation of the ϕX-174 DNA restriction fragment mixture by capillary gel electrophoresis at different temperatures in the isorheic separation mode: (A) 20; (B) 30; (C) 40; (D) 50°C. Conditions: isorheic mode, 20 μA; otherwise as in Fig. 2.

perature (eqn. 7), it also has an effect on the mobility of the sample components.

Fig. 4 compares the separations of the restriction fragment test mixture at different temperatures in the isorheic separation mode. In comparing these separations with those in Fig. 2, a different migration behavior is observed as the temperature is increased. In this instance, the migration time first increases with temperature, and then decreases above 40°C. This behavior can be understood by plotting the logarithm of migration time for different DNA fragments as a function of temperature, as shown in Fig. 5, and by referring back to eqn. 9. In this instance the two terms on the right-hand side of eqn. 9 combined describe the DNA migration properties. At low temperature (20°C), both the voltage and viscosity are high. The effect of the higher viscosity (eqn. 9, E_a/RT term) on migration will dominate over the voltage effect (eqn. 9, first term on the right-hand side) and lead to slower migration. On increasing the temperature of the gel-filled capillary column (30–40°C), the effect of voltage and viscosity on migration will be partially balanced, leading to a maximum migration time. At high temperature (50°C), the effect of the lower voltage on migration will prevail over the lower viscosity, leading to slower migration.

It can also be seen in Table I that the peak-height ratios for the higher molecular weight fragments in the isorheic mode decrease more (0.4 unit) than in the isoelectrostatic mode (0.12 unit). This is probably due to a greater decrease in efficiency, which can be explained by the combined effects of the decreasing apparent electric field [2] and possible conformational changes [22] with elevated temperature.

Effect of temperature on resolution

Referring back to Fig. 2, it is worth noting that good resolution is obtained between the 271 bp (peak 5) and 281 bp (peak 6) fragments. In other capillary electrophoretic systems where viscous hydrophilic polymers were used as sieving agents,

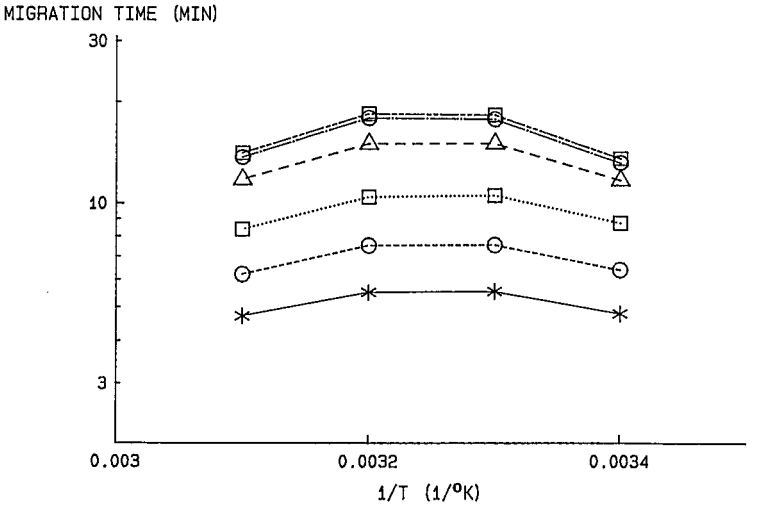

Fig. 5. Semi-logarithmic plot of the electrophoretic migration time of DNA restriction fragments as a function of the separation temperature in the isorheic separation mode. Conditions as in Fig. 4. Lines correspond to different sized DNA fragments: same order as in Fig. 3.

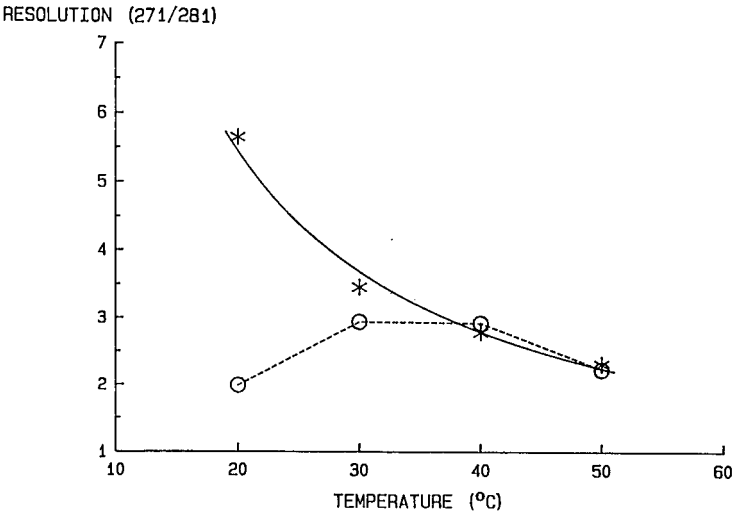

Fig. 6. Resolution between the 271 and 281 base pair DNA fragments as a function of the separation temperature using the (*) isoelectrostatic and (○) isorheic separation modes. Conditions as in Figs. 2 and 4.

these fragments could only be separated with the addition of special additives, such as intercalating agents, to the buffer [23]. Within the temperature range used in this study, a good separation of these two fragments was achieved in both the isoelectrostatic and isorheic separation modes.

Fig. 6 shows that the resolution between these two fragments is also a function of temperature. In the isoelectrostatic separation mode, the resolution in the lower molecular weight range decreases with temperature similarly to that observed with the higher molecular weight fragments (Table I). However, in the isorheic separation mode the resolution values of these low-molecular-weight fragments go through a maximum, in contrast to what was observed for the high-molecular-weight fragments.

CONCLUSIONS

According to theory, the migration of polyions in electrophoresis is driven by the potential difference between the two electrodes. In the isoelectrostatic and isorheic separation modes, the current and voltage are determined by the resistance of the capillary gel column at a given temperature, respectively.

Migration times decrease with increasing temperature in the isoelectrostatic mode and show a maximum in the isorheic mode. The resolution between the lower molecular weight DNA fragments (<300 bp) decreases in the isoelectrostatic separation mode and shows maxima in the isorheic mode at elevated temperature. However, the efficiency in the higher molecular weight range (>1000 bp) decreases in both modes with increasing temperature.

We are continuing these studies to determine the effect of other variables such

as column length, applied electric field, molecular weight of the polyion and the constant power separation mode (isoergic) in capillary gel electrophoresis.

ACKNOWLEDGEMENTS

The authors thank Professor Barry L. Karger and Dr. Herb Schwartz for stimulating discussions and for reviewing the manuscript. The help of Phyllis Browning in the preparation of the manuscript is also highly appreciated.

REFERENCES

1 J. W. Jorgenson and K. D. Lukacs, *Science (Washington, D.C.)*, 222 (1983) 266.
2 B. L. Karger, A. S. Cohen and A. Guttman, *J. Chromatogr.*, 492 (1989) 585.
3 S. Hjerten, *J. Chromatogr.*, 270 (1983) 6.
4 R. A. Wallingford, and A. G. Eving, *Anal. Chem.*, 58 (1988) 258.
5 M. J. Gordon, X. Huang, S. L. Pentoney, Jr., and R. N. Zare, *Science (Washington, D.C.)*, 242 (1988) 224.
6 J. A. Lux, H. F. Yin and G. Shomburg, *J. High. Resolut. Chromatogr.*, 13 (1990) 436.
7 A. Guttman, A. S. Cohen, D. N. Heiger and B. L. Karger, *Anal. Chem.*, 62 (1990) 137.
8 D. N. Heiger, A. S. Cohen and B. L. Karger, *J. Chromatogr.*, 516 (1990) 33.
9 R. J. Nelson, A. Paulus, A. S. Cohen, A. Guttman and B. L. Karger, *J. Chromatogr.*, 480 (1989) 111.
10 R. West, *Biopolymers*, 26 (1987) 607.
11 G. W. Slater and J. Noolandi, *Electrophoresis*, 9 (1988) 643.
12 S. Terabe, K. Otsuka and T. Ando, *Anal. Chem.*, 57 (1985) 834.
13 E. Grushka, R. M. McCormick and J. J. Kirkland, *Anal. Chem.*, 61 (1989) 241.
14 T. Tanaka, *Sci. Am.*, 244 (1981) 124.
15 C. R. Cantor, C. L. Smith and M. K. Mathew, *Annu. Rev. Biophys. Chem.*, 17 (1988) 287.
16 G. W. Slater and J. Noolandi, *Biopolymers*, 25 (1986) 431.
17 P. Grossmann and D. S. Soane, *Anal. Chem.*, 62 (1990) 1592.
18 F. W. Billmeyer, Jr., *Textbook of Polymer Science*, Wiley, New York, 3rd ed., 1984.
19 A. Guttman and N. Cooke, *Appl. Theor. Electrophor.*, in press.
20 A. Guttman, A. Arai, A. S. Cohen and B. L. Karger, presented at the *14th International Symposium on Column Liquid Chromatography, Boston, May 20–25, 1990*, paper P414.
21 B. L. Karger, A. S. Cohen, D. N. Heiger and K. Ganzler, presented at the *3rd International Symposium on High Performance Capillary Electrophoresis, San Diego, CA, February 3–6, 1991*, paper LM-4.
22 N. C. Stellwagen, *Biochemistry*, 22 (1983) 6186.
23 H. E. Schwartz, K. Ulfelder, F. J. Sunzeri, M. P. Busch and R. G. Brownlee, *J. Chromatogr.*, 559 (1991) 267.

Journal of Chromatography, 559 (1991) 295–305
Elsevier Science Publishers B.V., Amsterdam

CHROM. 23 554

Identification of DNA molecules by pre-column hybridization using capillary electrophoresis

JIUN WEI CHEN[a], AHARON S. COHEN and BARRY L. KARGER*
Barnett Institute, Northeastern University, Boston, MA 02115 (USA)

ABSTRACT

In this paper, we demonstrate the feasibility of using gel-filled capillary electrophoresis to perform Southern blotting with on-line detection and to study parameters that affect the hybridization of DNA molecules in solution. A fluorescence-tagged oligonucleotide was used as the probe for hybridization in solution with complementary DNA molecules prior to electrophoresis. The reaction mixture was subject to capillary electrophoresis in a polyacrylamide gel-filled capillary, and the hybridized species was identified on-line by UV absorption or laser-induced fluorescence detection. The effects of probe concentration and annealing temperature were studied.

INTRODUCTION

Capillary electrophoresis is of great interest for the analysis of oligonucleotides, DNA restriction fragments, DNA sequence analysis, peptide mapping, pharmaceuticals, and carbohydrates. Because of the small inner diameter of the capillary (usually 50–100 μm) and the efficient heat dissipation capability of the fused-silica capillary, very high electric fields (100–500 V/cm) can be used, and consequently, a very high efficiency and fast separation can be achieved [1,2].

This laboratory has developed polyacrylamide gel-filled capillary for the analysis of nucleic acids [3,4]. The high resolving power and speed of capillary format has drawn great interest in the study of capillary electrophoresis for fast and large scale DNA sequence analysis [5–7]. Recently, this laboratory has also demonstrated high efficiency separation of DNA fragments of restriction digests using little or no cross-linking polyacrylamide gel-filled (*i.e.* physical gel) capillaries [8]. Our most recent results further indicate that fast separation of restriction fragments can be easily achieved in less than 5 min with such columns. Separation of restriction fragments can also be obtained with dilute hydrophilic polymer networks [9,10].

Conventionally, Southern blotting is performed in order to identify the nucleotide sequence of a DNA molecule [11]. The process involves separation of DNA

[a] Present address: Department of Chemistry, University of California, Berkeley, CA 94720, USA.

0021-9673/91/$03.50

species with gel electrophoresis, transfer and immobilization onto a membrane support, and hybridization with a radioactively labelled probe. An autoradiogram is developed, and the molecules carrying complementary sequence to the probe are identified. Although a powerful tool, this method is a time-consuming and laborious process.

The goal of this study was to investigate the possibility of using capillary electrophoresis to perform on-line Southern blotting and to study parameters that affect DNA hybridization in solution. Several potential advantages can be expected from such an approach: (1) high speed identification of DNA molecules (1–5 min), (2) use of fluorescent tags rather than hazardous radioactive materials, (3) simultaneous identification of several species using various fluorescence-tagged probes, (4) low detection limits. For example, subattomolar detection is achievable using a laser-induced fluorescence detection system [5–7]. Thus, capillary electrophoresis has potential in the development of an automated ultra-sensitive tool for the detection of genetic mutations and infectious diseases.

EXPERIMENTAL

Apparatus

The capillary electrophoretic apparatus with UV or laser induced fluorescence detection, and the preparation of gel-filled capillaries for the separation of DNA molecules have been described previously [3,8]. A 30-kV, 400-μA direct current high-voltage power supply (Model PS/MJ30P0400-11; Glassman, Whitehouse Station, NJ, USA) was used to generate the potential across the capillary. For the UV detection of DNA molecules at 260 nm, a Spectra 100 (Spectra-Physics, San Jose, CA, USA) was used, while for the laser-induced fluorescence detection, an argon ion laser (Model 532AT; Ominichrom, Chino, CA, USA) was employed with the power level regulated at 2–4 mW. The laser light was filtered through a narrow-band pass filter (Model D1-488; Corion, Holliston, MA, USA), directed by a beam steerer (Model M670, Newport), and focused into the capillary with a 25 mm focal length lens (Model KBX043, Newport). The emitted fluorescent light was collected with a 40 × objective lens (Model M-Set, Newport) and passed through an interference filter (Model S10-520-R, Corion) and a colored glass filter (Model OG520, Schott Glass Technologies, Duryea, PA, USA). A photomultiplier tube (Model R928, Hamamatzu, San Jose, CA, USA) operated at 700 V, and a photon counter (Model 7070, Oriel) were used to detect the fluorescence signal. The data were stored in a PC computer through an analog-to-digital converter (Model 760, Nelson Analytical, Cupertino, CA, USA).

Gel-filled capillaries

Fused-silica tubing (Polymicro Technologies, Phoenix, AZ, USA) with inner diameter of 75 μm, outer diameter of 375 μm, effective length of 20–40 cm, and total length of 40–60 cm was first treated with methacryloxypropyltrimethoxysilane (Petrarch Systems, Bristol, PA, USA) and then filled with a carefully degassed solution of 9% acrylamide solution in 25 m*M* Tris–borate buffer, pH 8.0, 25 m*M* EDTA added with ammonium persulfate and N,N,N′,N′-tetramethylethylenediamine (TEMED).

Oligonucleotides and chemicals

Oligonucleotides pC1 (17-mer: GTAAAACGACGGCCAGT, identical to −20 universal M13 sequence primer) and pC2 (34-mer: TCGAATTCACTGGCCGTCGTTTTACAACGTCGTG) were synthesized on a DNA synthesizer (Cyclone, Milligen/Biosearch, Burlington, MA, USA) and purified by agarose gel electrophoresis. Joe-labelled M13 sequencing primer was either purchased from Applied Biosystems (Foster City, CA, USA) or synthesized on the Cyclone. The 5′ end of the oligonucleotide to be fluorescently labelled was modified with N-TFA-C6 Aminomodifier (Clontech, Palo Alto, CA, USA) and attached with activated fluorescent dye, Joe (Applied Biosystems). Unincorporated dye was separated from larger DNA molecules by size-exclusion chromatography with G-25. The Joe-labelled molecules were further purified by reversed-phase high-performance liquid chromatography (HPLC) with a C_8 column. Ultra-pure Tris base, urea, acrylamide, and EDTA were purchased from Schwartz/Mann Biotech (Cleveland, OH, USA). TEMED and ammonium persulfate were purchased from Bio-Rad (Richmond, CA, USA). DNA size standards were purchased from Pharmacia LKB (Piscataway, NJ, USA).

RESULTS

Effect of salt on electrokinetic injection

Although salt is often used to enhance hybridization of DNA molecules, it was known that in the presence of a significant concentration of salt in the sample preparation, the amount of DNA sample introduced by electrokinetic injection was greatly reduced [12]. Therefore, prior to hybridization, we examined the effect of solvent conditions on injection. Restriction digest ϕX 174 *Hae* III was separated on a 9%T, 0%C column, as previously described [8][a]. A serial dilution of the sample was made with distilled water. Since the commercial restriction digest contained 10 m*M* Tris–HCl buffer, the more dilute the DNA concentration, the less the amount of salt in the sample preparation. Interestingly, as seen in Table I, a much higher signal was observed when the DNA concentration in the sample vial was actually much lower. This result is due to a higher electric field drop created in the low conductivity sample solution, with more sample being introduced into the capillary for the given injection condition. As further shown in Table I, the relative peak heights of three different fragments injected under the same conditions from a solution containing different buffer concentrations were compared. Nearly a 500-fold difference in the sample introduction could be observed due to the difference in buffer concentration. Therefore, in order to avoid any misinterpretation caused by the differences during injection, all the DNA preparations used in this study were diluted with distilled water or with TBE (Tris–borate–EDTA) buffer of constant concentration, and no salt was added to the hybridization mixtures.

Identification of hybridized species

Unless otherwise specified, annealing of DNA molecules was achieved by following conventional molecular biology protocols: heating at 65°C for 10 min fol-

[a] C = g N,N′-methylene bisacrylamide (Bis)/T; T = (g acrylamide + g Bis)/100 ml solution.

TABLE I

EFFECT OF BUFFER CONCENTRATION ON ELECTROKINETIC INJECTION

Restriction digest, ϕX 174 *Hae* III, was separated on a 9%T, 0%C, non-denaturing gel as described in [8]. The peak heights corresponding to 234, 271, and 603 base-pairs (bp) fragments were compared. More DNA was injected when the sample was diluted with distilled water. A nearly 500-fold increase in peak height was observed when the sample was diluted 1000-fold. Injection was done electrokinetically at 15 kV for 5 s.

DNA concentration (μg/ml)	Tris–HCl concentration (m*M*)	Relative peak height		
		Fragment 234 bp	Fragment 271 bp	Fragment 603 bp
1000	10	1	1	1
500	5	5	6	5
100	1	33	27	24
20	0.2	139	139	119
5	0.05	436	442	364
1	0.01	346	282	282

lowed by slow cooling to room temperature in 30 min [13]. Equal amounts of Joe-labelled M13 universal sequencing primer and a complementary 34-mer, pC2, were mixed and annealed, as described above. As shown in Fig. 1, the species that was successfully hybridized was identified by UV absorption (Fig. 1C) and laser induced fluorescence detection (Fig. 1E). It is interesting to note that the molecules smaller than pC1 (Fig. 1D), (arising possibly from synthesis failure), were apparently also hybridized onto pC2, as seen by the extra peaks in Figure 1E. pC2, which served as the target molecule and was untagged, was not observed with laser induced fluorescence detection.

Dissociation of the hybridized species by urea and heat

Urea is often used as a denaturing reagent in the gels for DNA sequence analysis [13]. To demonstrate further that the third peak observed in Fig. 1C and E was indeed the hybridized species of Joe-labelled primer and pC2, we injected the same hybridization mixture as in Fig. 1C into a 7 *M* urea gel-filled capillary. As shown in Fig. 2, no hybridized species could be observed. The overall migration rate was slower in the urea gel than in the column without the denaturant due in part to the increased viscosity when urea was included.

To further demonstrate the identity of the third peak in Fig. 1C and E, the hybridization was driven to completion at low temperature, as described below. As shown in Fig. 3C, a single hybridized species was observed in the electropherogram. The same mixture was heated to 65°C for 5 min before injection and, as shown in Fig. 3D, two peaks corresponding to the single stranded species reappeared along with the residual hybridized species.

Effect of probe concentration and temperature on hybridization

With on-line detection, several parameters that affect DNA hybridization in solution can be conveniently studied using capillary electrophoresis. Various ratios of

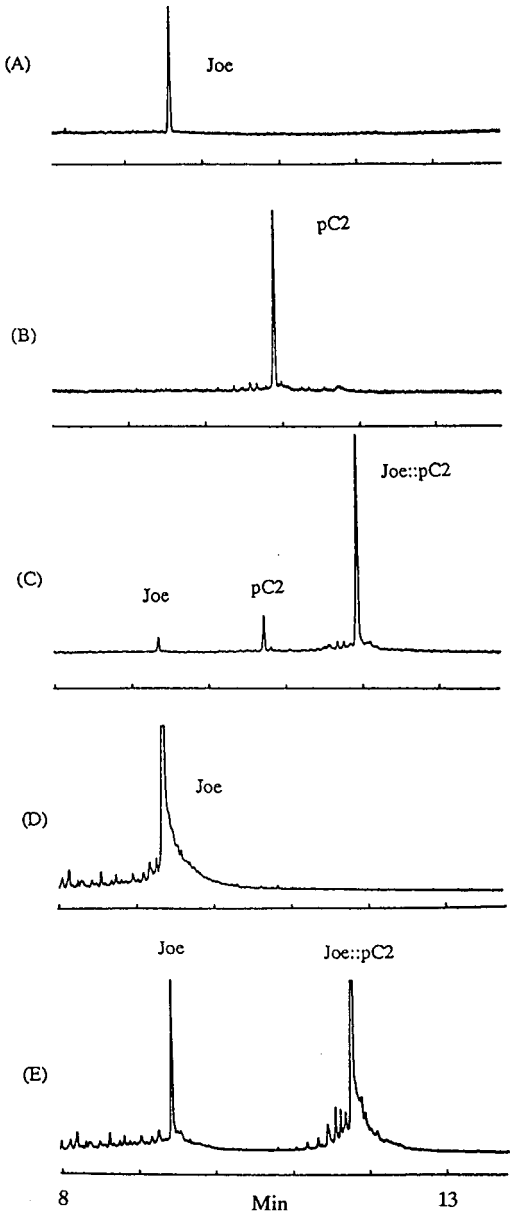

Fig. 1. Identification of DNA molecule by hybridization with a fluorescence-tagged oligonucleotide probe using capillary gel electrophoresis. (A) Joe-labelled 17-mer alone (5 μg/ml in 10 m*M* TBE). (B) pC2 alone (5 μg/ml in 10 m*M* TBE). (C) Equal amounts of Joe-labelled primer (10 μg/ml in 10 m*M* TBE) and pC2 (10 μg/ml in 10 m*M* TBE) were annealed prior to electrophoresis and were analyzed by UV absorption. (D) The same sample as (A) was analyzed by the laser system. (E) The same sample as (C) was analyzed by the laser system. The hybridized species was clearly identified either by UV (C) or by the laser system (E). The capillary was filled with 9%T, 0%C polyacrylamide gel with no urea. Total length of the capillary was 45 cm with an effective length of 25 cm. Injection was done electrokinetically at 13.5 kV for 5 s, and the electric field for electrophoresis was 300 V/cm.

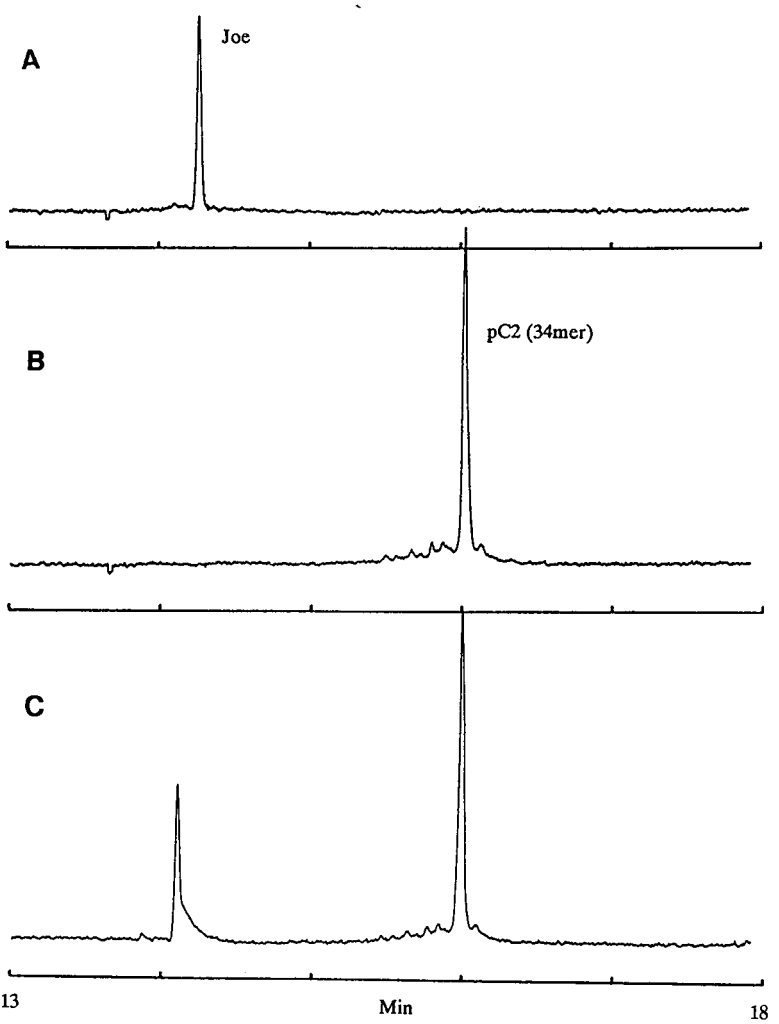

Fig. 2. Dissociation of the hybridized species in the urea gel. (A) Joe-labelled primer alone. (B) pC2 alone. (C) The same hybridization mixture as in Fig. 1 was analyzed in a 9%T, 0%C, 7*M* urea gel filled capillary with an effective length of 30 cm. Injection was done at 13.5 kV for 5 s, and the electric field for electrophoresis was 300 V/cm.

pC1 and complementary oligonucleotide, pC2, were annealed. As shown in Fig. 4, as expected, the amount of hybridized species increased as more probe was present. It is possible to drive the reaction to near completion with about a 10-fold molar excess of probe molecule.

In most molecular biology studies, heating followed by slow cooling is usually performed for the annealing of DNA molecules. However, as shown in Fig. 5, a much higher efficiency of hybridization is observed when the DNA mixture was incubated in dry ice without even heating. Indeed, a complete hybridization was often achieved with incubation in dry ice for *ca.* 10–15 min (data not shown).

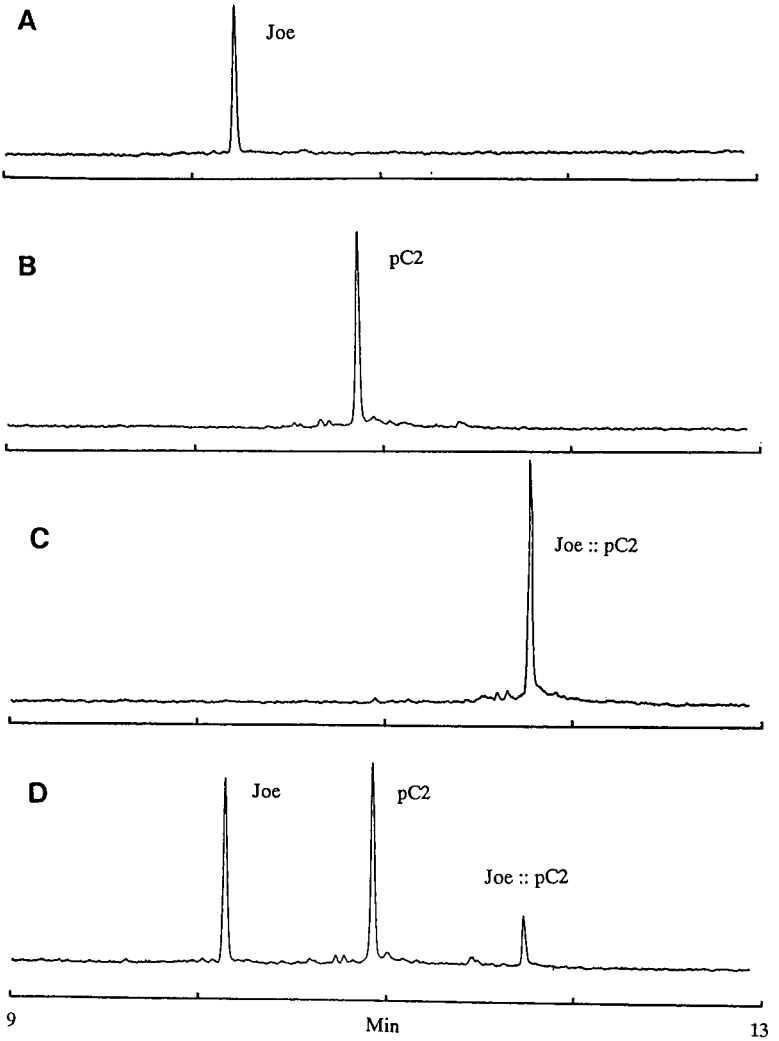

Fig. 3. Dissociation of the hybridized species by heat. (A) Joe-labelled primer alone. (B) pC2 alone. (C) Mixture of equal amounts of Joe-labelled primer and pC2 driven to a complete hybridization by incubating in dry ice. (D) After heating at 65°C for 5 min, the same mixture as in (C) was analyzed in the capillary. Two peaks corresponding to Joe-labelled primer and pC2 reappeared. The capillary was filled with 9%T, 0%C, non-denaturing gel. Total length of the capillary was 45 cm with an effective length of 25 cm. Injection was done at 13.5 kV for 5 s and the electric field for electrophoresis was 300 V/cm.

DISCUSSION

Since its development polymerase chain reaction (PCR) analysis has become one of the most important methodologies for molecular biology studies and also a powerful tool for the identification of genetic mutations and infectious agents [14]. However, very often, hybridization with a specific probe other than the primers used

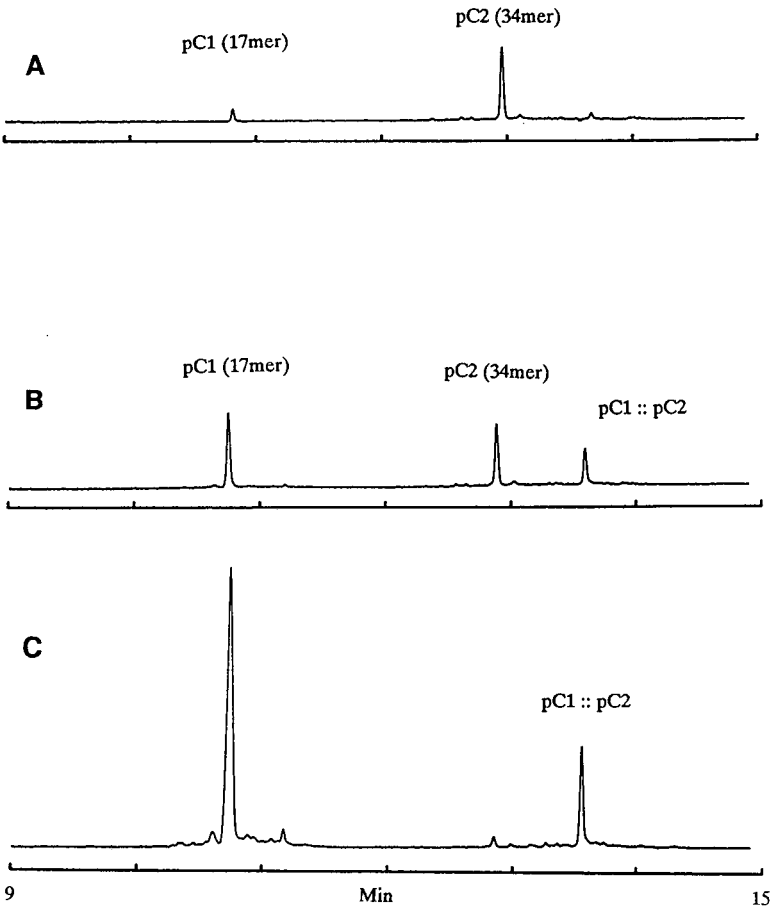

Fig. 4. Effect of probe concentration on hybridization. Various dilutions of pC1 and pC2 were prepared, and hybridization was performed with different molar ratios of pC1 and pC2. (A) Molar ratio of pC1 to pC2 is 2 to 5. (B) Molar ratio of pC1 to pC2 is 2 to 1. (C) Molar ratio of pC1 to pC2 is 10 to 1. The molar ratios of 1 to 5, 1 to 1, 4 to 1, and 20 to 1 have also been examined but not shown. A nearly complete hybridization was observed with a 10-fold molar excess of probe, as indicated by the disappearance of the peak corresponding to the target molecule, pC2. The electrophoretic conditions were the same as described in Fig. 3.

for the PCR reaction has been performed in order to assure the accuracy of the PCR products. Recent results obtained in this laboratory has shown that an ultra fast high-resolution separation of DNA fragments of less than 2000 bp can be easily achieved in less than 5 min. This makes capillary electrophoresis a potentially powerful tool for the analysis of PCR products. Moreover, with the highly sensitive laser induced fluorescence detection system and the possibility of performing on-line Southern blotting with a specific fluorescence tagged oligonucleotide probe, capillary electrophoresis has the possibility of becoming a screening tool for genetic mutations and infectious diseases in conjunction with PCR analysis. In this paper, we have demonstrated such a possibility with small single-stranded DNA molecules. For dou-

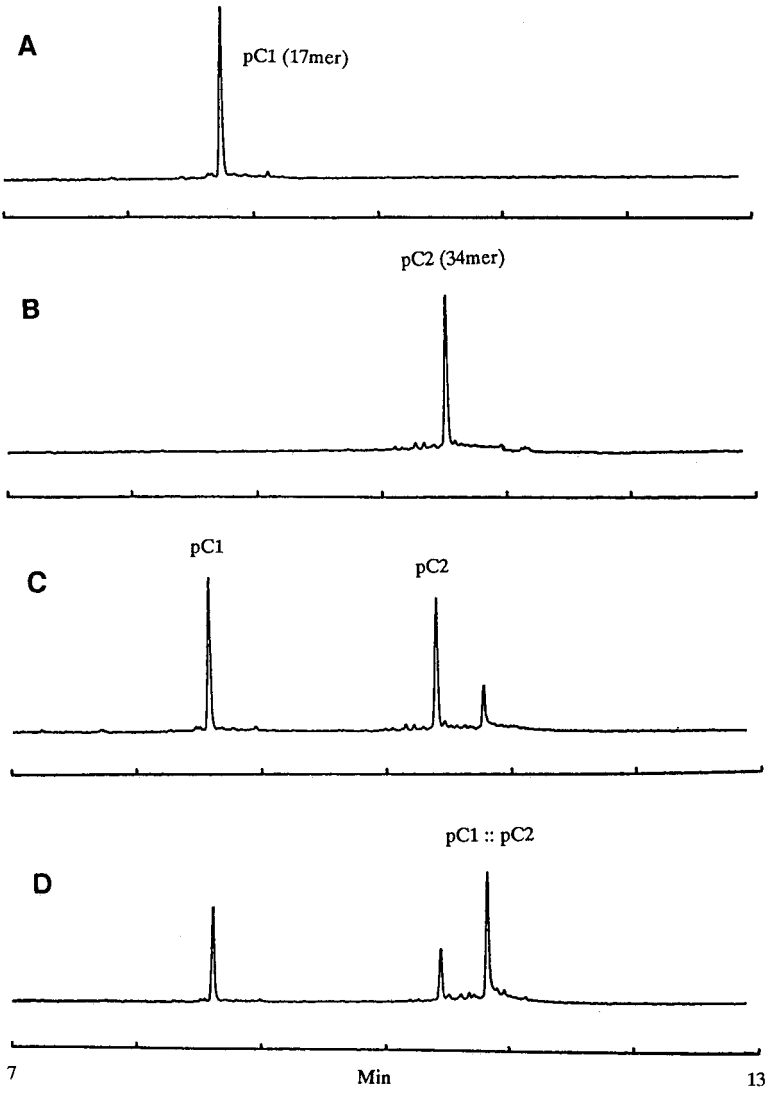

Fig. 5. Optimal incubation temperature for hybridization. (A) pC1 alone. (B) pC2. (C) Equal amounts of pC1 and pC2 were mixed and incubated in ice for 5 min before injection. (D) Equal amounts of pC1 and pC2 were mixed and incubated in dry ice for 5 min before injection. The extent of hybridization was greatly enhanced at low temperature and a nearly complete hybridization was achieved by incubating the mixture in dry ice for 10 min (data not shown). The electrophoretic conditions were the same as described in Fig. 3.

ble-stranded DNA molecules, however, we have observed rather inconsistent results. Further studies on the behavior of ds DNA and the possible effects of high electric field on "D-Loop" structure are needed. Nevertheless, potential applications can still be derived with similar approaches reported in this paper due to the fact that single-stranded products can be generated by asymmetric PCR reaction with appropriate

ratios of two primers and that single-stranded molecules are more accessible to hybridization with oligonucleotide probes.

It is well known that double-stranded DNA molecules migrate faster than single-stranded molecule of the same molecular weight. However, the hybridized species observed in this study apparently migrated more slowly than the single-stranded oligonucleotides. This may be due to the fact that the hybridized molecule still carried some single-stranded overhang on both ends.

It was quite surprising to note that a direct incubation at low temperature was actually the best annealing condition, although heating followed by slow cooling is recommended by most molecular biology protocols. However, in most molecular biology studies, hybridization has been done with membrane-bound DNA molecules, and any degree of annealing that sustains the washing procedure would generate identical positive responses on a subsequent autoradiogram. It is speculated that the high electric field (100–300 V/cm) used in capillary electrophoresis may disrupt molecules that are not perfectly annealed. Therefore, the higher annealing efficiency observed for low temperature may simply indicate the extent of perfectly annealed molecules. On the other hand, since the annealing in the study was performed without salt, it is also possible that low temperature provides a more favorable condition for DNA annealing in low ionic strength solutions. Interestingly, a similar result was reported by Casanova *et al.* [15] who found that −70°C was the best annealing condition for sequence analysis of double-stranded PCR products.

DNA molecules separated on a capillary can also be collected and immobilized on a membrane. Further confirmation with specific probes, similar to conventional Southern Blotting, could then be performed. Further studies are needed for identification of double stranded DNA molecules or even genomic DNAs using Southern Blotting with capillary gel electrophoresis.

ACKNOWLEDGEMENT

The authors gratefully acknowledge support of this work under DOE grant No.DE-FG02-90ER60985, Human Genome Project. Contribution number 479 from the Barnett Institute.

REFERENCES

1 B. L. Karger, A. S. Cohen and A. Guttman, *J. Chromatogr.*, 492 (1989) 585–614.
2 M. J. Gordon, X. Huang, S. L. Pentoney and R. N. Zare, *Science (Washington, D.C.)*, 242 (1988) 224–228.
3 A. S. Cohen, D. R. Najarian, A. Paulus, A. Guttman, J. A. Smith and B. L. Karger, *Proc. Natl. Acad. Sci. U.S.A.*, 85 (1988) 9660–9663.
4 A. Guttman, A. S. Cohen, D. N. Heiger and B. L. Karger, *Anal. Chem.*, 62 (1990) 137–141.
5 J. A. Luckey, H. Drossman, A. J. Kostichka, D. A. Mead, J. D'Cunha, T. B. Norris and L. M. Smith, *Nucl. Acids Res.*, 18 (1990) 4417–4421.
6 H. Swerdlow and R. Gesteland, *Nucl. Acids Res.*, 18 (1990) 1415–1419.
7 A. S. Cohen, D. R. Najarian and B. L. Karger, *J. Chromatogr.*, 516 (1990) 49–60.
8 D. N. Heiger, A. S. Cohen and B. L. Karger, *J. Chromatogr.*, 516 (1990) 33–48.
9 M. Zhu, D. L. Hansen, S. Burd and F. Gannon, *J. Chromatogr.*, 480 (1989) 311–319.
10 A. M. Chin and J. C. Colburn, *Am. Biotechnol. Lab.*, December (1989) 16.
11 E. M. Southern, *J. Mol. Biol.*, 98 (1975) 503–517.

12 S. Hjertén, *Arch. Biochem. Biophys.*, 1 (1962) 147–151.
13 T. Maniatis, E. F. Fritsch and J. Sambrook, *Molecular Cloning: A Laboratory Manual*, Cold Spring Harbor University Press, Cold Spring Harbor, 1982.
14 H. A. Erlich (Editor), *PCR Technology*, Stockton Press, New York, 1989.
15 J.-L. Casanova, C. Pannetier, C. Jaulin and P. Kourilsky, *Nucl. Acids Res.*, 18 (1990) 4028.

Journal of Chromatography, 559 (1991) 307–315
Elsevier Science Publishers B.V., Amsterdam

CHROM. 23 413

Assessment of capillary electrophoresis in pharmaceutical applications

Analysis and quantification of a recombinant cytokine in an injectable dosage form

NORBERTO A. GUZMAN*, HAIDER ALI, JOHN MOSCHERA, KHURSHID IQBAL and A. WASEEM MALICK

Pharmaceutical Research and Development, Hoffmann-La Roche Inc., Nutley, NJ 07110 (USA)

ABSTRACT

Several methods are available for determining the components present in a typical pharmaceutical dosage form. Although some of these methods are simple and have received wide pharmaceutical industry acceptance over many years, several limitations still need to be overcome. Capillary electrophoresis was examined as an alternative method for the determination of a recombinant cytokine in a pharmaceutical dosage form. The results show that capillary electrophoresis can separate the recombinant cytokine from its dosage form matrix adequately, rapidly and with minimum sample volume requirements. Owing to its high efficiency, high resolution and simplicity, capillary electrophoresis appears to be very applicable to pharmaceutical samples. For reliable quantification of the resulting data, however, it is essential to optimize the experimental conditions, such as separation buffer and capillary column temperature. The advantages and potential of capillary electrophoresis for the separation of active ingredients and excipients in pharmaceutical formulations are discussed.

INTRODUCTION

Many techniques have been developed for the assay and quality control of proteins and peptides in pharmaceutical formulations, such as radioimmunoassay (RIA), enzyme-linked immunosorbent assay (ELISA), bioassay, polyacrylamide gel electrophoresis (PAGE) and high-performance liquid chromatography (HPLC) (for a review, see refs. 1 and 2). Each of these techniques, however, has certain limitations, including the complexity and time-consuming nature of assay development, the relatively large amounts of sample required to reach a reasonable level of sensitivity and the high degree of assay variability. Consequently, we have evaluated capillary electrophoresis (CE), which is capable of high resolution and high detection sensitivity, as a complementary technique for the analysis of pharmaceutical formulations. In CE, a high-voltage electric field induced across a small-bore fused-silica capillary provides

0021-9673/91/$03.50

the driving force needed to separate the components of the assay sample [3–6]. The inherently high resolving power of CE not only permits the separation of the protein or peptide from its formulation excipients, but also makes it possible to assess minute changes in protein structure (*e.g.*, deamidation, oxidation) which might have profound effects on drug stability and bioactivity.

In this work, we examined the use of CE to separate and quantify two recombinant human cytokines (leukocyte A interferon and interleukin-1 α) in a formulation mixture and in an actual pharmaceutical dosage form.

EXPERIMENTAL

Reagents and samples

High-purity potassium hydroxide, sodium phosphate, sodium tetraborate, hydrochloric acid and lithium chloride were obtained from Sigma (St. Louis, MO, USA). Millex disposable filter units (0.22 μm) were purchased from Millipore (Bedford, MA, USA). Fused-silica capillary columns were obtained from Scientific Glass Engineering (Austin, TX, USA) and Polymicro Technologies (Phoenix, AZ, USA). Recombinant human leukocyte A interferon and recombinant interleukin-1 α purified bulk drug substances were prepared at Hoffmann-La Roche (Nutley, NJ, USA). Human serum albumin (Albuminar-25) was purchased from Armour Pharmaceutical (Kankake, IL, USA) and N-acetyltryptophan was obtained from Cyclo Chemical, a division of Travenol Labs. (Los Angeles, CA, USA). Triply distilled, deionized water was used for the preparation of buffer solutions. Capillary electrophoresis buffers were routinely degassed and sonicated under vacuum after filtration.

Assay samples

Formulation mixtures of recombinant leukocyte A interferon (400 μg/ml), recombinant interleukin-1 α (200 μg/ml) and a combination of recombinant leukocyte A interferon (400 μg/ml) and recombinant interleukin-1 α (200 μg/ml) were prepared by adding the appropriate amounts of the purified bulk drug substance to 0.05 *M* sodium phosphate buffer solution (pH 7.0) containing 500 μg/ml of human serum albumin (HSA) and 50 μg/ml of N-acetyltryptophan. A typical pharmaceutical liquid dosage form of recombinant human interleukin-1 α (200 μg/ml) was also prepared and used for CE analysis.

Instrumentation

The initial separation experiments were performed using a laboratory-made capillary electrophoresis apparatus similar to that described previously [3,4]. Samples were injected electrokinetically and the electropherograms were recorded and integrated using a Model L-6512 strip-chart recorder (Linseis, Princeton Junction, NJ, USA) at 20 cm/h, and a Model 3390 integrator (Hewlett-Packard, Avondale, PA, USA). For the controlled-temperature experiment a commercial instrument was used (P/ACE System 2000; Beckman Instruments, Palo Alto, CA, USA). In this instrument, the capillary is housed in a cartridge configured to allow a flow of recirculating liquid with Peltier temperature control of the capillary. Samples were injected by pressure and the data acquisition and analysis were carried out using System Gold Chromatography Software (Beckman Instruments, San Ramon, CA, USA).

Procedure

The CE separations were performed using a 0.05 *M* sodium tetraborate buffer (pH 8.3) containing 0.025 *M* lithium chloride. Alternative buffers used previously [3,4], such as 0.05 *M* sodium phosphate buffer (pH 7.0) and 0.05 *M* sodium tetraborate buffer (pH 8.3), were also used. Samples to be assayed were transferred to the appropriate application vessel, *i.e.*, a 1.5-ml microcentrifuge tube or P/ACE sample holder, and applied to the capillary as described below. On completion of each run, the capillary column was cleaned by injection of 0.1 *M* sodium hydroxide solution, followed by distilled water, and then regenerated with fresh buffer solution.

Running conditions

For the laboratory-made instrument, a 89 cm (41 cm to the detector) × 75 μm I.D. capillary column was used. Samples were injected electrokinetically at 10 kV for 12 s and then separated at 13 kV at ambient temperature. Under these conditions, *ca.* 12 nl of solution were injected into the capillary column. Monitoring of the samples was carried out at 210 nm.

For the P/ACE system 2000, a 57 cm (50 cm to the detector) × 75 μm I.D. capillary column was used. Samples were injected by a positive nitrogen pressure of 3500 Pa for 3 s and then separated at 10 kV at 20, 25 or 30°C. Under these conditions, *ca.* 15 nl of solution were injected into the capillary column. Monitoring of the samples was carried out at 200 nm.

RESULTS

Fig. 1 depicts the electropherograms of the two cytokine formulations tested: recombinant human leukocyte A interferon in a formulation mixture containing HSA and N-acetyltryptophan, and recombinant human interleukin-1 α in a pharmaceutical dosage form containing the same excipients. Both the leukocyte A interferon (peak 1) and the interleukin-1 α (peak 2) were well separated from the excipients HSA (peak 3) and N-acetyltryptophan (peak 4). Further, the separation and resolution demonstrated in these electropherograms were maintained when the formulation containing the interleukin-1 α was spiked with a comparable amount of leukocyte A interferon prior to analysis (Fig. 2).

The observed electropherograms for both cytokine samples were complex, indicating the presence of major and minor component peaks migrating in addition to the main components identified. It is interesting that leukocyte A interferon, which routinely assays at greater than 95% purity by PAGE and HPLC, was resolved into two peaks by CE. At present, the nature of the separation achieved and the identity of the second peak component are unknown. For the interleukin-1 α sample, the additional peak eluting just after the main cytokine peak most likely corresponds to its deamidation byproduct.

Buffer composition was observed to play an important role in the selectivity (*i.e.*, resolution and peak sharpeness) of separation. Although sodium phosphate buffer (pH 7.0) and sodium tetraborate buffer (pH 8.3) were able to resolve the various analytes present in the two kinds of samples (data not shown), an increased selectivity was apparent with the sodium tetraborate buffer when it was supplemented with 0.025 *M* lithium chloride. We are currently investigating the effects of salts such as lithium chloride in the separation of proteins and peptides by CE.

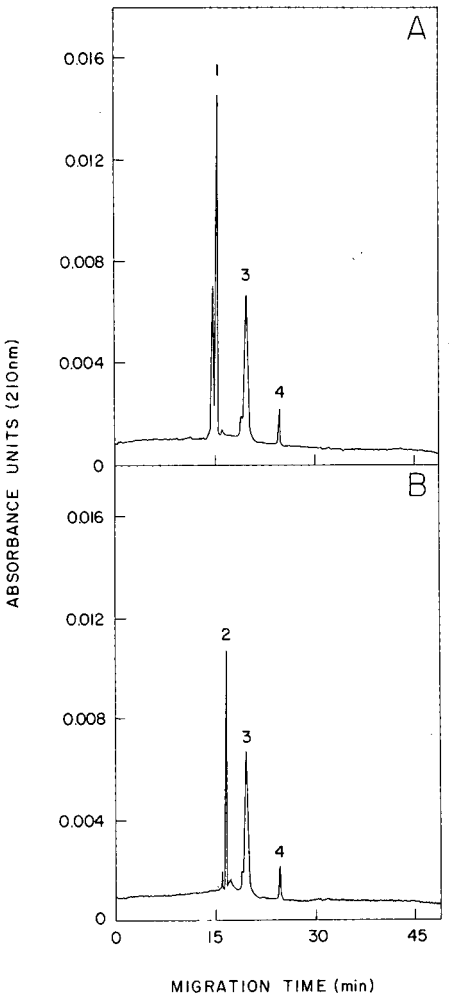

Fig. 1. Capillary electrophoresis profile of the cytokines interferon and interleukin. (A) Electropherogram of a formulation mixture containing recombinant leukocyte A interferon (peak 1), human serum albumin (peak 3) and N-acetyltryptophan (peak 4). (B) Electropherogram of an actual pharmaceutical dosage form containing recombinant interleukin-1 α (peak 2), human serum albumin (peak 3) and N-acetyltryptophan (peak 4).

In order to test the reproducibility when using the simple laboratory-made instrument at ambient running temperature, a solution of HSA was assayed six times over a period of *ca.* 4 h. As in the standard assay procedure, cleaning of the capillary column was carried out after every injection. Albumin was selected as a model protein as it is known to have an affinity for glass and might conceivably bind to the walls of the capillary column. Proteins in general are known to adsorb to fused silica [7]. As shown in Table I, the reproducibility of the electropherograms for both migration time and peak area recovery was excellent.

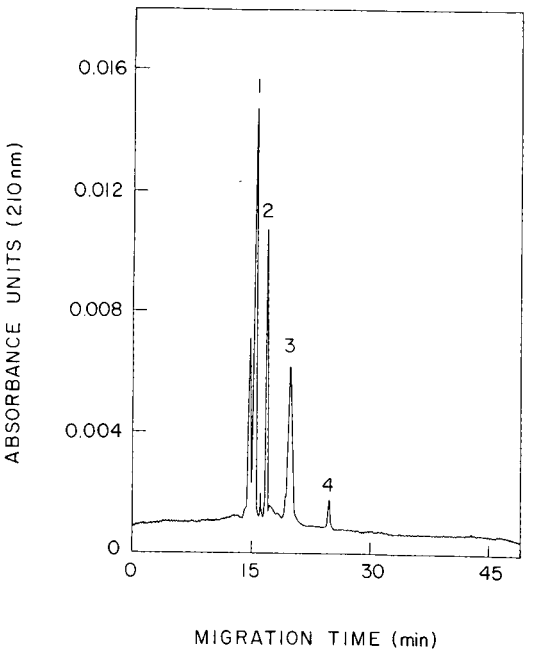

Fig. 2. Capillary electrophoresis profile of an actual pharmaceutical dosage form containing recombinant interleukin-1 α (peak 2), human serum albumin (peak 3), N-acetyltryptophan (peak 4) and spiked with recombinant leukocyte A interferon (peak 1).

The effect of variations in running temperature on the CE analysis was also investigated. Thermal experiments were performed using the P/ACE System 2000 CE instrument, which is constructed so as to allow fine temperature control of the capillary column. Separations were performed at 20, 25 and 30°C. The results of the temperature study are shown in Fig. 3 and Table II. The data shows that when the

TABLE I

PRECISION OF MIGRATION TIME AND ELECTROPHEROGRAM PEAK AREA FOR HUMAN SERUM ALBUMIN

Run No.	Migration time (s)	Peak area (units)
1	1489	15.77
2	1478	15.02
3	1487	16.52
4	1473	15.98
5	1483	16.09
6	1476	15.25
Mean	1481.00	15.77
Standard deviation	6.36	0.56
Relative standard deviation (%)	0.43	3.52

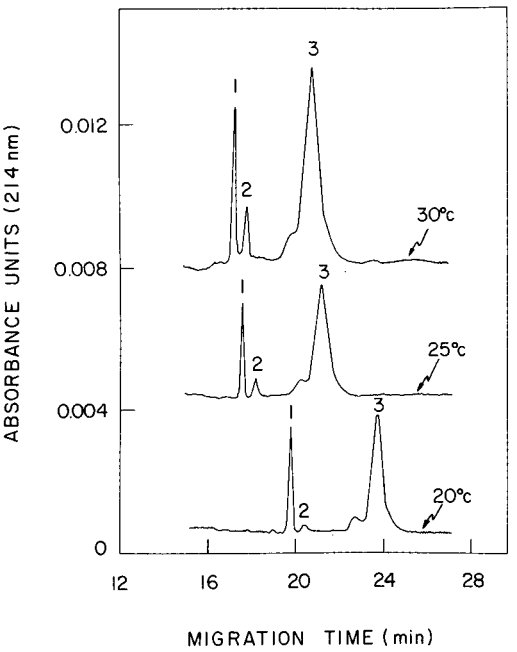

Fig. 3. Effect of temperature on migration times and peak areas of the sample components when subjected to 20, 25 and 30°C during separation. Electropherogram of an actual pharmaceutical dosage form containing recombinant interleukin-1 α, human serum albumin and N-acetyltryptophan. Peak 1 represents the intact interleukin-1 α, peak 2 its putative deamidation byproduct and peak 3 human serum albumin.

TABLE II

EFFECT OF TEMPERATURE ON THE MIGRATION TIMES AND PEAK AREAS OF ANALYTES BY CAPILLARY ELECTROPHORESIS

Temperature (°C)	Substance	Migration time (s)	Peak area (normalized percentage)
20	Interleukin	1178	20.32
	Deamidation product	1214	1.77
	Albumin	1425	77.91
25	Interleukin	1045	15.32
	Deamidation product	1081	3.27
	Albumin	1262	81.41
30	Interleukin	1020	12.59
	Deamidation product	1056	4.20
	Albumin	1232	83.21

temperature of the capillary column was increased the proteins migrated more rapidly, resulting in shorter separation times. The effects of an elevated running temperature on resolution and analyte recovery, however, were more complex. This is evident in the case of HSA (Fig. 3, peak 3), which at higher temperature shows an increase in peak area but a decrease in resolution. The interleukin-1 α (Fig. 3, peak 1), on the other hand, shows a decrease in recovery at higher temperature accompanied by an increase in the proportion of peak 2, its putative deamidation byproduct. On the basis of these findings, *i.e.*, diminished resolution and decreased stability, the use of an enhanced running temperature for these samples appears to be undesirable.

The effects of running conditions on the CE analysis are reflected in the observed relative standard deviations, which ranged between 0.4% and 2.0% for migration times and between 1.9% and 5.5% for peak areas, depending on the nature of the buffer, the separation temperature and the kind of instrument used (data not shown). The importance of temperature control in capillary electrophoresis for maintaining high resolution of the analytes and high efficiency of the technique has been described previously [8,9].

As interleukin-1 α apparently undergoes a temperature-dependent degradation in the capillary column during CE analysis, an attempt was made to generate a calibration graph for this cytokine under the most adverse conditions (30°C). Despite the enhanced degradation of the protein in the capillary column, the detection signal (peak area units) appears to be linear up to a cytokine concentration of 100 μg/ml. At the higher concentration tested (200 μg/ml), the observed peak area was slightly lower than expected. Hence, quantification of interleukin-1 α by CE appears to be at least feasible.

DISCUSSION

Protein and peptide components of a pharmaceutical formulation must be analyzed with an appropriate biological and/or chemical assay. The chemical assay of a protein or peptide drug substance in a pharmaceutical dosage form presents several unique problems. In general, pharmaceutical and diagnostic products are not present simply as pure substances but rather as complex formulated mixtures. Often, several chemical components or excipients are added for specific purposes, such as to enhance stability during storage, or to provide protection through a manufacturing process step (*i.e.*, freeze-drying or sterile filtration). Many of the excipients used in the formulations, however, are themselves proteinaceous in nature. In addition, because of the inherently strong biological potency of most of the protein and peptide drugs, the dosage forms usually contain only a few micrograms of the active drug. Commonly these drug substances must be protected by milligram amounts of excipients.

For a chemical assay, therefore, the method used should have sufficient sensitivity for measuring the low levels of drug substance in the dosage form and, at the same time, have the resolving power necessary to separate it from large amounts of excipients. Further, the method must have the consistent linearity required to encompass all dosage strengths expected. Unfortunately, many of the procedures currently available for the analysis of proteins and peptides in pharmaceutical dosage forms have some limitations. The assay methods used are frequently characterized as being nonspecific for the protein of interest, imprecise, subject to interference by other sub-

stances present, limited in sensitivity or non-linear over the range desired. Capillary electrophoresis, a method that offers many unique features, such as high resolution, high mass sensitivity (minimum sample requirements) and simplicity, may be able to address some of these limitations.

The experiments described here demonstrate that CE has the sensitivity and degree of resolution required for the analysis of two representative cytokines, interleukin-1 α and leukocyte A interferon, in typical formulation mixtures. Both cytokines were well separated from their excipients in a relatively short time and with a minimum sample requirement. The resulting electropherograms generated with either the simple CE apparatus, operating under ambient temperature conditions, or with the more sophisticated CE unit, using Peltier temperature control of the capillary column and operating at a specific isothermal temperature, show excellent reproducibility.

Capillary column temperature was observed to have an important influence on the electrophoretic results. With interleukin-1 α, for example, an enhanced operating temperature contributed to a faster migration rate resulting in a shorter separation time of the cytokine. Higher temperatures, however, also resulted in an increased degree of degradation of the cytokine, presumably through a deamidation pathway. Temperature influences diverse factors such as electric current, viscosity of the electrophoretic media, ionization of the migrating species, degree of electroosmotic flow, and the extent of surface adsorption of components to the capillary column. Each of these factors may contribute, to varying extents, to the overall characteristics of the run. Elevation of the running temperature in CE with increased current has been associated with parallel decreases in the viscosity of the electrophoretic buffer and in the efficiency of separation [8]. A higher running temperature may also affect the stability of the protein being analyzed. Deamidation of asparagine and/or glutamine residues is one of the most common non-enzymatic covalent modifications of proteins [10–15], and it is known that the rate of deamidation increases with temperature, and in the presence of certain buffer ions [11].

Finally, the CE running temperature seems to influence the recovery of proteins from the capillary column, as represented by relative absorbance (peak area). It is possible that at lower separation temperatures, protein adheres to the walls of the capillary more readily than at higher separation temperatures. On the other hand, it may also be possible that the amount of sample injected into the capillary column varies according to the method of injection and the temperature of the system. As a consequence, system and method differences may have a marked effect on the quantification of data. For samples such as interleukin-1 α dosage form, strict control of the temperature of the capillary column during separation is essential in order to apply CE as a quantitative analytical method. This is critical as the separation profile, and stability of the protein, appear to be influenced by as little as a 5°C variation in temperature.

CONCLUSIONS

Capillary electrophoresis has been clearly demonstrated to be a promising method for the separation of active ingredients and excipients in pharmaceutical formulations. Further, the incorporation of a temperature control system (during the

separation of analytes) is an important factor for maintaining constant column resistance, optimizing separation efficiency, reducing sample decomposition and maintaining a desired chemical equilibrium. The control of temperature is an essential parameter to yield an acceptable degree of reproducibility of the migration times during the analysis of the active ingredients of a dosage form. For quantification of proteins such as interleukin-1 α, which might be subject to degradation during separation, the running conditions must be modified to minimize degradation and appropriate standards developed. When the additional work has been completed, capillary electrophoresis should complement, if not surpass, existing methodology for the investigation of proteins in pharmaceutical dosage forms.

REFERENCES

1 F. M. Bogdansky, *Pharm. Technol.*, 11 (1987) 72-74.
2 Y.-C. J. Wang and M. A. Hanson, *J. Parenter. Sci. Technol.*, 42 (1988) S3–S25.
3 N. A. Guzman, L. Hernandez and B. G. Hoebel, *BioPharm.*, 2 (1989) 22–37.
4 N. A. Guzman, L. Hernandez and S. Terabe, in J. Nikelly and C. Horvàth (Editors), *Analytical Biotechnology. Capillary Electrophoresis and Chromatography (ACS Symposium Series*, 434), 1990, American Chemical Society, Washington, DC, 1990, Ch. 1, pp. 1–35.
5 R. A. Wallingford and A. G. Ewing *Adv. Chromatogr.*, 29 (1990) 1–76.
6 D. M. Goodall, D. K. Lloyd and S. J. Williams, *LC·GC*, 8 (1990) 788–799.
7 M. M. Bushey and J. W. Jorgenson, *J. Chromatogr.*, 480 (1989) 301–310.
8 R. J. Nelson, A. Paulus, A. S. Cohen, A. Guttman and B. L. Karger, *J. Chromatogr.*, 480 (1989) 111–127.
9 R. S. Rush, A. S. Cohen and B. L. Karger, *Anal. Chem.*, 63 (1991) 1346–1350.
10 A. B. Robinson and C. J. Rudd, *Curr. Top. Cell. Regul.*, 8 (1974) 27–295.
11 K. Ü. Yüksel and R. W. Gracy, *Arch. Biochem. Biophys.*, 248 (1986) 452–459.
12 T. Geiger and S. Clarke, *J. Biol. Chem.*, 262 (1987) 785–794.
13 K. Patel and R. T. Borchardt, *J. Parenter. Sci. Technol.*, 4 (1990) 300–301.
14 A. R. Friedman, A. K. Ichhpurani, D. M. Brown, R. M. Hillman, L. F. Krabill, R. A. Martin, H. A. Zurcher-Neely and D. M. Guido, *Int. J. Pept. Res.*, 37 (1991) 14–20.
15 H. T. Wright, *Crit. Rev. Mol. Biol.*, 26 (1991) 1–52.

Journal of Chromatography, 559 (1991) 317–324
Elsevier Science Publishers B.V., Amsterdam

CHROM. 23 418

Free solution capillary electrophoresis of proteins using untreated fused-silica capillaries

KONG-JOO LEE* and GWI SUK HEO

Organic Analytical Laboratory, Korea Standards Research Institute, P.O. Box 3, Daejonsi Daeduk Science Town 305-606 (South Korea)

ABSTRACT

Numerous efforts have been made to separate proteins by capillary zone electrophoresis (CZE). The most common optimization techniques are changing the pH of the running buffer, coating the capillary surface with a hydrophilic polymer, or using additives in the sample solution. Surface coatings and solution additives can reduce the adsorption of the protein onto the capillary surface, but they diminish the separation efficiency and the resolution of CZE. This paper reports the successful separation of proteins in a untreated fused-silica capillary by raising the pH of the running buffer and washing between runs with 1.0 *M* sodium hydroxide. Under these conditions, model proteins and proteins in human serum have been determined by CZE. It is shown that the results from CZE are compatible with those of sodium dodecyl sulphate–polyacrylamide gel electrophoresis.

INTRODUCTION

Small organic molecules, including amino acids, small peptides, bases and water-soluble vitamines, can be separated by capillary zone electrophoresis (CZE) or micellar electrokinetic capillary chromatography in untreated fused-silica capillaries [1–3]. When CZE is applied to the separation of multicharged proteins, however, adsorption becomes a serious problem [1].

Several strategies have been developed to overcome the problems caused by the adsorption of proteins onto the silanol surface of fused-silica capillaries. First, to remove the Coulombic interaction between the charged proteins and the silanol surface, running buffers of various pH values can be used. For fully protonated silanols, pH values lower than three have been used to remove the negative charges from the capillary surface [4]. Although some proteins can be separated, most are aggregated or precipitated under acidic conditions. In addition, separations of proteins without electroosmotic flow are insufficient. The use of higher pH values (above 9), where most of the proteins are negatively charged above their p*I* values is fairly successful in the separation of proteins [5,6]. Second, the use of a polymer-coated tube for CZE was described by Hjertén [7] and Zhu *et al.* [8]. Although capillaries coated with a hydrophilic polymer reduce the adsorption of the protein and the electroosmotic flow, the separations take longer and the peak resolution is decreased. Third, alkali

metal salts were used in the running buffer to minimize the adsorption of proteins by competition between potassium ions and proteins on the silanol surfaces [9]. As an increase in conductivity requires the use of a lower voltage, the separation times are very long (> 30 min). Finally, additives such as ethylene glycol were used in the sample solutions [6]. Combining a higher pH running buffer with additives, gave reproducible protein separations, except for ethylene glycol itself, which showed extra peaks by forming complexes with the borate buffer.

In this study, separations of model proteins of various p*I* values were performed using a high pH running buffer. Conventional protein analysis was performed with sodium dodecyl sulphate–polyacrylamide gel electrophoreis (SDS-PAGE), in which separations are based on the molecular weights of proteins [10]. The separation of proteins by CZE, which is mainly based on the p*I* values of proteins, are compared with the SDS-PAGE separation of modified human serum proteins. These results provide sound correlations between conventional gel electrophoresis and CZE.

EXPERIMENTAL

Apparatus

The CZE system used is similar to that described previously [1]. A high-voltage power supply (0–40 kV, Glassman, Whitehouse Station, NJ, USA; Model PS/EH 40R 2.5CTZR) was used to drive electrophoretic process across the capillary. The platinum wires connected to the anode and cathode of the power supply were immersed in 3 ml of buffer. This system was isolated in a Plexiglass box for operator safety.

A straight length of fused-silica capillary (Polymicro Technologies, Phoenix, AZ, USA), 100 cm long (63.5 cm to detector, 360 μm O.D. × 50 μm I.D.) was used as a separation tube. Detection was performed by the on-column measurement of UV absorption at 200 nm with an ISCO CV^4 UV detector (ISCO, Lincoln, NE, USA).

CZE procedure

Prior to each run the capillary was rinsed with 1 *M* sodium hydroxide solution, distilled water and running buffer. The capillary was filled with running buffer, usually 50 m*M* sodium borate buffer, pH 9.5, or various buffers as indicated in the figure legends. A sample was introduced by siphoning at a height of 15 cm. Using this sample injection techniques 5–15 nl of sample solution were carried into the capillary. The analysis was performed by applying a 20–30-kV voltage in the constant voltage mode.

Reagents

Proteins containing isoelectroic point (p*I*) standards (amyloglycosidase from *Aspergillus niger*, trypsin inhibitor from soybean, β-lactoglobulin A from bovine milk, carbonic anhydrase II from bovine erythrocyte, carbonic anhydrase I from human erythrocyte, myoglobin from horse heart and trypsinogen from bovine pancreas), SDS, acrylamide, glycine, N,N,N′,N′-tetramethylethylenediamine (TEMED), bovine serum and protein A-Sepharose were purchased from Sigma (St. Louis, MO, USA). The immunoaffinity matrix ALB-AWAY was from Kendrick Labs. (Madison, WI, USA). Human standard serum, SRM 909, was obtained from the National

Institute of Standards and Technology (NIST) (Gaithersburg, MD, USA). Samples of patient serum were gifts from Chungnam Medical School (Daejon, South Korea).

Sample preparation

Albumin-depleted serum were prepared using a immunoaffinity matrix (ALB-AWAY) as decribed previously [11]. Briefly, 10 μl of serum were incubated with 100 μl of 75 m*M* sodium phosphate buffer, pH 7.4, and 100 μl of pre-washed ALB-AWAY immunoaffinity gel for 2 h at room temperature. The supernanant liquid was separated and analyzed by CZE and SDS-PAGE.

Immunoglobulin G (IgG) was removed from human serum using protein A-Sepharose. Human serum (100 μl) was mixed with 0.15 *M* phosphate buffer (pH 8.0, 300 μl) and the mixture was shaken at room temperature for 4 h. The supernatant was kept for CZE and SDS-PAGE analysis.

IgG-binding protein A-sepharose gel was briefly washed with 0.1 *M* citrate buffer, pH 3.5, to obtain IgG. The supernatant containing IgG was analyzed.

Gel electrophoresis

The protein patterns of serum samples were analyzed by SDS-PAGE under non-reducing conditions. The proteins were separated on a 10% polyacrylamide slab gel by the Laemmli procedure [10]. The gels were stained with Coomassie Brilliant Blue.

RESULTS AND DISCUSSION

Separation of model proteins by CZE

The adsorption of proteins on an uncoated fused-silica capillary at neutral pH has been illustrated previously [1,8]. Although several workers have tried to overcome this problem by deactivating the silanol surface of the capillary using a low pH [4], high salt concentration [9], or by coating the surface with hydrophilic polymers [8], the reduction in electroosmotic flow diminishes the high separation efficiencies and fast separation which are the advantages of CZE.

The separation of proteins in an uncoated fused-silica capillary at alkaline pH using 50 m*M* sodium borate buffer, pH 9.5, is demonstrated in Fig. 1. In this buffer, the electropherogram of these model proteins at 22 kV showed sharp peaks. Glycine contamination in the model proteins gives two broad peaks, which are consistent with pure glycine at this pH.

This procedure is similar to that reported by Lauer and McManigill [5] in which the reproducibility was poor and the peaks deteriorated. In this experiment, the run-to-run reproducibility of migration time and peak height have been improved, as shown in Table I, by washing the capillary between analyses.

The coefficients of variation (C.V.) in retention time are less than 0.5% and those in peak height are less than 4%, except for the small peaks 3 and 7. Differences between these data and those reported previously [5] may be caused by differences in the nature of the chosen proteins. Depending on the nature of the proteins, including the p*I* value, hydrophobicity, molecular weight and structure, the adsorption of proteins during separation by CZE can be changed.

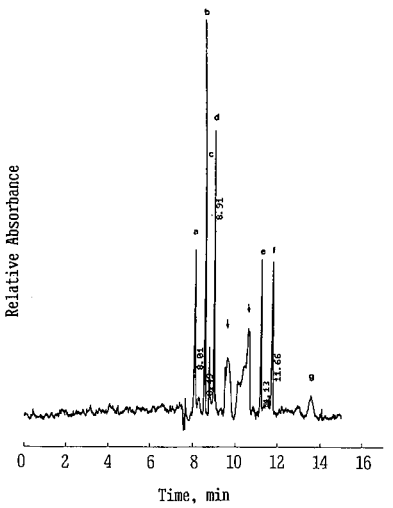

Fig. 1. Zone electrophoretic separation of seven model proteins on a 100 cm × 50 μm I.D. bare fused-silica column. Peaks: a = Trypsinogen, p*I* = 9.3, mol. mass = $24.5 \cdot 10^3$; b = myoglobin, p*I* = 6.8, 7.2, mol. mass = $17.5 \cdot 10^3$; c = carbonic anhydrase I, p*I* = 6.6, mol. mass = $29.7 \cdot 10^3$; d = carbonic anhydrase II, p*I* = 5.9, mol.mass = $29.7 \cdot 10^3$; e = trypsin inhibitor, p*I* = 4.6, mol.mass = $7.5 \cdot 10^3$; f = β-lactoglobulin A, p*I* = 5.1 mol.mass = $17.5 \cdot 10^3$; g = amyloglucosidase, p*I* = 3.6, mol.mass = $170 \cdot 10^3$. Conditions, buffer, 50 m*M* sodium borate buffer (pH 9.5); applied voltage, 22 kV; temperature, ambient; detection wavelength, 200 nm.

Protein separation of red blood cell lysate

Proteins in human red blood cell lysate were separated under alkaline conditions (50 m*M* sodium borate, pH 9.5) in uncoated fused-silica capillaries. A good reproducibiltiy of peak shape (Fig. 2) and migration time was observed (Table II), in which less than 0.7%. The first small sharp peak (a), which is considered to be carbonic anhydrase, and the second unknown peak are completely separated from large hemoglobin peak. These shapes were reproducible in seven consecutive runs, with

TABLE I

REPRODUCIBILITY OF MIGRATION TIME AND PEAK HEIGHT FOR THE ANALYSES OF MODEL PROTEINS WITH CZE

Conditions as in Fig. 1.

Peak	Retention time ($n = 5$)		Relative peak height ($n = 5$)	
	Average ± S.D. (min)	C.V. (%)	Average ± S.D.	C.V. (%)
a	7.97 ± 0.029	0.36	5.64 ± 0.08	1.42
b	8.45 ± 0.030	0.36	19.00 ± 0.31	1.63
c	8.63 ± 0.031	0.36	3.06 ± 2.05	67.00
d	8.87 ± 0.030	0.34	11.62 ± 0.29	2.5
e	11.09 ± 0.061	0.55	6.59 ± 0.23	3.49
f	11.62 ± 0.067	0.58	8.49 ± 0.33	3.89
g	13.47 ± 0.092	0.68	1.13 ± 0.14	12.40

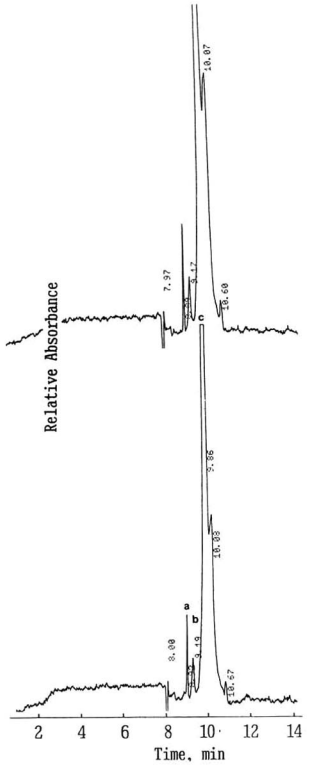

Fig. 2. Separation of proteins in human red blood cell lysate. First and seventh consecutive run. Other conditions as in Fig.1.

washing between runs with 1.0 *M* sodium hydroxide solution. This result is comparable to the data of Zhu *et al.* [8] in which they used a coated capillary for the same sample. With a coated capillary, the small peaks were not well separated from the haemoglobin peak. This indicates the possibility that the reduction in electroosmosis by coating the capillary decreases the separation efficiency of CZE.

TABLE II

REPRODUCIBILITY OF MIGRATION TIME FOR THE ANALYSES OF HUMAN RED BLOOD CELL LYSATE WITH CZE

Conditions as in Fig. 2.

Peak	Migration time ($n=5$)	
	Average ± S.D. (min)	C.V. (%)
a	8.858 ± 0.0620	0.70
b	9.112 ± 0.0453	0.50
c	9.782 ± 0.0655	0.67

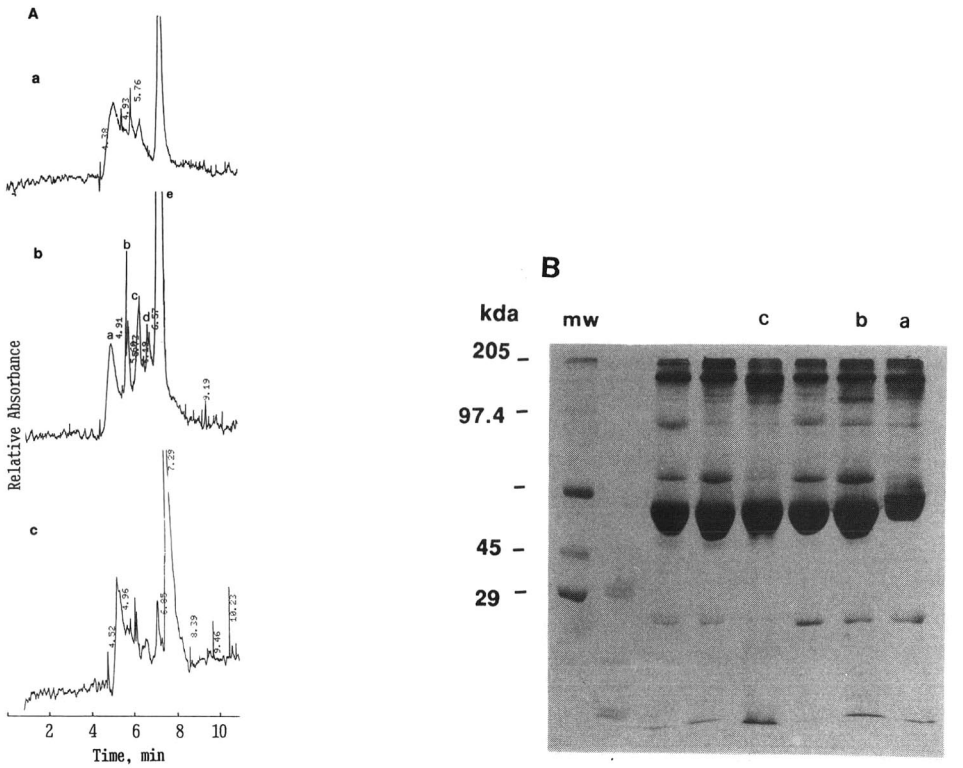

Fig. 3. (A) Separation of proteins with CZE from bovine serum (a), from NIST standard reference material (b) and human serum from a patient (c). Conditions as in Fig. 1, except the applied voltage = 30 kV. (B) Separation of proteins with SDS-PAGE under non-reducing conditions based on molecular mass. mw = Molecular mass; kda = kilodalton.

Comparison between CZE and conventional SDS-PAGE for the separation of proteins in human serum

Protein profiles of human serum in gel electrophoresis have been adopted for the diagnosis of diseases in the clinical laboratory. To estimate the possiblity of using CZE for this purpose, CZE electropherograms of serum proteins are compared with protein profiles of SDS-PAGE under non-reducing conditions in Fig. 3. Fig. 3A shows the CZE electropherograms of bovine serum, human serum from NIST standard reference material and from a hospital patient. The protein profiles in conventional SDS-PAGE in Fig. 3B correspond to those in Fig. 3A.

The reproducibility of migration time under alkaline condition with a 1 *M* sodium hydroxide solution wash in between analyses is shown in Table III. The C.V. value is $< 2\%$. It is obvious that the resolving power of this method with CZE is superior to that with the gel electrophoresis.

Modifications of the protein profiles in human serum have been performed by depleting IgG with protein A-sepharose or serum albumin with an immunoaffinity column (see under Experimental). The depletion of IgG is shown by the disapparance of the 160 kda molecular mass protein band corresponding to IgG in SDS-PAGE

TABLE III

REPRODUCIBILITY OF MIGRATION TIME FOR THE ANALYSES OF HUMAN SERUM WITH CZE

Conditions as in Fig. 3.

Peak	Migration time ($n=5$)	
	Average ± S.D.	C.V. (%)
a	4.90 ±0.0894	1.825
b	5.372±0.0584	1.087
c	5.916±0.0722	1.220
d	6.312±0.1128	1.787
e	6.908±0.1340	1.940

(Fig. 4B); the IgG peak, which is broad in CZE as a result of heterogeneity, is also missing (Fig. 4A). This indicates that the molecular mass distribution of IgGs is fairly homogeneous, but the p*I* values are varied. Serum albumin has been depleted with anti-human serum albumin antibody bound to the gel. The albumin peak in CZE (Fig. 5A) and the band is SDS-PAGE (Fig. 5B) are also simultaneously reduced. The identification of the peaks in CZE is possible by comparing these two methods. CZE can also be used to check the progress of biological reactions *in situ*.

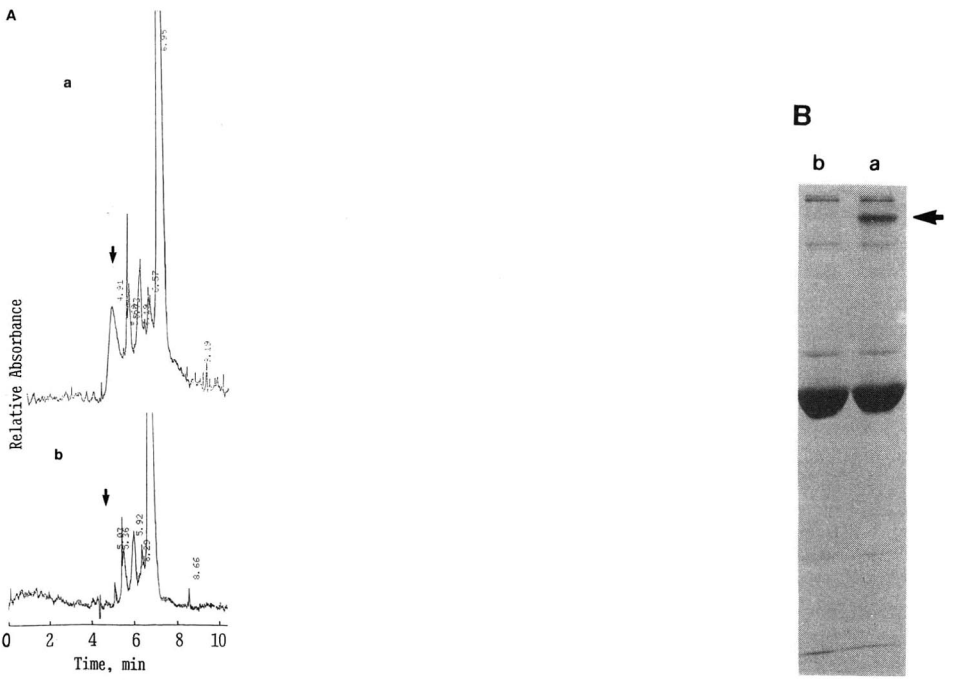

Fig. 4. Comparison between normal human serum (a) and IgG-depleted human serum (b). (A) CZE electropherogram under the same conditions as Fig. 3. (B) Protein profiles in SDS-PAGE. Arrow indicates the peak or band of IgG.

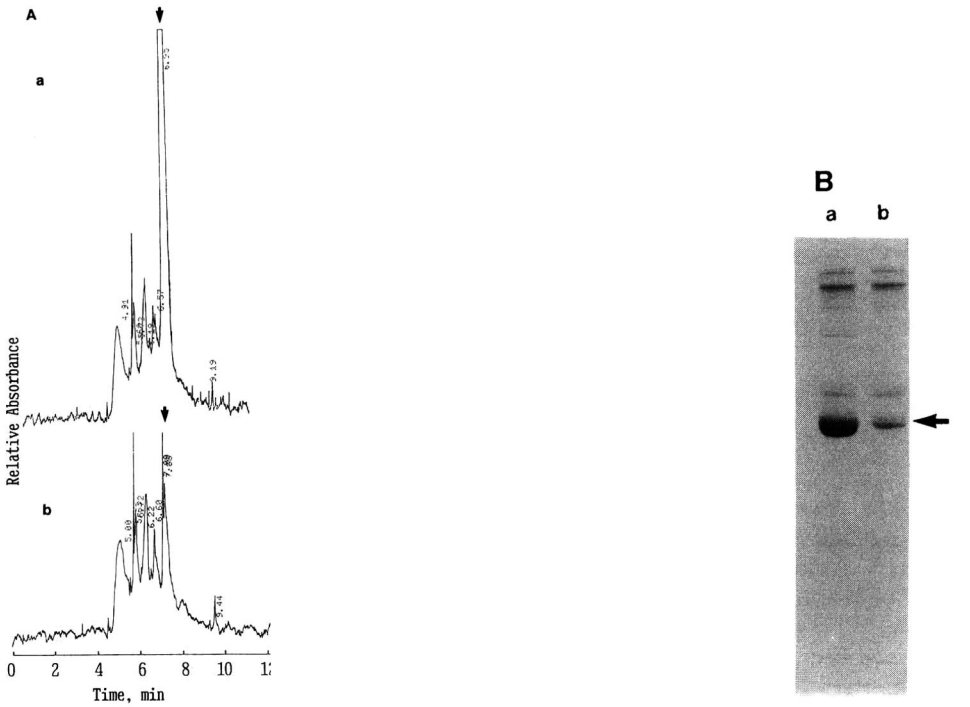

Fig. 5. Comparison between normal human serum (a) and albumin-depleted human serum (b). (A) CZE electropherogram under the same conditions as in Fig. 3. (B) Protein profiles in SDS-PAGE. Arrow indicates the peak and band of serum albumin.

In conclusion, proteins in model systems or in complicated biological samples can be determined in an uncoated fused-silica capillary under alkaline conditions. The reproducibility of the migration time and peak height is good (C.V. < 1%) except for a few proteins. The CZE electropherogram based on the p*I* values of proteins is compatible with the data obtained by SDS-PAGE, which is a separation technique based on molecular mass.

REFERENCES

1 K. D. Lukacs and J. W. Jorgenson, *Science (Washington, D.C.)*, 222 (1983) 266.
2 H. Nishi, F. Tsukasa, M. Matsuo and S. Terabe, *J. Chromatogr.*, 498 (1990) 313.
3 M. Yu and N. J. Dovinchi, *Anal. Chem.*, 61 (1989) 37.
4 R. M. McCormick, *Anal. Chem.*, 60 (1988) 2322.
5 H. H. Lauer and D. McManigill, *Anal. Chem.*, 58 (1986) 166.
6 M. M. Gordon, K.-J. Lee and R. N. Zare, *Anal. Chem.*, 63 (1991) 69.
7 S. Hjertén, *J. Chromatogr.*, 347 (1985) 191
8 M. Zhu, R. Rodriguez, D. Hansen and T. Wehr, *J. Chromatogr.*, 516 (1990) 123.
9 J. S. Green and J. W. Jorgenson, *J. Chromatogr.*, 478 (1989) 63.
10 V. K. Laemmli, *Nature (London)*, 227 (1990) 680.
11 A.. Burgess-Cassler, J. J. Johansen and N. C. Kendrick, *Clin. Chim. Acta*, 183 (1989) 359.

Journal of Chromatography, 559 (1991) 325–335
Elsevier Science Publishers B.V., Amsterdam

CHROM. 23 518

Detection of enzyme activity in fractions collected from free solution capillary electrophoresis of complex samples

NIELS BANKE*, KIM HANSEN and IVAN DIERS
Microbial Physiology, Novo Nordisk A/S, Novo Allé, DK-2880 Bagsvaerd (Denmark)

ABSTRACT

Crude fermentation broth from a fermentation of *Aspergillus oryzae* was analyzed using free solution capillary electrophoresis (FSCE) in a alkaline running buffer. Fractions as large as possible were collected after FSCE separation and analyzed for alkaline protease activity with Suc–Ala–Ala–Pro–Phe–*p*-nitroanilide as substrate. Two peaks were isolated; one of them was unknown and therefore was further investigated. After amplification of the activity by incubation with Suc–Ala–Ala–Pro–Phe–*p*-nitroanilide or casein as substrate, the reaction mixtures were analyzed by FSCE. In this way as little as 3 ng of enzyme were identified as an alkaline protease of the subtilisin family.

INTRODUCTION

For a long time we have been trying to analyze complex fermentation broth for secreted proteins and primary and secondary metabolites. The usual techniques have been thin-layer chromatography for the metabolites and sodium dodecylsulphate polyacrylamide gel electrophoresis (SDS-PAGE) with Western blotting, overlayer or direct staining technique for the proteins, all fairly time-consuming, laborious and semiquantitative methods.

Aspergillus oryzae is a filamentous fungius with a remarkable ability to secrete a large amount of different enzymatic activities [1]. We have become more and more interested in this organism as a host for "heterologous protein" products, such as the new lipase from *Humicola insolens* [1], found to be a new, very efficient remover of fat stains on cloth. In this context the proteolytic enzymes produced by the native host are undesirable and we therefore wanted to investigate some of the most important of these enzymes, and to be able to detect them when changing the fermentation process. We regard the alkaline proteases as the most aggressive enzymes for "heterologous protein" production and therefore first concentrated on the detection of these.

Free solution capillary electrophoresis (FCSE) is a new analysis technique anticipated to have a high resolution of charged components with a high and efficient sample capacity and therefore probably well suited for solving our problem.

We therefore tried to separate the complex *A. oryzae* fermentation broth into as many components as possible using FSCE and to identify and quantify some of the

0021-9673/91/$03.50

proteolytic enzymes in the fractions. The fractions collected by FSCE were very small, typically of the order of nanograms. Normally the electrical circuit has to be completed through the collection, which gives a high dilution, because the electrode needs to be in the buffer. It is possible to collect samples without dilution, using a capillary with an on-column frit structure, grounding the capillary on its side prior to its outlet [2]. However, normally the fractions are collected in 5–10 μl of buffer. By collecting the same fraction from several runs, higher concentrations are achieved [2–5]. The chance of successfully identifying and quantifying small amounts of enzyme can be increased by reacting the enzyme over many hours with a selected substrate.

In spite of these facts, fractions collected from high-performance capillary electrophoresis (HPCE) have been used for microsequencing on high-performance liquid chromatography (HPLC) [6,7], slab-gel electrophoresis (labeled with radioactivity [8]), determination of amino acid composition using HPLC [4], mass spectrometric analysis [3,4] and enzymatic analysis using HPLC [9]. However, in all these cases the fraction collected contained the main component.

Here we describe the FSCE separation of some minor side products from a complex fermentation broth and the collection and identification of their enzymatic activity by reaction with two different substrates. The detection of the reaction products from the enzymatic reaction was also achieved by FSCE analysis.

EXPERIMENTAL

Materials

The fermentation sample was from a four-day-old fermentation of *A. oryzae*, made in a 10-l laboratory fermenter, with a medium containing dextrin and soy flour. The main product of the fermentation was a neutral α-amylase with pI = 4.7; the concentration of α-amylase was 1.4 g/l. The broth is known to contain at least three proteases; the total amount was approximately 200 mg as estimated by SDS-PAGE.

Prior to analysis the sample was centrifuged for 10 min at 50 *g* (Digifuge, Heraeus-Christ, Germany) to remove the mycelium, and then sterile-filtered through a 0.45-μm filter (Millipore, Molsheim, France). The sample was stored at −18°C, before analysis, to avoid degradation. The purified alkaline protease used for "spiking" was a gift from Shamkant Anant Patkar, Novo Nordisk (Bagsvaerd, Denmark).

Boric acid, sodium dihydrogenphosphate, sodium hydroxide and maleic acid for the buffers were all of analytical grade from Merck (Darmstadt, Germany). Tris-(hydroxymethyl)aminomethane (Tris) of very high purity was from Sigma (St. Louis, MO, USA).

The casein substrate contained 3.5 g/l casein "nach Hammerstein" from Merck and 0.03 g/l benzoic acid (Merck) in 30 mM Tris–maleic acid buffer (pH 7).

The Suc–Ala–Ala–Pro–Phe–*p*-nitroanilide substrate contained 0.6 g/l Suc–Ala–Ala–Pro–Phe–*p*-nitroanilide from Sigma in 50 mM phosphate buffer (pH 7). It should be noted that the substrate is not a real peptide, but a peptide of Ala–Ala–Pro–Phe, which is blocked at the N-terminal by succinic acid and modified by *p*-nitroanilide at the C-terminal. The *p*-nitroanilide yields a yellow colour, when not connected to the peptide. Suc–Ala–Ala–Pro–Phe–*p*-nitroanilide is an artificial peptide substrate constructed for detection of alkaline proteases of the subtilisin family;

during protease detection the coloured free *p*-nitroanilide from the C-terminus of the peptide is released.

The FSCE analysis was performed on a Beckman P/ACE System 200 (Beckman Instruments, Palo Alto, CA, USA). The capillary was uncoated fused silica, 75 μm I.D., total length 57 cm, 50 cm to the detector, supplied by Beckman Instruments in a cartridge. The instrument was controlled and data were collected by P/ACE System 2000 software version 1.5 (Beckman Instruments) running on a Model 80 386 IBM Personal System/2 computer (IBM United Kingdom, Portsmouth, UK).

Methods

UV detection was at a fixed wavelength of 200 nm. The temperature of the capillary was maintained at 30°C by the liquid cooling system. Injection was made by applying an overpressure of 3.4 kPa to the injection end of the capillary.

The capillary was equilibrated before every run. It was first flushed for 2 min with 0.1 *M* sodium hydroxide, then for 0.3 min with water to remove the sodium hydroxide. It takes approximately 0.2 min to flush the whole capillary on this instrument (pressure 138 kPa). The water and the sodium hydroxide were flushed into a empty vial, to prevent changing the volume and pH of the buffer vial. The capillary was then flushed for 4 min with buffer, 2 min forward and 2 min reverse, to avoid changing the volume of the buffer vials when using the same buffer vials for more than one run.

For fraction collection a running buffer containing 33 m*M* phosphate at pH 9.5 was used, and 30 nl of the fermentation broth were injected. The separation was carried out using a constant voltage of 15 kV.

Before fraction collection, the sample was run normally to detect the migration time for the peak, which should be collected. The time (T_c) when the start of the peak is going to leave the capillary could then be calculated as $T_c = (57\text{ cm}/50\text{ cm}) \times T_d$, where T_d is the time when the peak passes the detector. When fractions were collected, the current was interrupted just before T_c. A new vial containing 10 μl of running buffer was placed in position at the detector end. The current was connected again and the peak forced to migrate into the collection vial. To avoid joule heating the small buffer volume in the vial, the voltage was fixed at 7.5 kV. In this case 0.6 min at 7.5 kV was used to move the peak to the collection vial.

To the vial with the collected peak, 10 μl of enzyme–substrate were added. The vial was incubated at room temperature (approximately 25°C) for 2–24 h. The conversion of substrate to product was followed simultaneously with FSCE. The casein and the Suc–Ala–Ala–Pro–Phe–*p*-nitroanilide substrates were treated in the same way. A 100 m*M* borate buffer (pH 8.35) was used as running buffer in the FSCE analysis. An 18-nl sample was injected, and 20 kV were applied constantly during separation.

RESULTS

Separation and identification of proteases

The fermentation broth was most efficiently separated after dilution three times with deionized water using a 25 m*M* phosphate buffer (pH 9.5) as running buffer at 15 kV. Fig. 1 shows the separation with 6 nl of diluted sample injected. The main compo-

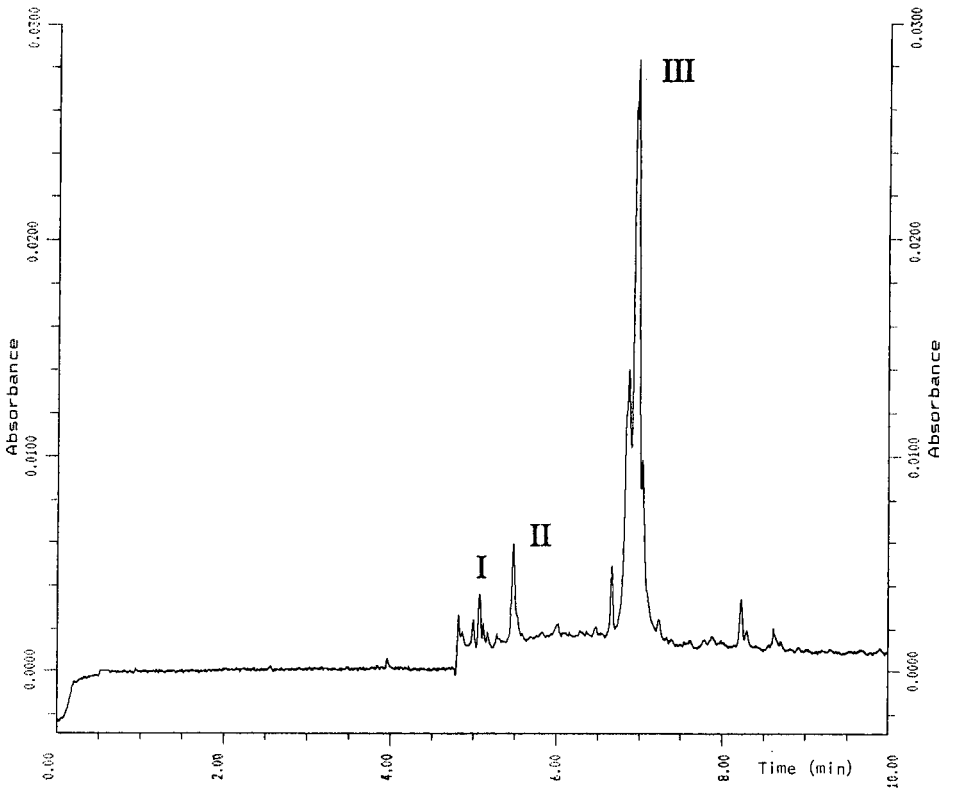

Fig. 1. FSCE pattern of fermatation broth from *Aspergillus oryzae* diluted three times with deionized water. The running buffer was 25 m*M* phosphate (pH 9.5), and a constant field of 15 kV (263 V/cm) was applied during separation. A 6-nl aliquot was injected, and detection was at 200 nm. I is an alkaline protease identified by "spiking" with a pure component, II is the peak investigated here for protease activity and III is the main product of the fermentation, a neutral α-amylase consisting of three or more non-baseline-separated peaks, caused by isoenzymes.

nent, the α-amylase (III, migration time 7 min), consists of three non-baseline-separated peaks, caused by isoezymes. The peak with migration time 5.0 min is identified as an alkeline protease (I) by "spiking" with purified alkaline protease from Shamkant Anant Patkar. The peak with migration time 5.5 min (II) is a subtilisin-like protease, identified by collection and enzymatic analysis.

Collection of fractions for identification

In order to obtain as much material as possible, undiluted broth was injected directly into the apparatus and the sample volume increased to 30 nl and the strength of the running buffer to 33 m*M*. By doing this the resolution becomes less efficient, because of greater dispersion. This is caused by the longer sample zone, the increased conductivity of the sample zone and more joule heating. To increase the amount of material further, the internal diameter of the separation capillary could also be in-

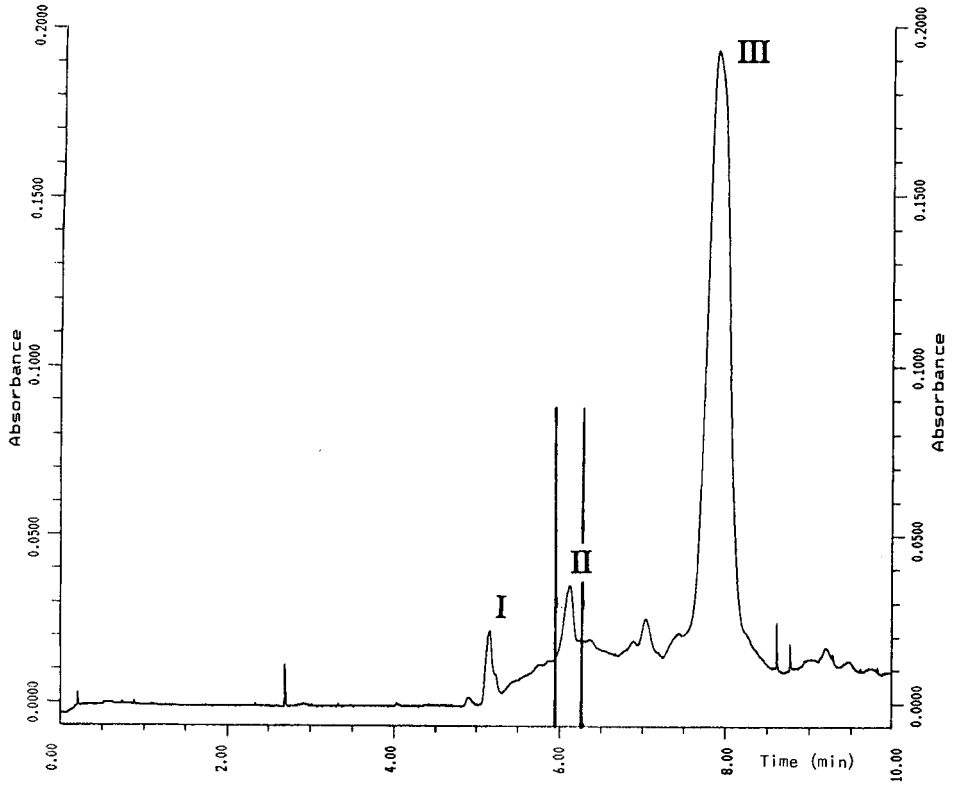

Fig. 2. FSCE pattern of fermentation broth from *Aspergillus oryzae* under fraction collection conditions. The running buffer was 33 m*M* phosphate (pH 9.5), and a constant field of 15 kV (263 V/cm) was applied during separation. A 30-nl aliquot was injected, and detection was at 200 nm. I is an alkaline protease, II is the peak investigated here for protease activity and III is the main product of the fermentation, a neutral α-amylase. The time window for collection of the peak with proteolytic activity is shown.

creased [7] or the same fraction could be collected from a number of runs [3–5], and in this way the concentration of the component in the collection vial can be increased. This was not necessary in this case, because enzymatic amplification was applied.

Fig. 2 shows the analysis of the sample using the conditions for fraction collection. The main product of the fermentation is the α-amylase (III), with a migration time of 8 min. The peak with migration time 5 min (I) is an alkaline protease identified as previously described. The peak with migration time 5.5 min (II) was also shown to possess proteolytic activity with Suc–Ala–Ala–Pro–Phe–*p*-nitroanilide. The time window used for the collection of the peak with protease activity is aslo shown in the figure.

The reproducibility of the method was tested by collection and analysis of the same peak (peak II, Fig. 2) in four independent runs. In all cases (not shown) the protease activity detected was equal in quantity and pattern of action. The alkaline protease, identified by "spiking" (peak I, Fig. 1), was also collected, and the protease activity detected (data not shown).

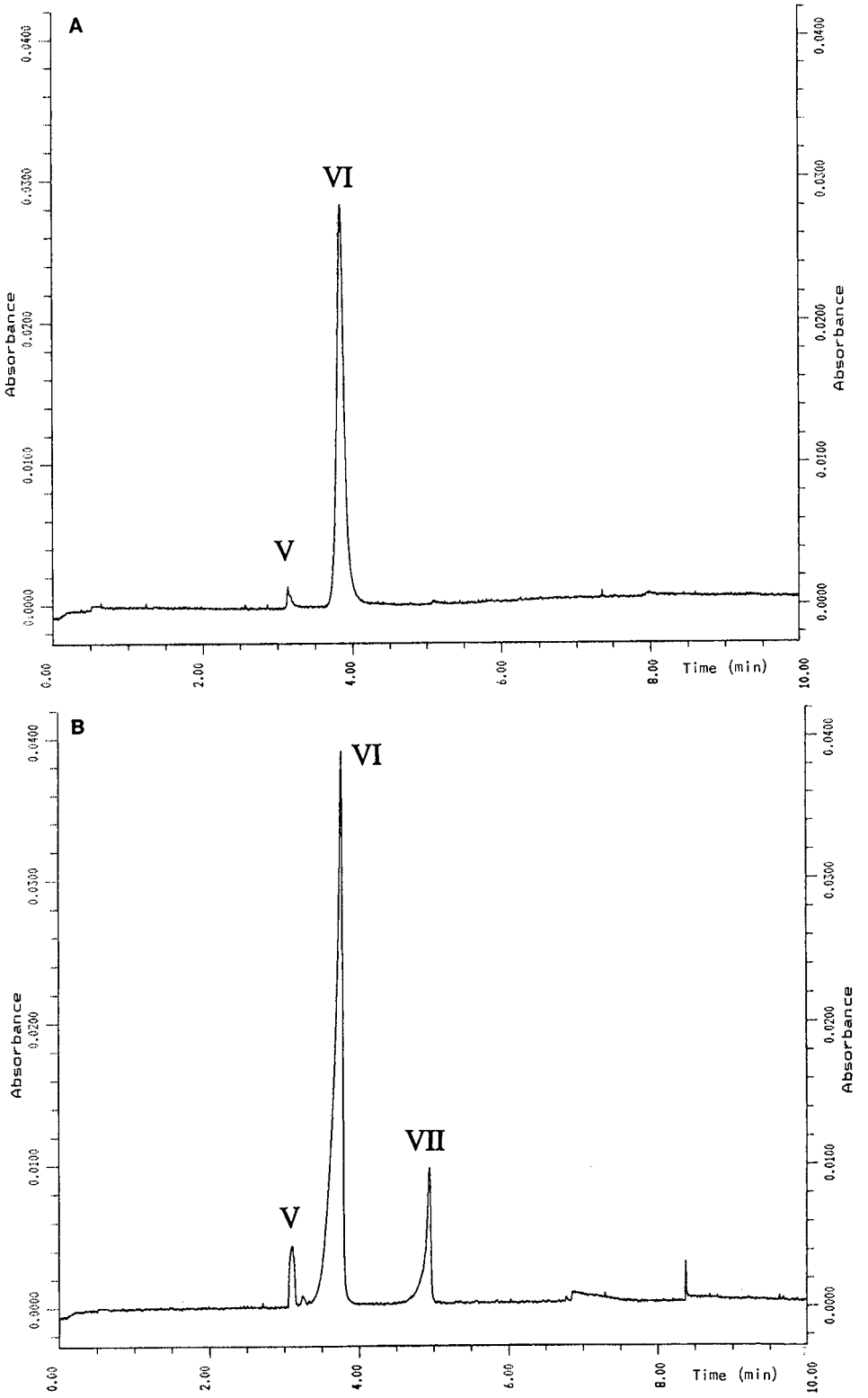
A
VI
V
Absorbance
0.0400
0.0300
0.0200
0.0100
0.0000
2.00
4.00
6.00
8.00
10.00
Time (min)
B
VI
VII
V
Absorbance
0.0400
0.0300
0.0200
0.0100
0.0000
2.00
4.00
6.00
8.00
10.00
Time (min)

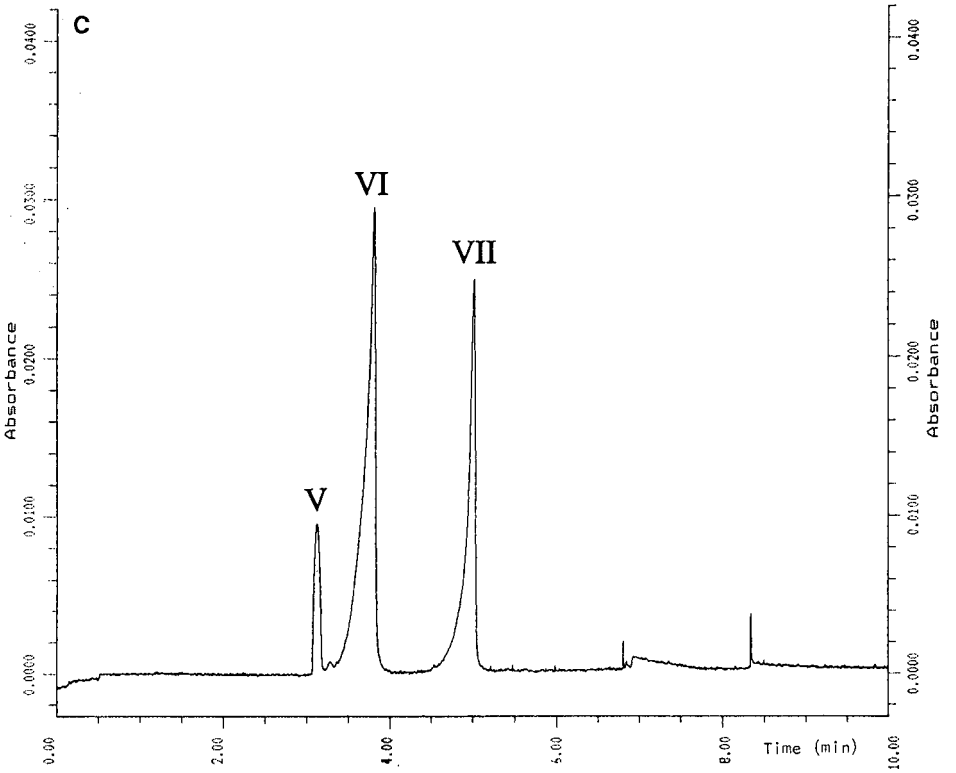

Fig. 3. FSCE enzyme assay patterns for fraction II collected by FSCE (Fig. 2), using Suc–Ala–Ala–Pro–Phe–*p*-nitroanilide substrate. Conditions as in Fig. 2. Peaks V = *p*-nitroanilide, VI = Suc–Ala–Ala–Pro–Phe–*p*-nitroanilide (substrate); VII = Suc–Ala–Ala–Pro–Phe. (A) Blank incubated for 8 h. (B) Incubation for 3 h. (C) Incubation for 8 h.

Enzymatic analysis of peak II (Fig. 2)

Suc–Ala–Ala–Pro–Phe–p-nitroanilide determinations. Fig. 3A–C shows the detection of proteolytic conversion of Suc–Ala–Ala–Pro–Phe–*p*-nitroanilide (VI) to *p*-nitroanilide (V) and Suc–Ala–Ala–Pro–Phe (VII). Fig. 3A is a blank (incubated for 8 h), Fig. 3B shows the conversion after 3 h of incubation and Fig. 3C the same after 8 h. It is obvious that Suc–Ala–Ala–Pro–Phe–*p*-nitroanilide is converted to only these two components. It is also apparent that quantitative determination is straightforward. The pattern of hydrolysis strongly indicates that peak II contains an alkaline protease of the subtilisin family, but it cannot be ruled out that it resulted from some kind of carboxypeptidase activity. To prove that the peak was due to a subtilisin-type enzyme, the proteolytic action in 100 m*M* borate buffer (pH 8.35) containing 0.6 g/l Suc–Ala–Ala–Pro–Phe–*p*-nitroanilide and 110 mg/l Savinase (subtilisin from Novo Nordisk) 30°C, was followed with FSCE over more than 7 h as shown in Fig. 4. The irregularity of the graph at 1.6 h of incubation is an instrumental error, caused by the injection of too much sample. The disappearance of the substrate and the emergence

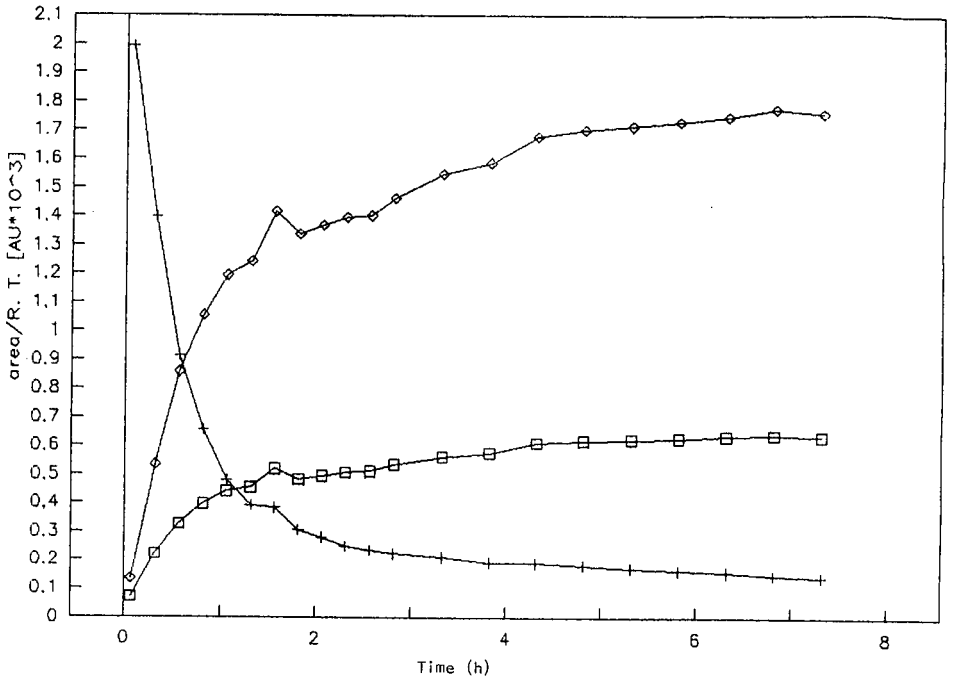

Fig. 4. FSCE enzyme assay as a function of time. Suc–Ala–Ala–Pro–Phe–*p*-nitroanilide in 100 m*M* borate buffer (pH 8.35) containing 110 mg/l Savinase. The degradation was followed on FSCE. Conditions as in Fig. 2. + = Suc–Ala–Ala–Pro–Phe–*p*-nitroanilide; ◇ = Suc–Ala–Ala–Pro–Phe; □ = *p*-nitroanilide.

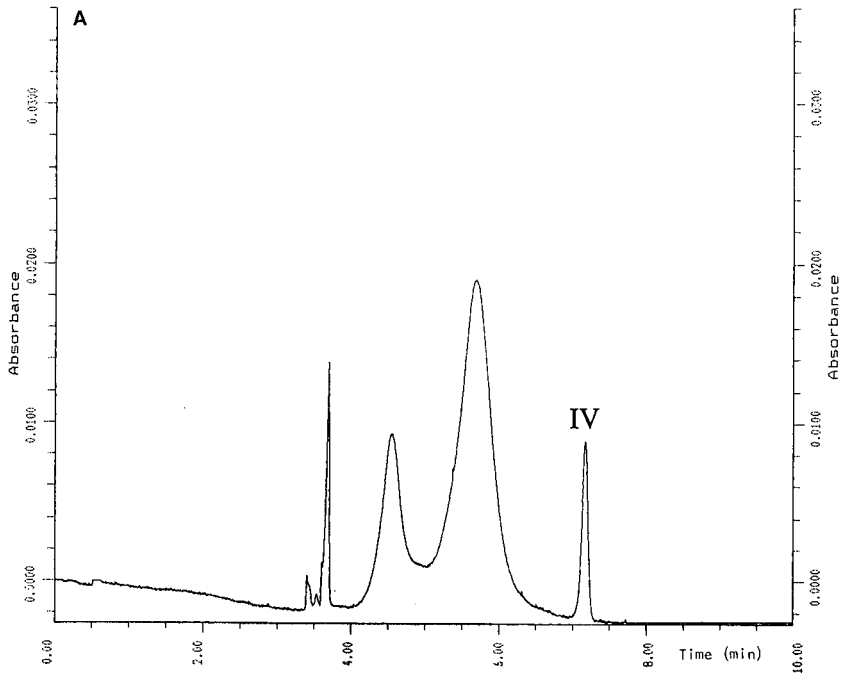

Fig. 5.

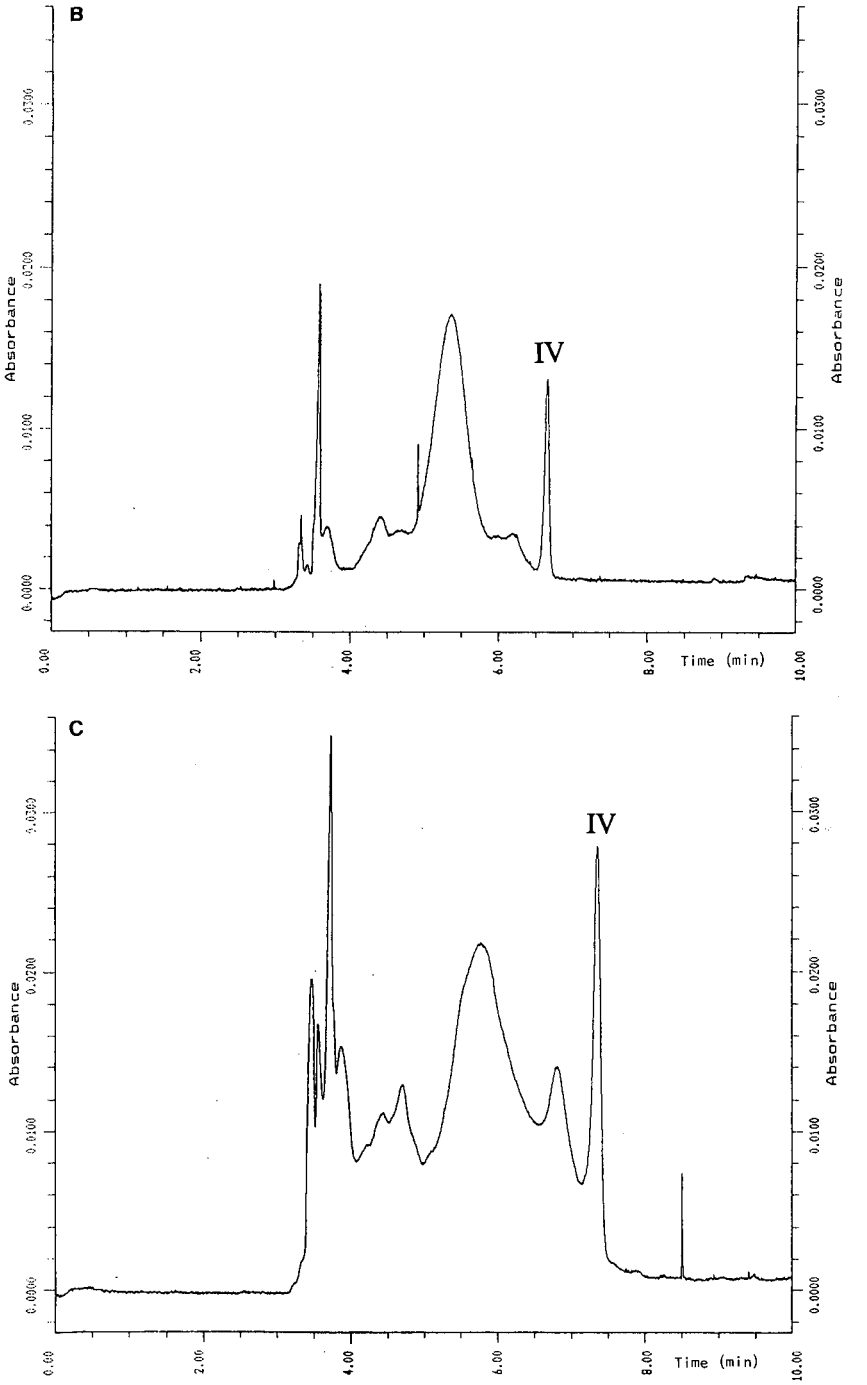

Fig. 5. FSCE enzyme assay patterns of fraction II collected by FSCE (Fig. 2), using casein as a substrate. The running buffer was 100 m*M* borate (pH 8.35), and a constant field of 350 V/cm was applied during separation. An 18-nl aliquot was injected, and detection was at 200 nm. The peak marked IV is benzoic acid, used as internal standard. (A) Blank incubated for 16 h; (B) incubation for 4.5 h; (C) incubation for 16 h.

of the products are, as expected, reciprocal events, and no internal standard is needed. There was no difference in reaction pattern between Savinase and peak II.

Casein determinations

To distinguish further between the action of a carboxypeptidase and an endoprotease, to which group the subtilisin family belongs, reactions with casein as substrate were carried out as described. The hydrolysis of casein is shown after 4.5 h (Fig. 5B) 16 h (Fig. 5C), and a blank (incubated for 16 h) is included for comparison (Fig. 5A). Benzoic acid in a concentration of 0.03 g/l was included (peak IV, Fig. 5A–C) to compensate for evaporation during the incubation. Unhydrolyzed casein is separated nicley (Fig. 5A) into two main components, the smallest of them being nearly completely degraded after 4.5 h (Fig. 5B) and both being heavily changed after 16 h of incubation (Fig. 5C), strongly confirming that peak II reacts like an endoprotease.

DISCUSSION

Throughout this work in which enzymatic activity was determined in collected fractions, blanks were included. The blanks, consisting of pure running buffer, were treated in exactly the same way as all the fractions, to take into account all changes except the ones caused by components in the fermentation broth. In particular, the changes caused by thermic degradation of the substrates could lead to wrong conclusions about protease activity if no blank was included.

Evaporation from the collection vials during the incubation was quite high, even if all vials were covered with special caps supplied by Beckman Instruments, and water was added to the bottoms of the vials to ensure high humidity around the sample. Evaporation, which increased the concentration of the substrate, increased during incubation. Benzoic acid (IV) was added as an internal standard to detect the evaporation from the sample during incubation. The peak areas increased during the incubation and varied from sample to sample, indicating that the internal standard is necessary for comparison, and that considerable evaporation occured.

Using borate as running buffer in the FSCE analysis created some difficulties with the two substrates, because the migration times varied. The capillary needed a very long time to achieve equilibrium with the borate ion, probably because borate complexes with the silanol groups of the capillary wall. The migration time was not stable even after a run of more than 20 h. Because of this only normalized areas (area/migration time) were compared [10].

The concentration of the collected protease is not known exactly, but the concentration is approximately 100 mg/l, estimated as the peak area at 200 nm (Figs. 1 and 2) and compared with the peak area of the α-amylase peak. This means that we were able to detect less than 3 ng of the protease and the concentration of the protease could under these assumptions be calculated to be 75 μg/l after substrate was added. We could probably have detected as little as 0.3 ng of the enzyme using this method.

The protease activity was detected by two different substrates. The Suc–Ala–Ala–Pro–Phe–*p*-nitroanilide substrate was chosen because it is specific for the alkaline subtilisin-like proteases, and also because it is normally easy to quantify by colorimetric measurements. The casein substrate containing nearly all possible pep-

tide bonds is fairly unspecific and can be used to detect all kinds of proteases but can only give a semiquantitative detection of the activity in the way we used it (FSCE).

REFERENCES

1 E. Boel, T. Christensen and H. F. Wöldike, *Eur. Pat.*, EP 0 238 023 A2 (1987).
2 X. Huang and R. N. Zare, *J. Chromatogr.*, 516 (1990) 185–189.
3 L. A. Kosobud, M. S. Chang and G. L. Schoenhard, presented at the *Third International Symposium on High Performance Capillary Electrophoresis, San Diego, CA, 1991*, poster PT-33.
4 R. E. Brown and J. Aliphon, Beckman Instruments, 1990, personal communication.
5 R. E. Brown and M. Carlquist, Beckman Instruments, 1990, personal communication.
6 A. Guttman, A. Paulus, A. S. Cohen, B. L. Karger, H. Rodriguez and W. S. Hancock, *Electrophoresis'88, Copenhagen, 1988*, VCH, Weinheim, 1988, pp. 151–159.
7 J. I. Ohms, presented at the *Third International Symposium on High Performance Capillary Electrophoresis, San Diego, CA, 1991*, last minute poster.
8 A. S. Cohen, D. R. Najarian, A. Paulus, A. Guttman, J. A. Smith, and B. L. Karger, *Proc. Natl. Acad. Sci. U.S.A.*, 85 (1988) 9660–9663.
9 D. J. Rose and J. W. Jorgenson, *J. Chromatogr.*, 438 (1988) 23–34.
10 R. G. Nielsen, G. S. Sittampalam and E. C. Rickard, *Anal. Biochem.*, 177 (1989) 20–26.

Journal of Chromatography, 559 (1991) 337–343
Elsevier Science Publishers B.V., Amsterdam

CHROM. 23 414

Analysis of a vaccine purification process by capillary electrophoresis

WILLIAM M. HURNI* and WILLIAM J. MILLER
Merck Sharp & Dohme Research Laboratories, West Point, PA 19486 (USA)

ABSTRACT

Free-zone capillary electrophoresis (CZE) was applied to the analysis of samples from the individual purification steps in the production of a licensed vaccine product. With this technique, real-time analysis can be performed to ensure that purification parameters are being met before proceeding to the next step. In addition to monitoring the product peak, a unique pattern of associated host cell contaminants also is displayed. This unique "fingerprint" at each step of the purification process may have practical utility for production in that it demonstrates lot-to-lot consistency in the manufacturing process of the vaccine.

INTRODUCTION

Recombinant products are produced in a host organism such as bakers' yeast (*Saccharomyces cerevisiae*). Whether the product is secreted into the growth medium or retained intracellularly, a reproducible purification process is required to bring the product to an acceptable level of purity. Typically, such a process is monitored at various stages by specific assays which may be based on serological reactivity, bioactivity or mass (*e.g.* UV or protein measurements). Although these assays can provide specific information about the functioning of the purification process, they give limited information about the reproducibility of the process. Therefore, other assays are required in order to measure impurities and the addition or removal of reagents used in the purification and formulation of the product.

We have evaluated the use of free-zone capillary electrophoresis (CZE) [1] for monitoring the purification of the recombinant hepatitis B vaccine expressed in *S. cerevisiae* (Recombivax HB®). Others have reported the use of CZE to measure the homogeneity and purity of final recombinant products [2,3]. Here we report the use of CZE to follow the purification of Recombivax HB by analyzing each step in the purification process for the amount of product, removal of impurities and additions and removal of reagents, thus establishing a 'fingerprint' for the entire process run.

0021-9673/91/$03.50

EXPERIMENTAL

Instrumentation

CZE analysis of the Recombivax HB production process was performed in an Applied Biosystems (Foster City, CA, USA) Model 270A capillary electrophoresis system using an uncoated open capillary 72 cm long (50 cm working length) × 50 μm I.D.

Materials

Samples for direct analysis from various stages in the production process for Recombivax HB and a thimerosal concentrate, used as a standard, were obtained from Merck Pharmaceutical (West Point, PA, USA). Triton X-100 (Triton), used as a standard, was purchased from Rohm and Haas (Philadelphia, PA, USA).

Capillary zone electrophoresis

All samples were analyzed at 30°C using 25 m*M* sodium phosphate running buffer at pH 7.25. A 27-kV electric field was applied across the capillary, with the detector end of the capillary being at a negative potential with respect to the inlet of the capillary. A typical running current was *ca.* 30 μA. Sample injection time was 1.5 s using vacuum, which results in a *ca.* 15-nl sample. A 2-min wash with 0.1 *M* sodium hydroxide solution followed by a 3-min wash with running buffer preceded each sample injection. Sample detection was by measurement of UV absorption at 200 nm.

RESULTS

Recombivax HB consists of 22-nm spherical lipoprotein particles of *ca.* $2 \cdot 10^6$ relative molecular mass (MW). Known as hepatitis B surface antigen (HBsAg) [4,5], each particle consists of *ca.* 100 226-amino acid polypeptides. Production of the polypeptides and assembly into HBsAg particles occurs within the recombinant yeast cells. The following is a partial list of the steps in the purification of HBsAg.

(A) Cell lysate. Yeast cells are ruptured and diluted in Triton.

(B) Filtered lysate. The *cell lysate* is clarified by microfiltration allowing the HBsAg to pass into the filtrate.

(C) Concentrated lysate. The *filtered lysate* is concentrated tenfold on a 100 kilodalton MW cut-off filter and Triton is removed by extraction with Amberlite.

(D) Silica product. The HBsAg is adsorbed on silica and eluted with borate buffer. It then is concentrated on a 100 kilodalton MW cut-off filter.

(E) HIC product. The HBsAg is adsorbed to a hydrophobic interaction chromatographic (HIC) column, then eluted with Triton in buffer.

(F) Amberlite product. The HBsAg-rich fractions from the HIC column are pooled and treated with Amberlite to remove Triton.

(G) Diafiltered Amberlite product. The *Amberlite product* is diafiltered with buffer over a 100 kilodalton MW cut-off filter.

(H) Thiocyanate product. The HBsAg product is diafiltered with 3 *M* potassium thiocyanate followed by buffer on a 100 kilodalton MW cut-off filter.

(I) Sterile Product. The pure HBsAg is diluted and sterile filtered.

(J) Formaldehyde product. The HBsAg product is treated with formalin and thimerosal is added as a preservative.

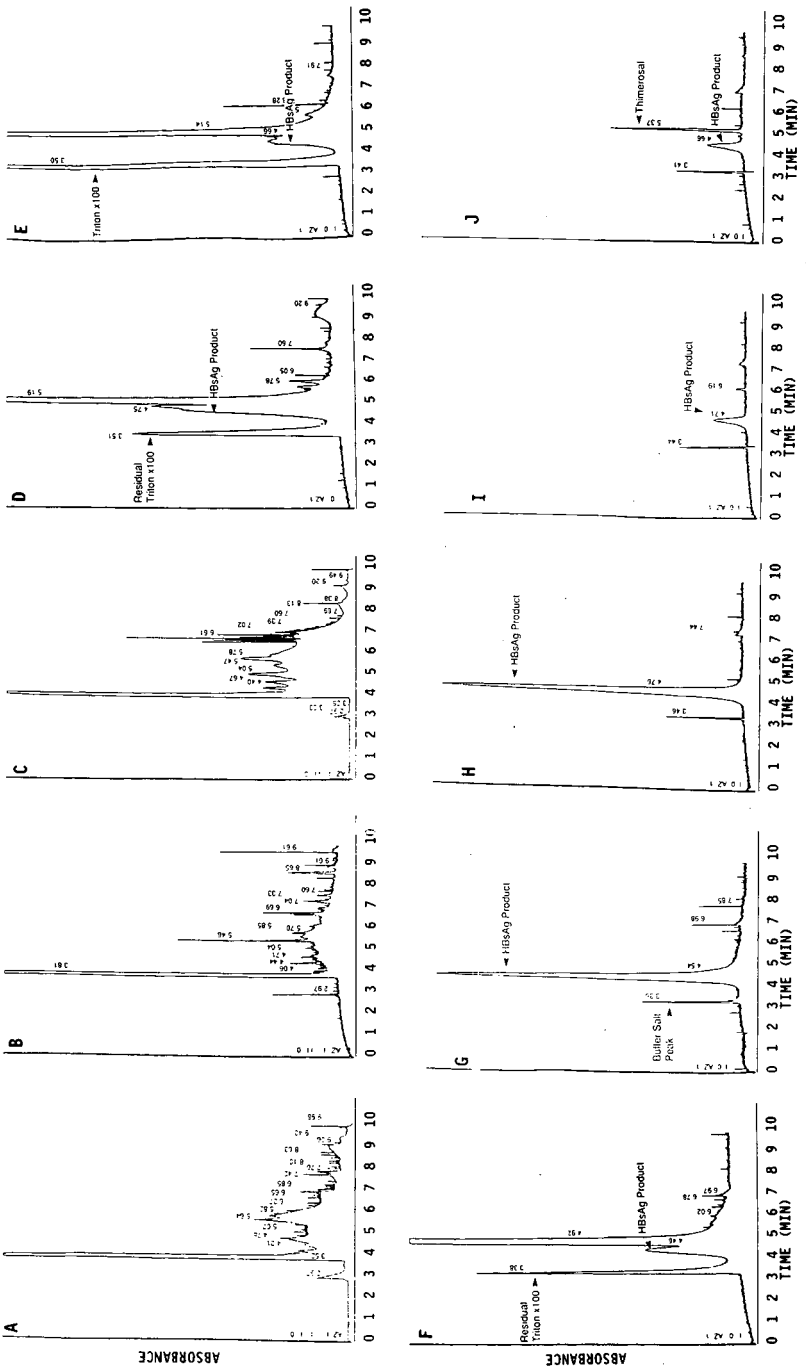

Fig. 1. Electropherograms of Recombivax HB hepatitis B vaccine production process steps. All electropherograms are plotted at attenuation 16 except for *cell lysate* and *concentrated lysate*, which are plotted at attenuation 128. (A) Cell lysate; (B) filtered lysate; (C) concentrated lysate; (D) silica product; (E) HIC product; (F) Amberlite product; (G) diafiltered Amberlite product; (H) thiocyanate product; (I) sterile product; (J) formaldehyde product.

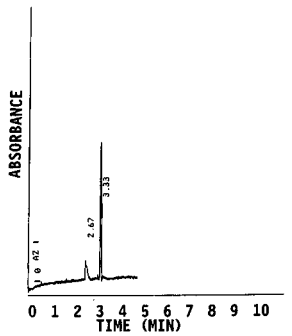

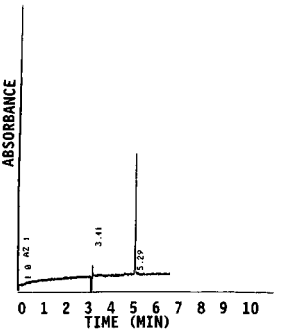

Fig. 2. Electropherogram of Triton X-100 at 50 μg/ml.

Fig. 3. Electropherogram of thimerosal at 16 μg/ml.

Fig. 1 shows ten individual electropherograms representing the above ten Recombivax HB production process steps. The *cell lysate* sample is crude, with both soluble and insoluble components. The *filtered lysate* shows that much of the protein has been removed by dilution and filtration. The *concentrated lysate* reflects a tenfold concentration. After the *silica product*, the protein load is greatly reduced. To facilitate direct comparison between electropherograms, all the remaining steps are plotted at the same attenuation. The first peak in the *silica product* electropherogram (3.51 min) is residual Triton. The following double peak (4.75 and 4.83 min) represents impurities and HBsAg. The large peak (5.19 min) is a buffer component with several small trailing impurity peaks. The *HIC product* electropherogram shows the addition of Triton (3.50 min). The double peak representing impurities and HBsAg is present as is the buffer component peak. The *Amberlite product* electropherogram shows reduction of the Triton peak (3.38 min). The HBsAg peak preceding the buffer component peak remains and the trailing impurity peaks are absent. The *diafiltered Amberlite product* electropherogram shows the removal of residual Triton as well as the buffer component compared with the previous electropherogram; additional impurities are also removed. The salt peak from the buffer used in the production process is resolved (3.36 min) and appears throughout the remainder of the process steps. The HBsAG product elutes 4.54 min. The *thiocyanate product* shows no change in the electropherogram from the preceding step. The *sterile product* electropherogram reflects a dilution made at this step with the HBsAg product at 4.71 min and the buffer salt peak at 3.44 min. The *formaldehyde product* electropherogram looks similar to the preceding electropherogram; however, it does show the addition of thimerosal (5.37 min).

Triton X-100, a commonly used detergent, can be determined by CZE at 3.3 min after injection. Fig. 2 shows a typical Triton peak at 3.33 min and represents an injection of 50 μg/ml of Triton. Linearity is good from 10 μg/ml and up to 10 mg/ml with a correlation coefficient (r) for a straight-line fit of 0.99900. The limit of detection is 10 μg/ml.

Thimerosal, a mercury-based preservative used in vaccine manufacture, can also be determined by CZE. Fig. 3 is an electropherogram showing thimerosal with a 16 μg/ml injection passing the detector at 5.29 min. The calibration graph shows good

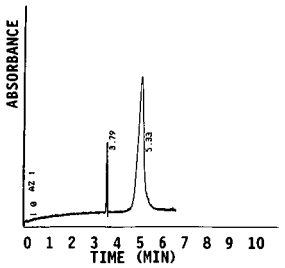

Fig. 4. Electropherogram of hepatitis B HBsAg at 100 μg/ml.

linearity from 3.2 μg/ml to 10 mg/ml with an r value for a straight-line fit of 0.99999. The limit of detection is 3μg/ml.

The recombinant HBsAg, which is the immunologically active component of Recombivax HB can be determined by CZE. Fig. 4 is an electropherogram showing a 100 μg/ml injection of HBsAg eluting at 5.33 min. A calibration graph for HBsAg shows excellent linearity between 5 and 200 μg/ml with an r of 0.99890.

DISCUSSION

There are several advantages of the use of CZE in the quality control of a production process, and they are evident as the Recombivax HB process is analyzed. A significant benefit which applies to the CZE analysis of all the process steps is that the results are available in less than 20 min. Quality control procedures currently used in the process consist of individual chemical and serological assays. The results of these assays typically follow one or more days after a particular process step has been completed. This time lag decreases process flexibility for action if a deviation is indicated. Additionally, each assay provides only a small "window" on the process step rather than the complete "fingerprint" that CZE analysis provides. With CZE analysis many types of problems can be identified and action taken while the process is ongoing. From an instrumentation point of view, CZE is very simple. A plain uncoated capillary is used, which can process hundreds of samples with virtually no maintenance. In our hands such an instrument can stand idle for days and be turned on, then samples processed within 20 min. The characteristics of this instrument are well suited to process monitoring.

(A) The *cell lysate* electropherogram is complex. It provides a "fingerprint" representing the initial yeast cell breakage. A significant change in the pattern would indicate an incomplete breakage of the yeast cells. With attenuation 128, Triton itself cannot be seen at the concentration used in the process. The large leading peak in the electropherogram is some component of the broken yeast cells. A large number of spiked peaks are apparent across the electropherogram and are attributed to insoluble particulates that flow by the detector.

(B) The *filtered lysate* step uses microfiltration, which allows the HBsAg product to pass through but retains large particulates. This electropherogram is analyzed at attenuation 16 as the bulk of the mass from the previous step has been removed by the filter. If the filter in this step were to have a partial or complete loss of integrity, it would be apparent from the "fingerprint", and corrective action could be taken.

Filter blockage also could be detected. The HBsAg cannot be seen at this step because it is too low in concentration.

(C) The electropherogram of the *concentrated lysate* reflects a tenfold concentration over a 100 000-dalton MW cutoff filter of the *filtered lysate* as well as passage across an Amberlite column to remove Triton added at the *cell lysate* step. Since the attenuation setting is high (128) to accommodate the concentration increase, residual Triton cannot be detected. The HBsAg cannot be identified definitively at this point in the process, but it is likely represented by the peak at 4.67 min.

(D) The *silica product* step retains the HBsAg, which then is eluted and analyzed. The first peak at 3.51 min is interpreted to be residual Triton from the *concentrated lysate* step, which bound to the Amberlite and subsequently coeluted with the HBsAg. The following double peaks are impurities and HBsAg product. The large peak (5.19 min) is a buffer component with some small trailing impurity peaks. The attenuation used to plot this electropherogram and all of the following electropherograms is 16.

(E) A hydrophobic interaction process step is used to further purify the HBsAg as *HIC product*. The HBsAg is removed using Triton. The first peak (3.50 min) reflects the addition of Triton and the second smaller peak (4.66 min) reflects the HBsAg product seen in the preceding electropherogram. The buffer component at 4.92 min remains. The trailing impurity peaks also have been reduced. Any problem with the affinity column or the addition of Triton would be detected easily by this analysis.

(F) The *Amberlite product* step is designed to remove most of the Triton from the product stream. The electropherogram for this step shows a substantial reduction in the Triton peak from its predecessor. The peaks for HBsAg and buffer component remain substantially unchanged. Any difficulties in this step would be apparent as a substantially larger Triton peak or perhaps a reduced HBsAg peak. Residual Triton and the remaining impurities are reduced by diafiltration over a 100 000-dalton MW cut-off filter.

(G) This *diafiltered Amberlite product* electropherogram shows the HBsAg peak (4.54 min) with the buffer component peak from the *Amberlite product* step removed. The remaining buffer salt peak (3.36 min) runs at the same location as Triton; after Triton removal, the salt peak becomes apparent.

(H) The *thiocyanate product* step consists of a 3-*M* potassium thiocyanate diafiltration followed by buffer diafiltration, which results in more complete disulfide bond formation in the HBsAg particle. The electropherogram remains unchanged from the preceding electropherogram, as might be expected.

(I) The *sterile product* step is the result of a dilution in buffer of the *thiocyanate product* material. As a result, the height and area of the HBsAg peak (20 μg/ml) are greatly reduced. The salt peak (3.44 min) remains as expected as the dilution was performed in buffer.

(J) The final step in this process, *formaldehyde product*, involves formalin treatment followed by the addition of the preservative thimerosal. This addition is represented by a peak at 5.37 min at this step. The HBsAg and the salt peaks are also present (4.66 and 3.41 min, respectively). From the electropherogram, the addition of thimerosal can be confirmed and determined, as can HBsAg, from calibration graph.

As demonstrated by the calibration graphs for Triton, thimerosal and HBsAg,

determination of a variety of macromolecules using CZE is possible. Questions about reproducible sample injection of very small volumes (*ca.* 15–30 nl) and flow-rates past the detector have been raised as possible problems. There are a significant number of laboratory-made CZE instruments in the field which may have contributed to the perception that quantification by CZE might be a problem. We did not find these issues apparent in our analyses.

While there is some variability in the migration time of HBsAg from step to step in the analysis process, this variability is small and without apparent trend. The variability seen may be due to instrument factors or to the association of HBsAg with various components of the process which might affect its migration time.

No significant shift in migration time is seen after potassium thiocyanate treatment. We understand the thiocyanate to be acting as a chaotropic agent, allowing for reformation of the disulfide bonds in the surface antigen particle with no change in charge. Additionally no significant change in migration time is seen after formaldehyde treatment, as one might expect owing to reactions with the free amino groups of arginine and lysine. There are seven such amino acids in each of the 100 polypeptides making up the HBsAg particle. Many of these may be within the interior of the HBsAg and unavailable for reaction. The size of HBsAg suggest that endosmotic flow may be the largest contributing factor to its migration.

In conclusion, CZE is a powerful and practical new tool for monitoring protein purification processes. It not only provides real-time analytical data to aid in control of the process but also provides the opportunity for intervention to correct problems that arise on a real-time basis. In addition, it provides a 'fingerprint' of each step, showing impurity removal and product enhancement and confirming additions of reagents where performed. Accumulation of composite process 'fingerprints' over a number of runs can demonstrate process reproducibility, which will have value for commercial products.

ACKNOWLEDGEMENTS

The authors thank Mr. John R. Telencho for providing Recombivax HB production process samples and most helpful cooperation, Dr. R. W. Ellis for helpful discussion and manuscript reviews and Susan Levandoski for excellent secretarial assistance.

REFERENCES

1 B. L. Karger, A. S. Cohen and A. Guttman, *J. Chromatogr.*, 492 (1989) 585–614.
2 R. G. Nielson and E. C. Rickard, *ACS Symp. Ser.*, 434 (1990) 36–49.
3 J. Frenz, S.-L.- Wu and W. S. Hancock, *J. Chromatogr.*, 480 (1989) 379–391.
4 D. Ganem and H. E. Varnus, *Ann. Rev. Biochem.*, 56 (1987) 651–693.
5 P. J. Kniskern, A. Hagopian, P. Burke, N. Dunn, D. L. Montgomery, L. D. Schultz, C. A. Schulman, C. E. Carty, R. Z. Maigetter, D. E. Wampler, E. D. Lehnman, S. Yamazaki, D. J. Kubek, E. A. Emini, W. J. Miller, W. M. Hurni and R. W. Ellis, in M. Z. Atassi (Editor), *The Application of Molecular Biology to the Development of Novel Vaccines. Immunobiology of Proteins and Peptides. 5. Vaccine Mechanism, Design, and Application (Advances in Experimental Medicine and Biology*, Vol. 251), Plenum Press, New York, London, 1989, pp. 83–98.

Journal of Chromatography, 559 (1991) 345–356
Elsevier Science Publishers B.V., Amsterdam

CHROM. 23 460

Application of high-performance capillary electrophoresis to the analysis of conformation and interaction of metal-binding proteins

HIDEYUKI KAJIWARA*
National Institute of Agrobiological Resources, Kannondai 2–1–2, Tsukuba, Ibaraki 305 (Japan)

ABSTRACT

A separation method using high-performance capillary electrophoresis was applied to the analysis of calcium- and zinc-binding proteins. Calcium-binding proteins (calmodulin, parvalbumin, thermolysin and proteolytic peptides of calmodulin), zinc-binding proteins (carbonic anhydrase and thermolysin), and internal standard proteins (carbonic anhydrase and lactoglobulin) were separated completely by capillary electrophoresis. Calcium- and zinc-binding proteins were obtained under Ca^{2+} and Zn^{2+}-containing conditions, respectively, cation-chelating conditions for the binding shift assay, and they showed that the binding shift depended on cations in the electrophoresis buffer in capillary zone electrophoresis and micellar electrokinetic chromatography. Two kinds of hydrophobic probes affected the electrophoretic mobility of calmodulin by interaction between its hydrophobic region and the hydrophobic probes under Ca^{2+}-containing conditions.

INTRODUCTION

High-performance capillary electrophoresis (HPCE) is developing rapidly and there are numerous demonstrating highly efficient separations of proteins and peptides [1]. Charged species will migrate electrophoretically towards the appropriate electrode and are separated by differences in their electrophoretic mobilities [2]. The rigorous description of the relationship between electrophoretic mobility and solute and solvent properties is given by the following equations [3,4]:

$$\mu = \frac{V}{E} = \frac{q}{6\pi r\eta}$$

where μ is the electrophoretic mobility, V is the migration velocity, E is the field strength, q is the net charge on the analyte, η is the solvent viscosity and r is the apparent Stokes radius of the analyte. Therefore, the electrophoretic mobility observed in a given solvent depends on the net charge and the apparent Stokes radius of the analyte.

Relatively new electrophoretic separation techniques, capillary zone electro-

0021-9673/91/$03.50

phoresis (CZE) [5] and micellar electrokinetic chromatography (MEKC) [6], are suitable fot the analysis of biological compounds. However, there has been no study concerning the conformation and the interaction of biological molecules such as calcium-binding proteins (CaBPs) using HPCE. It is clear that CaBPs are of importance as physiological regulators [7]. Studies from a number of laboratories have shown that many regulatory activities of Ca^{2+} ions are mediated by a signal CaBPs [8]. These proteins have remained highly conserved in structure and function [9]. Metal ions have an important role in biological reactions, *e.g.*, Zn^{2+} was shown to be essential for the active site of carbonic anhydrase [10] and thermolysin [11]. Herein, we report that the behaviour of CaBPs and zinc-binding proteins (ZnBPs) depends on cations and the interaction between the hydrophobic probes and the hydrophobic region on calmodulin (CaM) in HPCE. A preliminary report of the calcium-binding shift assay of CaBPs has been made [12].

EXPERIMENTAL

Reagents and materials

CaM (bovine testes) was obtained from Polyscience, parvalbumin (PV) (rabbit muscle), carbonic anhydrase (bovine erythrocyte) and lactoglobulin (bovine milk) from Sigma, arginylendopeptidase from Takara Shuzo, thermolysin (*Bacillus thermoproteolyticus* Rokko) from Seikagaku Kogyo, ethylenediaminetetraacetic acid (EDTA) from Dojin Chemical, N-[tris(hydroxymethyl)methyl]glycine (tricine) from Merck and N-(6-aminohexyl)-5-chloro-1-naphthalenesulphonamide (W-7) and 10-[3-(4-methylpiperazin-1-yl)propyl]-2-trifluoromethylphenothiazine (trifluoperazine) from Nacalai Tesque. All other chemicals were purchased from Wako.

Method

The protein runs were carried out in a fused-silica capillary of 50 μm I.D. and total length 122 cm (100 cm to the detector), which was filled with an electrophoresis buffer of 0.1 *M* tris(hydroxymethyl)aminomethane (Tris)–0.1 *M* tricine (pH 8.3) [13] or 50 m*M* Tris–384 m*M* glycine [14] (pH 8.3) with several additives (2 m*M* calcium chloride, zinc chloride and EDTA) for CZE. For MEKC, 0.1% sodium dodecyl sulphate (SDS) was added to 0.1 *M* Tris–0.1 *M* tricine (pH 8.3). Proteins (2.5 mg/ml) were dissolved in the electrophoresis buffer. To study the interaction between the hydrophobic probes (trifluoperazine or W-7) and the hydrophobic region on CaM, 50 μM of hydrophobic probes was added in the electrophoresis buffer. Detection was by UV absorption at 200 nm. A sample was introduced into the capillary by vauum injection for 1.0 s after washing with 1.0 *M* sodium hydroxide solution for 15 min and the electrophoresis buffer for 15 min, and electrophoresis was carried out at 30 kV (Applied Biosystems Model 270A).

RESULTS AND DISCUSSION

Binding shift assay in CZE

To obtain better separation and analytical efficiencies for proteins and peptides, three kinds of electrophoresis buffers, Tris–tricine, Tris–glycine and Tris–borate [15], were used for CZE. Two standard proteins (carbonic anhydrase and lactoglobulin)

and cation-binding proteins were separated well with Tris–tricine and Tris–glycine buffers (Fig. 1). However, Tris–borate buffer showed an unstable separation of proteins in the presence of EDTA in the electrophoresis buffer (data not shown).

The electropherogram for the CZE analysis of the Ca-binding shift assay is shown in Fig. 1. The first five peaks (1–5) and three other peaks (6–8) represented carbonic anhydrase and lactoglobulin, respectively. Although the broadening of lactoglobulin peaks occurred in this system, the accuracies of the migration time of two standard proteins were preserved. The peak of CaM was observed at 32.79 min in the presence of Ca^{2+} ions in a CZE separation, but the peak of CaM was observed at 44.42 min under Ca^{2+}-chelating conditions without any significant change of the

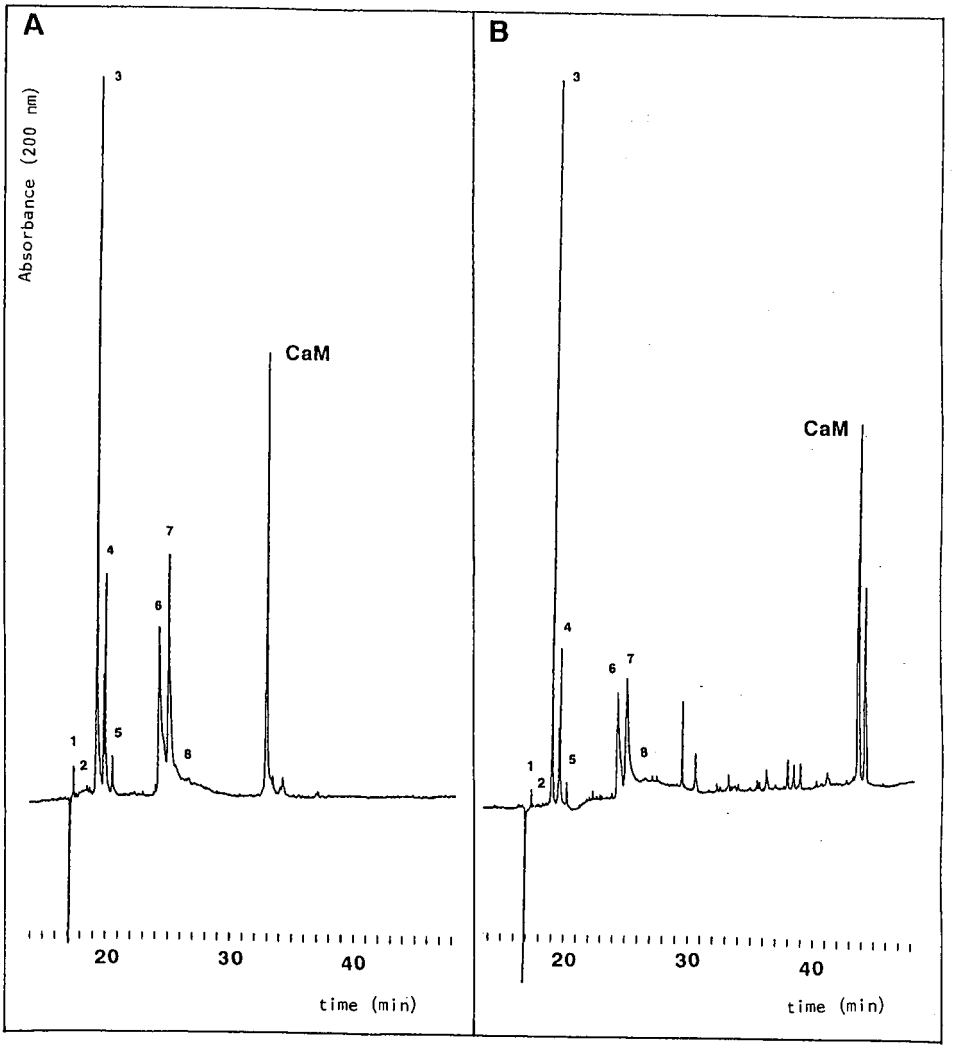

Fig. 1. CZE of carbonic anhydrase (1–5), lactoglobulin (6–8) and CaM for calcium-binding shift assay. Each protein (2.5 mg/ml) was dissolved in Tris–tricine electrophoresis buffer. (A) 2 m*M* calcium chloride in the electrophoresis buffer; (B) 2 m*M* EDTA in the electrophoresis buffer.

migration times of standard proteins. The migration velocity of CaM depended on the Ca^{2+} ions in the electrophoresis buffer, and it increased by Ca^{2+} binding to CaM. The migration velocity of CaM was altered through complexes of calcium-binding sites and Ca^{2+} ions. The complexing altered the net charge on CaM and the Stokes radius of CaM caused by conformational changes. The factor $k(+/-)$, the ratio of the net charge on protein between the Ca^{2+}-containing conditions and the Ca^{2+}-chelating conditions, can be calculated by the following equation:

$$k(+/-) = \frac{q(+)}{q(-)} = \frac{V(+)r(+)}{V(-)r(-)} = \frac{t(-)r(+)}{t(+)r(-)}$$

where + and − represent the presence and absence of Ca^{2+} ions in the electrophoresis buffer, respectively, and t is the migration time of CaM. The Stokes radius of CaM was 2.09 and 2.14 nm in the presence and absence of Ca^{2+} ions, respectively, in CaM [16]. The binding shift of CaM depended mainly on the ratio of the net charge on CaM between the Ca^{2+}-containing conditions and the Ca^{2+}-chelating conditions rather than the ratio of the Stokes radius of CaM between them, because there was only a 2% variance of the Stokes radius between the two sets of conditions. The electroendo-osmotic velocity might not be changed significantly because carbonic anhydrase and lactoglobulin showed same migration times under both conditions. The same phenomenon, a binding shift of CaM in Tris–glycine buffer (data not shown), was also observed. Several experiments on the calcium-binding shift assay of CaM as a function of Ca^{2+} concentration were performed between 2 and 0.2 m*M* calcium chloride, but there was no significant change in behaviour of the calcium-binding shift of CaM (data not shown).

The peak of PV was also shifted on addition of Ca^{2+} ions to the electrophoresis buffer (Fig. 2). The peak of PV was detected between five carbonic anhydrase peaks and three lactoglobulin peaks under Ca^{2+}-chelating conditions, but the peak of PV that contained three Ca^{2+} ions in its binding sites was detected between the peaks 3 and 4 of carbonic anhydrase.

Bovine CaM consists of 148 amino acids and has four specific calcium-binding sites [9]. Two calcium-binding sites (domains 1 and 2) out of the four could be isolated intact by arginylendopeptidase digestion. Four of the starred peaks in Fig. 3 disappeared completely from the electropherogram in the presence of Ca^{2+} ions in the electrophoresis buffer. A possible explanation of this disappearance is that the peptides that bound Ca^{2+} ions changed the net charge or the Stokes radius of the peptide, and therefore the migration velocity or migration direction of the peptide drastically changed. Peptide fragments obtained with trypsin (this protease did not preserve any calcium-binding sites of CaM) did not show the variance in eletropherograms between the two sets of conditions (data not shown).

Fig. 4 shows the Zn^{2+}-dependent variance for carbonic anhydrase. Higher peaks were obtained in the presence of Zn^{2+} ions in the electrophoresis buffer. An increase in the two peaks was not observed on addition of calcium chloride or sodium chloride to the electrophoresis buffer (data not shown). However, carbonic anhydrase did not show the complete binding shift that was observed in the calcium-binding shift assays of CaM and PV. Inactivation of protein by denaturation or a weak affinity of the active site for Zn^{2+} ions of carbonic anhydrase prevented the transition of the peak from a complete binding shift.

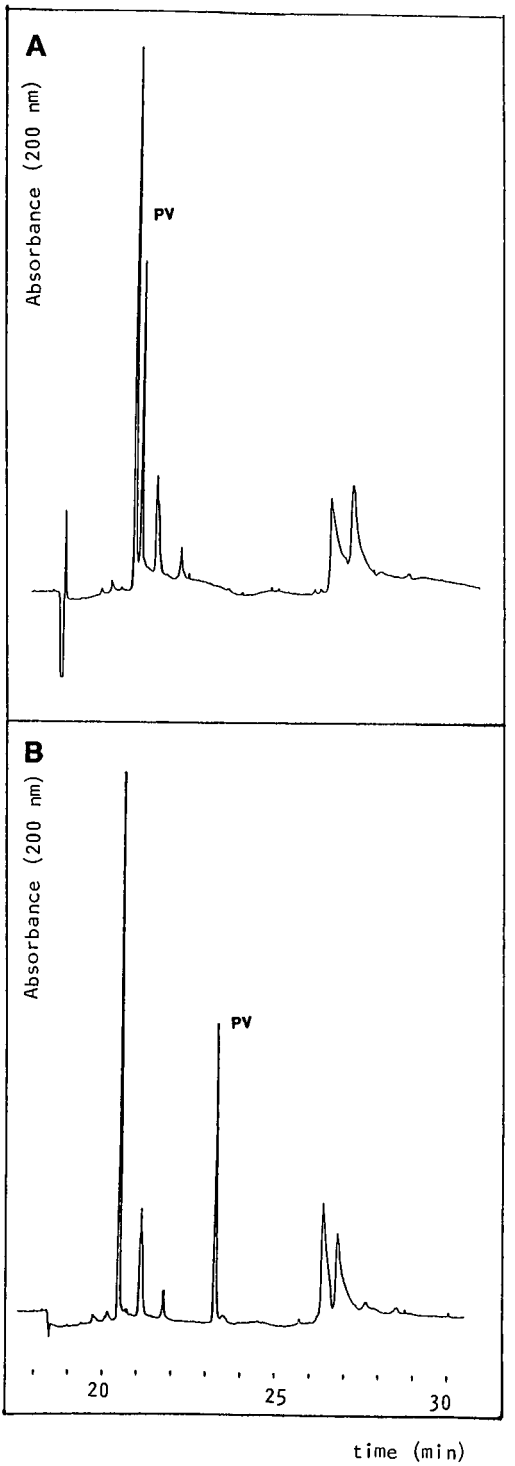

Fig. 2. CZE of carbonic anhydrase, lactoglobulin and PV for calcium-binding shift assay. Each protein (2.5 mg/ml) was dissolved in Tris–tricine electrophoresis buffer. (A) 2 m*M* calcium chloride in the electrophoresis buffer; (B) 2 m*M* EDTA in the electrophoresis buffer.

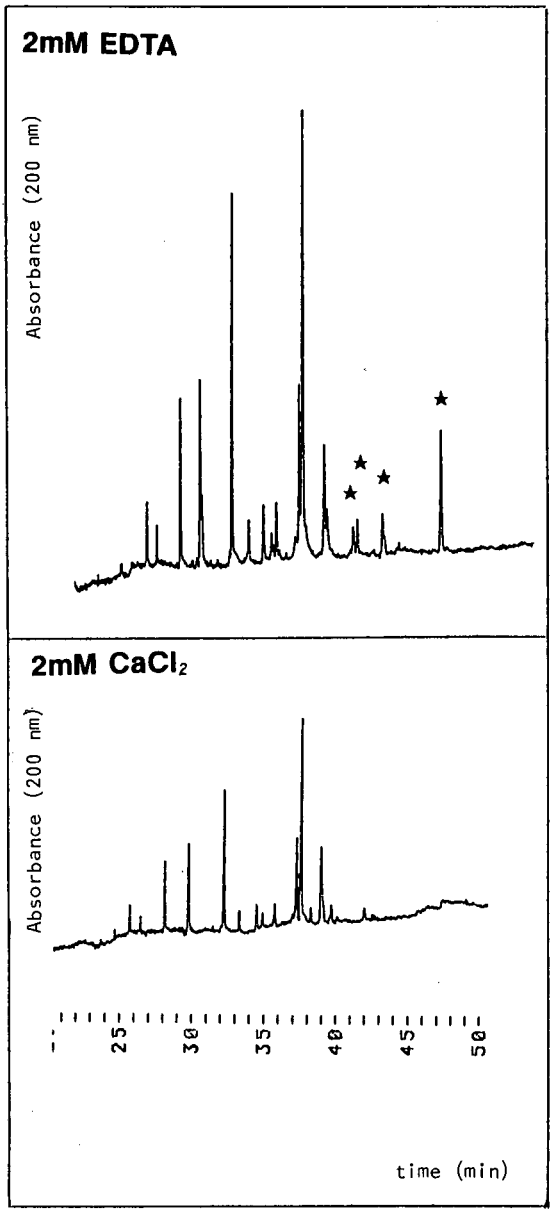

Fig. 3. Peptide mapping of proteolytic fragments of CaM by arginylendopeptidase in CZE. Top, 2 m*M* EDTA; bottom, 2 m*M* calcium chloride.

Thermolysin is a metalloproteinase that binds four Ca^{2+} ions for stability of conformation and one Zn^{2+} ion for the active site [11]. This protease is stable in 1% SDS or 8 *M* urea, and the proteinase activity is preserved. In the presence of EDTA, thermolysin was detected as a broad peak in a Tris–tricine electrophoresis buffer

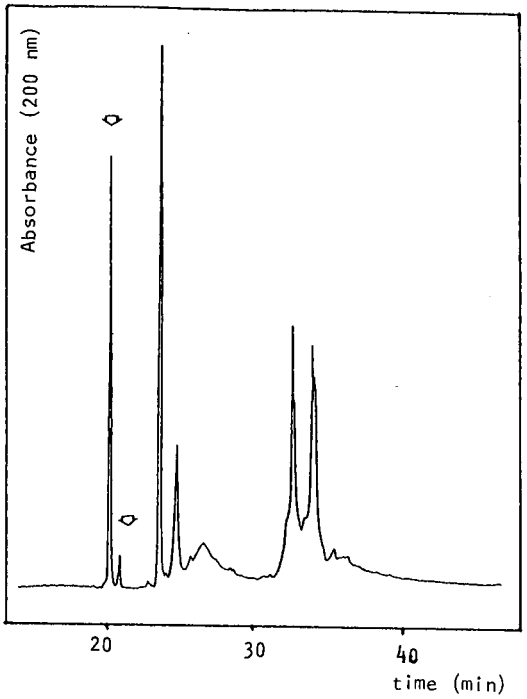

Fig. 4. Partial binding shift of carbonic anhydrase in CZE with 2 m*M* zinc chloride in the electrophoresis buffer. Arrowhead peaks increased in height.

system (Fig. 5). This broadening of the thermolysin peak might reflect the instability of the protein conformation. When 2 m*M* zinc chloride was added to the electrophoresis buffer, the peak of thermolysin varied and relatively sharp peaks were detected. Ca^{2+} ions changed the electropherogram drastically: the peak appeared as a single, sharp peak in the front of the endoosmotic flow peak. In the presence of both cations, the electropherogram did not change significantly and it showed the same electrophoresis pattern as for the addition of Ca^{2+} ions in the electrophoresis buffer. A drastic conformational change occurred because of binding of Ca^{2+} ions and this caused a drastic change in the net charge of thermolysin. These electropherograms for calcium- and zinc-binding shift assays indicate that Ca^{2+} and Zn^{2+} ions were essential for the thermolysin to create an appropriate active site and conformation.

Binding shift assay in MEKC

Variance of the electrophoretic mobility of CaM was also observed in MEKC (Fig. 6). The conformation of CaM remained even in the presence of 0.1% SDS and the migration velocity was greatly changed between the Ca^{2+}-containing conditions and the Ca^{2+}-chelating conditions. This change in electrophoretic mobility might be mainly affected by the hydrophobicity rather than the net charge or the Stokes radius of CaM.

PV also showed the calcium-binding shift in MEKC, although the binding shift

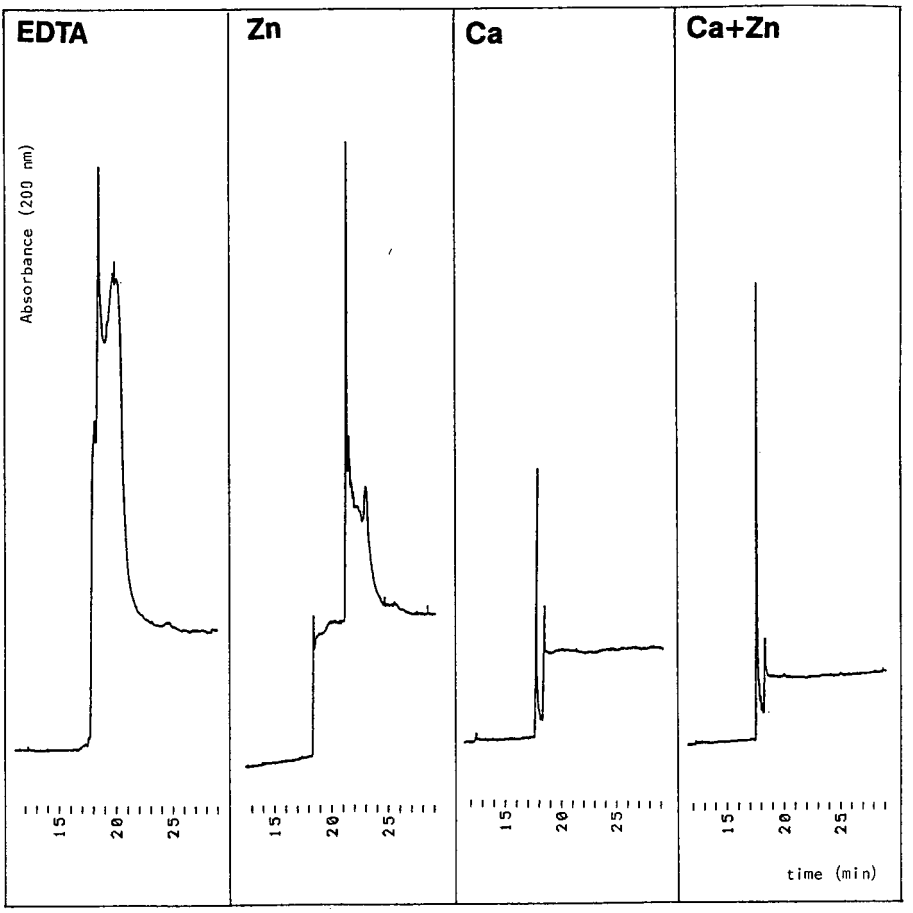

Fig. 5. CZE of thermolysin in the presence of 2 m*M* EDTA, 2 m*M* zinc chloride and 2 m*M* calcium chloride.

of PV in MEKC was less than that of CaM (Fig. 7). These results suggested that the hydrophobicity of PV was not changed so much by Ca^{2+} binding to PV.

A binding shift assay in MEKC was performed for thermolysin (Fig. 8). Under cation chelating conditions, the peak of thermolysin was detected after 80 min in electrophoresis runs. In the presence of Ca^{2+} ions, the migration time of thermolysin drastically changed and the peak of thermolysin was detected at the front of the water peak in MEKC containing 0.1% SDS. The migration velocity of thermolysin was faster than that of the water peak in the presence of 0.1% SDS. When the micellar concentration in the electrophoresis buffer was increased, the peak of thermolysin shifted backwards, depending on the concentration of SDS.

Interaction between hydrophobic probes and the hydrophobic region on CaM

As shown in Fig. 6, the appearance of a hydrophobic region on the surface of CaM by binding of Ca^{2+} ions was suggested by the binding shift assay of CaM in

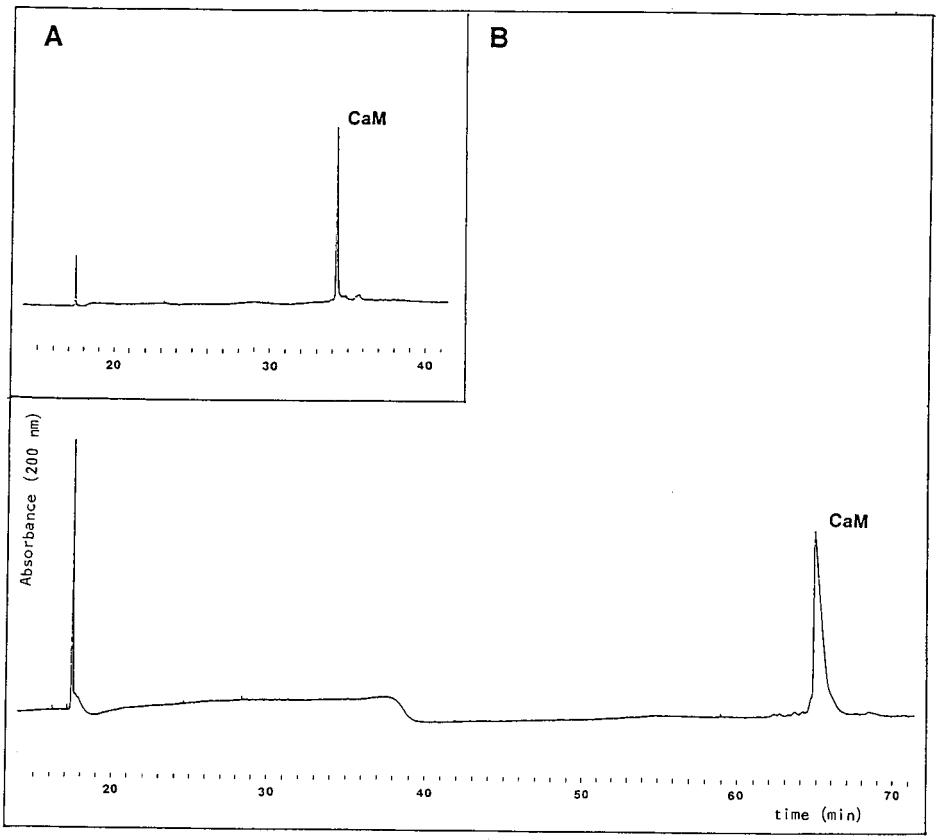

Fig. 6. Binding shift assay of CaM in MEKC. (A) 2 m*M* calcium chloride in the electrophoresis buffer; (B) 2 m*M* EDTA in the electrophoresis buffer.

MEKC. Two kinds of hydrophobic probes were mixed with the electrophoresis buffer (50 μM) and both conditions of Ca^{2+}-containing and Ca^{2+}-chelating conditions were compared (Table I). Only in the presence of Ca^{2+} ions did a hydrophobic region appear on the surface of CaM and the interaction between hydrophobic probes and the hydrophobic region on CaM could be observed. Therefore, a shift of the CaM peak occurred in the presence of Ca^{2+} ions, and the interaction between each standard protein and the hydrophobic probes must be same whether the hydrophobic probes interacted with standard proteins or not. The means of the migration time shown in Table I represent at least five repeated HPCE experiments; two major peaks of carbonic anhydrase (3 and 4) and lactoglobulin (6 and 7) (Fig. 1) were selected for the calculation as reference peaks.

The ratio of the migration time in the presence and absence of trifluoperazine, Ca/Ca(Trif), indicated the shift being caused by hydrophobic probe under Ca^{2+}-containing conditions. Theoretically, the difference in migration time, Ca/Ca(Trif) – EDTA/EDTA(Trif), of carbonic anhydrase and lactoglobulin must be 0% because of the identical interactions between the protein and the hydrophobic probes. The value

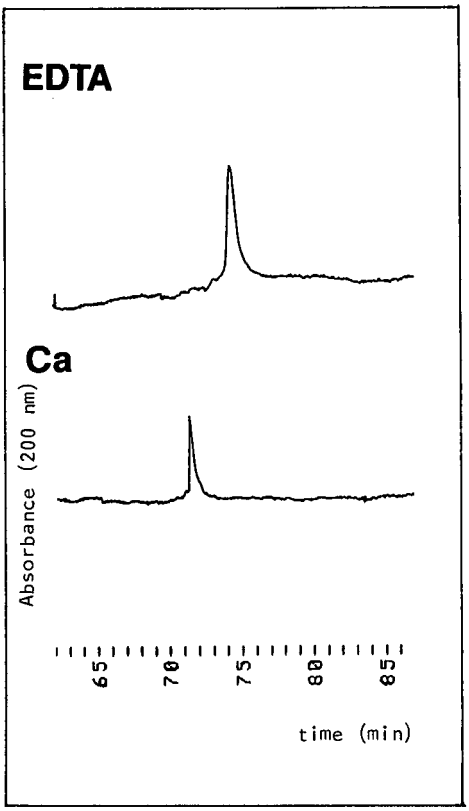

Fig. 7. Calcium-binding shift assay of PV in MEKC. The migration time of PV was 71.34 and 74.34 min in the presence of calcium chloride and EDTA, respectively.

of Ca/Ca(Trif) − EDTA/EDTA(Trif) was, however, −0.64%, 0.47%, 0.72% and 0.42% for the reference peaks, but the value was 1.22% for CaM.

A similar calculation was performed to investigate the interaction between CaM and W-7. The value of Ca/Ca(W-7) − EDTA/EDTA(W-7) was 2.03% for CaM. According to the calculations, a significant interaction between the hydrophobic probes and the hydrophobic region on CaM occurred in HPCE.

CONCLUSIONS

CaBPs (CaM, PV and thermolysin) and ZnBPs (carbonic anhydrase and thermolysin) varied the migration velocity depending on suitable cations in the electrophoresis buffer in CZE and MEKC. An interaction between the hydrophobic region of CaM and the hydrophobic probes was observed in CZE. The binding shift assay in HPCE is a simple and rapid technique for the analysis of conformation and interaction of proteins.

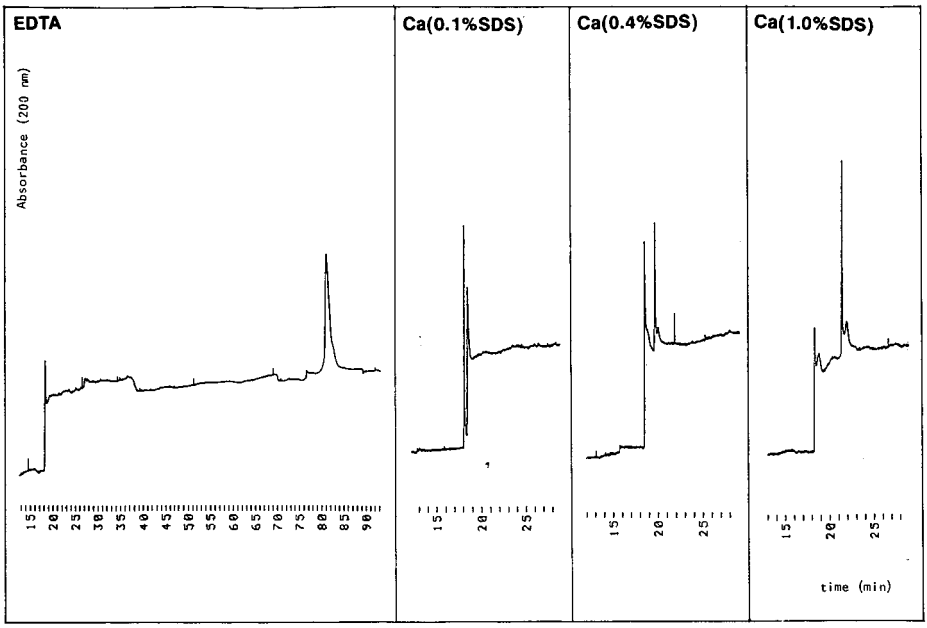

Fig. 8. Cation-binding shift assay of thermolysin in MEKC. EDTA or calcium chloride (2 m*M*) was added to the electrophoresis buffer. The concentration of SDS was 0.1%, 0.4% and 1.0%.

TABLE I

BINDING SHIFT ASSAY OF CaM DEPENDING ON THE INTERACTION BETWEEN THE HYDROPHOBIC PROBES, TRIFLUOPERAZINE (Trif) AND W-7, AND THE HYDROPHOBIC REGION ON CaM

Parameter	Carbonic anhydrase 1	Carbonic anhydrase 2	Lacto-globulin 1	Lacto-globulin 2	Calmodulin
Ca	19.126 min	19.802 min	24.007 min	24.949 min	32.789 min
EDTA	18.891 min	19.544 min	23.958 min	24.994 min	44.415 min
Ca/EDTA	100.58%	100.66%	99.55%	99.17%	73.34%
Ca(Trif)	17.801 min	18.411 min	22.424 min	23.295 min	29.735 min
EDTA(Trif)	18.842 min	19.504 min	24.309 min	25.273 min	43.962 min
Ca(Trif)/EDTA(Trif)	101.23%	101.14%	98.84%	98.75%	72.47%
Ca/Ca(Trif)	100.14%	100.26%	99.79%	99.83%	102.78%
EDTA/EDTA(Trif)	100.78%	100.73%	99.07%	99.41%	101.56%
Ca/Ca(Trif) − EDTA/EDTA(Trif)	−0.64%	0.47%	0.72%	0.42%	1.22%
Ca(W-7)	19.229 min	19.909 min	24.331 min	25.308 min	32.602 min
EDTA(W-7)	19.002 min	19.677 min	24.220 min	25.268 min	45.020 min
Ca(W-7)/EDTA(W-7)	100.44%	100.43%	99.72%	99.41%	71.88%
Ca/Ca(W-7)	100.42%	100.42%	99.63%	99.54%	101.54%
EDTA/EDTA(W-7)	100.28%	100.17%	99.77%	99.77%	99.51%
Ca/Ca(W-7) − EDTA/EDTA(W-7)	0.14%	0.25%	−0.14%	−0.23%	2.03%

ACKNOWLEDGEMENTS

The author thanks Drs. H. Hirano, S. Komatsu and K. Oono for discussions and encouragement.

REFERENCES

1 W. G. Kuhr, *Anal. Chem.*, 62 (1990) 403.
2 P. D. Grossman, J. C. Colburn, H. H. Lauer, R. G. Nielsen, R. M. Riggin, G. S. Sittamoalm and E. C. Rikard, *Anal. Chem.*, 61 (1989) 1186.
3 P. D. Grossman, J. C. Colburn and H. H. Lauer, *Anal. Biochem.*, 179 (1989) 28.
4 P. D. Grossman, K. J. Wilson, G. Petrie and H. H. Lauer, *Anal. Biochem.*, 173 (1988) 265.
5 R. G. Nielsen and E. C. Rickard, *J. Chromatogr.*, 56 (1990) 99.
6 H. Nishi, N. Tsumagari and S. Terabe, *Anal. Chem.*, 61 (1989) 2434.
7 N. D. Moncrief, R. H. Kretsinger and M. Goodman, *J. Mol. Evol.*, 30 (1990) 522.
8 Y. Sami and K.-Y. Ling, *Science (Washington, D.C.)*, 249 (1990) 1441.
9 H. Kasai, Y. Kato, T. Isobe, H. Kawasaki and T. Okuyama, *Biomed. Res.*, 1 (1980) 248.
10 M. Sociaky, N. Limozin, D. Filippi-Foveau, J. M. Gulian and G. Laurent-Tabusse, *Biochimie*, 58 (1976) 1071.
11 K. Titani, M. A. Hermodson, L. H. Ericsson, K. A. Walsh and H. Neurath, *Nature New Biol.*, 238 (1972) 35.
12 H. Kajiwara, H. Hirano and K. Oono, *J. Biochem. Biophys. Methods*, 22 (1991) 263.
13 H. Schagger and G. V. Jagow, *Anal. Biochem.*, 166 (1987) 368.
14 B. J. Davis, *Ann. N.Y. Acad. Sci.*, 121 (1964) 321.
15 *Counter-migration Capillary Electrophoresis (CMCC) in DNA Restriction Fragment Analysis, Application Note No. 28*, Applied Biosystems, Tokyo, 1990.
16 C. B. Klee, *Calcium and Cell Function*, Academic Press, New York, 1980.

Journal of Chromatography, 559 (1991) 357–366
Elsevier Science Publishers B.V., Amsterdam

CHROM. 23 454

Electrophoretic mobility modeling of proteins in free zone capillary electrophoresis and its application to monoclonal antibody microheterogeneity analysis

BRUCE JON COMPTON*
Bristol-Myers Squibb Co., Industrial Division, P.O. Box 4755, Syracuse, NY 13221-4755 (USA)

ABSTRACT

A semi-empirical model for describing the electrophoretic mobility of proteins in free solution is derived. Protein mobility is found to be influenced, as dictated by the Debye–Hückel–Henry theory, by protein valence, size and shape, and by solution ionic strength, pH, viscosity and temperature. Protein valence, the most important mobility determining parameter intrinsic to the protein, is calculated for a given pH from its amino acid content using the Henderson–Hesselbalch equation. Electrostatic charge suppression causes actual valence to be less than that calculated. To equate the two an experimentally determined proportionality constant (F_Z) is introduced. Consequently, F_Z can be applied to the calculated valence and mobility–pH titration curve for a protein, resulting in the actual mobility of the protein at any given pH. The model further predicts that the molecular weight (M) dependency of mobility should be a continuous function of $M^{-1/3}$ to $M^{-2/3}$, depending on the magnitude of the protein molecular weight and buffer ionic strength under investigation. Many aspects of the model are demonstrated by its application to the resolution of immunoglobulin G isoelectrotypes, normally only resolved using isoelectric focusing.

INTRODUCTION

Capillary zone electrophoresis (CZE) in free solution has proved useful for the analysis of non-volatile thermally labile molecules such as proteins. The method is characterized by a high theoretical plate count (the generation of greater than 10^5 plates/min [1]) and, in the free solution mode, operational simplicity. Application for the resolution of immunoglobulin isoelectrotypes or other proteins which exhibit microheterogeneity would appear logical, and CZE has been used, for example, in work on the analysis of proteins such as human growth hormone (rhGH), tissue plasminogen activator and CD4, tryptic digest of rhGH [2,3], and transferrin variants [4].

A question that comes to mind when considering therapeutic applications is whether it would be possible to predict conditions under which CZE in free solution is capable of distinguishing between a native protein and a variant (or degradant) which differs from the native form because of, for example, multiple deamidation events (Gln to Glu or Asn to Asp). To address this question a general model describing protein electrophoretic mobility is needed.

0021-9673/91/$03.50

One of the benefits of working with recombinant or well characterized proteins is that either their primary sequence or at least their amino acid content is known or easily obtained from commercial data bases. In principle, this sequence data can be used to determine a theoretical titration curve for the protein, which gives the calculated protein valence (Z_c) as a function of pH. Z_c should always be greater than actual protein valence (Z_a) because of electrostatic charge suppression [5,6], but a direct proportionality is postulated to exist between the two [7–10]. This proportionality constant (F_Z), is expected to be dependent on both the nature of the protein and its environment.

The molecular weight (M) of a protein can also be calculated from the sequence data and with some assumptions about the partial specific volume of the protein, can be used to calculate an equivalent radius (r_e), which is then equated to the protein's Stokes radius (r) after the application of a correction factor such as a frictional ratio. With this information, a classic model based on the Debye–Hückel–Henry theory (DHHT, [11–14]) is employed to predict electrophoretic mobility (u) of the protein.

The rationale for this approach is historically well developed, since much work has been done confirming the usefulness of the DHHT for describing the electrophoretic mobility of amphoteric species such as proteins [15,16]. In this previous work the critical parameter of protein valence (Z) was obtained either by direct titration or by measurements of membrane potentials, while size parameters were obtained through diffusion measurements [7–16]. The use of Z_c and r_e rather than Z and r to calculate u sacrifices accuracy but eliminates the need to measure Z and r experimentally, a task requiring considerable amounts of material and time.

THEORY

Electrophoretic mobility model

In electrolyte solution under unit field strength (1 V/m) the Debye–Hückle–Henry theory can be used to develop a general expression for protein mobility (u) such that

$$u = (Ze/6\pi nr)(1/1 + kr)\phi(kr) \tag{1}$$

where Ze, the product of the protein valence and e, the charge of an electron ($1.602 \cdot 10^{-19}$ C), gives protein net charge, n is solution viscosity (0.000895 kg/ms, water at 25°C), r is the Stokes radius (distance in m from the particle center to where solvent slippage occurs), $\phi(kr)$ is Henry's function [11], and k, the Debye parameter (m^{-1}), is $2^{1/2}Ne(e_0e'RT)^{-1/2}I^{1/2}$, where N is Avogadro's number, e_0 is the fluid dielectric constant (78.54, water 25°C), e' is permittivity of free space ($8.854 \cdot 10^{-12}$ C^2/Jm), R is the gas constant (8.314 J/K mol), T is absolute temperature, and I is solution ionic strength (mol/m^3). I is further defined as $\sum C_i/2z_i^2$, where C_i is ion concentration (mol/m^3), and z_i the valence of fluid ions. The magnitude of $\phi(kr)$ varies from 1.0 to 1.5 in a sigmoidal fashion as kr increases from zero to infinity.

The Debye parameter (k) represents the reciprocal thickness of the ionic atmosphere surrounding the protein [17]. The expression $1/1+kr$ indicates that the mobility of a protein has ionic strength (I) dependency, sometimes overshadowed in CZE by experimental complications [18]. This dependency is not a strict inverse

proportionality but can be expressed from eqn. 1 directly as

$$u = \frac{Ze\phi(kr)(e_0e'RT)^{1/2}}{6\pi nr(1 + 2^{1/2}Ner)I^{1/2}} \tag{2}$$

Eqn. 1 can be made more useful, but more approximate, by expressing the size dependency of mobility using protein molecular weight rather than radius, as discussed by Oncley [19], through the relationship

$$r_e = (3Mv/4\pi N)^{1/3}(f/fo) \tag{3}$$

where r_0 is equivalent radius (m), v is protein partial specific volume and (f/fo) is a frictional ratio discussed below. Substitution of eqn. 3 into eqn. 1 gives eqn. 4

$$u = \frac{K(1)Z}{K(2)\mathrm{M}^{1/3} + K(3)\mathrm{M}^{2/3}} \tag{4}$$

where terms $K(1) = e\phi(kr)$, $K(2) = 6\pi n(f/fo)(4\pi N/3v)^{-1/3}$ and $K(3) = 6\pi n(2^{1/2}Ne) \cdot (e_0e'RT)^{-1/2}(f/fo)^2(4\pi N/3v)^{-2/3}I^{1/2}$.

The equivalent radius is made equal to Stokes radius by the frictional ratio (f/fo), such that $r_e(f/fo) = r$, which corrects for protein asymmetry and hydration [19]. The frictional ratio usually varies from 1.0 (ideal behavior) to 1.7 for globular proteins having non-spherical dimensions, to greater than 3 for a cylindrical protein such as myosin.

Eqn. 4 indicates that a protein's valence is its most important attribute with regard to determining its mobility. Molecular weight exhibits an inverse influence which varies continuously from $M^{1/3}$ to $M^{2/3}$ depending on the magnitude of the molecular weight and ionic strength [coefficient $K(3)$] range under examination.

Calculation of protein valence

As mentioned, one benefit of investigating therapeutic proteins is that they are usually well characterized with respect to their primary sequence, amino acid content and modifications (glycosylation, phosphorylation, etc.). With this information it is possible to calculate the protein's theoretical valence–pH titration curve using the Henderson–Hasselbalch equation. This gives its calculated net valence (Z_c) at a given pH. In this work the extended method of Sillero and Ribeiro [20] is used and the expression used to calculate Z_c is as follows:

$$Z_c = \sum_{n=1-4} \frac{Pn}{1 + 10^{\mathrm{pH} - \mathrm{p}K(Pn)}} - \sum_{n=1-5} \frac{Nn}{1 + 10^{\mathrm{p}K(Nn) - \mathrm{pH}}} \tag{5}$$

where pH refers to the buffer, Pn and Nn the integral number of each amino acid of that type, and p$K(Pn)$ and p$K(Nn)$ its respective ionization potential. The pK values and the respective number of each charged amino acid type in native chimeric L6 are given in Table I.

TABLE I

LIST OF IONIZATION CONSTANTS OF AMINO ACIDS

Amino acid type		pK_a	Charged amino acid content of cL6
P1	HIS	6.4	22
P2	tNH_2	8.2	4
P3	LYS	10.4	100
P4	ARG	12.0	30
N1	tCOOH	3.2	4
N2	ASP	4.0	46
N3	GLU	4.5	64
N4	CYS	9.0	32
N5	TYR	10.0	62

As mentioned in the introduction, the magnitude of Z_c is expected to be greater then actual protein charge (Z_a) due to electrostatic charge suppression. Though the ionization constants used by Sillero and Ribeiro are taken from peptides, Z_c is a simple sum of the individual charges of amino acids and its calculation does not account completely for electrostatic interactions which can modify an amino acid's (side chain or terminal) ionization potential by 2–3 units [5,6]. A similar bias has been described in the past for studies which attempted to equate protein valances obtained from titration, membrane potentials, and mobility measurements. Valence measurements from membrane potentials gave results consistent with mobility measurements while titration results overestimated protein valence [9].

Because of electrostatic considerations, the differences between Z_c and Z_a are most pronounced at electrolyte pH values at which the protein has an appreciable charge, *i.e.* far from the isoelectric point (p*I*) of the protein. Consequently, titration curves for proteins flatten out at pH values far from the p*I* of the molecule, at pHs where the proteins should still be gaining appreciable charge [5].

Some additional evidence for this discrepancy can be seen in the recent work of the derivation of an empirical expression for predicting peptide mobility as a function of sequence and size [21]. It was found that a non-linear relationship [$\ln(Z_c + 1)$] between calculated charge and mobility existed. This relationship must be valid since it empirically relates Z_c to u. However, a contradiction arises since it is well documented that a direct relationship exists between u and Z_a as predicted from fundamental principles and determined experimentally by a variety of means, for such diverse entities as ions and particles. This discrepancy can be accounted for when one considers that the difference between Z_c and Z_a increases at pH values far from the p*I* of the peptide and that this difference was not accounted for when deriving the empirical expression.

The proportionality that exists between Z_c and Z_a for any given protein under a particular set of conditions such as solution pH [5,6], is expressed by $Z_c = Z_a F_Z$. Since F_Z is independent of pH, it can be determined for one solution pH and, along with the theoretical titration curve and eqn. 4, be used to calculate u for other pH conditions. This in turn allows optimization of conditions for resolving protein variants.

One problem associated with this approach is that in the calculation of Z_c no consideration is given for variations in amino acid ionization potentials as a function of buffer type and ionic strength. These differences are factored into F_Z and accordingly, a given value for F_Z is expected to be valid only for the experimental conditions —*i.e.*, solution ionic strength, dielectric constant and temperature— under which it is determined.

EXPERIMENTAL

CZE was conducted on a Bio-Rad HPE 100 system (Bio-Rad Labs., Richmond, CA, USA) with a 25 μm I.D. coated capillary, with 0.20 m between electrode reservoirs and 0.172 m from the injection reservoir to detector. Reagent-grade sodium orthophosphate buffer was used (Fisher Scientific, Pittsburg, PA, USA). Detection was by ultraviolet absorption at 200 nm. Sample concentrations were generally 100 μg/ml, made up with a diluent that gave a final sample solution of 10% ionic strength of the electrophoresis buffer used in any particular experiment. Most experiments were conducted with + 12 000 V at the injector reservoir which, based on the lack of current variation during the initiation of a run, did not cause appreciable capillary heating. All samples were loaded by electromigration, the potential and duration of which varied with experiment. All experimental conditions were studied using triplicate sample introductions and reported as mean results of the main electrophoretic band. The use of coated capillaries reduced electroendoosmosis to non-measurable levels [22].

Immunoglobulin G (IgG) monoclonal antibody chimeric L6 (human-murine, estimated p*I* 10.2) was either produced at the Bristol-Myers Squibb Syracuse site or obtained from Oncogen (Seattle, WA, USA). Samples were stored at −70°C in phosphate buffered saline at 5 mg/ml. For use, samples were thawed on a rotary shaker at 32°C for 2 h, diluted appropriately, and analyzed as above. All other samples and materials were purchased from Sigma (St. Louis, MO, USA).

RESULTS AND DISCUSSION

Fundamental models for calculating the electrophoretic mobility of proteins require charge and size information obtainable only through tedious membrane potential and diffusion studies. Because buffer type and ionic strength affect protein p*I*, these studies must be carried out under conditions identical to the electrophoretic studies [10,16]. This experimentally derived information often allows exact calculation of protein mobility from first principles [9,12], and as such is useful for demonstrating the validity of these principles. However, this approach is not practical for optimizing protein resolution in CZE, therefore, an effort has been made to use readily available sequence information to calculate protein valence and size. This results in a calculated valence–pH titration curve for the protein which, when corrected for by experimentally determined F_Z, allows calculation of a protein's actual valence and mobility at all pH values.

This approach has been developed specifically to address the CZE resolution of protein isoelectrotypes often encountered when developing therapeutic proteins such as antibodies and growth factors. This is a special case of a protein which exhibits microheterogeneity with regard to charge, but not size, presumably due to variations in

primary sequence, for instance, from protein degradation though deamidation, or alternatively in charged carbohydrate portions of the molecule [2–4,23]. In either case, this semi-empirical model is intended to allow quantitative prediction on how best to optimize a CZE resolution of isoelectrotypes.

The electrophoretic mobility model developed here has resulted in eqn. 4, which indicates that u is directly proportional to protein charge Z and inversely proportional to molecular weight in a continuous fashion from $M^{1/3}$ to $M^{2/3}$, depending on the magnitude of M and the solution ionic strength (I). Protein charge is the most sensitive parameter governing mobility, and is directly controlled through adjustments to solution pH, such that achievement of resolution of similar sized native proteins in CZE is most practically brought about by controlling this parameter. Additional selectivity can be achieved through the specific interactions of various ions on specific proteins.

The calculated mobility and valence–pH relationship of a protein is obtained using eqns. 4 and 5 and values in Table I, examples for which are shown in Fig. 1 and 2 for IgG chimeric L6. Fig. 1 further illustrates the constant bias postulated between experimental mobility results and u calculated using the DHHT and Z_c. This bias is accounted for by modifying Z_c using F_Z; in this case F_Z, which is determined by directly ratioing calculated and measured mobility for a solution pH of 2.5, is 5.66. Once this correction is made to Z_c, mobility is seen to be directly proportional to protein valence. As previously mentioned, this bias between experimental and calculated mobility and direct proportionality between mobility and Z, as determined using titration and membrane potentials, has been previously demonstrated for a number of proteins.

The titration curves further indicate the appropriate choice of buffer pH for optimum mobility discrimination between isoelectrotypes, as shown in Fig. 2 for hypothetical desamido forms of cL6. The figure indicates that resolution of these

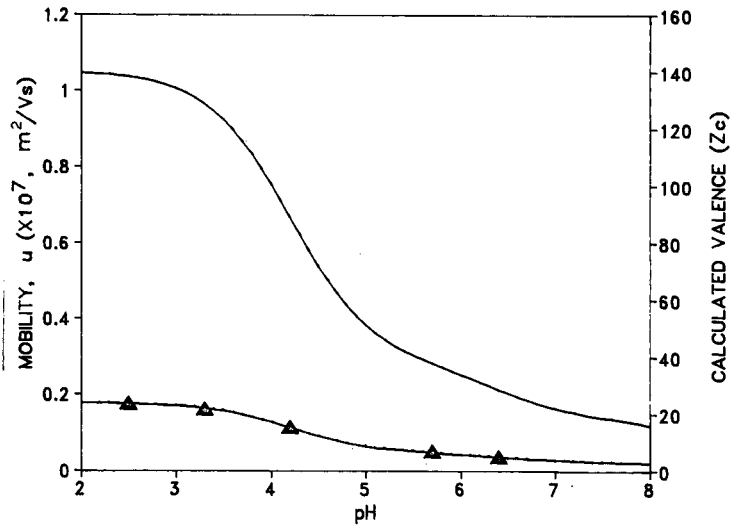

Fig. 1. Calculated (solid line) and experimental (triangles) mobilities for cL6. The calculated results were obtained from eqns. 4 and 5 using constants and parameters given in Table I. The calculated values, when corrected for a F_Z of 5.66, gave the mobilities shown by the dashed line.

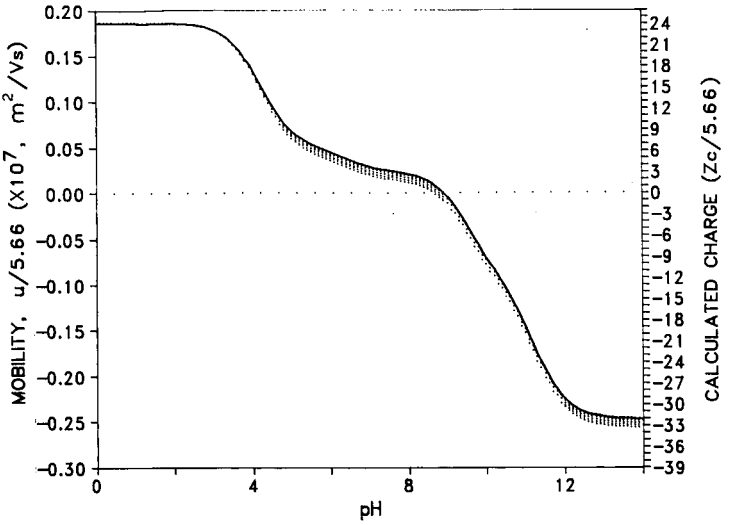

Fig. 2. Calculated mobility and valence titration curve for native and hypothetical deamidated cL6 from eqns. 4 and 5 and Table I. The solid line shows the mobility for the native form while each subsequent dashed line is the mobility for deamidated cL6 occurring at intervals of 5 (by the sequential substitution of 5 Glu for 5 Gln residues per curve).

degradants is best achieved at pH values between 4 and 8, or above 12. The expected time of migration (t) of native and deamidated cL6 under the experimental conditions can be calculated from $t = (L_t L_d)/Vu$, where L_t and L_d are total capillary length and length to detector, respectively.

The validity of this prediction is shown by the electropherograms in Fig. 3 for

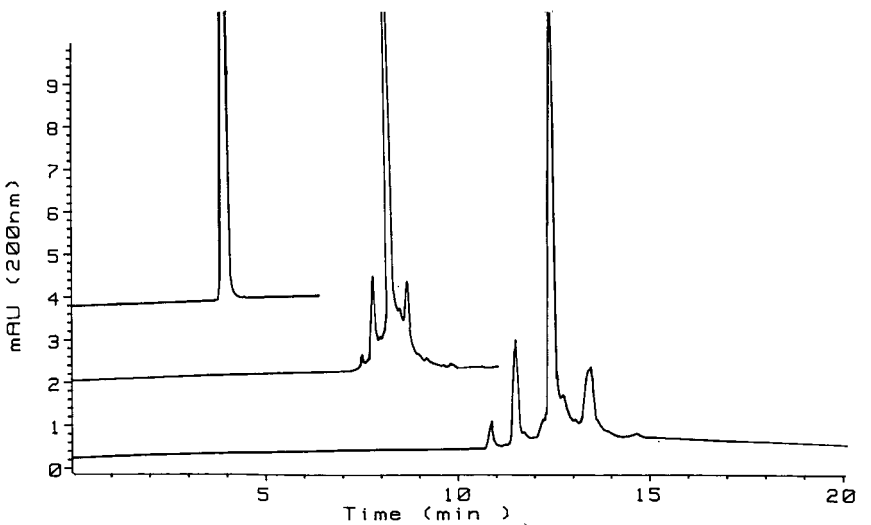

Fig. 3. Electropherograms of cL6 at (left-to-right) pH 2.5, 5.6 and 6.4 showing resolution of isoelectrotypes as predicted in Fig. 2.

native cL6. This information has been used to develop a method for determining the lot-to-lot reproducibility of various cL6 lots as well as how cL6 isoelectrotypes vary with production and storage conditions. This method is comparable to rapid isoelectric focusing and analytical ion-exchange chromatographic methods previously described for highly basic antibodies [23].

At pH values above 7, cL6 did not migrate sufficiently to be detected within 30 min. Electrolyte conditions above pH 6 were avoided to minimize hydrolysis of the capillary coating and electroendoosmosis. Fig. 3 also indicates that the valence–pH relationship can be further exploited such that at the pI of the IgG isoelectrotypes, essentially infinite resolution occurs as the more acidic isoelectrotypes undergo charge reversal and migrate in an opposite direction to those with higher pI.

For an exact solution, the mobility model requires input of the protein partial specific volume (v), frictional ratio (f/fo), an indirect measure of protein asymmetry, and Henry's function $\phi(kr)$. The protein partial specific volume falls between 0.745 and 0.750 [19,24,25] for natural proteins and f/fo is between 1.0–1.7 for globular proteins [19]. Literature values for IgGs indicate $v = 0.74$, irrespective of species origin [26]. The magnitude of f/fo is taken here to be 1.0, though it has been noted from light scattering studies that IgGs are highly assymmetric [27]. For this work the magnitude of Henry's function $\phi(kr)$ is taken to be 1.05, as calculated from Henry's work [11]. As indicated by the notation for the function, $\phi(kr)$ varies as a function of solution ionic strength and protein radius.

Besides changing solution pH, two other means of controlling u, as seen in eqn. 4, are by varying fluid viscosity (n) and ionic strength (I); the former has a general effect on u and the latter modifies the Debye–Hückel parameter and protein charge by changing both F_Z and the protein's pI. While increasing fluid viscosity decreases u by increasing the frictional factor of the protein and thus tends to accentuate differences in protein size, little enhancement of resolution is expected since the size dependency of u is rather weak. For instance, as mentioned previously, various empirical models have been developed to explain electrophoretic results [21,28] and indicate a molecular weight dependency ranging from $M^{-1/3}$ to $M^{-2/3}$. The $M^{-1/3}$ dependency is an ideal lower limit for small molecules in low-ionic-strength buffer. Larger molecules in high ionic strength buffer will exhibit a $M^{-2/3}$ dependency as seen in Offord's model [28]. For intermediate sized molecules in medium-strength buffer, a $M^{-1/2}$ dependency is seen in Lauer's model. The transition from a $M^{-1/3}$ to $M^{-2/3}$ dependency is shown in Fig. 4 for various ionic strengths of aqueous solutions at 25°C, by showing how the ratio of the coefficients [$K(3)/K(2)$] varies with these parameters. For any given experimental condition, eqn. 4 reduces to $u = K(4)ZM^{-n}$, where n varies from 1/3 to 2/3 and $K(4)$ is an aggregate of $K(1–3)$.

In conclusion, the semi-empirical model presented here indicates that a proteins primary sequence data and F_Z can be used to calculate u for a protein at a variety of pH conditions. The model utilizes the observation that the calculated valence Z_c of a particular protein is proportional to its actual valency Z_a by F_Z. In this application F_Z also incorporated the frictional ratio f/fo which was taken to be unity. In reality, the model indicates that the mobility of a protein, and variants of that protein, at any given pH can be calculated directly from its theoretical titration curve if its mobility is measured at any one pH since mobility is directly proportional to protein valence.

One of the main benefits of the model is that it shows that the molecular weight

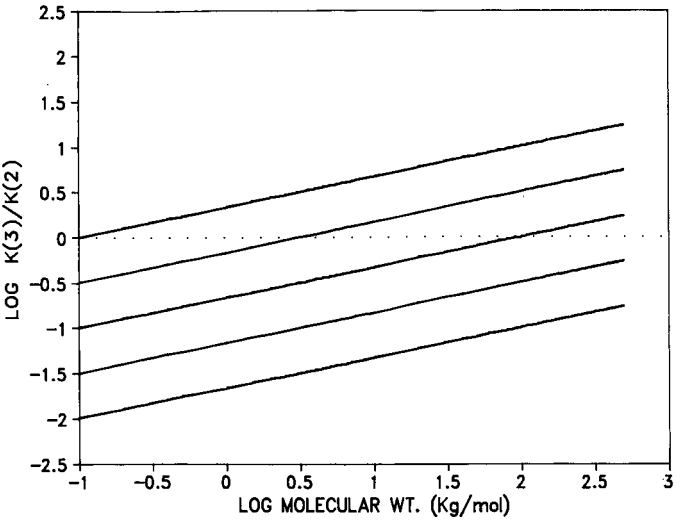

Fig. 4. Plot of the ratio of the $M^{-2/3}$ and $M^{-1/3}$ coefficients [$K(3)/K(2)$] from eqn. 4 showing the molecular weight dependency of u as a function of both M and I, at I = 0.1, 1.0, 10, 100 and 1000 mol/m^3 (bottom-to-top).

influence on mobility is a complex function of both the magnitude of protein molecular weight and the buffer ionic strength. This reconciles differences in previous empirically derived models, which is a necessity if the model developed here is to be considered valid.

REFERENCES

1 B. Nickerson and J. W. Jorgenson, *J. High Resolut. Chromatogr. Chromatogr. Commun.*, 11 (1988) 553.
2 J. Frenz, S.-L. Wu and W. S. Hancock, *J. Chromatogr.*, 480 (1989) 379.
3 S.-L. Wu, G. Teshima, J. Cacia and W. S. Hancock, *J. Chromatogr.*, 516 (1990) 115.
4 F. Kilàr and S. Hjertén, *J. Chromatogr.*, 480 (1989) 351–357.
5 J. B. Matthew, *Ann. Rev. Biophys. Biophys. Chem.*, 14 (1985) 387.
6 C. Tanford and J. G. Kirkwood, *J. Am. Chem. Soc.*, 79 (1957) 5333.
7 J. Th. G. Overbeek, in H. Mark and E. J. W. Verweys (Editors), *Advances in Colloid Science*, Vol. 3, Wiley-Interscience, New York, 1950, pp. 97–134.
8 L. G. Longsworth, *Ann. N.Y. Acad. Sci.*, 41 (1941) 267.
9 G. S. Adair and M. E. Adair, *Trans. Faraday. Soc.*, 36 (1940) 23.
10 R. K. Cannan, A. Kibrick and A. H. Palmer, *Ann. N.Y. Acad. Sci.*, 41 (1941) 243.
11 D. C. Henry, *Proc. R. Soc. London, Ser. A*, 133 (1931) 106–124.
12 A. Tiselius and H. Svensson, *Trans. Faraday Soc.*, 36 (1940) 16.
13 G. J. Wei and V. A. Bloomfield, *Anal. Biochem.*, 101 (1980) 245.
14 R. A. Mosher, D. Dewey, W. Thormann, D. A. Saville and M. Bier, *Anal. Chem.*, 61 (1989) 362.
15 H. A. Abramson, *J. Gen. Physiol.*, 15 (1931–32) 575.
16 H. A. Abramson, M. H. Gorin and L. S. Moyer, *Chem. Rev.*, 24 (1939) 345.
17 W. J. Moore, *Physical Chemistry*, Prentice-Hall, NJ, 4th ed., 1972, p. 455.
18 H. T. Rasmussen and H. M. McHair, *J. Chromatogr.*, 516 (1990) 223.
19 J. L. Oncley, *Ann. N.Y. Acad. Sci.*, 41 (1941) 121–150.
20 A. Sillero and J. M. Ribeiro, *Anal. Biochem.*, 179 (1989) 319–325.
21 P. D. Grossman, J. C. Colburn and H. H. Lauer, *Anal. Biochem.*, 179 (1989) 28.

22 M. Zhu, D. L. Hansen, S. Burd and F. Gannon, *J. Chromatogr.*, 480 (1989) 311.
23 B. J. Compton, J. S. Gerald, D. A. Lowe and R. P. Elander, *Biotech. Tech.*, 3 (1989) 349.
24 L. D. Ward and D. J. Winzor, *Arch. Biochem. Biophys.*, 209 (1981) 650.
25 A. A. Zamyatnin, *Ann. Rev. Biophys. Bioeng.*, 13 (1984) 145–165.
26 I. Pilz, G. Puchwein, O. Kratky, M. Herbst, O. Haager, W. E. Gall and G. M. Edelman, *Biochemistry*, 9 (1970) 211.
27 J. Yguerabide, H. F. Epstein and L. Stryer, *J. Mol. Biol.*, 51 (1970) 573.
28 R. E. Offord, *Nature (London)*, 211 (1966) 591.

Journal of Chromatography, 559 (1991) 367–383
Elsevier Science Publishers B.V., Amsterdam

CHROM. 23 487

Capillary zone electrophoresis of proteins with hydrophilic fused-silica capillaries

WASSIM NASHABEH and ZIAD EL RASSI*
Department of Chemistry, Oklahoma State University, Stillwater, OK 74078-0447 (USA)

ABSTRACT

Fused-silica capillaries having surface-bound hydroxylated polyether functions were developed for the separation of proteins by capillary zone electrophoresis. In one approach, the hydrophilic coatings consisted of two layers: a glyceropropylpolysiloxane sublayer covalently attached to the inner surface and a polyether top layer. In a second approach, the capillary wall was coated with polysiloxane polyether chains the monomeric units of which at both ends were covalently attached to the capillary inner surface with possible interconnection. These coatings yielded capillaries with different electroosmotic flow characteristics. The relatively long polyether chains of the various coatings were effective in shielding the unreacted surface silanols, thus minimizing solute–wall adsorption. As a consequence, high separation efficiencies were obtained in the pH range 4.0–7.5, which allowed the separation of widely differing proteins, the characterization of heterogeneous proteins and the fingerprinting of crude protein mixtures. The various coatings were stable and exhibited reproducible separations from run-to-run, day-to-day, and column-to-column. Furthermore, a procedure was developed for restoring collapsed capillaries after prolonged use.

INTRODUCTION

Capillary zone electrophoresis (CZE) with its high resolving power and unique selectivity is well placed to play an important role in the separation and characterization of proteins. However, since its debut [1–3], researchers have soon realized that CZE of proteins with fused-silica capillaries is hampered by solute adsorption onto the capillary inner walls, which often gives rise to band broadening and low recovery of the separated analytes.

Several attempts have been made to alleviate the problem of solute–wall interactions. The major approaches have been: (i) capillary surface treatments [4–11], (ii) the use of running electrolytes at high [12,13] or low pH [6], *i.e.* above or below the isoelectric points of proteins, (iii) the addition of high salt concentrations to the running electrolytes [14] using high pH, and (iv) the use of zwitterionic buffers with high salt concentrations [15]. Among all these approaches, surface modification is the method that affords the highest flexibility as far as selectivity modulation with pH changes is concerned. Indeed, approach (ii) limits the selectivity of the system to a narrow pH range and may result in protein denaturation at low pH or capillary degradation at high pH; approach (iii) may not be effective at medium pH range (5 to

0021-9673/91/$03.50

7) and in addition may produce system overheating due to the high ionic strength of the running electrolyte. On the other hand, method (iv), although effective in reducing solute adsorption, does not allow high sensitivity detection due to increased background in UV of most zwitterions when used at elevated concentrations.

Thus far, several coatings have been developed for CZE of proteins. These coatings are polyacrylamide [4], methylcellulose [4], glycol [5], glycerol-glycidoxypropyl [6], poly(vinylpyrrolidinone) [6], polyethylene glycol (PEG) [7], maltose [8], aryl pentafluoro (AFP) groups [9], polyethyleneimine (PEI) [10], and vinyl-bound polyacrylamide [11]. The PEI coating provided positively charged surface and was useful for the separation of basic proteins. This mimic the idea of operating untreated fused-silica capillaries with high pH, whereby the proteins and the surface have the same charge, which then prevent adsorption by coulombic repulsion. All other coatings were of the neutral type and produced acceptable results in terms of protein separations.

This report is concerned with the investigation of surface modification procedures that yield stable and inert capillaries having moderate electroosmotic flow. The capillary surface modification reported here entails the covalent attachment of polyether chains of various length to the inner surface of fused-silica capillaries via siloxane bonds, either directly using polyether chains with trimethoxysilane groups at both ends or by attaching a top polyether layer to a polysiloxane sublayer already anchored to the capillary inner surface. The first type of coatings is referred to as interlocked coatings, the second as fuzzy coatings. The coated capillaries were evaluated in protein CZE and characterized in terms of efficiency and electroosmotic flow over a wide range of pH. In addition, a procedure was developed for restoration of collapsed capillaries after prolonged use.

EXPERIMENTAL

Instrument

The capillary electrophoresis instrument used in this study resembles that reported earlier [16,17]. It was constructed from a Glassman High Voltage (Whitehouse Station, NJ, USA) Model HP30P3 high-voltage power supply of positive polarity and a Linear (Reno, NV, USA) Model 200 UV–VIS variable-wavelength detector equipped with a cell for on column detection. In all experiments, the wavelength was set at 210 nm. The electropherograms were recorded with a computing integrator interfaced with a floppy disk drive and a CRT monitor from Shimadzu (Columbia, MD, USA).

Reagents and materials

Cytochrome *c* from horse heart, lysozyme from chicken egg white, ribonuclease A and α-chymotrypsinogen A, both from bovine pancreas, myoglobin from horse skeletal muscle, carbonic anhydrase from bovine erythrocytes, iron saturated transferrin from human serum, β-lactalbumin from bovine milk, and crude trypsin inhibitor and lipoxidase, both from soybean were purchased from Sigma (St. Louis, MO, USA). Table I compiles the relative molecular mass (M_r)and p*I* values of these proteins. γ-Glycidoxypropyltrimethoxylsilane (Z-6040) was a gift from Dow Corning (Midland, MI, USA). Polyethylene glycol diglycidyl ether (M_r 600) was purchased

TABLE I

PROTEINS USED IN THIS STUDY

Protein	M_r	p*I*
Lysozyme	14 100	11.0
Cytochrome *c*	12 400	10.7
Ribonuclease A	13 700	9.4
α-Chymotrypsinogen A	25 500	9.5
Myoglobin	17 500	6.8–7.3
Carbonic anhydrase	31 000	5.3
Transferrin	79 550	5.2–6.1
α-Lactalbumin	14 200	4.8
Trypsin inhibitor	20 100	4.5
Lipoxidase	102 400	5.7

from Polysciences (Warrington, PA, USA). Polyethylene glycol (PEG) of M_r 200, 600 and 2000, boron trifluoride etherate and phenol were obtained from Aldrich (Milwaukee, WI, USA). Reagent-grade sodium phosphate monobasic, sodium hydroxide, hydrochloric acid, dioxane, and N,N-dimethylformamide (DMF) were from Fisher Scientific (Pittsburgh, PA, USA). Fused-silica capillaries of 50 μm I.D. and 375 μm O.D. were obtained from Polymicro Technology (Phoenix, AZ, USA). Deionized water was used to prepare the running electrolyte. All solutions were filtered with 0.2-μm Uniperp Syringeless filters from Genex (Gaithersburg, MD, USA) to avoid capillary plugging.

Capillary modification

Fused-silica capillaries of 80 cm long were treated using the following procedures.

Polyether fuzzy coatings. Fused-silica capillaries were first filled with an aqueous solution at 10% (v/v) γ-glycidoxypropyltrimethoxysilane and allowed to react at 96°C for 40 min. This treatment was repeated four times. Subsequently, the capillary was filled with 0.01 *M* HCl and then heated at 95°C for 40 min. After washing successively with water and dioxane, the capillary was flushed with a solution of dioxane at 1% (v/v) boron trifluoride. Following, the capillary was filled with an equimolar solution of polyethylene glycol diglycidyl ether (M_r 600) and PEG 2000 or PEG 600 in dioxane. The modified capillaries were stored in HPLC-grade methanol.

Polyether interlocked coatings. DMF solutions containing PEG 200 with trimethoxysilane at both ends were introduced into the capillary and allowed to react at 100°C for 1 h. This treatment was repeated twice. All capillaries were stored in HPLC-grade methanol.

Restoration of deteriorated capillaries. After prolonged use, the performance of the various hydrophilic capillaries declined due to hydrolytic degradation of some of their coatings. The feasibility of recoating a deteriorated capillary to restore its protective hydrophilic layer was assessed with polyether interlocked coatings. In this regard, the collapsed capillary was flushed with 1.0 *M* NaOH and then heated at 95°C for 30 min; a step that removed the remaining of the coating via nucleophilic cleavage of the siloxane bonds (Si–O–Si–C) [18]. Following, the capillary was successively washed with water, filled with 0.1 *M* HCl and then heated at 95°C for 30 min. After

washing with water and DMF, the capillary was filled with the coating reagent and allowed to react as described above.

Reproducibility. The coated capillaries were evaluated for the reproducibility of protein migration times from run-to-tun, day-to-day and column-to-column. From run-to-run (on the same day), the relative standard deviation (R.S.D.) was calculated based on four successive measurements separated by 20 min equilibration with the running electrolyte. From day-to-day the R.S.D. was calculated based on a total of 9 measurements made on three different days (3 sets of 3 measurements each) and from column-to-column, the R.S.D. was estimated using data collected (2 sets of 6 measurements each) from two columns prepared on different days.

RESULTS AND DISCUSSION

Surface modification

Fig. 1A and B depict the idealized structure of the fuzzy and interlocked hydrophilic coatings, respectively. Both types of coatings are essentially hydroxylated polyether chains covalently attached to the capillary inner surface. The fuzzy coatings (see Fig. 1A) consist of two layers: a cross-linked glyceropropylpolysiloxane sublayer

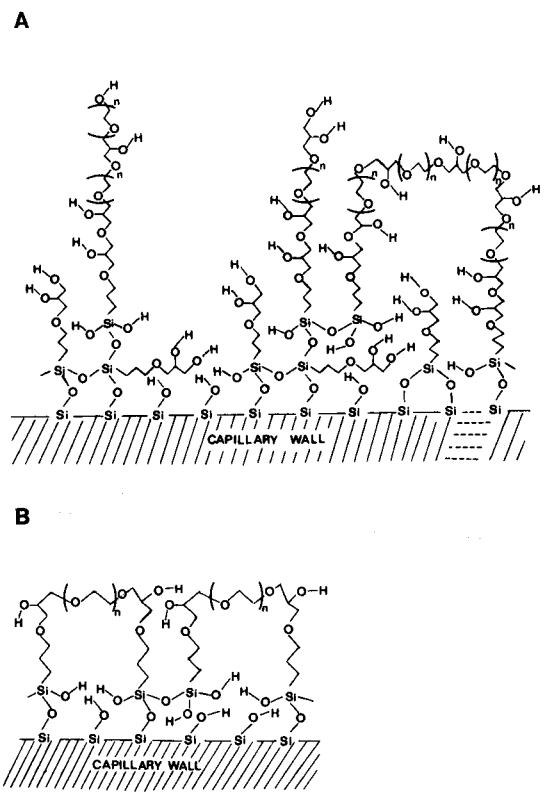

Fig. 1. Schematic illustration of the idealized structures of fuzzy (A) and interlocked (B) polyether coatings of fused-silica capillaries.

covalently attached to the capillary inner-surface, and a hydrophilic polyether top layer. The fuzzy top layer is the result of the different ways in which the PEG 600 diglycidyl ether can react with the PEG 600 or 2000 leading to polyether chains of different lengths with either one end or two ends covalently attached to the sublayer. On the other hand, the interlocked coatings consist of polyether polysiloxane chains whose monomeric units at both ends are covalently attached to the surface with possible interconnection. The following capillary codings will be utilized throughout the text to designate each type of coatings. F-2000 and F-600 denote capillaries with fuzzy coatings having PEG 2000 or PEG 600 moieties, respectively, whereas I-200 refers to capillaries with interlocked coatings having PEG 200 polyether chains.

Electroosmotic flow

The above two schemes of surface modification yielded capillaries with different electroosmotic flow characteristics. Fig. 2A and B illustrate the results obtained at 17 and 20 kV over the pH range 4.0–7.5 using phenol as the inert tracer. At both running voltages, the fuzzy coatings exhibited lower electroosmotic flow than the interlocked ones indicating that the concentration of unreacted surface silanols is relatively low for the capillaries with fuzzy polyether coatings. This is because the fuzzy coatings have an additional cross-linked polysiloxane sublayer that the interlocked coatings do not have. On the other hand, for the two fuzzy coatings, *i.e.* F-600 and F-2000, which should have the same surface concentration of unreacted silanols, F-600 exhibited a higher flow-rate than F-2000 under otherwise identical conditions. The difference in the flow-rate between the two fuzzy coatings may be related to the size of the polar top layer. The polyether chains of the polar top layer in F-600 are shorter than those in F-2000, and as a result they were less effective in masking the ionized surface silanols (*i.e.* unreacted silanols) toward the atmospheric binding of electrolyte cations. In view of Manning's counterion condensation theory [19], salt counterions are

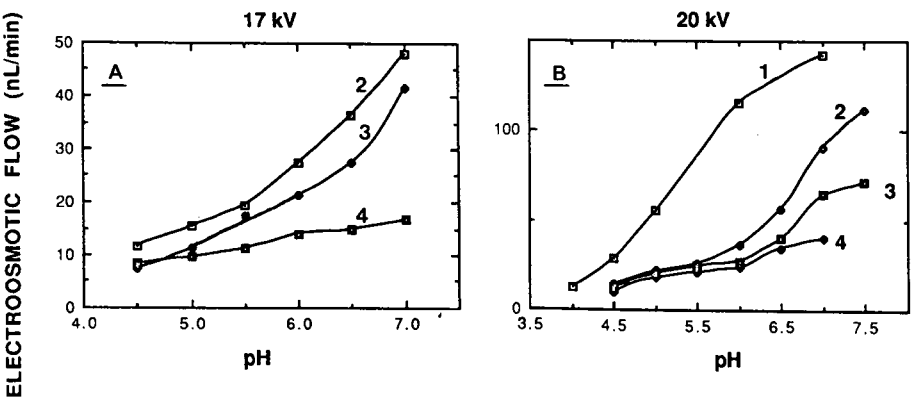

Fig. 2. Plots of electroosmotic flow-rates obtained on coated and uncoated capillaries *versus* pH of the electrolyte at 17 kV in A and 20 kV in B. Fused-silica capillaries: 1 = untreated; 2 = I-200; 3 = F-600; 4 = F-2000. All tubes were 50 cm (to the detection point), 80 cm total length × 50 μm I.D.; electrolyte, 0.1 *M* phosphate solutions at different pH. At 17 kV, currents were 21, 22, 23, 24, 34 and 38 μA at pH 4.5, 5.0, 5.5, 6.0, 6.5 and 7.0, respectively. At 20 kV, currents were 26, 28, 29, 30, 33, 45, 50 and 70 μA at pH 4.0, 4.5, 5.0, 5.5, 6.0, 6.5, 7.0 and 7.5, respectively. Inert tracer: phenol.

territorially or atmospherically bound, *i.e.* they are retained by the electrostatic field at the capillary surface, but remain free to move within a certain layer above it. The atmospheric binding of electrolyte cations to the negatively charged silanols generates an electric double layer adjacent to the capillary walls, which migrates toward the cathode when an electric potential is applied to the capillary. Since the cations are solvated, they pull solvent with them, thus producing the electroosmotic or bulk flow.

On the other hand, when compared to untreated fused-silica capillaries at an applied voltage of 20 kV (see Fig. 2B), the electroosmotic flow was reduced on the average by a factor of 3.6, 2.9 and 2.3 for F-2000, F-600 and I-200, respectively. It should be noted that the difference in flow-rate among the various coatings was greater in magnitude at pH 5.0 and above due to increasing ionization of the unreacted surface silanols (see Fig. 2A and B).

In principle, changing the applied voltage should produce proportional changes in the rate of the electroosmotic flow. However, the comparison of Fig. 2A and B shows that increasing the applied voltage by a factor of 1.17, *i.e.* from 17 to 20 kV yielded a larger increase in the electroosmotic flow. On average, the flow increased by a factor of *ca.* 1.5 for the coated capillaries over the pH range studied when going from 17 to 20 kV. Capillary internal temperature was found to increase in non-linear fashion with the applied voltage [20]. On the other hand, solvent viscosity decreases exponentially with increasing temperature and since the electroosmotic flow is inversely proportional to viscosity, this decrease in viscosity may have caused the jump in flow at 20 kV when compared to 17 kV.

Evaluation of coated capillaries with basic proteins

Figs. 3, 4 and 5 depict typical electropherograms of four model basic proteins

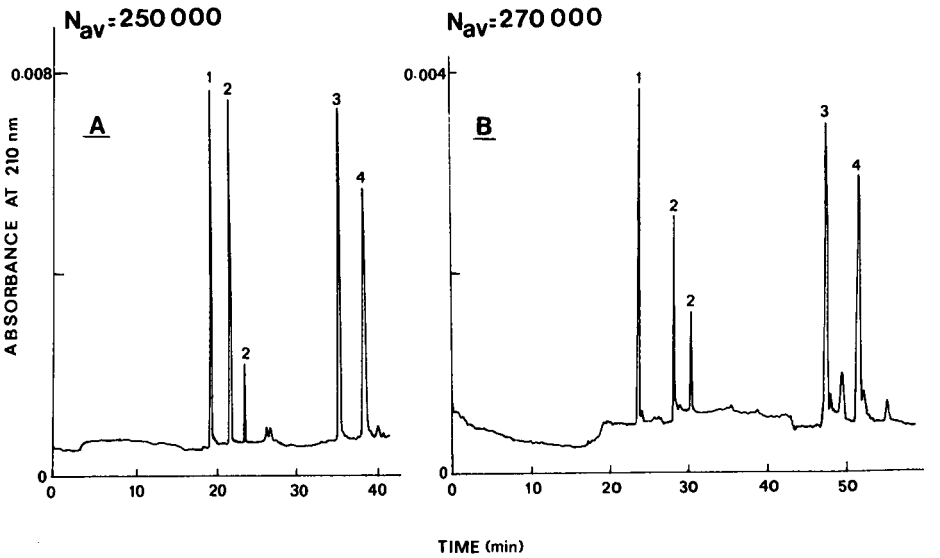

Fig. 3. Electropherograms of basic proteins obtained on the fuzzy 2000 coated capillary. Capillary, 50 cm (to detection point), 80 cm total length × 50 μm I.D.; electrolyte, 0.1 *M* phosphate solutions at pH 6.0 in A and 7.0 in B; running voltage, 17 kV; currents were 24 and 38 μA at pH 6.0 and 7.0, respectively. Proteins: 1 = lysozyme; 2 = cytochrome *c*; 3 = ribonuclease A; 4 = α-chymotrypsinogen A.

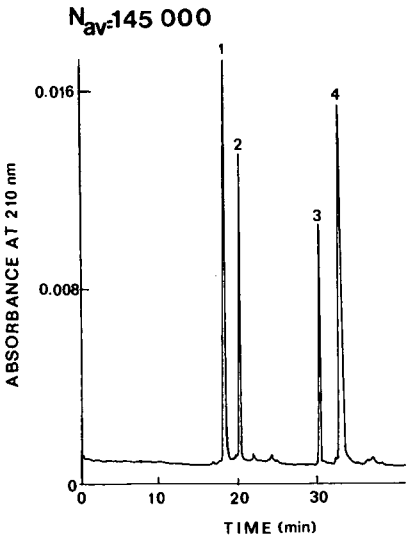

Fig. 4. Electropherogram of basic proteins obtained on fuzzy 600 coated capillary at pH 6.0. All other conditions as in Figs. 2 and 3.

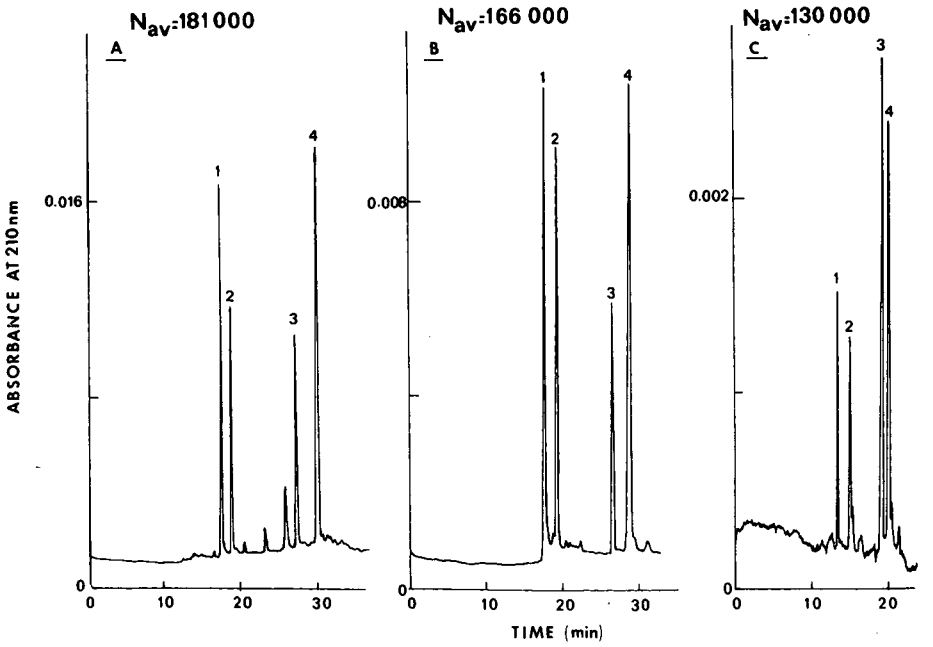

Fig. 5. Electropherograms of basic proteins obtained on interlocked 200 coated capillary at pH 5.0 (A), pH 6.0 (B) and pH 7.0 (C). All other conditions as in Figs. 2 and 3.

performed on F-2000, F-600, and I-200 coated capillaries, respectively, at an applied voltage of 17 kV using 0.1 *M* phosphate solutions as the running electrolyte at different pH. The average plate count per meter, N_{av}, is indicated on each electropherogram. These efficiency values may indicate that interaction between the proteins and the inner surface proper of the capillaries has been greatly reduced. Based on the results of electroosmotic flow with the various capillaries (see Fig. 2), some unreacted silanols remained on the capillary inner surface. These silanols which were accessible for the atmospheric binding of small counterions, may be less exposed for the territorial binding of large polyionic solutes such as proteins. The relatively long polyether chains of the various coatings are believed to hinder the access of macromolecules to the unreacted silanols. Indeed, according to Manning's counterion condensation theory [19], charges must be within the Bjerrum length in order to undergo electrostatic interactions. This length is defined as the distance at which two unit charges interact with an energy of k_BT (k_B is Boltzman's constant and T is absolute temperature) in the relevant dielectric medium and its value is 7.14 Å in water at 25°C.

Referring to Fig. 5, the N_{av} obtained on I-200 was slightly lower at pH 7.0 than at pH 5.0; a trend that was also observed on F-600 and F-2000. This may be due to increasing ionization of unreacted surface silanols and/or Joule heating with increasing pH. Raising the electrolyte pH from 5.0 to 7.0 would lead to increasing protein interactions with the residual ionized silanols, which in turn would cause lower separation efficiencies. On the other hand, due to increasing the ionic strength of the running electrolyte with increasing pH, the current almost doubled when the pH of phosphate solution was raised from 5.0 to 7.0. Higher currents lead to increasing center-to-wall temperature difference, thereby producing a more pronounced radial viscosity gradient inside the capillary. As a result, radial variations in the overall velocity profiles (*i.e.*, the sum of electrophoretic and electroosmotic velocity) of the separated proteins would also increase in magnitude at high currents. These perturbations in the velocity profiles may produce mass transfer resistances that broaden the migrating solute zones and cause lower separation efficiencies. The effect of temperature gradients on CZE separation efficiency is well documented [21–23].

The values of N_{av} obtained on F-600 and I-200 capillaries were quite comparable, but lower than those obtained on F-2000 under otherwise identical conditions (see Figs. 3, 4 and 5). This may be due to the higher electroosmotic flow with F-600 and I-200 when compared to F-2000. Under these conditions, mass transfer resistances due to heat-induced perturbations in the overall velocity profiles are amplified. Another possible explanation is that the F-600 and I-200 coatings are not as effective as F-2000 coatings in shielding the unreacted surface silanols toward the protein solutes. It has been shown that a slight solute–wall adsorption can cause separation efficiency to decline [24].

In CZE of proteins, capillary internal Joule heating due to passage of current through the electrolyte inside the tube could also denature the biomacromolecules. Increasing the voltage from 17 to 20 kV using 0.1 *M* phosphate solutions at pH 6.0, 6.5 and 7.0 resulted in increasing the current from 24 to 33 μA, from 34 to 45 μA and from 38 to 50 μA, respectively. At this higher voltage, and independently of the nature of the coating, α-chymotrypsinogen A did not elute from the capillary when pH 6.5 or 7.0 were used, while the peaks of cytochrome *c* and lysozyme, and to a lesser extent that of ribonuclease A, exhibited a significant drop in efficiency. At pH

6.0, increasing the voltage from 17 to 20 kV did only result in lowering the separation efficiency. This may be due to the binding of proteins to the coating proper by hydrophobic interactions. It has been shown in liquid chromatography of proteins that hydrophobic interactions are induced and/or increased with increasing temperature due to heat-induced conformational changes [25,26]. These interactions which are the result of temperature effects arising from Joule heating can be viewed as the major contributors to band broadening at elevated voltage.

To examine the influence of the running voltage on separation efficiencies, the four basic proteins (*i.e.* lysozyme, cytochrome *c*, ribonuclease A, and α-chymotrypsinogen A) were analyzed on an I-200 capillary at different voltages using 0.1 *M* phosphate, pH 7.0. The results are illustrated in Fig. 6 by a plot of average plate count per meter *versus* applied voltage. As in the preceding experiment, α-chymotrypsinogen A did not elute from the capillary at an applied voltage of 20 kV. It is seen that an applied voltage in the range 10–13 kV yields higher efficiency than at elevated voltage. However, the tradeoff is longer analysis time. A running voltage of 16–17 kV seems to be a compromise, whereby protein separation can be carried out relatively fast without sacrificing separation efficiencies. The relatively high separation efficiency obtained at lower running voltage may result from diminished Joule heating of the system. Similar observations were recently reported by Cobb *et al.* [11] with capillaries having polyacrylamide coatings.

To evaluate the effect of ionic strength on separation efficiencies, the voltage was kept low (*i.e.* 10 kV) so that a wide range of phosphate concentrations in the running electrolyte can be investigated without overheating the system. This set of experiments was performed on an I-200 capillary at pH 7.0. The results are depicted in Fig. 7 by a plot of N_{av} *versus* the phosphate concentrations in the running electrolyte. As can be seen in Fig. 7, N_{av} first increased, passed through a maximum and then decreased with increasing phosphate concentrations. Again, the sharp decrease in separation efficiency at high ionic strength (*i.e.*, at 0.25 *M*; see Fig. 7) can be related to

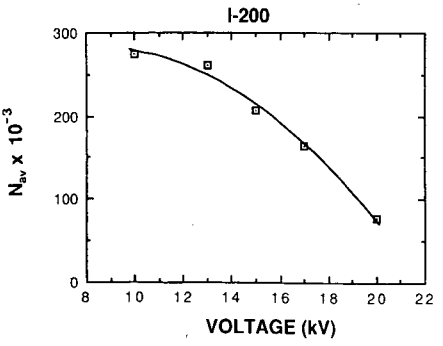

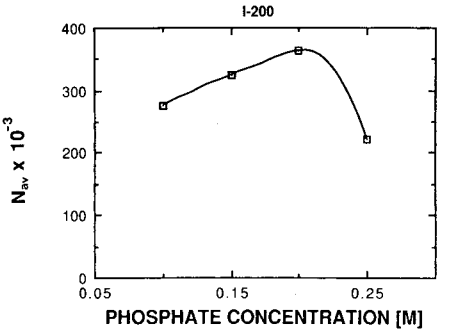

Fig. 6. Plot of average plate count per meter *versus* applied voltage obtained on an I-200 capillary. Electrolyte, 0.1 *M* phosphate solution, pH 7.0; currents were, 7, 20, 28, 38, and 50 μA at 10, 13, 15, 17 and 20 kV, respectively. All other conditions as in Figs. 2 and 3.

Fig. 7. Plot of average plate count per meter *versus* the ionic strength of the running electrolyte obtained on an I-200 capillary. Electrolytes, phosphate solutions at different ionic strength, pH 7.0; running voltage 10 kV; currents were, 7, 18, 35 and 50 μA at 0.1, 0.15, 0.2 and 0.25 *M* phosphate, respectively. All other conditions as in Figs. 2 and 3.

effects associated with system heating. At this lower voltage, *i.e.* 10 kV, and using 0.25 *M* phosphate, α-chymotrypsinogen A eluted from the capillary despite that the current was as high as with 0.1 *M* phosphate and 20 kV (*i.e.* 50 μA); conditions under which the same protein was tightly bound to the capillary (see above). It seems that for the same current passing through the running electrolyte, a higher ionic strength would stabilize protein structure, and consequently protein hydrophobic interaction with the coating due to heat-induced conformational changes would be reduced.

To compare the three types of coatings, peak capacity, n, was calculated for each capillary based on the following assumptions: (i) all capillaries can generate 100 000 theoretical plates per column on the average over the pH range 4.5–7.0, (ii) the hypothetical proteins differ among each others by their pI values, which span 4–11, (iii) lysozyme is the first eluting peak, and (iv) the analysis time is set arbitrarily to 150 min, time at which the center of the last eluting peak appears in the detector. The peak capacity, n, was calculated using the equation $n = 1 + (N_{av}/16)^{1/2} \ln (t_f/t_i)$, and the results are depicted in Fig. 8 for the pH range 4.5 to 7.0. In this equation, t_i is the migration time of lysozyme and t_f is that of phenol (*i.e.* the inert tracer); a migration time interval within which the elution of basic and slightly neutral proteins may take place. On the other hand, the migration times of acidic proteins are assumed to

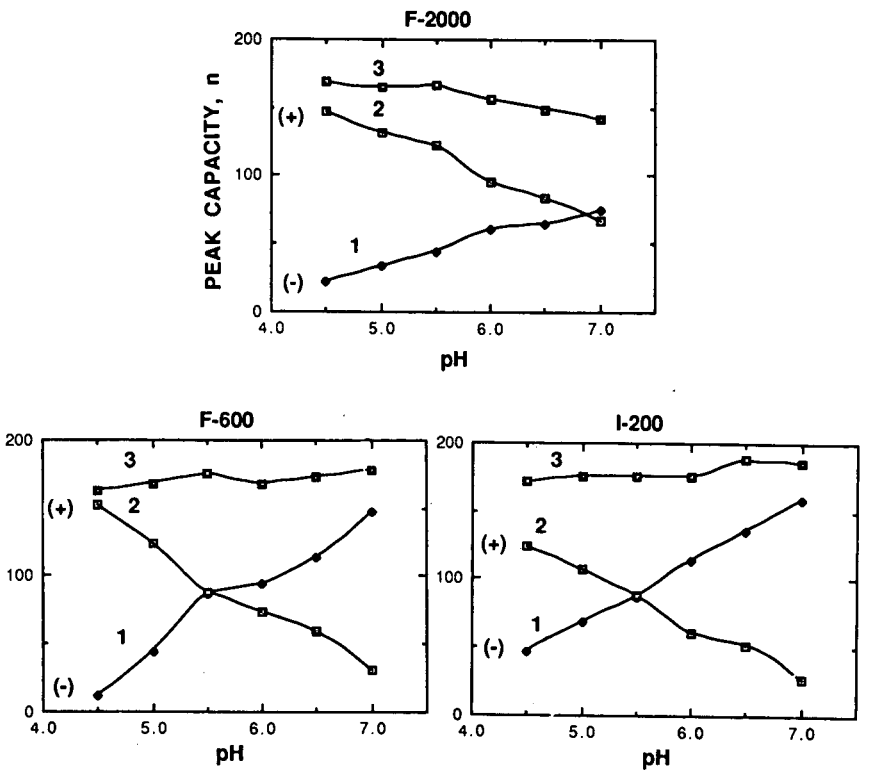

Fig. 8. Comparison of peak capacity, n, of the different coatings over the pH range 4.5 to 7.0 using lysozyme and phenol migration times as 17 kV (see text for details). 1 = n for negatively charged proteins; 2 = n for positively charged proteins; 3 = total n.

lie between the migration times of phenol, t_i, and that of the last eluting peak, t_f, set arbitrarily to 150 min. The migration times of lysozyme and phenol used in calculating peak capacity were those obtained from experiments performed on the various capillaries with a migration distance of 50 cm (*i.e.* distance from injection end to detection point) using 0.1 *M* phosphate solutions at pH ranging from 4.5–7.0, and a running voltage of 17 kV. Referring to Fig. 8, it can be seen that F-2000 capillaries require an electrolyte of pH 7.0 to elute an equal number of positively and negatively charged proteins, whereas this situation is reached at pH 5.5 for I-200 and F-600 capillaries. Due to the oversimplifications in the calculations, the peak capacity may not be realistic. Nevertheless, to obtain similar behavior in terms of peak capacity, it seems wise to state that a tube with relatively low electroosmotic flow requires the use of an electrolyte pH that is two or more units higher in value than with a capillary having 2.5 to 3 times higher electroosmotic flow. Another difference is that at any pH the peak capacity for positively charged proteins on the F-2000 capillary is always greater than that with F-600 and I-200. On the other hand, the peak capacity for the negatively charged proteins is higher with F-600 and I-200 than with F-2000.

Fig. 9 illustrates the overall and the electrophoretic mobilities of two model proteins (*i.e.* lysozyme and ribonuclease A) as well as the electroosmotic mobility of neutral solutes over the pH range studied with F-2000, F-600 and I-200 coated capillaries. In all cases (see Fig. 9), the electrophoretic mobility of the two test proteins decreased sharply between pH 5.5 and 6.0 indicating the deprotonation of an imidazole and/or the dissociation of a carboxylic side chain group. Furthermore, the electrophoretic mobility of proteins was virtually independent of the nature of the coatings under otherwise identical conditions. This is an indication of quasi-homosystems; meaning that the various coatings are quite effective in shielding the surface proper of the capillary toward the protein solutes. On the other hand, the overall mobility, $\mu_{overall}$, which is the sum of electroosmotic and electrophoretic mobilities, varied from one coating to another. The electroosmotic flow was relatively low with F-2000 capillary, and since this flow increased slightly with the pH at 17 kV, the overall mobility of the proteins almost paralleled their electrophoretic mobility (see Fig. 9). This may represent an advantage when dealing with unknown substances in the sense that their basicity or acidity can be assessed from simple $\mu_{overall}$–pH plot. On the other hand, the overall mobility of the same proteins followed different patterns on F-600 and I-200 mainly due to their higher electroosmotic flow. For lysozyme, the overall mobility increased between pH 4.5 and 5.5, decreased at pH 6.0 and then increased between pH 6.0 and 7.0. For ribonuclease A, a sharp increase in the overall mobility occurred in the pH range 6.0–7.0.

Reproducibility and stability of the coatings

These studies were carried out on F-600 and I-200 capillaries that are representative of fuzzy and interlocked coatings, respectively. Table II summarizes the run-to-run, day-to-day and column-to-column migration reproducibility expressed in terms of percent relative standard deviation (R.S.D.) with four basic proteins at pH 6.5. It should be noted that the column-to-column reproducibility reflects columns made on two different days. It can be seen that the interlocked 200 is slightly more reproducible than the fuzzy coatings simply because the surface modification is accomplished in a single step in the former, whereas it takes three steps to make the latter.

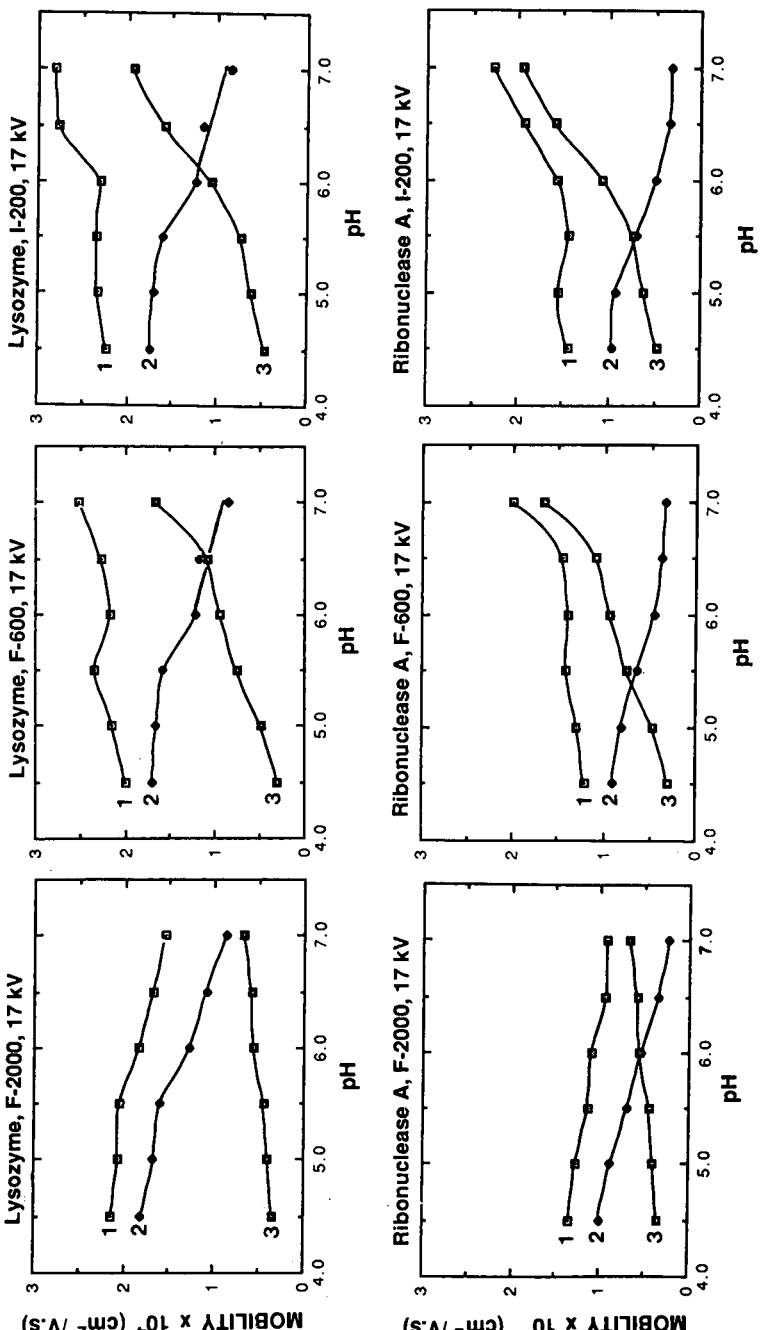

Fig. 9. Plots of overall and electrophoretic mobilities of lysozyme and ribonuclease A as well as electroosmotic mobility *versus* pH on the different coatings. Electrolytes, 0.1 *M* phosphate solutions at different pH. 1 = overall mobility; 2 = electrophoretic mobility; 3 = electroosmotic mobility. All other conditions are the same as in Figs. 2 and 3.

TABLE II

REPRODUCIBILITY OF MIGRATION TIMES OF PROTEINS ON F-600 AND I-200 CAPILLARIES

Capillary, 50 cm (to the detection point), 80 cm total length × 50 μm I.D.; electrolyte, 0.1 *M* phosphate solution, pH 6.5; applied voltage, 17 kV; current, 38 μA (see Experimental for details).

Protein	R.S.D. (%)					
	F-600			I-200		
	Run to run	Day to day	Column to column	Run to run	Day to day	Column to column
Lysozyme	1.6	1.4	4.2	0.9	1.6	1.5
Cytochrome *c*	0.2	0.6	6.7	0.9	1.8	2.2
Ribonuclease A	1.5	1.2	5.4	1.0	1.9	2.8
α-Chymotrypsinogen A	1.8	2.3	4.5	1.0	2.0	2.3

The different coatings were quite stable. In fact, the various columns exhibited constant performance for several weeks when operated at pH 6.0 or below, and for more than 80 h when used in the pH range 6.5–7.0.

Restoration of capillary coatings

After prolonged use, the various capillaries lost some of their coatings by hydrolytic degradation, and consequently they exhibited strong interactions with the proteins and high electroosmotic flow nearing that obtained with uncoated capillaries. Fig. 10A illustrates the separation of 8 acidic and basic standard proteins spanning a wide range of molecular weights. This electropherogram is typical of what can be obtained on an original I-200 coating that is still exhibiting constant performance in terms of efficiency, resolution and electroosmotic flow characteristics. We have chosen several proteins for better assessment of the feasibility of restoring a collapsed capillary. Fig. 10B represents a typical electropherogram obtained on the same capillary after it has lost some of its coating, whereby a significant drop in efficiency and resolution as well as a pronounced increase in electroosmotic flow can be noticed.

In an attempt to restore the performance of the capillary, the coating that remained was stripped off the inner wall of collapsed capillary column by treatment with aqueous solutions of sodium hydroxide. The naked capillary thus obtained was then recoated as described in the experimental section. It can be seen from Fig. 10C that the column can be restored to its orginal performance in every regard. To assess the reproducibility of this procedure, we have performed the restoration several times on collapsed I-200 capillaries and each time obtained similar results to those reported in Fig. 10C. The procedure developed here for restoring capillary coatings is expected to be applicable to other type of coatings provided that they are attached to the capillary inner surface via siloxane bonds.

Referring to Fig. 10A and C, it should be noted that human serum transferrin is a heterogeneous glycoprotein consisting of at least five isoforms [27,28] that differ among each other in sialic acid content. It can be seen that the present electrophoretic

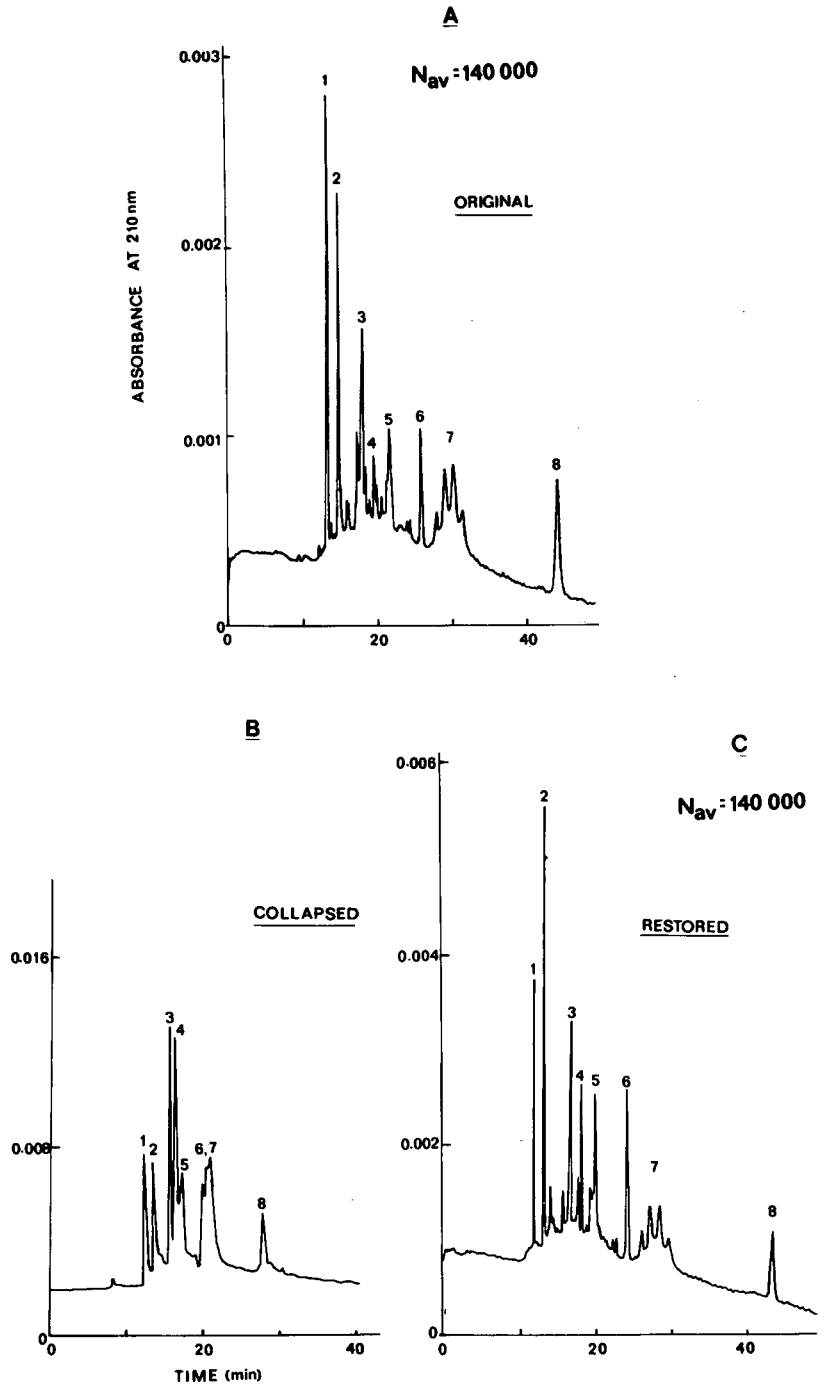

Fig. 10. Electropherograms of basic and acidic proteins obtained on original (A), collapsed (B) and restored (C) I-200 capillaries. Electrolyte, 0.1 *M* phosphate solution, pH 7.0; running voltage, 17 kV. All other conditions as in Fig. 3. Proteins: 1 = lysozyme; 2 = cytochrome *c*; 3 = ribonuclease A; 4 = α-chymotrypsinogen A; 5 = myoglobin; 6 = carbonic anhydrase; 7 = transferrin; 8 = α-lactalbumin. In both cases N_{av} was calculated on the well defined peaks, *i.e.* peaks 1, 2, 4, 6 and 8.

system is capable of separating these isoforms. Furthermore, most of the commercial standard proteins are somewhat microheterogeneous or not highly pure as manifested by the presence of small peaks that elute before or after the main peaks when the selectivity of the electrophoretic system is adequate (*e.g.* myoglobin, cytochrome *c*, etc.; *cf* Figs. 4–6 and 10).

Applications

As discussed above, the I-200 capillaries exhibited relatively higher electroosmotic flow than F-600 and F-2000 capillaries, and similarly to the fuzzy coatings they showed no significant solute–wall interactions over a wide range of pH. In CZE, the primary goal of surface modification of fused-silica capillaries is to minimize protein–wall interactions without completely inhibiting the electroosmotic flow. A reduction in the flow by a factor of 2.0 to 2.5 with respect to the untreated capillary is ideal in order to analyze both positively and negatively charged species in the positive polarity mode. This characteristic added to the "neutrality" of the inner wall is advantageous in capillary electrophoresis with on-line detection. As in slab gel electrophoresis the electropherogram, which is the written record of the experiment, should contain the maximum information about a given mixture. The presence of a moderate electroosmotic flow in capillary zone electrophoresis with coated capillaries permits the achievement of this goal. For a crude mixture whereby the p*I* values of all the components are not known, the presence of electroosmotic flow is essential to analyze and

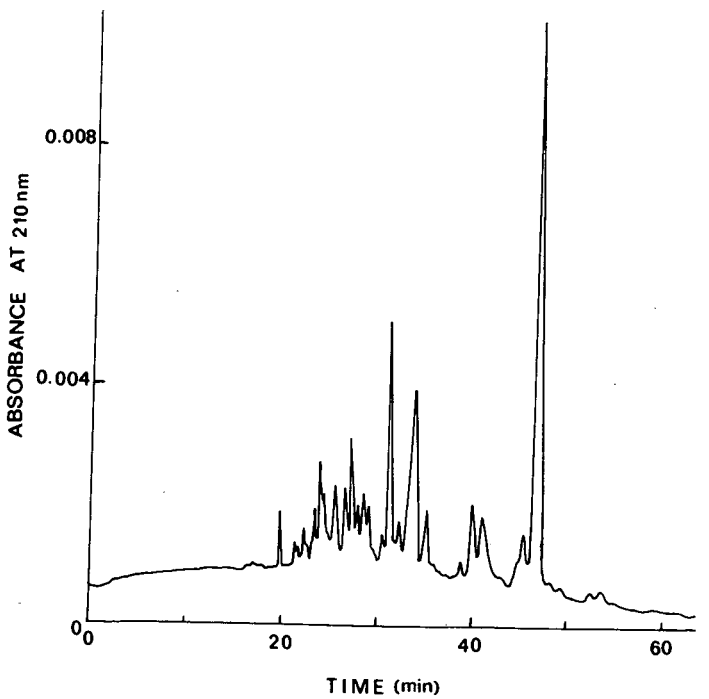

Fig. 11. Electropherogram of crude soybean trypsin inhibitor. Capillary, I-200; electrolyte, 0.1 *M* phosphate solution, pH 6.5; running voltage, 17 kV. All other conditions as in Figs. 2 and 3.

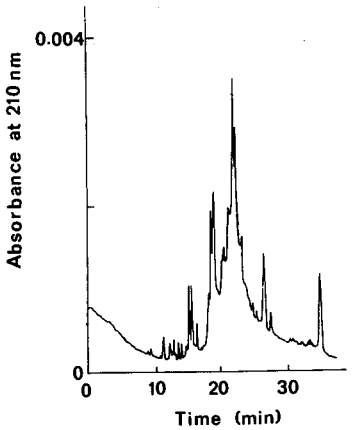

Fig. 12. Electropherogram of commercial soybean lipoxidase. Capillary, I-200, 0.1 *M* phosphate solution, pH 7.0; running voltage 17 kV. All other conditions as in Figs. 2 and 3.

characterize (fingerprinting) the mixture. This is in part the advantage of I-200 capillaries over the fuzzy capillaries.

Fig. 11 represents a typical electropherogram of crude soybean trypsin inhibitor (Sigma T-9128) performed on I-200 capillaries. It can be seen that the mixture contains at least 23 minor components and one major component. Another example of the usefulness of I-200 in analyzing complex protein mixture is shown in Fig. 12, which illustrates the electropherogram of commercial lipoxidase (Sigma L-8383), the unsaturated-fat oxidase. The microheterogeneity of lipoxidase was recently assessed by others [29] using several high-performance liquid chromatography techniques. The commercial protein gave also multiple peaks when chromatographed by reversed-phase, anion-exchange or metal chelate interaction chromatography [29].

The F-600 capillaries would also be useful in the above applications; however, longer analysis time would be expected under otherwise identical conditions. In a recent publication from our laboratory [17], F-2000 capillaries were used successfully at high voltage for the tryptic mapping of glycoproteins and the separation of oligosaccharide chains cleaved from glycoproteins. On the other hand, F-2000 capillaries may prove useful in isoelectric focusing or isotachophoresis whereby the presence of low electroosmotic flow may not be deleterious and good resolution of the solute bands could still be achieved.

ACKNOWLEDGEMENTS

The financial supports from the College of Arts and Sciences, Dean Incentive Grant Program, and in part from the Agricultural Station at Oklahoma State University, grant No. CSRS OKL 02109, are gratefully acknowledged.

REFERENCES

1 F. E. P. Mikkers, F. M. Everaerts and T. P. E. M. Verheggen, *J. Chromatogr.*, 169 (1979) 11.
2 S. Hjertén, *J. Chromatogr.*, 270 (1983) 1.

3 J. W. Jorgenson and K. D. Lukacs, *Anal. Chem.*, 53 (1981) 1298.
4 S. Hjertén, *J. Chromatogr.*, 347 (1985) 191.
5 J. W. Jorgenson, *Trends Anal. Chem.*, 3 (1984) 51.
6 R. M. McCormick, *Anal. Chem.*, 60 (1988) 2322.
7 G. J. M. Bruin, J. P. Chang, R. M. Kuhlman, K. Zegers, J. C. Kraak and H. Poppe, *J. Chromatogr.*, 471 (1989) 429.
8 G. J. M. Bruin, R. Huisden, J. C. Kraak and H. Poppe, *J. Chromatogr.*, 480 (1989) 339.
9 S. A. Swedberg, *Anal. Biochem.*, 185 (1990) 51.
10 J. K. Towns and F. E. Regnier, *J. Chromatogr.*, 516 (1990) 69.
11 K. A. Cobb, V. Dolnik and M. Novotny, *Anal. Chem.*, 62 (1990) 2478.
12 H. H. Lauer and D. McManigill, *Anal. Chem.*, 58 (1986) 166.
13 Y. Walbroehl and J. W. Jorgenson, *J. Microcolumn Sep.*, 1 (1989) 41.
14 J. S. Green and J. W. Jorgenson, *J. Chromatogr.*, 478 (1989) 63.
15 M. Bushey and J. W. Jorgenson, *J. Chromatogr.*, 480 (1989) 301.
16 W. Nashabeh and Z. El Rassi, *J. Chromatogr.*, 514 (1990) 57.
17 W. Nashabeh and Z. El Rassi, *J. Chromatogr.*, 536 (1991) 31.
18 K. K. Unger, *Porous Silica*, Elsevier, Amsterdam, 1979, p. 86.
19 G. S. Manning, *Q. Rev. Biophys.*, 11 (1978) 179.
20 J. W. Jorgenson, *ACS Symp. Ser.*, 335 (1987) 182.
21 J. H. Knox and I. H. Grant, *Chromatographia*, 24 (1987) 135.
22 F. Foret, M. Deml and P. Bocek, *J. Chromatogr.*, 452 (1988) 602.
23 E. Grushka, R. M. McCormick and J. J. Kirkland, *Anal. Chem.*, 61 (1989) 241.
24 M. Martin and G. Guiochon, *Anal. Chem.*, 56 (1984) 614.
25 S. Hjertén, *J. Chromatogr.*, 87 (1973) 325.
26 Z. El Rassi, A. L. Lee and Cs. Horvath, in J. A. Asenjo (Editor), *Separation Processes in Biotechnology*, Marcel Dekker, New York, 1990, p. 447.
27 S. Petren and O. Vesterberg, *Biochim. Biophys. Acta*, 994 (1989) 161.
28 F. Kilar and S. Hjertén, *J. Chromatogr.*, 480 (1989) 351.
29 Y. Kato, K. Nakamura and T. Hashimoto, *J. Chromatogr.*, 354 (1986) 511.

Journal of Chromatography, 559 (1991) 385–390
Elsevier Science Publishers B.V., Amsterdam

CHROM. 23 488

High-performance capillary electrophoresis as a fast in-process control method for enzyme-labelled monoclonal antibody conjugates

SARAH J. HARRINGTON*, RUDOLF VARRO and THOMAS M. LI
Syva Company, 900 Arastadero Road, M/S S3–3, Palo Alto, CA 94303 (USA)

ABSTRACT

High-performance capillary electrophoresis (HPCE) was evaluated as a method for characterizing enzyme–antibody conjugates. Alkaline phosphatase (AP) and immunoglobulin G (IgG), individually and in a mixture, were used as standards to identify the components of an AP–IgG conjugate separation. 0.5% Methyl cellulose was added to the running buffer to separate and identify the conjugate, unreacted AP and unreacted IgG. Due to its speed and resolution, HPCE appears to be a good candidate for in-process evaluations of conjugates for immunoassays.

INTRODUCTION

The purpose of this study was to evaluate high-performance capillary electrophoresis (HPCE) as a quality control instrument for the characterization of enzyme–antibody conjugates. The results of a conjugation process may include unwanted material such as unreacted antibody and enzyme, and protein aggregates. The conjugate is usually purified using liquid chromatography after the conjugation procedure [1].

This study utilized capillary zone electrophoresis (CZE) for the separation of proteins. The separation mechanism of CZE is based on electrophoretic mobilities of the sample components which are affected by solvent characteristics including pH, ionic strength, and viscosity.

Alkaline phosphatase (AP) and immunoglobulin G (IgG) were the enzyme and antibody compounds to be conjugated. The relative molecular mass of AP is very close to that of IgG. Their mass–charge ratios may also be similar making CZE separation of an unreacted mixture of AP and IgG difficult. A linear polymer, methyl cellulose, was introduced into the running buffer to facilitate separation. Methyl cellulose (MC) has been previously added to HPCE buffers to enhance separations [2], but it has not been reported for monoclonal antibody separations or as an in-process method for diagnostic product development. HPCE could be used as a quick procedure for evaluating the success of the conjugation (independent of immunoassay performance).

0021-9673/91/$03.50

EXPERIMENTAL

Materials

The Beckman P/ACE 2000 capillary electrophoresis system (Palo Alto, CA, USA) using an IBM PS/2 with P/ACE software and Microsoft Windows interface was used throughout this study. IgG monoclonal antibody (produced in-house) from mouse ascites (3G1, IgG_1 subclass) and alkaline phosphatase (from calf intestine, lot 12056526–08, Boehringer Mannheim, Mannheim, Germany) were used as standards and in the conjugation procedure. Methyl cellulose (15 cP at 2% solution in water; Aldrich, Milwaukee, WI, USA) was used as an additive in the running buffer to create a molecular sieve [2].

The sample buffer was 0.1 *M* borax with 0.5 m*M* sodium dodecyl sulfate (SDS) at pH 10. At this pH, all proteins are negatively charged and are repelled from the wall of the uncoated capillary [3]. The running buffer consisted of 0.5% MC in 0.1 *M* borax with 0.5 m*M* S.D.S. (pH 10).

Methods

Samples were injected using a one second pressure injection into a 27 cm × 75 μm I.D. capillary. The proteins were separated at a current of 5 kV and the temperature was reduced to 15°C. A 280-nm wavelength detector filter was used.

At the beginning of each day, the capillary was pre-rinsed for 5 min. After separation, post-run rinses were used to clean the capillary. This procedure included a 1-min sodium hydroxide rinse, followed by a 1-min water rinse, and a final 3 min rinse using the running buffer.

The IgG was thiolated with S-acetylthioglycolic acid N-hydroxysuccinimide ester (Sigma, St. Louis, MO, USA). The AP was maleimidated with succinimidyl 4-(N-maleimidomethyl)cyclohexane-1-carboxylate (Pierce, Rockford, IL, USA). The conjugate was prepared by reacting the thiolated IgG with maleimidated alkaline phosphatase. This method [4] produces a conjugate consisting of one enzyme and one antibody molecule.

IgG (160 000 relative molecular mass) and AP (140 000 relative molecular mass) were tested alone and in equal amounts as a standard mixture. The electropherogram of the standard AP + IgG mixure was compared to the migration pattern of the conjugate.

The conjugate was tested before and after purification by fast protein liquid chromatography (FPLC) using a Superose 6 column (Pharmacia LKB, Piscataway, NJ, USA). The purification procedure separates the conjugate from unreacted IgG, unreacted AP and from large protein aggregates.

After the conjugate was purified by FPLC, absorbance readings at 280 nm (Perkin-Elmer Lambda 4B spectrophotometer, Norwalk, CT, USA) were cross-matched with enzyme-linked immunosorbent assay (ELISA) results to test for the location of the conjugate fractions. Based on ELISA and absorbance readings, two different fractions selected from the FPLC separation were tested. One fraction represented the main conjugate peak, while another fraction consisted mostly of unreacted IgG and AP.

RESULTS

Figs. 1 and 2 show the electropherograms of IgG and AP, respectively. The migration time for IgG was 4 min as shown in Fig. 1, while AP has a longer migration time of 4.5 min (Fig. 2). The small peak prior to the first major peak (found in all

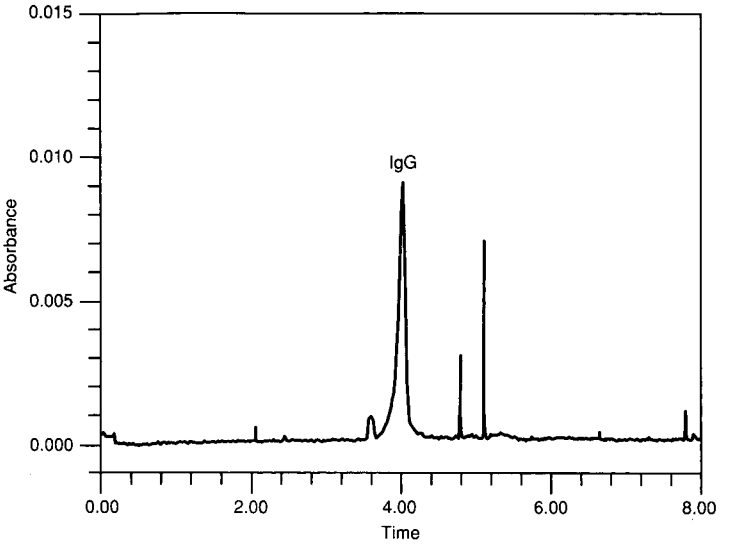

Fig. 1. Analysis of IgG (160 000 relative molecular mass) in 0.5% methyl cellulose in 0.1 *M* borax buffer in 0.5 m*M* SDS at pH 10. Conditions as given under Experimental. For all figures, time (*x*-axis) is in min, and absorbance (*y*-axis) is at 280 nm.

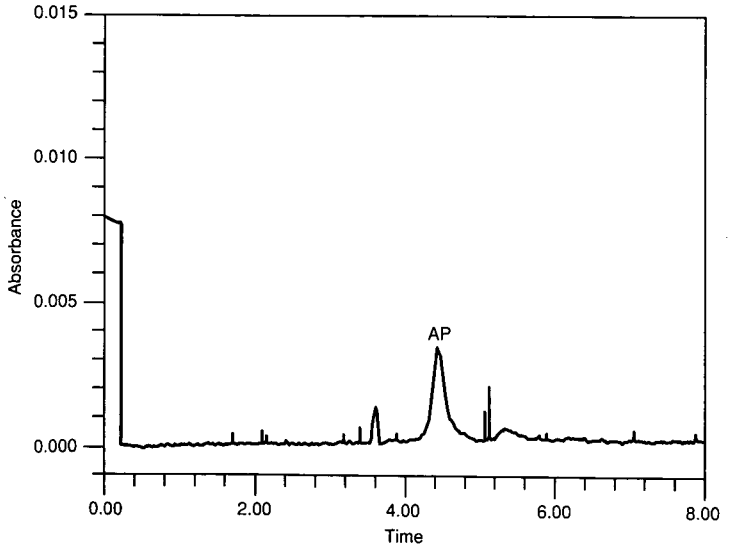

Fig. 2. HPCE of alkaline phosphatase (AP). Relative molecular mass is 140 000. Conditions are as in Fig. 1.

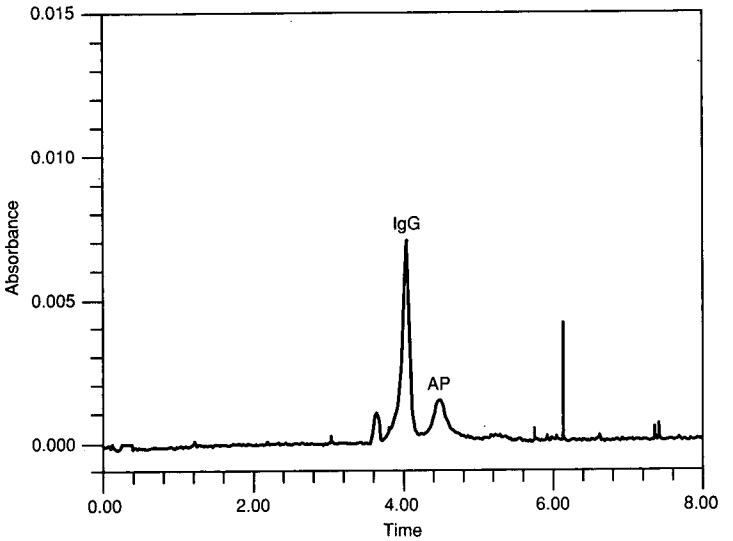

Fig. 3. Separation of the standard mixture of AP + IgG (1:1).

figures) may be due to a refractive index change caused by the front edge of the sample buffer.

By comparing the AP + IgG standard mix in Fig. 3 to the individual runs (Figs. 1 and 2), the first major peak can be identified as IgG (4 min) and the second major peak is AP (4.5 min). The electropherogram of the AP + IgG standard mix was a single peak when MC was not added to the running buffer (data not shown).

Fig. 3 can also be used to identify the components of the unpurified conjugate in

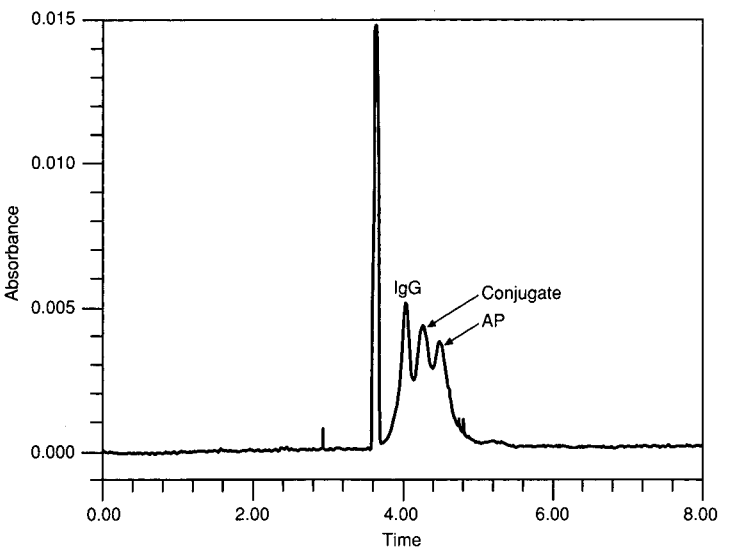

Fig. 4. Separation of unpurified AP–IgG conjugate containing the conjugate and unreacted AP and IgG.

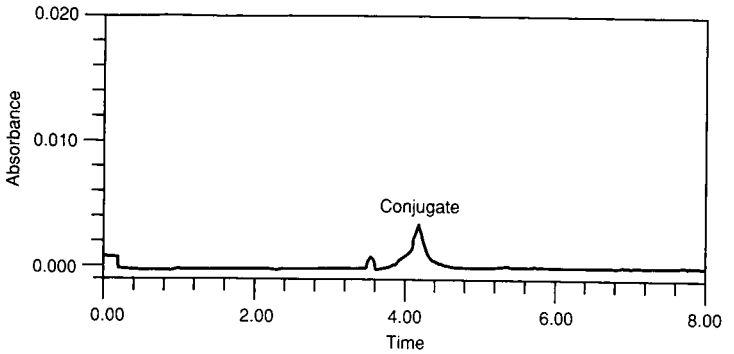

Fig. 5. Electropherogram of a sample from the FPLC purification of AP–IgG conjugate. Represents the fraction with the highest concentration of conjugate.

Fig. 4. Of the three main peaks in Fig. 4, the AP – IgG conjugate appears to be the middle peak located between the unreacted AP and IgG.

The results of the ELISA and absorbance readings correlated well with the migration times of samples from the FPLC fractions obtained during the purification of the conjugate. The electropherogram of a sample containing the main conjugate peak is shown in Fig. 5. This profile can be compared to the one in Fig. 6 showing a sample from a FPLC fraction containing unreacted AP and IgG.

CONCLUSIONS

The high resolution capabilities of HPCE were demonstrated with the separation and identification of components of a conjugate mix and the purified conjugate fractions. Using MC in the running buffer, separation of proteins with similar mass–charge ratios and relative molecular masses was possible. The electropherogram of the conjugate mix (Fig. 4) reveals a triple peak separation. The AP–IgG conjugate was identified as the middle peak between the smaller, unreacted conjugate components. Therefore, MC seems to improve resolution between compounds with similar mass–charge ratios by decreasing electroosmotic flow and enhancing differences in electrophoretic mobilities.

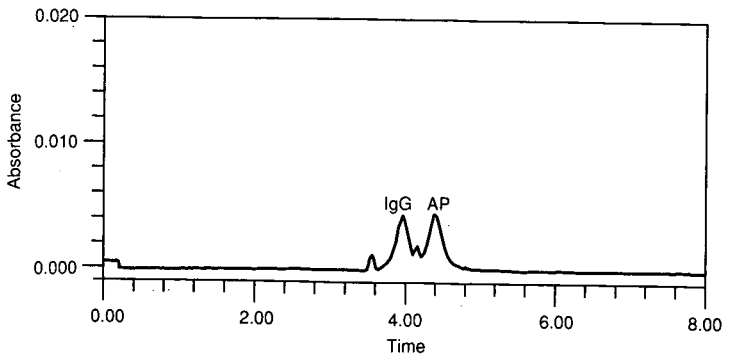

Fig. 6. Profile of a sample from the FPLC purification of AP–IgG conjugate. Fraction primarily contains unreacted AP and IgG.

Along with MC, other factors, such as temperature and SDS concentration enhanced resolution. Decreasing the temperature to 15°C increases migration times, but may also increase resolution.

The capillary electrophoresis system was able to verify the success of the conjugate preparation and purification procedure. Due to its speed and resolution, HPCE appears to be a good candidate for in-process evaluations of conjugates for immunoassays.

ACKNOWLEDGEMENTS

We would like to thank Beckman Instruments for the loan of the P/ACE 2000 capillary electrophoresis system used in this study.

REFERENCES

1 E. Ishikawa, M. Imagawa, S. Hashida, S. Yoshitake, Y. Hamaguchi, and T. Ueno, *J. Immunol.*, 4 (1983) 209.
2 M. Zhu, D. L. Hansen, S. Burd, and F. Gannon, *J. Chromatogr.*, 480 (1989) 311.
3 H. H. Lauer and D. McManigill, *Anal. Chem.*, 58 (1986) 166.
4 R. J. S. Duncan, P. D. Weston and R. Wriggleworth, *Anal. Biochem.*, 132 (1983) 68.

Journal of Chromatography, 559 (1991) 391–399
Elsevier Science Publishers B.V., Amsterdam

CHROM. 23 492

Capillary zone electrophoresis studies of motilin peptides

Effects of charge, hydrophobicity, secondary structure and length

JAMES R. FLORANCE*, ZENON D. KONTEATIS, MARK J. MACIELAG, RALPH A. LESSOR and ALPHONSE GALDES

BOC Group Technical Center, 100 Mountain Avenue, Murray Hill, NJ 07974 (USA)

ABSTRACT

Motilin is a gut hormone, which is involved in gastrointestinal motility. Capillary electrophoresis studies were made on 24 peptides that are N-terminal, C-terminal or internal fragments of motilin. The isoelectric point, total charge and hydrophobicity were calculated for all of the peptides. The effects of buffers and pH on migration time and resolution were studied. These included citrate buffer, pH 2.5; phosphate buffer, pH 7.0 and borate buffer, pH 10.0. A capillary zone electrophoresis method was developed to resolve 14 of the motilin peptides. Secondary structure predictions were made using the Chou–Fasman method. Circular dichroism spectra were collected to confirm presence of α-helix in several fragments. Effects of charge, hydrophobicity, secondary structure and length of the motilin fragments on migration time were studied.

INTRODUCTION

Motilin is a 22-residue peptide hormone (FVPIFTYGELQRLQEKERNKGQ) that is synthesized in the antrum of the stomach. Its biological effect is to stimulate phase III migrating motor complex (MMC) which increases gut motility [1]. Recently a two-dimensional NMR study was published which had suggested a three-dimensional structure for native motilin [2]. A circular dichroism study was also done indicating that an α-helix was present in native motilin in hexafluoropropanol–water (30:70).

Motilin contains ten charged residues distributed throughout the peptide. Capillary zone electrophoresis (CZE), with separation determined predominantly by charge and mass, seemed to be an ideal technique for analysis of motilin peptides as an alternative to reversed-phase high-performance liquid chromatography (RP-HPLC). No HPLC or CZE studies have been reported on motilin peptides. Previous CZE studies have been done on factors affecting resolution in a series of heptapeptides. These factors included charge, hydrophobicity and amino acid sequence of the peptides [3–5].

0021-9673/91/$03.50

In the present study a series of 24 motilin fragments were synthesized where Leu replaces Met-13 using the standard 9-fluorenylmethyoxycarbonyl (FMOC) [6] solid-phase peptide method. A number of factors including charge, hydrophobicity and secondary structure were correlated with CZE migration times.

METHODS

Capillary electrophoresis was carried out under the following conditions. Instrument: Applied Biosystems (ABI, Foster City, CA, USA) 270 CZE; injection: 2 s vacuum injection, samples *ca.* 10 μg/ml; buffers: pH 2.5 20 m*M* sodium citrate, pH 7.0 50 m*M* sodium phosphate, pH 9.4 50 m*M* sodium borate; voltage: 30 kV, *ca.* 20–30 mA with anode at the autosampler end; capillary: 72 cm (48 cm to detector) × 50 μm, 30°C; detection: UV at 200 nm; running procedure: 2 min wash with 0.1 *M* NaOH, followed by a 5-min buffer wash, then sample injection.

The purity of the motilin peptides was confirmed by gradient RP-HPLC. The primary structure of all peptides was confirmed by quantitive amino acid analysis and fast atom bombardment mass spectrometry (FAB-MS). In addition the primary sequence of motilin 1-14 was confirmed by peptide sequencing.

The secondary structure was predicted using PROSEC (CHEMLAB, Molecular Design Limited, Hayward, CA, USA) a program which is based on Chou–Fasman methods [7]. Helical wheels were also generated for the regions of the peptides that were predicted to contain α-helix. The isoelectric point (p*I*) was calculated using MacVector (International Biotechnology, New Haven, CT, USA). The pK_a and pK_b values used for the calculation of p*I* are based on published data with several modifications [8][a]. The total charges on the peptides were calculated at pH increments of 0.1 units using a program called PIAA, supplied by Applied Biosystems.

The total hydrophobicity values were calculated by summing up the Kyte and Doolittle (K&D) parameters for each residue in the peptide [10]. The charge/mass ratio was calculated using the total calculated charge divided by the molecular mass of the peptide.

All figures were plotted with R/S1 using the MAKEGRAPH function (Bolt, Beranek and Newman, Cambridge, MA, USA) and lines were drawn using the least-squares linear fitting program from R/S1 called FITLINE.

The circular dichroism (CD) spectra were recorded on a Jasco 720 instrument (Japan Spectroscopic Co., Tokyo, Japan) using conditions as listed in the legend to Fig. 2.

RESULTS AND DISCUSSION

The isoelectric points and total charges for the 24 N-terminal, C-terminal and internal peptide fragments of motilin are shown in Table I. The charges range from +0.36 to +4.36 at pH 2.5, −2 to +2 at pH 7.0 and −2.5 to +1.4 at pH 10.0. The

[a] The following values were used for pK_a and pK_b values: Asp 3.86, Glu 4.25, Tyr 10.10, Lys 9.80, Arg 12.48, NH_3 end 8.00 and COOH end 3.00. They are taken with some modifications from ref. 9.

TABLE I

ISOELECTRIC POINT AND CALCULATED TOTAL CHARGE AT pH 2.5, 7.0 AND 10.0

Motilin fragment	p*I*	Calculated charge		
		pH 2.5	pH 7.0	pH 10.0
1-5	5.496	0.398	−0.002	−0.376
1-7	5.496	0.398	−0.003	−0.542
1-9	3.625	0.382	−1.001	−1.542
1-10	3.625	0.382	−1.001	−1.542
1-11	3.625	0.367	−1.999	−2.542
1-12	6.135	1.382	−0.001	−0.543
1-13	6.135	1.367	−0.999	−1.543
1-14	6.135	1.367	−0.999	−1.543
1-15	4.292	1.351	−1.997	−2.543
1-16	6.278	2.351	−0.998	−1.617
1-19	6.365	3.351	0.002	−0.617
1-22	8.673	4.351	1.002	0.309
15-22	8.730	3.367	1.001	0.476
12-22	9.81	4.367	2.001	1.475
10-22	9.81	4.367	2.001	1.475
8-22	8.73	4.351	1.003	0.475
6-22	8.673	4.351	1.002	0.309
3-22	8.673	4.351	1.002	0.309
7-19	6.365	3.351	0.002	−0.617
5-17	4.568	3.351	0.002	−0.617
1-5/17-22	8.899	2.382	0.999	0.550
1-7/19-22	8.797	1.398	0.997	0.384
2-14	6.135	1.367	−0.999	−1.543
3-14	6.135	1.367	−0.999	−1.543

isoelectric points range from 3.6 to 9.8. The p*I* values for the 24 motilin peptides provided a large and varied data base for this CZE study.

Table II lists the migration times at pH 2.5, pH 7.0 and pH 10.0. A marker such as mesityl oxide was not used, so electrophoretic mobilities were not calculated. The migration times range from 5.2 to 13.7 min at pH 2.5; 5.2 to 8.9 min at pH 7.0; 4.7 to 7.3 min at pH 10.0. The greatest resolution for motilin peptides was found in citrate buffer at pH 2.5.

Table III lists the residues that were involved in the predicted secondary structure (α-helix, β-turn and β-sheet). The rationale for including the secondary structure predictions was to study if the secondary structure in these small model peptides would affect CZE migration time. Most of the motilin fragments larger than Mot_{1-14} are predicted to have a helical region, except Mot_{15-22} and $Mot_{1-5/17-22}$. Many of the peptides are predicted to contain a β-turn.

Fig. 1 shows the log of $q/mw^{2/3}$ plotted against the migration time for the 24 peptides. This plot yields a linear relationship ($R = 0.89$), with several outlying points including Mot_{1-14}. Interestingly Mot_{1-14} is predicted to contain regions of α-helix from residues 8-14. Mot_{1-15}, Mot_{1-16} and Mot_{1-19} are also predicted to contain α-helix but are not outlying points in Fig. 1.

TABLE II

CZE MIGRATION TIMES OF MOTILIN PEPTIDES

CZE performed with an ABI 270A at 30 kV, 30°C, with a 72 cm × 50 μm capillary. Buffers were pH 2.5 citrate, pH 7.0 phosphate, and pH 10.0 borate. UV detection at 200 nm.

Motilin fragment	Migration times (min)		
	pH 2.5	pH 7.0	pH 10.0
1-5	10.9	8.99	6.48
1-7	12.3	7.80	6.33
1-9	13.7	8.63	7.15
1-10	12.6	7.31	7.37
1-11	13.7	7.06	4.76
1-12	8.67	7.11	6.11
1-13	9.16	7.22	6.08
1-14	5.96	5.3	6.2
1-15	10.45	5.3	6.77
1-16	7.92	5.29	5.89
1-19	7.13	5.13	5.86
1-22	6.89	5.61	5.47
15-22	5-21	5.52	5.34
12-22	5.29	5.48	4.76
10-22	5.47	5.78	
8-22	5.84	6.81	5.35
6-22	5.96	5.26	5.62
3-22	6.32	5.24	5.67
7-19	6.75	5.61	6.28
5-17	7.78	5.52	7.15
1-5/17-22	7.13	5.82	
1-7/19-22	9.6	5.85	5.80
2-14	9.78	6.41	6.09
3-14	9.39	6.79	6.08

Fig. 2 shows a circular dichroism spectra of Mot_{1-22} and Mot_{1-14} in 20 m*M* acetic acid pH 3.8 with 20% hexafluoropropanol (HFP). HFP tends to induce or stabilize helical regions of peptides. A secondary structure prediction package for CD data from Jasco called SSE-338 was used to calculate amounts of secondary structure including α-helix in Mot_{1-14} and Mot_{1-22}. This prediction package is based on published methods [11]. The CD results with 20% HFP indicate that Mot_{1-14} contains 47% α-helix, while Mot_{1-22} contains 42% helix. These values are similar to the Chou–Fasman predictions of *ca.* 50% α-helix for both peptides. CD studies done in the absence of HFP indicate that both 1-14 and 1-22 still maintain some small amount of helical content.

All CZE studies were performed in aqueous buffers with no addition of HFP.

Table IV lists the Kyte and Doolittle [10] values for the total hydrophobicity, log (q/mw$^{2/3}$) and the number of residues in the 24 motilin peptides. The calculated charge at pH 2.5 and the K&D hydrophobicity values are 1.3, 2.9 for Mot_{1-14} and 2.3, −4.5 for Mot_{1-16}, respectively. Motilin 1-19 and 1-22 and many of the other motilin peptides have more negative calculated hydrophobicity and greater positive charges but are well correlated with the linear relationship in Fig. 1. The deviation of Mot_{1-14} may be due to differences in charge and hydrophobicity.

TABLE III

PREDICTED SECONDARY STRUCTURE OF MOTILIN PEPTIDES USING CHOU–FASMAN METHOD

	1	10	20
Motilin (Leu-13)	FVPIFTYGELQRLQEKERNKGQ		

Motilin fragment	Residues contained in secondary structure		
	α-Helix	β-Turn	β-Sheet
1-5			
1-7			
1-9			
1-10		5-9	3-9
1-11		5-9	3-9
1-12		5-9	3-9
1-13		5-9	3-9
1-14	8-14	5-9	3-9
1-15	8-15	5-9	3-9
1-16	8-16	5-9	3-9
1-19	8-19	5-9	3-9
1-22	8-20	5-9, 17-22	3-9
15-22			
12-22	12-20	17-22	
10-22	10-20	17-22	
8-22	8-20	17-22	
6-2	8-20	17-22	
3-22	8-20	3-7, 17-22	3-9
7-19	8-19		
5-17	10-17	7-11	
1-5/17-22		17-22	
1-7/19-22	3-7/19-20		
2-14	8-14	5-9	3-9
3-14	8-14	5-9	3-9

Fig. 3 depicts the migration time *versus* hydrophobicity. The data points are not well correlated with a linear function ($R = 0.67$). The plot indicates that the more hydrophobic (less hydrophilic) the peptide, the longer the migration time. Presumably the hydrophilicity is related to the relative charge of the peptide and thus CZE migration time.

Fig. 4 is a plot of the log $(q/\mathrm{mw}^{2/3})$ *versus* hydrophobicity. The relationship can be fitted to a linear function with $R = 0.81$. Many of the deviating points, such as motilin 1-9, 1-10 and 1-11, have small charge/mass ratios (due to high percentage of charged residues) as well as large hydrophobicities.

Fig. 5 is an electropherogram of 14 of the motilin fragments. This figure indicates the resolving power of CZE. Many of the peptide fragments differ by only one residue, while others have only a small difference in total charge.

In this study several different factors affecting CZE of motilin peptides were investigated. These included the affects of charge/mass; hydrophobicity and secondary structure on migration time.

The CZE migration times for this series of 24 motilin peptides is linearly corre-

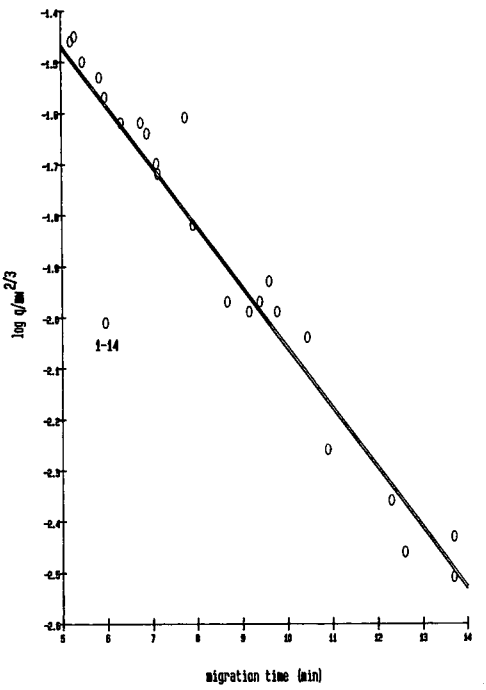

Fig. 1. Log (q/mw$^{2/3}$) *versus* CZE migration time (min) for 24 motilin peptide fragments run at 30 kV in pH 2.5 citrate buffer.

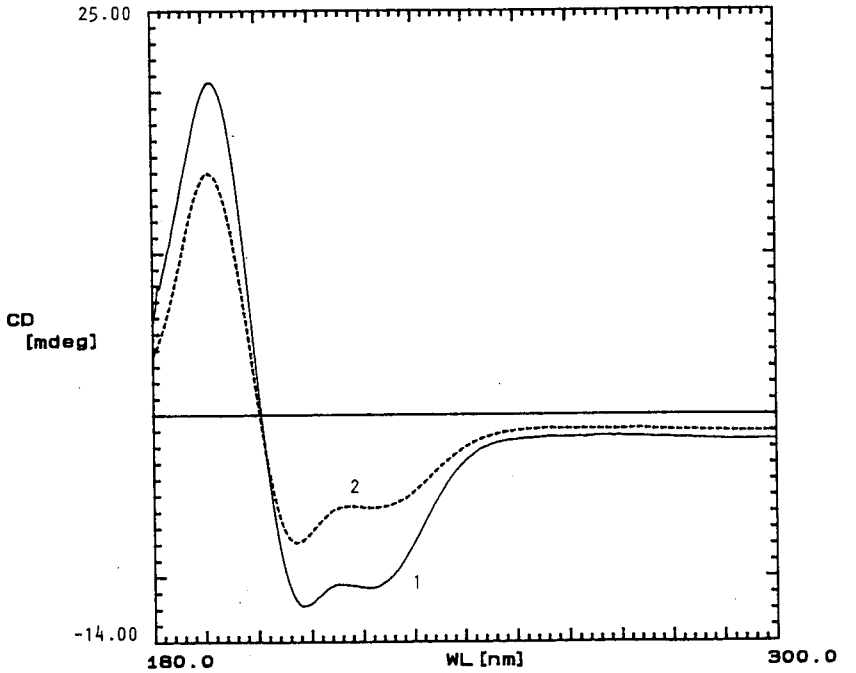

Fig. 2. Circular dichroism spectra, ellipticity (millidegree) *versus* wavelength (WL) (nm) of Mot_{1-22} and Mot_{1-14}. Sample is 0.7 mg/ml in 20 mM acetic acid pH 3.8 with 20% hexafluoropropanol. CD method: Scan 300 to 180 nm at 50 nm/min using a step of 0.1 nm/data. Bandwidth 1.0 nm, sensitivity 20 millidegree with response of 8 s. Path length of cell was 0.1 mm, temperature was 25°C. Curves: 1 = Mot_{1-22}; 2 = Mot_{1-14}.

TABLE IV

MASS/CHARGE RATIO, HYDROPHOBICITY AND NUMBER OF RESIDUES IN MOTILIN PEPTIDES

Motilin fragment	Log(q/mw$^{2/3}$)	Hydrophobicity (Kyte and Doolittle)	Number of residues
1-5	−2.26	12.7	5
1-7	−2.36	10.7	7
1-9	−2.43	6.8	9
1-10	−2.46	10.6	10
1-11	−2.51	7.10	11
1-12	−1.97	2.60	12
1-13	−1.99	6.40	13
1-14	−2.01	2.90	14
1-15	−2.04	− 0.60	15
1-16	−1.82	− 4.50	16
1-19	−1.72	−16.00	19
1-22	−1.64	−23.80	22
15-22	−1.46	−26.70	8
12-22	−1.45	−30.90	11
10-22	−1.50	−30.60	13
8.22	−1.53	−34.50	15
6.22	−1.57	−36.50	17
3-22	−1.62	−30.80	20
7-19	−1.62	−31.15	13
5-17	−1.61	−21.05	12
1-5/17-22	−1.70	−6.60	11
1-7/19-22	−1.93	−4.10	11
2-14	−1.99	0.10	13
3-14	−1.97	1.70	12

lated with the log of the charge/mass ratio when q/mw$^{2/3}$ is plotted, with several exceptions. When q/mw is plotted the linear correlation is less (R = 0.86). Similar results have been shown in CZE studies of other peptides [12]. The correlation between migration time and hydrophobicity is poor. In this series, the hydrophobicity is not a major factor in determining migration in CZE, although generally more hydrophobic motilin peptides have longer migration times. The hydrophobicity of these fragments has a higher correlation with the charge/mass ratio than with the migration time. The N-terminal region of $Mot_{1\text{-}22}$ and similar fragments is hydrophobic, while the carboxy terminal region is hydrophilic. In general the 24 fragments have charged groups that are distributed throughout the length of the peptides, but there is no correlation between the number of residues and CZE migration time.

In the motilin family of peptides, the presence of secondary structure doesn't appear to be a major factor in deviations from linearity in Fig. 1. Smaller peptides such as motilin 1-5, 1-7, 1-9, 1-11, 1-12 and 1-13 are not predicted to contain α-helix and are not outlying points. An exception is $Mot_{1\text{-}14}$ which contains helix and also has a much faster migration time than would be expected from the charge/mass ratio. Presumably a small peptide containing a significant amount of helical structure could possess an altered hydrodynamic profile compared to a peptide having no secondary structure. This could possibly affect migration time and offer an explanation for the

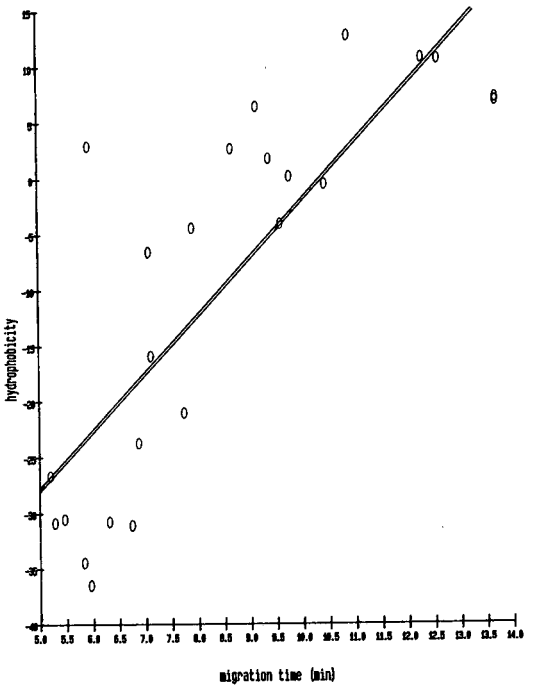

Fig. 3. Hydrophobicity (Kyte and Doolittle parameters) *versus* CZE migration time (min) for 24 motilin fragments at 30 kV in pH 2.5 citrate buffer.

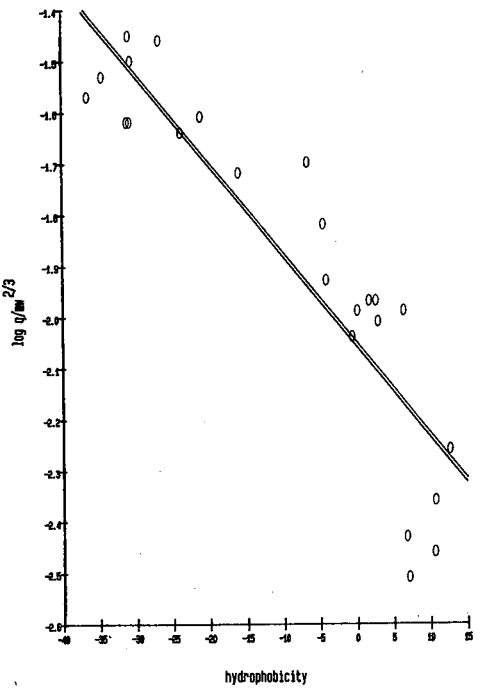

Fig. 4. Log (q/mw$^{2/3}$) *versus* hydrophobicity (K&D parameters) for 24 motilin fragments.

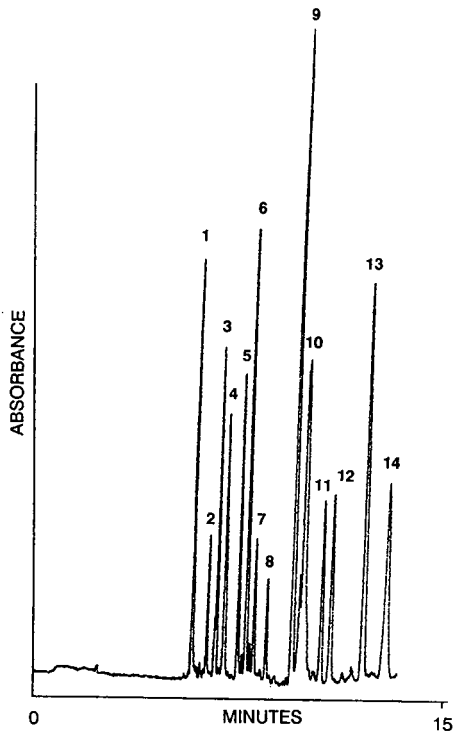

Fig. 5. Electropherogram of fourteen motilin peptides. 1 = Mot_{15-22}; 2 = Mot_{10-22}; 3 = Mot_{1-14}; 4 = Mot_{3-22}; 5 = Mot_{1-22}; 6 = Mot_{1-19}; 7 = Mot_{1-16};8 = Mot_{1-12}; 9 = Mot_{3-14}; 10 = Mot_{2-14}; 11 = Mot_{1-15}; 12 = Mot_{1-5}; 13 = Mot_{1-7} 14 = Mot_{1-9}. Conditions as described in Methods using pH 2.5 citrate buffer at 20 kV. Absorbance range 0–0.01 a.u.f.s. Each motilin peptide was run individually to correlate migration times in the mixture.

deviation of Mot_{1-14} seen in Fig. 1. It is not clear why a peptide with a similarly predicted helical content such as Mot_{1-16} is linearly correlated in Fig. 1. Further CD studies will be needed to confirm helical content and to evaluate the contributions of secondary structure to CZE migration time in the motilin peptides.

REFERENCES

1 V. Bormans, G. Vantrappen and T. L. Peeters, *Regul. Pept.*, 15 (1986) 143–153.
2 N. Khan, A. Graslund, A. Ehrenberg and J. Shriver, *Biochem.*, 29 (1990) 5743–5751.
3 P. D. Grossman, K. J. Wilson, G. Petrie and H. H. Lauer, *Anal. Biochem.*, 173 (1988) 265–270.
4 P. D. Grossman, J. C. Colburn and H. H. Lauer, *Anal. Biochem.*, 179 (1989) 28–33.
5 R. G. Nielsen, R. M. Riggin and E. C. Rickard, *J. Chromatogr.*, 480 (1989) 393–401.
6 E. Atherton and R. C. Sheppard, in D. Rickwood and B. D. Hames (Editors), *Solid-Phase Peptide Synthesis*, IRL Press, Oxford, 1989, pp. 25–37.
7 P. Y. Chou and G. D. Fasman, *Ann. Rev. Biochem.*, 47 (1978) 251–370.
8 International Biotechnology, Inc., New Haven, CT, 1991, personal communication.
9 A. L. Lehninger, *Biochemistry*, 2nd ed., Worth Publishers, New York, 1970.
10 J. Kyte and R. F. Doolittle, *J. Mol. Biol.*, 157 (1982) 105–110.
11 J. T. Yang, C. C. Wu and H. G. Martinez, *Methods Enzymol.*, 130 (1986) 208–269.
12 R. G. Nielsen and E. C. Rickard, *J. Chromatogr.*, 516 (1990) 99.

Journal of Chromatography, 559 (1991) 401–410
Elsevier Science Publishers B.V., Amsterdam

CHROM. 23 457

Fractionation of the human recombinant tissue plasminogen activator (rtPA) glycoforms by high-performance capillary zone electrophoresis and capillary isoelectric focusing

KALVIN W. YIM

Department of Pharmaceutical Research and Development, Genentech Inc., S. San Francisco, CA 94080 (USA)

ABSTRACT

This paper reports the fractionation of recombinant human tissue plasminogen activator (rtPA) glycoforms, a complex mixture to demonstrate the high resolving power of capillary zone electrophoresis (CZE) and capillary isoelectric focusing (cIEF). rtPA is a glycoprotein with a complex carbohydrate structure. The electropherograms and IEF patterns have been discussed in light of the known carbohydrate structures of rtPA. rtPA was treated with neuraminidase which removes the sialic acids from the carbohydrate chains. The desialylated rtPA was analyzed by both CZE and IEF and the results were compared to those of untreated rtPA. The usefulness of CZE and cIEF in the characterization of glycoproteins proteins is also discussed.

INTRODUCTION

Zone electrophoresis and isoelectric focusing in the slab-gel format are well established high resolution separation techniques for proteins. Capillary zone electrophoresis (CZE) and capillary isoelectric focusing (cIEF) are their counterparts in the capillary format. Giddings [1] has shown that the upper limit of N (number of theoretical plates) for electrophoretic separations is proportional to the applied voltage. So in theory, higher applied voltages result in narrower peaks. The highly efficient heat transfer from small diameter capillaries allows the application of high voltages and results in high resolution and short analysis times [2]. The purpose of this paper is to evaluate the resolving power of cIEF and CZE, using the glycoforms of rtPA as a test mixture.

Glycoforms are glycoproteins sharing an identical polypeptide but differing with respect to the structure, location and incidence of individual oligosacccharides. It is becoming increasingly obvious that protein glycosylation patterns may be important – if not essential – to their function or therapeutic efficacy. The oligosaccharides can influence a protein's clearance rate, its specific ativity and its immunogenicity [3].

Recombinant human tissue plasminogen activator (rtPA) is a fibrin-specific plasminogen activator which has been approved for the treatment of myocardial

0021-9673/91/$03.50

infarction. It has a polypeptide molecular mass of about 60 000 and consists of 527 amino acids. The carbohydrate structures of Chinese hamster ovary (CHO)-derived rtPA have been elucidated [4]. The amino acid sequence of rtPA has four potential N-glycosylation sites, as predicted by the consensus sequence Asn–X–Ser/Thr [5]; these residues are: 117, 184, 218 and 448. rtPA is not glycosylated at Asn-218 (X is a proline residue). rtPA exists as two glycosylation variants designated Type I and II. Type I rtPA is glycosylated at asparagine residues 117, 184 and 448 whereas Type II rtPA is glycosylated only at asparagine resides 117 and 448. The nature of the carbohydrate as Asn-117 was found to be high mannose oligosaccharide. At ASN-448 the carbohydrates comprise biantennary, 2,4-branched triantennary, 2,6-branched triatennary and tetraantennary N-acetyllactosamine oligosaccharides. In Type I rtPA, the carbohydrates as Asn-184 are of the same complex types of oligosaccharide as at Asn-448. All of the hybrid and N-acetyllactososamine-type oligosaccharides can contain sialic acid attached to galactose. This paper reports the results of the application of capillary electrophoretic methods to the resolution of a complex mixture of similar forms of a protein. Both free zone and isoelectric focusing methods have been successfully applied using columns whose inner surface have been covalently coated with polymer.

EXPERIMENTAL

All capillary electrophoresis was performed using the HPE 100 high-performance capillary electrophoresis system from Bio-Rad Labs. (Hercules, CA, USA). All the capillaries were purchased from Bio-Rad Labs. The capillaries were enclosed in microsampler cartridges. The capillaries used in the CZE and IEF experiments were 20 cm and 14 cm long respectively. The internal surfaces of the capillaries were coated with a covalently bonded linear polymer and the internal diameters of the capillaries were 25 μm. Detection was performed by UV at 200 nm in the CZE mode and at 280 nm in the IEF mode.

Sample preparation

rtPA (approximately 5 mg/ml) was obtained by adding a suitable amount of water for injection (WFI) into a vail of lyophilized Activase rtPA. Type I and Type II rt-PA were obtained by partially separating rtPA into two fractions on a lysine-Sepharose column using an arginine gradient [6]. Type I was collected from the leading edge of the first peak and Type II was collected from the trailing of the second peak. They were concentrated by Centriprep and then dialysed into 10 m*M* sodium phosphate buffer, pH 2.5. The final sample concentrations were 2.85 mg/ml and 3.05 mg/ml, for Type I and Type II rtPA respectively. The Type I/Type II mixture sample was prepared by mixing equal volumes of the above samples. The dialysed samples were then diluted to obtain an approximate concentration of 0.5 mg/ml rtPA in 2% ampholyte (pH 6–8) containing 2% 3-[(3-cholamidopropyl)dimethylammonio] 1-propanesulfonate (CHAPS) and 0.36 mg/ml of urea. The IEF calibration mixture was obtained from Pharmacia LKB (Piscataway, NJ, USA) and reconstituted with an ampholyte solution (pH 3–10) containing N,N,N′,N′-tetramethylethylenediamine (TEMED) as a spacer. The final concentrations of the ampholyte and TEMED were 1 and 0.4%, respectively.

IEF conditions

The capillary was first washed with 100 μl of 10 m*M* phosphoric acid and then rinsed with 100 μl of deionized water. The sample (10–20 μl) was introduced into the capillary. The purge block was first washed with 1 ml of deionized water and then with 1 ml of catholyte (20 m*M* sodium hydroxide). A microcentrifuge tube (the anode reservoir) was filled with the anolyte (10 m*M* phosphoric acid) and inserted into the microsampler housing. The focusing voltage and time were 12 kV and 2 min. At the end of the focusing step, the purge block was purged with 1 ml of the mobilizer (10 m*M* sodium hydroxide and 80 m*M* sodium chloride). The mobilizing voltage was set at 8 kV.

CZE conditions

The capillary was washed with 100 μl of 10 m*M* phosphoric acid and then rinsed with 100 μl of the running buffer. The purge block reservoir was then flushed with 1 ml of buffer. Volumes of 10–50 μl of sample was added to a microcentrifuge tube and placed into the microsampler housing and the loading cycle started. The loading voltage was 8 kV and loading time was 8 s. The sample was then replaced by buffer and the run started. The run voltage was set at 6 kV. The rtPA sample was the same as described above in the IEF section. The running buffer consisted of 0.1 *M* ammonium phosphate pH 4.6 with 0.01% Triton X-100 (chemically reduced to minimize UV absorbance) and 0.2 *M* ε-aminocaproic acid (EACA).

RESULTS AND DISCUSSION

Since the total volume of a 14 cm × 25 μm capillary is only about 60 nl, the difficulties associated with collection and characterization of proteins separated by capillary electrophoretic methods lead to the need for calibration of the system by markers of known properties. Fig. 1 is the cIEF of a mixture of some p*I* markers to illustrate the features of a typical IEF pattern. cIEF is a three-step process. In the first

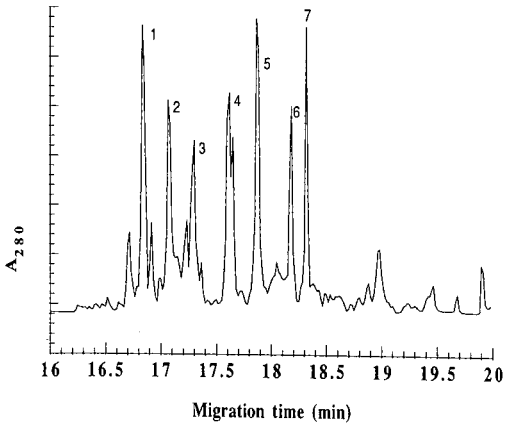

Fig. 1. IEF pattern of a mixture of p*I* markers in 1% (pH 3–10) ampholyte solution containing 0.4% TEMED. Peaks: 1 = lectin (8.6); 2 = lectin (8.4); 3 = lectin (8.2); 4 = horse myoglobin (7.3); 5 = horse myoglobin (6.8); 6 = human carbonic anhydrase (6.6); 7 = bovine carbonic anhydrase (5.8).

step, the sample is mixed with an ampholyte solution and introduced into a capillary by pressure loading. The second step is the focusing step. After the high voltage is applied, sample components are focused in a pH gradient formed by the carrier ampholytes according to their isoelectric points. The third step is the mobilization step where the separated zones are mobilized cathodically [7,8], by adding sodium chloride to the catholyte thus eluting to the focused species electrophoretically. As a result, focused bands with shorter migration times have higher p*I* and *vice versa*.

Fig. 2A and B are the cIEF patterns of Type I and Type II rtPA, respectively. It is observed that, despite the fact that rtPA is purified to homogeneity (with respect to the polypeptide chain), these samples can be resolved in a narrow pH range (6–8) into as many as 20 peaks. This microheterogeneity is expected on the basis of the known carbohydrate structures present in rtPA [4], illustrated in Figs. 3 and 4. If there is only one glycosylation site, the number of glycoforms is simply the number of different oligosaccharide structures at that site (site heterogeneity). Thus, a given subset of Type II rtPA glycoforms may have a biantennary oligosaccharides at Asn-448 with no sialic acid residue, while another subset may have a tetraantennary oligosaccharides with 4 sialic acids residues etc.. However, the number of glycoforms increases dramatically with the number of glycosylation sites due to the number of permuta-

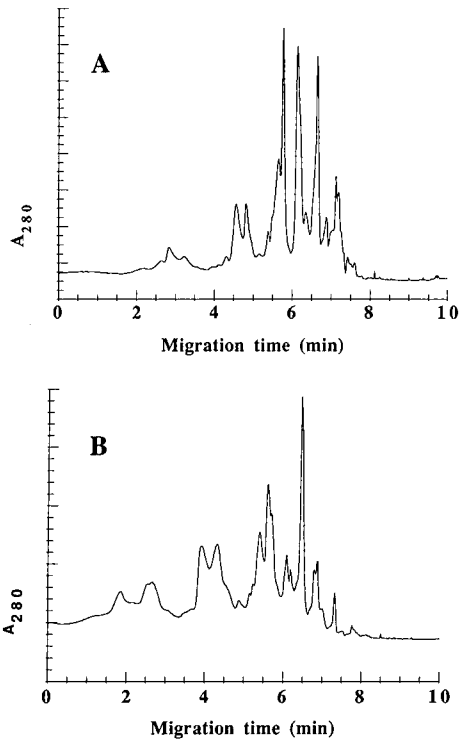

Fig. 2. IEF patters of (A) Type I rtAP and (B) Type II rtPA obtained at 280 nm using a Bio-Rad coated silica capillary (14 cm × 25 μm). The focusing voltage was 12 kV and mobilization voltage was 8 kV. The ampholyte solution contained 2% ampholyte (pH 6–8), 2% CHAPS and 6 *M* urea.

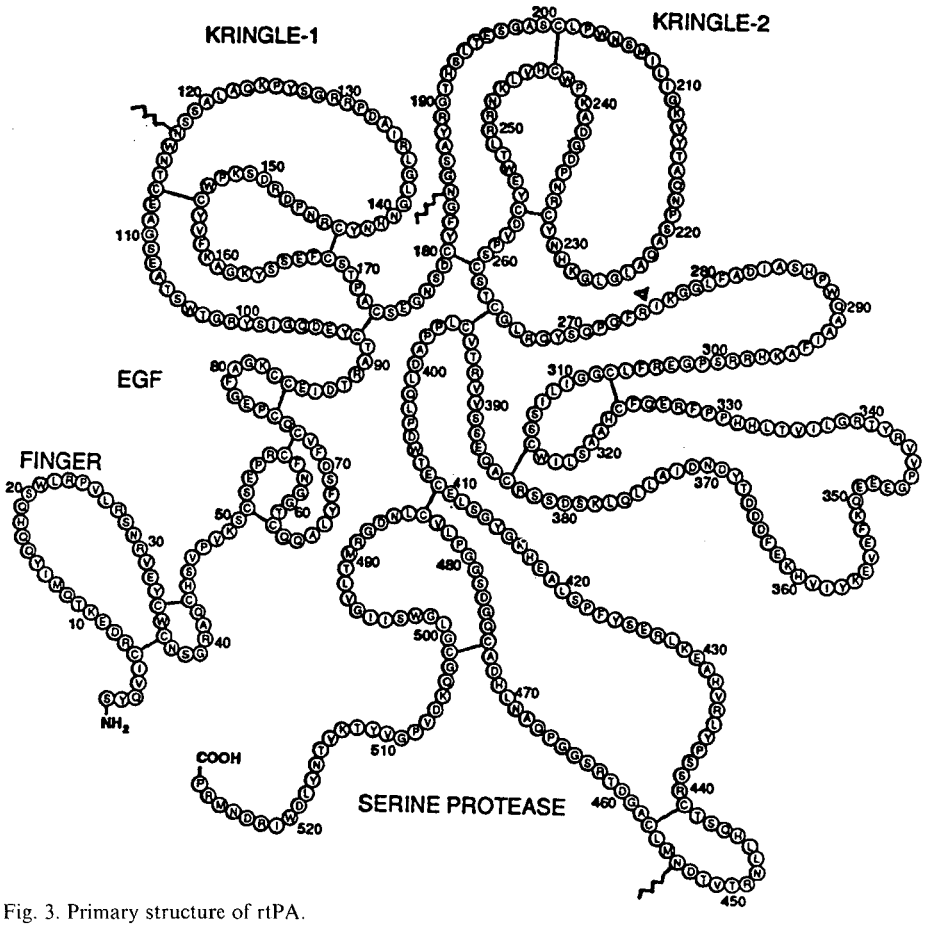

Fig. 3. Primary structure of rtPA.

tions of heterogeneity at each site. Each peak in the IEF pattern may represent a combination of glycoforms having the same p*I*, since there are probably more glycoforms than peaks. Type I and Type II rtPA are expected to contain different subsets of glycoforms; as a result, their IEF patterns are different, as observed. That cIEF can discriminate such subtle differences between two complex and yet similar mixtures (Type I and Type II rtPA) suggests that this technique could be very useful in studying subtle changes in protein molecules (*e.g.* deamidation, conformational changes etc.).

One might expect the IEF patterns to be additive, (*i.e.* the arithmetic sum of the IEF patterns of Type I and Type II rtPA should yield the IEF pattern of the mixture), if the run-to-run migration time reproducibility is good. However, this additivity is not observed. If one could scan the IEF pattern in the capillary without having to mobilize the focused bands, this additivity could very well have been observed. But since the current methodology requires a mobilization step to move the focused bands through the detector, an additional variable is introduced. The migration time of a

HIGH MANNOSE

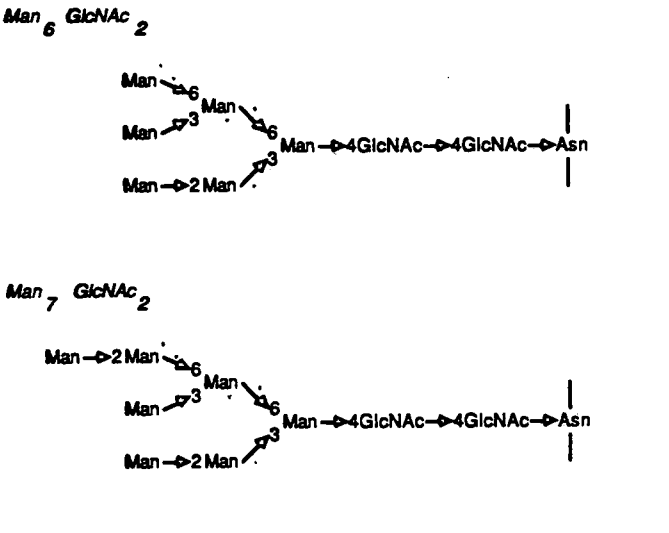

COMPLEX

Biantennary

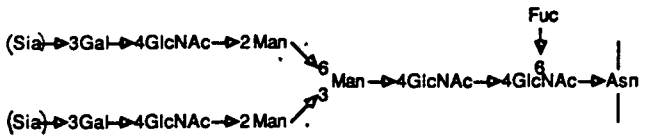

Triantennary

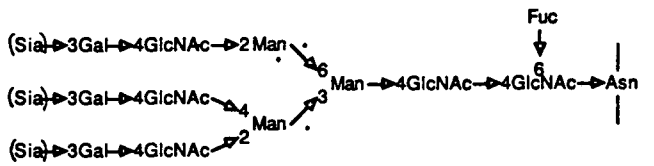

Tetraantennary

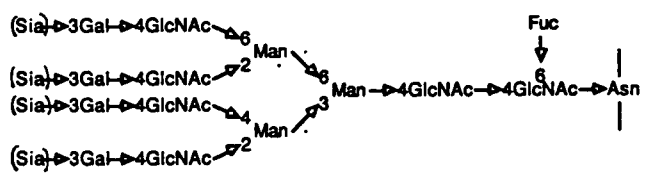

Fig. 4. Schematic structures of some of the Asn-linked oligosaccharides present in rtPA (see ref. 2 for details).

focused protein band appears to depend not only on the p*I* but also on the nature of the protein, its concentration and the amount of time it has been focused and possibly the viscosity of the band and the mobilization conditions, all of which affect the mobilization step. In short the absolute migration time of a focused band is quite variable. This variability in migration time makes correlation of p*I* *vs.* migration time very difficult to assess. However, the reproducibility of the IEF pattern of rtPA between runs was quite good, except that the migration times were shifted. So if one could correct for this variability (*e.g.* by use of a internal standard p*I* marker), then the "corrected" IEF pattern would be much more reproducible. The ideal situation would be to bracket the analyte sample between two internal standard p*I* markers, not unlike the use of p*I* markers in conventional IEF gels. This approach is being investigated currently.

When one overlays the IEF patterns of Type I and Type II rtPA over that of the mixture, one can see that the patterns overlap quite well but only after some shifting in migration times. That is, if the IEF pattern of Type II rtPA was shifted −0.86 min and added to the IEF pattern of Type I rtPA, the resultant pattern compares favorably with the IEF pattern of a mixture of Type I and Type II rtPA after it shifted 3.3 min. Fig. 5 shows the overlay of the time-shifted IEF patterns. While this is only a simulation exercise, it suggests that cIEF patterns may be compared from run to run if the time shift problem can be corrected for by the use of internal standards.

Fig. 6 is the IEF of a neuraminidase treated rtPA sample. The microheterogeneity is considerably reduced and the resulting peaks have migration times which are shorter. This observation is consistent with the fact that when all the sialic acid residues are removed (data not shown), the p*I* of the desialylated rtPA is increased. The simplification of the pattern indicates that the large cause of the microheterogeneity in the p*I*'s of the glycoforms of untreated rtPA are due to different levels of sialylation.

Fig. 7A and B are the capillary zone electropherograms of Type I and Type II rtPA, respectively. It can been seen that Type II rtPA dominates the front part of the

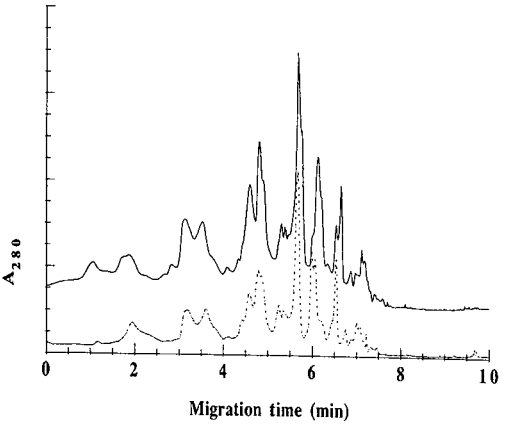

Fig. 5. Comparison of the IEF of a mixture of Type I and Type II rtPA (- - -) with the arithmetic sum (——) of the IEF patterns of Type I and Type III rtPA.

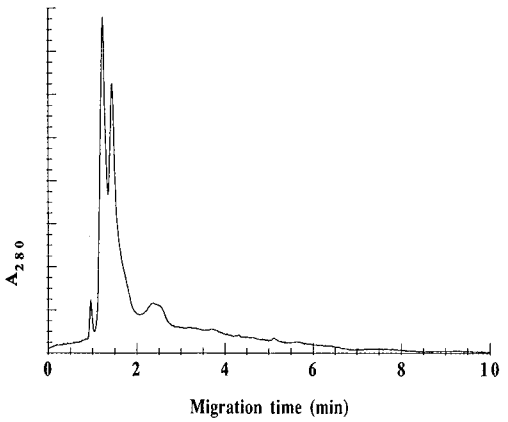

Fig. 6. IEF of a neuraminidase-treated rtPA sample. A Bio-Rad coated silica capillary (14 cm × 25 μm) was used, the focusing voltage was 12 kV and mobilization voltage was 8 kV, the ampholyte solution contained 2% ampholyte (pH 6–8), 2% CHAPS and 6 *M* urea,

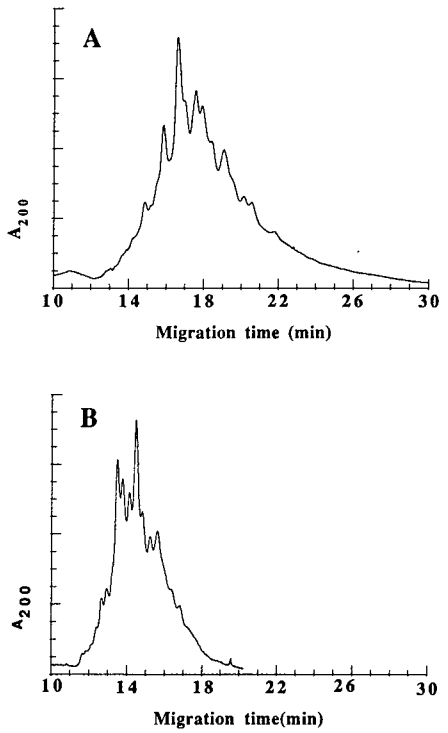

Fig. 7. CZE of (A) Type I rtPA and (B) Type II rtPA obtained at 200 nm. Samples were introduced electrophoretically at 8 kV for 8 s. The run voltage was set at 6 kV. The rtPA sample was the same as described above in the IEF section. The running buffer consisted of 0.1 *M* ammonium phophate pH 4.6 with 0.01% Triton X-100 (chemically reduced to minimize UV absorbance) and 0.2 *M* EACA.

rtPA profile and Type I dominates the back part of the rtPA profile. The resolution of the glycoforms was not was good as in the IEF mode, but still about 15 peaks could be recognized. It should be noted that the separation was done on a very short capillary (20 cm); a longer capillary (*e.g.* 50 cm) should give better separations. A publication [9] reported that an earlier attempt to separate the glycoforms was not successful. It was observed that rtPA solubility is too low in many common buffers and hence successful CZE could not be accomplished in them. The addition of 0.2 *M* EACA solubilizes rtPA and led to the success of the CZE experiment. It appears the choice of buffer components is crucial to the success of CZE of proteins.

Fig. 8 is the overlay of the CZE of rtPA sample with that of a desialylated rtPA sample. The CZE of the desialylated rtPA sample is much simpler than that of rtPA and the migration time is also much shortened. This is the expected result: the desialylated rtPA becomes more positively charged and hence has higher mobility. The loss of the sialic acid residues again reduces the charge heterogeneity and results in the simpler profile. The removal of sialic acid only reduces that charge heterogeneity but does not alter the other causes of carbohydrate heterogeneity. The appearance of two to three peaks in the desialylated rtPA coud possibly be attributed to the heterogeneity of molecular mass of these glycoforms resulting in differences in mobility. Fig. 9 is an overlay of the CZE of a mixture of rtPA and desialylated rtPA with the arithmetic sum of the CZE patterns of the two run separately. The fact that the two profiles are very similar indicates that CZE of proteins can be performed more reproducibly and data analysis using CZE is consequently much more straightforward.

CONCLUSIONS

This paper reports the successful fractionation of rtPA by capillary zone electrophoresis and cIEF. The results confirm the existence of different glycoforms and are consistent with the known carbohydrate structures of rtPA. A key to the success-

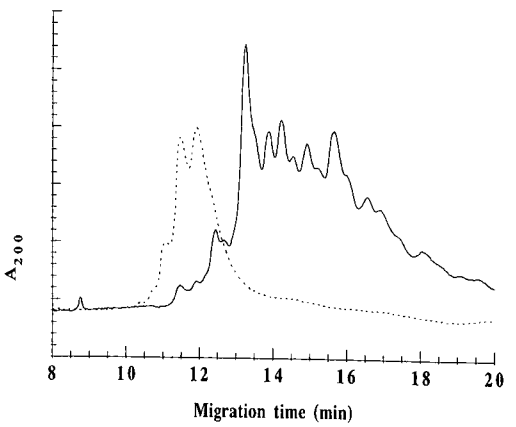

Fig. 8. Overlay of CZE patterns of rtPA (——) and desialylated rtPA (- - -) obtained at 200 nm. Samples were introduced electrophoretically at 8 kV for 8 sec. The run voltage was set at 6 kV. The rtPA samples were the same as described above in the IEF section. The running buffer consisted of 0.1 *M* ammonium phosphate pH 4.6 with 0.01% Triton X-100 (chemically reduced to minimize UV absorbance) and 0.2 *M* EACA.

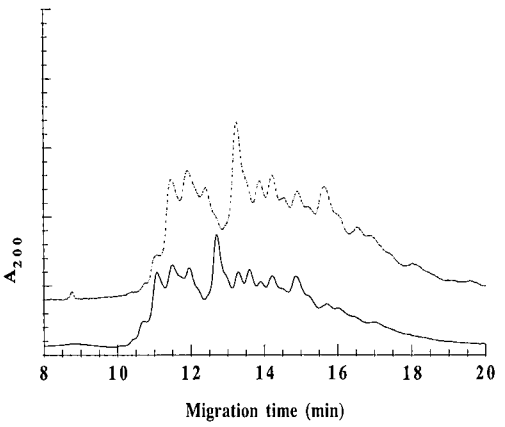

Fig. 9. Comparision of the CZE of a mixture of rtPA and desialyated rtPA (——) with the arithmetic sum of the CZE patterns of rtPA and desialylated rtPA (- - -).

ful separation of these glycoforms was to increase the solubility properties of rtPA in order to obtain high enough sample concentration for the electrophoretic sample loading method. rtPA solubility is too low in many common buffers and hence successful CZE could not be accomplished in them. The addition of 0.2 *M* EACA solubilizes rtPA and led to the success of the CZE experiment. After the optimum buffer was found, both techniques worked well as expected. In summary, we have investigated the glycoforms of rtPA using capillary zone electrophoresis and capillary IEF. The information obained provides a rapid method for evaluating the complexity of rtPA and at the same time validates the usefulness of these two techniques in protein characterization.

ACKNOWLEDGEMENTS

The author wishes to thank Dr. Andy Jones for his support, valuable discussions and for suggesting the use of EACA for the solubilization of rtPA; Ann Mac and Huong Doung for technical assistance, Jonathan Briggs for the rtPA samples; M. Zhu and Dr. M. Spellman for valuable discussions.

REFERENCES

1 J. C. Giddings, *Sep. Sci.*, 4 (1969) 181.
2 J. W. Jorgenson and K. D. Lukacs, *Science (Washington, DC)*, 222 (1983) 266.
3 T. E. Rademacher, R. B. Parekh, and R. A. Dwek, *Ann. Rev. Biochem.*, 57 (1988) 785.
4 M. W. Spellman, L. J. Basa, C. K. Leonard, J. A. Chakel and J. V. O'Connor, *J. Biol. Chem.*, 264 (1989) 14100.
5 R. Kornfeld, S. Kornfeld, *Ann. Rev. Biochem.*, 54 (1985), 631.
6 M. Einarsson, J. Brandt and L. Kaplan, *Bochim. Biophys. Acta*, 830 (1985) 1.
7 S. Hjertén, J. Liao and K. Yao, *J. Chromatogr.*, 387 (1987) 127.
8 M. Zhu, and S. Hjertén, *J. Chromatogr.*, 346 (1985) 265.
9 S. L. Wu, G. Teshima, J. Cacia and W. Hancock, *J. Chromatogr.*, 516 (1990), 115.

Journal of Chromatography, 559 (1991) 411–429
Elsevier Science Publishers B.V., Amsterdam

CHROM. 23 462

High-performance capillary electrophoresis of proteins from the fluid lining of the lungs of rats exposed to perfluoroisobutylene

L. R. GURLEY*, J. S. BUCHANAN, J. E. LONDON, D. M. STAVERT and B. E. LEHNERT
Los Alamos National Laboratory, Life Sciences Division, Mail Stop M880, Los Alamos, NM 87545 (USA)

ABSTRACT

Measurements of the biochemical constituents in the fluid lining of the lung can be used for diagnosing and assessing lung disorders. To facilitate such measurements, a high-performance capillary electrophoresis (HPCE) method has been developed by which the proteins in lung fluid can be analyzed. The lung fluid was obtained by a bronchoalveolar lavage procedure using 48 ml of physiological saline to wash out the lung fluid of rats. The proteins were precipitated from the fluid with 10 volumes of acetone and concentrated by dissolution in 2 ml of water containing 0.2% of trifluoroacetic acid. Aliquots of these samples (5 μl) were then injected into a Bio-Rad HPE-100 capillary electrophoresis instrument fitted with a 50 cm × 50 μm I.D. coated capillary filled with 0.1 *M* phosphate buffer (pH 2.5). With phosphate buffer in the outlet electrode chamber (cathode) and water in the inlet electrode chamber (anode), the proteins were loaded into the capillary electrophoretically for 10 s at 10 kV constant voltage. The inlet electrode chamber was then filled with phosphate buffer and HPCE was performed at 8 kV constant voltage. Six major protein fractions were resolved in 35 min, and were detected by UV absorption at 200 nm. The procedure was used to compare the lung fluid proteins of normal untreated rats with those of rats exposed by inhalation to perfluoroisobutylene (PFIB) at a concentration of 100 mg/m^3. It was found that PFIB induced pulmonary edema involving a translocation of blood compartment proteins into the lung's alveolar compartment. Comparison of the HPCE fractions with similar fractions obtained by high-performance liquid chromatography confirmed albumin, transferrin and IgG as three major proteins translocated into the alveolar space after PFIB exposure.

INTRODUCTION

Perfluoroisobutylene (PFIB) is a toxic compound that can be generated by pyrolysis of tetrafluoroethylene polymers, such as Teflon [1]. Brief inhalation exposure to low concentrations of PFIB can result in profound lung injury, incapacitation and death. Hence there is concern about the toxicity of smoke from such polymeric materials during their thermal decomposition [1]. The hallmark feature of such acute lung injury is a breach in the permeability characteristics of the lung's air–blood barrier, which is manifested by pulmonary edema [2–5]. However, as is the case with the toxic gas phosgene [6], there can be a latency period of up to several hours following exposure to PFIB that exists before the development of clinically significant

0021-9673/91/$03.50

lung injury [2]. Such latency periods offer a period of opportunity in which therapeutic intervention could be implemented to abate the otherwise ensuing life-threatening lung damage if only the nature of the injury was understood. Hence it is important to develop new methods to study the mechanisms of action of PFIB [7,8]. With this in mind, we have recently developed a method for the analysis of lung fluid proteins by high-performance capillary electrophoresis (HPCE). This paper describes the development of the separation of lung fluid proteins by zone electrophoresis in free solution using low-pH buffers in coated silica capillaries.

EXPERIMENTAL

Animal exposure to PFIB

Adult, male Fischer 344 rats (Harlan Sprague Dawley, Indianapolis, IN, USA) were exposed to an atmosphere containing 100 mg/m^3 of PFIB for 10 min. The apparatus and operation of the exposure system are described in detail elsewhere [9]. Exposure was accomplished by withdrawing 1 ml of PFIB (Fluoro Corp., Newport, TN, USA) from its storage cylinder with a gas-tight syringe. The syringe was placed in a syringe pump and attached to a dilution air manifold. HEPA-filtered air was metered into a glove-box at 2–3 l/min and the exposure atmosphere generation began with the starting of the syringe pump, which was capable of delivering up to 0.024 ml/min of neat agent into the airstream. Downstream, a series of baffles assured complete gas mixing and an automatic sampling device withdrew atmosphere samples every 30 s for measurements of PFIB concentration using a dual-column gas chromatograph fitted with an electron-capture detector (Model 140B, Valco Instruments) sensitive to 1 ppb of PFIB. The rats were placed in Teflon animal exposure tubes, passed into the glove-box through an airlock and the atmosphere was directed to the holding tubes for exposure for 10 min. After exposure, fresh air was directed to the animals until gas chromatographic sampling indicated the absence of PFIB. The animals were then returned to their cages and provided food and water *ad libitum* for 24 h before being killed. Control animals were subjected to air only by the same protocol.

Lung fluid sampling

The extracellular lining fluid was washed from the bronchial tree and alveoli of the lungs of rats using a bronchoalveolar lavage procedure [10]. Twenty-four hours after exposure, rats were killed following intraperitoneal injections of 50 mg of pentobarbital sodium. Prior to total apnea, the rats were exsanguinated via carotid artery transection, and the trachea was subsequently cannulated with a blunt, 18-gauge needle secured with ligature. The lungs and trachea were excised from the thoracic cavity *en bloc*, and the heart and esophagus were removed.

The lavage protocol consisted of six sequential lung wash cycles with 8 ml of 0.15 *M* sodium chloride solution per wash at room temperature. This saline solution was prepared with chromatography-grade water. The lavage was performed by gently massaging the lungs during infusion and aspiration of the saline during each cycle [11]. Retrieved lavage fluid from each lung was pooled in a centrifuge tube maintained on ice. Typically, $\geqslant$97% of the instilled fluid volume was recovered from each lung [12]. The lavage fluid was centrifuged at 300 *g* for 10 min at 4°C to sediment the lung

free cells. The supernatant fluid was removed by aspiration, placed in another centrifuge tube and centrifuged at 2300 *g* for 10 min to sediment any remaining acellular solid material. The supernatant fluid obtained was designated the bronchoalveolar lavage fluid (BALF). This BALF was frozen in glass tubes and stored at − 70°C until used for chromatography and HPCE studies.

HPLC of lung fluid samples

Reversed-phase high-performance liquid chromatography (HPLC) was performed on BALF preparations as described in detail elsewhere [13]. Briefly, a 12-ml sample of BALF from control rats or a 1-ml sample from PFIB-exposed rats was made 0.2% in trifluoroacetic acid (TFA) and 6 *M* in guanidine hydrochloride by adding these reagents to the lavage fluid. The addition of these solubilization reagents was necessary to clarify the cloudiness of the samples caused by the large amount of proteinaceous material in the fluid following acute lung injury [14]. These samples were then diluted with an equal volume of phosphate-buffered saline [13] containing 0.2% TFA and pumped at a flow-rate of 1 ml/min through the HPLC column followed by 2 ml of water containig 0.2% TFA to rinse the sample from the pumps and lines.

The HPLC system consisted of a μBondapak Radial-PAK C_{18} flexible-walled cartridge (10 cm × 8 mm I.D.) contained in a Z-Module radial compression device (Waters Assoc., Milford, MA, USA) [15] which had been equilibrated with water containing 0.2% of TFA. The BALF constituents were loaded on the top of the column by adsorption to the hydrophobic packing and the phosphate, salts and guanidine were passed through to waste. Chromatography of the BALF constituents was accomplished by a series of acetonitrile gradients and isocratic steps that progressed from water–0.2% TFA to 65% acetonitrile–0.2% TFA followed by further isocratic elution with methanol [13]. The elution solvents were pumped at 1 ml/min using a Waters Assoc. Model 6000A solvent-delivery system equipped with three pumps. Control of the gradients was achieved by computer [13], and the eluted BALF constituents were detected by UV absorbance at 206 nm using a Waters Assoc. Model 490 flow spectrophotometer attached to a strip-chart recorder.

Preparation of BALF proteins of HPCE

Our experience has been that a sample containing a complex mixture of proteins needs to have a total protein concentration of at least 0.1 μg/μl to achieve good UV detection of the individual components separated by HPCE [16]. The BALF protein concentration was too dilute for analysis by HPCE so it was necessary to concentrate the BALF proteins. Initial attempts to concentrate the sample by membrane filtration methods resulted in component loss (probably owing to membrane adsorption) and protein precipitation. We therefore attempted to use precipitation methods to remove the proteins from the BALF so they could be redissolved in a small volume of electrophoresis buffer at higher concentrations. During this early stage of our investigation we were using phosphate-buffered saline as the lavage fluid, which was customary [13,14]. This caused a serious problem when we used acetone to precipitate the proteins because the phosphate salts were also precipitated. As sodium chloride was not precipitated in acetone–water (90:10), we performed the lavage with unbuffered 0.15 *M* sodium chloride solution. With this BALF we could precipitate

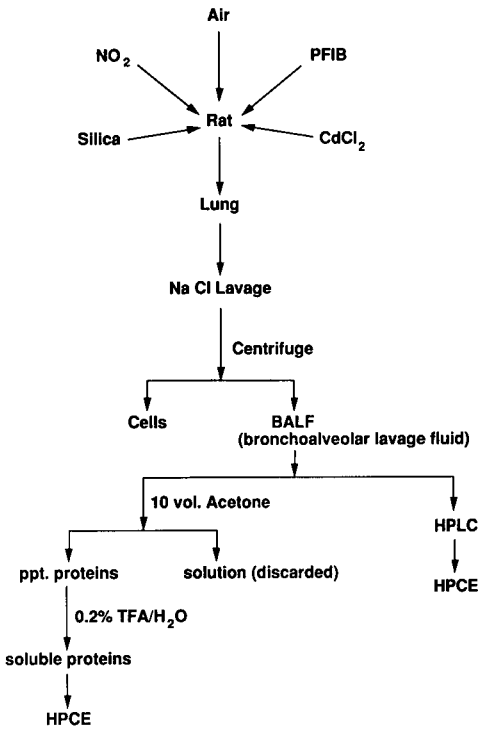

Fig. 1. Diagram of the protocol for the analysis of lung fluid proteins by HPCE and HPLC.

the proteins by adding acetone without precipitating the salt. HPLC analysis of saline lavage samples indicated that there were no differences between this lavage fluid and that obtained with phosphate-buffered saline.

The following protocol was therefore used to prepare BALF proteins for HPCE (Fig. 1). Saline BALF was obtained as described above and 10 volumes of acetone were added to 20 ml of the BALF. The proteins were precipitated overnight at 4°C. The precipitate was recovered by centrifugation at 1300 *g* for 10 min in a International Clinical Centrifuge. The supernatant acetone was discarded and the precipitate was washed once with 10 ml of acetone. The precipitate was again recovered by centrifugation. The acetone wash was discarded, the protein pellet was drained for 10 min and the proteins were dissolved in 1 ml of 0.2% TFA in water and frozen until used for HPCE. TFA is a good solubilizing agent for the proteins and it does not interfere with the electrophoresis at low pH. Because the salts in the sample have been removed, the electrophoresis sample has a low conductivity, which is advantageous for loading the sample into the capillary by electroinjection.

HPCE of BALF proteins

HPCE was performed using a Model HPE-100 high-performance electrophoresis system (Bio-Rad Labs., Richmond, CA, USA) fitted with a 50 cm × 50 μm I.D. silica capillary tube whose internal surface was chemically modified to produce a patented hydrophilic coating. Coatings of this nature have been reported by several

laboratories to eliminate electroendoosmosis and protein adsorption [17–19]. The cathode, anode and capillary buffers were 0.1 *M* sodium phosphate (pH 2.5) (Bio-Rad Labs.) unless specified otherwise. Detection of the separated proteins traversing the capillary was accomplished by in-tube monitoring of the peptide bond absorbance at 200 nm with spectrophotometer sensitivity settings ranging from 0.005 to 0.050 a.u.f.s.

To evaluate the performance of this instrument, a standard mixture of nine polypeptides was subjected to electrophoresis in a 20 cm × 25 μm I.D. coated capillary. This mixture contained bradykinin, angiotensin II, α-MSH, TRH, LHRH, [2–5] leucine enkephalin, bombesin, methionine enkephalin and oxytocin (Bio-Rad Labs.). When this standard mixture was electroinjected for 8 s at 8 kV and subjected to electrophoresis at 8 kV, nine completely resolved peaks were obtained in the order listed above.

To perform HPCE on BALF proteins, the proteins that were precipitated from 20 ml of BALF were dissolved in 1 ml water containing 0.2% of TFA and loaded into the capillaries by electroinjection [20]. To accomplish this, the cathode chamber and the 50 cm × 50 μm I.D. coated capillary were filled with 0.1 *M* phosphate buffer (pH 2.5) and the anode chamber was filled with water. Then 5 μl of sample were injected into the loading chamber at the anode end between the capillary and the water. Power was applied to the capillary for 10 s at 10 kV (constant voltage) and *ca.* 28 μA. This activity carried the cations (including the positively charged protonated proteins) into the capillary. Under these low ionic strength sample conditions the proteins were concentrated and stacked in the capillary during this loading step [21]. The excess of sample in the loading chamber and the water in the anode chamber were then replaced with 0.1 *M* phosphate buffer (pH 2.5) and electrophoresis was performed by applying power to the capillary at 8 kV (constant voltage) and ca. 23 μA. Electrophoresis normally took 35 min under these conditions. HPCE was also performed on 1 mg/ml standard solutions of rat albumin (Sigma, St. Louis, MO, USA), rat transferrin (Cappel, Westchester, PA, USA) and rat immunoglobulin G (IgG) (Sigma) dissolved in water containing 0.2% of TFA.

RESULTS

Performance of polypeptides and proteins in the HPE-100 system

The performance of the HPE-100 instrument was evaluated by subjecting a mixture of nine polypeptide standards to zone electrophoresis in a 20 cm × 25 μm I.D. coated capillary using 0.1 *M* phosphate buffer at pH 2.5. Repetitive electrophoresis of this standard produced fractions whose peak heights varied by only 3.0% (relative standard deviation). We have been unable to obtain such high quantitative precision with proteins, however. Our experience with either plasma proteins (in this paper) or with histone proteins [16] has shown that proteins in general produce much broader peaks than do small polypeptides and that electroinjection produces more variation in the quantity of loaded proteins than it does in the quantity of loaded quantity polypeptides.

Repetitive electrophoresis revealed a variability of 7.2% in the mobility of the nine polypeptide standards. This variability was also experienced with proteins, which made it impossible to identify unequivocally protein fractions by comparing

their mobilities with those of external standards. Therefore, to identify the peaks in a complex protein mixture, it was necessary to "spike" samples with an internal standard protein to facilitate assignments of known proteins to specific peaks in an electropherogram.

From previous experiments we expected BALF from PFIB-treated rats to have >10-fold increases in plasma proteins [8]. We therefore examined the effect that protein sample concentration might have on a protein's mobility. From our experience with histone proteins [16] we had determined that proteins could not be resolved in the small 20 cm × 25 μm I.D. capillaries used for polypeptides. Therefore, this experiment was performed in a 50 cm × 50 μm I.D. coated capillary in which transferrin was loaded for 10 s at 10 kV and then subjected to electrophoresis at 12 kV. It was found that the mobility of transferrin was reduced by only 1% by a fivefold increase in load, whereas it was reduced by 15% by a tenfold increase in load. Hence there appears to be a threshold in the 0.5–1.0 μg/μl range above which there is a significant decrease in protein mobility.

These experiments served to define the limits of performance for the electrophoresis of proteins in the HPE-100 system. Most important, they illustrate the great differences in performance experienced between the electrophoresis of polypeptides and that of proteins in this HPCE system.

HPCE of BALF proteins under acid conditions

Initial experiments on the HPCE of BALF proteins indicated that electrophoresis in 25-μm capillaries resulted in frequent capillary plugging. As a result, we chose to conduct our studies using the 50 cm × 50 μm I.D. coated capillary in which we could conduct 20–50 runs before noticing any degradation of the electropherograms. These studies also indicated that electrophoresis at 12 kV, the operational upper limit for the HPE-100, produced frequent sparking which resulted in degradation of the electropherogram. Consequently, we chose to conduct our studies by loading the BALF proteins at 10 kV for 10 s and then performing electrophoresis at 8 kV.

To determine the optimum pH to resolve the BALF proteins under acid conditions, samples were subjected to electrophoresis in various 0.1 *M* phosphate buffers having a pH range of 2.5–5.0 (Fig. 2). We found that the proteins ran the fastest at pH 2.5 and also achieved the best resolution at this pH (Fig. 2A). Higher pH runs produced peak tailing (Fig. 2B) and at pH ⩾3.75 the fractions moved so slowly that resolution was totally lost due to diffusion (Fig. 2C–F). Therefore, pH 2.5 was found to be the optimum condition for the electrophoresis of this set of proteins under acid conditions in phosphate buffer.

HPCE of the major blood compartment proteins

Albumin, transferrin and immunoglobulin G (IgG) are the major plasma proteins expected to be found in BALF proteins [22]. These proteins were subjected to HPCE (Fig. 3a–c) and the electropherogram of their mixture (Fig. 3d) was compared with that of BALF proteins (Fig. 3e). The order of mobility of the plasma proteins (from fastest to slowest) was albumin, transferrin and IgG. Albumin ran as a single peak while transferrin contained two components. IgG ran as a slow-moving broad fraction. Owing to the 7% variability in mobilities in this HPCE system (discussed above), it was impossible to determine unequivocally which fractions in the BALF

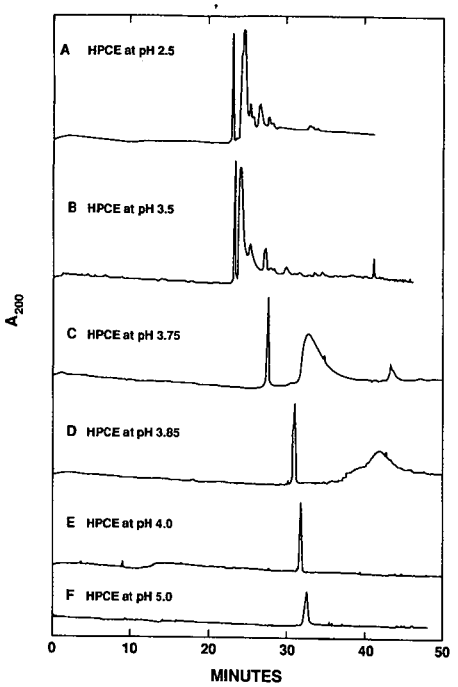

Fig. 2. HPCE of BALF proteins under acid conditions. Rat BALF proteins dissolved in 0.2% TFA were loaded by electroinjection for 10 s at 10 kV into a 50 cm × 50 μm I.D. coated capillary fitted in a Bio-Rad Labs. HPE-100 instrument. Electrophoresis was then performed at 8 kV (constant voltage) in 0.1 *M* phosphate buffer of pH 2.5–5.0.

electropherogram were these plasma proteins by comparison with the external standard runs.

Identification of blood compartment proteins in BALF protein samples

To identify the blood compartment proteins in the BALF protein electropherogram, albumin, transferrin or IgG was individually added to different samples of BALF proteins. These "spiked" samples were then subjected to HPCE. Each plasma protein in the electropherogram of the whole BALF protein sample was located by the increase in the fraction's peak height (Fig. 4b–d). The location of these three plasma proteins was identified in the BALF protein electropherogram (Fig. 4a). The second and largest BALF peak was found to contain albumin. The first transferrin peak was found to be a trailing shoulder on the third BALF peak and the second transferrin peak was found to be in the fourth BALF peak. IgG was not detectable in the BALF proteins (Fig. 4a). However, the area of the electropherogram trailing the fifth BALF protein peak (>26 min) is usually above the baseline. Because of the broad nature of the IgG peak (Fig. 4d) a small amount of IgG might be difficult to detect.

HPLC of BALF proteins

Our laboratory has previously developed an HPLC method for the analysis of

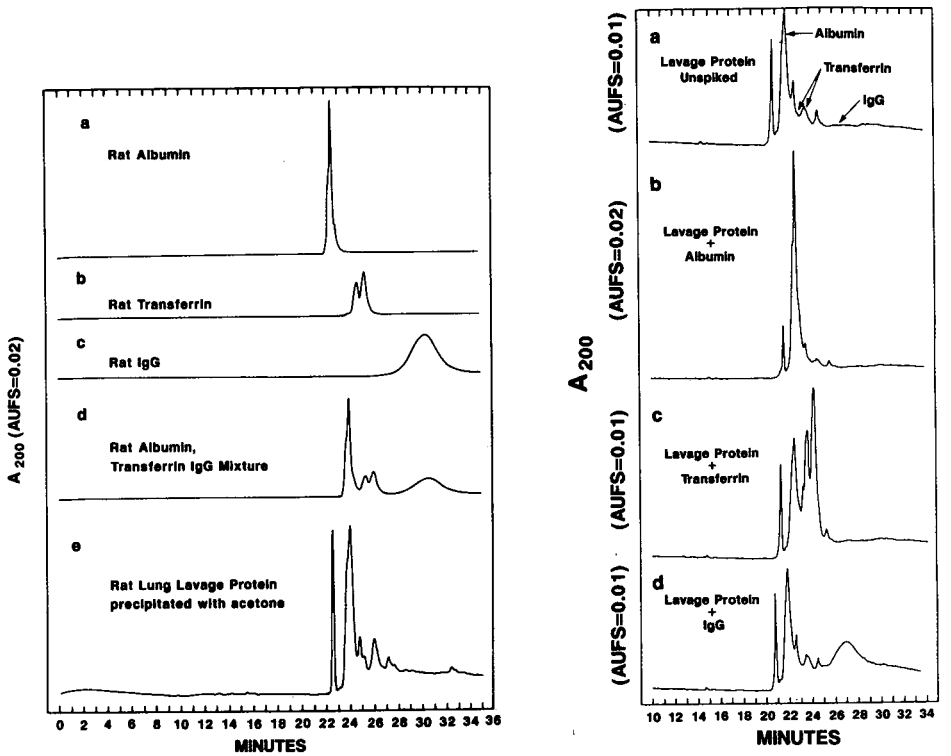

Fig. 3. HPCE of major blood compartment proteins. Rat (a) albumin, (b) transferrin and (c) IgG dissolved in 0.2% TFA at 1 mg/ml were subjected to HPCE at pH 2.5 as described in Fig. 2. (d) A mixture of these blood proteins was compared with (e) BALF proteins.

Fig. 4. Identification of blood compartment proteins in the HPCE electropherogram of BALF proteins. (a) BALF proteins were subjected to HPCE at pH 2.5 as described in Fig. 2. (b) Albumin, (c) transferrin and (d) IgG were individually added to different samples of BALF proteins. The fractions in the BALF electropherogram that contained these proteins were identified by the increase in the peak height of the fraction.

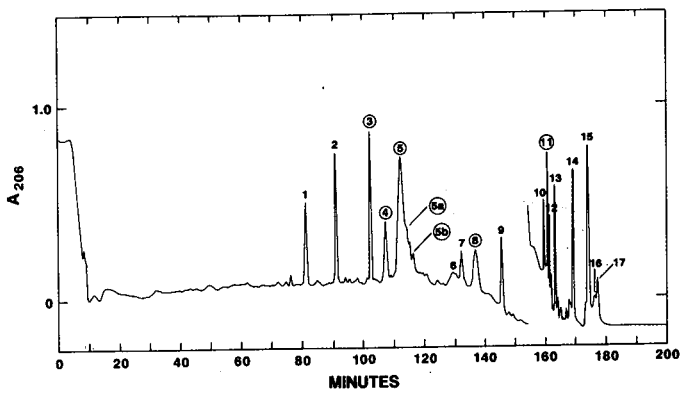

Fig. 5. HPLC of BALF proteins. A 12-ml sample of BALF was loaded directly onto a μBondapak Radial-PAK C_{18} reversed-phase column. Fractions were eluted at 1 ml/min with a series of acetonitrile gradients and isocratic steps that progressed from water–0.2% TFA to 65% acetonitrile–0.2% TFA in 155 min. Following this, additional fractions were eluted with methanol (the break in the baseline at 155 min is the result in a baseline adjustment due to the change in solvents). Fractions of 1 ml of effluent were collected and dried for HPCE analysis. Fractions circled were detected by HPCE.

BALF proteins [13]. Nine of the HPLC fractions were found to contain protein [13]. To determine the identity of the HPLC fractions in the HPCE electropherogram, the HPLC fractions were prepared directly from BALF. This was accomplished by subjecting 12 ml of BALF to reversed-phase HPLC (Fig. 5). Fractions of 1 ml of the column effluent were collected for 200 min and evaporated to dryness. Each of these samples was then dissolved in 30 μl of water containing 0.2% of TFA and used for HPCE analysis. In this chromatogram, transferrin has been shown to elute in peak 4, albumin in peak 5 and IgG among the cluster of peaks 6–9.

HPCE of the HPLC fractions of BALF proteins

Each of the seventeen HPLC fractions marked in Fig. 5 were subjected to HPCE (Fig. 6). HPLC fractions 3, 4, 5, 5a, 5b, 8 and 11 produced significant HPCE electropherograms. HPLC peak 3 was found to produce a single peak by HPCE, indicating that it is probably homogeneous as it elutes from the HPLC column. HPLC peak 4 (the transferrin peak) was found to be a single peak in the BALF. Commercial preparations of transferrin prepared from plasma contained two HPCE peaks (Fig. 3b). HPLC peak 4 was also found to be contaminated with some albumin migrating ahead of the transferrin.

HPLC peak 5 (the albumin peak) was found to contain two HPCE fractions. Commercial preparations of albumin prepared from serum contain one HPCE peak

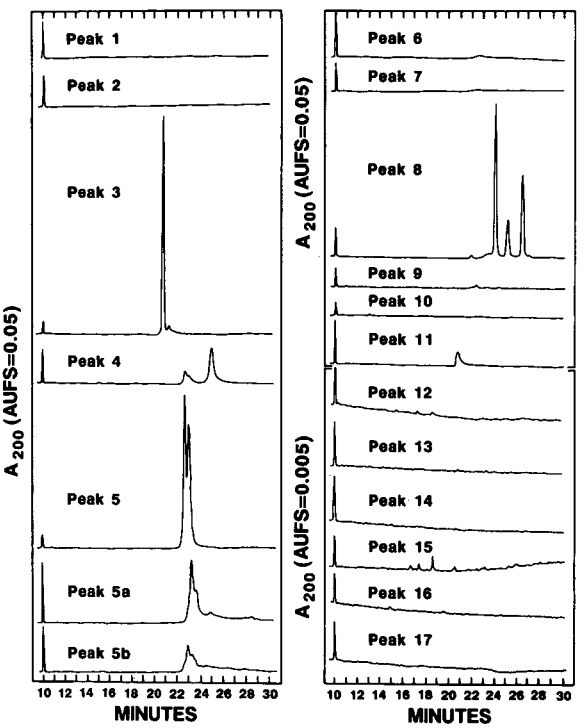

Fig. 6. HPCE of HPLC fractions of BALF proteins. The HPLC fractions (numbered 1–17 in Fig. 5) were subjected to HPCE at pH 2.5 as described in Fig. 2. The peak at 10 min in these chromatograms is produced by guanidine eluted from the HPLC column.

(Fig. 3a). Thus, either BALF modifies the albumin in some way to produce an albumin component with an altered electrophoretic mobility, or the BALF contains another major component (not yet identified) that elutes with albumin from the HPLC column. The trailing shoulders of HPLC peak 5 (peaks 5a and 5b in Fig. 5) appeared also to have slower moving HPCE components. For example, HPLC peak 5a appears to contain the second HPCE albumin peak plus a slower moving shoulder and HPLC peak 5b appears to contain the second HPCE albumin peak plus two slower moving shoulders. Hence the albumin-containing HPLC peak 5 probably contains at least four different components.

Among the cluster of peaks eluting from the HPLC column at high acetonitrile concentrations (peaks 6–9 in Fig. 5), only HPLC peak 8 produced an HPCE electropherogram. This HPLC fraction produced three well resolved HPCE fractions that eluted between 24 and 27 min. We know from previous experience that IgG and IgM will elute from the HPLC column in this part of the chromatogram [13–15]. However, the HPCE components of HPLC peak 8 (Fig. 6) do not resemble the HPCE components of IgG (Fig. 3c) in any way. The HPCE components are well defined and move significantly faster than the poorly defined, slower moving IgG.

Among the HPLC fractions eluted with methanol (peaks 10–17 in Fig. 5) only peak 11 produced a fraction detectable by HPCE (Fig. 6). This was expected as protein was found previously in this cluster of HPLC fractions (peaks 10–13 in Fig. 5) [13]. However, it was surprising that no HPCE fractions were found in the last cluster of HPLC fractions (peaks 15–17 in Fig. 5). These HPLC fractions have been shown to contain significant amounts of both protein and phospholipid [13]. Consideration should therefore be given to the possibility that phospholipids might interfere with the HPCE of those proteins, perhaps by hydrophobic interactions with the capillary wall.

Identification of HPLC fractions in the HPCE electropherogram of BALF proteins

Each HPLC fraction that was detected by HPCE is circled in Fig. 5. To determine where those HPLC fractions occur in the HPCE electropherogram of whole BALF proteins, samples of BALF proteins were "spiked" with HPLC fractions 3, 4, 5, 8 and 11 and then subjected to HPCE. The fractions in the BALF electropherogram that contained the HPLC components were identified by the increase in the HPCE peaks (Fig. 7). The first HPCE peak was identified as HPLC peak 3 (Fig. 7b). The fourth HPCE peak was identified as HPLC peak 4 (Fig. 7c). As the mobility of HPCE peak 4 and the elution of HPLC peak 4 correspond to those of transferrin, it is reasonable to identify those fractions as containing transferrin.

The second, large HPCE peak was identified as HPLC peak 5 (Fig. 7d). The trailing shoulder of HPLC peaks 5a and 5b were also identified in the second HPCE peak (Fig. 7e and f). As the mobility of HPCE peak 2 and the elution of HPLC peak 5 correspond to those of albumin, it is reasonable to identify these fractions as containing albumin.

The three HPCE fractions found in HPLC peak 8 were identified in the BALF protein electropherogram as the third, fourth and fifth HPCE peaks (Fig. 7g). This means that the fourth HPCE peak contains not only transferrin, but also some other component. The HPLC peak 11 was found to have an electrophoretic mobility faster than the first HPCE peak (Fig. 7h). As this fraction is not normally seen in the HPCE

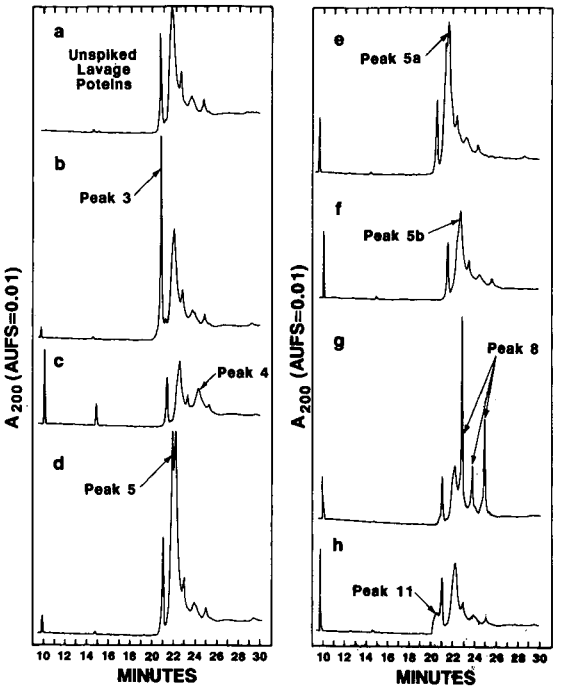

Fig. 7. Identification of HPLC fractions in the HPCE electropherograms of BALF proteins. Each HPLC fraction circled in Fig. 5 was detected by HPCE in Fig. 6. These seven HPLC fractions (peaks 3, 4, 5, 5a, 5b, 8 and 11) were individually added to separate samples of BALF proteins and subjected to HPCE. The fractions in the BALF electropherogram that contained the HPLC components were identified by the increase in peak height in the HPCE fraction. The peak at 10 min in these chromatograms is produced by guanidine eluted from the HPLC column.

of BALF proteins (Fig. 7a), this component is either present at concentrations too low for detection in the HPLC system or it is not recovered by acetone precipitation during the preparation of BALF proteins for HPCE.

Guanidine hydrochloride in HPLC fractions

During the course of these experiments is was observed that all HPCE electropherograms of samples prepared by HPLC contained a sharp peak at 10 min (Figs. 6 and 7). As guanidine hydrochloride was added to BALF as a solubilizing agent before performing HPLC on these samples, we subjected a guanidine hydrochloride standard to HPCE to determine its electrophoretic mobility in our system. It was found to migrate at the position of the 10-min peaks seen in Figs. 6 and 7 and had a high sensitivity for detection at 200 nm. Its presence as a contaminant from the HPLC system was surprising as it is highly charged under the acid conditions of HPLC (pH 2) and was expected to pass through the hydrophobic C_{18} column in the void volume.

Another surprising feature was that the guanidine was present in all fractions regardless of their position in the HPLC chromatogram (Fig. 6). Hence it was necessary to determine whether the guanidine was adsorbed to the proteins being eluted from the column or whether it was adsorbed directly to the column itself and bled from the column throughout the entire elution gradient. To do this, a new C_{18} col-

umn that had never been exposed to proteins was injected with sample solvent containing guanidine and eluted with the acetonitrile gradient containing TFA. Column effluent taken at 115 min (the time albumin normally elutes) was found to contain the 10-min guanidine peak, thus demonstrating that the guanidine was adsorbed directly to the HPLC column. Purging the C_{18} column with 100% acetonitrile removed all guanidine from the column (data not shown) and also removed any TFA from the column [13].

This suggests that the adsorption of guanidine to the C_{18} packing may be facilitated by ion pairing between TFA and guanidine, which formed an uncharged more hydrophobic species capable of interacting with the C_{18} column. Equilibrium of guanidine between the TFA on the column and that in the solvent might account for the constant bleeding of guanidine into the eluting solvents and the inability to flush out the guanidine before the TFA is removed from the system at the end of the HPLC trace.

HPCE of BALF proteins from PFIB-treated rats

Having characterized the HPCE profile of BALF proteins from control (unexposed) rats, HPCE was performed on the BALF proteins of rats exposed to PFIB (Fig. 8). Because of the acute edema in the lungs 24 h after PFIB treatment, we expected to find a great increase in plasma proteins in the PFIB samples [8]. Thus the

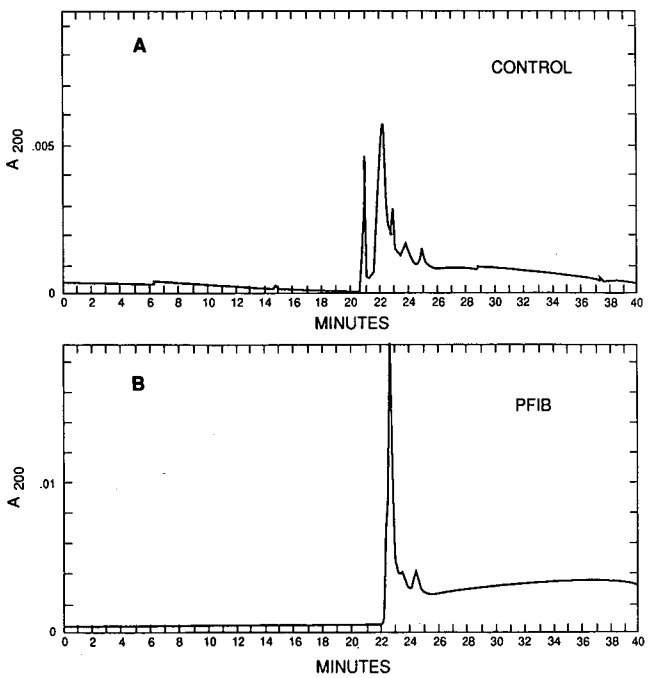

Fig. 8. HPCE of BALF proteins from control and PFIB-treated rats. Proteins were precipitated with acetone from the BALF of control (air-exposed) and PFIB-exposed rats. The amount of BALF used to prepare the protein sample from the PFIB-exposed rat was one tenth of that used for the preparation of the control sample. (A) HPCE of BALF proteins from control rats; (B) HPCE of BALF proteins from PFIB-treated rats.

PFIB proteins subjected to HPCE (Fig. 8B) amounted to the protein taken from one tenth the amount of BALF which was used for the HPCE of control proteins (Fig. 8A). This was necessary to keep the protein concentration in the PFIB sample within the concentration range of the analytical instrument. Examination of the electropherogram of the PFIB sample revealed that the first HPCE peak was missing while the second HPCE peak (albumin) was greatly increased. The increase in peak height was four times that of the control. Since one tenth the amount of BALF was used for the PFIB sample, this increase amounts to a *ca.* 40-fold increase in albumin. There was also an increase in the peak height of the PFIB transferrin peak (fourth peak at 23.5 min) to three times that of control. This indicated that transferrin was increased roughly 30-fold. A similar increase was observed for the fifth peak at 24.5–25 min. Following these peaks there was a high background in the electropherogram of the PFIB sample in the region from 26 to 30 min where one would expect to find IgG.

From this HPCE profile it is concluded that the first HPCE peak is not increased by PFIB treatment. It may either be lost from detection by the reduction in the PFIB sample size or it may actually decrease owing to PFIB treatment. The great increase in plasma proteins in the PFIB sample detected by HPCE confirmed similar increases observed in these proteins in PFIB samples analyzed by HPLC in our preliminary studies [8].

HPCE analysis of HPLC fractions of BALF proteins from PFIB-treated rats

Because of the profound changes in the HPCE profile of the BALF proteins from PFIB-treated rats observed in Fig. 8, a more detailed analysis was performed by comparing the HPCE analysis of individual HPLC fractions obtained from the BALF of treated and untreated animals. To do this, 12 ml of BALF from a control rat and 1 ml of BALF from a PFIB-treated rat were subjected to HPLC fractionation (Fig. 9A and E and Fig. 10A and G). The numbered fractions in these chromatograms were collected and subjected to HPCE (Fig. 9B–D and F–J and Fig. 10B–F and H–L).

The HPLC profile (Fig. 9E) confirmed the conclusion drawn from the HPCE profile (Fig. 8B) that the HPLC peak 3 did not increase after PFIB treatment. In contrast, there was a very large increase in the amounts of HPLC peaks 4 (transferrin) and 5 (albumin) and the peak cluster 6–10 that followed. In addition, two new fractions, A and B, were observed to appear in the HPLC profile after PFIB treatment. We have observed the appearance of these two new peaks during other cases of pulmonary edema caused by agents such as cadmium and nitrogen dioxide [14].

We were unable to detect the new A and B fractions by HPCE (Fig. 9F and G). However, small amounts of contaminating transferrin (HPLC peak 4) and albumin (HPLC peak 5) were observed in the A and B samples. HPLC peak 3, which migrates at 20 min by HPCE (Fig. 9B), was undetectable after PFIB treatment (Fig. 9H). This result was the same as that observed when performing HPCE on acetone-precipitated proteins (Fig. 8B). We conclude that this fraction is decreased by PFIB treatment because, if it remained the same as the control, we would expect to see a small HPCE peak at 20 min in Fig. 9H. This fraction (HPLC peak 3) was contaminated with transferrin and albumin (Fig. 9H).

Transferrin (HPCE peak 4) was greatly increased by PFIB treatment (Fig. 9E). HPCE analysis of this HPLC fraction revealed that, in addition to transferrin, this

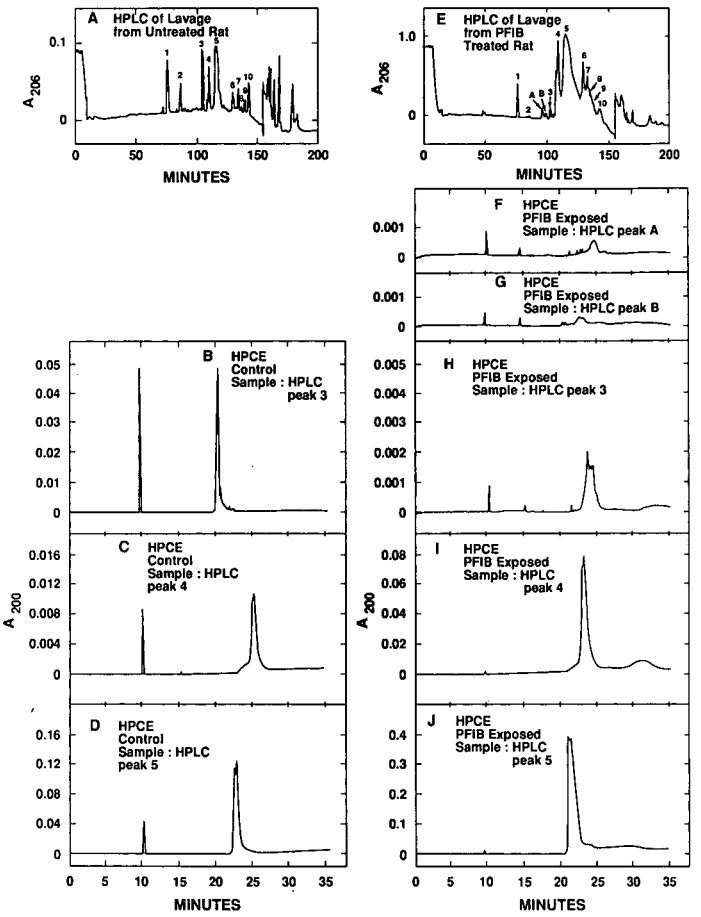

Fig. 9. HPCE of HPLC fractions of BALF taken from unexposed rats and from rats exposed to PFIB. BALF from unexposed and PFIB-exposed rats were subjected to HPLC (A and E, respectively). HPLC peaks 3, 4 and 5 from untreated rats were subjected to HPCE (B, C and D, respectively). HPLC peaks A, B, 3, 4 and 5 from PFIB-treated rats were subjected to HPCE (F, G, H, I and J, respectively).

HPLC fraction contained an HPCE fraction at 30 min that resembled IgG (Fig. 9I). This was surprising as IgG is normally eluted in the HPLC peak cluster 6–10 [13–15]. Albumin (HPLC peak 5) was also greatly increased by PFIB treatment (Fig. 9E). HPCE analysis of this HPLC fraction showed no significant amount of IgG-like material in this fraction (Fig. 9J).

PFIB treatment increased the amount of material in the HPLC peak cluster 6–10 (Fig. 10G). HPCE analysis of these peaks indicated that all these HPLC peaks from PFIB-treated animals were contaminated with albumin and perhaps transferrin (Fig. 10H–L). Hence the HPLC peaks 6–10 are riding on top of the tailing shoulder of the massive albumin peak (Fig. 10G). Even though most of these HPLC peaks are undetectable by HPCE (Fig. 6 and Fig. 10B–F), the large increase in the peak heights of these fractions in Fig. 10G suggests that these fractions are probably increased by PFIB treatment (Fig. 10G). No IgG-like peaks were observed in the HPCE analysis of this peak cluster (Fig. 10H–L).

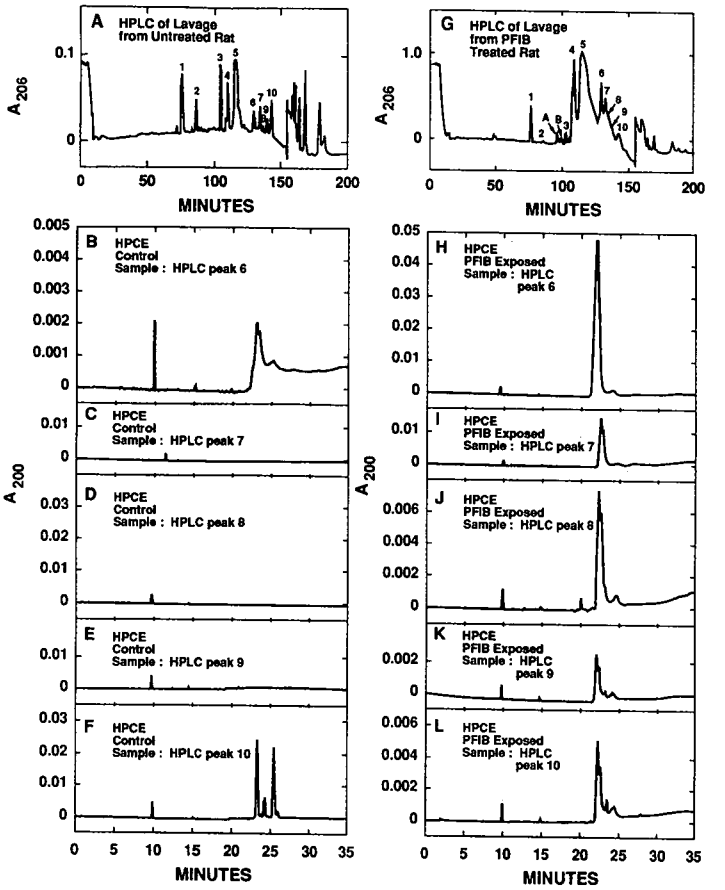

Fig. 10. HPCE of HPLC fractions of BALF taken from unexposed rats and from rats exposed to PFIB (this is a continuation of Fig. 9). BALF from unexposed and PFIB-exposed rats were subjected to HPLC (A and G, respectively). HPLC peaks 6, 7, 8, 9 and 10 from untreated rats were subjected to HPCE (B, C, D, E and F, respectively). HPLC peaks 6, 7, 8, 9 and 10 from PFIB-treated rats were subjected to HPCE (H, I, J, K and L, respectively).

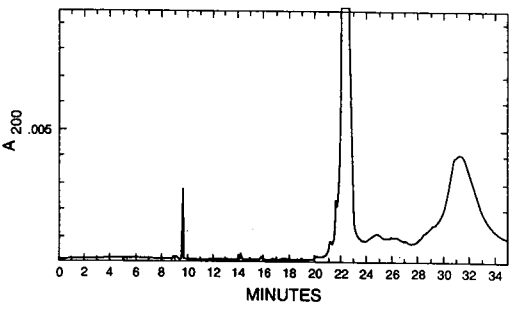

Fig. 11. HPCE of the HPLC transferrin peak from a PFIB-exposed rat. The HPLC transferrin fraction from a PFIB-exposed rat (such as peak 4 in Fig. 9E) was collected and subjected to HPCE. Guanidine eluted at 9.6 min, transferrin at 22.3 min and the IgG-like protein at 31.2 min.

To confirm that an IgG-like substance was induced in the transferrin HPLC peak by PFIB, the BALF of another PFIB-exposed rat was subjected to HPLC and its transferrin peak was subjected to HPCE (Fig. 11). Again the IgG-like peak was observed late in the electropherogram after the transferrin peak. Thus, HPCE provides the only method for detecting the appearance of this IgG-like substance during lung injury.

DISCUSSION

In this paper we have described the development of an HPCE system for the analysis of BALF proteins, identified the major blood compartment proteins in the electropherogram, characterized the HPCE fractions with respect to the BALF proteins fractionated by HPLC and demonstrated the usefulness of HPCE in analyzing BALF protein changes induced by a hazardous toxic gas such as PFIB. The most effective application of HPCE was found to be its use as a second-dimensional analysis system following a first-dimensional fractionation of BALF proteins by HPLC. An excellent example of this application was the discovery of an IgG-like protein hidden in the HPLC transferrin fraction of PFIB-treated rats. The absence of this component in controls (untreated rats) indicates that PFIB has mediated a major breach in the air–blood barrier of the lung allowing the escape of large proteins into the alveolar space.

Another example of the usefulness of HPCE in the second dimension was the discovery that a single peak which was eluted at high acetonitrile concentrations from the HPLC column actually contained three components that were well resolved by HPCE. In a similar manner, the single albumin peak obtained by HPLC was found to be subfractionated into two major and two minor components by HPCE. An interesting reversal of this observation was demonstrated with transferrin. Using HPCE, serum-derived transferrin standards were found to contain two components, but only one component was found in BALF proteins.

Another effective application of HPCE was found to be its use as a quality control system for analysis of the purity of BALF components prepared by HPLC. Because of the large amounts of albumin and transferrin in the BALF protein mixture, the preparations of other BALF components were sometimes found to be contaminated by these proteins. Such contamination will be detrimental to the accurate amino acid analysis, amino acid sequencing and immunological analysis which will be necessary for the identification of the unknown components in BALF. HPCE will provide a rapid and simple method to document the purity of the preparations used for such endeavors.

The use of HPCE in this manner has also revealed an unexpected contaminant in the HPLC fractions of BALF proteins. This contaminant is guanidine, which was added to the BALF as a solubilizing agent. This reagent has been used for some time to dissociate complex mixtures of proteins for HPLC fractionation. Because of its highly charged nature, it has been presumed that all the guanidine was eluted immediately from the hydrophobic reversed-phase HPLC column leaving the proteins guanidine free when they were eluted. With HPCE we have shown that this is not so. Under many circumstances the presence of residual guanidine in the HPLC fractions may be irrelevant. However, if guanidine is detrimental to the further use of these HPLC preparations, HPCE can be used to determine quickly whether is is present.

Another important application of this HPCE system will be its use as an assay method to guide the development of new HPLC systems for the isolation and preparation of the subfractions of BALF proteins which are unresolved by present HPLC systems. HPCE will be particularly attractive in this role as it is fast and can be automated for use with the large number of fractions generated by HPLC.

The HPCE system has its share of limitations as an analytical method at this early stage in its development. Quantitative reproducibility is the most serious. Quantitative analysis appears to be fairly good for polypeptides. However, HPCE does not meet the standards of reproducibility for proteins that is expected by most researchers. The reasons for this difference remain unclear. This is not simply a problem encountered only with BALF proteins. We find the problem equally a nuisance when attempting to perform HPCE on histone proteins which have a very different nature from BALF proteins [16]. We suspect that the problem involves variations in electroinjection, but we have not yet been able to identify the varying parameter.

Another limitation of HPCE is sample concentration. While sample volumes required by the system are very small (5 μl for the HPE-100), the concentration of the protein in the sample must be high if UV detection is used to monitor the electrophoresis. For complex mixtures of proteins, this concentration should be at least 0.1 mg/ml in order to detect most of the components. With BALF proteins, we found it necessary to concentrate the samples by either precipitation, evaporation or reversed-phase HPLC before we could use HPCE for analysis. In addition to these concentration steps, electroinjection itself produces another helpful concentration by stacking the proteins in the capillary [21]. If some other method of injection is employed for HPCE, one should expect to have to use protein sample concentrations considerably greater than 0.1 mg/ml.

The reproducibility of mobilities cannot be relied upon for identification of closely migrating components. This is a general problem with HPCE, which we found to be as true for polypeptides as for proteins. In chromatography we have commonly used radiolabeled internal standards to circumvent this problem, but the present lack of sensitive radioactivity detection for HPCE systems makes this impractical. However, we found that identification of the various components could usually be made by "spiking" the samples with a known internal standard and detecting the fraction in the electropherogram by the increase in its peak height.

A number of BALF fractions which were isolated by HPLC were not detectable by HPCE. This may be due to the presence of hydrophobic interactions between some lung constituents and the coating of the capillary. The resulting adsorption might remove the more hydrophobic components, such as lipids and surfactants, from the sample during electrophoresis. Another possible explanation for the loss is that some components were not charged under the acidic conditions of this HPCE system. The absence of electroosmotic flow caused by the capillary coating would prevent uncharged components from reaching the detector. Hence it may be necessary to analyze some HPLC samples in uncoated capillaries which produce electroendoosmosis.

While the shortcomings of the HPCE of proteins need to be clearly recognized, we have nevertheless, found that this new technology offers effective new ways to analyze a complex mixture of proteins. With the BALF proteins, HPCE has significantly pushed back the frontier of analysis of lung fluid samples.

The use of HPCE together with HPLC has enabled us to characterize the effects

of PFIB on the fluid lining of the lung. We found that, 24 h after PFIB exposure, the resulting pulmonary edema is accompanied by a massive outpouring of plasma components into the alveolar compartment. BALF albumin was increased >40-fold and BALF transferrin was increased >30-fold. There was also a significant amount of an IgG-like protein in the BALF after PFIB treatment that was undetectable in controls. The great increase in these proteins in the BALF indicate that PFIB has caused a breach in the air–blood barrier in the lung that is large enough to permit the translocation of large macromolecules such as IgG from the bood to the alveolar compartment.

Two new unidentified components (labeled A and B in the HPLC traces) were found in the BALF after PFIB treatment. These two components have been found in BALF after other treatments that cause pulmonary edema [14]. Hence it is suspected that their origin may also be the blood compartment.

There was one major component of normal BALF that was found to be lost from the BALF of PFIB-treated lungs. This component has not yet been identified. It is easily detectable by both HPLC and HPCE. It elutes early from the reversed-phase C_{18} HPLC column, indicating that it is not very hydrophobic. It is the fastest migrating component in BALF proteins subjected to HPCE, indicating that it is highly positively charged. Previous work has shown that this component contains protein [13,14].

When we exposed rats to other edema inducing agents this component has not increased greatly like albumin and transferrin [14]. There was a small loss of this component in cadmium-injured lungs and a small increase in nitrogen dioxide-injured lungs [14]. Hence this component does not appear to be derived from the blood compartment, but rather is likely a product of the lung cells and/or the lung's extracellular matrix. Its loss after PFIB treatment may reflect damage to the cells producing it. HPCE may play an important role in uncovering the nature of IgG in BALF. When serum-derived IgG standards are subjected to HPLC they elute late in the chromatogram [13,14]. However, the only IgG-like substance we observed by HPCE was found in the early-eluting HPLC transferrin peak from PFIB-treated rats (Fig. 11). The late-eluting components in the HPLC chromatogram contained three HPCE peaks that did not have the electrophoretic properties of IgG. We therefore suspect that IgG may be altered or degraded in normal lung fluid. HPCE should provide a useful new method to examine this possibility and to determine if toxic agents such as PFIB interfere in the process.

This work demonstrates that HPCE can be effectively used for the analysis of lung proteins. It is expected that in the future this method will be refined to a point where it will be a major analytical tool by which the pulmonary biologist, biochemist and toxicologist can elucidate the mechanisms of lung injury.

ACKNOWLEDGEMENTS

This work was performed under the auspices of the US Department of Energy and was supported in part by the Institute of Chemical Defense, US Army Medical Research and Development Command, Project No. 87 pp 7832, and fellowships from the US Department of Energy's Teacher Research Associates Program and the American Society for Biochemistry and Molecular Biology's High School Teacher Summer Fellowship Program.

REFERENCES

1 Y. Alarie, *Annu. Rev. Pharmacol. Toxicol.*, 25 (1985) 325.
2 D. M. Stavert, D. Archuleta, G. Wood, M. J. Behr and B. E. Lehnert, *Toxicologist*, 10 (1990) 203.
3 B. E. Lehnert and D. M. Stavert, in *Proceedings of the 1990 Science Conference on Chemical Defense Research*, 1991, in press.
4 R. Sebring, D. M. Stavert and B. E. Lehnert, *Toxicologist*, 10 (1990) 204.
5 B. E. Lehnert and D. M Stavert, paper presented at the *1989 US Army Chemical Research, Development, and Engineering Center Scientific Conference on Chemical Defense Research, Aberdeen Proving Ground, MD, November 14–17, 1989.*
6 W. D. Currie, G. E. Hatch and M. F. Frosolono, *Fundam. Appl. Toxicol.*, 8 (1987) 107.
7 J. R. Brainard, S. A. Kinkead, E. M. Kober, D. M. Stavert and B. E. Lehnert, in *Proceedings of the 1990 Scientific Conference on Chemical Defense Research*, 1991, in press.
8 L. R. Gurley, J. E. London, Y. E. Valdez, N. M. Lehnert, D. M. Stavert and B. E. Lehnert, *Toxicologist*, 10 (1990) 203.
9 B. E. Lehnert and D. M. Stavert, in D. H. Moore (Editor), *Proceedings of the Workshop on Acute Lung Injury and Pulmonary Edema*, U.S. Army Medical Research Institute of Chemical Defense, Aberdeen Proving Ground, MD, May 4–5, 1989, pp. 153–188.
10 B. E. Lehnert and P. E. Morrow, *Immunol. Commun.*, 13 (1984) 313.
11 J. D. Brain and R. Frank, *J. Appl. Physiol.*, 34 (1973) 75.
12 B. E. Lehnert and P. E. Morrow, *Exp. Lung Res.*, 9 (1985) 1.
13 L. R. Gurley, W. D. Spall, J. G. Valdez, J. E. London, L. A. Dethloff and B. E. Lehnert, *Anal. Biochem.*, 172 (1988) 465.
14 L. R. Gurley, J. E. London, L. A. Dethloff, D. M. Stavert and B. E. Lehnert, in T. E. Hugli (Editor), *Techniques in Protein Chemistry*, Academic Press, New York, 1989, pp. 479–489.
15 G. J. Fallick and C. W. Rausch, *Am. Lab.*, 11, Nov. (1979) 87.
16 L. R. Gurley, J. E. London and J. G. Valdez, *J. Chromatogr.*, 559 (1991) 431.
17 S. Hjerten, *J. Chromatogr.*, 347 (1985) 191.
18 J. S. Green and J. W. Jorgenson, *J. Chromatogr.*, 352 (1986) 337.
19 G. J. M. Brain, J. P. Chang, R. H. Kuhlman, K. Zegers, J. C. Kraak and H. Poppe, *J. Chromatogr.*, 471 (1989) 429.
20 J. D. Olechno, J. M. Y. Tso, J. Thayer and A. Wainright, *Am. Lab.*, 22, Dec. (1990) 30.
21 S. Hjerten, S. Jerstedt and A. Tiselius, *Anal. Biochem.*, 11 (1965) 219.
22 G. George and G. E. R. Hook, *Environ. Health Perspect.*, 55 (1984) 227.

Journal of Chromatography, 559 (1991) 431–443
Elsevier Science Publishers B.V., Amsterdam

CHROM. 23 493

High-performance capillary electrophoresis of histones

L. R. GURLEY*, J. E. LONDON and J. G. VALDEZ
Los Alamos National Laboratory, Life Sciences Division, Mail Stop M880, Los Alamos, NM 87545 (USA)

ABSTRACT

A high-performance capillary electrophoresis (HPCE) system was developed for the fractionation of histones. This system involves electroinjection of the sample and electrophoresis in 0.1 *M* phosphate buffer (pH 2.5) in a 35 cm × 50 μm I.D. coated capllary. Electrophoresis was accomplished in 9 min, separating a whole histone preparation into its components in the following order of decreasing mobility: (MHP) H3, H1 (major variant), H1 (minor variant), (LHP) H3, (MHP) H2A (major variant), (LHP) H2A, H4, H2B and (MHP) H2A (minor variant), where MHP is the more hydrophobic component and LHP is the less hydrophobic component. This order of separation is very different from that found in acid–urea polyacrylamide gel electrophoresis and in reversed-phase high-performance liquid chromatography and, thus, brings the histone biochemist a new dimension for the qualitative analysis of histone samples.

INTRODUCTION

The separation of histones by zone electrophoresis in a starch gel matrix was first introduced by Neelin and Connell over 30 years ago [1]. Since that time, the gel electrophoresis of histones, particularly in polyacrylamide gels, has been widely practiced [2–12] because it is inexpensive to implement and simple to operate [13]. On the other hand, the gel preparation is tedious, the electrophoresis is time consuming and quantification involves staining, destaining and scanning desitometry, which is labor intensive, time consuming, and semi-quantitative [13].

The advent of high-performance capillary electrophoresis (HPCE) [14,15] potentially offers a new opportunity to raise the electrophoretic fractionation and analysis of histones to a performance level superior to that of gel electrophoresis. The advantages of HPCE should include high resolution, rapid analysis time, on-line detection and computer-based quantification. Most important, HPCE has the potential for the analysis of very small samples in the femtomole range [15]. In our laboratory, the ability to perform analyses on such small samples is attractive because it would facilitate the analysis of histones from the small numbers of cells acquired by flow cytometry cell sorting. For these reasons, we have initiated a program to develop HPCE methods to fractionate nucleoproteins. This paper describes the development of the separation of histones by zone electrophoresis in free solution using low-pH buffers in coated silica capillaries.

0021-9673/91/$03.50

EXPERIMENTAL

Cel cultures and histone preparation

Chinese hamster cells (line CHO) were grown exponentially in suspension culture as described by Tobey *et al.* [16]. Chromatin was prepared from whole-cell homogenates as described by Gurley *et al.* [17]. Histones were extracted from the chromatin with 0.2 *M* sulfuric acid, recovered by acetone precipitation and stored as a lyophilized powder at −70°C until used for HPCE [17].

To prepare purified histones for high-performance liquid chromatography (HPLC), 3×10^8 nuclei were prepared from CHO cells using the detergents Nonidet P-40 and sodium deoxycholate in hypotonic solution as described by Gurley *et al.* [18]. The nuclei were then dissolved for 2 h in 1 ml of reagent containing 6 *M* guanidine · HCl, 0.2% trifluoroacetic acid (TFA), 0.155 *M* NaCl, 0.026 *M* HCl and 0.025% dithiothreitol according to the method of Jackson and Gurley [19]. Undissolved residual nuclei were sedimented by centrifugation at 8000 *g* for 10 min. The supernatant fluid containing soluble DNA and proteins was decanted into 9 ml of water containing 0.2% TFA. The residual undissolved nuclei were dissolved in 1 ml of dissolving reagent for 1 h and then centrifuged as before. Only a trace of nuclear material remained undissolved. The supernatant fluid was decanted into the water–0.2% TFA containing the first decantate. The DNA in the solution was precipitated overnight at 4°C due to the acidic conditions of the solution. The DNA was sedimented by centrifugation at 8000 *g* for 2 h. The 11 ml of supernatant fluid, containing the total complement of proteins from the cell nuclei, was stored at −70°C. When used for HPLC, this solution was thawed and centrifuged for 2 h at 8000 *g* to remove any residual DNA clouding the sample.

HPLC of histones

The guanidine-soluble DNA, salts and other chemical reagents in the dissolved nuclei samples were separated from the nuclear proteins by size-exclusion HPLC. This was accomplished as described by Jackson and Gurley [19] using a Waters HPLC system equipped with a Bio-Sil TSK guard column followed by a Bio-Sil TSK size-exclusion column (Bio-Rad Labs). The sample was injected into the guard column and was eluted through the two columns with water–0.2% TFA at a flow-rate of 0.5 ml/min. The guard column adsorbed any soluble DNA remaining in the sample and the proteins were separated from the salts and other chemical reagents by size-exclusion HPLC on the Bio-Sil TSK column [19]. The effluent protein fraction was either lyophilized to a dry powder and stored at −70°C for future use or it was injected directly into a reversed-phase μBondapak CN HPLC column (Waters Assoc.) [20] which adsorbed the proteins on the top of the column [21].

The histone proteins were fractionated and purified by reversed-phase HPLC on the μBondapak CN column using gradient elution with acetonitrile containing 0.2% of TFA as described by Gurley *et al.* [22]. This column fractionated the histones into the five basic types, H1, H2A, H2B, H3 and H4, and the H2A and H3 histones were subfractionated into two variants of each, the less hydrophobic (LHP) H2A and (LHP) H3 and the more hydrophobic (MHP) H2A and (MHP) H3 [20–22]. Each of these seven individual histone fractions was collected and either lyophilized to dryness or evaporated to dryness while centrifuging in a vacuum chamber (Speed-Vac)

and stored at −70°C [22] until used to identify the individual histones fractionated by HPCE.

HPCE of histones

HPCE was performed using a Model HPE-100 high-performance electrophoresis system manufactured by Bio-Rad Labs. Experiments were performed using 20 cm × 25 μm I.D., 35 cm × 50 μm I.D., and 50 cm × 50 μm I.D. capillary tubes whose inside surfaces were chemically modified to produce a patented hydrophilic coating. Coatings of this nature have been reported by several laboratories to eliminate electroendoosmosis and protein adsorption [23–25]. Cathode, anode and capillary buffers were 0.1 *M* sodium phosphate (pH 2.5) (Bio-Rad Labs.) unless specified otherwise. Detection of the separated proteins traversing the capillary was accomplished by in-tube monitoring of the peptide bond absorbance at 200 nm with a spectrophotometer setting of 0.005 a.u.f.s. To evaluate the peformance of this instrument, a standard mixture of nine polypeptides was subjected to electrophoresis. This mixture contained bradykinin, angiotensin II, α-MSH, TRH, LHRH, [2–5] leucine enkephalin, bombesin, methionine enkephalin and oxytocin (Bio-Rad Labs).

Samples were prepared for HPCE by dissolving lyophilized histone powder in water containing 0.2% of TFA at a concentration of 0.1 μg/μl. Poly-L-lysine hydrobromide, Type VI, molecular mass 13 000 (Sigma) was added to some of these solutions at a concentration of 0.05 μg/μl to serve as an internal mobility marker during electrophoresis. These samples were loaded into the capillaries by electroinjection [26]. To accomplish this, the cathode chamber and capillary were filled with 0.1 *M* phosphate buffer and the anode chamber was filled with water. Then 5 μl of sample were injected into the loading chamber at the anode end between the capillary and the water. Power was applied to the capillary at 10 kV (constant voltage) and *ca.* 38 μA for 10 s. This actively carries the cations (including the positively charged protonated proteins) into the capillary. Under these low ionic strength sample conditions, the proteins are concentrated and stacked in the capillary during this loading step [27]. The excess of sample in the loading chamber and the water in the anode chamber were then replaced with 0.1 *M* phosphate buffer and electrophoresis was performed by applying power to the capillary at 10 kV (constant voltage) and *ca.* 41 μA. Electrophoresis normally took 10 min using the 35 cm × 50 μm I.D. coated capillary.

RESULTS

20 cm × 25 μm I.D. capillary

The performance of the HPE-100 high-performance electrophoresis instrument is typically evaluated by subjecting a mixture of nine polypeptides to zone electrophoresis in a 20 cm × 25 μm I.D. coated capillary using 0.1 *M* phosphate buffer (pH 2.5). In our laboratory repetitive electrophoresis of this standard produced fractions whose peak heights varied by only 3.0% (relative standard deviation) and whose mobilities varied by 7.2%. This high performance led us to choose these operating conditions for our first attempts to separate histones by HPCE. We found that when whole histones were dissolved in water containing 0.2% of TFA (as they are when recovered from an HPLC column) we could electroinject them into the capillary in 10 s at 10 kV. However, electrophoresis at 10 kV produced a single peak of unresolved

proteins. By decreasing the electrophoresis voltage we found that this single peak contained the various histone fractions which had mobilities ranging over 2 min at 4 kV, but they could not be resolved under these conditions (Fig. 1A).

It was thought that perhaps protein–protein interactions in the capillary might cause a degradation of resolution. To prevent this, NaCl was added to the electrophoresis buffer. Preliminary experiments indicated that when NaCl concentrations greater than 0.12 *M* was used, the electrophoresis was inhibited owing to the elevated conductivity of the buffer. However, when 0.12 *M* NaCl was used, histone electrophoresis was accomplished. Histone resolution at 4 kV was better in the presence of 0.12 *M* NaCl (Fig. 1B) than it was without NaCl (Fig. 1A). However, it was not adequate for analytical use.

50 cm × 50 μm I.D. Capillary

Another possible cause of the poor resolution might be protein interactions with the capillary walls. To reduce the magnitude of this effect we performed the electrophoresis in a larger diameter capillary having the dimensions of 50 cm × 50 μm I.D. After electroinjection at 10 kV, the histones were subjected to electrophoresis

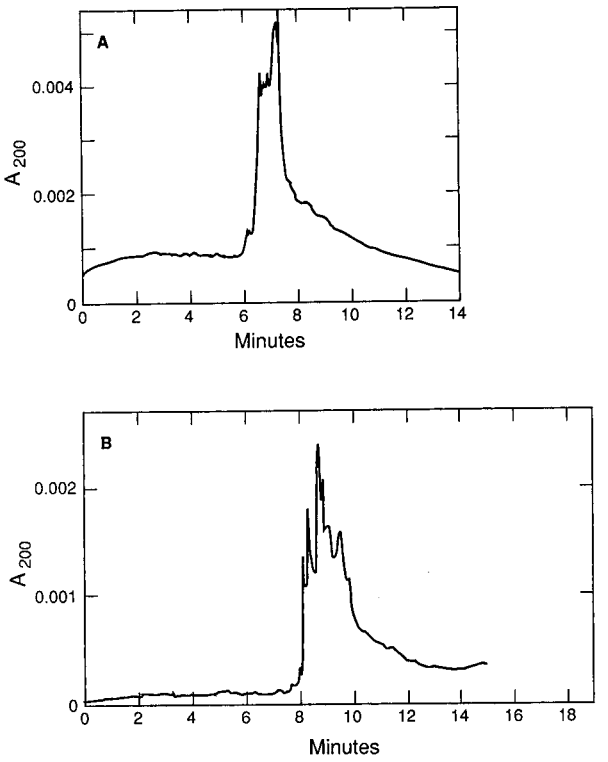

Fig. 1. HPCE of whole histones in a 20 cm × 25 μm I.D. coated capillary. Samples were electroinjected for 10 s at 10 kV. Electrophoresis was performed at 4 kV in 0.1 *M* phosphate buffer (pH 2.5) (A) without NaCl or (B) containing 0.12 *M* NaCl. Resolution was monitored at 200 nm with a detector response time of 1 s and a chart speed of 1 cm/min.

at four different voltages (4, 6, 8 and 10 kV). We found that the resolution of the histones was far superior in this 50 μm I.D. capillary (Fig. 2A) than in the 25 μm I.D. capillary (Fig. 1A). Reducing the electrophoresis voltage from 10 to 6 kV appeared to improve the resolution. However, close inspection indicated that although the peaks are spread further apart at 6 kV than at 10 kV, the longer electrophoresis time permitted diffusion to spread the bands so that no significant increase in resolution was accomplished at the lower voltages.

NaCl was added to the electrophoresis buffer in the 50 cm × 50 μm I.D. capillary. There was a small increase in the resolution when the NaCl concentration was increased from 0 *M* (Fig. 2A) to 0.12 *M* (Fig. 2B). The most noticeable effect of NaCl was with the largest fraction, which was latter identified as H2B. When the

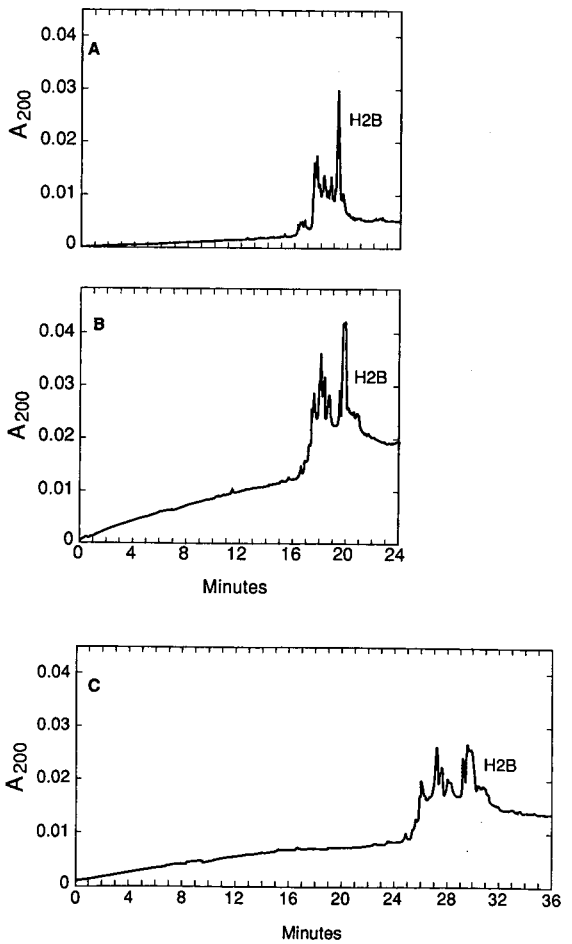

Fig. 2. HPCE of whole histones in a 50 cm × 50 μm I.D. coated capillary. Samples were electroinjected for 10 s at 10 kV. Electrophoresis was performed at 10 kV in 0.1 *M* phosphate buffer (pH 2.5) (A) without NaCl and (B) containing 0.12 *M* NaCl, and (C) at 7 kV in 0.1 *M* phosphate buffer (pH 2.5) containing 0.12 *M* NaCl. Resolution was monitored as in Fig. 1.

electrophoresis voltage was reduced from 10 to 7 kV in the presence of 0.12 *M* NaCl, the H2B peak was observed to undergo partial resolution into more fractions (Fig. 2C). Unfortunately, the longer electrophoresis time at 7 kV permits too much band broadening due to diffusion, thus destroying the overall resolution of the whole sample (Fig. 2C).

35 cm × 50 μm I.D. capillary

Since diffusion appeared to be a significant factor in the degradation of the electropherogram, we used a shorter capillary (35 cm × 50 μm I.D.) to reduce the time of the run. With the shorter capillary, the histones migration took less than 8 min at 10 kV (Fig. 3B) whereas with the 50-cm capillary it took 15–17 min (Fig. 3A). This capillary size appeared to give the best resolution of the three examined, so we adopted this capillary to investigate other operational parameters.

pH of the electrophoresis buffer

All the previous experiments were performed at pH 2.5. To determine if this pH was the optimum condition for resolving the histones, the pH was varied in the 35 cm × 50 μm I.D. capillary from 2.0 to pH 5.0 (Fig. 4). We found that histones moved the fastest at pH 2.0 (Fig. 4A) and the slowest at pH 3.5 (Fig. 4E). The best resolution was obtained at pH 2.5 (Fig. 4B). Runs at higher pH produced greater overlapping frac-

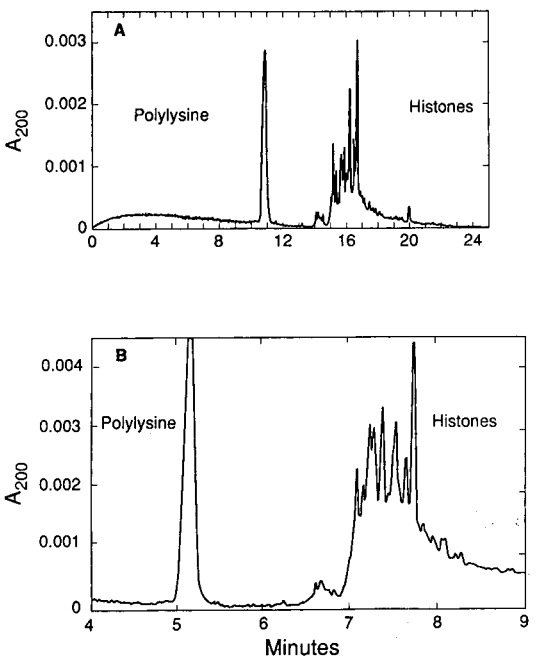

Fig. 3. HPCE of whole histones in a 35 cm × 50 μm I.D. coated capillary. Samples were electroinjected for 10 s at 10 kV and electrophoresed at 10 kV. A comparison is shown between electrophoresis in (A) a 50 cm × 50 μm I.D. and (B) a 35 cm × 50 μm I.D. capillary. Resolution was monitored as in Fig. 1 except that the chart speed of (A) 1 cm/min was increased to (B) 6 cm/min in order to facilitate visualization of the resolution of the closely spaced bands in the 35 cm × 50 μm I.D. capillary.

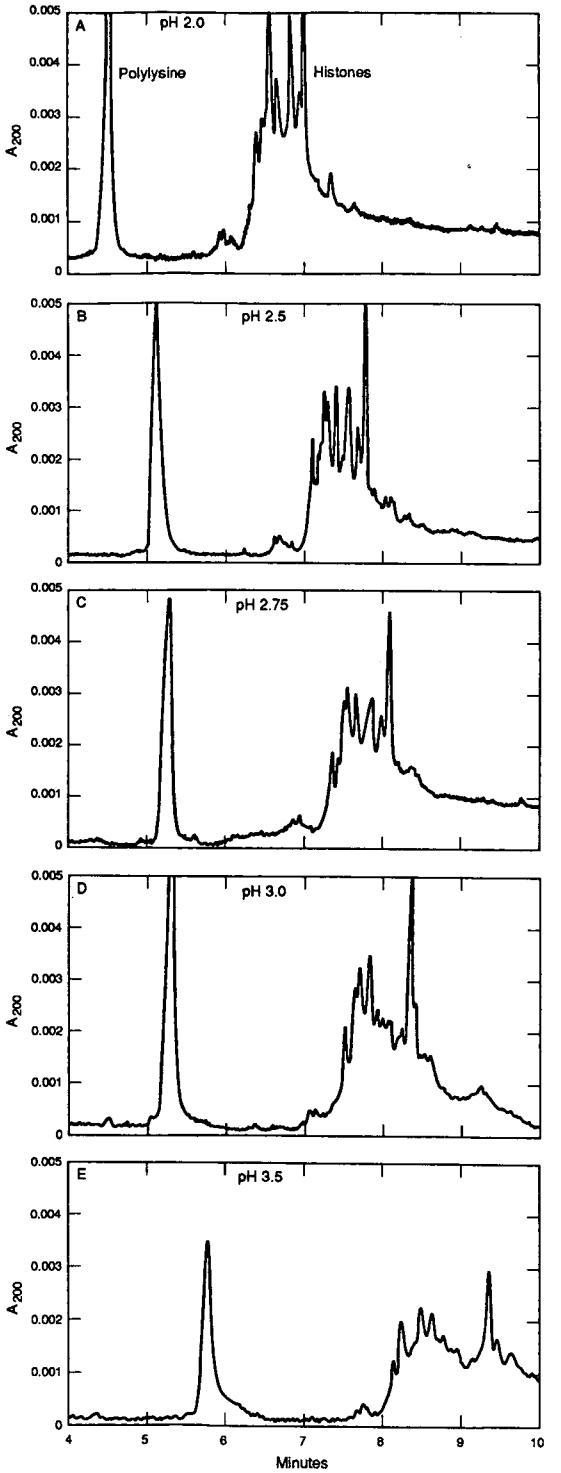

Fig. 4. HPCE of whole histones in a 35 cm × 50 μm I.D. coated capillary at various pH values. All samples were electroinjected for 10 s at 10 kV. Electrophoresis was performed in 0.1 *M* phosphate buffer at pH (A) 2.0, (B) 2.5, (C) 2.75, (D) 3.0 and (E) 3.5. Resolution was monitored at a chart speed of 3 cm/min.

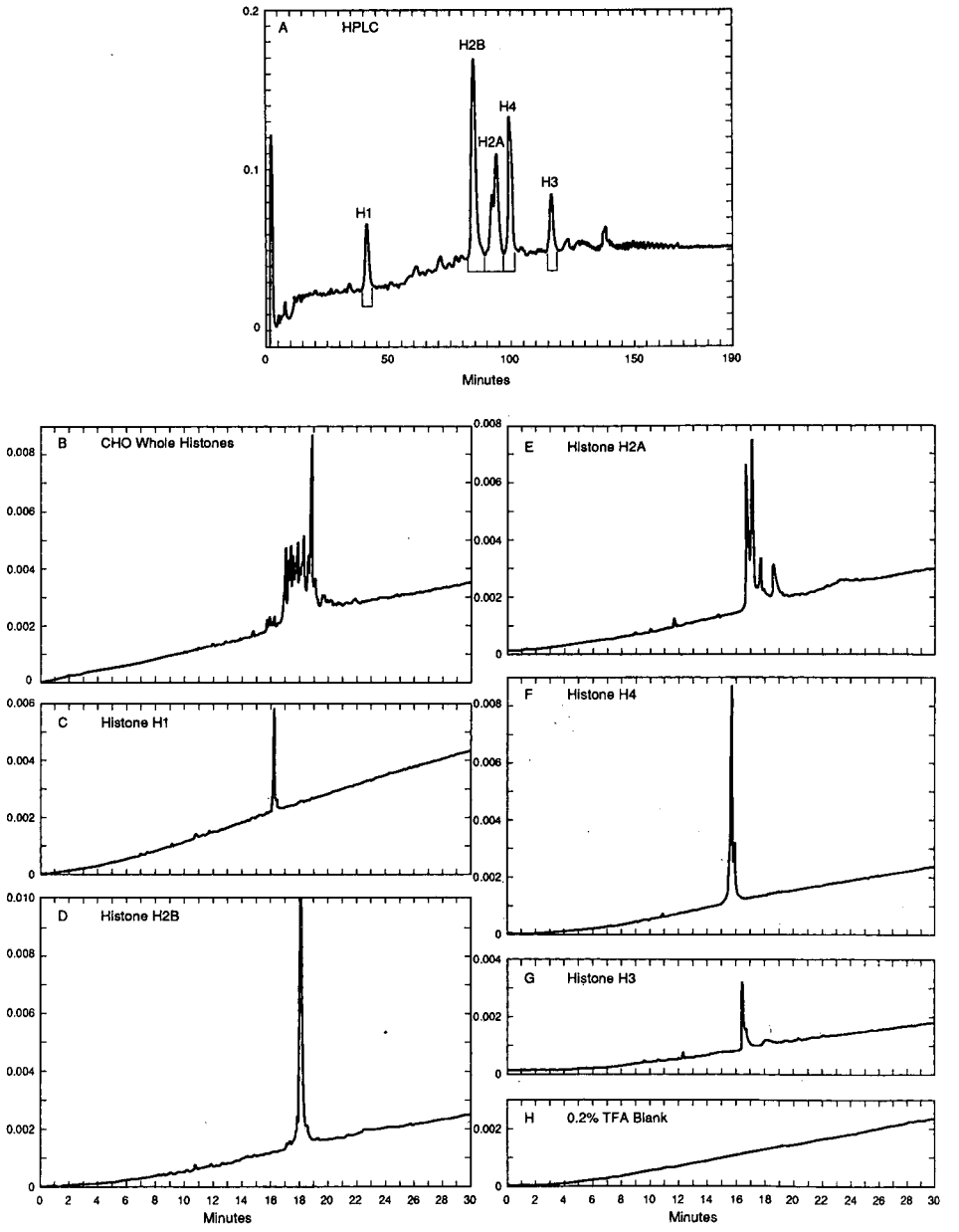

Fig. 5. HPCE of histone fractions in a 50 cm × 50 μm I.D. coated capillary. (A) The histones of CHO nuclei were fractionated into the five histone classes (H1, H2B, H2A, H4 and H3) by reversed-phase HPLC. (B) Whole unfractionated histones, (C) H1, (D) H2B, (E) H2A, (F) H4, (G) H3 and (H) a 0.2% TFA blank solution in which these histones were dissolved were subjected to HPCE in 0.1 *M* phosphate buffer (pH 2.5) at 10 kV. Resolution was monitored as in Fig. 1.

tions and above pH 3.5 the electropherogram became a broad, unresolved smear. Therefore, pH 2.5 appears to be the optimum condition for this set of proteins.

Identification of the histone fractions

Our first attempt to identify the individual histone fractions in the electropherograms was made while using the 50 cm × 50 μm I.D. capillary. Purified histone fractions (H1, H2A, H2B, H3 and H4) were obtained from CHO nuclei by HPLC (Fig. 5A). Each of these five fractions was subjected to electrophoresis at pH 2.5 (Fig. 5, C–G) and compared with a whole histone preparation (Fig. 5B) and a water–0.2% TFA blank, the solvent in which the samples were dissolved (Fig. 5H). The fractions were found to be pure by HPCE, H1 and H2B migrating as a single peak, H2A migrating as four variants which are known to exist for this histone, histone H4 migrating as a single peak with a presumptive acetylated form following it and H3 migrating as a single peak with its presumptive acetylated form following it. The fractions had migration times varying from 16 to 20 min (Fig. 5, C–G). The whole histones had migration times from 17 to 20 min. We pointed out at the beginning of the paper that there was a 7.2% variability in the mobility of standards. This variability made it impossible to use the mobility of the individual histone fractions to identify the histone fractions in the whole histone electropherogram in Fig. 5B.

In some experiments, polylysine was added to samples as an internal standard in the hope that this mobility variation could be normalized as a ratio of the mobility of the fractions to that of polylysine (Fig. 3). However, this did not reduce the variability sufficiently to provide unequivocal assignments based on the individual fraction mobilities.

This problem was overcome by adding individual histone fractions to the whole histone sample. Seven individual histone fractions were isolated by HPLC (Fig. 6A). Each of these fractions was mixed with a separate sample of whole histone containing polylysine and loaded into a 35 cm × 50 μm I.D. capillary for 10 s at 10 kV. The samples were then subjected to electrophoresis at 10 kV for 10 min. Each fraction in the electropherogram of the whole histone sample was located by the increase in the fraction's peak height (Fig. 6, B–H). From these data, the order of mobility of each histone fraction was determined (Fig. 7). From the fastest to the slowest, they are (MHP) H3, H1 (major variant), H1 (minor variant), (LHP) H3, (MHP) H2A (major variant), (LHP) H2A, H4, H2B, (MHP) H2A (minor variant). Under these conditions, all the fractions move past the detector within 1 min. Two unidentified fractions are detectable in the whole histone electropherogram, one between the (LHP) H2A and H4 and the other between the H4 and H2B (Fig. 7). The whole histone preparations also contain a cluster of unidentified high-mobility minor components which precede the histones at 7 min and a cluster of unidentified low-mobility minor components which follow the H2B at 8 min (Fig. 7).

DISCUSSION

These experiments represent the development of the first application of HPCE to histone analysis. The optimum conditions that we have found to date involve sample electroinjection for 10 s at 10 kV and electrophoresis at 10 kV under acid conditions at pH 2.5 in 0.1 *M* phosphate buffer in a 35 cm × 50 μm I.D. coated

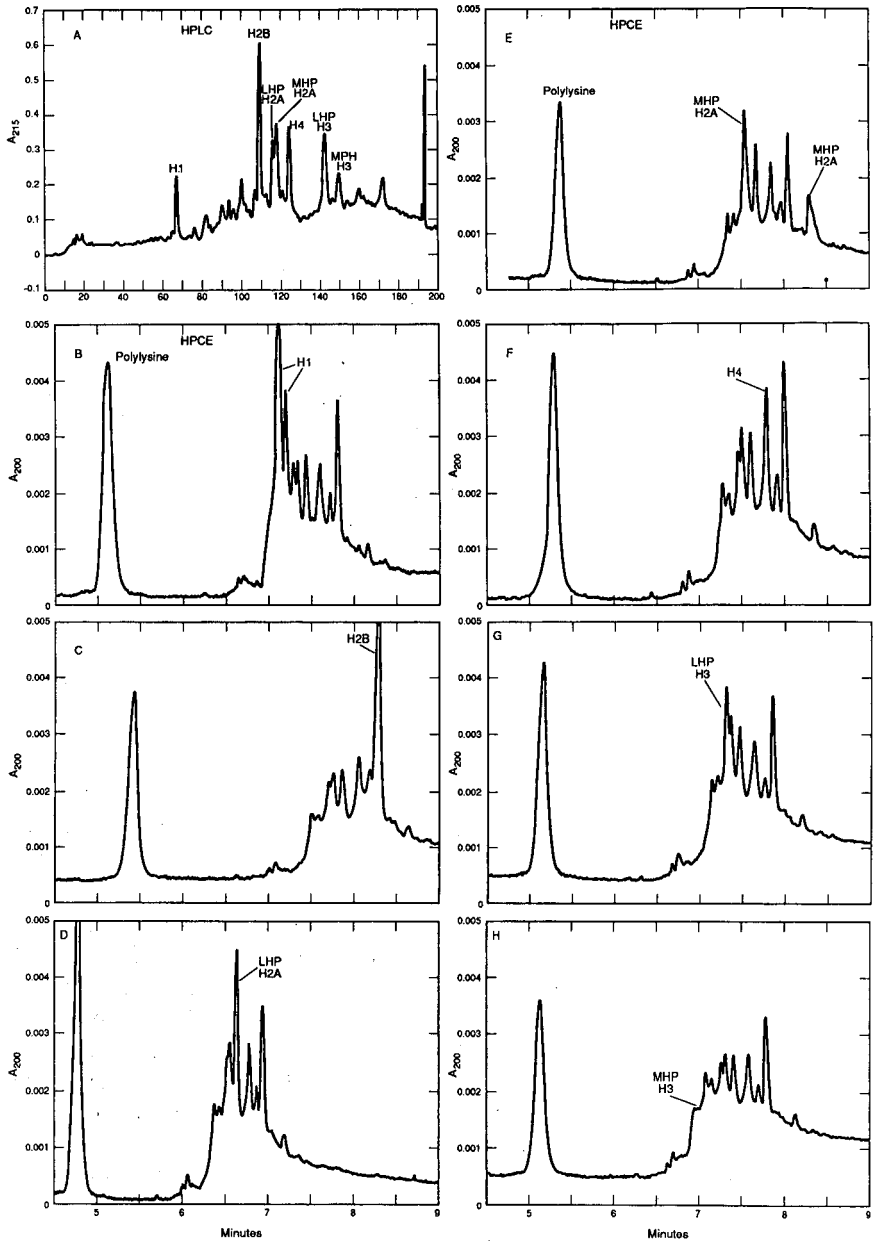

Fig. 6. HPCE of whole histones spiked with individual histone fractions using a 35 cm × 50 μm I.D. coated capillary. (A) The histones of CHO nuclei were fractionated into the five histone classes (H1, H2B, H2A, H4 and H3) and two variants each of H2A and H3, which are indicated as the less hydrophobic (LHP) and more hydrophobic (MHP) forms. (B–H) A sample of each of these fractions was evaporated to dryness and added to a separate whole histone preparation together with polylysine (internal standard) and subjected to HPCE in 0.1 *M* phosphate buffer (pH 2.5) at 10 kV. Resolution was monitored at a chart speed of 6 cm/min. (B) Histone H1 (C) H2B, (D) LHP-H2A, (E) MHP-H2A, (F) H4, (G) LHP-H3 and (H) MHP-H3 were identified in the whole histone electropherograms by the increase in the peak height of an individual component.

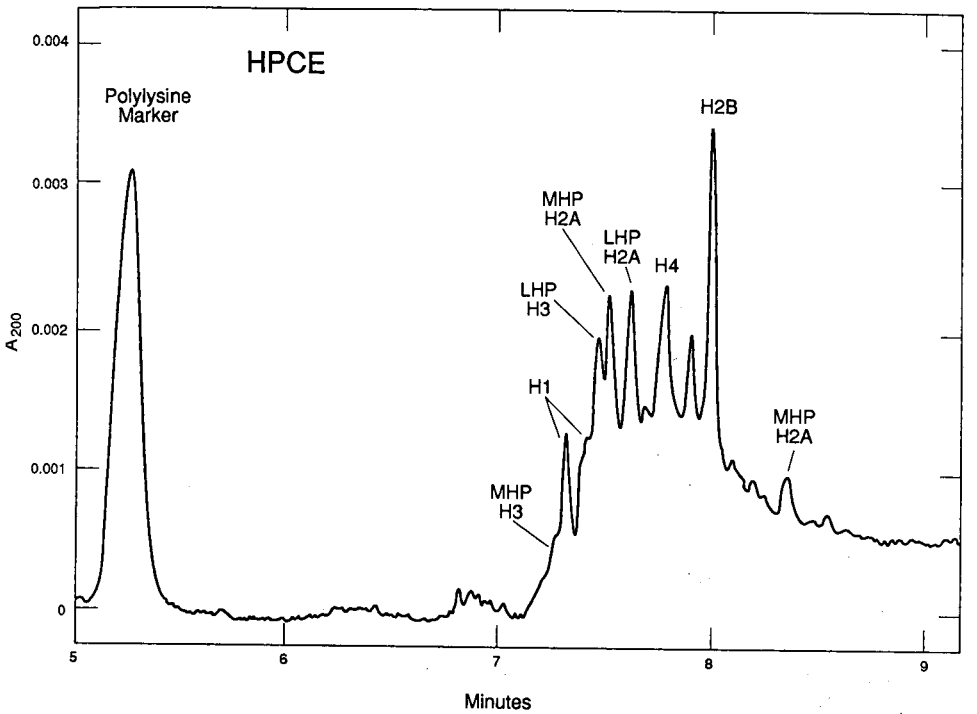

Fig. 7. Assignment of histone fractions obtained by HPCE of a whole histone sample. HPCE was performed in a 35 cm × 50 μm I.D. coated capillary. The sample was dissolved in 0.2% TFA and electroinjected for 10 s at 10 kV. Electrophoresis was performed at 10 kV in 0.1 *M* phosphate buffer (pH 2.5). Resolution was monitored at 200 nm with a detector response time of 1 s and a chart speed of 6 cm/min. Polylysine was added to the sample as an internal mobility standard.

capillary. Some of the criteria for high performance are met by this system. Small sample volumes (5 μl) can be used and electrophoresis is accomplished in a short time (9 min). In-capillary detection by UV absorption at 200 nm is possible provided that the sample is concentrated enough (0.1 μg/μl). This permits the use of computers to perform on-line data analysis of the electropherograms. This procedure also fulfills our need to be able to perform analysis on the histones from a small number of cells, such as those acquired by flow cytometry cell sorting. For example, a 5-μl sample at 0.1 μg/μl is the amount of histones we can obtain from 55 000 CHO cells.

The order in which the histone fractions migrate in HPCE is very different from that found in acid–urea polyacrylamide gel electrophoresis [8,12] or in reversed-phase HPLC (Figs. 5A and 6A). For this reason, HPCE brings the histone biochemist a new dimension for the qualitative analysis of histone samples. It also provides a quick method of quality control for evaluating the purity of isolated individual histone fractions. For example, we demonstrated that histone fractions isolated by reversed-phase HPLC were pure (Fig. 5).

The apparent greater amount of H2B compared with the other histone fractions (Fig. 7) may reflect heterogeneity in that band. When we added 0.12 *M* NaCl to the electrophoresis buffer and decreased the voltage to 7 kV, this fraction broadened

and appeared to develop a slower moving component as a trailing shoulder (Fig. 2C). Further work will be required te determine what this extra component is. Also, two other unknown components were observed in whole histone preparations, one preceding and the other following H4. These also need to be identified. As they are readily separated by HPCE, we shall be able to use this method as an assay for them. This will enable us to search chromatograms for their presence and then verify their purity during isolation.

The system has two problems that need to be dealt with further: narrowly spaced bands and broadly diffused bands. These problems are not restricted to the HPCE of histones, as we have also encountered them with the HPCE of plasma proteins. As we do not encounter these problems when performing HPCE on small peptide standards, they appear to be problems associated strictly with macromolecular proteins. These problems interfere most seriously during quantitative analysis. For example, at the beginning of the Results section we pointed out that we could obtain peak heights that varied by only 3.0% when using small peptide standards. This high precision has not been obtainable for histones or other proteins, however.

To improve the HPCE of histones, a system needs to be found that will separate the bands further apart in a shorter time. At present, all the histone fractions pass the detector within 1 min. The use of longer capillaries did not increase their resolution because it also increased the time taken to traverse the capillary, thus broadening the bands due to diffusion. However, the close bands would not be such a problem if the protein bands were narrow like those of small peptides. Hence the most serious problem to be solved is that of band broadening.

It may be that the broader protein bands result from incomplete stacking of the proteins during the electroinjection step. It has been suggested that protein–protein interactions may cause such an interference. Our experience with polylysine argues against this reasoning, however. We found that polylysine, having a molecular mass of 13 000, produced a broad band like a protein (Fig. 7). We would not expect this highly positively charged macromolecule to produce significant intermolecular interactions. An alternative suggestion is that the hydration shell around the proteins may be much greater than that around the small peptides, thus preventing the high degree of concentration from occurring during the stacking process. If this in the case, it may be difficult in the HPCE of proteins to produce the narrow bands observed with peptides and we shall be forced to find a system that produces bands spaced further apart in order to increase resoluton.

Although the HPCE of proteins has several shortcomings at this early stage of development, capillary electrophoresis still offers the potential for further development into an important high-performance analytical system for the histones. This work lays the groundwork and experience for further experiments to solve the resolution and quantification problems associated with the application of this new technology to protein biochemistry.

ACKNOWLEDGEMENTS

This work was performed under the auspices of the US Department of Energy's Office of Health and Environmental Research.

REFERENCES

1 J. M. Neelin and G. E. Connell, *Biochim. Biophys. Acta*, 31 (1959) 539–541.
2 H. C. McAllister, Jr., Y. C. Wan and J. L. Irvin, *Anal. Biochem*, 5 (1963) 321–329.
3 M. G. Ord, J. H. Raaf, J. A. Smit and L. A. Stocken, *Biochem. J.*, 95 (1965) 321–331.
4 A. Macpherson and K. Murray, *Biochim. Biophys. Acta*, 104 (1965) 574–580.
5 G. F. Vande Woude and F. F. Daivs, *Anal. Biochem.*, 12 (1965) 441–451.
6 G. R. Shepherd and L. R. Gurley, *Anal. Biochem.*, 14 (1966) 356–363.
7 L. R. Gurley and G. R. Shepherd, *Anal. Biochem.*, 14 (1966) 364–375.
8 S. Panyim and R. Chalkley, *Arch. Biochem. Biophys.*, 130 (1969) 337–346.
9 E. L. Smith, R. J. DeLange, and J. Bonner, *Physiol. Rev.*, 50 (1970) 159–170.
10 L. R. Gurley and R. A. Walters, *Biochemistry*, 10 (1971) 1588–1593.
11 L. A. Boland and E. W. Johns, *Eur. J. Biochem.*, 35 (1973) 546–553.
12 L. R. Gurley, J. A. D'Anna, S. S. Barham, L. L. Deaven and R. A. Tobey, *Eur. J. Biochem.*, 84 (1978) 1–15.
13 R. M. McCormick, *Anal. Chem.*, 60 (1988) 2322–2328.
14 V. Berry and R. Shansky, *LC · GC*, 7 (1989) 860–865.
15 V. Berry, R. Shansky and P. Kinkade, *LC · GC*, 7 (1989) 929–931.
16 R. A. Tobey, D. F. Peterson, E. C. Anderson and T. T. Puck, *Biophys. J.*, 6 (1966) 567–581.
17 L. R. Gurley, J. G. Valdez, D. A. Prentice and W. D. Spall, *Anal. Biochem.*, 129 (1983) 132–144.
18 L. R. Gurley, M. D. Enger and R. A. Walters, *Biochemistry*, 12 (1973) 237–245.
19 P. S. Jackson and L. R. Gurley, *J. Chromatogr.*, 326 (1985) 199–216.
20 L. R. Gurley, D. A. Prentice, J. D. Valdez and W. D. Spall, *Anal. Biochem.*, 131 (1983) 465–477.
21 L. R. Gurley, W. D. Spall, J. G. Valdez, P.S. Jackson, J. Meyne and F. A. Ray, in K. M. Gooding and F. E. Regnier (Editors), *HPLC of Biological Macromolecules* (*Chromatographic Science Series*, Vol. 51) Marcel Dekker, New York, 1990, pp. 529–570.
22 L. R. Gurley, D. A. Prentice, J. G. Valdez and W. D. Spall, *J. Chromatogr.*, 266 (1983) 609–627.
23 S. Hjertén, *J. Chromatogr.*, 347 (1985) 191–198.
24 J. S. Green and J. W. Jorgenson, *J. Chromatogr.*, 352 (1986) 337–343.
25 G. J. M. Bruin, J. P. Chang, R. H. Kuhlman, K. Zegers, J. C. Kraak and H. Poppe, *J. Chromatogr.*, 471 (1989) 429–436.
26 J. D. Olechno, J. M. Y. Tso, J. Thayer, and A. Wainright, *Am. Lab.*, 22, No. 18, Dec. (1990) 30–37.
27 S. Hjertén, S. Jerstedt and A. Tiselius, *Anal. Biochem.*, 11 (1965) 219–223.

Journal of Chromatography, 559 (1991) 445–453
Elsevier Science Publishers B.V., Amsterdam

CHROM. 23 470

Rapid protein analysis by capillary electrophoresis

FU-TAI A. CHEN
BAT, Beckman Instruments Inc., 2500 Harbor Blvd. D-20-A, Fullerton, CA 92634 (USA)

ABSTRACT

Rapid protein analysis by free-zone capillary electrophoresis in an untreated fused-silica column is presented. Separation of model proteins by the proposed method shows that the retention times of these proteins correlate well with each of their isoelectric points. By using a high voltage gradient, most proteins could be separated in 200 s with excellent reproducibility. Similarly, human serum proteins could be resolved and determined in less than 100 s.

INTRODUCTION

Zone electrophoresis on paper, starch gel, cellulose acetate, agarose and polyacrylamide gels has been used for the separation of proteins and polynucleotides during the last 40 years. It is one of the most important and versatile tools for the structural analysis of proteins and DNA. Analysis of the resulting gel required staining with a dye to reveal the molecules, or the molecules are labelled with radioisotopes or fluorphores. It is a labor-intensive, skill-dependent and a relative slow procedure. Recent developments with capillary columns represent an important technical advance in analytical zone electrophoresis [1]. It is well suited for automation with real-time data analysis. Sample amounts are in the nanoliter range, and microliters of buffer reagent are consumed for each run.

Earlier attempts to electrophorese proteins in untreated fused-silica capillaries resulted in broad and irreproducible migration of all sample zones [2]. Protein–silica surface interaction, and ion-exchange mechanism proposed by Lauer and McManigill [3] and Green and Jorgenson [4], is believed to be responsible for degrading the efficiency and reproducibility of protein separation. Thus, the separation of proteins by capillary electrophoresis (CE) requires the buffer pH to be above the isoelectric points of the sample proteins [3] or below 2.5 [5] or under neutral conditions with high ionic strength [2]. Chemical modification of the silica surface resulted in many successful high-efficiency protein separations under limited pH conditions [6–8]. The object of this work was to perform protein analysis by CE, reproducibly, with high efficiency, in an untreated fused-silica column. This paper summarizes our approach to rapid protein separations by CE.

0021-9673/91/$03.50

EXPERIMENTAL

Materials

All model proteins were obtained from Sigma Biochemicals (St. Louis, MO, USA) and Serva Biochemicals (Westbury, NY, USA). Protein samples were dissolved in buffer containing 75 m*M* sodium chloride, 20 m*M* potassium phosphate and 0.01% sodium azide (PBS). Each protein concentration was 200–500 μg/ml. Serum samples were diluted 1:20 in PBS. Dimethylformamide (DMF) (0.01%, v/v) was added to the sample diluent as a neutral marker.

Capillary electrophoresis system

A P/ACE 2000 system (Beckman, Palo Alto, CA, USA) was used with P/ACE system software controlled by an IBM PS/2 Model Z-50 computer. Data analysis was performed on System Gold™ software (Beckman, San Ramon, CA, USA). The P/ACE 2000 system contains built-in 200-, 206-, 214-, 280- and 340-nm narrow-band filters for on-line detection and quantification. Electrophoreses were performed in a fused-silica tube, 25 or 37 cm × 25 μm I.D., supplied by Polymicro Technologies (Phoenix, AZ, USA). The detection window is located at 6.5 cm from the column outlet. The capillary was assembled in the Beckman cartridge format.

Capillary electrophoresis procedures

Samples were placed on the inlet tray of the P/ACE 2000 instrument and introduced into the capillary by pressure injection for 8–10 s. The system can be programmed to run samples in a random access manner for up to ten different assay methods. Proteins were monitored at 200 or 206 nm. The temperature of the capillary during electrophoresis was kept constant at 22°C. The buffer used for model protein separation was 150 m*M* borate of pH 10.5 and 100 m*M* borate of 11.5. The buffer for human serum protein analysis was a Beckman proprietary buffer of pH 10.0. All buffers were filtered through a 0.45-μm filter. Between runs, the capillary was washed with 1.0 *M* sodium hydroxide solution and water, followed by reconditioning with running buffer. All the washing, rinsing and reconditioning procedures were performed on the P/ACE system.

RESULTS AND DISCUSSION

Protein analysis by CE under both high salt buffer and high pH conditions can achieve a fast separation without compromising resolution. Borate buffer of 150 m*M* (pH 10.5) allows the separation of protein species by CE with moderate success, as shown in Fig. 1. Peak-width analysis indicates significant protein–silica surface interactions. Titration of proteins such as ribonuclease showed that the pK_a of the side-chain amino group in the lysine residue is between 10 and 10.2 whereas that of the guanidyl group of arginine residues is well above 12.0 [9]. Hence, a significant portion of most protein contains positively charged moieties at a buffer pH of 10.5. Increasing the pH of the borate buffer to 11.5 reduces the number of positively charged side-chain lysine moieties sifnigicantly (by *ca.* one order of magnitude). A well resolved separation of the same protine mixture could be achieved simply by raising the pH of the borate buffer to 11.5, as shown in Fig. 2. Fig. 3A shows the separation of another

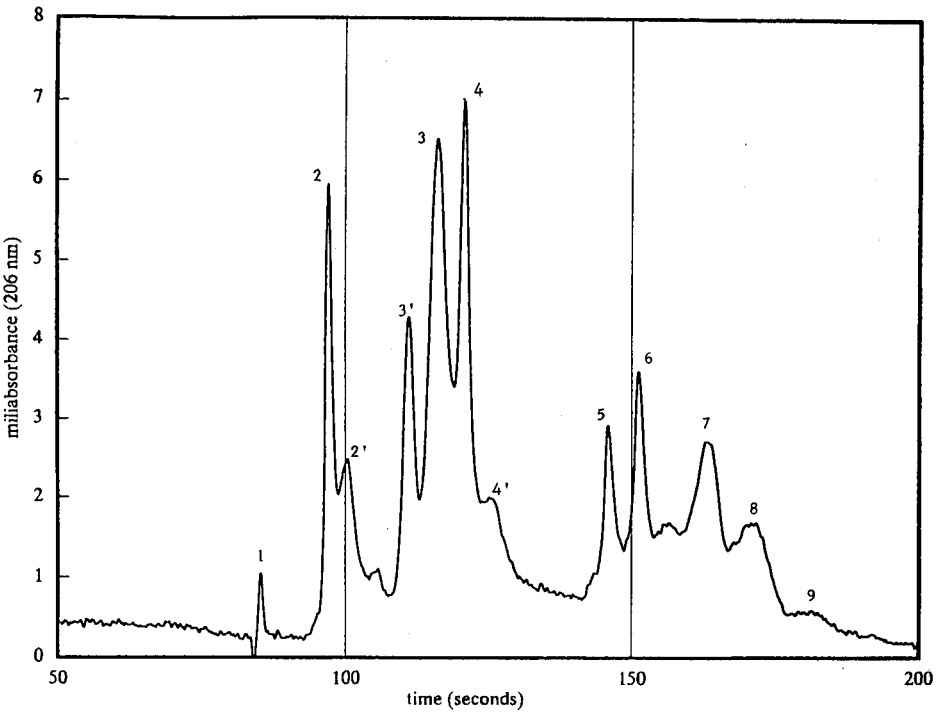

Fig. 1. Electropherogram of model proteins. Conditions: untreated fused-silica capillary, 25 cm × 25 μm I.D.; applied potential, 15 kV; buffer, 150 m*M* borate (pH 10.5). Peaks: 1 = DMF (neutral marker); 2 = bovine ribonuclease A; 3 = whale myoglobin; 4 = horse myoglobin; 5 = conalbumin; 6 = β-lactoglobulin; 7 = bovine serum albumin; 8 = ferritin; 9 = α-amyloglycosidase. Peaks 2′, 3′ and 4′ are impurities from 2, 3 and 4, respectively.

model protein mixture with a separation efficiency of more than 100 000 theoretical plates for all protein species. Addition of bovine ribonuclease to the above protine mixture (Fig. 3B) shows that its p*I* can be estimated to be 9.5.

Analysis of human serum protein by CE in an untreated capillary column has been attempted [10,11]. Our group has achieved a serum protein analysis by CE that reproduces the separation patterns obtained by using conventional agarose gel-based electrophoresis. With a high voltage gradient of 800 V/cm, a fast serum protein separation is achieved in less than 100 s without compromising the resolution (Fig. 4). Each of the serum protein fractions can be clearly identified; γ-globulin appears first, followed by β, α_2- and α_1-globulin, albumin and a minute amount of prealbumin.

A substantially better resolution of serum protein separation can be obtained with a higher ionic strength of the same buffer, as is evident from Fig. 5. Good resolution is evident for both the β- and α-globulin regions. Transferrin is resolved from β-lipoprotein and haptoglobin appears well above the shoulder of α_2-macroglobulin. The addition of a high salt concentration to the buffer appears to minimize protein–protein interactions which may be responsible for peak broadening in protein separation by CE in general.

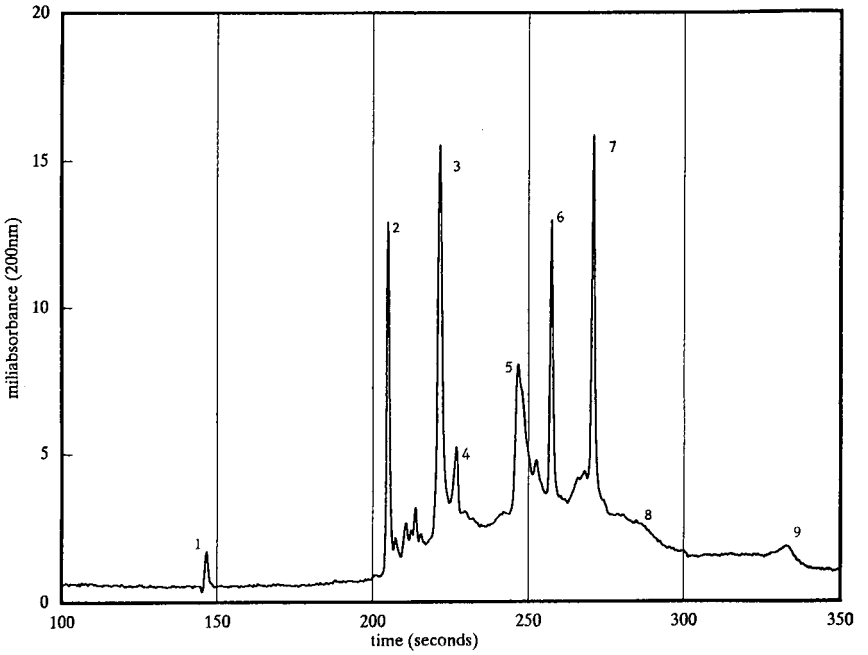

Fig. 2. Electropherogram of model proteins as in Fig. 1. Conditions: untreated fused-silica capillary 37 cm × 25 μm I.D.; applied potential, 12 kV; buffer, 100 m*M* borate (pH 11.5).

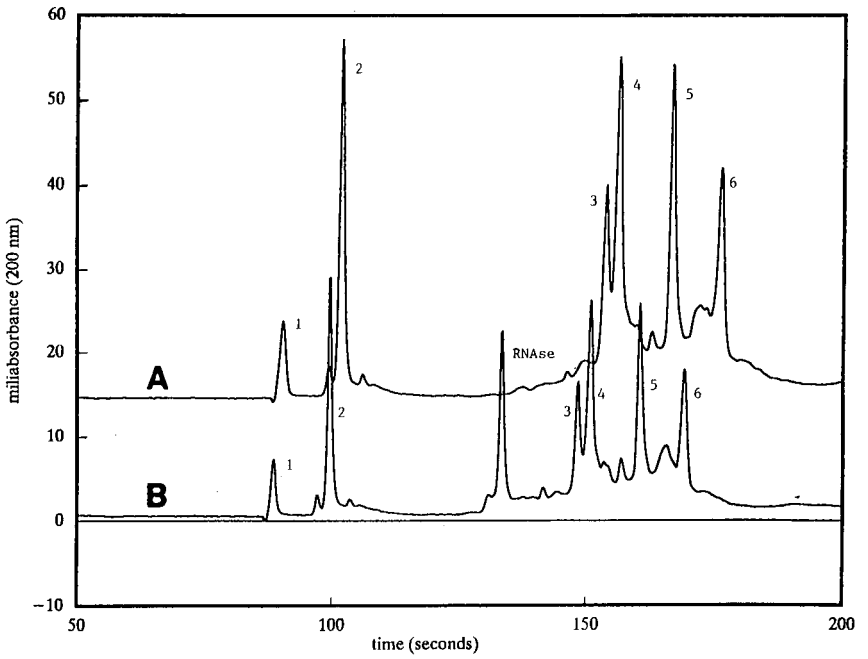

Fig. 3. Electropherogram of model proteins. Conditions: untreated fused-silica capillary, 25 cm × 25 μm I.D.; applied potential, 15 kV; buffer, 100 m*M* borate (pH 11.5). Peaks: (A) 1 = DMF; 2 = bovine trypsin inhibitor; 3 = whale myoglobin; 4 = human carbonic anhydrase; 5 = bovine carbonic anhydrase; 6 = soybean trypsin inhibitor; (B) same as (A) with addition of bovine ribonuclease A between peaks 2 and 3 at 130 s.

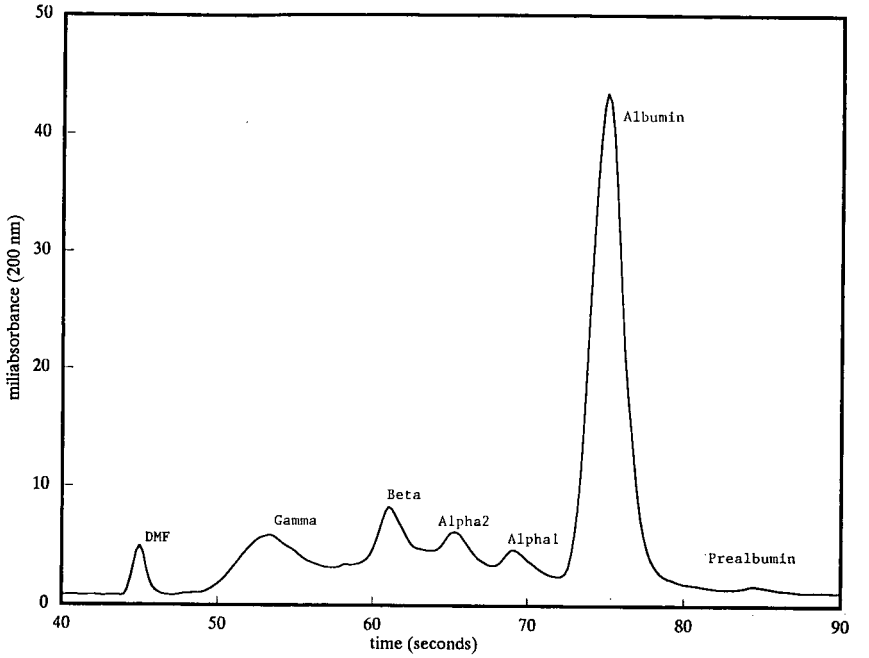

Fig. 4. Electropherogram of a normal control serum protein. Conditions: untreated fused-silica capillary, 25 cm × 25 μm I.D.; applied potential, 20 kV; buffer, pH 10.0.

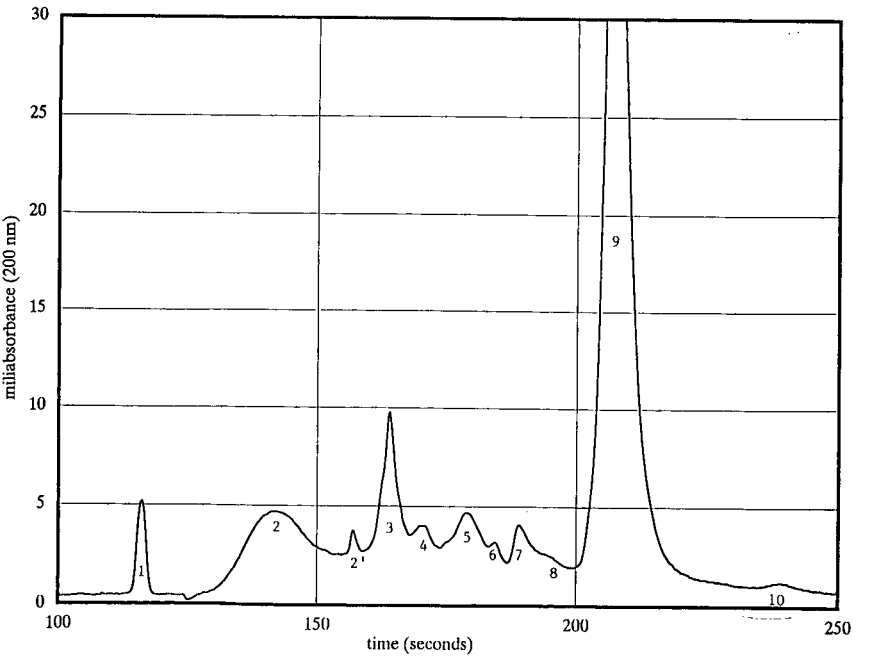

Fig. 5. Electropherogram of a normal control serum protein. Conditions: untreated fused-silica capillary 25 cm × 25 μm I.D. applied potential, 10 kV; buffer, as in Fig. 4 with a higher buffer strength (pH 10.0). Peaks: 1 = DMF; 2 = γ-globulin; 3 = transferrin; 4 = β-lipoproteins; 5 = haptoglobin; 6 = α_2-macroglobulin; 7 = α_1-antitrypsin; 8 = α_1-lipoproteins; 9 = albumin; 10 = prealbumin; 2′ = complements.

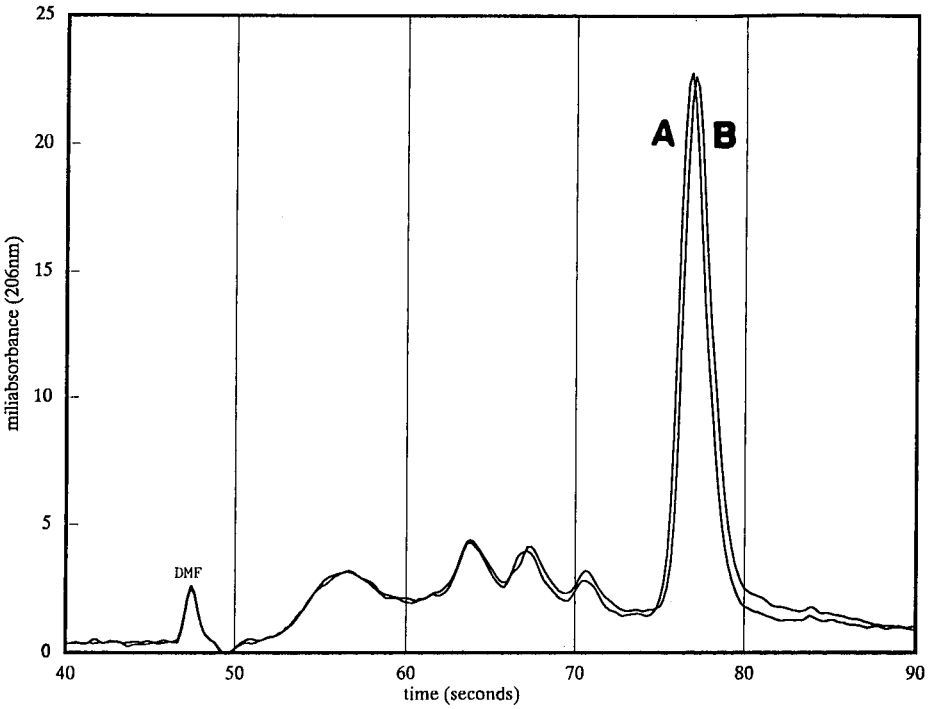

Fig. 6. Reproducibility of rapid capillary electrophoresis: (A) first run; (B) ninth run. Conditions as in Fig. 4.

The reproducibility of serum protein separation by capillary electrophoresis with nine-repeated runs is exhibited in Fig. 6. Between runs, the capillary was washed with base and water. The relative standard deviation (R.S.D.) of the migration time of each protein fraction is less than 1% regardless of the voltage gradient, as shown in Fig. 7. Washing of the capillary between runs ensures reproducibility. Without washing, however, the R.S.D. of the migration time of each protein fraction is significantly higher at a voltage gradient of 200 V/cm, as shown in Fig. 8A. Presumably a slow build-up of proteins on the capillary wall is responsible for the gradual increase in migration time. At a voltage gradient of 800 V/cm, the R.S.D. of the migration time of each protein fraction is less than 1% with nine repeated runs, regardless of post-run washing (Figs. 7B and 8B). Rapid serum protein separation results in a shorter residence time of protein species in the capillary, which may be responsible for reduced protein adsorption on the capillary wall.

In conclusion, the results presented demonstrate the utility of rapid protein analysis by capillary electrophoresis in an untreated fused-silica column. With a high salt concentration and a high pH buffer, the apparent isoelectric point of an unknown protein can be determined. A fast protein separation by CE has been achieved without compromising resolution. The potential of this method for clinical diagnostic applications, serum protein analysis in particular, is promising.

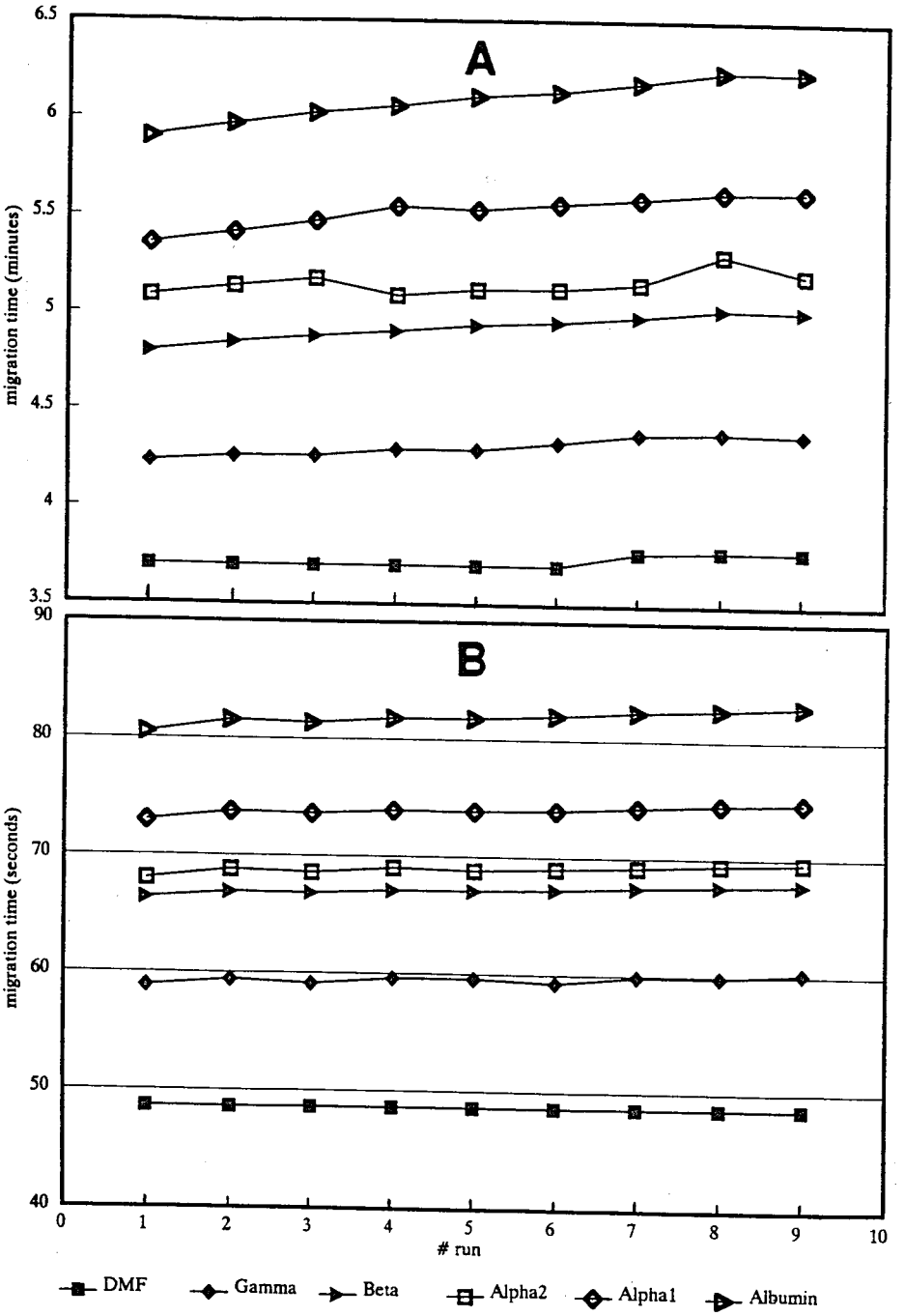

Fig. 7. Migration time of each protein fraction with washed capillary for nine repeated runs. Conditions as in Fig. 4 except the voltage gradients were (A) 200 and (B) 800 V/cm.

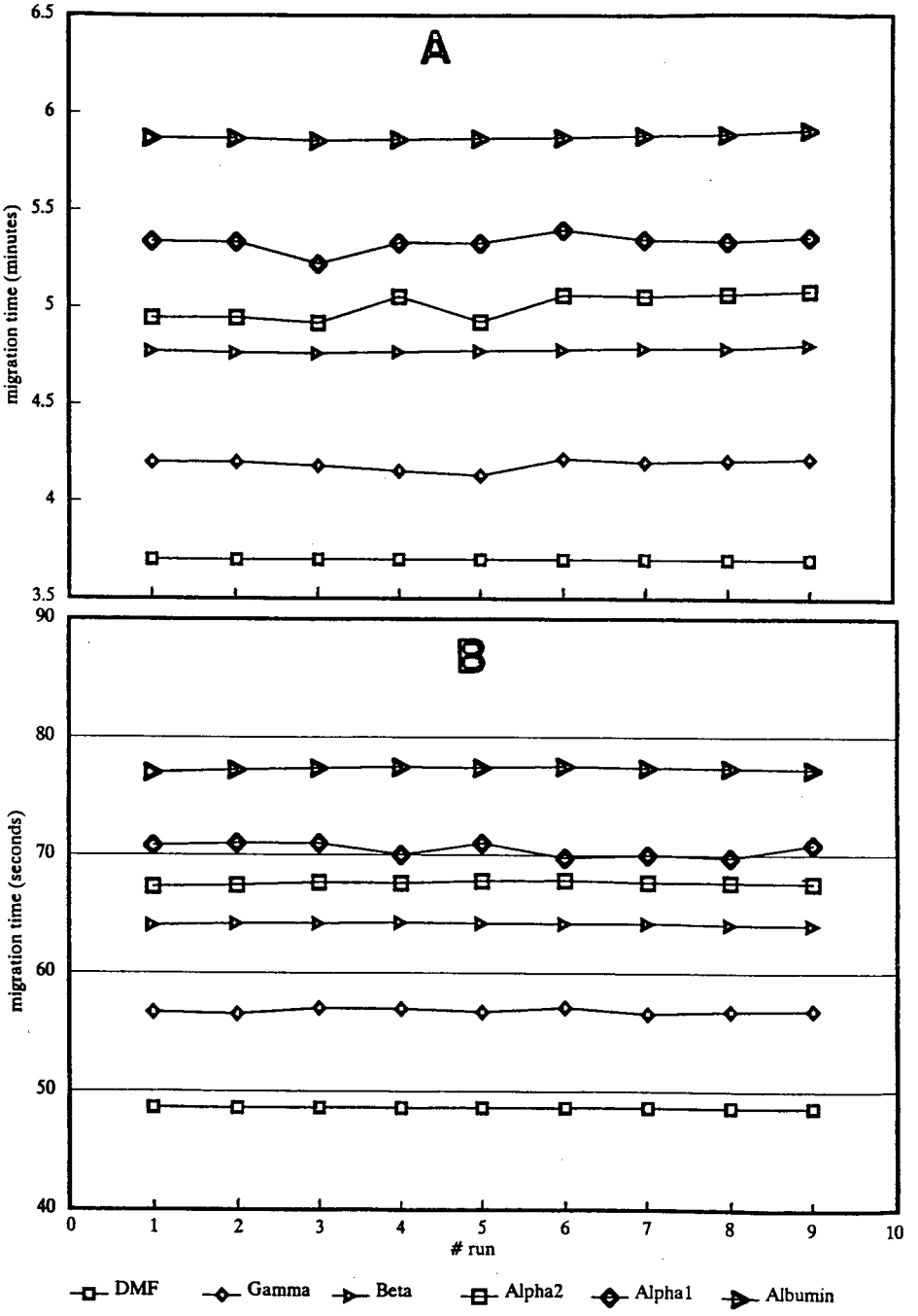

Fig. 8. Migration time of each protein fraction with unwashed capillary for nine repeated runs. Conditions as in Fig. 4 except the voltage gradients were (A) 200 and (B) 800 V/cm.

ACKNOWLEDGEMENT

I express many thanks to Dr. Jim Sternberg for his continuing interest in and encouragement of this work.

REFERENCES

1 J. W. Jorgenson and K. D. Lukacs, *Science, (Washington, D.C.)*, 222 (1983) 266.
2 J. W. Jorgenson and K. D. Lukacs, *Anal. Chem.*, 53 (1981) 1298.
3 H. H. Lauer and D. McManigill, *Anal. Chem.*, 58 (1986) 166.
4 J. S. Green and J. W. Jorgenson, *J. Chromatogr.*, 478 (1989) 41.
5 R. McCormick, *Anal. Chem.*, 60 (1988) 2322.
6 S. Hjerten, *J. Chromatogr.*, 347 (1985) 191.
7 M. Novotny, K. A. Cobb and J. Liu, *Electrophoresis*, 11 (1990) 735.
8 J. K. Towns and F. Regnier, *J. Chromatogr.*, 516 (1990) 69.
9 C. Tanford and J. D. Hauenstein, *J. Am. Chem. Soc.*, 78 (1956) 5287.
10 F.-T. A. Chen, C. M. Liu, Y. Z. Hsieh and J. C. Sternberg, *Clin. Chem.*, 37 (1991) 14.
11 M. J. Gordon, K.-J. Lee, A. A. Arias and R. N. Zare, *Anal. Chem.*, 63 (1991) 69.

Journal of Chromatography, 559 (1991) 455–465
Elsevier Science Publishers B.V., Amsterdam

CHROM. 23 489

Capillary electrophoresis for diagnosis and studies of human disease, particularly metabolic disorders

EGIL JELLUM*, ANNE KARINE THORSRUD and ELLEN TIME
Institute of Clinical Biochemistry, Rikshospitalet, 0027 Oslo 1 (Norway)

ABSTRACT

High-performance capillary electrophoresis (HPCE) has been used in a multicomponent analytical system designed to diagnose and study human diseases, particularly metabolic disorders. Comparative analyses, using HPCE, high-performance liquid chromatography (HPLC) and an automated amino acid analyser, were carried out on urine and blood samples from patients with homocystinuria, cystinuria, glutathione synthetase deficiency and adenylosuccinase deficiency. HPCE of the sulphur-containing amino compounds, derivatized with monobromobimane and detected by fluorescence spectroscopy, was a quick and simple alternative to classical amino acid analysis. The detection of the characteristic succinylpurines associated with adenylosuccinase defect was equally well achieved with HPLC and HPCE (absorbance detector). Owing to the possible connection between deficiency of taurine (2-amino-1-ethanesulphonic acid) in the heart and the development of cardiomyopathy and heart failure, a simple HPCE method was developed for the determination of taurine in sub-milligram samples of biopsies of the myocardium. The homologue 3-amino-1-propanesulphonic acid was the internal standard, and derivatives of 9-fluorenylmethyl chloroformate and fluorescence detection were used. It is suggested that the potential of HPCE to analyse small volumes should be exploited in biomedicine and clinical diagnosis to analyse sub-milligram samples of tissue biopsies and cells.

INTRODUCTION

Several human diseases, in particular metabolic disorders, often lead to the accumulation of characteristic metabolites in serum, urine and cells. Multicomponent analytical techniques, including chromatography and electrophoresis, are suitable to detect diagnostically important changes in the biochemical "profiles" thus obtained. The profiling techniques currently used in this laboratory include gas chromatography (GC), gas chromatography–mass spectrometry (GC–MS), high-performance liquid chromatography (HPLC) with a computerized diode-array detector, automated amino acid analysis and high-resolution two dimensional electrophoresis. DNA techniques (Southern blotting and polymerase chain reaction) and certain enzyme assays have also been included in the analytical system. The techniques currently in use [1,2] can diagnose more than 100 different disorders.

The latest addition to the analytical repertoire in this laboratory is high-performance capillary electrophoresis (HPCE) [3]. Comparative studies have been carried out to learn more about the potential of HPCE in the clinical laboratory. Some

0021-9673/91/$03.50

disorders related to the metabolism of amino acids, nucleotides and the tripeptide glutathione have been selected for this purpose, and HPCE has been used to determine taurine (2-amino-1-ethanesulphonic acid) in sub-milligram samples of biopsies of heart muscle.

EXPERIMENTAL

Chemicals

Monobromobimane (MB; Thiolyte) was from Calbiochem. (La Jolla, CA, USA). L-Cysteine, L-cystine, D,L-homocysteine, DL-homocystine, reduced glutathione (GSH), dithiothreitol (DTT, Clelands's reagent), taurine and 3-amino-1-propanesulphonic acid were from Sigma (St. Louis, MO, USA). 9-Fluorenylmethyl chloroformate (FMOC) was from Fluka (Buchs, Switzerland). All other chemicals were commercial products of analytical-reagent grade.

Instruments

The HPCE equipment used for most of the analysis was made by SpectroVision (Chelmsford, MA, USA) and consisted of a DA-30 power supply (maximum 30 kV), an FD-300 dual monochromator fluorescence detector and a DS-4 sample delivery system. Manual injection was performed using the electrokinetic technique. The capillary was 40 cm × 0.075 mm I.D. in most of the experiments, except in Fig. 4, where a 0.10 mm I.D. capillary was used. The applied voltage was about 24 kV, giving a current of approximately 150 μA using 0.05 mol/l sodium phosphate buffer at pH 7.5. The fluorescence detector was set at 375 nm (excitation) and 480 nm (emission) for measuring the MB-labelled compounds, and the corresponding settings were 265 and 305 nm for the FMOC-labelled compounds.

In some experiments (see Fig. 6) a Beckman P/ACE Systems 2000 HPCE instrument, version 1.50 (Beckman Instruments, Palo Alto, CA, USA) was used (kindly made accessible by Knut Sletten and Vidar Syversen, Biotechnology Center, University of Oslo, Oslo, Norway). The absorbance detector was set at 214 nm, the capillary was 0.075 mm I.D. and a constant voltage of 20 kV gave a current of about 90 μA using a 0.05 mol/l sodium phosphate buffer, pH 2.5. Pressure injection for 3.8 s, giving a volume of about 20 nl, was used.

The HPLC instrument was an LDC liquid chromatograph with two Consta-Metric pumps (Laboratory Data Control, FL, USA) and the diode-array detector was a 2140 rapid spectral detector (LKB, Bromma, Sweden) with an IBM-XT personal computer. The column was of the reversed-phase LC-18 type. Details of the experimental procedures used for the HPLC analysis of urine have been described elsewhere [1,2].

The GC–MS instrument was a Hewlett-Packard 5970 mass-selective detector coupled to a gas chromatograph with an automated sample injection system (HP 5890 GC with HP 7673A 100 sample injector) and an HP 300 data system. A 30 m fused-silica capillary column coated with SP-1000 (Supelco, Bellefonte, PA, USA) was used. The experimental procedures have been described elsewhere [1,2].

A Biotronic automatic amino acid analyser (Biotronic, Maintal, Germany) with an ion-exchange chromatography column and classical post-column ninhydrin detection was used. All samples, including urine, were deproteinized with sulphosal-

icylic acid prior to analysis [1,2]. The total elution time was about 130 min; the total cycle time, including the regeneration of the ion-exchange column, was about 180 min.

Standards

The standard solution of thiol-containing compounds contained 0.2 mmol/l each of cysteine, homocysteine, GSH and the drug penicillamine, in 0.05 mol/l phosphate buffer, pH 7.5. To prevent oxidation of the thiol groups, DTT was added to a final concentration of 0.8 mmol/l. For MB derivatization, 15 μl of Thiolyte MB in acetonitrile (50 mmol/l) were added to 250 μl of standard solution and injected into the HPCE instrument after 10 min.

Standard solutions (5 mmol/l) of taurine and the internal standard (3-amino-1-propanesulphonic acid), in 0.05 mol/l phosphate buffer, pH 7.5, were used. For derivatization 10 μl of each standard were mixed with 50 μl of the FMOC reagent (5 mmol/l, dissolved in acetonitrile) and 50 μl of 0.05 mol/l phosphate buffer, pH 7.5. After 20 min at room temperature the derivatization was complete.

Urine analysis: thiol compounds

Urine samples were reduced with DTT (2.5 mmol/l of urine) for 15 min, diluted with equal parts of the running buffer (sodium phosphate buffer, 0.05 mol/l), adjusted to pH 7.5, and filtered through a 0.22-μm filter. To an aliquot (250 μl) of each filtrate, 50 μl of Thiolyte MB in acetonitrile (50 mmol/l) were added. Injection was performed after 10 min.

Analysis of red blood cells: thiol compounds

Red cells from centrifuged citrate blood (15 min at 2500 rpm, 750 *g*) were diluted with equal parts of water and further lysed by freezing and thawing. Proteins were precipitated by the addition of a perchloric acid solution (1 mol/l) and removed by centrifugation. The supernatant was neutralized to pH 7.5, reduced with DTT, filtered and labelled with MB as described for urine.

Direct analysis of urine: UV-absorbing compounds

Urine from healthy controls and from patients with various metabolic disorders was analysed directly after filtration through a 0.22-μm filter and centrifugation to remove air bubbles.

Determination of taurine in heart muscle biopsies

Human heart biopsies, 1–3 mg, sufficient for several analyses, were obtained by standard surgical procedures routinely performed in this hospital. Rat heart biopsies were also used during method development. The sample size generally used for taurine determination was about 0.5–1 mg of tissue. After weighing the biopsies, the internal standard (3-amino-1-propanesulphonic acid) was added and the mixture was homogenized in 50 μl of phosphate buffer (0.05 mol/l, pH 7.5) in a specially designed glass micro-homogenizer with a ground glass, manually operated pestle. To the homogenate was added perchloric acid (20 μl of a 1 mol/l solution) and the precipitated proteins were removed by centrifugation (Beckman Microfuge). The supernatant was neutralized to pH 7.5 with a few microlitres of 1 mol/l aqueous trisodium phosphate

solution and mixed with a five-to-ten-fold excess on a molar basis of the FMOC reagent (5 mmol/l in acetonitrile). After 20 min at room temperature the derivatized amino compounds were separated by HPCE and detected by fluorescence spectroscopy as described.

RESULTS

Diagnosis of some disorders related to thiol-containing amino compounds

Separation of standards. HPCE gives a baseline separation of MB-labelled homocysteine, cysteine, the drug penicillamine and the tripeptide GSH (elution order) in less than 10 min, as shown in Fig. 1. The reagents, MB and DTT, are eluted together in the first peak, well separated from the other four compounds.

Homocystinuria. This is a disorder with various causes, all resulting in the accumulation of homocyst(e)ine in serum and urine. Clinical symptoms include disloca-

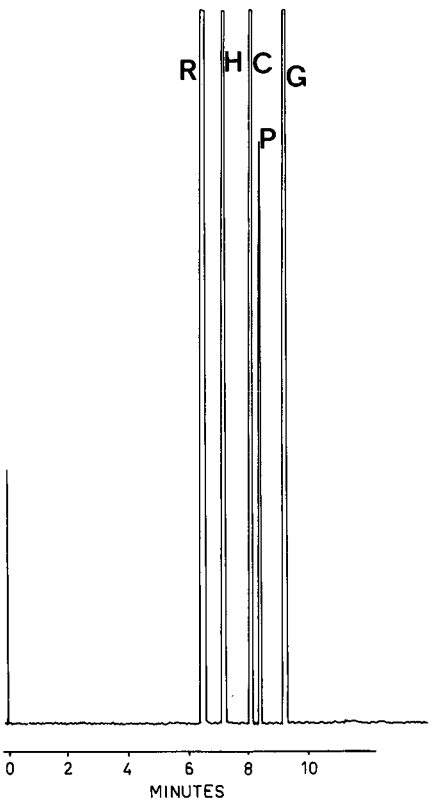

Fig. 1. Separation of thiol-containing compounds by HPCE. The standard compounds were derivatized with MB as described in the text. A SpectroVision HPCE instrument with a fluorescence detector was used, and the capillary was 40 cm × 0.075 mm I.D. A voltage of 25 kV gave a current of about 150 μA (0.05 mol/l phosphate buffer, pH 7.5). Peaks: R = reagent peak; H = homocysteine; C = cysteine; P = penicillamine; G = glutathione.

tion of the eye-lens, osteoporosis, lengthening of the bones and increased tendency to thrombosis [4]. The underlying biochemical defect may be cystathionine β-synthetase deficiency (the most frequent), or other mechanisms including failure to remethylate homocysteine to methionine [4]. Fig. 2A shows the diagnosis of homocystinuria (remethylation defect) using traditional amino acid analysis with ion-exchange chromatography and post-column ninhydrin detection. The control urine did not contain detectable amounts of homocystine, in contrast to that of the patient. The HPCE electropherogram of DTT-reduced and MB-labelled urine from the same patient is shown in Fig. 2B. Only three peaks are seen, corresponding to the reagent peak, homocysteine and cysteine. The increased cysteine peak, compared to controls, is secondary and is usually seen in homocystinuria.

Cystinuria. This is due to a defect in the cellular transport mechanism of the dibasic amino acids cystine, lysine, ornithine and arginine [5]. The defect leads to a high concentration of these four amino acids in urine because their normal reabsorption mechanism in the kidneys does not function. Cystine is only sparingly solu-

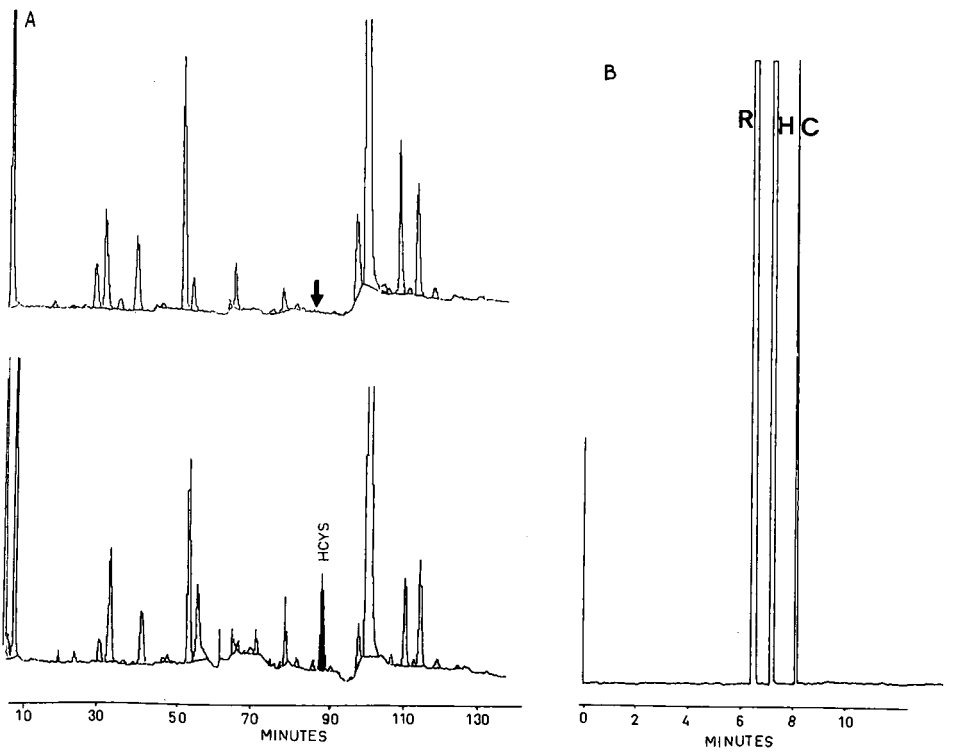

Fig. 2. (A) Amino acid analysis by classical ion-exchange chromatography of urine from a control (upper panel) and a patient with homocystinuria (lower panel). (B) HPCE analysis of urine from the patient. The sample was reduced with DTT and derivatized with MB before separation. Experimental conditions and symbols as described in the text and in Fig. 1.

ble in water, and when the concentration in urine exceeds about 300 mg/l at pH 6, crystallization may begin. Kidney-stone formation is therefore the usual clinical symptom in classical cystinuria. Variant forms of this disorder are also known [5].

The laboratory diagnosis of cystinuria is usually carried out in two steps. First, a simple colour test is performed using sodium nitroprusside after the addition of a reducing agent to the urine. Following a positive test (red colour), quantitative amino acid analysis is required to differentiate between cystinuria and homocystinuria (the latter also gives a positive nitroprusside test). Fig. 3A shows a typical amino acid chromatogram of urine from a patient with cystinuria, with large amounts of the four dibasic amino acids being excreted. The mixed disulphide homocysteine–cysteine is usually a secondary finding, as seen from the figure. Fig. 3B shows the separation by HPCE of the DTT-reduced and MB-labelled compounds. Large amounts of cysteine and some homocysteine are seen, and as only thiol groups react with the MB-reagent, no other amino acids show up on the electropherogram. Note the difference in elution time; this is about 130 min in the classical amino acid analysis and less than 10 min for the HPCE separation.

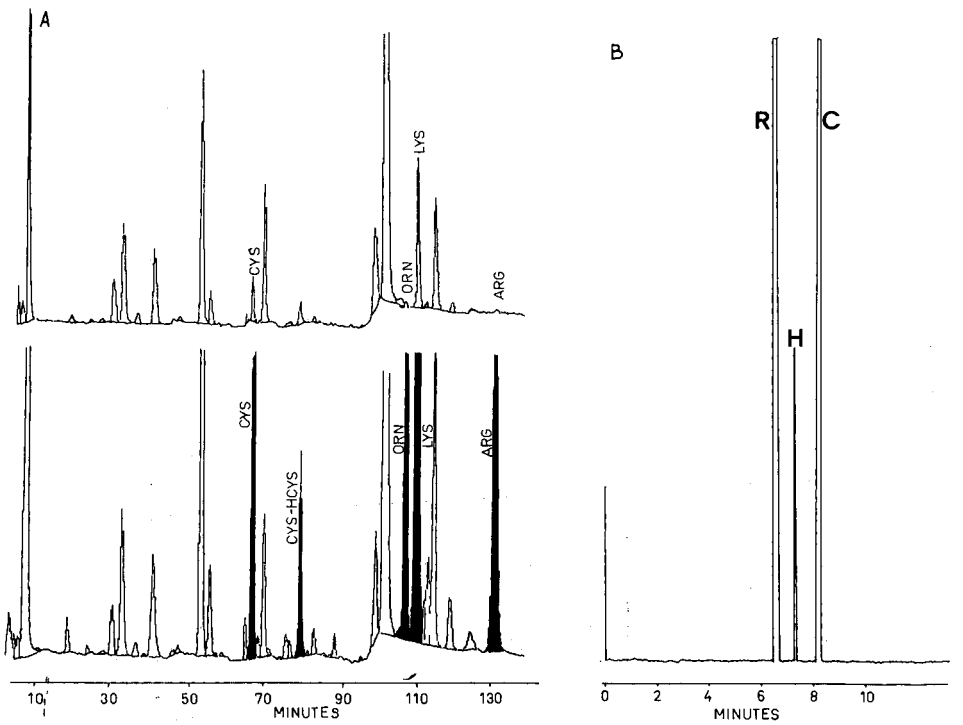

Fig. 3 (A) Amino acid analysis by classical ion-exchange chromatography of urine from a control (upper panel) and a patient with cystinuria (lower). (B) HPCE analysis of urine from the patient. The sample was reduced with DTT and derivatized with monobromobimane before separation. Experimental conditions and symbols as in Fig. 1.

Glutathione synthetase deficiency. Glutathione synthetase deficiency [6] or "pyroglutamic aciduria" as the disease was called previously [7], is associated with the massive urinary excretion of 5-oxoproline (pyroglutamate), severe metabolic acidosis and defective central nervous system function, sometimes of fatal consequence. The enzyme defect causes a deficiency of the tripeptide GSH (GSH = τ–Glu–Cys–Gly) in all cells, with overproduction of 5-oxoproline in a modified τ-glutamyl cycle as a secondary consequence [6]. GSH is believed to exert anti-oxidant properties and a lack of this protectant may lead to the oxidative damage of cells, particularly in the brain.

Laboratory diagnosis of this disorder includes the identification of large amounts (up to 30 g/l) of 5-oxoproline in urine using GC–MS [7]. GSH is normally present at a high concentration (2–3 mmol/l) in all cells [6], but is normally absent in serum and urine. The second step in the laboratory diagnosis, following the finding of 5-oxoproline in the urine, is therefore to confirm the lack of GSH in cells. Red blood cells are often the material of choice, and classical amino acid analysis gives the confirmatory diagnosis, *i.e.* lack of GSH (and its oxidized form). The same result can be achieved in a simpler and much faster way using HPCE, as shown in Fig. 4. The lack of GSH in the red cells of the patient compared with control is readily seen. Note that because MB-labelling which only reacts with thiol groups is used, and as GSH

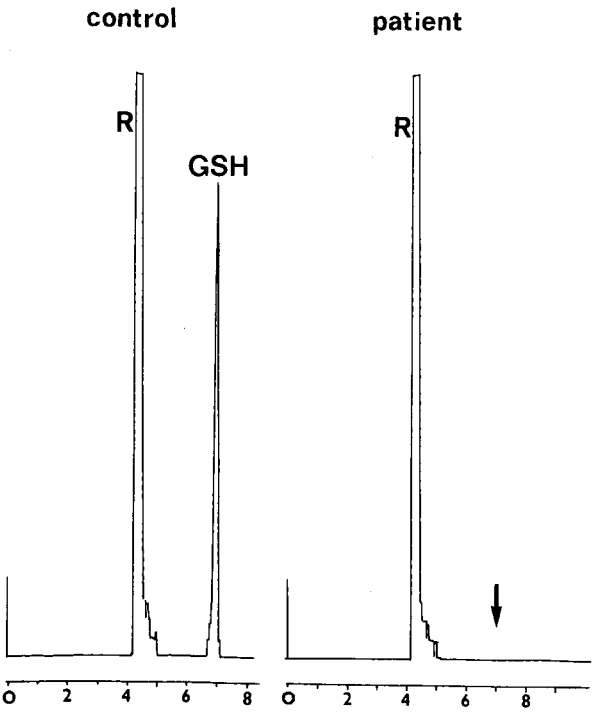

Fig. 4. HPCE analysis of GSH in red blood cells from a control (left) and a patient with GSH synthetase deficiency (right). Experimental procedures as described in the text. The capillary was 40 cm × 0.10 mm I.D., which explains the retention times being slightly different from those shown in Fig. 1. Note the absence of GSH in the cells of the patient.

normally is present at very high concentrations compared with most other cellular constituents, the only peak that is clearly visible at the attenuation level used is the GSH peak.

Adenylosuccinase deficiency. This is a rare disorder in the biosynthesis of purine nucleotides and gives rise to severe psychomotor delay and autism [8]. The diagnostic metabolites present in increased amounts in urine are the succinylpurines adenylosuccinate and succinylamino-imidazole-carboxamid ribotide. These compounds are readily detected by HPLC [1,8], but not by GC–MS. Urine from a patient with this disorder was first analysed in this laboratory by a routine HPLC system with diode-array detection, and then by HPCE using UV absorbance detection as described earlier. (The urine sample was kindly provided by Dr. Jaeken, University of Leuven, Leuven, Belgium.)

Figs. 5 and 6 show that the separation time (13–16 min) and efficiency of the HPLC and HPCE techniques are comparable, the former giving a more reliable identification due to the use of diode-array detection and spectral comparison. Sample pre-treatment included clean-up on a Bond Elute cartridge before HPLC [1], but filtration only (0.22-μm filter) before HPCE.

HPCE determination of taurine in biopsies of heart muscle

Recent reports [9–11] have caused an increased interest in the aminosulphonic acid taurine [NH_2–CH_2–CH_2–SO_3H], because of its possible role in the development of cardiomyopathy. It now seems clear that this compound is an essential amino acid in cats. Taurine-depleted cats develop retinal degeneration, cardiomyopathy, altered white-cell function and abnormal growth and development [11]. Evidence for a taurine-deficiency cardiomyopathy in humans is also beginning to appear [10], and there seems to be a direct link between decreased taurine concentration in the myocardium and decreased myocardial mechanical function, at least in the cat [9].

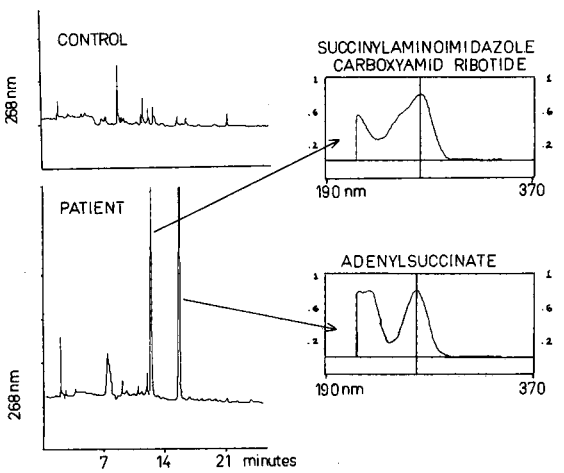

Fig. 5. Left: HPLC profiles of urine from a control (upper panel) and a patient with adenylosuccinase deficiency (lower panel). Right: Characteristic absorption spectra of the excreted succinyl purines as recorded by the LKB 2140 rapid spectral detector. The LC-18 reversed-phase column (Supelcosil) was eluted with a gradient system as follows: start solution 5 mmol/l sulphuric acid, end solution acetonitrile–water (4:6, v/v), flow-rate 1.0 ml/min.

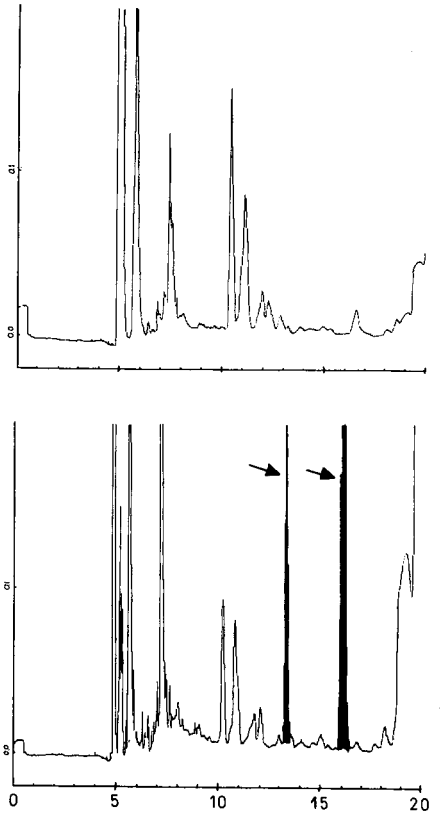

Fig. 6. HPCE profiles of urine from a control (upper panel) and from a patient with adenylosuccinase deficiency (lower panel). Same patient as in Fig. 5. A Beckman P/ACE Systems 2000 HPCE instrument with an absorbance detector set at 214 nm was used (see text). The succinyl purines are marked with arrows (see also Fig. 5).

The treatment of advanced cardiomyopathy in humans may involve heart transplantation, which is carried out routinely in this hospital. In view of the possible link between cardiomyopathy and lack of taurine in the heart muscle, there is a need for a method to determine taurine in small samples of biopsies from the myocardium. HPCE may be a suitable method for this purpose, as indicated in Fig. 7. The electropherogram in Fig. 7A shows baseline separation of equal amounts of the FMOC derivatives of taurine and the very closely related internal standard that was chosen, [NH_2–CH_2–CH_2–CH_2–SO_3H]. Fig. 7B shows the determination of taurine in sub-milligram sample of biopsy of human heart muscle to which the internal standard had been added. As the heart contains a millimolar concentration of taurine (about 5 mmol/l), the attenuation of the HPCE instrument could be kept low. At this level of sensitivity only one other major peak appears, tentatively identified as GSH (present at 2–3 mmol/l in many cells).

These initial results are now being pursued in a collaborative study, and a quantitative HPCE method which require only sub-milligram amounts of tissue will be used to study patients with cardiomyopathy and other myocardial failures.

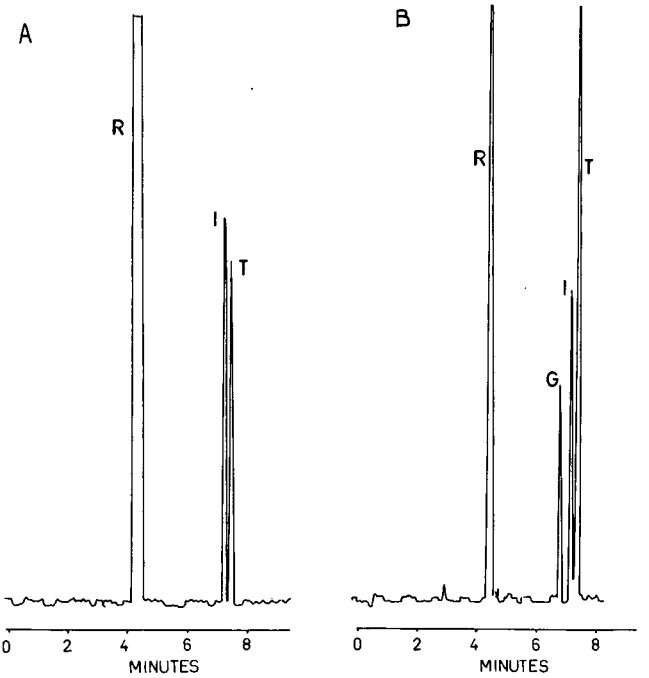

Fig. 7. (A) HPCE separation of taurine and the internal standard. (B) HPCE analysis of a sub-milligram biopsy of human heart muscle, to which the internal standard was added before derivatization with FMOC and electrophoresis. Peaks: R = reagent peak; I = internal standard; T = taurine; G = tentatively identified as GSH. The taurine concentration was calculated to be about 5 mmol/kg wet weight of tissue.

DISCUSSION

HPCE has been used to analyse urine and blood samples from some selected cases with different metabolic disorders, and to determine the aminosulphonic acid taurine in sub-milligram tissue samples (myocardial biopsies). The results have been compared with traditional automated amino acid analysis (ion-exchange chromatography), and with the HPLC (reversed-phase LC-18) and GC–MS methods routinely used in this laboratory for the diagnosis of metabolic diseases.

The selected diseases included homocystinuria, cystinuria and GSH synthetase deficiency. The diagnostic metabolites in these cases are sulphur-containing amino acids and the tripeptide GSH. MB-labelling (after reduction of the disulphides) of the thiol groups yielded derivatives that were quickly formed, baseline-separated and readily detected by HPCE with fluorescence detection. The conclusion to these experiments is that if clinical symptoms and preliminary spot tests raise the suspicion that a patient may suffer from any one of the above-mentioned disorders, confirmatory diagnosis may be made in less than 30 min by HPCE (including sample preparation) compared with 3 h by traditional amino acid analysis (including regeneration of the column). HPCE would in these cases perhaps be the method of choice.

Comparative analyses on samples from a patient with the rare disorder adenylosuccinase deficiency were carried out using HPLC with diode-array detection and

HPCE with absorbance detection. The diagnostic metabolites in this disorder are two different succinylpurines which have strong UV absorbance. Derivatization is therefore not required. In this instance little is gained by using HPCE, as both methods require about 20–30 min analysis time, including sample pretreatment. It should be noted, however, that none of the procedures has been optimized. As the HPLC diode-array detector allowed spectral comparison, in contrast to the HPCE equipment, HPLC is preferred over HPCE in this instance.

In these examples the diagnostic goals can easily be achieved with methods other than HPCE. The advantage of HPCE is, however, the small sample volume required, *i.e.* 1–10 nl. This opens up the possibility of analysing small tissue biopsies, small numbers of cells and even perhaps further down to the analysis of a single cell [12]. However, when dealing with cells and body fluids, the concentration of an interesting metabolite is often low, *e.g.* of the order of μmol/l to nmol/l. If 1 nl of unconcentrated sample is injected into the capillary column of an HPCE instrument, the detector must then be able to detect $10^{-6}/10^{-9} = 10^{-15}$ mol and $10^{-9}/10^{-9} = 10^{-18}$ mol, respectively. At present, the way to achieve such a sensitivity is to use a laser-induced fluorescence dtector [12,13]. Unfortunately, the ordinary lamp-based fluorescence detector currently available in this laboratory is not nearly as sensitive, and so far these studies have been limited to clinical problems with metabolites that are present at much higher concentrations. Such an example is the study of the role of taurine in the development of cardiomyopathy. The preliminary results shown in this paper clearly indicate that HPCE may become the method of choice for this purpose.

In conclusion, at these early stages of the application of HPCE to biomedical problems, it has been shown that the method can offer a quick and simple alternative to existing methods such as amino acid analysis. We believe, however, that it is at the cellular level that the full potential of HPCE will become apparent. Thus, the use of HPCE to analyse, for example, amniotic cells directly and without cultivation for prenatal diagnosis, can be foreseen, and it seems likely that the use of HPCE to analyse tissue biopsies will expand, particularly when laser-induced fluorescence becomes more generally available.

REFERENCES

1 E. Jellum, E. A. Kvittingen, O. Thoresen, G. Guldal, L. Horn, R. Seip and O. Stokke, *Scand. J. Clin. Lab. Invest.*, 46 (Suppl. 184) (1986) 11.
2 E. Jellum and A. K. Thorsrud, *J. Chromatogr.*, 488 (1989) 105.
3 J. Jorgenson and K. D. Lukacs, *Anal. Chem.*, 53 (1981) 1298.
4 S. H. Mudd, H. L. Levy and F. Skovby, in C. R. Scriver, A. L. Beaudet, W. S. Sly and D. Valle (Editors), *The Metabolic Basis of Inherited Disease*, McGraw-Hill, New York, 6th ed., 1989, p. 693.
5 S. Segal and S. O. Thier, in C. R. Scriver, A. L. Beaudet, W. S. Sly and D. Valle (Editors), *The Metabolic Basis of Inherited Disease*, McGraw-Hill, New York, 6th ed., 1989, p. 2479.
6 A. Meister and A. Larsson, in C. R. Scriver, A. L. Beaudet, W. S. Sly and D. Valle (Editors), *The Metabolic Basis of Inherited Disease*, McGraw-Hill, New York, 6th ed., 1989, p. 855.
7 E. Jellum, T. Kluge, H. C. Borresen, O. Stokke and E. Eldjarn, *Scand. J. Clin. Lab. Invest.*, 26 (1970) 327.
8 J. Jaeken and G. Van den Berghe, *Lancet*, 10 (1984) 1058.
9 P. D. Pion, M. D. Kittleson, Q. R. Rogers and J. G. Morris, *Science*, 237 (1987) 764.
10 A. Tenaglia and R. Cody, *Am. J. Cardiol.*, 62 (1988) 136.
11 R. L. Hamlin and C. A. Buffinton, *Vet. Clin. North Am. Small Anim. Pract.*, 19 (1989) 527.
12 R. T. Kennedy, M. D. Oates, B. R. Cooper, B. Nickerson and J. W. Jorgenson, *Science*, 246 (1989) 57.
13 J. Liu, Y-Z Hsieh, D. Wiesler and M. Novotny, *Anal. Chem.*, in press.

Journal of Chromatography, 559 (1991) 467–477
Elsevier Science Publishers B.V., Amsterdam

CHROM. 23 633

Characterization of polyethylene glycol modified proteins using charge-reversed capillary electrophoresis

ROBERT L. CUNICO[a], VICTORIA GRUHN*, LILIA KRESIN and DANUTE E. NITECKI
Cetus Corporation, 1400 53rd Street, Emeryville, CA 94608 (USA)
and
JOHN E. WIKTOROWICZ
Applied Biosystems Inc., San Jose, CA 95134 (USA)

ABSTRACT

A capillary electrophoretic method employing a charge reversal technique [J. E. Wiktorowicz and J. C. Colburn, *Electrophoresis*, 11 (1990) 769] has been developed to characterize polyethylene glycol (PEG)–proteins. A removable coating is applied to a standard fused-silica capillary in order to change the negative charge of the capillary surface to a positive charge. This prevents the adsorption of basic and PEG–proteins. The positive electrode is positioned at the detector end of the capillary, orienting electroosmotic flow towards the detector. Automated reconditioning procedures prior to each analysis give relative standard deviations in migration time and area of less than 2%, with most analysis times under 20 min. As the number of PEGs conjugated to a protein increases, the net positive charge and migration time of the copolymer decrease. Resulting peak widths are broad, reflecting the broad molecular mass distribution of PEGs and the heterogeneous nature of the PEG conjugates. This method can be used to monitor process steps, optimize reaction conditions, determine extent of modification, or assess product quality and consistency. Examples of PEG derivatized molecules characterized in our laboratory by charge-reversed capillary electrophoresis are tryptophan, Lys–Trp–Lys, lysozyme, myoglobin, RNase and immunoglobulin G; the size of the attached monomethoxy-PEG molecules varied from 0.15 kDa to 10 kDa (10^3 dalton).

INTRODUCTION

Recombinant proteins are often produced in cells such as *Escherichia coli* which are not capable of glycosylation. Many unglycosylated proteins have limited solubility and a tendency to aggregate at neutral pH [1]. Polyethylene glycol (PEG) is a man-made polymer that can be covalently bound to a protein, typically via active ester reaction with the ε amino group of lysine or the protein's N-terminal primary amine. Covalent attachment of PEG to proteins results in conjugates that have: (a) increased pharmacokinetic half-life [1], (b) reduced immunogenicity [2,3] and (c) increased solubility [2]. Examples of such modified proteins are PEG–adenosine

[a] Present address: Bay Bioanalytical Laboratory, 280 Beechnut Dr., Hercules, CA 94547, USA.

0021-9673/91/$03.50

deaminase (Pegademase), recently approved by the Food and Drug Administration (FDA) for the treatment of severe combined immunodeficiency syndrome (SCIDS [4]) and PEG–asparaginase [5]. Characterization of PEG-proteins is a challenging analytical problem. By coupling a homogeneous polymer (the protein), to a heterogeneous polymer (the PEG) one creates an extremely heterogeneous mixture that must be characterized by class. For example, a protein such as myoglobin, with 20 reactive amino groups, derivatized with a 10 kDa (10^3 dalton) PEG that contains a mixture of 8 kDa sized PEG, may result in a mixture of greater than 10^{33} kinds of molecules. There are simply too many possible combinations to make an exhaustive analysis of each distinct PEG–protein conjugate feasible. Methods which have been used to characterize PEG–proteins include high-performance liquid chromatography (HPLC) [1,6], NMR [7], isoelectric focusing (IEF) [2] and sodium dodecylsulfate-polyacrylamide gel electrophoresis (SDS-PAGE). None of these methods is capable of exploiting both the charge and mass changes that are the result of PEG conjugation, in contrast to capillary electrophoresis (CE).

Previously reported CE methods employing an unmodified capillary and low pH buffers [8], buffers using a pH above the pI of the protein [9], or addition of organic modifiers to the sample matrix [10] are not applicable to the characterization of PEG conjugated proteins. Others describe coatings that slow or eliminate electroosmotic flow [11–14], which is not always desirable, as electroosmotic flow can be used to increase effective separation length and improve resolution. In this paper we describe an application of CE, using a charge-reversed, coated capillary, to the separation and characterization of six different PEG conjugated species. An amino acid, a tri-peptide, and four proteins of varying size were chosen in order to reflect a wide range of size and charge characteristics.

EXPERIMENTAL

Apparatus and materials

CE was performed on an Applied Biosystems Model 270A (ABI, Foster City, CA, USA). The capillary column consisted of fused-silica tubing (Polymicro Technologies, Phoenix, AZ, USA), 50 μm I.D., 360 μm O.D., with a total column length of 72 cm (52 cm to the detector). Approximately 0.5 cm of the polymide coating was burned off at a distance of about 20 cm from the detector end of the column to create a detector window. The UV data (215 nm) were analyzed using a Nelson Analytical data system (Perkin-Elmer/Nelson, Cupertino, CA, USA).

D-Tryptophan, Lys–Trp–Lys, myoglobin from horse heart, lysozyme from chicken egg-white, RNase from bovine pancreas and human immonoglobulin G (IgG) were purchased from Sigma (St. Louis, MO, USA); sodium phosphate (monobasic) was purchased from Fisher Scientific (Forest Lawn, NJ, USA); phosphoric acid, sodium phosphate (dibasic) and analytical grade ethylene glycol were purchased from Mallinckrodt (Paris, KY, USA). The 2 kDa and 10 kDa methoxy-PEGs (mPEGs) were obtained from Union Carbide; 2-(2-methoxy-ethoxy)ethanol was obtained from Aldrich (Milwaukee, WI, USA); Microcoat was obtained from Applied Biosystems (Foster City, CA, USA). All buffer solutions were filtered through 0.2-μm sterile polysulfone syringe filters (Gelman Scientific, Ann Arbor, MI, USA) and vacuum degassed before use. Water was HPLC grade.

Reagent synthesis

Both N-hydroxysuccinimide (NHS) and *p*-nitrophenyl (pNP) activated PEG esters were used for conjugation. The 6 kDa NHS active esters were obtained by using methoxy-PEG-glutarate prepared from mPEG and glutaric anhydride, followed by activation with dicyclohexylcarbodiimide and N-hydroxy-succinimide [15,16]. The 2 kDa and 10 kDa pNP active esters were synthesized as shown using a method described by Veronese *et al.* [17]:

$$\text{mPEG-OH} + \text{Cl-CO-O-C}_6\text{H}_4\text{-NO}_2 \rightarrow \text{mPEG-O-CO-O-C}_6\text{H}_4\text{-NO}_2$$

The 0.15 kDa PEG ester was synthesized as follows. In a well cooled flask containing 200 ml of dry diethyl ether, 20.2 g (0.1 mol) of *p*-nitrophenyl chloroformate was dissolved together with 12 ml (0.1 mol) of 2-(2-methoxy ethoxy)ethanol. Pyridine, 20 ml, was added slowly, causing a precipitate to form. The reaction was allowed to stand at ambient temperature for several hours. The precipitate was filtered and discarded. The mother liquor was diluted to 300 ml with diethyl ether, washed 3 times with water, 3 times with sodium chloride and dried over magnesium sulfate. The solvent was removed *in vacuo*; pale yellow oil resulted. Yield was 16.67 g. Analysis using a method described by Aldwin and Nitecki [18] indicated 87% active ester by weight. It should be noted that the molecular mass of the reagent (PEG ester) is 0.28 kDa but the resulting attached PEG residue is 0.15 kDa; with larger mPEG molecules the molecular weight change is negligible. To avoid confusion we will refer to both the PEG ester and its conjugate by the molecular mass of the PEG residue (*i.e.* 0.15 kDa).

Amino acid, peptide, and protein conjugation

The NHS ester reactions with ribonuclease, lysozyme, myoglobin and IgG were carried out in N-[2-hydroxyethyl]piperazine-N′-3-propane sulfonic acid (EPPS) buffer pH 8.5 at ambient temperature for 30 min; reactions were quenched by lowering the pH to 5.0 with acetic acid. In order to achieve various degrees of PEG conjugation, the PEG-ester was added to the protein solutions at different molar ratios ranging from 1:1 to 5:1, respectively. The activated pNP esters were mixed with tryptophan, Lys–Trp–Lys, myoglobin or IgG in 0.1 *M* 4-(2-hydroxyethyl)-1-piperazine-ethane sulfonic acid (HEPES) buffer, pH 8.5. Typically, varying amounts of PEG ester calculated as a molar ratio of the PEG ester-to-target molecule were added to 5 mg/ml protein solutions and allowed to react overnight. Reactions times and activated ester-to-target molecule molar ratios were varied as noted in the Figures. Reactions were stopped by dilution (1:1) into pH 2.0 electrophoresis buffer (0.1 *M* phosphate, 10% ethylene glycol). The pNP esters are considerably slower reacting than the more commonly used NHS esters [19]. This feature allows analysis of the kinetics of the conjugation, as shown in the myoglobin time course electropherograms. The activity of the PEG–pNP esters was checked by following the appearance at 400 nm of the characteristic yellow color of *p*-nitrophenyl anion formed at pH above 8.0 [18]. In general, the percentage by weight of active esters was greater than 70%.

Procedures

Capillaries were first treated with 1.0 *M* NaOH for 20 min by drawing the solution into the capillary by vacuum, followed by 5 min with 0.1 *M* NaOH, according to the manufacturer's protocol. After a 5-min wash with water, the capillary was

coated for 20 min with Micro-coat in 2% ethylene glycol. In order to keep a consistent coating on the capillary surface, the capillary was washed between injections with 0.1 *M* NaOH for 1 min and reconditioned for two minutes with Micro-coat in 2% ethylene glycol. Samples were injected by application of vacuum for two seconds. This corresponded to an injection size of approximately 8 nl. Electrophoresis was performed at −30 kV (400 V/cm) for 15–40 min. The concentrations of the PEG conjugated species were on the order of 1–2.5 mg/ml.

RESULTS

Fig. 1 shows a schematic diagram of the capillary surface under both normal (Fig. 1A) and charge-reversed (Fig. 1B) conditions. Proteins and PEG–proteins below their isoelectric points are positively charged and can interact with the negatively charged capillary surface. After coating, the net charge on the capillary wall is positive, causing a reversal in electroosmotic flow (μ_{eo}). By reversing the polarity, the analytes can be swept by the detector as usual. The charged PEG–proteins are now repulsed from the capillary wall. Electroosmotic flow is fast enough to overcome the electrophoretic mobility (μ_{ep}) of the positively charged species. Since mobility is countered by electroosmotic flow, those species with greater net positive charge exhibit longer migration times, according to eqns. 1 and 2, where μ_{app} is the apparent electrophoretic mobility; μ_{ep} is the true electrophoretic mobility; vel_{app} is the peak velocity; V is the field strength; t_{app} is the peak migration time, and k is a constant reflecting the total length of the capillary, the length to the detector, and the applied voltage. In eqn. 2, q is the net positive charge, R_s is the Stokes radius, and n is the intrinsic viscosity.

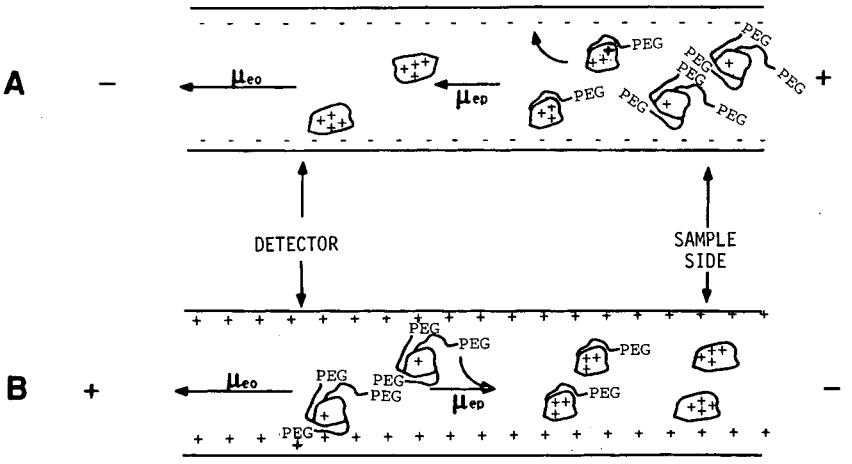

Fig. 1. Diagram of the capillary under (A) normal and (B) charge-reversed conditions. Note the electrode polarity, the direction of electroosmotic flow (μ_{eo}), the cationic PEG–protein electrophoretic mobility (μ_{ep}) and its attraction to the capillary surface.

$$\mu_{app} = \frac{vel_{app}}{V} = k\frac{1}{t_{app}} \quad (1)$$

$$\mu_{ep} = \frac{q}{6\pi R_s n} \quad (2)$$

CE of PEG esters, tryptophan and Lys–Trp–Lys

p-Nitrophenyl active PEG esters are stable and uncharged at pH 2.0 and adsorb strongly in the UV region. In the experiments described here, they migrated with the mesityl oxide neutral marker. The *p*-nitrophenol formed during conjugation, either by hydrolysis or as a by-product of the conjugation, served as a convenient neutral marker, being uncharged below pH 5.0. Uridine-5′-diphosphoglucose (UDPG) served as a negatively charged marker in the PEG ester electropherograms in order to compare relative migration rates of the PEG esters. Since the 0.15 kDa, 2 kDa and 10 kDa PEG esters all migrated with the neutral marker, we have concluded that the polyethylene glycol moiety was not interacting with the Micro-coat on the walls of the capillary. There was some peak broadening observed with the 10 kDa ester. This appeared to be the result of a greater mass of the larger PEG being injected in order to obtain the same number of moles (0.046 mol) on the capillary (*e.g.* 46 mg/ml for the 10 kDa PEG and 1 mg/ml for the 0.15 kDa PEG). When a minimum amount of the 10 kDa PEG was injected, the peak width more closely resembled that of the smaller PEG ester.

The amino acid tryptophan has one primary amino group available for modification. When a PEG is attached to this amine, the resulting conjugate is neutral at pH 2.0. The 0.15 kDa, 2 kDa and 10 kDa PEG–tryptophan conjugates all migrated with the neutral marker. Thus, similar to unreacted PEGs, in the case of uncharged conjugates, migration proved to be independent of size.

The Lys–Trp–Lys tripeptide has a molecular mass of 0.46 kDa and three amino groups available for conjugation. Upon PEG conjugation, three mono-PEG species, three di-PEG species and one tri-PEG species are expected. We found that as the molar ratio of the 0.15 kDa PEG ester-to-peptide was increased stepwise, the relative triplet height (Fig. 2) remained constant. Thus, the triplet migrating at 13–14 min most likely reflects the three possible mono-conjugates of Lys–Trp–Lys: the N-terminal α-amino, the N-terminal lysine ε-amino, and the C-terminal lysine ε-amino. At higher PEG ester-to-peptide ratios, the amount of di-PEG species (8.2 min) increased. The PEG-tripeptide was uncharged and migrated with the *p*-nitrophenol (6.0 min). The three possible di-PEG species apparently could not be resolved. When the Lys–Trp–Lys tripeptide was conjugated with 2 kDa and 10 kDa PEGs, the resulting products migrated closer to the neutral marker. The larger molecules migrated faster, consistent with eqn. 2.

CE of myoglobin

Myoglobin (17 kDa) showed essentially no change in mobility when conjugated with the 0.15 kDa PEG. When modified with the 2 kDa and 10 kDa PEGs, however, the myoglobin conjugates (which are larger) migrated faster (Fig. 3). A PEG ester-to-protein molar ratio of 5:1 was used in this reaction. By observing the appearance of the various PEG conjugated species of myoglobin as a function of reaction time, we assigned the number of PEGs attached to myoglobin for each peak (Fig. 4a). Since no

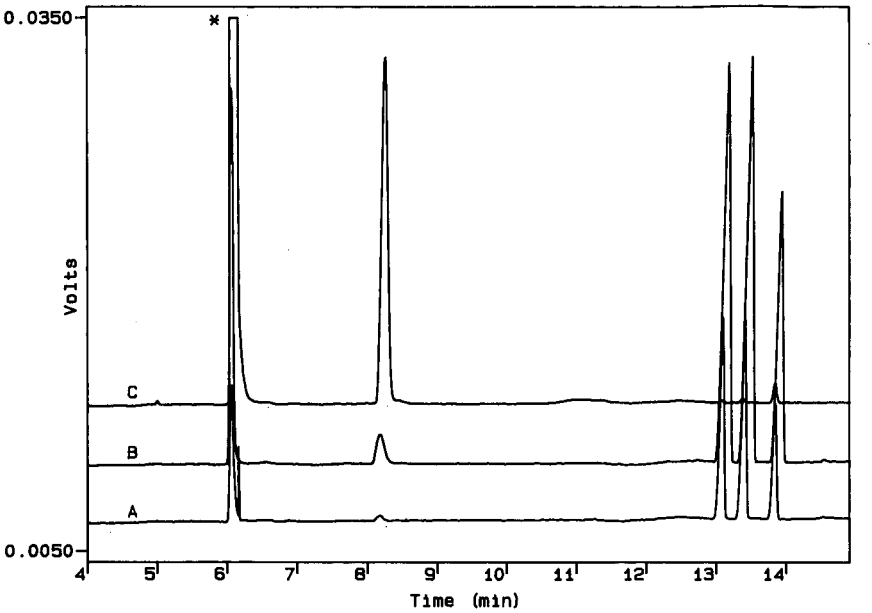

Fig. 2. High-performance capillary electrophoresis of Lys–Trp–Lys conjugated with 0.15 kDa PEG using pNP esters. The PEG ester-to-peptide molar ratio in these reactions was: (A) 1:1, (B) 3:1, (C) 10:1. The electropherograms were obtained using a 72 cm × 50 μm I.D. fused-silica capillary tube; 100 m*M* phosphate, 10% ethylene glycol, pH 2.0, −30 kV, 45 μA, UV detection at 215 nm. The hydrolyzed *p*-nitrophenol (*) was used as a neutral marker. Unmodified Lys–Trp–Lys migrated at 37.5 min.

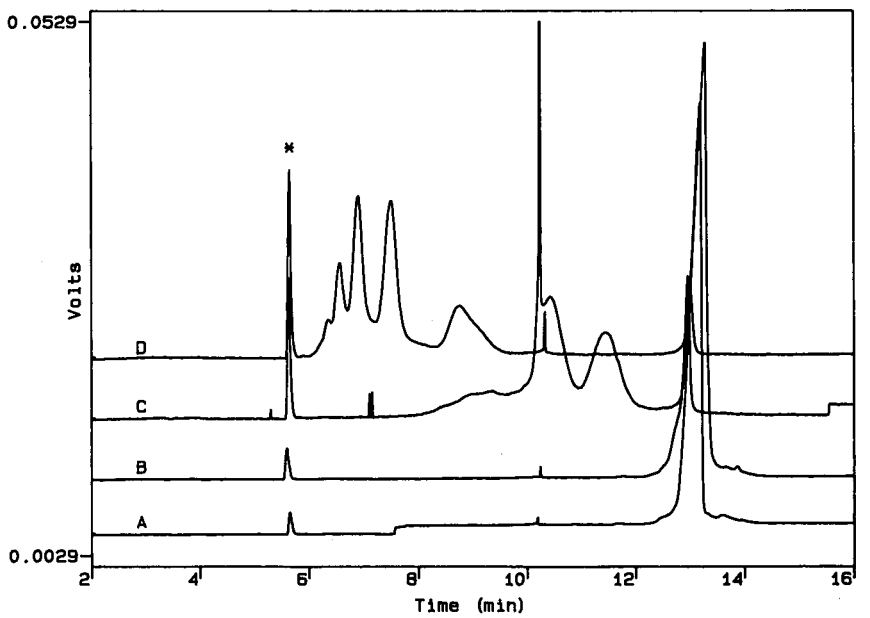

Fig. 3. High-performance capillary electrophoresis of myoglobin conjugated with pNP esters. The PEG ester-to-protein molar ratio in these reactions was 5:1. (A) Unmodified myoglobin, (B) 0.15 kDa PEG, (C) 2 kDa PEG, (D) 10 kDa PEG. Electrophoresis conditions are described in Fig. 2. Hydrolyzed *p*-nitrophenol (*) was used as a neutral marker. The peak at 10.1 min is not identified, and may be a system-related artifact.

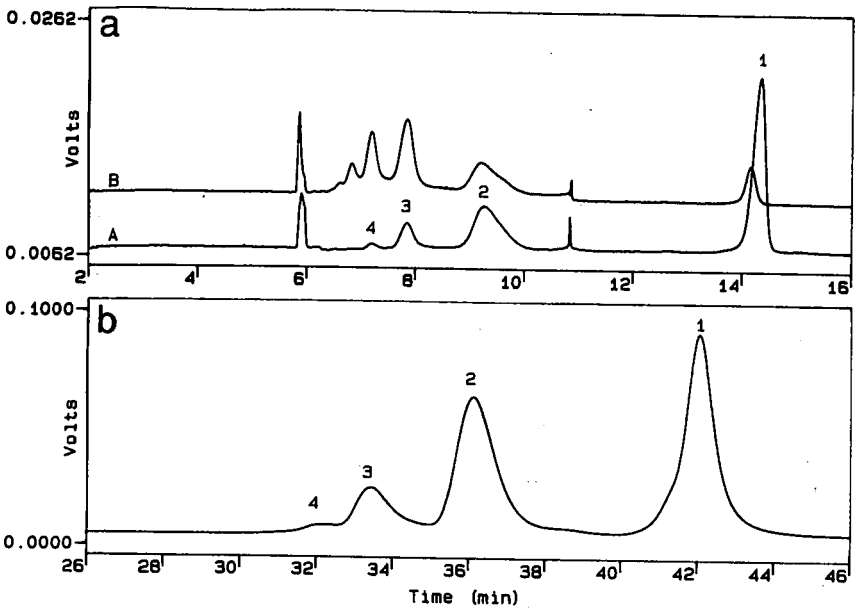

Fig. 4. (a) High-performance capillary electrophoresis of (A) myoglobin conjugated with 10 kDa PEG, 1 h reaction time, (B) myoglobin conjugated with 10 kDa PEG, 20 h reaction time. The PEG pNP ester-to-protein molar ratio in these reactions was 3:1. Reactions were stopped by the addition of pH 2.0 buffer. Electrophoresis conditions are described in Fig. 2. Peaks are identified as (1) unmodified myoglobin; (2) 1-PEG; (3) 2-PEG; (4) 3-PEG. (b) Size-exclusion chromatography of myoglobin conjugated with 6 kDa PEG using the NHS ester. The PEG ester-to-protein molar ratio in this reaction was 1:1. Chromatography was performed on two Dupont Zorbax GF-250 columns in series (25 cm × 9.4 mm I.D. each); 0.1 *M* sodium sulfate, 0.01 *M* sodium phosphate, pH 7.0; UV detection was at 280 nm. Peaks are identified as (1) unmodified myoglobin; (2) 1-PEG; (3) 2-PEG; (4) 3-PEG.

significant peaks appeared between 10 and 14 min of migration time, the peak that migrated at 9.4 min was assigned a mono-PEG identity. These experiments were done at a low pNP–PEG-to-myoglobin ratio (3:1) and stopped at various points by dilution into pH 2.0 buffer in order to favor a lower PEG-to-protein ratio.

When a similar experiment was performed using the NHS ester of 6 kDa PEG (ester-to-protein molar ratio 3:1), the same pattern of PEG conjugated species was observed. The electropherogram and sizing HPLC chromatogram of the myoglobin conjugates (Fig. 4b) were very similar. Using UV-RI size exclusion HPLC compositional analysis described by Kunitani *et al.* [6], weight composition of the PEG myoglobin conjugates formed was determined. Based on the found weight PEG per weight protein, the mole ratio in this sample was calculated to be 1.24. By using the PEG assignments shown in Fig. 4, we obtained a similar value by first correcting the areas of the myoglobin conjugate peaks for migration time, then summing the area percents of each peak multiplied by its conjugation number [*i.e.* 1(Area% 1-PEG) + 2(Area% 2-PEG)...]. This gave a value of 1.27, which is consistent with the sizing HPLC results.

CE of IgG

IgG is a large (150 kDa) protein. Conjugation with 0.15 kDa PEG should

decrease the net positive charge on IgG but have little effect on the mass. Net positive charge at pH 2.0 was calculated using a program that sums the fractional charges from each charged amino acid at pH values from 1 to 14. The number of charged amino acids was estimated from sequence data found in the literature [20]. IgG conjugation with 0.15 kDa PEG changed the charge-to-mass less than 1%, while conjugation with the 10 kDa PEG changed it almost 10%. Thus, resolution of the 0.15 kDa PEG from unmodified IgG was poor. The PEG ester-to-IgG molar ratio in this reaction was 10:1.

Effects of pH

Based on the known amino acid composition of myoglobin, a theoretical charge-to-mass ratio was calculated at unit pH values from 1 to 13 for myoglobin conjugates with one to four 10 kDa PEG molecules (Fig. 5). Net positive charge and pI were calculated using a program that sums fractional charges, as described earlier. The largest difference in charge-to-mass ratio is observed at very low (1 to 3) and very high (> 10) pH values. At extreme pH values charge interactions with the capillary wall or stripping of the coating phase may be a problem. Thus, the ideal working pH range appeared to be between pH 2 and 6. According to Fig. 5, as the pH of the separation buffer is increased, the difference in charge-to-mass between the myoglobin conjugates becomes smaller. The conjugates should migrate closer together, decreasing resolution. Data from a series of electropherograms of 10 kDa PEG–myoglobin at different pH values are summarized in Table I. At low pH, the net positive charge on the myoglobin is greatest, effecting the largest difference in charge-to-mass. This improved the separation between the various PEG conjugated species. The electroosmotic flow was also faster at lower pH, decreasing analysis time. Each PEG conjugate is uncharged at its p*I* (*e.g.* 4-PEG myoglobin p*I* is 6.9). As the pH of the separation buffer approached this p*I*, the 4-PEG myoglobin migrated closer to the neutral marker. Thus, as the pH of the separation buffer increased, the resolution between the PEG conjugates decreased, as predicted earlier. In general, as the net positive charge on a protein approaches 0, it should migrate with the neutral marker, thus providing a simple way to measure its p*I*. For the PEG-conjugated proteins discussed here, this is

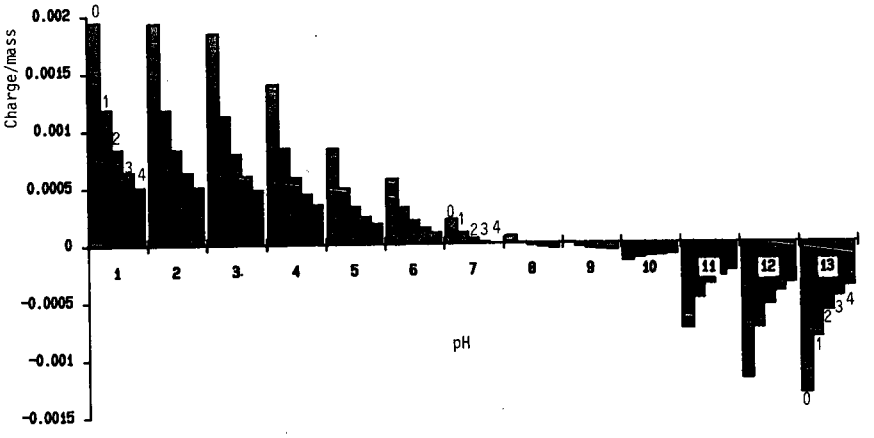

Fig. 5. Charge-to-mass *vs.* pH for myoglobin conjugated with 10 kDa PEG. Based on the assignments given in Fig. 4, data represents 0 to 4 PEGs per molecule myoglobin; 0 = 0 PEGS, 1 = 1 PEG, 2 = 2 PEGs, etc.

TABLE I

CE MIGRATION DATA OF 10 kDa PEG–MYOGLOBIN

72 cm × 50 μm I.D. capillary, 100 m*M* phosphate pH 2.0, 10% ethylene glycol, −30 kV, 45 μA, UV detection at 215 nm.

System pH	Migration time (min)					
	Neutral marker	Myoglobin +				
		0-PEG (p*I* 8.9)	1-PEG (p*I* 7.9)	2-PEG (p*I* 7.5)	3-PEG (p*I* 7.2)	4-PEG (p*I* 6.9)
2	5.87	14.17	9.23	7.85	7.20	6.84
4	7.35	15.48	9.93	8.80	8.35	8.11
5	9.38	13.27	10.95	10.44	10.36	9.79
6	11.66	15.33	14.82	14.37	14.37	14.37

not applicable in the case of very small PEG (0.15 kDa) attached to large (10 kDa or 150 kDa) proteins.

Reproducibility

Sequential injections of 10 kDa PEG–myoglobin were made in order to examine migration time and peak area reproducibility. Between each injection, the wash procedure described in the Experimental section was used to maintain a consistent surface on the capillary. The relative standard deviation (R.S.D.) of migration times for a series of 6 injections was 0.1%, while the R.S.D. of peak areas was 1.8%.

DISCUSSION

If the separation of PEG conjugates were based solely on differences in charge, then the size of the PEG used for conjugation would have no effect on electrophoretic mobility. This is not the case. If the separation were based only on size, then changes in pH would have little effect on relative migration times; this also is not the case. The separation mechanism appears to be governed by both size and charge. Eqn. 2 is consistent with this proposal. In order to test the validity of eqn. 2, the electrophoretic mobility of three PEG conjugated proteins and the PEG conjugated tripeptide were plotted in relation to their respective charge-to-Stokes radii ratios (Fig. 6). Electrophoretic mobility was corrected for capillary length and electroosmotic flow velocity by using eqn. 3, where μ_{ep} is the electrophoretic mobility; L and I are the capillary length and the length to the detector; t_0 and t are the migration times of the neutral marker and the sample; and V is the applied voltage.

$$\mu_{ep} = \frac{IL(1/t_0 - 1/t)}{V} \tag{3}$$

Protein Stokes radii were obtained from the literature; Stokes radii of the PEG were calculated from eqn. 4, using known values of PEG intrinsic viscosity [21], where R is the Stokes radius; M is the molecular weight; and $[n]$ is the intrinsic viscosity.

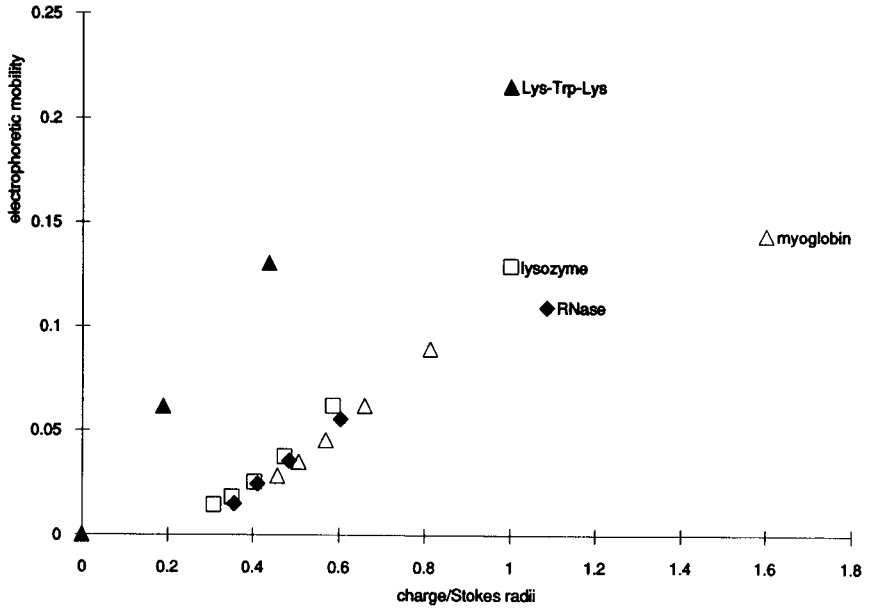

Fig. 6. Electrophoretic mobility ($cm \cdot s \cdot kV^{-1}$) *vs.* charge/Stokes radius. Data from lysozyme and RNase conjugated with 6 kDa PEG using the NHS ester. The PEG ester-to-protein molar ratios in these reactions were 1:1 and 3:1, myoglobin conjugated with 10 kDa PEG and Lys–Trp–Lys conjugated with 0.15 kDa PEG, using the pNP ester. The PEG ester-to-analyte molar ratio in these reactions was 3:1.

$$R = \left[\frac{30\,M[n]}{\pi(6.02 \cdot 10^{23})}\right]^{1/3} \tag{4}$$

Conjugate Stokes radii were calculated from eqn. 5, where R_s is the conjugate Stokes radii; $R_{protein}$ is the Stokes radii of the protein (or peptide); and R_{PEG} is the Stokes radii of the PEG.

$$R_s = \sqrt{(R_{protein})^2 + (R_{PEG})^2} \tag{5}$$

In theory, all the data should lie upon a single straight line, yet they do not. This may be a function of our ability to accurately estimates Stokes radii. The PEG conjugates exhibit a linear relationship, although the tripeptide conjugate relationship has a different slope than that of the protein conjugates. Other factors such as conformation can influence electrophoretic mobility (μ) and hence affect the relationship between μ, and size and charge. It is possible that this relationship may be improved by an independent measurement (*e.g.* dynamic light scattering) of the Stokes radii.

CONCLUSIONS

Capillary electrophoresis with charge-reversed capillaries provides a fast, simple and accurate method for determining the degree of PEG modification of amino acids,

peptides and proteins. The separation is governed by the size of the PEG and the net positive charge on the conjugate at the separation pH and is consistent with eqn. 2. The distribution of unmodified, mono-modified, di-modified and multi-modified PEGs can be determined by this method. This method can be used to determine the p*I* of a protein, to study reaction kinetics, monitor process steps, and to analyze a final product for purposes of quality control.

REFERENCES

1 N. V. Katre, M. J. Knauf, D. P. Bell, P. Hirtzer, Z. Luo and J. D. Young, *J. Biol. Chem.*, 263 (1988) 15064.
2 N. V. Katre, *J. Immunol.*, 144 (1990) 209.
3 C. C. Jackson, J. L. Charlton, K. Kuzminski, G. M. Lang and A. H. Sehon, *Anal. Biochem.*, 165 (1986) 114.
4 *New Drug Approvals in 1990*, Pharmaceutical Manufacturers Association, Washington, DC, January 1991.
5 E. Teske, G. R. Rutteman, P. van Heerde and W. Misdorp, *Eur. J. Cancer*, 26 (1990) 891.
6 M. Kunitani, D. Dollinger, D. Johnson and L. Kresin, *J. Chromatogr.*, 588 (1991) in press.
7 L. Banci, I. Bertini, P. Caliceti, L. Monsu Scolaro, O. Schiavon and F. M. Veronese, *J. Inorg. Biochem.*, 39 (1990) 149.
8 P. D. Grossman, J. C. Colburn, H. H. Lauer, R. G. Nielsen, R. Riggin, G. S. Sittampalam and E. C. Rickard, *Anal. Chem.*, 61 (1989) 1186.
9 G. H. Lauer and D. McManigill, *Anal. Chem.*, 58 (1986) 166.
10 M. J. Gordon, K. Lee, A. A. Arias and R. N. Zare, *Anal. Chem.*, 63 (1991) 69.
11 J. W. Jorgenson, K. D. Lukacs, *Science (Washington, D.C.)*, 222 (1983) 266.
12 S. J. Hjerten, *J. Chromatogr.*, 347 (1985) 191.
13 S. J. Hjerten, K. Elenbring, F. Kilar, J. L. Liao, A. J. C. Chen, C. J. Siebert and M. D. Zhu, *J. Chromatogr.*, 403 (1987) 47.
14 R. M. McCormick, *Anal. Chem.*, 60 (1988) 2322.
15 S. Zalipsky, C. Gilon and A. Zilkha, *Eur. Polym.*, 19 (1983) 1177.
16 G. W. Anderson, J. E. Zimmerman and F. M. Callahan, *J. Am. Chem. Soc.*, 86 (1986) 1839.
17 F. M. Veronese, R. Largajolli, E. Boccu, C. A. Benassi and O. Schiavon, *Appl. Biochem. Biotech.*, 11 (1985) 141.
18 L. Aldwin and D. E. Nitecki, *Anal. Biochem.*, 164 (1987) 494.
19 D. E. Nitecki and L. Aldwin, in C. G. Gebelein (Editor), *Polymers in Biotechnology, ACS Symposium Series*, Washington, DC, 1991, in press.
20 G. D. Fasman (Editor), *Handbook of Biotechnology and Molecular Biology, III-Proteins*, CRC Press, Cleveland, OH, 3rd ed., 1986.
21 *Catalog of Polymer Standards fior Research and Development*, American Polymer Standards Corporation, Mentor, OH, 1987, p. 23.

Journal of Chromatography, 559 (1991) 479–488
Elsevier Science Publishers B.V., Amsterdam

CHROM. 23 486

Optimizing separation parameters in capillary isoelectric focusing

MINGDE ZHU, ROBERTO RODRIGUEZ and TIM WEHR*
Bio-Rad Laboratories, 3300 Regatta Boulevard, Richmond, CA 94804 (USA)

ABSTRACT

Several modifications have been developed for capillary isoelectric focusing (IEF) to improve separation and detection of proteins. A basic compound was incorporated into the ampholyte mixture to block the segment between the monitor point and capillary end during focusing, enabling detection of basic proteins during mobilization. Use of a low-p*I* zwitterionic mobilization agent increased mobilization efficiency of the acidic region of the pH gradient, improving detection of acidic proteins. Mobilization with a neutral-p*I* zwitterion selectively mobilized neutral and basic proteins with improved resolution. Observation of colored proteins in glass capillaries mounted on thermosensitive liquid crystal was used to determine the heat generation patterns along the capillary and the effect of salt on the IEF process. The presence of salt in the sample resulted in long focusing and mobilization times. Incorporation of a non-ionic detergent in the sample plus ampholyte mixture reduced precipitation and improved reproducibility in capillary IEF of γ-globulins.

INTRODUCTION

Isoelectric focusing (IEF) is widely used for separation of complex protein mixtures based on differences in isoelectric points. Conventional IEF performed in gel media can provide extremely high resolution, separating proteins with isoelectric point differences as small as 0.02 p*I* units [1]. The technique is limited by the time required for preparing, running and staining the gel, and non-linearity of the staining reaction.

Isoelectric focusing in capillaries was first described by Hjertén and Zhu [2]. In this variation of the technique, a mixture of proteins in the ampholyte solution is introduced into a gel-free capillary by pressure and focused at high field strength. Detection of proteins by on-tube UV monitoring requires a means of mobilizing focused zones past a monitoring point. This can be accomplished by replacement of a basic catholyte with acid or replacement of an acidic anolyte with base [2]. More commonly, mobilization is accomplished by addition of salt to the catholyte or anolyte [3]. Compared to conventional gel isoelectric focusing, capillary IEF is rapid (separations are typically complete within 15–20 min) and mobilized zones can be detected directly by on-tube monitoring. Capillary IEF requires the use of internally-coated capillaries since the magnitude of electroendosmosis in uncoated capillaries

0021-9673/91/$03.50

prevents attainment of stable focused zones [2,4]. Capillary IEF has been applied to the separation of hemoglobins [2], transferrins [5,6], and immunoglobulins [7,8].

Capillary IEF has several limitations. First, positioning the monitor point at some distance from the end of the capillary prevents detection of proteins which focus between the monitor point and the capillary end during mobilization. Second, when mobilizing focused zones by addition of salt to either of the electrolytes, the mobilization efficiency of proteins which focus at the distal end of the tube is low. These proteins may appear as broad peaks or be undetected. Third, the presence of salts in the sample changes the distribution of the pH gradient during focusing, and increases the time required for focusing and mobilization. We have developed improvements to the capillary IEF process which address each of these limitations.

EXPERIMENTAL

Materials

Cytochrome *c* (horse heart) and γ-globulins (bovine) were obtained from Sigma (St. Louis, MO, USA). Hemoglobins A, F, S and C were obtained from Isolab (Akron, OH, USA). Phycocyanin, the IEF protein standard mixture, Bio-Lyte pH 3/10 ampholytes, and N,N,N′,N′-tetramethylethylenediamine (TEMED) were all obtained from Bio-Rad Labs. (Richmond, CA, USA). The monoclonal antibody preparation was donated by a local biotechnology company. Reduced Trition X-100 was obtained from Aldrich (Milwaukee, WI, USA). Temperature sensitive liquid crystal sheets (25–30°C) were obtained from Edmund Scientific (Barrington, NJ, USA).

Capillary isoelectric focusing

Instrumental capillary IEF was performed with the Microsampler 100 high performance capillary electrophoresis system (Bio-Rad Labs.). Fused-silica capillaries (14 cm or 20 cm length × 25 μm I.D.) were coated internally with linear polyacrylamide covalently attached to the wall using a modification of the method of Hjertén [4]. Capillaries were purged with water and 10 m*M* phosphoric acid between separations. Samples were mixed with ampholytes at a final ampholyte concentration of 2%. Prior to focusing, the capillary was filled with the sample + ampholyte mixture by pressure loading. Focusing was performed at 6 kV constant voltage (unless indicated otherwise) using 10 m*M* phosphoric acid as anolyte and 20 m*M* sodium hydroxide as catholyte. When focusing was complete (as determined by the rate of current drop), cathodic mobilization was initiated by replacing the 20 m*M* sodium hydroxide catholyte with the appropriate mobilization catholyte. Mobilization was performed at 8 kV constant voltage (unless indicated otherwise). Mobilized zones were detected by on-tube monitoring at 280 nm.

To monitor the IEF process visually under various experimental conditions with colored proteins, 14 cm × 200 μm I.D. glass capillaries were used. These were coated by the same procedure used for 25 μm I.D. fused-silica capillaries. The IEF protein standard mixture (containing the colored proteins cytochrome *c*, myoglobin, hemoglobins A and C, and phycocyanin) was diluted 1:10 in 2% Bio-Lyte 3/10 ampholytes. Heat generation along the length of the glass capillary during the IEF process was monitored by mounting the capillary on a 0.7 × 12 cm piece of temperature-sensitive liquid crystal sheet. Focusing and mobilization were carried out under constant voltage 3.5 kV with a current limit of 25 μA.

RESULTS AND DISCUSSION

The IEF process

The mechanism of isoelectric focusing centers on the formation of a stable pH gradient in the capillary by the ampholytes upon application of high voltage. A protein will migrate along the gradient to the point where the pH is equivalent to its isoelectric point and migration ceases. Zone broadening is minimized, since diffusion of the protein away from the zone results in acquisition of charge; because of this focusing effect, zones are very sharp. Ideally, the pH gradient spans the entire length of the capillary and the gradient range is defined by the chemical composition of the ampholytes. A significant level of electroendosmosis would interfere with formation of a stable pH gradient and the attainment of focusing protein zones. Therefore, the use of coated capillaries is an absolute requirement for high-resolution capillary IEF. Because the entire capillary is filled with sample during loading, and because the focused zones are very narrow, the protein concentration in the focused zones can be 200- to 300-fold higher than in the unfocused sample. Therefore, of all modes of capillary electrophoresis, capillary IEF shows greatest potential for micropreparative applications.

At the completion of the focusing stage, only hydroxyl ions enter capillary at the cathodic end and only protons enter the capillary at the anodic end. When cathodic mobilization is initiated by addition of sodium chloride to the catholyte, the movement of chloride ions into the capillary causes a reduction in the hydroxyl ion concentration at the cathodic end of the capillary. As the pH drops, focused proteins and carrier ampholytes acquire charge and thus are mobilized towards the cathode [3]. By a similar mechanism, addition salt to the anolyte in anodic mobilization causes a pH increase in capillary and migration of proteins and ampholytes towards the anode. Because the pH gradient is maintained during mobilization, zone broadening and loss of resolution are minimal. In the mobilization electropherogram of hemoglobin variants presented in Fig. 1, the separation of hemoglobin A (p*I* 7.10) and hemoglobin F (p*I* 7.15) indicates a resolving power of about 0.02 p*I* units.

Use of TEMED in the focusing step

In a high-performance capillary electrophoresis system, good detector stability requires placement of the monitor point some distance from the electrode. This distance is 2.8 cm in the Microsampler 100 system. Since mobilization is in one direction only, proteins which focus in this "blind" segment distal to the monitor point will be undetected during mobilization. Using a 14 cm capillary, this blind segment accounts for 20% of the pH gradient. For example, when using pH 3–10 ampholytes, proteins with p*I* values above 8.6 (*e.g.* cytochrome *c*, Fig. 2A) will not be detected. Yao-Jun and Bishop [9] have described the use of TEMED in the ampholyte mixture to extend the pH range in gel isoelectric focusing. We have used this approach to block the blind segment of the capillary and shift the pH gradient so that it occupies only the segment of the capillary proximal to the monitor point. In Fig. 2B, TEMED was added to the ampholyte + sample mixture at a final concentration of 0.5%. This basic compound filled the cathodic segment of the capillary during focusing, shifting the pH gradient away from the blind segment. In this case cytochrome *c* (p*I* 9.6) was detected during mobilization. Addition of TEMED will reduce resolution somewhat due to increased steepness of the pH gradient after focusing.

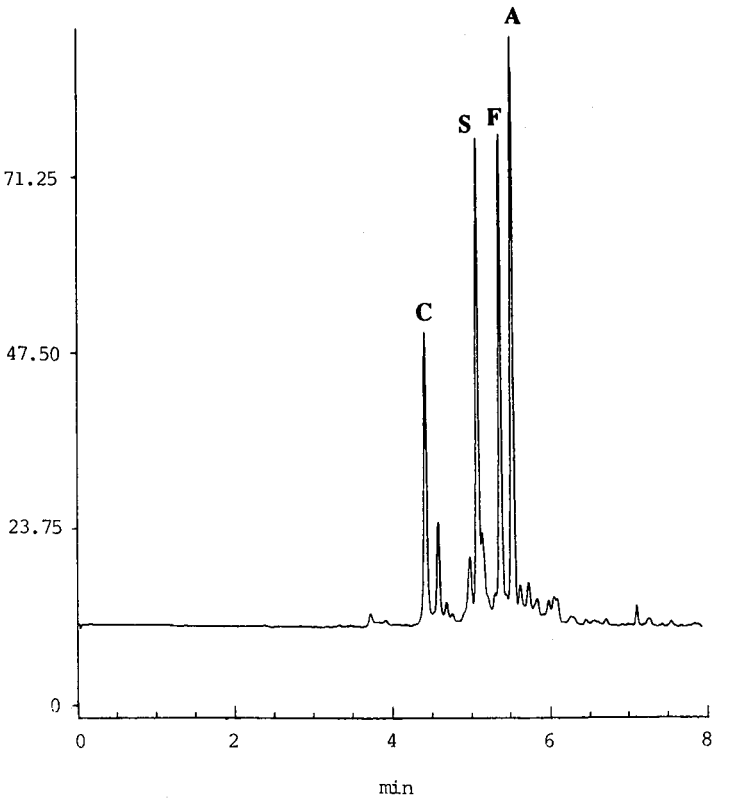

Fig. 1. Separation of hemoglobin variants by capillary IEF in a 12 cm × 25 μm coated capillary using pH 3–10 ampholytes. Focusing and mobilization were carried out at 8 kV constant voltage. Protein concentration was approximately 250 μg/ml for each protein. Isoelectric points are: hemoglobin A, p*I* 7.10; hemoglobin F, p*I* 7.15; hemoglobin S, p*I* 7.25; hemoglobin C, p*I* 7.50.

Alternative mobilization agents

The ideal mobilization mechanism should cause focused zones to maintain their relative order and distance during migration, *i.e.* zones should be mobilized as a train past the monitor point (Fig. 3A). In practice, salt mobilization causes movement of sodium or chloride ions into the capillary at one end. The pH change occurs at this end initially, then gradually progresses deeper into the capillary. The rate of change depends upon the amount of co-ion moving into the capillary, the mobility of the co-ion, and the buffering capacity of the carrier ampholytes. The actual slope of the pH gradient changes across the capillary, becoming shallower in the direction opposite to mobilization. Therefore protein zones at the far end of the capillary are mobilized with lower efficiency and are more likely to exhibit diffusion and defocusing (Fig. 3B). For example, the acidic protein phycocyanin (p*I* 4.65) was not detected during cathodic mobilization with sodium chloride (Fig. 4A). The shallower pH gradient at the far end of the capillary may provide better resolution for proteins which are mobilized, however.

We have developed an alternative mobilization technique employing zwitter-

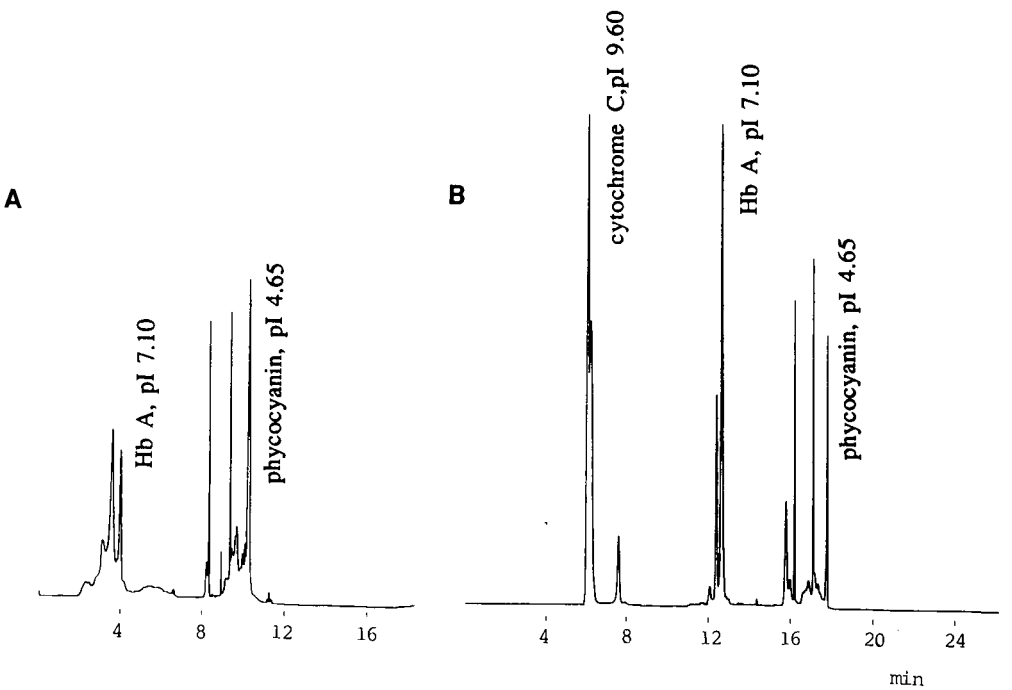

Fig. 2. Use of TEMED to block the blind segment. (A) Separation of cytochrome *c*, hemoglobin A, and phycocyanin without TEMED (cytochrome *c* undetected). (B) Separation with 0.5% TEMED added to sample + ampholyte mixture. Protein concentrations were approximately 300 μg/ml for each component.

ionic agents which allows protein zones across the entire pH gradient to be mobilized with good efficiency. The procedure is identical to sodium chloride mobilization except that the basic catholyte or acidic anolyte is replaced with a solution of a zwitterion of a given isoelectric point. We believe that zwitterion mobilization occurs via two mechanisms. First, movement of the zwitterion into the capillary causes a pH shift in the same fashion as sodium chloride mobilization. Second, the zwitterion migrates to a point in the gradient equivalent to its isoelectric point, where migration ceases and an ever-widening zwitterion zone displaces contiguous zones towards the monitor point.

In the example shown in Fig. 4B, mobilization was initiated by replacing the catholyte (20 m*M* NaOH) with a p*I* 3.22 zwitterion in basic solution. In this case, proteins across the entire pH gradient were mobilized and acidic proteins such as phycocyanin were detected. This approach can also be used to selectively mobilize portions of a broad pH gradient. For example, a zwitterion with a p*I* value near neutrality mobilizes only neutral and basic proteins. In Fig. 5A, proteins across the pH gradient were detected using a p*I* 3.22 zwitterion in basic solution while in Fig. 5B, only proteins with p*I* values greater than that of the p*I* 6.90 mobilization zwitterion were detected.

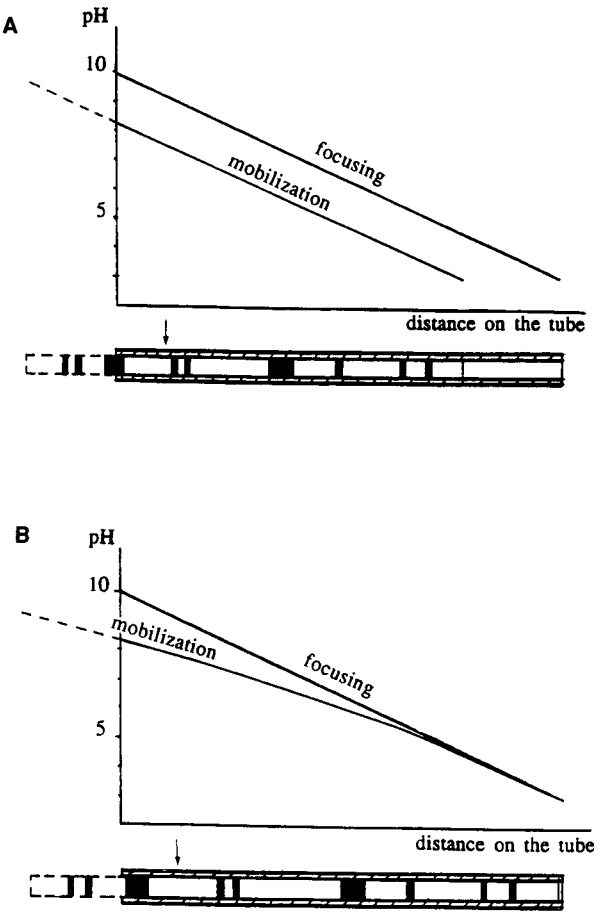

Fig. 3. Variation of pH with distance along the capillary after focusing and during mobilization. (A) Ideal profile (zones mobilize as a train); (B) actual profile (mobilization of zones at the far end of the tube is minimal).

Effect of salt in capillary IEF samples

Ionic species are usually present in biological samples; these can be neutral salts, buffers, or ionic detergents. The effect of salt on the IEF process was observed in a 200 μm I.D. glass capillary using colored proteins (cytochrome *c*, myoglobin, hemoglobin variants, phycocyanin). Under standard conditions without added salt, these proteins formed focused zones distributed across the entire length of a 14 cm capillary using a pH 3–10 ampholyte gradient. When the experiment was repeated with the addition of 100 m*M* NaCl to the sample + ampholyte mixture, focused zones were confined to the central 3–4 cm of the capillary. The time required for focusing and mobilization increased 4- to 5-fold and mobilized zones were more diffuse. Generation of heat during the IEF process was monitored in 200 μm capillaries mounted to temperature sensitive liquid crystal sheets. It was observed that heat

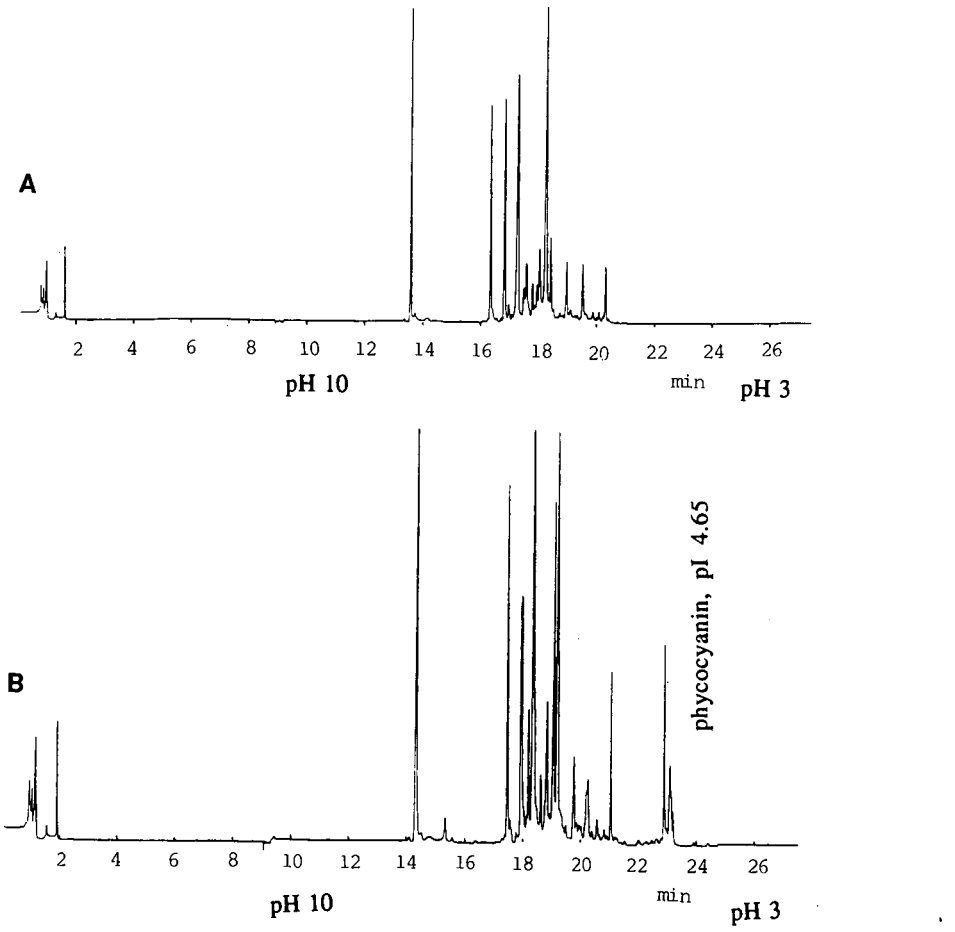

Fig. 4. Comparison of different mobilization agents. (A) Mobilization with sodium chloride (phycocyanin undetected); (B) mobilization with p*I* 3.22 zwitterion in basic solution. IEF protein standards mixture was diluted 1:50 in 2% pH 3–10 ampholytes.

generation closely follows the focusing process. Primary focused zones appeared initially at the margins of the capillary and heat generation was evident due to the increased electrical resistance in these segments. As focusing proceeded, heat generation extended to the central part of the capillary and, a steady state, heat was generated across much of the length of the tube. In contrast, when the sample + ampholyte contained 100 m*M* salt, initial current was very high, which increased the risk of overheating. Later in focusing, heat generation was localized in the central segment of the capillary containing the ampholyte gradient. Confinement of protein zones in a small segment of the capillary where heat generation was localized increased the risk of protein precipitation. For this reason, desalting of biological samples prior to capillary IEF is recommended.

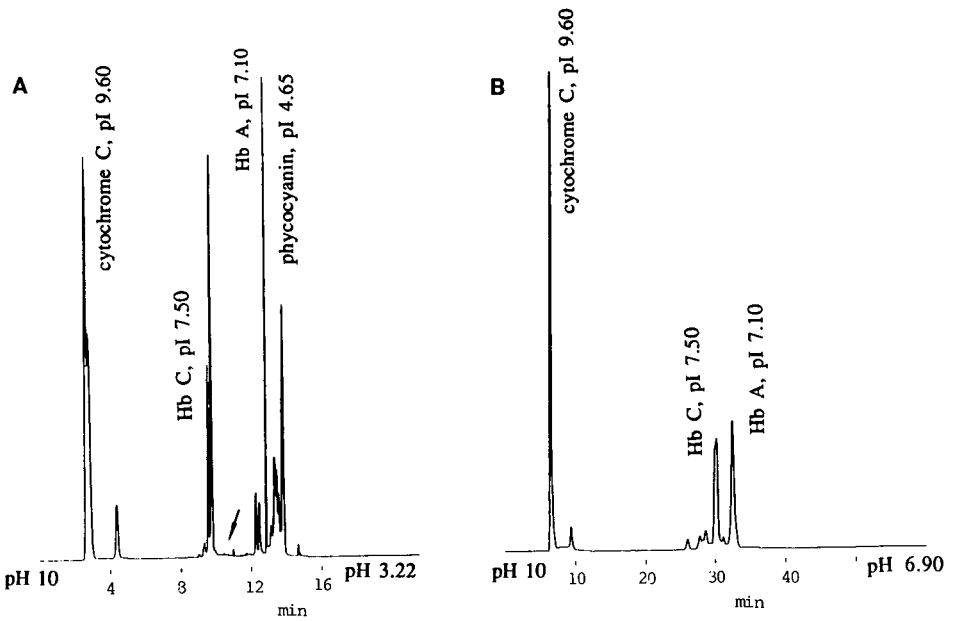

Fig. 5. Comparison of mobilization agents. (A) Mobilization with p*I* 3.22 zwitterion in basic solution; (B) mobilization with p*I* 6.90 zwitterion. Protein concentrations were approximately 300 μg/ml for cytochrome *c* and phycocyanin, and approximately 150 μg/ml for hemoglobins A and C.

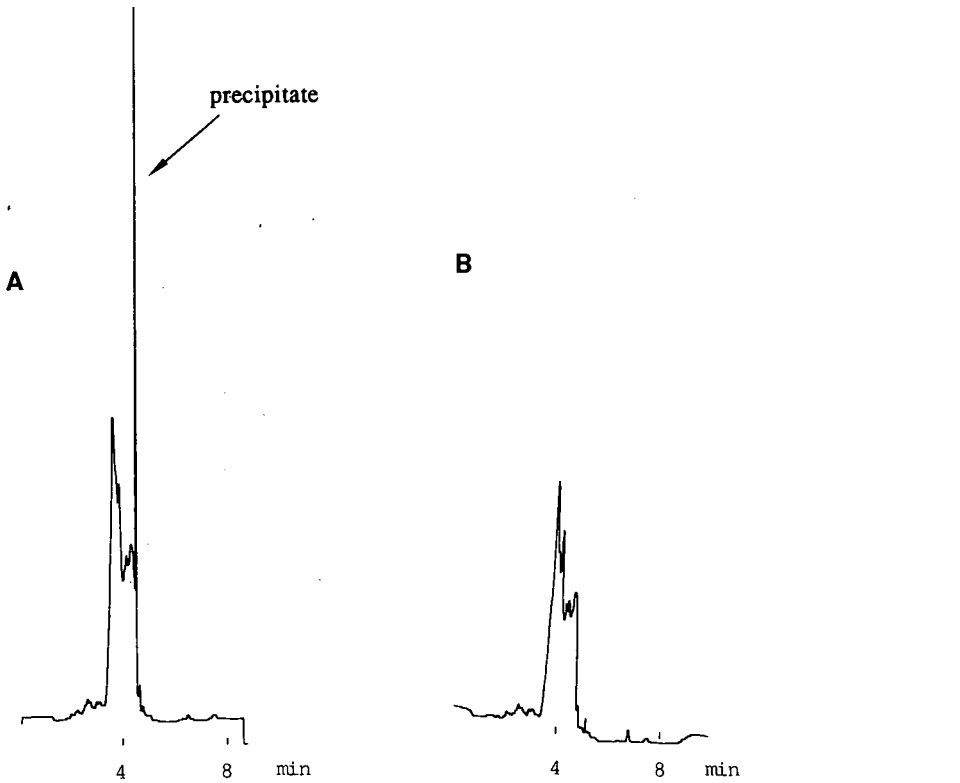

Fig. 6. Separation of monoclonal antibody preparation (A) with and (B) without precipitation.

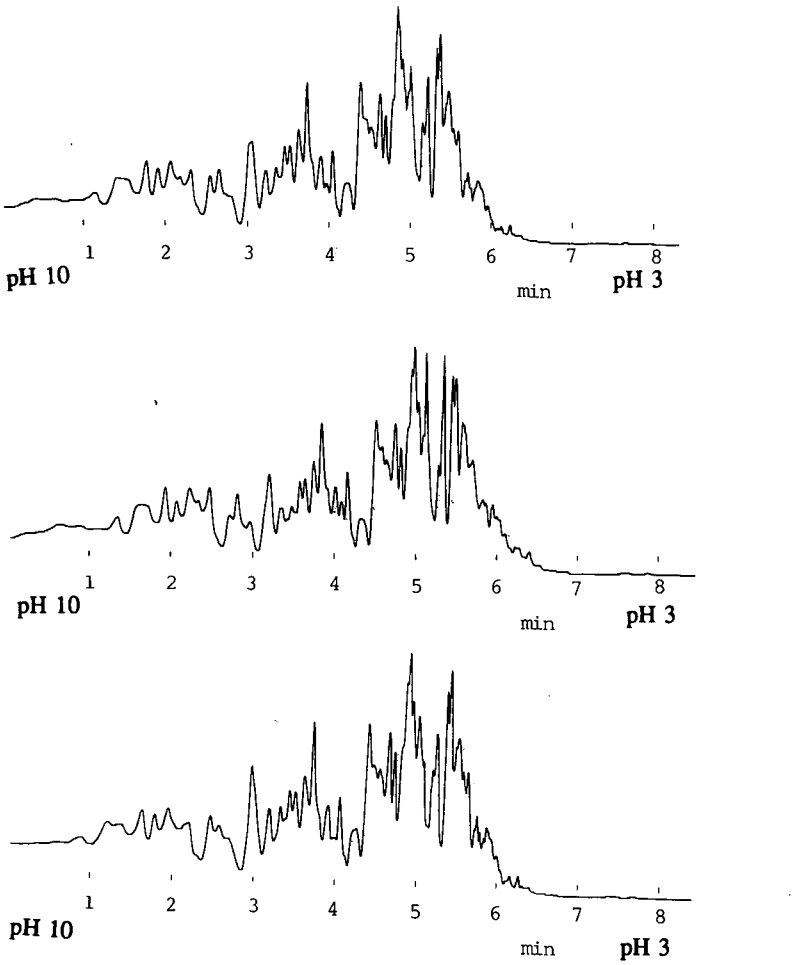

Fig. 7. Replicate separations of γ-globulins. Sample + ampholyte mixture was supplemented with 1% reduced Triton X-100.

Protein precipitation in capillary IEF

Protein precipitation has been a common problem in conventional gel isoelectric focusing, and capillary IEF is no exception. In both versions of the technique, proteins are confined in zones at extraordinarily high concentrations in a state of zero net charge, conditions which favor reduced solubility and aggregation. Moreover, stabilizing counterions are stripped from the protein as it is focused, and heat generation is localized in the focused zone. In capillary IEF, precipitation can cause poor reproducibility of peak size and migration time. Very sharp peaks or spikes are evidence of particulate precipitates passing the monitor point (Fig. 6). Protein precipitation can be suppressed by adding nonionic detergents or ethylene glycol to the sample + ampholyte solution [3,10]. We found that protein solubility was enhanced and reproducibility was improved in IEF separations of γ-globulins by addition of Triton X-100 to the sample + ampholyte mixture (Fig. 7).

CONCLUSIONS

Capillary IEF is a high-resolution separation technique which can resolve protiens based on small differences in isoelectric point. In the most common approach, focused proteins are detected by cathodic mobilization past a monitor point. Basic proteins which normally focus beyond the monitor point were detected by including TEMED in the ampholyte + sample mixture to displace the gradient towards the anode. Using sodium chloride as the mobilizing agent, acidic proteins at the far end of the gradient were mobilized with poor efficiency. An alternative mobilizing technique using zwitterionic agents enabled acidic proteins to be detected as sharp peaks. The same technique could be used for selective mobilization of neutral and basic proteins with enhanced resolution. The presence of salt in the sample resulted in increased focusing and mobilization time, and increased risk of precipitation. Desalting of biological samples to 10 m*M* salt concentration prior to analysis is recommended. Precipitation could be reduced by incorporating a non-ionic detergent in the sample + ampholyte mixture. With these improvements, the capillary IEF technique provided reproducible high-resolution separations of difficult samples such as immunoglobulins.

REFERENCES

1 P. G. Righetti, *Isoelectric Focusing: Theory, Methodology and Applications*, Elsevier, Amsterdam, 1983.
2 S. Hjertén and M. Zhu, *J. Chromatogr.*, 346 (1985) 265–270.
3 S. Hjertén, J.-L. Liao and K. Yao, *J. Chromatogr.*, 387 (1987) 127–138.
4 S. Hjertén, *J. Chromatogr.*, 347 (1985) 191–198.
5 F. Kilar and S. Hjertén, *J. Chromatogr.*, 480 (1989) 351–357.
6 F. Kilar and S. Hjertén, *Electrophoresis*, 10 (1989) 23–29.
7 S. Hjertén, K. Elenbring, F. Kilar, J.-L. Liao, A. Chen, C. Siebert and M. Zhu, *J. Chromatogr.*, 403 (1987) 47–61.
8 T. Wehr, M. Zhu, R. Rodriguez, D. Burke and K. Duncan, *Am. Biotech. Lab.*, 8 (1990) 22–29.
9 G. Yao-Jun and R. Bishop, *J. Chromatogr.*, 234 (1982) 459–462.
10 R. E. Jones, W. A. Hemmings and W. Page Faulk, *Immunochemistry*, 8 (1971) 299–301.

Journal of Chromatography, 559 (1991) 489–497
Elsevier Science Publishers B.V., Amsterdam

CHROM. 23 420

Capillary isotachophoresis with concentration-gradient detection

An application to the separation of synthetic peptides

THERESA McDONNELL and JANUSZ PAWLISZYN*
The Guelph–Waterloo Centre for Graduate Work in Chemistry, University of Waterloo, Waterloo, Ontario N2L 3G1 (Canada)

ABSTRACT

The purity of several synthetic peptides was determined by capillary isotachophoresis with the concentration-gradient detector. The results of the separations are complimentary to those obtained by reversed-phase high-performance liquid chromatography. Detection of low concentration of underivatized peptides (nmol) is facilitated by the universal and low volume optical detector. A simple slider injector was designed for this inexpensive system.

INTRODUCTION

Interest in high-resolution capillary isotachophoresis (cITP) has been rapidly growing over the past few decades [1–7]. This method performs the separation of small quantities of ionic components of a sample in a complex buffer system. It has significant applications in biochemical and medical separations. Instrumentation for cITP traditionally includes a PTFE separation capillary, an injector and one or more detectors [1]. Common injectors include valves and taps which both yield reproducible injection volumes with little or no mixing, but which are complex and expensive. Widely used detectors include UV absorption, and those based on conductivity and fluorescence [1,2]. These measure respective zone properties and have poor resolution; therefore, the performance of the technique is often limited by the detection system.

In this paper we describe simple cITP instrumentation which was constructed in-lab with a few starting materials and access to a machine shop. In our design we use the universal concentration-gradient detector which detects the refractive index gradients associated with high concentration gradients formed at the narrow boundary between two zones of analytes [8–11]. Applications of this inexpensive instrumentation to the separation and determination of the purity of synthetic peptides are described.

0021-9673/91/$03.50

EXPERIMENTAL

The ITP system consisted of an injector and separation capillary, and the concentration-gradient detection system consisting of a laser, a focusing lens and a position sensor [12]. The laser beam is focused directly into the separation capillary and is then intercepted by the position sensor.

Capillary isotachophoresis instrumentation

Fig. 1 shows the assembly of the homemade sliding injector. It was built in a student science shop. Two polytetrafluoroethylene resin rods, 10 cm × 1.9 cm diameter are require to construct the plunger and the house. The size can be varied based on the dimensions required.

The plunger was made first, by machining one rod on a lathe to the required diameter, in this case 6.4 mm. The plunger must be machined to a smooth surface so that it can easily slide into the housing. A "head" is left on one end of the plunger (2 in Fig. 1), while the other end remains bare so that it can slide into the injector housing. The length of the plunger must be longer than the housing by a distance slightly greater than the predetermined sliding distance. The exact length of the plunger is adjusted later. The house for the plunger is made next using the second PTFE rod. A hole is drilled through the rod with a diameter about 0.25 mm smaller than that of the plunger. Then the hole is smoothed with a reamer on the lathe so that the plunger fits in tightly. A tight fit allows vertical motion of the plunger upon applying a force, but prevents free movement of the plunger as well as leakage between the plunger and the

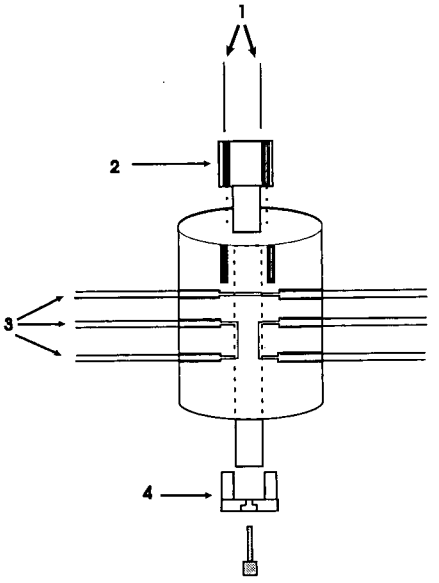

Fig. 1. Diagram of the injector showing the plunger in its housing. 1 = Two rods extending from the head of plunger down into the house which guides the movement of the plunger and prevents horizontal rotation; 2 = plunger head; 3 = capillaries joined tightly into holes drilled in housing, by a butt-type connection; 4 = screw cap on plunger.

house. Two aluminium rods were inserted through the plunger head, down into the housing to prevent horizontal rotation during the sliding motion. These are shown in Fig. 2 and labelled 1.

Three parallel holes are drilled through one side of the housing, and then through the opposite face, with a diameter equal to that of the separation capillary, in this case 0.30 mm. The plunger, aligned in the housing, is also marked with drill bits to map out the placement of the grooves and canal, and is then removed in order to drill the canal and to cut the grooves. The holes in the housing sides are enlarged partway into the housing with a diameter equal to the outer diameter of the capillaries used, 0.76 mm. The plunger and housing are depicted, partially assembled, in Fig. 1. The capillaries fit into the housing by a butt-type connection (Fig. 1). Next, a screw cap is made for the plunger end, which determines the exact distance that the plunger slides.

The diameter of the hole drilled through the plunger, 0.30 mm, as well as the diameter of the plunger, 6.4 mm, determine the volume of the liquid injected. In this injector, about 0.5 μl is injected between the leading and tailing electrolyte. This volume can be varied by replacing the entire injector. Alternatively, a different plunger with a different-diameter hole drilled through it can replace the existing one.

During construction of the injector, care must be taken so that dead volumes are not created between the plunger and housing which may attract either micro gas bubbles from the electrolyte, or a thin layer of liquid. Either situation would decrease reproducibility and affect zone length. The dead volumes can be eliminated by a properly constructed tight fit or by placing narrow O-rings on the plunger brackering the sample hole.

To prepare for an ITP separation, the injector was first rinsed with leading electrolyte (LE), tailing electrolyte (TE) and sample. This was done while the injector was in the up position (Fig. 2A). The LE was filled by syringe action into the capillaries on one face of the injector, and the TE on the other. For example, the tailing electrolyte was filled in through capillary 3 on the bottom (Fig. 2A) up through the small groove

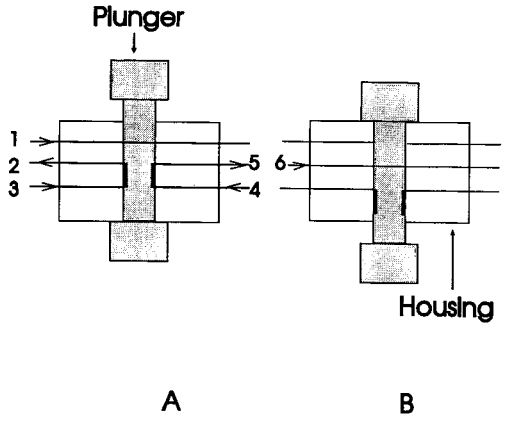

Fig. 2. Two stages of operation of the injector. (A) Stage 1. The plunger is in the up position in the housing, the rinse/fill position of the LE, TE and sample. (B) Stage 2. The plunger slides down in housing. The sample trapped in the plunger is now sandwiched between the LE and TE. The ITP separation follows. 1 = Fill with sample; 2,3 = fill with TE in through 3 and out through 2; 4,5 = fill with LE in through 4 and out through 5; 6 = separation capillary with sample in plunger.

cut in the plunger and out of the centre drainage capillary 2. Similarly, on the opposite side of the injector, the leading electrolyte is filled in through 4 on the bottom and out through 5. Excess LE exists through the separation capillary. The sample is rinsed into capillary 1, through the canal in plunger and exits by a drain capillary. When the rinsing is complete the two ends of the separation capillary are attached to two buffer reservoirs containing membranes.

The sample in the canal of the plunger is then injected (Fig. 2B) as the plunger slides down. The canal in the plunger is now aligned with the middle holes in the housing, 2 and 5. The canal, capillaries 2 and 5 now form the separation capillary 6 in Fig. 2B. The sample is now trapped between the LE contained in 5, and the TE in 2. The voltage is immediately applied.

The separation capillary is made of tetrafluoroethylene (TFE, Cole Parmer, Chicago, IL, USA) tubing, 0.30 mm I.D. × 0.76 mm O.D. The total length of the capillary is 33.0 cm and the length from the injector to the detector is 12.0 cm. This separation capillary was isolated on an XYZ translation stage (Model MR3 linear XYZ translation stage, Klinger Scientific, Montreal, Canada). Two buffer reservoirs were located at either end of the separation capillary. In both reservoirs, membranes (type EPA; Osmonics, Minnetonka, MN, USA) are used to prevent hydrodynamic flow within the capillary. If present, this flow will interfere with the separation. The injector, XYZ translation stage and detector were fastened securely to a stable table, to eliminate any vibrations or movements which would interfere with the optical detector [12].

The current is monitored at the grounded end of the separation capillary, by measuring a drop of voltage across a 1-kΩ resistor, using a digital multimeter (HM 8011-2, Hameg, Germany). A voltage-stabilized high-voltage power supply (Spellman, Plainview, NY, USA) is used to drive the separation. A plexiglass box houses the high-voltage end to shield the user and instruments. The potential is applied to platinum wires embedded into the buffer reservoirs. The negative end of the capillary is grounded.

Gradient detection instrumentation

Concentration-gradient detection was used and is described in further detail elsewhere [8–12]. The optical arrangement consists of a light source which is a helium–neon laser (Model GLG5261, NEC, Japan) and photodiode position sensor. The laser beam is focused to a small spot size of 40 μm directly into the separation capillary, by a focusing lens of focal length 38.10 mm. The probe beam is arranged so that the far field intensity profile points to the centre between two photodiodes placed close together [11]. When irradiated uniformly, the photodiodes generate equal amounts of photocurrent. Upon encountering a concentration gradient, for example at the boundary between two zones, the laser probe beam is deflected and the amount of light reaching the diodes is not equal. The difference in photocurrent associated with the two diodes corresponds to the magnitude of deflection of the laser beam. The difference in photocurrent generated by the diodes is converted to a voltage by a single operational amplifier. The data is collected by an IBM DACA board, in a PC-AT compatible personal computer, using the software ASYST (Asyst Softwares Technology, Rochester, NY, USA).

Reagents

For anionic separations, HCl (ACS reagent grade, Caledon Lab., Georgetown, Canada) was used as leading electrolyte. Counter ion was ammediol, 2-amino-2-(hydroxymethyl)-1,3-propanediol (J. T. Baker, Phillipsburg, NJ, USA). The ammediol was recrystallized twice from ethanol. An additive was added as stabilizer to the leading electrolyte, in this case 0.05% (w/v) polyvinyl alcohol (PVA, molecular mass 10 000; Sigma, St. Louis, MO, USA) was added.

All solutions were prepared from deionized water. The leading electrolyte was prepared by first dissolving the stabilizer in deionized water, and then adding HCl to the desired concentration. Counter ions were added last, and the pH of the solution was monitored by a Corning pH meter (Model 220, Suffolk, UK). Enough counter ion was added to reach a pH of 8.9.

The tailing electrolyte was β-alanine (Sigma), adjusted to a pH of 10.3 with $Ba(OH)_2$ (BDH, Toronto, Canada).

Solutions were filtered twice using 0.2-μm pore size cellulose acetate filters (Sartorius, Göttingen, Germany), and degassed before use by purging with helium. If solutions are not degassed, microbubbles from during the separation which block the passage of current and hinder the reproducibility of the separations. In addition, the presence of CO_2 in the solution will degrade the performance of the separation by the formation of carbonate ion [1]. Carbonate can be separated as a band immediately behind chloride ion and before the first sample, or it may interfere with the separation and distort zones. The effects of carbonate ion are decreased by the use of high-pH tailing electrolyte. The tailing electrolyte must therefore be bubble-free which is effectively done by purging with helium between separations. Also, between injections the separation capillary was washed twice with leading and tailing electrolyte. If the capillary is not rinsed twice, the separations are not reproducible.

DISCUSSION

Fig. 3 illustrates the trace generated when the concentration gradient detector is applied to detect the three boundaries formed in a cITP separation of a mixture of two amino acids between a leading and tailing ion. In this separation, the refractive index of each successive zone was higher than the previous one, from leading to tailing ion. This creates three positive deflections of the probe beam as the zone boundaries migrate by the detector. The broad base in the last valine/tailing electrolyte peak, corresponding to the boundary, is present because of a large temperature gradient between these two zones. In ITP separations, each of the zones has a characteristic temperature associated with it. If the difference in these temperatures is large (dT/dx), then the corresponding large refractive index gradient (dn/dx) is expected to distort the concentration-gradient information. However, it is easy to distinguish between the peaks associated with the concentration and temperature gradients since the latter will be broader, because of higher thermal diffusivities compared to mass diffusivities.

The concentration of analytes in separated zones is governed by the Kahlrausch regulating function which states that the concentration of a pure zone of one ionic species becomes adapted to the concentration of the LE. At a steady state, the concentration of components in zones is similar in magnitude and independent of the initial concentration of components in the injected sample mixture. At low concentra-

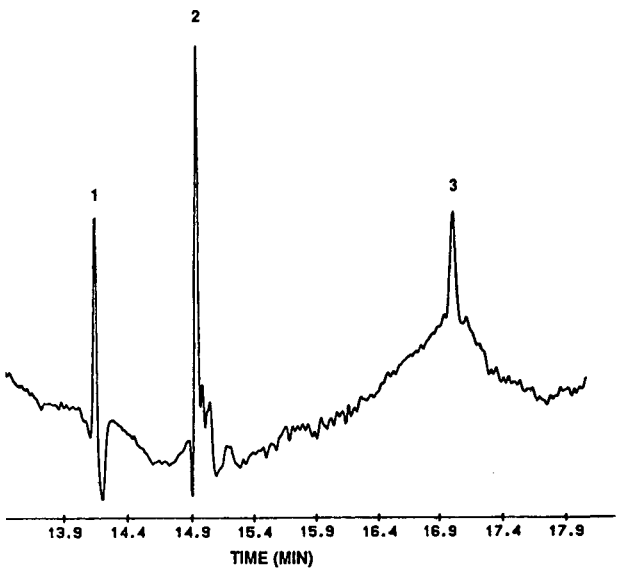

Fig. 3. cITP separation of two amino acids with concentration gradient detection. The leading ion is chloride ion (3 m*M*), counter ion is ammediol pH 8.9, tailing ion is β-alanine (3.0 m*M*) adjusted to pH 10.3 with $Ba(OH)_2$. Sample components are glutamic acid 0.3 m*M*, and valine 0.3 m*M*. Applied voltage is 5 kV.

tion of LE (2 m*M* chloride ion) and low concentration of sample, the concentrating effect of the LE on the sample will not be large. The final volume of each component and therefore the final zone length will be decreased only slightly since mass balance must be applied. For example, four components of a crude preparation of a synthetic peptide (not purified after solid-phase synthesis) were separated by cITP and detected with the high spatial resolution gradient detector (Fig. 4A) at a low LE concentration. This figure shows three major components forming the longest zones, composed of the peptide of interest and possible peptide fragments. The peptides are marked by boundaries 2–3, 3–4 and 4–5. The less than 0.5 mm zone marked by boundaries 1–2 is an impurity comprising about 7% of the total crude preparation. Similar results have been obtained by reversed-phase high-performance liquid chromatography (HPLC); however, the separation required a much longer separation time and more expensive instrumentation. Notice that the gradient detector is capable of marking the 0.5-mm zone indicating its high resolution. Fig. 4 illustrates the excellent compatibility of combining the universal non-destructive concentration gradient detector with cITP to determine the degree of peptide purity. Pure fractions can be collected for micro-preparative work, for example to determine biological activity, since the diameter of the capillaries used are large. cITP with the gradient detector offers an alternative method to reversed-phase HPLC for the separation and collection of pure components of a sample. HPLC, the most widely used chromatographic method for pure sample collection, primarily separates analytes on the basis of polarity. In contrast, cITP separates analytes on the basis of differences in ionic mobility in an electric field and therefore offers a method of separation complimentary to that available by HPLC [7].

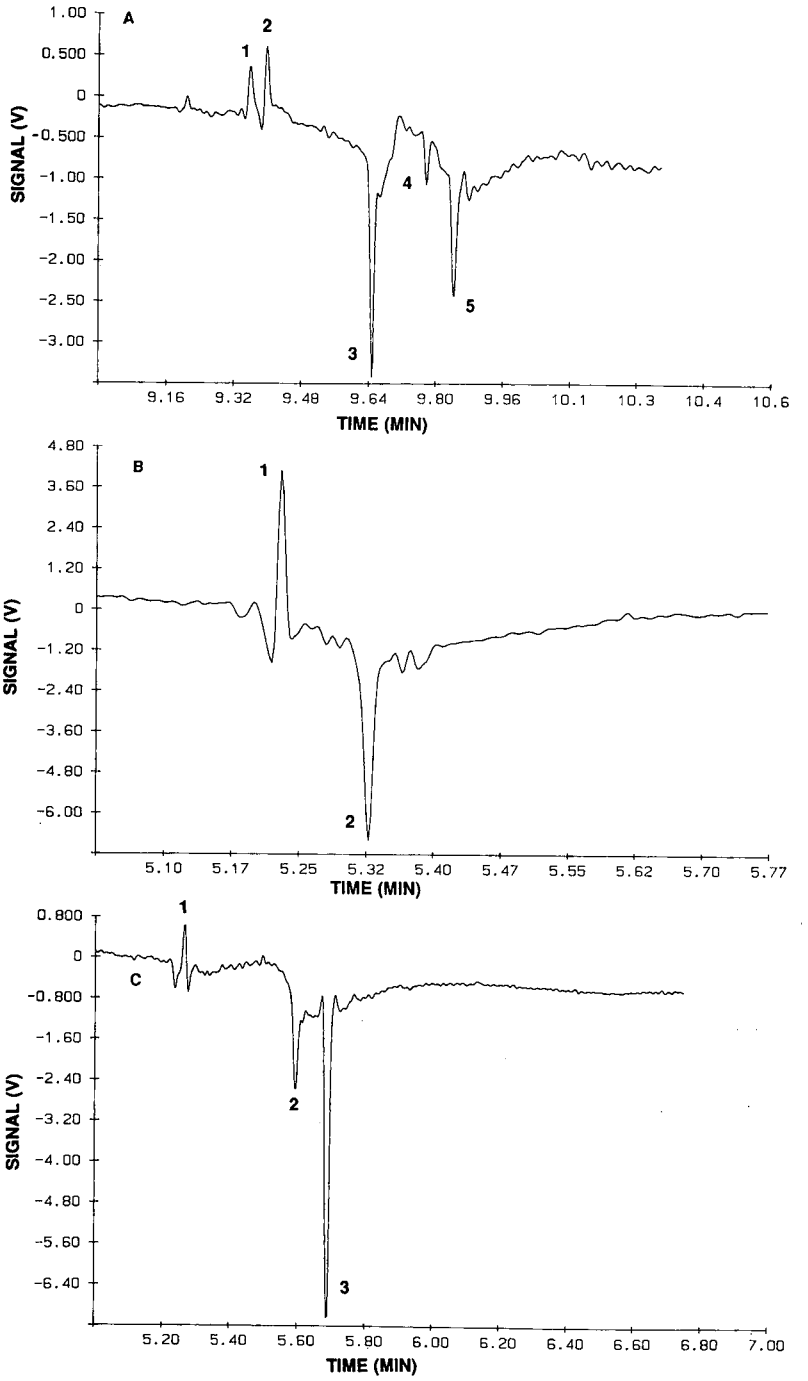

Fig. 4. cITP of crude synthetic peptide. Leading ion is chloride ion 2 mM, counter ion is ammediol pH 8.9, tailing ion is β-alanine 1.6 mM adjusted to pH 10.3 with $Ba(OH)_2$. (A) Injection of 0.5 μl of 0.6 mM concentration of a crude preparation of the linear peptide, 12 kV. (B) Injection of 0.5 μl of 0.3 mM concentration of the purified linear peptide, 12.5 kV. (C) Injection of 0.5 μl of 0.6 mM concentration of two other components of the crude preparation from (A), 13.5 kV.

In addition, the gradient detector can be used to mark the zones of pure sample components to facilitate effective identification with other spectroscopic methods [6].

Stages of a peptide purification scheme were examined with ITP and the concentration-gradient detector. The peptide of interest, Glu–Pro–Val–Thr–Leu–Asp–Leu–Lys–Tyr, formed in the crude separation shown in Fig. 4A has biological activity making it is possible therapeutic agent towards conditions such as emphysema and connective-tissue disorders. This peptide was isolated by reversed-phase HPLC, and the degree of purity of 0.2 nmol of the peptide was determined (Fig. 4B) by ITP with the concentration-gradient detector. The presence of two major boundaries, labelled 1–2 indicate one component, the peptide of interest. On either side of the boundaries marking the peptide zone there are a few small peaks. These are likely impurities which have formed into their own distinct zones. The signal-to-noise ratio of these peaks is very small versus the boundaries labelled as 1–2. The concentration-gradient detector gives a signal related to the molecular-mass difference between species, and therefore generates a large signal with a large molecular-weight difference and a corresponding small signal, such as the ones seen on either side of the two major peaks, with a small molecular-weight difference [8]. The small refractive index gradient of the unlabelled peaks indicates that these impurities have only small differences in refractive index between them and the LE or TE. These must be much smaller in size and molecular mass than the peptide and could be small ions, amino acids or fragments of peptides.

Other major fractions from the peptide synthesis, which were not the peptides of interest forming the main product, were also collected after separation by reversed-phase HPLC. They were isolated in order to check for possible biological activity. These were separated by ITP and detected by the concentration gradient detector (Fig. 4C). The three boundaries labelled as 1–2–3 map out the two major fractions, as zone 1–2 and zone 2–3. At least one of these two pure fractions is composed of a peptide which may also have some biological activity. The first boundary, 1, between the leading ion and highest-mobility component, shows a dip in the baseline around the boundary. This occurs because of a large temperature difference between the two zones, as discussed previously.

A portion of the peptide of interest was cyclized yielding a crude mixture of approximately 80% cyclized and 20% linear peptide. This crude mixture was separated using ITP (Fig. 5) under conditions similar to those previously described of high voltage and low concentrations. Three major boundaries are present and some smaller signals from impurities such as ions or peptide fragments. The first zone marked by boundaries 1–2 comprises 20% of the total distance between peaks 1–3, having a zone length of 1.0 mm. This is the linear unreacted peptide. The second zone marked by boundaries 2–3 has a zone length of 4.0 mm, comprising about 80% of the total distance and is the desired cyclized peptide. The results from ITP with the concentration gradient detector confirm the chromatogram obtained for the same mixture by reversed-phase HPLC.

The simple instrumentation described in this paper is a valuable and practical tool for the determination of peptide purity and collection of samples for micro-preparative work. The instrumentation can be easily adapted to capillary isoelectric focusing, a similar electrophoretic technique which has both self-sharpening and concentrating properties. In this method sharp zones of analytes along a pH gradient

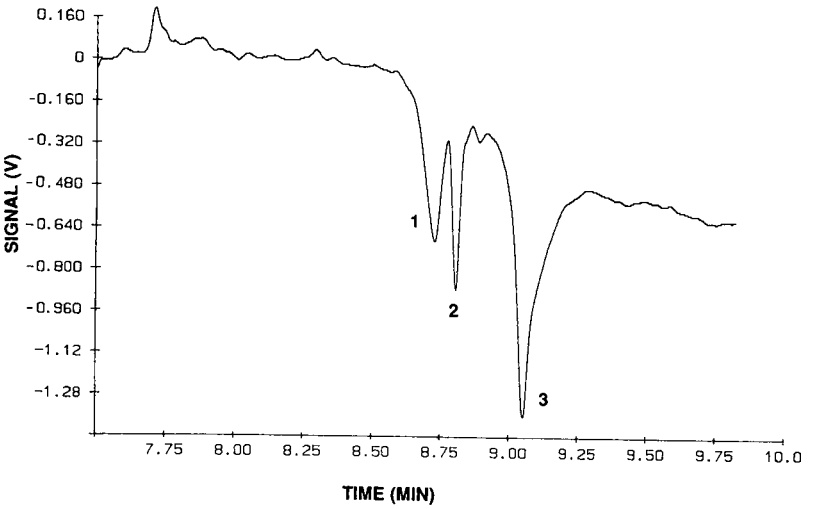

Fig. 5. cITP separation of a cyclized and linear peptide, 13 kV. Leading ion is chloride ion 2 mM, counter ion is ammediol pH 8.9, tailing ion is β-alanine 1.6 mM, adjusted to pH 10.3 with $Ba(OH)_2$. Injection was 0.5 μl of 0.45 mM of the mixture.

are formed, which can be effectively detected with the concentration-gradient detector. The cost of the system can be decreased to about US$ 150 by replacing the HeNe laser with a diode laser.

ACKNOWLEDGEMENTS

The Natural Sciences and Engineering Research Council of Canada supported this work. Beckman Instruments Inc. provided the high-voltage power supply. Dr. Lajoie, Peter Belshaw and Anna Crivici provided the synthesized peptides.

REFERENCES

1 F. Everaerts, J. Beckers and Th. P. E. M. Verheggen, *Isotachophoresis*, Elsevier, Amsterdam, New York, 1976.
2 P. Bocek, M. Demi, P. Gebauer and V. Dolnik, *Analytical Isotachophoresis*, VCH, Weinheim, 1988.
3 F. Everaerts (Editor), *Analytical Isotachophoresis —Proceedings of the 2nd International Symposium on Isotachophoresis, Eindhoven, September 9–11, 1980*, Elsevier, Amsterdam, 1980.
4 S. Hjalmarsson and A. Baldesten, *Crit. Rev. Anal. Chem.*, 11(4) (1981) 264.
5 J. Beckers and F. Everaerts, *J. Chromatogr.*, 508 (1990) 3–17, 19–26.
6 R. Smith, J. Loo, C. Edmonds, C. Barinaga and H. Udseth, *Anal. Chem.*, 61 (1989) 228.
7 P. Hermann, R. Jannasch and M. Lebl, *J. Chromatogr.*, 351 (1986) 283–293.
8 J. Pawliszyn, *Spectrochem. Acta Rev.*, 13 (1990) 311–354.
9 J. Pawliszyn, *Anal. Chem.*, 58 (1986) 243.
10 J. Pawliszyn, *Anal. Chem.*, 58 (1986) 3207.
11 J. Pawliszyn, *Rev. Sci. Instrum.*, 58, No. 2 (1987) 245.
12 T. McDonnel and T. Pawliszyn, *Anal. Chem.*, 63 (1991) 1884–1889.

Journal of Chromatography, 559 (1991) 499–504
Elsevier Science Publishers B.V., Amsterdam

CHROM. 23 464

Isotachophoretic analysis of flavonoids and phenolcarboxylic acids of relevance to phytopharmaceutical industry

ULRIKE SEITZ and GÜNTHER BONN*
Institute of Radiochemistry, University of Innsbruck, Innrain 52a, A-6020 Innsbruck (Austria)
PETER OEFNER
Department of Urology, University of Innsbruck, Anichstrasse 35, A-6020 Innsbruck (Austria)
and
MICHAEL POPP
Bionorica/Plantamed, Kerschensteinerstrasse 11-15, W-8430 Neumarkt (Germany)

ABSTRACT

Using capillary isotachophoresis, the rapid analysis of flavonoids and phenolcarboxylic acids was accomplished in the nanomole range. Optimum separations were achieved at pH 9.5 with a leading electrolyte containing 15 m*M* hydrochloric acid, 30% methanol and 0.2% hydroxypropylmethylcellulose. Under these conditions, the content of rutin could be determined in a methanolic extract of *Sambuci flos*, which is a common constituent of phytopharmaceutical products.

INTRODUCTION

Flavonoids are ubiquitous secondary plant metabolites. Their structures are based on 2-phenylbenzopyrone. The individual flavonoids vary in their degree of saturation and the pattern of substitution. In plants they exist mostly as mono- or diglycosides [1]. Flavonoids possess many pharmacological properties, of which antiphlogistic, spasmolytic, antiallergic, diuretic and anthelmintic activities are only a few [1]. In plants, flavonoids are often accompanied by phenolcarboxylic acids such as the analogues of cinnamic acid [2]. Because of the importance of flavonoids as remedies for inflammatory processes, their analysis is of considerable interest.

Existing methods commonly used for the analysis of flavonoids are high-performance liquid chromatography [3–7], thin-layer chromatography [8–11] and gas chromatography [12]. However, these analytical techniques tend to be time-consuming and laborious. Based on our experience with capillary isotachophoresis in the analysis of organic acids [13–17], its utility as a simple, rapid and economic alternative for the analysis of flavonoids and phenolcarboxylic acids in plant extracts was evaluated.

In the present study we investigated the influence of the pH and the percentage

0021-9673/91/$03.50

of methanol in the leading electrolyte on the resolution of flavonoids and phenolcarboxylic acids for their analysis in plant extracts.

EXPERIMENTAL

Sample pretreatment

All reference standard solutions were prepared from chromatographic- or analytical-reagent-grade chemicals (Sigma, St. Louis, MO, USA; Carl Roth, Karlsruhe, Germany) in methanol–water (80:20, v/v) at a concentration of 1 mg/ml. Flavonoids were extracted from 1 g of dried, pulverized flowers of *Sambucus nigra* (Caprifoliaceae) by means of 10 ml of methanol (Art. 6009, Merck, Darmstadt, Germany) for 5 min in a water bath kept at a temperature of 60°C. Subsequently, the sediment was filtered off (Art. 311642, Schleicher & Schuell, Dassel, Germany).

Isotachophoretic conditions

Isotachophoretic analyses were carried out on a LKB (Bromma, Sweden) Model 2127 tachophor equipped with a 250-mm PTFE capillary of 0.5 mm I.D.

The leading electrolyte was 15 m*M* hydrochloric acid (Art. 9057, Merck) in either water or mixtures of water and methanol (Art. 6009, Merck). The pH was adjusted to 8.5–9.5 by the addition of 2-amino-2-methyl-1,3-propanediol (Ammediol, A-2676, Sigma). The terminating electrolyte was 10 m*M* glycine (161-0718, Bio-Rad, Richmond, CA, USA) in methanol–water (30:70, v/v) adjusted to pH 10.6 by adding barium hydroxide (Art. 1737, Merck). Barium hydroxide precipitates the bicarbonate ions, which originate from dissolved carbon dioxide in alkaline media. Hydroxypropylmethylcellulose (HPMC, viscosity of 2% solution 4.000 centipoises, H7509, Sigma) was added to both the leading and the terminating electrolyte to reduce electroendosmosis.

The samples were injected through the inlet membrane into the leading electrolyte by means of 10-μl Hamilton syringes (Hamilton Bonaduz, Bonaduz, Switzerland). Usually separations were started at a current of 210 μA, which was gradually reduced to 60 μA shortly before the separated anions could be detected by means of their conductivity and differential conductivity. Analyses were carried out at a temperature of 20°C and took about 30 min.

RESULTS AND DISCUSSION

The phenolic nature of flavonoids indicates that the addition of organic solvents to the electrolytes may have a significant impact on their separation. Although flavonoids are soluble in alkaline media [1], their solubility is increased considerably by dissolving them in methanol, which belongs, like water, to the group of amphiprotic solvents with relatively high dielectric constants. Moreover, the acid–base characters of water and methanol do not differ much [18]. As long as the percentage of methanol does not exceed 30%, standard buffer solutions in water can be used to calibrate the pH meter in order to measure the pH of a methanol–water mixture correctly [19]. No corrections of the observed pH have to be made.

Using aqueous alkaline buffers, the investigated compounds, namely caffeic acid, luteolin, ferulic acid, chlorogenic acid, kaempferol, isoquercitrin, hyperosid and

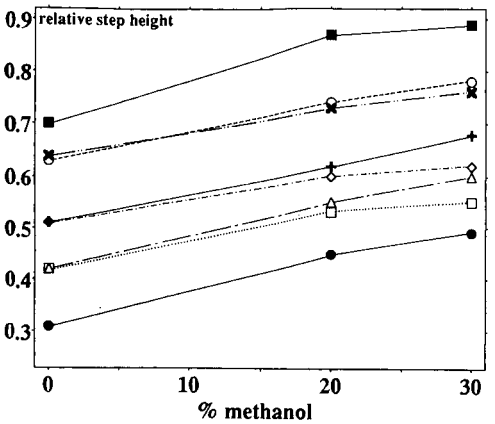

Fig. 1. Impact of the content of methanol in the running buffers on relative step heights (glycine = 1). Leading electrolyte: 15 m*M* hydrochloric acid–ammediol–0.2% HPMC, pH 9.5. Terminating electrolyte: 10 m*M* glycine–barium hydroxide–0.2% HPMC, pH 10.6. (●) Caffeic acid; (□) luteolin; (△) ferulic acid; (◇) chlorogenic acid; (+) kaempferol; (×) isoquercitin; (○) hyperosid; (■) rutin.

rutin, were resolved poorly. Owing to the change in solvation, resolution increased significantly upon addition of 20% methanol to the electrolytes. As Fig. 1 illustrates, optimum separability was obtained at a content of 30% methanol. This even allowed the separation of kaempferol and chlorogenic acid, which could not be resolved under aqueous conditions.

The parameter which primarily influences the effective mobilities of the analytes is the degree of dissociation. Because of their phenolic nature, an alkaline buffer system was chosen in order to ensure an adequate degree of dissociation of the flavonoids of interest. Fig. 2 shows the isotachophoretic analysis of a mixture of flavonoids and phenolcarboxylic acids commonly found in plant extracts at three different pH values of the leading electrolyte. The mixture contained caffeic acid, luteolin, chlorogenic acid, kaempferol, isoquercitrin and rutin. From the steepness of the steps in the conductivity signal it is evident that the highest resolution was obtained at a pH of 9.5. In addition, the third isotachopherogram indicates that the successful separation of flavonoids and phenolcarboxylic acids into individual zones is based on differences in negative charge and molecular weight. Compounds with lower molecular weight and larger numbers of free hydroxyls generally had greater mobility.

Fig. 3 shows the relative step heights of the investigated compounds in relation to glycine at pH 8.5, 9.0 and 9.5. The relative step heights of all compounds increased gradually with increasing pH of the leading electrolyte. However, as the change in mobility was not uniform, flavonoids such as kaempferol and isoquercitrin, which could not be separated at lower pH values, were resolved at a pH of 9.5. These results are contrary to those reported by Hiraoka *et al.* [20], who observed optimum resolution under neutral conditions.

By inhibiting electrode reactions and suppressing electroendosmosis, which is highest at high pH, surface-active compounds have a significant impact on boundary sharpness in isotachophoresis. While the investigated flavonoids were resolved rather

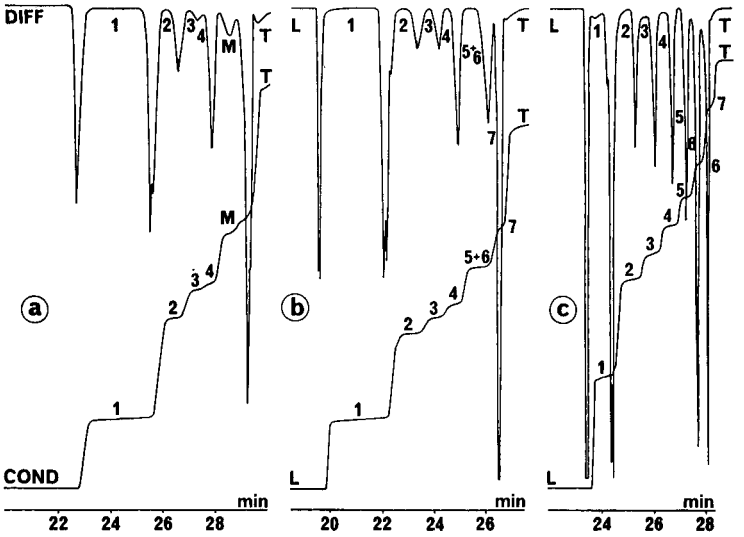

Fig. 2. Isotachopherograms of a standard solution of flavonoids and phenolcarboxylic acids at pH 8.5 (a), 9.0 (b) and 9.5 (c). Leading electrolyte (L): 15 m*M* hydrochloric acid–ammediol–0.2% HPMC in methanol–water (30:70, v/v). Terminating electrolyte (T): 10 m*M* glycine–barium hydroxide–0.2% HPMC in methanol–water (30:70, v/v), pH 10.6. Detection: conductivity (COND) and differential conductivity (DIFF). Current: 60 μA. Chart speed: 10 mm/min. Injection volumes: 2 μl. Zone identification: 1 = bicarbonate ions; 2 = caffeic acid; 3 = luteolin, 4 = chlorogenic acid; 5 = kaempferol; 6 = isoquercitin; 7 = rutin; M = mixed zones of kaempferol, isoquercitrin and rutin.

poorly when only 0.1% HPMC was added to the electrolytes, 0.2% HPMC was found to suppress electroosmotic flow efficiently and to ensure a constantly high resolution. Moreover, the increase in bulk viscosity might have also contributed to the enhanced boundary sharpness by reducing diffusion and convection effects.

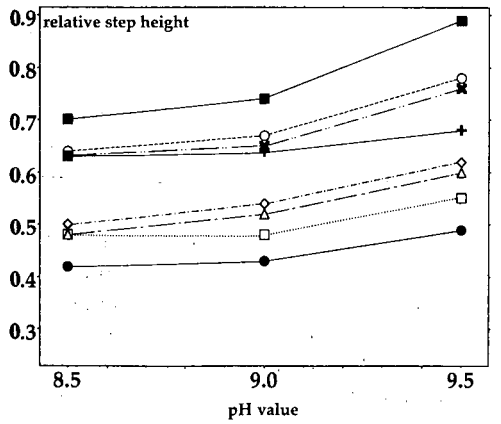

Fig. 3. Impact of the pH of the leading electrolyte on relative step heights (glycine = 1). Leading electrolyte: 15 m*M* hydrochloric acid–ammediol–0.2% HPMC in methanol–water (30:70, v/v). Terminating electrolyte: 10 m*M* glycine–barium hydroxide–0.2% HPMC in methanol–water (30:70, v/v), pH 10.6. Symbols as in Fig. 1.

Fig. 4. Isotachophoretic analysis of a methanolic extract of *Sambuci flos*. Leading electrolyte: 15 m*M* hydrochloric acid–ammediol–0.2% HPMC in methanol–water (30:70, v/v), pH 9.5. Terminating electrolyte: 10 m*M* glycine–barium hydroxide–0.2% HPMC in methanol–water (30:70, v/v), pH 10.6. Detection: conductivity (COND) and differential conductivity (DIFF). Current: 60 μA. Chart speed: 10 mm/min. Injection volume: 3 μl. Zone identification: R = rutin.

Fig. 4 shows the presence of rutin, which is the flavonoid of greatest interest to phytopharmaceutical industry, in a methanolic extract of *Sambuci flos*. Its identity was confirmed by the injection of an additional small amount of a standard solution, which resulted in an increase in the length of the respective zone.

Quantitative information was obtained by measuring the zone length. The calibration curve for rutin revealed a detection limit of 3.8 nmol and linearity over its biological concentration range. In least-square linear regression analysis, the representative equation of the line and the regression coefficient were $y = 50.286x + 2.667$ and $r^2 = 0.994$, respectively.

By allowing the rapid and reproducible determination of flavonoids in plant extracts, the developed isotachophoretic method may serve as a valuable tool in assessing quality in the phytopharmaceutical industry.

REFERENCES

1 E. Steinegger and R. Hänsel, *Lehrbuch der Pharmakognosie und Phytopharmazie*, Springer, Berlin, 1988, p. 394.
2 H. Wagner, S. Bladt and E. M. Zgainski, *Drogenanalyse*, Springer, Berlin, 1983, p. 164.
3 P. Pietta, E. Manera and P. Ceva, *J. Chromatogr.*, 357 (1986) 233.
4 F. A. Blouin and Z. M. Zarins, *J. Chromatogr.*, 441 (1988) 443.
5 B. Heimhuber, R. Galensa and K. Herrmann, *J. Chromatogr.*, 439 (1988) 481.
6 P. G. Pietta, P. L. Mauri, E. Manera and P. L. Ceva, *Chromatographia*, 28 (1989) 311.
7 M. C. Pietrogrande, C. Bighi, G. Blo, Y. D. Kahie, P. Reschiglian and F. Dondi, *Chromatographia*, 27 (1989) 625.

8 P. Spiegel, Ch. Dittrich and K. Jentzsch, *Sci. Pharm.*, 44 (1976) 129.
9 A. Hiermann and Th. Kartnig, *J. Chromatogr.*, 140 (1977) 322.
10 P. P. Schmid, *J. Chromatogr.*, 157 (1978) 217.
11 A. Hiermann, *J. Chromatogr.*, 174 (1979) 478.
12 W. Greenaway, S. English, E. Wollenweber and F. R. Whatley, *J. Chromatogr.*, 481 (1989) 352.
13 P. J. Oefner, G. Bonn and G. Bartsch, *Fresenius' Z. Anal. Chem.* 320 (1985) 175.
14 P. J. Oefner, P. Pohl and G. Bonn, *Ann. N.Y. Acad. Sci.*, 529 (1988) 193.
15 P. J. Oefner, S. Wongyai, G. Bonn and G. Bartsch, in D. S. Coffey and W. Gardner (Editors), *Cytopathology/Flow Cytometry and Prognostic Indicators of Prostate Cancer*, Elsevier, New York, 1988, p. 374.
16 G. Bonn, P. J. Oefner and O. Bobleter, *Fresenius' Z. Anal. Chem.*, 331 (1988) 46.
17 P. Oefner, R. Häfele, G. Bartsch and G. Bonn, *J. Chromatogr.*, 516 (1990) 251.
18 F. M. Everaerts, J. L. Beckers and Th. P. E. M. Verheggen, *Isotachophoresis: Theory, Instrumentation and Application*, Elsevier, Amsterdam, 1976, p. 87.
19 J. L. Beckers, *Thesis*, Eindhoven University of Technology, Eindhoven, 1973, p. 93.
20 A. Hiraoka, K. Yoshitama, T. Hine, T. Tateoka and T. N. Tateoka, *Chem. Pharm. Bull.*, 35 (1987) 4317.

Journal of Chromatography, 559 (1991) 505–513
Elsevier Science Publishers B.V., Amsterdam

CHROM. 23 463

Determination of thiopental in human serum and plasma by high-performance capillary electrophoresis–micellar electrokinetic chromatography

PETER MEIER and WOLFGANG THORMANN*
Department of Clinical Pharmacology, University of Bern, Murtenstrasse 35, CH-3010 Bern (Switzerland)

ABSTRACT

The quantitation of thiopental in human serum and plasma was investigated using high-performance capillary electrophoresis (HPCE) in a micellar configuration and the results were compared with reversed-phase high-performance liquid chromatography (HPLC). Thiopental and an internal standard (carbamazepine for HPCE and thiamylal for HPLC) were extracted from serum or plasma using pentane and a phosphate buffer (pH 6.4). HPCE analysis took place in a phosphate–borate buffer with 50 m*M* sodium dodecyl sulphate using an automated instrument and HPLC was performed with a C_8 column and a mobile phase of phosphate buffer–acetonitrile (65:35, v/v). HPCE and HPLC data from 66 patient samples compared well based on linear regression analysis. However, estimates obtained with the inclusion of the internal standard were lower than those based on the sample peak only. This example allows the elucidation of the advantages of using HPCE as an assay methodology for the therapeutic monitoring of thiopental and other drugs.

INTRODUCTION

The barbiturate thiopental is used for anaesthetic and pre-anaesthetic medication and for the treatment of head trauma with severe brain injury. It has a low therapeutic index and is therefore prone to cause poisoning. Monitoring its concentration in body fluids is important for the optimization of pharmacotherapy. The therapeutic range of thiopental is not yet clearly established, but plasma concentrations in the range 1–40 μg/ml have been found to be efficient in many treatments [1,2]. Several immunoassays [3–5] and chromatographic methods [6–9] have been developed for the determination of thiopental in serum. The immunological techniques are attractive because of their ease of performance, speed of analysis and sensitivity. However, these assays are not specific and sensitive enough to monitor thiopental in the presence of other barbiturates, including its metabolite pentobarbital. Chromatographic procedures, and high-performance liquid chromatography (HPLC) in particular, have been successfully applied to the determination of thiopental, although they are rather time-consuming.

High-performance capillary electrophoresis (HPCE) and micellar electrokinetic

0021-9673/91/$03.50

capillary chromatography (MECC; an interface between electrophoresis and chromatography) have been shown to be attractive approaches to the determination of drugs in body fluids [10–15]. It has previously been shown that barbiturates in human urine and serum can be determined by an HPCE–MECC technique where the separation is based on a combination of differential partitioning and differences in electrophoretic mobilities [16]. This paper reports the determination of thiopental in human plasma using HPCE–MECC (abbreviated as HPCE throughout this paper) and data are compared with those obtained by reversed-phase HPLC.

EXPERIMENTAL

Drugs and chemicals

Thiopental (Pentothal, containing 6% sodium carbonate) was from Abbott Labs. (Cham, Switzerland) and thiamylal, carbamazepine and sodium dodecyl sulphate (SDS) were from Sigma (St. Louis, MO, USA). Methanol and acetonitrile (both HPLC grade) were from Rathburn Chemicals (Walkerburn, UK); *n*-pentane (99% pure), potassium dihydrogenphosphate, sodium dihydrogenphosphate, sodium borate and phosphoric acid (85%) were from Merck (Darmstadt, Germany). Bovine plasma, used as the calibration material, was prepared by centrifugation (1500 *g* for 10 min) of bovine blood which was obtained from the local slaughter house.

Patient samples

Patient samples were received from the Department of Anesthesiology and Intensive Care, Inselspital (Bern, Switzerland) from patients undergoing short-term thiopental infusion (100 mg/min for 6–9 min). Blood samples were drawn during the infusion period and at increasing time intervals over a period of 24 h thereafter.

Preparation of standard solutions

Methanolic standard solutions of thiopental (100 μg/ml), thiamylal (20 μg/ml) and carbamazepine (2 mg/ml) were prepared and stored at 4°C. Blank and patient sera were spiked by the addition of known aliquots of these standard solutions to body fluids prior to sample extraction.

Extraction procedure

Liquid–liquid extraction of thiopental and the internal standards was achieved with pentane at pH 6.4, as described by Elbling *et al.* [17]. Briefly, 0.5 ml of patient serum spiked with 100 μl of a solution containing the internal standard (or 0.5 ml of bovine plasma spiked with thiopental and internal standard), 1 ml of pH 6.4 phosphate buffer (about 0.07 *M*) and 5 ml of *n*-pentane were added to a 11-ml screw-capped Sovirel test-tube. After vigorous shaking for 10 min and centrifugation at 1500 *g* for 10 min the upper (organic) phase was transferred into a centrifuge glass tube with a short conical bottom and then evaporated to dryness under a gentle stream of nitrogen at 40°C. For HPCE (HPLC) the residue was dissolved in 200 μl of running buffer (200 μl of mobile phase) and vortexted for about 60 s.

HPCE

A Model 270A capillary electrophoresis system (Applied Biosystems, San Jose,

CA, USA) was used. This apparatus features automated capillary rinsing, sampling and execution of the electrophoretic run. For these experiments it was equipped with a 50 μm I.D. fused-silica capillary of 50 cm effective separation length. A Model D-2000 chromato-integrator (Merck-Hitachi, Darmstadt, Germany) was used for recording the pherograms and for quantitation by peak-area measurements. The integrator sampling period was set to one data point per 200 ms. As an alternative a PC integration pack (version 2.50, Kontron Instruments, Zürich, Switzerland), together with a Mandax AT 286 computer system, were used for data acquisition, raw data storage and integration of the signals. The pack features automatic range switching and a dynamic sampling rate allowing sampling every 10 ms for quickly changing signals. Before each run the capillary was rinsed with 0.1 *M* sodium hydroxide (1 min) and buffer (2 min). The running buffer, if not stated otherwise, was composed of 50 m*M* SDS, 9 m*M* sodium borate and 15 m*M* sodium dihydrogenphosphate (pH about 7.8). Injection of the sample was by vacuum suction (typically 2 s). In most experiments a constant voltage of 30 kV (current 55–60 μA) was applied, the temperature was set at 40°C and detection occurred at 290 nm. Under these conditions, thiopental and carbamazepine (internal standard) eluted after about 4 and 7.5 min, respectively, and the total analysis time was about 10.5 min.

HPLC

HPLC analyses were performed using a Model M45 solvent delivery system, a WISP 712 autosampler (both from Waters Assoc., Milford, MA, USA), a reversed-phase C_8 column (Nucleosil 5 C_8, 250/8/4, Macherey Nagel, Oensingen, Switzerland) and a Spectroflow Model 757 UV detector (Kratos Analytical, Ramsey, NJ, USA). Chromatograms were recorded and integrated by a Model 3390A integrator (Hewlett-Packard, Basel, Switzerland). The integrator sampling rate was set to five data points per min (peak width 0.20 min). The mobile phase consisted of a mixture of an aqueous phosphate buffer (0.2 m*M* phosphoric acid and 0.175 m*M* potassium dihydrogenphosphate) and acetonitrile (65:35, v/v). Thiamylal served as the internal standard, the injection volume was 5 μl, the flow-rate was 1.2 ml/min, the temperature was ambient and detection was at 290 nm. Under these conditions, thiopental and thiamylal eluted after about 10 and 12 min, respectively, and the total analysis time was 15 min. After each sample series the column was first rinsed with mobile phase (30 min) and then for about 60 min with a mixture of acetonitrile–water (35:65, v/v).

RESULTS AND DISCUSSION

The electropherograms in Fig. 1 represent the analysis of a model mixture of seven barbiturates (20 μg/ml each) detected at 215, 254 and 290 nm. This result confirms the HPCE data with fast-scanning polychrome detection reported elsewhere [16]. Thiopental is monitored at 290 nm selectively and with the highest sensitivity. Peak 5a represents an isomer of thiopental found in the commercial thiopental product (Fig. 2), a barbiturate which can also be detected by HPLC [9]. Each component is characterized by its retention and migration behaviour, with barbital being the fastest and pentobarbital the slowest of the components investigated. For detection at 290 nm, none of these barbiturates can be used as an internal standard for the determination of thiopental. Therefore, thiamylal (Fig. 2), which was often used for the HPLC

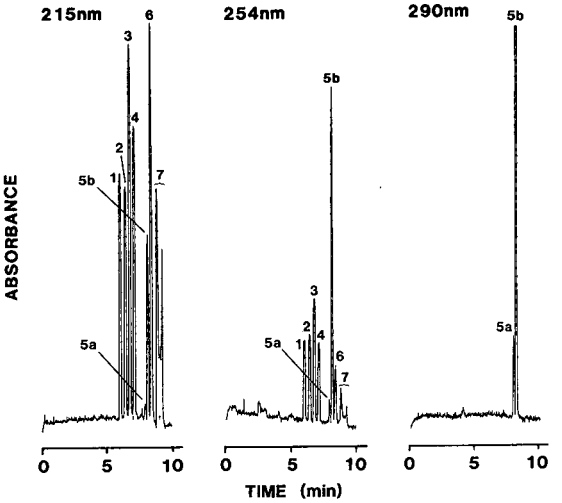

Fig. 1. HPCE data of a model mixture of seven barbiturates (20 μg/ml each) monitored at three different wavelengths. The injection time was 5 s and the applied voltage was a constant 20 kV (current 35 μA). Peaks: 1 = barbital; 2 = allobarbital; 3 = phenobarbital; 4 = butalbital; 5a = isomer of thiopental; 5b = thiopental; 6 = amobarbital; 7 = pentobarbital.

determination of thiopental [9,17], was considered. Retention of that compound, however, was found to be only slightly larger than thiopental. Modifications of the buffer composition, such as pH, SDS concentration (between 20 and 100 m*M*) and addition of methanol (up to 10%, v/v) did not sufficiently alter the separation of the two compounds to obtain full resolution in a capillary of 50 cm length. Resolution was attained with much longer columns, but the analysis times became too long for practical purposes. Therefore, carbamazepine (a compound also used in HPLC [7]) was used as the internal standard for all HPCE determinations of thiopental reported here.

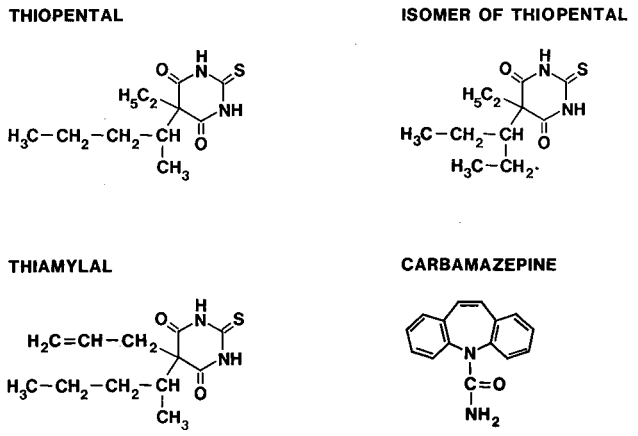

Fig. 2. Structures of thiopental, its isomer, thiamylal and carbamazepine.

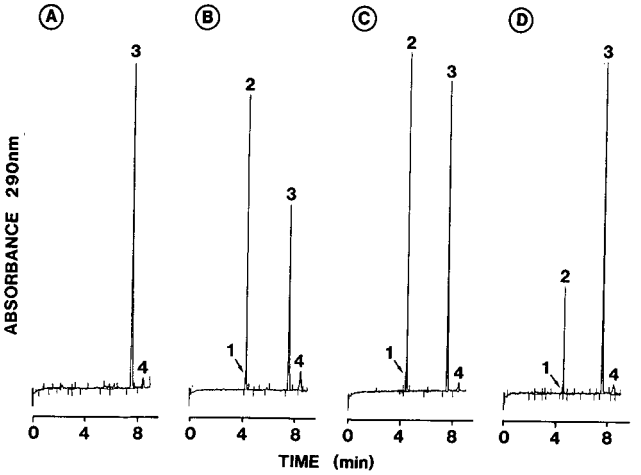

Fig. 3. Electropherograms of two calibration samples [(A) bovine plasma spiked with carbamazepine (0.4 mg/ml); (B) bovine plasma spiked with internal standard and 40 μg/ml thiopental] and two patient samples [(C) 23.6 μg/ml; (D) 6.4 μg/ml thiopental]. All experiments were performed with a 2-s injection and a constant 30-kV voltage (55–60 μA). Peaks: 1 = isomer of thiopental; 2 = thiopental; 3 = carbamazepine; 4 = unknown compound.

Fig. 3 shows typical electropherograms obtained after the extraction of two calibration (panels A and B) and two patient (panels C and D) samples. Thiopental (2), its isomer (1), carbamazepine (3) and an unknown compound (4) were detected (290 nm) within about 8 min of current flow beginning. Typical chromatograms of the HPLC determination of thiopental with thiamylal as the internal standard are shown in Fig. 4. Here excellent separation of the two barbiturates and the isomer of thiopental was obtained with an analysis time of about 12 min. All the calibration chromatograms contained an unknown peak (1) in front of the isomer and all data panels showed an impurity of unknown origin (4) which eluted between thiopental (3) and thiamylal (5). Comparison of the data in Figs. 3 and 4 reveal that the HPCE peaks are significantly sharper than those monitored in HPLC.

The reproducibility of the HPCE determination of thiopental is given in Table I. Here typical means and the relative standard deviations of ten consecutive injections evaluated with the D-2000 chromato-integrator and the PC integration pack are given. Different capillaries (and samples) were used for the two sets of data. With both methods the carbamazepine peak was integrated with a higher reproducibility than that of thiopental. The peak of the isomer in front of that of thiopental may be attributed to this difference. Retention times, although gradually increasing within the sets of ten injections, showed the best reproducibility of all parameters tested. These data are comparable to those reported with model compounds [18].

The quantitation of thiopental in human serum was performed (i) by the internal standard method and (ii) by direct calibration with the thiopental peak, *i.e.* without the inclusion of an internal standard. Calibration graphs were constructed with spiked bovine plasma in the concentration range 2–60 μg/ml (six data points). Peak areas were used as the basis for data evaluation, providing graphs with good

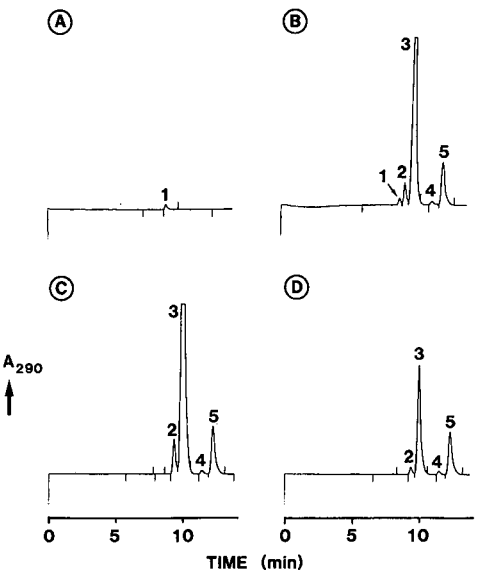

Fig. 4. Chromatograms of (A) bovine plasma blank, (B) bovine plasma spiked with thiamylal (internal standard, 4 μg/ml) and 40 μg/ml thiopental, and (C, D) of two patient samples [(C) 31.4 μg/ml thiopental; (D) 7.1 μg/ml thiopental] spiked with thiamylal (4 μg/ml). Peaks: 1 = unknown compound extracted from bovine plasma; 2 = isomer of thiopental; 3 = thiopental; 4 = unknown impurity; 5 = thiamylal.

linearities and small y-intercepts. Table II lists the statistical data of seven HPCE and HPLC calibrations which were based on peak-area measurements using the D-2000 and the HP 3390A instruments, respectively. Evaluations based on the inclusion of the internal standards are referred to as "ratio", whereas those with calibration using peak areas of thiopental only are referred to as "area". An increased concentration range to 80 μg/ml thiopental (or higher) could best be fitted with a quadratic regression analysis (data not shown). Similar results were obtained when (i) peak heights

TABLE I

REPRODUCIBILITY DATA FOR TEN CONSECUTIVE INJECTIONS

Integration method	D-2000 chromato-integrator[a]		PC integration pack[b]	
	Mean	Relative standard deviation (%)	Mean	Relative standard deviation (%)
Retention time of thiopental (min)	4.617	0.95	5.22	1.11
Area of thiopental (μV s)	39965	3.73	81420	6.93
Area of carbamazepine (μV s)	69180	2.04	39000	3.54
Area ratio thiopental/carbamazepine	0.577	2.08	2.087	5.22
Thiopental concentration (μg/ml)	25.83	1.93	–	–

[a] Patient sample spiked with carbamazepine (0.4 mg/ml).
[b] Calibration sample spiked with thiopental (40 μg/ml) and carbamazepine.

TABLE II

STATISTICAL EVALUATION OF SEVEN CALIBRATION GRAPHS

Calibration graph	Slope	y-Intercept	Correlation coefficient
HPCE ratio[a]	40.177 ± 4.087	−0.022 ± 2.878	0.977 ± 0.003
HPCE area[b]	0.00136 ± 0.000938	−2.990 ± 3.778	0.994 ± 0.007
HPLC ratio[a]	4.035 ± 0.690	0.159 ± 0.904	0.994 ± 0.013
HPLC area[b]	6.186 ± 0.565	−0.659 ± 1.133	0.998 ± 0.001

[a] Data evaluation with inclusion of internal standard.
[b] Data evaluation without inclusion of internal standard.

were used as the basis for data evaluation and (ii) the PC integration pack was used instead of the integrators.

Sixty-six serum samples of four patients obtained during and within about 24 h after short-term (see under Experimental) thiopental infusion were analysed using the two methods. A comparison of all the data evaluated on the basis of peak-area ratios,

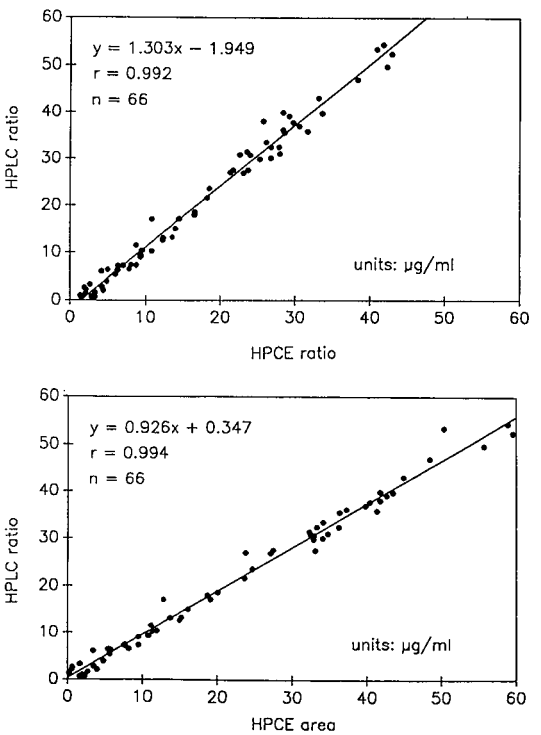

Fig. 5. Comparison of HPCE and HPLC data of 66 patient samples. The acronym "area" represents data evaluated based on thiopental areas and without inclusion of internal standard, whereas "ratio" stands for evaluation based on area ratios (inclusion of internal standard). All electropherograms were integrated with the D-2000 instrument.

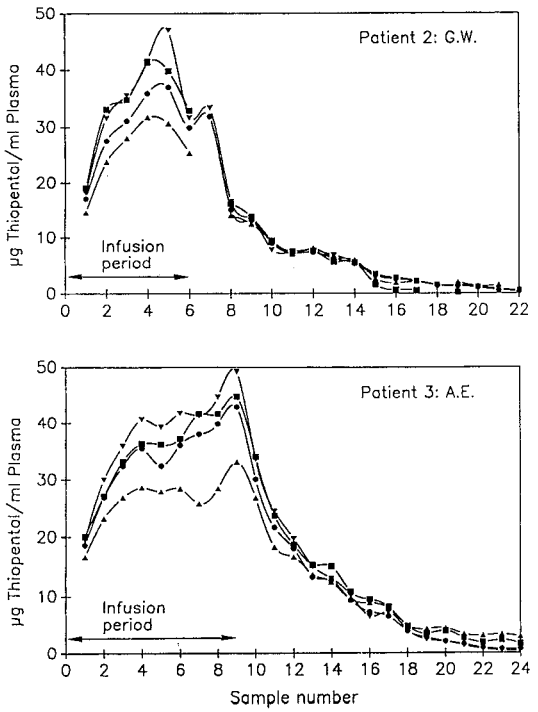

Fig. 6. HPCE and HPLC data of two patients plotted as a function of sample number which were obtained during thiopental infusion and (at increasing time intervals) over about 24 h thereafter. Other conditions are identical to those in Fig. 5. Symbols: (●) HPLC ratio; (▲) HPCE ratio; (■) HPCE area; (▼) HPLC area.

i.e. with calibrations established using the ratio of the area of thiopental divided by the area of the internal standard, are presented in the upper panel of Fig. 5. The data show a good linear correlation which, however, is not identical to the line of equality. It is interesting that the correlation of HPLC data based on area ratios with HPCE data obtained without the use of the internal standard correlated better (lower panel of Fig. 5). Linear regression analysis of the HPCE data based on area ratios *versus* those based on the thiopental peak area only (slope 1.40; y-intercept -2.39; correlation coefficient 0.994; $n = 66$) showed much stronger deviations from the line of equality than the same analysis of the HPLC results (slope 1.15; y-intercept -0.68; correlation coefficient 0.999; $n = 24$). The discrepancy of the estimates obtained by the different procedures is also seen by plotting the thiopental concentrations of single patients as a function of sample number (Fig. 6). No explanation has yet been found to account for these differences, which are most pronounced in the HPCE data obtained with the inclusion of the internal standard.

CONCLUSIONS

The results reported in this paper suggest that HPCE can be easily used for the determination of thiopental in human serum or plasma. After extraction, this barbit-

urate can selectively and sensitively be monitored at 290 nm. Peak integration can be executed with a stand-alone integrator or a PC integration pack, both developed for the evaluation of chromatograms. For the concentration range 2–60 μg/ml and using different quantitation procedures, such as peak areas with and without internal standard, calibration graphs using bovine plasma spiked with thiopental always showed good linear correlations. HPLC and HPCE data from 66 patient samples compared well based on linear regression analysis. However, the graphs always deviated from the line of equality. The reasons for this behaviour are the subject of on-going investigations. For therapeutic drug monitoring, such differences are relatively insignificant. Using HPCE instead of HPLC for the therapeutic monitoring of thiopental has several important advantages. These are a high degree of automation, small sample size, no requirement for large amounts of organic solvents and rapidity of analysis. Furthermore, HPCE allows a fast change from one buffer configuration to another separation medium.

ACKNOWLEDGEMENTS

Valuable discussions with and reception of the patient sera from Drs. P. O. Maitre, M. Bührer and D. R. Stanski of the Department of Anesthesiology and Intensive Care, Inselspital (Bern, Switzerland) are gratefully acknowledged. The authors also thank T. Schär, Y. Aebi and R. Stotzer for technical assistance. This work was partly sponsored by the Research Foundation of the University of Bern and the Swiss National Science Foundation.

REFERENCES

1 A. Forbes, G. J. M. Alexander, J. G. O'Grady, R. Keays, R. Gullan, S. Dawling and R. Williams, *Hepatology*, 10 (1989) 306.
2 R. F. Shaw, *Barbiturates, Abused Drugs Monograph Series*, Abbott Labs., Diagnostics Division, Irving, TX, 1988, and references cited therein.
3 B. E. Pape, P. L. Cary and L. C. Clay, *Ther. Drug Monit.*, 5 (1983) 473.
4 A. T. Watson, J. E. Manno and B. R. Manno, *J. Anal. Toxicol.*, 7 (1983) 257.
5 D. L. Colbert, D. S. Smith, J. Landon and A. M. Sidki, *Clin. Chem.*, 30 (1984) 1765.
6 R. Gill, A. A. T. Lopes and A. C. Moffat, *J. Chromatogr.*, 226 (1981) 117.
7 C. Salvadori, R. Farinotti, Ph. Duvaldestin and A. Dauphin, *Ther. Drug Monit.*, 3 (1981) 171.
8 G. K. Shiu and E. M. Nemoto, *J. Chromatogr.*, 227 (1982) 207.
9 D. R. Stanski, P. G. Burch, S. Harapat and R. K. Richards, *J. Pharm. Sci.*, 72 (1983) 937.
10 M. C. Roach, P. Gozel and R. N. Zare, *J. Chromatogr.*, 426 (1988) 129.
11 Y. Tanaka and W. Thormann, *Electrophoresis*, 11 (1990) 760.
12 T. Nakagawa, Y. Oda, A. Shibukawa and H. Tanaka, *Chem. Pharm. Bull.*, 36 (1988) 1622.
13 T. Nakagawa, Y. Oda, A. Shibukawa, H. Fukuda and H. Tanaka, *Chem. Pharm. Bull.*, 37 (1989) 707.
14 H. Nishi, T. Fukuyama and M. Matsuo, *J. Chromatogr.*, 515 (1990) 245.
15 H. Nishi and S. Terabe, *Electrophoresis*, 11 (1990) 691.
16 W. Thormann, P. Meier, C. Marcolli and F. Binder, *J. Chromatogr.*, 545 (1991) 445.
17 W. F. Ebling, L. Mills-Williams, S. R. Harapat and D. R. Stanski, *J. Chromatogr.*, 490 (1989) 339.
18 K. Otsuka, S. Terabe and T. Ando, *J. Chromatogr.*, 396 (1987) 350.

Journal of Chromatography, 559 (1991) 515–528
Elsevier Science Publishers B.V., Amsterdam

CHROM. 23 432

Determination of small drug molecules by capillary electrophoresis–atmospheric pressure ionization mass spectrometry

I. MONIKA JOHANSSON[a], ROBERT PAVELKA and JACK D. HENION*
Drug Testing and Toxicology, Cornell University, 925 Warren Dr., Ithaca, NY 14850 (USA)

ABSTRACT

Capillary electrophoresis (CE) separations are reported for sulfonamides and benzodiazepines in an uncoated fused-silica capillary. The capillary column exit was connected to a liquid junction–ion spray interface combination coupled to an atmospheric pressure ionization (API) triple quadrupole mass spectrometric (MS) system. On-line UV detection occurred 20 cm from the inlet of the capillary and with the API mass spectrometer (CE–API-MS) after the entire length of the capillary (100 cm). The separations were made using volatile buffers composed of ammonium acetate (15–20 m*M*) with 15–20% of methanol to facilitate ionization under electrospray conditions. This study showed that the major metabolite of flurazepam in man, N-1-hydroxyethylflurazepam, could be detected and characterized in human urine by CE–UV–MS following the administration of a single oral dose of 30 mg of flurazepam dihydrochloride. The presence of additional flurazepam metabolites in human urine was observed by using the system, suggesting that a combination of UV with MS detection should be useful for metabolic studies. In addition to molecular weight determination of compounds, structural information may be obtained by utilizing on-line tandem mass spectrometry (CE–UV–MS–MS). This was demonstrated for sulfamethazine where the protonated molecule species was transmitted into the collision cell of the tandem triple quadrupole mass spectrometer. Collision-induced dissociation of the protonated sulfamethazine molecule yielded structural information characteristic of the sulfa drug following the on-column injection of 2 pmol of sulfamethazine.

INTRODUCTION

The development and use of capillary electrophoresis (CE) as a separation technique has expanded in recent years [1]. In CE, charged compounds are separated under the influence of a high electrical field in small-diameter capillary tubes filled with buffer. Efficient separations, short analysis times and low sample consumption make CE a very attractive separation technique. The most common detectors for CE include UV absorbance or fluorescence detectors, but an increasing number of applications utilizing mass spectrometric (MS) detection have been reported [2–14].

Developments in CE–MS interfacing have been based either on electrospray or

[a] Present address: University of Uppsala, Equine Drug Research Laboratory, Ulleråker, S-750 17 Uppsala, Sweden.

0021-9673/91/$03.50

ion spray ionization at atmospheric pressure [2–11] or on continuous-flow fast atom bombardment (CF-FAB) [12–14]. The CE–MS inferface is needed to facilitate coupling of the low CE buffer flow to the mass spectrometer or to introduce the matrix required for the CF-FAB process. The make-up liquid is introduced either by a liquid junction [3,7–9,11,13,14] or as a sheath flow arrangement [4–6,10,12]. Here we have used a pneumatically assisted electrospray (ion spray) interface with the liquid junction coupling described previously [9]. The buffer in the liquid junction is typically the same as the separation buffer for CE and provides a suitable make-up buffer flow to sustain a stable spray to the API mass spectrometer. The advantage of using a mass spectrometer as the detector is that molecular weight information can be obtained in addition to the migration time for a compound. It is also possible to obtaine structural information from the analytes by tandem mass spectrometry (MS–MS).

The coupling of CE with electrospray ionization requires some compromise to be made with the electrophoretic buffer in order to obtain a high ion current response. Involatile buffers such as sodium citrate, phosphate and borate commonly used in CE separations are not generally suitable in combination with MS. The ion evaporation mechanism which produces gas-phase ions under these conditions operates best with volatile buffers at low concentration [15]. In addition, a high content of an organic solvent such as methanol or acetonitrile in the running buffer is desirable to facilitate the ion spray process [16]. A review of atmospheric pressure ionization mass spectrometry (API-MS) has been published recently [17].

In this work, we used a commercially available CE instrument interfaced to the API-MS system. The instrumental set-up and the use of the system for characterizing tryptic digests has been presented in a previous paper [11]. This paper describes an investigation using the CE–API-MS system for analyzing human urine extracts containing benzodiazepines and for characterizing sulfonamides. The convenience of using a UV detector in-line with the API-MS system is discussed and the utility of the technique is demonstrated for the detection of flurazepam metabolites in human urine.

EXPERIMENTAL

Chemicals

Fused-silica capillary tubing with dimensions of 75 μm I.D. and 375 μm O.D. was obtained from Polymicro Technologies (Phoenix, AZ, USA). The benzodiazepines chlordiazepoxide, flurazepam, diazepam, prazepam and oxazepam were obtained as Quik-Chek Drug Solutions (Alltech, Deerfield, IL, USA). The metabolite of flurazepam, N-1-hydroxyethylflurazepam, was kindly supplied by Hoffman-La Roche (Nutley, NJ, USA). β-Glucuronidase and the sulfonamides sulfanilamide, sulfamethazine, sulfathiazole, sulfamerazine, sulfadimethoxine and sulfamethoxazole were obtained from Sigma (St. Louis, MO, USA). Sequencing-grade trifluoroacetic acid (TFA) was obtained from Aldrich (Milwaukee, WI, USA). Optima grade methanol was obtained from Fisher Scientific (Fair Lawn, NJ, USA). Water was purified in-house with a Barnstead Nanopure system. All other chemicals were of analytical-reagent or reagent grade and were used without further purification.

Capillary electrophoresis instrumentation

A Beckman (Palo Alto, CA, USA) P/ACE System 2000 capillary electrophoresis system was used. The total length of the capillary was 100 cm with the UV detector operated at 254 nm and positioned 20 cm from the inlet. Two modifications were made to the commercial CE instrumentation. The first was the installation of a simple switch to by-pass the safety lock between the capillary ends. No measurement of the current by the P/ACE 2000 could be made during CE–MS operation with this modification. The current through the system was measured by an external ammeter before or after the CE–MS separation. The second modification was that the capillary cartridge temperature control system was bypassed during CE–MS operation [11]. The CE instrument was equipped with a 30-kV high-voltage power supply. The standard pressure inejction feature of this system was preferred for sample injection in this work.

Mass spectrometry

A Sciex (Thornhill, Ontario, Canada) TAGA 6000E triple quadrupole mass spectrometer equipped with an API source was used. The capillary end from the CE system was coupled via a liquid junction to a pneumatically assisted electrospray (ion spray) interface [16] and the API-MS system. The same interface was used by Lee and co-workers [3,7–9]. The only modification in this work was that the inner capillary in the ion spray interface consisted of uncoated fused silica (75 μm I.D.) instead of stainless steel [11]. During CE–MS operation the liquid junction and the ion spray interface were floated at +4 kV and the mass spectrometer was operated in the positive-ion mode of detection. When the high voltage was maintained at 30 kV at the capillary inlet, the 4-kV potential maintained on the ion spray interface produced a potential difference across the separation capillary of 26 kV.

Gas-phase ions generated from the ion spray interface via the ion evaporation mechanism [15] were sampled into the mass spectrometer by a potential difference of about 3 kV set between the ion spray interface and the ion sampling orifice. The sampling orifice was a 100-μm diameter hole in the end of a conical skimmer extended toward the atmosphere. To minimize solvent cluster formation, this system utilizes a gas curtain of ultrapure nitrogen applied to the atmospheric side of the skimmer. For full-scan CE–MS work, the first quadrupole (Q1) was scanned from either m/z 250 or 300 to m/z 400 in about 5 s in steps of 1 u. For CE–MS–MS work, ultrapure argon (AIRCO, BOC Group, Murray Hill, NJ, USA) was used as the collision gas and was introduced into the collision cell (Q_2) at a target gas thickness of 2×10^{14} atoms/cm^2. The collision gas energy used for the MS–MS experiments was 70 eV. Both quadrupole mass analyzers were maintained at unit mass resolution in this work.

Infusion of the sulfonamides dissolved in the CE buffer [20 m*M* ammonium acetate (pH 6.8) containing 20% of methanol] were made with a Harvard (South Natick, MA, USA) syringe pump. During infusion, at a flow-rate of 4 μl/min, the first quadrupole was scanned from m/z 100 to 450.

Methods

Rinsing of the CE capillary was performed by pressurizing the inlet at 138 kPa. New capillaries were flushed with 9 column volumes of 1 *M* sodium hydroxide, 3 column volumes of distilled water, 3 column volumes of 0.1 *M* hydrochloric acid, 3

column volumes of distilled water and 9 column volumes of electrophoretic buffer. Between analyses the capillary was rinsed with 1.5 column volumes of 0.1 *M* sodium hydroxide followed by 9 column volumes of buffer.

The low-pH buffers were prepared from a solution of ammonium acetate to which trifluoroacetic acid (TFA) was added to give the desired pH. Methanol was then added to the buffer. The buffer concentrations reported in this work are the total concentration of ammonium acetate in the buffer. The electrophoretic buffers were filtered through a 0.45-μm Miller-HV filter unit prior to use (Millipore, Bedford, MA, USA).

The electroosmotic flow, v_{eo}, was calculated by measuring the migration time, $t_o = V/v_{eo}$ and V is the volume of the capillary. The calculation for column efficiency was based on $N = 5.54\ (t/w_{0.5})^2$, where N is the number of theoretical plates, t is the migration time for the compound and $w_{0.5}$ is the peak width at half-height.

The ion spray interface was positioned within 1 cm of the ion sampling orifice of the API-MS system. The position of the ion spray interface was adjusted while infusing flurazepam ($5 \cdot 10^{-6}$ *M*) or sulfamethazine ($2 \cdot 10^{-4}$ *M*) dissolved in the electrophoretic buffer through the capillary. Flurazepam was infused using the 138-kPa pressure (rinse feature) of the CE instrument and sulfamethazine was infused using the 3.45-kPa pressure typically used for injection. The singly charged ion at m/z 388 (flurazepam) or m/z 279 (sulfamethazine) was monitored and the mass spectrometric tuning parameters were adjusted to give the optimum ion current signal form the API-MS system.

Urine extraction and sample introduction

Urine samples were treated with β-glucuronidase prior to extraction. Two ml of 1.0 *M* potassium acetate solution (pH 5.0) containing $2 \cdot 10^6$ units/l of β-glucuronidase were added to 5 ml of urine in a 16 × 125 mm screw-capped test-tube and the treated urine was incubated at 65°C for 2 h. After incubation, the urine was cooled to ambient temperature and the pH adjusted to 9.5 with concentrated ammoniua solution. The urine was then extracted with 3.0 ml of 1-chlorobutane on a mixer at slow rotation for 15 min. The liquid phases were separated by centrifugation at 2500 *g* for 10 min. The upper organic layer was transferred to silanized, conical-bottomed centrifuge tubes and evaporated at 65°C under a gentle stream of nitrogen. Each extract was dissolved in 100 μl of electrophoretic buffer containing ammonium acetate (0.2 m*M*) adjusted to pH 1.3 with TFA in 15% (v/v) methanol. The extracts and standards were introduced into the capillary by pressurizing the inlet end of the capillary to 3.45 kPa. Injection volumes typically ranged from 5-to 28 nl.

RESULTS AND DISCUSSION

Benzodiazepines and sulfonamides are drugs that are often present at high concentrations in human urine after therapeutic doses. They are therefore suitable candidates for analysis by capillary electrophoresis with the present system. Although the amount of sample needed for CE separations and detection is very small, the sample concentration in the injection vial must be fairly high because only a few nanoliters are introduced into the capillary. A benefit of CE, however, is that the chemical derivatization of these drug classes often required for gas chromatographic (GC)–MS analyses [18–20] is not needed in CE–MS.

Sulfonamides

Sulfa drugs are used in the treatment for bacterial infections. There are, for example, veterinary preparations sold in the USA, for the treatment of large animals, that contain a mixture of three sulfa drugs, sulfamethazine and sulfathiazole together with either sulfamerazine or sulfanilamide. In the doping control of racehorses there is considerable interest in separating and detecting these and related substances in equine urine [21].

Fig. 1 shows the electropherograms obtained with (A) UV and (B) mass spectrometric detection for the separation of a synthetic mixture of six sulfonamides using an electrophoretic buffer consisting of 20 m*M* ammonium acetate (pH 6.8) containing 20% (v/v) of methanol. Minor structural variations between the sulfonamides result in different dissociation constants, pK_a = 5.6–10.4 [22,23]. The sulfonamides are separable by CE because they are negatively charged to different extents in the electrophoretic buffer. Changes in selectivity with pH in ion-pair high-performance liquid chromatographic (HPLC) separations of sulfonamides have been studied. It was found that dramatic changes in retention order may occur due to different selectivities

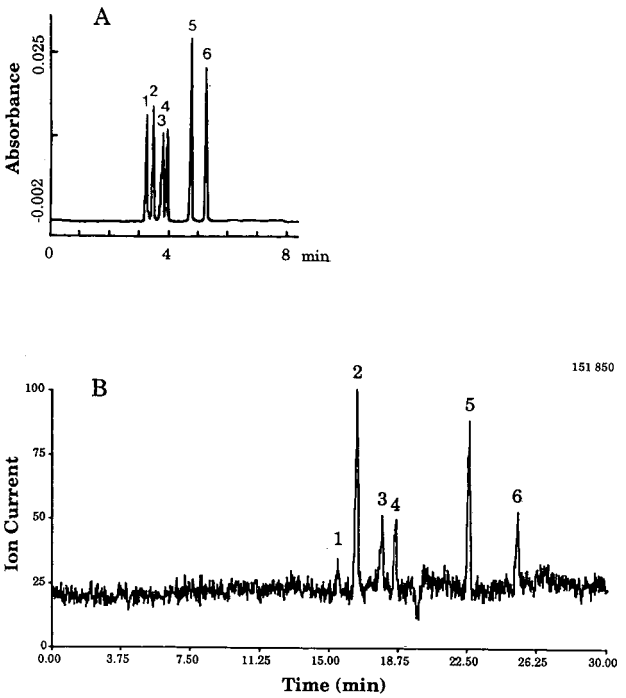

Fig. 1. (A) CE–UV and (B) CE–SIM–MS total selected ion current electropherograms for the separation of six sulfonamides. Capillary, uncoated fused silica, 100 cm × 75 μm I.D.; voltage, 26 kV; buffer, 20 m*M* ammonium acetate (pH 6.8) containing 20% (v/v) of methanol; injection, 5.5 nl of a $4 \cdot 10^{-4}$ *M* solution (2 pmol) of each drug. Peaks: 1 = sulfanilamide, *m/z* 190 $[M+NH_4]^+$ (pK_a = 10.4); 2 = sulfamethazine, *m/z* 279 $[M+H]^+$ (pK_a = 7.4); 3 = sulfathiazole, *m/z* 256 $[M+H]^+$ (pK_a = 7.27); 4 = sulfamerazine, *m/z* 265 $[M+H]^+$ (pK_a = 6.90); 5 = sulfadimethoxine, *m/z* 311 $[M+H]^+$ (pK_a = 5.9); 6 = sulfamethoxazole, *m/z* 254 $[M+H]^+$ (pK_a = 5.6). (A) CE–UV electropherogram at 254 nm; detection after 20-cm capillary. (B) CE–SIM–MS total selected ion current electropherogram; detection after 100-cm capillary.

in acid and ion-pair partition of the sulfonamides to the hydrophobic silica support coated with either 1-pentanol or butyronitrile [24].

The first peak in Fig. 1, sulfanilamide (pK_a = 10.4), is neutral in the electrophoretic buffer used and migrates with the electroosmotic flow. All the other sulfonamides are negatively charged under these CE conditions and migrate towards the positively charged anode. They are all carried towards the detector due to the electroosmotic flow (0.27 μl/min). The same migration order for the sulfonamides was obtained at pH 7.0 with 30 m*M* sodium dihydrogenphosphate–10 m*M* sodium tetraborate buffer [25]. The ammonium acetate–methanol buffer used in this study was chosen because volatile buffers benefit detection by API-MS. Fig. 1A shows the separation of 2 pmol (380–680 pg) of each sulfonamide within a 20-cm capillary length with UV detection at 254 nm and Fig. 1B shows the sulfonamides following elution from the 100-cm capillary length with API-MS detection under selected ion monitoring (SIM) conditions. The ammoniated molecular ion $[M + NH_4]^+$ for sulfanilamide and the protonated molecular ion $[M + H]^+$ for the other sulfonamides were monitored with the mass spectrometer operated in the positive-ion mode of detection. One advantage of using UV on-line with the API-MS system was that only after 4 min an indication was given as to whether the CE separation was taking place satisfactorily.

With the exception of sulfanilamide, the sulfonamides are partly negatively charged in the electrophoretic buffer and hence also partly negatively charged when they reach the ion spray interface. The sulfonamides contain two or more nitrogen atoms and a higher response was obtained when the API-MS system was operated in the positive-ion detection mode compared with the negative-ion detection mode. The relative response for positive- and negative-ion modes of detection is shown in Fig. 2.

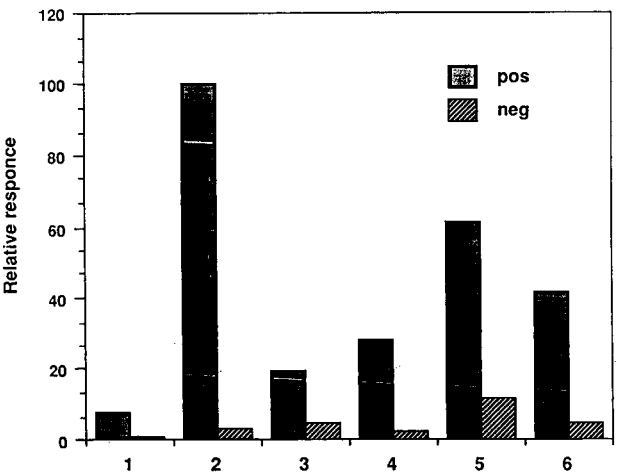

Fig. 2. Relative response of the sulfonamides by ion spray-MS operated under positive- and negative-ion modes of detection. The sulfonamides were dissolved in 20 m*M* ammonium acetate buffer (pH 6.8) containing 20% (v/v) of methanol to give a concentration of $2 \cdot 10^{-4}$ *M* and infused at a flow-rate of 4 μl/min. 1 = Sulfanilamide, *m/z* 190 $[M + NH_4]^+$, *m/z* 170 $[M - H]^-$; 2 = sulfamethazine, *m/z* 279 $[M + H]^+$, *m/z* 277 $[M - H]^-$; 3 = sulfathiazole, *m/z* 256 $[M + H]^+$, *m/z* 254 $[M - H]^-$; 4 = sulfamerazine, *m/z* 265 $[M + H]^+$, *m/z* 263 $[M - H]^-$; 5 = sulfadimethoxine, *m/z* 311 $[M + H]^+$, *m/z* 309 $[M - H]^-$; 6 = sulfamethoxazole, *m/z* 254 $[M + H]^+$, *m/z* 252 $[M - H]^-$.

These data were obtained from infusion of the individual sulfonamides into the API-MS system. The sulfonamides were dissolved in the electrophoretic buffer, 20 m*M* ammonium acetate (pH 6.8) containing 20% (v/v) of methanol, to give an infusion concentration of $2 \cdot 10^{-4}$ *M*. The position of the ion spray interface relative to the ion sampling orifice of the mass spectrometer and the applied potential was carefully adjusted to determine the optimum ion current response for the sulfonamides in the positive and negative-ion modes of detection, respectively. Sulfamethazine gave the highest response of the sulfonamides studied and was normalized to 100%.

One advantage provided by MS–MS is that structural information may be obtained for the analyte of interest. This is illustrated in Fig. 3 for sulfamethazine where the same synthetic mixture containing six sulfonamides was re-injected. The $[M+H]^+$ ion at *m/z* 279 for sulfamethazine was monitored with the first quadrupole (Q1), collision-induced dissociation (CID) was performed in the second quadrupole (Q2), and the third quadrupole (Q3) was scanned from *m/z* 10 to 350 in 6 s. Both mass-analyzing quadrupoles were maintained at unit mass resolution. The full-scan total ion electropherogram and the daughter-ion mass spectrum for 2 pmol (600 pg) of sulfamethazine was acquired to produce the data shown in Fig. 3. The migration time for sulfamethazine in Fig. 3A (16.5 min) agrees with peak 2 (sulfamethazine)

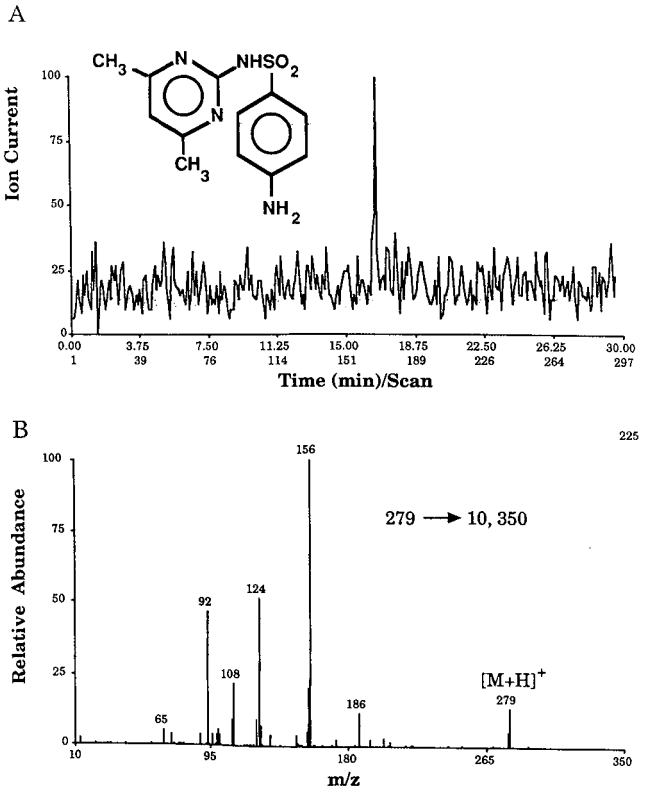

Fig. 3. (A) CE–MS–MS total ion electropherogram and (B) daughter-ion mass spectrum for sulfamethazine from a synthetic mixture of sulfonamides containing 600 pg each (2 pmol). Sample, injection volume and conditions as in Fig. 1.

observed in Fig. 1B. The CE–MS–MS trace shown in Fig. 3B displays structurally important fragment ions at *m/z* 186, 156, 124, 108, 92 and 65, which are characteristic of many sulfa drugs. The most abundant ion observed at *m/z* 156 is common to the mass spectra of sulfa drugs and is formed by cleavage of the sulfonamide–nitrogen bond [21,26]. All the expected MS–MS fragments for sulfamethazine are present compared with previous analyses by LC–MS–MS [21]. It should therefore be possible to use CE–UV–MS–MS for the determination of sulfa drugs in equine urine in the same way as was demonstrated for sulfadimethoxine in racehorse plasma and urine extracts by LC–MS–MS.

Benzodiazepines

Four benzodiazepines were separated using a 15 m*M* ammonium acetate buffer adjusted with TFA to pH 2.5 and containing 15% (v/v) of methanol. The separation of 1.4-2.0 pmol (554 pg each) of four benzodiazepines is shown in Fig. 4A with UV detection at 254 nm after a 20-cm capillary length and in Fig. 4B with API-MS from an experiment in which the mass spectrometer was operated under SIM conditions utilizing a 100-cm length of the capillary. A high separation efficiency was obtained,

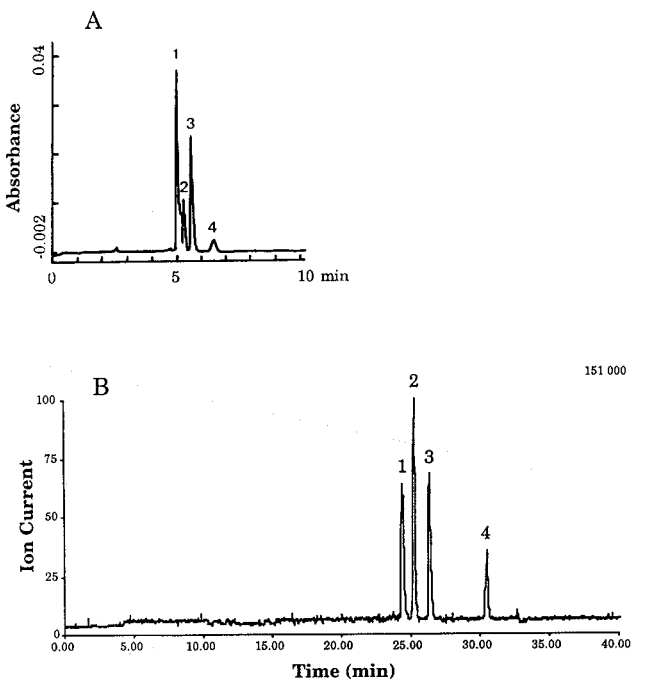

Fig. 4. (A) CE–UV and (B) CE–SIM-MS total selected ion current electropherograms from the separation of four benzodiazepines. Capillary uncoated fused silica, 100 cm × 75 μm I.D.; voltage, 26 kV; buffer, 15 m*M* ammonium acetate adjusted to pH 2.5 with TFA and containing 15% (v/v) of methanol; injection, 28 nl of a 20 μg/ml solution of each drug (1.4–2.0 pmol). Peaks: 1 = chlordiazepoxide, *m/z* 300 $[M+H]^+$; 2 = flurazepam, *m/z* 388 $[M+H]^+$; 3 = diazepam, *m/z* 286 $[M+H]^+$; 4 = prazepam, *m/z* 325 $[M+H]^+$. (A) CE–UV electropherogram at 254 nm, detection after 20-cm capillary; (B) CE–SIM-MS total selected ion electropherogram, detection after 100-cm capillary.

as evidenced from the 70 000–140 000 theoretical plates calculated from the CE–MS selected ion current electropherogram. The improved separation observed in Fig. 4B results from the longer residence time of the analytes in the capillary prior to MS detection.

Chlordiazepoxide, diazepam and prazepam have pK_a values between 4.6 and 2.7, and flurazepam has two pK_a values, 1.9 and 8.2 [22]. They exhibit varying degrees of positive charges in the electrophoretic buffer and migrated towards the negatively charged cathode under the experimental conditions. They were all detected as the $[M+H]^+$ ions by API-MS, with flurazepam giving the highest ion current response.

All benzodiazepines are extensively metabolized in humans. Chlordiazepoxide, diazepam and prazepam are excreted in urine mainly as glucuronide conjugates of oxazepam [22]. For flurazepam the main metabolite found in urine was the glucuronide conjugate of N-1-hydroxyethylflurazepam [22,27–29]. Oxazepam and N-1-hydroxyethylflurazepam could be analyzed with CE using a low pH in the electrophoretic buffer. The migration time in an electrophoretic buffer composed of 0.2 m*M* ammonium acetate adjusted with TFA to pH 1.3 and containing 15% (v/v) of methanol was 13 min for oxazepam and 11 min for N-1-hydroxyethylflurazepam at 20 cm with an applied voltage of 260 V/cm capillary. The capillary length for MS detection was 100 cm in the present instrumental set-up and the migration time for the compounds is thus about five times longer for API-MS detection. N-1-Hydroxyethylflurazepam was chosen for further studies owing to its predominance as a major metabolite of flurazepam and its shorter migration time. It should also be possible to detect oxazepam in human urine with the same approach as decribed below, but a shorter capillary would be preferred to shorten the overall analysis time.

A CE–MS total ion electropherogram for a synthetic mixture containing flurazepam and N-1-hydroxyethylflurazepam is shown in Fig. 5A. The amount injected was 2.2 ng for each compound and the electrophoretic buffer was 0.2 m*M* ammonium acetate adjusted with TFA to pH 1.3 and containing 15% (v/v) of methanol. The mass spectrometer was scanned from *m/z* 300 to 400. The mass spectra for peak 1 (Fig. 5B) and peak 2 (Fig. 5C) show *m/z* 388 and 333, respectively, as the most abundant ions, which correspond to the singly charged molecular ion $[M+H]^+$ for flurazepam and its metabolite, N-1-hydroxyethylflurazepam, respectively. For both compounds the isotope distribution expected for a compound containing one chlorine atom was observed.

Detection of N-1-hydroxyethylflurazepam in human urine

Urine samples were collected before and 2,4 and 7 h after the oral administration of 30 mg flurazepam dihydrochloride (one tablet of Dalmane) to a healthy volunteer. The major urinary metabolite of flurazepam, N-1-hydroxyethylflurazepam, accounts for 30–55% of an orally administered dose of flurazepam [27]. N-1-Hydroxyethylflurazepam is present mainly as the glucuronide conjugate, so the urine samples were first treated with β-glucuronidase, then extracted as described under Experimental and the extract was analyzed by CE–UV–MS.

The CE–UV and CE–MS electropherograms for the analysis of a human urine extract are shown in Fig. 6A and B, respectively. These data were obtained from the injection of the 4-h urine extract with an electrophoretic buffer of 0.2 m*M* ammonium acetate adjusted with TFA to pH 1.3 and containing 15% (v/v) of methanol. The

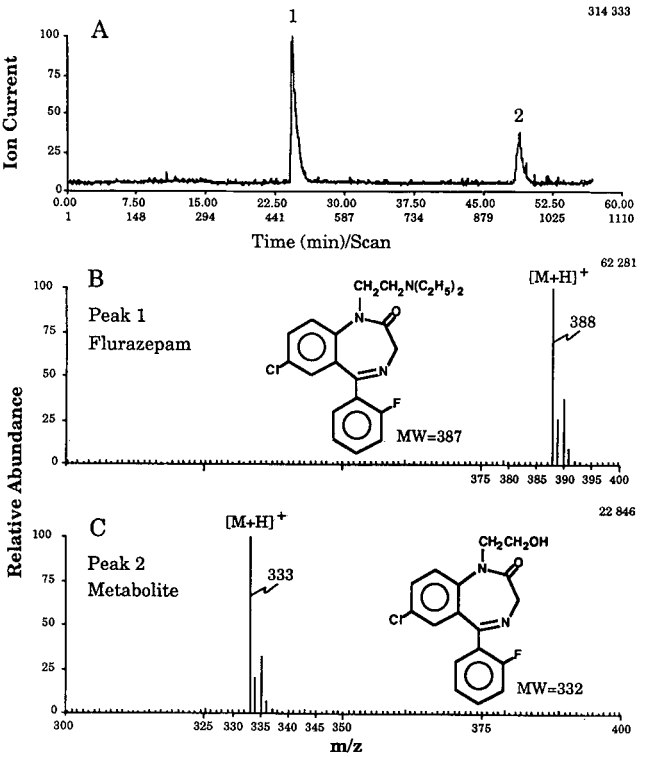

Fig. 5. (A) Full-scan CE–MS total ion current profile and mass spectra of (B) flurazepam and (C) metabolite. Capillary, uncoated fused silica 100 cm × 75 μm I.D. buffer, 0.2 m*M* ammonium acetate adjusted to pH 1.3 with TFA and containing 15% (v/v) of methanol; voltage, 26 kV; current, 8 μA; injection, 11 nl of a 200 μg/ml solution of each compound. Peaks: 1 = flurazepam (2.2 ng, 8 pmol); 2 = N-1-hydroxyethylflurazepam (2.2 ng, 7 pmol). MW = Molecular weight.

mass spectrometer was operated in the SIM mode, while the ions at m/z 388 for flurazepam and *m/z* 333 for N-1-hydroxyethylflurazepam were monitored. Only one component, corresponding to N-1-hydroxyethylflurazepam, was observed in the MS electropherogram (Fig. 6B). The concentration of N-1-hydroxyethylflurazepam in the 4-h urine was estimated to be 4 μg/ml from extracts of blank urine to which flurazepam and N-1-hydroxyethylflurazepam had been added prior to treatment with β-glucuronidase and extraction. Aliquots of 5.0 ml of urine were extracted with 1-chlorobutane and, after evaporation of the solvent, the residues were dissolved in 100 μl of electrophoretic buffer. Only 5 nl were injected, corresponding to about 1 ng of N-1-hydroxyethylflurazepam assuming a 100% recovery of N-1-hydroxyethylflurazepam via extraction by 1-chlorobutane. 1-Chlorobutane has been used in the screening procedure for basic drugs in blood or tissues prior to GC–MS analysis and has been shown to give clean extracts with up to 96.7% recovery of flurazepam in blood [30].

The third peak in the UV electropherogram observed at 254 nm (Fig. 6A) was N-1-hydroxyethylflurazepam. The first two peaks in Fig. 6A appear to be other metabolites of flurazepam present in the urine, as the extract of the urine collected before

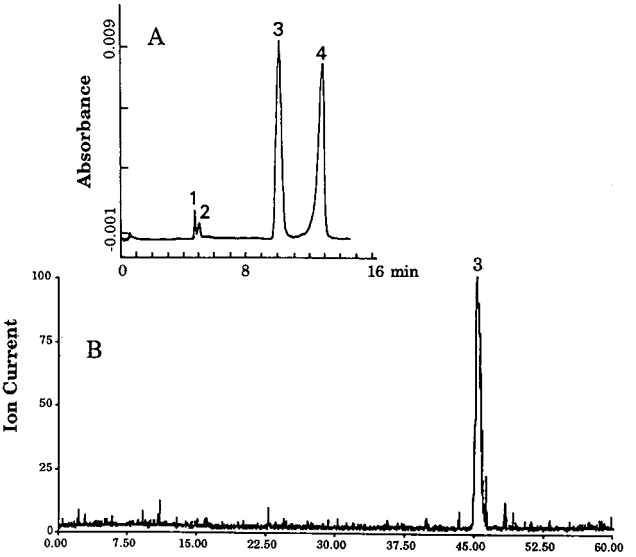

Fig. 6. (A) CE–UV and (B) CE–SIM-MS total selected ion current electropherogram from the analysis of an extract of human urine collected 4 h after the administration of a 30-mg oral dose of flurazepam dihydrochloride (one tablet of Dalmane). Injection volume, 5 nl; electrophoretic conditions as in Fig. 5. Peaks as in Fig. 7. (A) CE–UV electropherogram at 254 nm, detection after 20-cm capillary; (B) CE–SIM-MS total selected ion electropherogram, detection after 100 cm capillary.

administration of flurazepam (blank urine) did not show any peaks in this region. The blank urine extract was very clean, showing one peak corresponding to peak 4 in Fig. 6A. Peak 4 has the same migration time as a neutral compound (benzyl alcohol) and from this peak the electroosmotic flow and the electrophoretic mobility of individual components in the urine may be calculated. Peaks with the same migration times were found in the 7-h urine extract. The concentration of N-1-hydroxyethylflurazepam in the 7-h urine was estimated to be 0.5 μg/ml from extracts of blank urine to which 1-hydroxyethylflurazepam had been added. The m/z 333 peak observed in the MS electropherogram of the 7-h urine extract had a 3:1 signal-to-noise ratio and thus represents the practical detection limit for N-1-hydroxyethylflurazepam using the CE–MS system described. A detection limit of 0.5 μg/ml in urine has previously been reported for N-1-hydroxyethylflurazepam in a study of urinary metabolites of flurazepam in man by HPLC [29]. In CE–SIM-API-MS it would be possible to decrease the detection limit about tenfold by dissolving the extract residue in a smaller volume and introducing more than 5 nl of sample into the capillary column.

A full-scan CE–MS total ion current electropherogram of the 2-h urine extract was obtained (Fig. 7B). The on-line UV detector (Fig. 7A) indicated the presence of the same four components as observed in the 4- and 7-h urine extracts. The same electrophoretic buffer, 0.2 mM ammonium acetate adjusted with TFA to pH 1.3 and containing 15% (v/v) of methanol, was used and the mass spectrum was scanned from m/z 250 to 400. The peak at a migration time of 52 min corresponded to N-1-hydroxyethylflurazepam. Extracted ion current profiles of the $[M+H]^+$ ions for N-1-

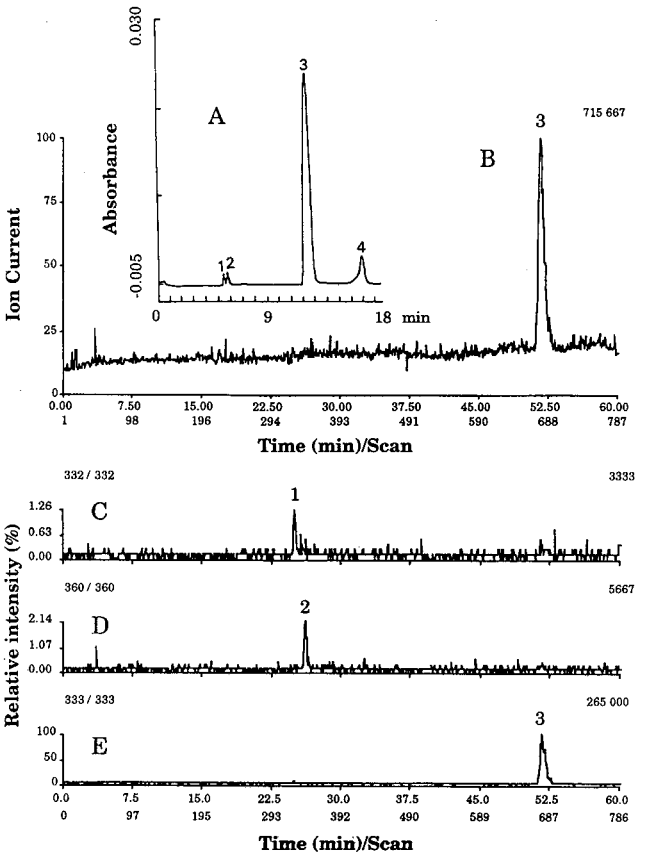

Fig. 7. (A) CE–UV and (B) full-scan CE–MS total ion current and (C–E) extracted ion current profiles from the analysis of an extract of human urine collected 2 h after the administration of a 30-mg oral dose of flurazepam dihydrochloride. (A) CE–UV electropherogram at 254 nm, detection after 20-cm capillary (B) full-scan acquisition from m/z 250 to 400, 5 s per scan, detection after 100-cm capillary. Peaks: 1 = didesethylflurazepam, m/z 332 $[M+H]^+$ (C); 2 = monodesethylflurazepam, m/z 360 $[M+H]^+$ (D); 3 = N-1-hydroxyethylflurazepam, m/z 333 $[M+H]^+$ (E); 4 = "neutral fraction" in the urine extract. No peak corresponding to flurazepam (m/z 388) was observed. Injection volume, 5 nl; electrophoretic conditions as in Fig. 5.

hydroxyethylflurazepam (Fig. 7E) and two possible metabolites of flurazepam, didesethylflurazepam at m/z 332 (Fig. 7C) and monodesethylflurazepam at m/z 360 (Fig. 7D), were observed. The flurazepam metabolites didesethylflurazepam and monodesethylflurazepam account for 0.5–13% of the dose in human urine [27]. No indication of the $[M+H]^+$ ion for flurazepam at m/z 388 was observed. The combination of UV and API-MS detection gave more information than could be obtained with only one of these detection methods. The UV electropherogram indicated the presence of two flurazepam metabolites (peaks 1 and 2 in Figs. 6A and 7A) and with API-MS detection the molecular weight of the metabolites could be determined and their identity proposed.

A change in migration time for N-1-hydroxyethylflurazepam was observed during the course of the day. This instability appeared to be due to column temperature variation. The first analytical determination in the morning produced longer migration times than those observed later in the day. We conclude that heat generated inside the unthermostated capillary resulted in decreased migration times during the course of the day owing to the decrease in viscosity of the buffer. The standard CE instrument used in this work normally thermostatically controls the entire electrophoretic capillary. For the CE–MS experiments described in this work, the thermostat control could not be utilized owing to the need to extend the capillary to the mass spectrometer. The electroosmotic flow-rate was 0.051–0.077 μl/min, calculated from the "neutral fraction" observed in the UV electropherograms. When MS is used for CE detection, small changes in migration times do not matter because the $[M+H]^+$ ion facilitates monitoring of the identity of the sample components. For unknown compounds MS–MS can facilitate the structural characterization of unknown compounds.

CONCLUSIONS

This study has shown that benzodiazepines and sulfonamides may be separated by CE with buffer systems compatible with the ion spray-API mass spectrometer system. The major metabolite of flurazepam in man, N-1-hydroxyethylflurazepam, can be monitored in human urine extracts after a single 30-mg oral dose of flurazepam dihydrochloride. The structural characterization of sulfamethazine was also demonstrated by CE–UV–MS–MS experiments.

It is an advantage to use UV detection on-line with API-MS detection for the analysis of human urine extracts containing flurazepam metabolites. The metabolites provide a good UV response at 254 nm, and the presence of metabolites other than N-1-hydroxyethylflurazepam was indicated in the UV electropherograms. With API-MS the identification of mixture component molecular weights was possible for the determination of these additional metabolites. Another advantage of the present CE–UV–API-MS system was the pressure injection system of the CE system, which allowed optimization of the position of the interface and MS tuning parameters while delivering a solution of a test analyte through the entire CE–UV–MS system. Rinsing of the capillary between analyses and sample injection could then be done without changing the position of the interface because the pressure injection system utilizes only the inlet end of the capillary.

In this study, small sample volumes (5–28 nl) were introduced into the CE capillary. The small injection volumes demand fairly concentrated samples to permit MS of dectection. For sulfonamides and the major metabolite of flurazepam, N-1-hydroxyethylflurazepam, their concentration in urine should be sufficient to allow analysis conditions does not appear to be practical at present unless the capillary column capacity or MS sensitivity is increased. It appears that the latter could be addressed by using an ion trap mass spectrometer equipped for ion spray sample introduction, and we are investigating this possibility [31].

ACKNOWLEDGEMENTS

We thank Beckman Instruments for providing the capillary electrophoresis instrument and Dr. P. F. Sorter (Hoffmann-La Roche, Nutley, NJ, USA) for providing the standard of N-1-hydroxyethylflurazepam. We also thank Eastman Kodak, Sciex and the Swedish Trotting Association for partial financial support of this work. This work was supported by grants to one of us (I.M.J.) from the Swedish Medical Research Council, the Swedish Academy of Pharmaceutical Sciences and the Royal Swedish Academy of Sciences, which are gratefully acknowledged.

REFERENCES

1 W. G. Kuhr, *Anal. Chem.*, 62 (1990) 403R.
2 J. A. Olivares, N. T. Nguyen, C. R. Yonker and R. D. Smith, *Anal. Chem.*, 59 (1987) 1232.
3 E. D. Lee, W. Mück, T. R. Covey and J. D. Henion, *J. Chromatogr.*, 458 (1988) 313.
4 R. D. Smith, J. A. Olivares, N. T. Nguyen and H. R. Udseth, *Anal. Chem.*, 60 (1988) 436.
5 R. D. Smith, C. J. Barinaga and H. R. Udseth, *Anal. Chem.*, 60 (1988) 1948.
6 R. D. Smith, J. A. Loo, C. J. Barinaga, C. G. Edmonds and H. R. Udseth, *J. Chromatogr.*, 480 (1989) 211.
7 E. D. Lee, W. Mück, T. R. Covey and J. D. Henion, *Biomed. Environ. Mass Spectrom*, 18 (1989) 253.
8 W. M. Mück and J. D. Henion, *J. Chromatogr.*, 495 (1989) 41.
9 E. D. Lee, W. Mück, J. D. Henion and T. R. Covey, *Biomed. Environ. Mass Spectrom*, 18 (1989) 844.
10 J. A. Loo, H. K. Jones, H. R. Udseth and R. D. Smith, *J. Microcolumn Sep.*, 1 (1989) 223.
11 I. M. Johansson, E. C. Huang, J. D. Henion and J. Zweigenbaum, *J. Chromatogr.*, 554 (1991) 311–327.
12 M. A. Moseley, L. J. Deterding, K. B. Tomer and J. W. Jorgenson, *J. Chromatogr.*, 480 (1989) 197.
13 N. J. Reinhoud, W. M. A. Niessen, U. R. Tjaden, L. G. Gramberg, E. R. Verheij and J. van der Greef, *Rapid Commun. Mass Spectrom.*, 3 (1989) 348.
14 R. M. Caprioli, W. T. Moore, M. Martin, B. B. DaGue, K. Wilson and S. Moring, *J. Chromatogr.*, 480 (1989) 247.
15 B. A. Thomson and J. V. Iribarne, *J. Chem. Phys.*, 71 (1979) 4451.
16 A. P. Bruins, T. R. Covey and J. D. Henion, *Anal. Chem.*, 59 (1987) 2642.
17 E. C. Huang, T. Wachs, J. J. Conboy and J. D. Henion, *Anal. Chem.*, 62 (1990) 713A.
18 O. Gyllenhaal, U. Tjärnlund, H. Ehrsson and P. Hartvig, *J. Chromatogr.*, 156 (1978) 275.
19 H. Maurer and K. Pfleger, *J. Chromatogr.*, 422 (1987) 85.
20 M. Japp, K. Garthwaite, A. V. Geeson and M. D. Osselton, *J. Chromatogr.*, 439 (1988) 317.
21 J. D. Henion, B. A. Thomson and P. H. Dawson, *Anal. Chem.*, 54 (1982) 451.
22 A. Wade (Editor), *Clark's Isolation and Identification of Drugs*, pharmaceutical press, London, 2nd ed. 1986.
23 R. Elofsson, S. O. Nilsson and A. Ågren, *Acta Pharm. Suec.*, 7 (1970) 473.
24 I. M. Johansson and K.-G. Wahlund, *Acta Pharm Suec.*, 14 (1977) 459.
25 A. Wainright, *J. Microcolumn Sep.*, 2 (1990) 166.
26 W. Garland, B. Miwa, G. Weiss, G. Chen, R. Saperstein and A. MacDonald, *Anal. Chem.*, 52 (1980) 842.
27 J. A. F. deSilva and N. Strojny, *J. Pharm. Sci.*, 60 (1971) 1303.
28 J. A. F. deSilva, C. V. Puglisi, M. A. Brooks and M. R. Hackman, *J. Chromatogr.*, 99 (1974) 461.
29 R. E. Weinfeld and K. F. Miller, *J. Chromatogr.*, 223 (1981) 123.
30 E. H. Foerster, D. Hatchett and J. C. Garriott, *J. Anal. Toxicol.*, 2 (1978) 50.
31 S. A. McLuckey, G. J. van Berkel, G. L. Glish, E. C. Huang and J. D. Henion, *Anal. Chem.*, 63 (1991) 375–383.

Journal of Chromatography, 559 (1991) 529–536
Elsevier Science Publishers B.V., Amsterdam

CHROM. 23 468

Migration behaviour of catechols and catecholamines in capillary electrophoresis

C. P. ONG, S. F. PANG, S. P. LOW, H. K. LEE and S. F. Y. LI*
Department of Chemistry, National University of Singapore, Kent Ridge Crescent, Singapore 0511 (Singapore)

ABSTRACT

The migration behaviour of selected catechols and catecholamines in micellar electrokinetic chromatography (MEKC) was investigated. For the MEKC separation of the compounds, electrophoretic media with sodium dodecyl sulphate in phosphate–borate buffer were used. The migration behaviour of the catechols and catecholamines at different concentrations of micellar solution and at different pH of the electrophoretic media was investigated. The results successfully demonstrated the use of MEKC for the separation of a mixture of two catechols and six catecholamines.

INTRODUCTION

Catechols and catholamines play important roles as neurotransmitters in the central and peripheral autonomic nervous systems and as hormones exerting endocrine and exocrine effects. It is not surprising, therefore, that the lack of sufficient amounts of some of these compounds in the body can have a severe impact on both the quality and duration of life.

High-performance capillary electrophoresis (HPCE) is a fairly new technique and has become complementary to or a substitute for high-performance liquid chromatography (HPLC) for analytical purposes [1–8]. One of the reasons for its popularity is the exceptionally high separation efficiency achievable with this technique, which is based on a simple instrumental set-up. The characteristic of HPCE is that the separation takes place in a small capillary tube which is favourable for minimizing thermal zone distortion when high field strengths are required in order to obtain short run times and high resolution. At the same time, the capillary tube minimizes zone broadening generated by convection, which can be effectively suppressed in narrow-bore tubes.

Capillary electrokinetic chromatography was introduced by Terabe *et al.* [1] in 1984 by pumping micelles electroosmotically in a capillary electrophoresis system to effect the chromatographic separation of neutral compounds. In this system, ionic surfactants are added to the operating buffer at concentrations exceeding the critical micelle concentration. This technique, termed micellar electrokinetic capillary chro-

0021-9673/91/$03.50

matography (MEKC) by Burton *et al.* [2], has been used extensively for selective separations of both neutral and ionic compounds while retaining the advantages of the capillary electrophoresis format. Separation in MEKC is based on the chromatographic principle of partitioning the solute between the carrier (micelle) and the surrounding aqueous medium, and the differential migration of the two phases. MEKC is most frequently performed with anionic surfactants, *e.g.*, sodium dodecyl sulphate (SDS). In addition, experimental parameters, such as pH of the buffer solution, concentration of the micelle and the applied voltage, can help to increase the separation efficiency.

Although the capillary electrophoretic analysis of catechols and catecholamines have explored in previous investigations [3–8], the main emphasis was on the development of highly sensitive electrochemical techniques for capillary electrophoresis. The migration behaviour of catechols and catecholamines in MEKC has rarely been investigated. In this work, the separation of a mixture of two catechols and six catecholamines using the MEKC technique was studied. The effects of surfactant concentration and pH on the migration behaviour were investigated.

EXPERIMENTAL

The experiments were performed on a laboratory-built MEKC instrument. The power supply used was a Spellman (Plainview, NY, USA) Model RHR 30PN10/RVC capable of delivering up to 30 kV. A fused-silica capillary (45 cm effective length × 50 μm I.D.) obtained from Polymicro Technologies (Phoenix, AZ, USA) was used as the separating tube. On-column detection of the peaks was carried out on a Micro UVis detector (Carlo Erba, Milan, Italy) with the wavelength set at 210 nm. A Linear Instruments (Irvine, CA, USA) Model 252A/MM chart recorder was used to record the chromatograms. Sample solution was introduced by gravity feed. An injection time of 5 s at a height of 12 cm was used.

All chemicals were of analytical-reagent grade. The buffer solution was prepared by dissolving sodium dihydrogenphosphate dihydrate and sodium tetraborate in water purified with a Milli-Q system (Millipore, Bedford, MA, USA) electrophoretic medium consisting of SDS micelles in phosphate–borate buffer was prepared as described previously [9]. The structures of the two catechols and six catecholamines investigated are shown in Fig. 1. A standard solution of the catechol moieites and Sudan III was prepared in HPLC-grade methanol (J. T. Baker, Phillipsburg, NJ, USA) at a concentration of 1000 ppm for each of the species. All these chemicals were supplied by Aldrich (Milwaukee, WI, USA).

RESULTS AND DISCUSSION

Effect of pH

The results obtained for the migration times at different pH values are shown in Fig. 2. With the exception of 3,4-dihydroxyphenylacetic acid (DHPAA) and DL-3,4-dihydroxyphenylglycol (DHPG), a general trend of a decrease in migration times with increase in pH was observed. It should be noted that with a decrease in pH, a substantial decrease in electroosmostic velocity, v_{eo}, and migration velocity of the SDS micelles, v_{mc}, would be expected [10]. In fact, our attempt to study the migration

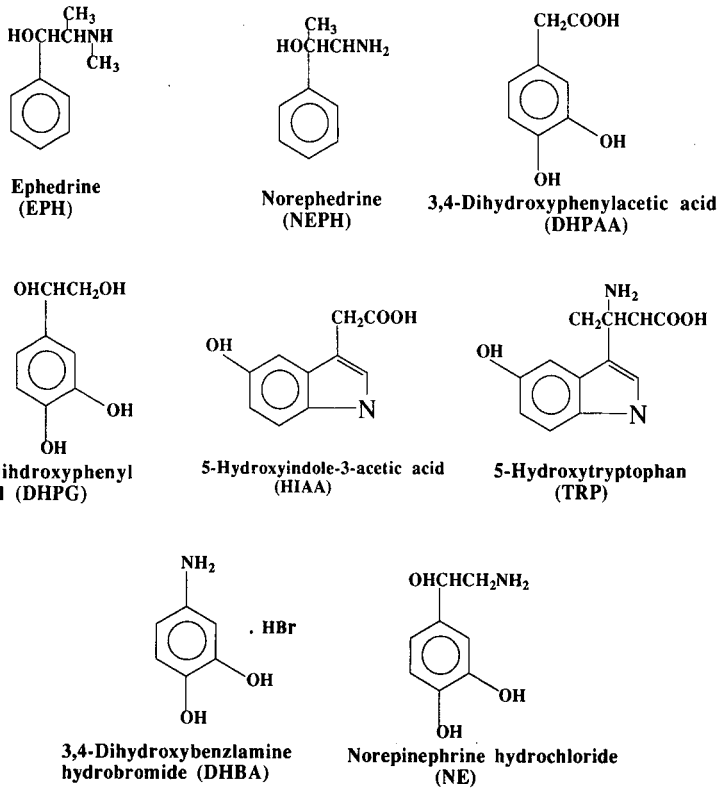

Fig. 1. Structures of the catechols and catecholamines investigated.

behaviour of the catechols and catecholamines at pH 5 failed to provide any satisfactory results. Sudan III, ephedrine (EPH), norepinephrine (NEPH) and 5-hydroxytryptophan (TRP) were not detected even after a prolonged analysis time of more than 1 h. At this pH, it is believed that v_{mc} approaches zero and subsequently solutes which have interacted with the SDS micelles, together with Sudan III, would not migrate within a reasonable time.

In addition to being affected by the changes in v_{mc} and v_{eo} due to variations in pH, another possible reason for the variation of migration times could be the differences in the extent of ionization of the various compounds in the pH range investigated. In fact, from the results shown in Fig. 2, it seems that this effect plays a more important role than the former.

At low pH (*i.e.*, pH 6), protonation of the amino group in some of these species is possible. These positively charged protonated species would form ion pairs with the anionic micelles. As a result of the strong electrostatic attraction of the SDS micelles towards the anode, an increase in migration times would be expected for these species. Among the catechols and catecholamines investigated, only EPH, NEPH, TRP and norepinephrine (NE) seemed to be affected. This effect is more pronounced for EPH as the protonation of its secondary amino group is highly favourable. Therefore, a large variation of migration time was observed for EPH. On the other hand,

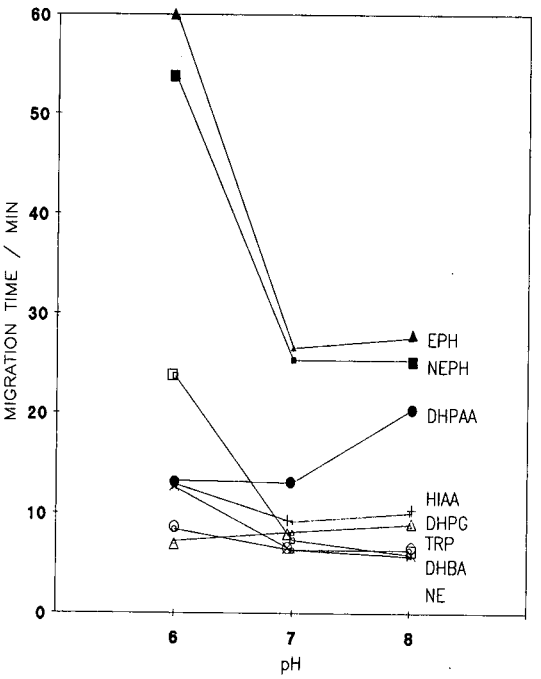

Fig. 2. Plot of migration times of the catechols and catecholamines with variation of pH. Experiments were carried out at 80 m*M* SDS.

for NE, as a result of possibility of bond rotation, the amino group can readily form intrahydrogen bonds with the phenolic OH groups, which consequently render effective protonation of this species. Therefore, this effect is less significant for NE. A similar observation is noted for TRP; because of the close proximity of the amino group with its carboxylate group, protonation to a certain extent would also be affected. However, owing to the presence of the basic pyrrole ring, protonation is still possible and migration behaviour as shown in Fig. 2 is observed.

As the pH of the electrophoretic media increases, protonation of these amino groups would be inhibited. Therefore, it would be reasonable to expect to observe a decrease in migration times as shown in Fig. 2 for species that tend to protonate less at higher pH. With DHPAA and DHPG, instead of decreases in their migration times with increasing pH, the reverse trend was observed. From their structures, it can be seen that both species possess an acidic hydrogen (i.e., the carboxylate in DHPAA and the OH in DHPG). These acidic hydrogens at higher pH would tend to ionize and thus result in negatively charge species. These negatively charged species, like the anionic SDS micelles, would be electrophoretically attracted to the anode. However, it should be noted that larger variations in migration times were observed for DHPAA than DHPG with changes in pH. This can be explained by the fact that as the pK_a for DHPG (aliphatic alcohol) is larger than that for DHPG, the extent of ionization would be higher in the latter. As a result, DHPAA was more affected than DHPG by pH changes. In contrast to DHPAA and DHPG, even though TRP pos-

sesses a carboxylate group, owing to the close proximity of the two basic groups (namely the amino group and the pyrrole ring) ionization of this carboxylate group would be highly unfavourable. Thus no significant increase in the migration time was observed for TRP.

For DHBA and HIAA, because of the possibility of intrahyrogen bonding, either between the two adjacent phenolic OH groups (as in DHBA), or between the carbonyl group and the phenolic OH group (as in HIAA), the hydrogen is now no longer available for ionization. Therefore, marginal decreases in migration times were observed. This is in response to the increase in the v_{eo} for the system at higher pH.

Effect of SDS concentration

The results obtained for the investigation of the effect of SDS concentration on the migration of the catechols and catecholamines are shown in Fig. 3. For EPH, NEPH and DHPAA, with an increase in SDS concentration their migration times increased correspondingly. The increase in migration times for these compounds is explained in terms of their high lipophilicity [11]. This observation is in agreement with the trend observed above. As protonation of NEPH and EPH may be still possible at pH 7, ion pairing with the SDS micelles would be likely to occur. Thus, with increase in SDS concentration, there would be a corresponding increase in the probability of interaction. Therefore, the migration times were found to increase. For the other compounds, only marginal changes with increase in SDS concentration were observed. These observations suggest that there is minimum interaction between these species and the SDS micelles. One of the possible reasons could be the presence of polar substituent groups in these species. All these species possess, in addition to the two phenolic OH groups, additional polar substituent groups, which makes them

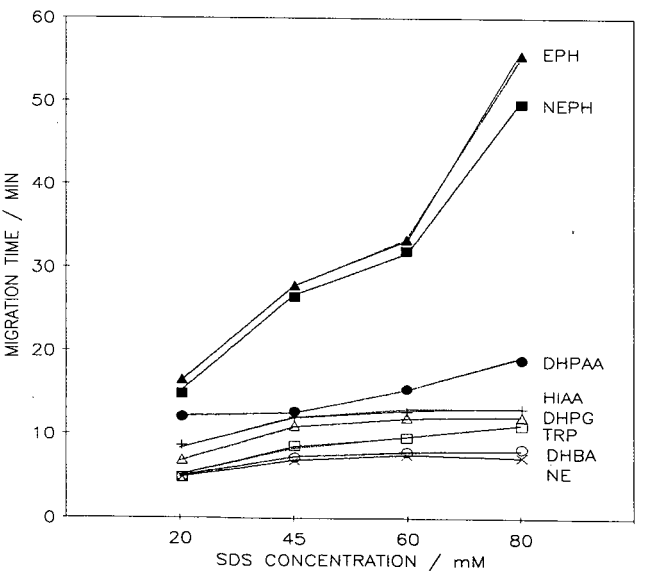

Fig. 3. Plot of migration times of the catechols and catecholamines with variation in SDS concentration. Experiments were carried out at pH 7.00.

hydrophilic. These species would tend to be solvated more by the aqueous phase and effective solubilization by the SDS micelles would be affected. As a result, their migration times would be shorter.

Migration order

Optimum separation for this group of catechols and catecholamines was obtained using an 80 m*M* SDS concentration and the corresponding chromatogram is shown in Fig. 4. It can be seen that all the peaks are satisfactorily separated. The usual peak broadening and tailing of peaks observed in the HPLC separation of this group of compounds are not seen here. In Table I, the ratios t_0/t_{mc}, where t_0 and t_{mc} are the migration times of an insolubilized species and that of the micelle respectively, obtained at various SDS concentrations are listed. From Table I, it is worth noting that the t_0/t_{mc} ratio obtained using 80 m*M* SDS was the smallest among the four sets of conditions. It is known that a smaller t_0/t_{mc} ratio usually offers a wider elution range which, to a certain extent, would enhance the separation of peaks [12].

Many complex equilibria are thought to occur in this system [5,8], including ion-pair formation in solution, penetration of the ion pair into the micelle interior, solubilization of the ion pair by insertion of the monomer end ino the micelle, solubilization of the ion pair with the catechols or catecholamines penetrating into the micelle, solubilization of the free cation at the anionic surface of the micelle and partitioning of catechols and catecholamines through complexation with boric acid present in the buffer. Therefore, elucidation of the solubilization mechanism would be

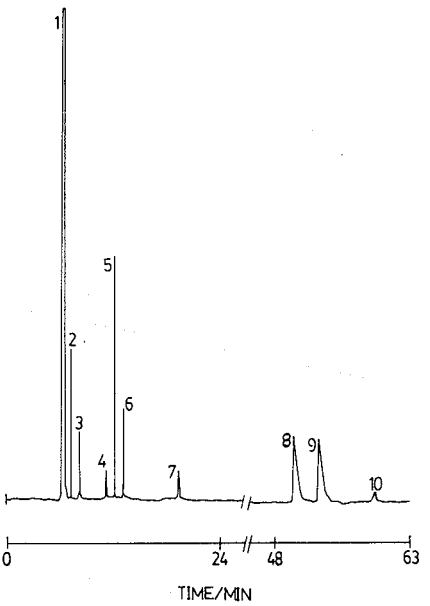

Fig. 4. Electrokinetic chromatogram of the catechols and catecholamines. Peaks: 1 = methanol; 2 = Ne; 3 = TRP; 4 = DHBA; 5 = DHPG; 6 = HIAA; 7 = DHPAA; 8 = NEPH; 9 = EPH; 10 = Sudan III. Electrophoretic solution, 80 m*M* SDS in 0.1 *M* borate–0.05 *M* phosphate buffer (pH 7.0); separation tube, 45 cm × 50 μm I.D. fused-silica capillary; voltage, 15 kV; detection wavelength, 210 nm.

TABLE I

EXPERIMENTAL t_0/t_{mc} RATIOS OBTAINED AT VARIOUS SDS CONCENTRATION

SDS concentration (m*M*)	t_0/t_{mc}
20	0.19
45	0.19
60	0.19
80	0.11

difficult. However, the migration order observed in Fig. 4 can be briefly explained by noting the dominant interactions.

At pH 7, protonation of the amino group in EPH, NEPH and TRP would be likely to occur. Consequently, long migration times are observed for these species. For the other compounds, because of the presence of the polar groups, they tend to be solvated more by the aqueous phase and therefore they migrate faster. With DHPAA and 5-hydroxyindole-3-acetic acid (HIAA), because of the orientation of the substituent groups, intrahydrogen bonding is possible (*i.e.*, for DHPAA between the carboxylate group and the phenolic OH, and for HIAA between the carbonyl and the phenolic groups). As a result, they are solvated less by the aqueous phase. Hence they migrate more slowly than all the other compounds except EPH and NEPH.

Two of the cationic species (NE and DHBA) show relatively short migration times. It has been documented by Wallingford and Ewing [5] that cations interact with free SDS monomers (DS^-) to form ion pairs. The neutral ion pairs would be very hydrophobic and can be solubilized by the micelles, and hence longer migration times would be expected for the cations. However, the two cationic compounds under invesigation did not seem to have formed ion pairs with the SDS. The reason could be that owing to the presence of *o*-dihydroxyl groups, the compounds may form complexes with boric acid present in the buffer solution [5,8]. Consequently, NE and DHBA exist in the form of net-neutral complexes, which do not interact strongly with the SDS micelles. Therefore, they show very short migration times.

On the other hand, for the other two cationic compounds, NEPH and EPH, formation of the borate complexes did not take place as they do not possess *o*-dihydroxyl groups. As a result, they interact with SDS through the formation of ion pairs as expected, thus resulting in the longer migration times obtained for these two species.

For the neutral compounds, TRP and HIAA, there is no tendency to form complexes with borate or to interact with the SDS micelles. They are polar and would remain in the aqueous phase. Hence they have short migration times. It was also noted that TRP migrated faster than HIAA. This can be attributed to the fact that the primary amine group in TRP increases its hydrophobicity.

With DHPG, which is non-ionic, the dominant factor that determines its migration order may be its ability to form a net-anionic complex with boric acid. This net-anionic complex was found to migrate more slowly than the neutral species (borate complexes of NE and DHBA, and TRP). This could be due to the fact that electrophoretic effects predominate as the anions were attracted by the positive electrode and hence the migration time would be longer for this species. As for DHPAA,

although there is also a tendency to form a net-anionic complex with boric acid, the effect due to intrahydrogen bonding may be dominant, as discussed earlier. Consequently, DHPAA shows an even longer migration time than that of DHPG.

The results obtained in this work successfully demonstrated the use of MEKC for the separation of catecholamines. The interesting trends observed in their migration behaviour at different pH values and SDS concentrations demonstrated the versatility of the MEKC technique. From the results obtained, it is believed that this technique possesses immense potential for the separation of other groups of complicated mixtures.

ACKNOWLEDGEMENT

We thank the National University of Singapore for financial support.

REFERENCES

1 S. Terabe, K. Otsuka, K. Ichikawa, A. Tsuchiya and T. Ando, *Anal. Chem.*, 56 (1984) 111.
2 D. E. Burton, M. J. Sepaniak and M. P. Maskarinec, *J. Chromatogr. Sci.*, 24 (1986) 347.
3 R. A. Wallingford and A. G. Ewing, *Anal. Chem.*, 59 (1987) 1762.
4 R. A. Wallingford and A. G. Ewing, *Anal. Chem.*, 60 (1988) 258.
5 R. A. Wallingford and A. G. Ewing, *J. Chromatogr.*, 441 (1988) 299.
6 R. A. Wallingford and A. G. Ewing, *Anal. Chem.*, 61 (1989) 98.
7 R. A. Wallingford and A. G. Ewing, *J. Microcolumn Sep.*, 1 (1989) 23.
8 S. Tanaka, T. Kaneta and H. Yochida, *Anal. Sci.*, 6 (1990) 467.
9 C. P. Ong, C. L. Ng, N. C. Chong, H. K. Lee and S. F. Y. Li, *J. Chromatogr.*, 516 (1990) 263.
10 K. Otsuka and S. Terabe, *J. Microcolumn Sep.*, 1 (1989) 150.
11 H. Nishi, N. Tsumagari, T. Kakimoto and S. Terabe, *J. Chromatogr.*, 465 (1989) 331.
12 S. Terabe, K. Otsuka and T. Ando, *Anal. Chem.*, 57 (1985) 834.

Journal of Chromatography, 559 (1991) 537–545
Elsevier Science Publishers B.V., Amsterdam

CHROM. 23 469

Separation of Dns-amino acids and vitamins by micellar electrokinetic chromatography

C. P. ONG, C. L. NG, H. K. LEE and S. F. Y. LI*
Department of Chemistry, National University of Singapore, Kent Ridge, Singapore 0511 (Singapore)

ABSTRACT

Fifteen Dns-amino acids were analysed by micellar electrokinetic chromatography (MEKC). All the amino acids were satisfactorily separated within *ca.* 26 min with 40 m*M* sodium dodecyl sulphate in phosphate–borate buffer (pH 7.56). The migration behaviour of the amino acids at different pH values and SDS concentrations was examined. In addition, attempts were made to separate a mixture of amino acids and vitamins simultaneously in a single run by MEKC. Detection for this mixture was carried out with an on-column fluorescence detection system with the capability of performing multi-wavelength programming.

INTRODUCTION

Interest in the use of high-performance capillary electrophoresis (CE) as a separation technique in chromatography has been rapidly increasing over the years. Its popularity has been attributed largely to its high separation efficiency with a relatively simple instrumental set-up [1–3].

Micellar electrokinetic chromatography (MEKC), one of the many modes of CE, was first initiated by Terabe *et al.* [3] in 1984. This mode of separation involves the addition of a surfactant to the carrier electrolyte solution. The introduction of MEKC has since expanded the scope of applications in CE. The usefulness and versatility of MEKC have been demonstrated by the numerous papers published since [4—7]. The main advantage of this technique is largely due to the extra partition mechanism for solutes to distribute between the aqueous and the micellar phases in the electrophoretic media. As a result, higher selectivity is often observed, particularly for non-ionic species.

The analysis of vitamins and amino acids has been carried out using a wide range of chromatographic techniques, such as ion-exchange chromatography for amino acids [8] and normal-phase high-performance liquid chromatography (HPLC) for vitamins [9]. To date the simultaneous analysis of this two groups of compounds by HPLC has rarely been explored. One of the reasons could be that each group requires a different HPLC mode for optimum separation and therefore sequential analysis would be needed if HPLC is used. In this work, attempts were made to analyse these two groups of compounds simultaneously using MEKC.

0021-9673/91/$03.50

The first part of the paper reports the use of an MEKC system with on-column fluorescence detection for the separation of fifteen Dns-amino acids (Dns = dansyl = 5-dimethylaminonaphthalene-1-sulphonyl). The separation of the amino acids is achieved by optimizing the pH and the concentration of the sodium dodecyl sulphate (SDS) in the electrophoretic media. The retention characteristics of the amino acids at various SDS concentrations and pH conditions were also examined. In the second part of the investigation, the separation of a mixture of amino acids and vitamins simultaneously in a single analysis using MEKC was studied. An on-column fluorescence detection system which permits programming of the excitation and emission wavelengths during the analysis was used for this investigation.

EXPERIMENTAL

A Spellman (Plainview, NY, USA) Model RM15P10KD power supply capable of delivering up to 15 kV was used. A fused-silica capillary (50 μm I.D. $\times$ 60 cm effective length) obtained from Polymicro Technologies (Phoenix, AZ, USA) was used as the separation tube. Detection of the Dns-amino acids was carried out on a Shimadzu (Kyoto, Japan) Model RF-535 fluorescence detector. For the detection of mixtures containing Dns-amino acids and vitamins, a Shimadzu Model RF-551 fluorescence detector capable of multi-wavelength programming was used. In both instances, the detector cells were modified as described elsewhere [10]. Briefly, the on-column micro fluorescence flow cell was fabricated by replacing the quartz cell with a separating capillary tube. A section of the polyimide coating on the capillary *ca.* 5 mm was removed to form the detection window. A slit was made for the incident light to improve the background signal. A Linear Instruments (Irvine, CA, USA) Model 252A/MM chart recorder was used to record the chromatograms.

All chemicals were of analytical-reagent grade or better. The buffer solution was prepared by dissolving sodium dihydrogenphosphate dihydrate and sodium tetraborate in water purified with a Milli-Q system (Millipore, Bedford, MA, USA). The electrophoretic medium containing sodium dodecyl sulphate (SDS) micelles was prepared as described previously [3]. Standard solutions of Dns-amino acids and Dns-amino acids–vitamins mixtures were prepared in HPLC-grade methanol (J. T. Baker, Phillipsburg, NJ, USA) at a concentration of 500 ppm for each of the species. The Dns-amino acids were supplied by Sigma (St. Louis, MO, USA) and the other chemicals by Fluka (Buchs, Switzerland).

Sample solution was introduced manually by gravity feed. This was carried out by placing the tip of the capillary at the high-potential end in a sample vial at a height 10 cm higher than the buffer reservoir. The time for each injection was 5 s.

RESULTS AND DISCUSSION

In previous investigations using MEKC, Sudan III has been the most commonly used marker to obtain the migration time of the micelles, which is used for calculating the capacity factors of the solutes. In this work, as Sudan III could not be detected at the wavelength at which the system was operating, migration times, t_r, rather than the capacity factors were used throughout. The two parameters used for the optimization of the separation of the Dns-amino acids were pH and SDS concentration. For

each of these parameters, a series of experiments were conducted to study their effect on the separation of the amino acids.

All the Dns-amino acids possess, in addition to their original ionizable groups, two other groups, namely the dimethylamino group and the α-carboxyl group from the Dns group. As all the amino acids investigated have the same Dns group attached to them, its effect on the migration behaviour would be expected to be the same. Therefore, the major factor that influences the migration order of these amino acids would be largely due to the differences in their main structural parent chains.

Effect of SDS

The results obtained for the migration times at different SDS concentrations are shown in Fig. 1. There was no apparent change in the migration order of any of the Dns-amino acid in all three sets of experiments. This observation is in agreement with the fact that as these experiments were carried out at the same pH, the extent of ionization of the Dns-amino acids would be the same in all three sets of experiments. In Table I, the log *P* (partition coefficient) values for some amino acids are listed according to the migration order observed. Even though not all the log *P* values are available, a distinct migration pattern could be observed. It can be seen that there is a good correlation between the migration order and the log *P* values. This relationship strongly suggests that the separation is primarily due to differences in hydrophobicity rather than differences in charge for these amino acids. This observation is typically observed in many MEKC applications in which the presence of micelles in the electrophoretic media influences the elution of the solutes. The extent of solubilization of the compounds into the neutral cavity of the micelles would be largely dependent on the hydrophobicity of the solutes. The more hydrophobic species would tend to be strongly associated with the micelles. As the anionic micelles are attracted by the

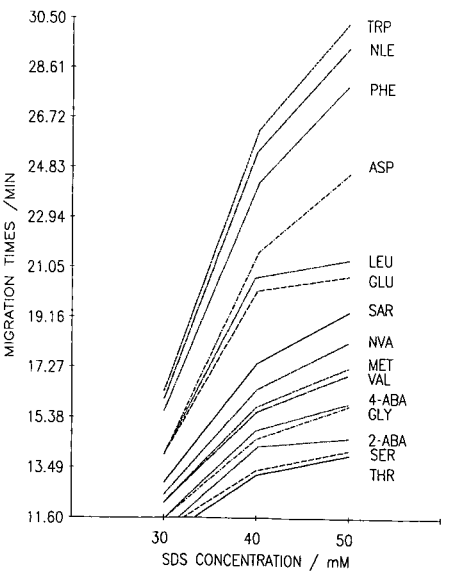

Fig. 1. Plot of migration times against SDS concentration. Experiments were carried out at pH 7.56.

TABLE I

LOG *P* [11] AND pK_a [12] VALUES FOR SOME AMINO ACIDS

Migration order	Amino acid	Log $P^{a,b}$	pK_a[b]
1	Thr	–	–
2	Ser	–	9.15
3	α-Aba	−1.81	–
4	Gly	−1.34	9.78
5	γ-Aba	–	–
6	Val	−1.41	9.72
7	Met	–	9.21
8	Nva	−0.98	–
9	Sar	–	–
10	Glu	–	4.07
11	Leu	−0.74	9.70
12	Asp	–	3.86
13	Phe	−0.59	–
14	Nle	−0.51	–
15	Trp	0.30	9.39

[a] Measured using *n*-butanol.
[b] – = Not available.

negative electrophoretic attraction towards the positive electrode, the solubilized species would tend to migrate more slowly than the hydrophilic species. For example, with Dns-Trp, its high log *P* value (0.3) would favour stronger interaction with the micelles in comparison with the other amino acids. Consequently, it would be highly incorporated in the micelles and thus would have a longer migration time, as observed in Fig. 1. On the other hand, Gly was one of the first few amino acids to migrate as it has the smallest log *P* values (−1.81). The trend observed is in good agreement with the results previously obtained by reversed-phase HPLC [8].

The migration behaviour of the other Dns-amino acids listed in Table I (*i.e.*, those amino acids for which the log *P* values are not available) can be categorized into the following groups: group I, consisting of Dns-Thr, Dns-Ser and Dns-Met; group II, consisting of Dns-γ-Aba and Dns-Sar; and group III, consisting of Dns-Glu and Dns-Asp.

The characteristic feature of the amino acids in group I is that each possesses at least one polar substituent group, which makes them hydrophilic. Consequently, these amino acids would tend to be solvated more by the aqueous phase and effective solubilization by the micelles would be inhibited. Therefore, their migration times were shorter than those of most of the other amino acids. For example, for Dns-Met, even though it has the same number of methylene groups in its alkyl chain as Dns-Nva, a shorter migration time was observed. The difference in the migration times between these two species could be largely due to the presence of the polar sulphur atom in the alkyl chain in Dns-Met, which makes it more hydrophilic. Similar results were obtained for Dns-Thr and Dns-Ser. Further, it was noted that the extent of solvation of these two amino acids by the aqueous phase seems more pronounced than for Dns-Met. The fact that their hydroxyl groups are at the terminus enables

these amino acids to form hydrogen bonds more readily with the aqueous phase. Subsequently, these two amino acids were found to have the shortest migration times.

An interesting trend was observed for the amino acids in group II. Both Dns-γ-Aba and Dns-Sar were found to have a longer migration times than expected. For example, for Dns-Sar, the increase in hydrophobicity due to the additional methyl group could not have resulted in such a large increase in migration time when compared with Dns-Gly. A longer migration time was also observed for Dns-γ-Aba when compared with Dns-α-Aba. A possible reason for the longer migration times observed could be that these amino acids are generally more basic than the others and therefore they would be susceptible to protonation. These positively charged species would be very prone to ion-pair formation with the micelles. Consequently, owing to the negative electrophoretic attraction towards the anode, longer migration times would be expected for these amino acids. Among the two amino acids in group II, this effect seems more pronounced for Dns-Sar. The reason is probably its secondary amino group, which makes it more basic and therefore protonation would be more favorable for Dns-Sar. As a result, Dns-Sar was found to migrate more slowly. For Dns-γ-Aba, unlike the other of amino acids, its carboxylate group is not attached to α-carbon. This would make its amino group more basic than that in Dns-α-Aba. Consequently, it is possible for Dns-γ-Aba to undergo preferential protonation, and therefore it would have a longer migration time than Dns-α-Aba.

Dns-Glu and Dns-Asp are the two diacid amino acids in group III. In view of the extra methylene group in the alkyl chain of the more hydrophobic Dns-Glu, it would be reasonable to expect it to migrate more slowly than Dns-Asp. However, the opposite was observed. Further, on comparing their migration order with that of some of the amino acids having the same number of carbons in the alkyl chain, it was observed that both Dns-Asp and Dns-Glu have longer migration times. In addition, because of the presence of the additional carboxylic group in these two species, which could have made them more hydrophilic, these species would be expected to be less solubilized by the micelles and therefore they should have shorter migration times. However, the results obtained contradict this expectation. This anomalous behaviour can be explained by the differences in pK_a values. From Table I, it can be seen that the pK_a values of these two amino acids are significantly smaller than those of the other amino acids. Therefore, dissociation of the carboxylic group in these compounds is possible and these negatively charged, dissociated species would be electrostatically attracted to the anode. Consequently, because of this negative electrophoretic attraction, they would tend to migrate more slowly. As the pK_a value of Asp (3.86) is lower than that of Glu (4.07), the extent of ionization in Asp would be expected to be higher. Therefore, Asp would experience a stronger interaction with the anode and hence a longer migration time is expected for Asp. Further, it is worth noting that even under conditions where dissociation of these compounds is not favourable, the migration order for these two "neutral" amino acids would remain the same (*i.e.*, t_r for Asp would be longer than t_r for Glu). The behaviour can be explained by their tendency to form hydrogen bonds. The two carboxylic groups in these species are oriented in such a position that intramolecular hydrogen bonding would be possible. As a result, it is expected that the two polar carboxylic groups in these species would be in a "cage-like" configuration. This caging effect would render the species less hydrophilic. As the two carboxylic acids are in closer proximity in Asp than in Glu

(*i.e.*, they are separated by one less methylene group), stronger intramolecular hydrogen bonding would be expected. Hence Asp would be more hydrophobic than Glu, and therefore would have a longer migration time.

From Fig. 1, it was also noted that with an increase in SDS concentration a corresponding increase in the migration times was observed for all the amino acids in all three sets. This is because an increase in SDS concentration would result in an increase in solubilization of the species by the micelles. Therefore, longer migration times would be expected.

Effect of pH

The results obtained for the migration times at different pH values are shown in Fig. 2. It can be seen that with increase in pH from 6.6 to 7.5, a corresponding decrease in the migration times was observed for all the Dns-amino acids. With a further increase in pH to 8.0, a reversal of this trend was noted. This interesting effect is largely due to the presence of two different types of ionizable amino and carboxylate groups in these compounds. At low pH, it is reasonable to expect the amino group to be protonated. These positively charged protonated species would then form ion pairs with the anionic micelles. As the pH of the electrophoretic medium increases, the extent of protonation would be lowered and in this event the species would no longer be able to effectively form ion pairs with the micelles. Therefore, a decrease in the migration times was observed as the pH increased. On the other hand, at higher pH, ionization of the carboxylate group in these compounds would be favourable. As the negatively charged amino acids would be attracted to the anode via electrophoretic interaction, therefore, at pH 8 the amino acids would elute at longer migration times, as observed in Fig. 2.

It is worth noting that in spite of the reversal in the trend observed with changes

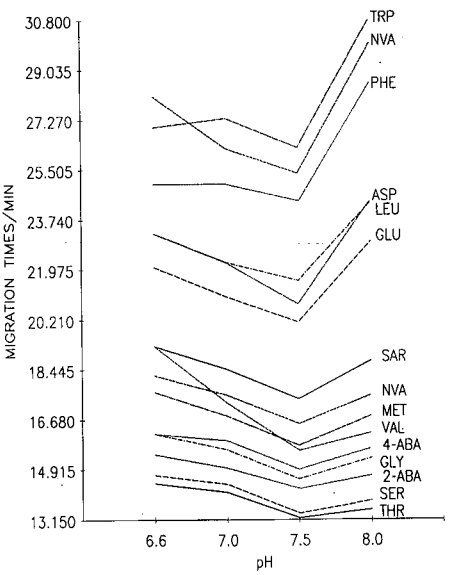

Fig. 2. Plot of migration times against pH. Experiments were carried out at 40 m*M* SDS.

in pH, with the exception of the group consisting of Dns-Met, Dns-Val and Dns-Nva and the pair Dns-Nle and Dns-Trp, the migration order of the amino acids remained unchanged in the pH range investigated. For these pH values hydrophobicity is one of the principal factors dominating the migration order.

For Dns-Met, Dns-Val and Dns-Nva, crossover of peaks was observed with changes in pH. At lower pH, preferential protonation of the amino group in some of the amino acids would be possible. This would subsequently lead to the formation of ion pairs between the positively charged amino acids and the micelles. Hence longer migration times would be expected for these species. With Dns-Val, the highly branched, electon-donating isopropyl group attached to the α-carbon would enhance the basicity of the amino group. This is in contrast to Dns-Val, which has a straight, less electron-donating alkyl chain, and Dns-Met, which contains an electron-withdrawing sulphur group. As a result, protonation of the basic Dns-Val would be more favourable than that of the other two amino acids. Consequently, because of the possibility of ion-pair formation in Dns-Val, a longer migration time was observed. From Fig. 2, it can be seen that this is more apparent at lower pH. On increasing the pH, protonation of Dns-Val would be inhibited. Under such circumstances, the migration would now be governed by hydrophobicity. Therefore, at higher pH, Dns-Val would be expected to migrate faster than Dns-Met and Dns-Val as it has the smallest log *P* among the three amino acids.

A change in migration order was also observed in Dns-Nle and Dns-Trp. It was noted that at lower pH (i.e., pH 6.6), Dns-Trp, in spite of its large log *P* value, was found to have a migration time smaller than that of Dns-Leu. A possible reason could be the basicity of the pyrrole ring, which makes it susceptible to protonation at this pH. Consequently, this would lead to the formation of ion pairs with the micelles, therefore inhibiting effective solubilization by the micelles and giving a longer migration time. However, unlike with Dns-Val, ion-pair formation in Dns-Trp seems to result in a shorter migration time. This discrepancy can be attributed to the fact that as the pyrrole ring in Dns-Trp is more basic than Dns-Val, the extent of protonation would be greater. Consequently the electrophoretic repulsion experienced by the more positively charged Dns-Trp would then be more pronounced. As a result, Dns-Trp would migrate faster, as is observed in Fig. 2.

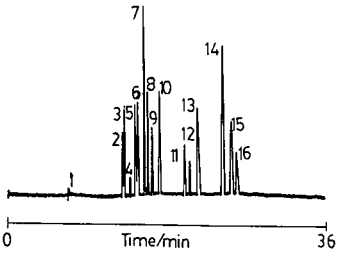

Fig. 3. Electrokinetic chromatogram obtained for the fifteen Dns-amino acids. Peaks: 1 = methanol; 2 = Dns-Thr; 3 = Dns-Ser; 4 = Dns-α-Aba; 5 = Dns-Gly; 6 = Dns-γ-Aba; 7 = Dns-Val; 8 = Dns-Met; 9 = Dns-Nva; 10 = Dns-Sar; 11 = Dns-Glu; 12 = Dns-Leu; 13 = Dns-Asp; 14 Dns -Phe; 15 = Dns-Nle; 16 = Dns-Trp. Electrophoretic conditions: 40 m*M* SDS in 0.1 *M* borate–0.05 *M* phosphate buffer (pH 7.56); separation tube, 60 cm × 50 μm I.D. fused-silica capillary; applied voltage, 15 kV; excitation wavelength, 325 nm; emission wavelength, 550 nm.

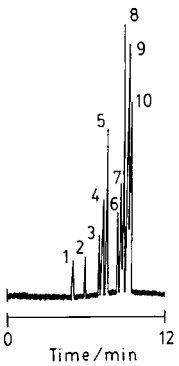

Fig. 4. Electrokinetic chromatogram obtained for a mixture of seven selected Dns-amino acids and two vitamins. Peaks: 1 = methanol; 2 = vitamin B_6; 3 = Dns-Thr; 4 = Vitamin B_2; 5 = Dns-γ-Aba; 6 = Dns-Glu; 7 = Dns-Leu; 8 = Dns-Asp; 9 = Dns-Phe; 10 = Dns-Nle. Electrophoretic conditions: 40 m*M* SDS in 0.1 *M* borate–0.05 *M* phosphate buffer (pH 7.56); separation tube, 60 cm × 50 μm I.D. fused-silica capillary; applied voltage, 15 kV. Wavelength programme: 0.1 min, excitation wavelength 340 nm, emission wavelength 400 nm; 6.1 min, excitation wavelength 325 nm, emission wavelength 550 nm; 7.10 min, excitation wavelength 370 nm, emission wavelength 440 nm; 7.40 min, excitation wavelength 325 nm, emission wavelength 550 nm.

The optimum separation of the fifteen Dns-amino acids was obtained at pH 7.56 with 40 m*M* SDS. The corresponding chromatogram obtained is shown in Fig. 3. All the peaks were satisfactorily separated within 30 min.

Dns-amino acids and vitamins

In an earlier investigation, Nishi *et al.* [13] successfully separated a group of vitamins. In this work, the separation of a mixture of amino acids and water-soluble vitamins in a single analysis was attempted. The unique feature of this investigation is the use of a multi-wavelength programmable fluorescence detector. The excitation and emission wavelengths for detection were programmed to give maximum sensitivity for each of the species in the mixture.

A typical chromatogram obtained is shown in Fig. 4. It can be seen that all the peaks were satisfactorily separated. The conditions used for the optimum separation of the vitamins and Dns-amino acids were similar to those used in Fig. 3 (*i.e.*, 40 m*M* SDS in an electrophoretic medium at pH 7.56). The migration order for the seven selected Dns-amino acid would therefore be expected to be the same as that obtained earlier. It was noted that vitamin B_6 has the shortest migration time. This is largely due to the presence of the three hydroxyl groups, which makes vitamin B_6 even more hydrophilic than Dns-Thr. For vitamin B_2, because of its bulkier substituent group, effective solubilization by the micelles would be hindered. Hence, a shorter migration time was observed vitamin for B_2 compared with the other Dns-amino acids.

The separation of these two groups of compounds in a single analysis by MEKC is, to our knowledge, the first attempt in which a multi-wavelength programmable fluorescence detector has been used. In view of the encouraging results obtained in this investigation, it is believed that the inherently high efficiency of MEKC and the versatility of the wavelength-programmable fluorescence detector can be exploited for the separation of complicated mixtures.

ACKNOWLEDGEMENTS

We thank the National University of Singapore for financial support. We also express our gratitude to Schmidt Scientific (Singapore) and Shimadzu (Asia Pacific) for their generous loan of the Shimadzu RF551 fluorescence detector.

REFERENCES

1 J. W. Jorgenson and K. Lukacs, *Anal. Chem.*, 53 (1981) 1298.
2 T. Tsuda, K. Normura and G. Nakagawa, *J. Chromatogr.*, 264 (1983) 385.
3 S. Terabe, K. Otsuka, K. Ichikawa, A. Tsuchiya and T. Ando, *Anal. Chem.*, 56 (1984) 111.
4 A. Guttman, A. Paulus, A. S. Cohen, N. Grinberg and B. L. Karger, *J. Chromatogr.*, 448 (1988) 41.
5 E. Gassmann, J. E. Kuo and R. N. Zare, *Science(Washington, D.C.)*, 230 (1985) 813.
6 P. Gozel, E. Gassmann, H. Michelsen and R. N. Zare, *Anal. Chem.*, 59 (1987) 44.
7 C. P. Ong, C. L. Ng, N. C. Chong, H. K. Lee and S. F. Y. Li, *J. Chromatogr.*, 516 (1990) 263.
8 J. M. Wilinson, *CRC Handbook of HPLC for the Separation of Amino Acids, Peptides and Proteins*, Vol. 1, CRC press, Boca Raton, FL, 1985, p. 339.
9 S. Hara, T. Ando and Y. Nakayama, *J. Liq. Chromatogr.*, 12 (1989) 729.
10 T. Tsuda and Y. Kobayashi, *J. Chromatogr.*, 515 (1990) 357.
11 C. Hansch and A. Leo, *Substituent Constants For Correlation Analysis in Chemistry and Biology*, Wiley, New York, 1979.
12 R. C. Weast (Editor), *CRC Handbook of Chemistry and Physics*, CRC Press, Boca Raton, FL, 68th ed., 1987, p. C699.
13 H. Nishi, T. Fukuyama, M. Matsuo and S. Terabe, *J. Chromatogr.*, 498 (1990) 313.

Journal of Chromatography, 559 (1991) 547–558
Elsevier Science Publishers B.V., Amsterdam

CHROM. 23 471

Electrochromatographic solid-phase extraction for determination of cimetidine in serum by micellar electrokinetic capillary chromatography

HELENA SOINI[a], TAKAO TSUDA[b] and MILOS V. NOVOTNY*
Department of Chemistry, Indiana University, Bloomington, IN 47405 (USA)

ABSTRACT

A highly effective electrochromatographic solid-phase extraction and preconcentration method is reported for the determination of cimetidine in serum in the concentration range 0.233–11.4 μg/ml. Preconcentrated samples were determined by micellar electrokinetic capillary chromatography while ranitidine was used as an internal standard. Sample preparation included retention of the analyte on a C_{18} solid-phase cartridge, followed by elution assisted by an applied voltage of 150 V. From 0.5-ml serum samples, 20–50-μl aliquots were collected for electrophoretic analysis. Within the studied concentration range, the method was linear and provided adequate precision.

INTRODUCTION

Cimetidine, N-cyano-N-methyl-N′-[2(5-methyl-1H-imidazoyl-4-yl)methylthioethyl]guanidine, is a histamine H_2 receptor antagonist which is used to reduce acid secretion in treatment of gastrointestinal ulcers [1]. This pharmaceutical has traditionally been determined in serum by high-performance liquid chromatography (HPLC) [2—11]. Unfortunately, some analytical problems are encountered with this chromatographic approach. Cimetidine exhibits a high retention with most HPLC systems and, in addition, asymmetric and broad peaks are often experienced owing to undesirable interaction with the packing materials. Typical column efficiencies are seldom sufficient to separate cimetidine adequately from various interfering serum or plasma constituents.

Isolation of cimetidine as a pure component from serum is difficult owing to its neutral character (pK_a = 6.8) [12] and high solubility in water. In some instances, laborious, multiple extractions with methylene chloride have been reported [2] to be necessary. An alternative approach has been solid-phase extraction with Extrelut [6]

[a] On leave from Analytical Department, Orion Pharmaceutica, P.O. Box 65, 02101 Espoo, Finland.
[b] On leave from Department of Applied Chemistry, Nagoya Institute of Technology, Gokiso-cho, Showa-ku, Nagoya-shi, 466, Japan.

0021-9673/91/$03.50

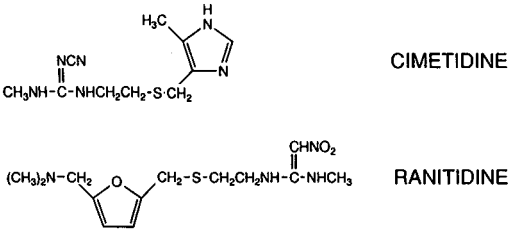

Fig. 1. Structures of cimetidine and ranitidine.

or a reversed-phased material [5,7–11]. In this general procedure, large volumes of solvent can be avoided, while the occurrence of coextracted blood constituents is also suppressed. However, relatively large volumes of either acetonitrile or methanol (1–5 ml) must be reduced to the permissible injection volumes (40–100 μl) for HPLC.

Capillary electromigration techniques, with their relatively high efficiencies and various selective mechanisms, now offer interesting alternatives in drug analysis. As such techniques are relatively new, only few quantitative methods for determining drug substances in serum or plasma have been reported [13–18]. At this stage of development, small sample volumes (of the order of nanoliters) are essential in capillary zone electrophoresis (CZE) or micellar electrokinetic capillary chromatography (MECC), so that very low levels of therapeutic drugs can be reached only through highly sensitive detection methods, such as laser-induced fluorescence measurements of derivatized samples [17].

This investigation concerns the use of cimetidine as a model compound in exploring certain analytical merits of MECC in serum analysis. Sample purification and preconcentration are accomplished through electrochromatography, which combines certain advantages of electrophoresis and sorptive interactions [19]. In its more modern version, the separation modes of electrochromatography have been explored with slurry-packed reversed-phase microcapillaries, where the model compounds were separated under various conditions of pressurized flow and applied electrical field [20–23]. A potential role of electrochromatography in sample pretreatment has also been predicted previously [23].

During our analyses of cimetidine, ranitidine (Fig. 1) has been used as an internal standard. In order to determine the drug levels in the range 0.2–10 μg/ml, sample preconcentration proved essential. We therefore combined a traditional solid-phase extraction with electrically driven elution to provide a sample treatment compatible with electrophoretic analysis. We have termed this method "electrochromatographic solid-phase extraction". Various experimental variables were further explored to ensure quantitative results, while the capabilities of providing pharmacologically relevant measurements were also considered.

EXPERIMENTAL

Chemicals

Cimetidine and ranitidine were a gift from Orion Pharmaceutica (Espoo, Finland). Hexadecyltrimethylammonium bromide (HTAB) and tris(hydroxymethyl)

aminomethane (TRIZMA base) were purchased from Sigma (St. Louis, MO, USA), glacial acetic acid, rosaniline hydrochloride (Magenta) and tetrahydrofuran (THF) from Fisher Scientific (Fair Lawn, NJ, USA), trifluoroacetic acid from Mallinkrodt (Paris, KY, USA), sodium hydrogenphosphate from Aldrich (Milwaukee, WI, USA) and acetonitrile (OmniSolv) from EM Science (Cherry Hill, NJ, USA). VWR 50-μl micropipets (Drummond Scientific, Broomall, PA, USA), and Kimble 20-μl microcapillary pipets (Toledo, OH, USA) were used for sample collection. Supelclean LC-18 1.0-ml SPE tubes (C_{18}, 100 mg, 40-μm particle size, 20-μm porous polyethylene frits) were obtained from Supelco (Bellefonte, PA, USA). Tuberculine 1-ml disposable syringes (Becton Dickinson, Rutherford, NJ, USA) were used for pressing liquids through sample cartridges. Nylon 66 membranes (0.2 μm) (Alltech, Deerfield, IL, USA) were used for filtering all buffer solutions. Water was purified by distillation and ion exchange.

Micellar electrokinetic capillary chromatography

A laboratory-made capillary electrophoresis apparatus described previously [24] was used. A high-voltage power supply (0–60 kV) was a product of Spellman High Voltage Electronics (Plainview, NY, USA). Negative voltages, -18 to -23 kV, were used (positive ground). The uncoated fused-silica capillary was 60 cm $\times$ 50 μm I.D. $\times$ 180 μm O.D. from Polymicro Technologies (Phoenix, AZ, USA). The polyimide coating was removed in a small area about 15 cm from the capillary end to form an on-column flow cell for UV detection. The detector was a Jasco UVIDEC-100-IV (Japan Spectroscopic, Tokyo, Japan) adjusted to 228 nm. Sample injection was performed hydrodynamically by dipping the capillary end into the sample solution for 10–15 s. The height difference between the injection point and buffer level was 13.5 cm to produce the necessary pressure gradient. The buffer system included the cationic detergent HTAB (9.8 m*M*), TRIZMA base (3.3 m*M*) and sodium hydrogenphosphate (9.4 m*M*) at pH 6.4.

A new capillary was rinsed with water for 30 min and, overnight, with 0.1 *M* sodium hydroxide solution. After a short wash with water, the buffer was stabilized for several hours, followed by injections of cimetidine standard solutions. The same buffer solution was used for at least 2 days continuously. When changing the buffer, rinsing for 15 min was performed. A short rinse with the buffer between injections was found to be necessary. The capillary remained in the buffer solution overnight.

When the separation system lost its efficiency, a short rinse with water (10 min), 45% trifluoroacetic acid (2 h) and water (10 min) restored its original characteristics. When using an acid wash, equilibration with the analytical buffer containing cationic detergent was easily established within 2 h. However, an alkaline wash was necessary with overnight equilibration.

Spiked serum samples

Stock cimetidine and ranitidine standard solutions of 5 mg/ml in methanol were prepared. Additional working standard solutions were prepared by appropriate dilutions. Cimetidine standard solutions (50 μl) were added to 0.5 ml of serum. In all samples, 5 μg per 5 μl of ranitidine were added as an internal standard (concentration 10 μg/ml in serum).

Electrochromatographic solid-phase extraction

Samples were concentrated on the reversed-phase C_{18} (commercially packed cartridges, 6 mm I.D.). Solvents and samples were moved by means of a disposable 1-ml syringe in the voltage "off" mode (Fig. 2). The general procedure for the solid-phase extraction included the steps of conditioning, retention, washing and elution, as described previously [25,26].

The cartridge was subsequently activated with methanol (1 ml) by a syringe suction (downflow) (Fig. 2). The remaining methanol was further removed with 1.0 ml of water, while the cartridge was conditioned to pH 7.7 with 1.0 ml of buffer (10 m*M* TRIZMA–3.2 m*M* acetic acid, buffer TAC-2). Serum (0.5 ml) was diluted (1:1) with a buffer (40 m*M* TRIZMA–13 m*M* acetic acid, buffer TAC-8). Sample was dispensed by means of a 1.0-ml syringe, from the bottom of the cartridge to the upflow direction, followed by washing with 1.0 ml of water in the same direction. Finally, water in the cartridge was compensated for in the suction mode with 160 μl of the elution solvent [tetrahydrofuran–buffer, 5 m*M* TRIZMA–1.7 m*M* acetic acid (pH 7.7) (50:50)].

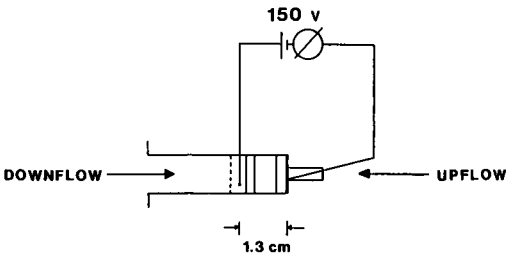

Fig. 2. Electrochromatographic solid-phase extraction set-up. Retention of the drug: voltage off/upflow direction with pressure. Elution: voltage on/flow towards negative electrode (downflow).

During elution of the sample, an electrical field was applied as a driving force. The cartridge was set in a horizontal position between the platinum electrodes, as shown in Fig. 2 (a hole was drilled in the cartridge for the positive electrode, which was in contact with the elution solvent). The negative electrode was sharpened and attached to the front part of the polyethylene frit.

RESULTS AND DISCUSSION

While developing the solid-phase electrochromatographic technique, several situations had to be recognized during retention and elution of the analytes of interest. These were different from the previously used elution mode using a pressure gradient.

Preconcentration of cimetidine on a hydrophobic octadecyl phase was previously found to be effective [5,7–11]. The interaction between cimetidine and the C_{18} phase is strong at pH 7.7 where cimetidine appears in its neutral, secondary amine form. However, the known disadvantages of the C_{18} phase are its limited selectivity and the ionic activity of the free silanol groups [27]. Consequently, the roles of TRIZMA buffer during the cartridge conditioning and as a diluting buffer for the serum

sample were assessed as necessary to both adjusting pH and covering the active silanol sites, in order to prevent strong interactions with cimetidine molecules [25].

When introducing the serum samples into the cartridge at the same side (upflow, Fig. 2) as that where the analytes were driven out (downflow, Fig. 2) with the eluting solvent, the elution volume and time could be effectively decreased. This is analogous to the coupled-column backflush mode in HPLC [28]. Water served for washing out the salts, while leaving part of the serum proteins on the cartridge.

During the electrically driven elution, solvents of medium polarity were necessary to overcome the interactions between the solute of interest and the octadecyl moieties [25,26]. While selecting the percentage and type of eluting solvent, rosaniline (aromatic primary amine) was used as a marker due in spiked cimetidine aqueous samples or the serum samples. Eluting colored zones were observed visually and the cimetidine concentrations were measured in collected (colored) sample fractions. Cimetidine and the dye eluted together. According to these results, the solvent-to-buffer ratio was selected. Tetrahydrofuran, acetonitrile and methanol were all tested in a 50:50 solvent–50% buffer [3.7 m*M* TRIZMA–1.8 m*M* acetic acid (pH 7.7)] ratio. Table I summarizes certain important characteristics of these studied solvents.

For the three different solvents, fractions were evaluated for their content of cimetidine (contained originally at 1.85 μg per 0.5 ml of serum). For the elution procedure driven by 150 V, the retention and elution steps were repeated 3–6 times with each solvent. Fig. 3 shows the corresponding elution profiles. Tetrahydrofuran with the lowest dielectric constant and the largest elution strength on ODS (Table I) resulted in the most effective medium.

The electrically driven elution (150 V) was further compared with a pressurized elution (syringe action). While the cimetidine elution trends were similar (Fig. 4), there was a substantial difference in precision (5.9 *vs.* 18.9% in favor of the electrically driven elution). In addition, it was considerably easier to collect precisely the relatively small volumes in the electrical mode. Table II shows the calculated concentration factors together with standard deviations (S.D.s) acquired when cimetidine peak heights were compared with those in the standard solutions and serum samples.

Elution flow stability was found to be influenced by the applied voltage and percentage and type of solvent, and also the mobility of ions in the buffer solution. At

TABLE I

PROPERTIES OF SOLVENTS USED IN ELECTROCHROMATOGRAPHIC MEASUREMENTS

Solvents[a]	Elution strength on ODS[b]	Viscosity, η(cP) (25°C)[c]	Dielectric constant, ε (20°C)[c]
THF	3.7	0.55[d]	7.6
ACN	3.1	0.34	37.5
CH_3OH	1.0	0.55	32.6[e]

[a] THF = tetrahydrofuran; ACN = acetonitrile; CH_3OH = methanol.
[b] Ref. 29.
[c] Ref. 30.
[d] 20°C.
[e] 25°C.

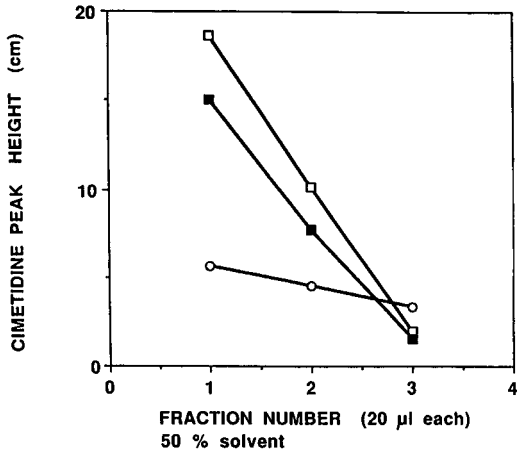

Fig. 3. Elution profiles of cimetidine with different solvent–buffer (50:50) compositions on a 100-mg C_{18} cartridge. Cimetidine peak heights were measured in three successively collected 20-µl sample fractions (n = 3–6). □ = THF; ■ = acetonitrile; ○ = methanol.

150 V, flow-rates were stable and Joule heating was insignificant. With a voltage increase to 200 V, bubbles were generated with all the solvents studied. The tetrahydrofuran–buffer mixture used was found to be the most stable and effective. The flow-rates experienced with the methanol–buffer medium were highly variable, while the elution strength was also insufficient.

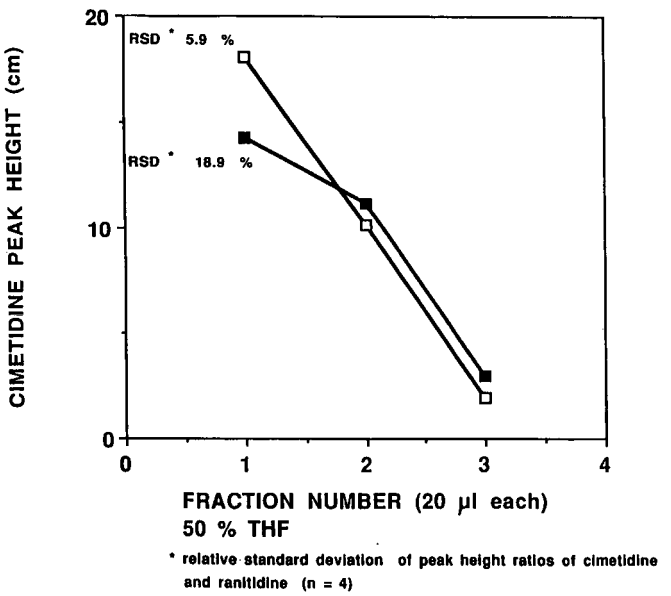

Fig. 4. Elution profiles of cimetidine with (□) the electrical elution mode, R.S.D. = 5.9% (n = 4), and (■) pressure mode, R.S.D. = 18.9% (n = 4). Cimetidine peak heights were measured in the fractions obtained. For calculation of precision data, the cimetidine–ranitidine peak-height ratio was evaluated.

TABLE II

CONCENTRATION FACTORS FOR CIMETIDINE IN SERUM SAMPLE: ENRICHMENT BY ELECTRICAL (E) AND PRESSURE (P) ELUTION MODE

Solvent (50%)	Elution mode	Concentration factor	S.D.	n	Flow-rate (μl/min)
THF	E	13	2	6	40
THF	P	8	2	5	–[a]
ACN	E	10	3	3	60
MeOH	E	4	2	3	30–60

[a] Not measured.

Tsuda [22] reported the use of a pressurized system to avoid bubbles in electrochromatography. In our experience, a non-pressurized system is effective provided that the high-mobility ions (*e.g.*, buffers containing sodium or potassium) are avoided. Otherwise, inappropriately high flow-rates, cartridge overheating and formation of bubbles typically occur.

For precise sample introduction, it is desirable to match the composition of the solution eluting from the cartridge with that of a buffer used in the analytical MECC. Table III summarizes the types and concentrations of the respective buffers. Hexadecyltrimethylammonium bromide (HTAB) was used here at concentrations above the critical micelle concentration. The flow direction was oriented toward the positive electrode, as reported earlier by Liu *et al.* [31]. Under stable MECC conditions, the precision [relative standard deviation (R.S.D.)] of the cimetidine retention was 2.5% (n = 6), and for the cimetidine–ranitidine peak-height ratio, the R.S.D. was 1.0% (n = 6) (concentration 3.7 μg/ml).

The method was found to be linear ($r > 0.999$) using both 20- and 50-μl collected fraction volumes. The linear regression calibration data for the peak-height ratios of cimetidine and the internal standard ranitidine from electrochromatographically extracted serum samples are shown in Table IV.

TABLE III

BUFFERS, SOLVENTS AND CONDITIONS USED

Parameter	Eluting solvent	MECC buffer
THF	50%	–
TRIZMA	3.7 mM	3.3 mM
Acetic acid	1.8 mM	–
HTAB	–	9.8 mM
NaH_2PO_4	–	9.4 mM
pH	7.7	6.4
Flow direction	To cathode	To anode
Voltage, current	+ 150 V, 0.5 mA	– 20 kV, 11–13 μA
Tube radius	6 mm	50 μm

TABLE IV

LINEAR REGRESSION CALIBRATION DATA FOR SPIKED CIMETIDINE SERUM SAMPLES

Range (μg/ml)	No. of points, *n*	Correlation coefficient, *r*	*x*-Axis intercept	*y*-Axis intercept	Collected volume (μl)
0.233–11.4	6	0.9991	0.126	−0.016	50
0.233–11.4	5	0.9993	0.047	−0.004	20

Precision was studied with repeated analyses of 0.5-ml serum samples at concentrations of 0.47 and 3.7 μg/ml. The R.S.D. values were 9.2% and 4.5% ($n = 4$), respectively. The peak-height ratios for cimetidine and the internal standard ranitidine were also measured. Accuracy (relative error) was calculated by using the linear regression calibration graph for the measurement data. The results are shown in Tables V and VI. Means (x), standard deviation (S.D.) values and R.S.D. values were calculated ($n = 4$).

Drug recovery was estimated by comparing the peak heights of cimetidine in the first eluted 20- or 50-μl fractions with a standard solution sample, which was

TABLE V

PRECISION AND ACCURACY FOR SPIKED SERUM SAMPLES (0.47 μg/ml OF CIMETIDINE)

	Cimetidine–ranitidine peak-height ratio	Added (μg)	Found (μg)	Relative error (%)
	0.076	0.233	0.262	+12.4
	0.079	0.233	0.276	+18.5
	0.082	0.233	0.289	+24.0
	0.066	0.233	0.219	− 6.0
x	0.076		0.261	+12.2
S.D.	0.007		0.03	13
R.S.D. (%)	9.2		11.6	
n	4		4	4

TABLE VI

PRECISION AND ACCURACY FOR SPIKED SERUM SAMPLES (3.7 μg/ml OF CIMETIDINE)

	Cimetidine–ranitidine peak-height ratio	Added (μg)	Found (μg)	Relative error (%)
	0.402	1.85	1.71	−7.6
	0.428	1.85	1.83	−1.1
	0.446	1.85	1.91	+3.2
	0.414	1.85	1.77	−4.3
x	0.423		1.81	−2.5
S.D.	0.019		0.085	4.6
R.S.D. (%)	4.5		4.7	
n	4		4	4

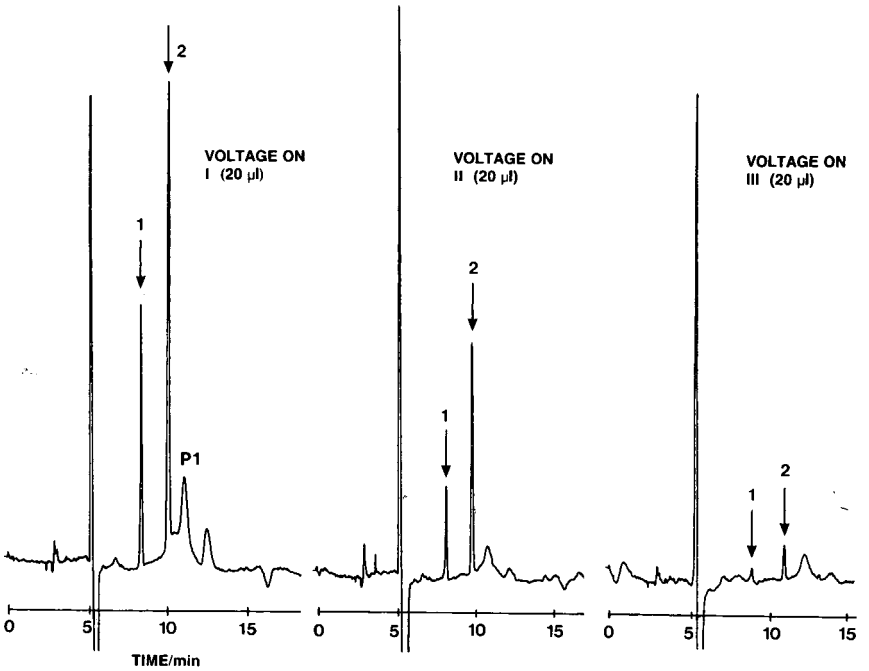

Fig. 5. Series of electropherograms for successively collected 20-μl fractions (I–III) after electrical elution (3.7 μg/ml of cimetidine in serum). 1 = Cimetidine; 2 = ranitidine; P1 = unknown serum background component.

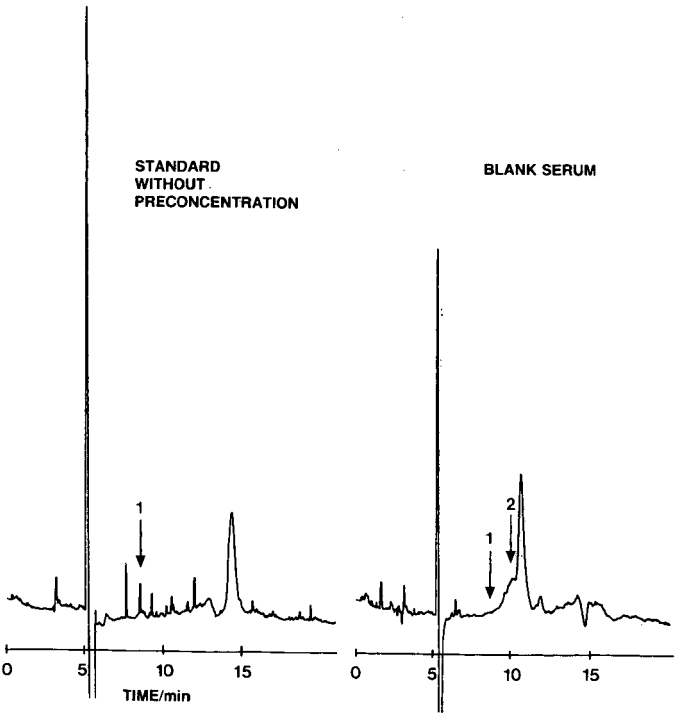

Fig. 6. Cimetidine standard (11.4 μg/ml) in THF–buffer (50:50) without preconcentration and a blank serum extract after electrochromatographic preconcentration. 1 = Cimetidine; 2 = ranitidine.

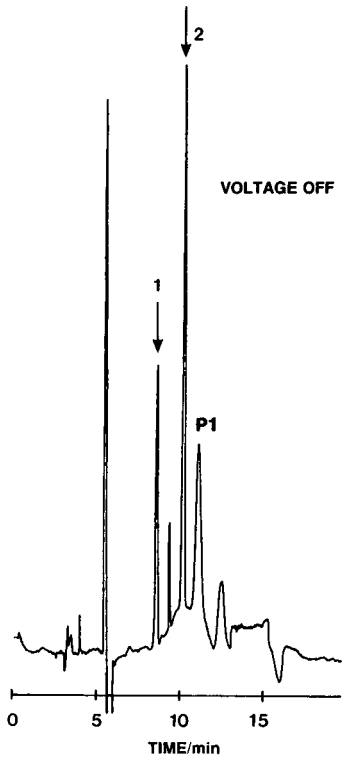

Fig. 7. Electropherogram of a cimetidine serum sample enriched by pressure elution. 1 = Cimetidine; 2 = ranitidine; P1 = unknown serum background compound.

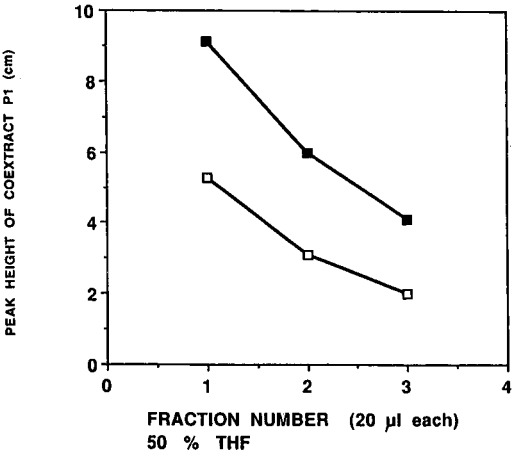

Fig. 8. Elution profiles of unknown serum background component P1 in the (□) electrochromatographic elution (150 V) and (■) pressure elution modes.

prepared in the eluting solvent [THF–buffer (50:50)]. Recoveries were 74% (S.D. = 15%, n = 4) and 93% (S.D. = 2%, n = 4) for 20- and 50-μl samples, respectively. Fig. 5 shows electropherograms for three successive electrically eluted 20-μl sample fractions. Fig. 6 compares the cimetidine standard (11.4 μg/ml) prepared in an elution solvent mixture without preconcentration with a blank serum extract after electrical preconcentration.

The electrochromatographic mode of elution appeared to have a beneficial effect on sample purification. Fig. 7 shows the appearance of an unidentified serum component (labeled P1) in the electropherogram of the cimetidine serum sample eluted by pressure. Electrochromatographic elution decreased the amount of this unwanted component by *ca.* 40% [Fig. 5, I (20 μl)]. Fig. 8 shows the elution profiles of compound P1 in both elution modes for three successively eluted 20-μl fractions.

Overall, the proposed electrochromatographic solid-phase extraction procedure serves to achieve a *ca.* 10–15-fold increase in sample concentration for cimetidine, while decreasing the occurrence of interfering peaks. Through the use of internal standards, satisfactory analytical results could be obtained. Further, such results were achieved with just a laboratory-built apparatus, and considerably better accuracy and reproducibility are to be expected from the rapidly emerging commercial instruments.

ACKNOWLEDGEMENTS

This work was supported by Grant No. GM24349, from the National Institute of General Medical Sciences, U.S. Department of Health and Human Services, and a grant-in-aid from Dow Chemical Co. One of us (H.S.) has been a recipient of a graduate fellowship from the Academy of Finland.

REFERENCES

1 R. N. Brodgen, R. C. Heel, T. M. Speight and G. S. Avery, *Drugs*, 15 (1978) 93.
2 W. C. Randolph, V. L. Osborne, S. S. Walkenstein and A. P. Intoccia, *J. Pharm. Sci.*, 66 (1977) 1148.
3 G. W. Mihaly, S. Cockbain, D. B. Jones, R. G. Hanson and R. A. Smallwood, *J. Pharm. Sci.*, 71 (1982) 590.
4 J. Fleitman, G. Torosian and J. H. Perrin, *J. Chromatogr.*, 229 (1982) 255.
5 J. A. Apffel, U. A. Th. Brinkman and R. W. Frei, *J. Liq. Chromatogr.*, 5 (1982) 2413.
6 M. Kozma and L. Vereczkey, *J. Chromatogr.*, 273 (1983) 223.
7 J. M. Bartlett and A. B. Segelman, *J. Chromatogr.*, 255 (1983) 239.
8 V. Nitsche and H. Mascher, *J. Chromatogr.*, 273 (1983) 449.
9 Q. Lin, G. L. Lensmeyer and F. C. Larson, *J. Anal. Toxicol.*, 9 (1985) 161.
10 R. Chiou, R. J. Stubbs and W. F. Bayne, *J. Chromatogr.*, 377 (1986) 441.
11 H. A. Strong and M. Spino, *J. Chromatogr.*, 442 (1987) 301.
12 D. H. Newton and R. B. Kluza, *Drug Intell. Clin. Pharm.*, 12 (1978) 549.
13 S. Fujiwara and S. Honda, *Anal. Chem.*, 58 (1986) 1811.
14 D. E. Burton, M. J. Sepaniak and M. P. Maskarinec, *J. Chromatogr. Sci.*, 24 (1986) 347.
15 T. Nakagawa, Y. Oda, A. Shibukawa and H. Tanaka, *Chem. Pharm. Bull.*, 36 (1988) 1622.
16 X. Huang, M. J. Gordon and R. N. Zare, *J. Chromatogr.*, 425 (1988) 385.
17 M. C. Roach, P. Gozel and R. N. Zare, *J. Chromatogr.*, 426 (1988) 129.
18 T. Nakakawa, T. Oda, A. Shibukawa, H. Fukuda and H. Tanaka, *Chem. Pharm. Bull.*, 37 (1989) 707.
19 E. Heftman (Editor), *Chromatography*, Van Nostrand, New York, 3rd ed., 1975.
20 T. Tsuda, K. Nomura and G. Nakagawa, *J. Chromatogr.*, 248 (1982) 241.
21 T. S. Stevens and H. J. Cortes, *Anal. Chem.*, 55 (1983) 1365.
22 T. Tsuda, *Anal. Chem.*, 59 (1987) 521.

23 T. Tsuda, *Anal. Chem.*, 60 (1988) 1677.
24 J. W. Jorgenson and K. Lukacs, *Anal. Chem.*, 53 (1981) 1928.
25 K. C. Van Horne (Editor), *Handbook of Sorbent Extraction Techniques*, Analytichem International, Harbor City, CA, 1985.
26 M. Zief and R. Kiser (Editors), *Solid-Phase Extraction Manual*, J. T. Baker, Phillipsburg, NJ, 1988.
27 A. Nahum and Cs. Horváth, *J. Chromatogr.*, 203 (1981) 53.
28 R. W. Frei and K. Zech (Editors), *Selective Sample Handling and Detection in High-Performance Liquid Chromatography, Part A* (*Journal of Chromatography Library*, Vol. 39A), Elsevier, Amsterdam, 1988. Ch. 2.
29 P. A. Krieger, *High Purity Solvent Guide*, Burdick & Jackson Labs., McGaw Park, IL, 1984.
30 T. J. Bruno and P. D. N. Svoronos (Editors), *CRC Handbook of Basic Tables for Chemical Analysis*, CRC Press, Boca Raton, FL, 1989, p. 89.
31 J. Liu, J. F. Banks and M. Novotny, *J. Microcolumn Sep.*, 1 (1989) 136.

Author Index Vol. 559

Vol. 559

journal of chromatography news section

IN MEMORIAM

In February 1991, the scientific community lost one of its unique individuals when Bob Brownlee, 47-year-old chromatographer/entrepreneur died. For those who knew him, Bob was also a naturalist, philosopher and philanthropist. He was founder of Brownlee Labs (now part of Applied Biosystems), Microphoretic Systems, the Bay Area Chromatography Colloquium, and the Robert Brownlee Foundation for pre-college science education. Bob held more than a dozen patents dealing with analytical instrumentation. He published scientific papers on several topics, including the ecology of monarch butterflies, insect pheromones, chromatography, electrophoresis and detection of viral DNA.

In 1966 Bob graduated from San Jose State University with a B.S. in chemistry. From 1966 to 1969 Bob worked at Stanford Research Institute isolating and identifying natural products, principally insect pheromones. In 1969, he began a short lived career as a graduate student in entomology at SUNY College of Environmental Science and Forestry in Syracuse, New York. Bob then moved to Europe and worked for three years in Italy as a chromatography specialist. This was followed by employment by Hewlett Packard in Waldbronn, Germany. In 1976, with a few thousand dollars, he returned to Italy where he started his own company, Brownlee Labs, specializing in HPLC columns. The next year he returned to California, where he steadily increased the size of his company. Among his innovations were a cartridge system for HPLC columns and a dual syringe, micropump for HPLC and SFC. In 1984 Brownlee Labs merged with Applied Biosystems.

In 1987 he founded Microphoretic Systems where he designed, manufactured and marketed the first fully automated capillary electrophoresis instrument. At both Brownlee Labs and Microphoretic Systems, Bob created a unique, family type environment for his employees. When faced with complicated legal issues and the withdrawal of support from a major financial and marketing partner, his company went bankrupt. Although plagued by ill health, he began to participate and fund research into microclimatic controls upon monarch migration. He was an active participant in the Robert Brownlee Foundation (among the 8 largest endowments in the Silicon Valley) which he funded with proceeds from the sale of Brownlee Labs.

Bob was a visionary whose ideas were often complete elegant solutions to complicated problems. He was an unusual combination of scientist and businessman with an often unconventional, intuitive approach. Bob had many interests outside of science. He loved music, animals, good design, good food and his friends and family. He will be remembered for his generosity, his travel experiences, his deep interest in scientific adventures, his absent-mindedness, and his loyalty to friends.

Franklin Sunzeri, *San Jose, CA, USA*
Herb Schwartz, *Beckman Instruments, Palo Alto, CA, USA*

SHORT CONFERENCE REPORT

HPCE '91, 3rd INTERNATIONAL SYMPOSIUM ON HIGH PERFORMANCE CAPILLARY ELECTROPHORESIS, SAN DIEGO, CA, USA, FEBRUARY 3–6, 1991

It has gradually become a tradition that with the high performance capillary electrophoresis meetings a few pictures of the participants are published. The gang is not subjected to fundamental changes and thus some of the faces inevitably become familiar, even to those who did not participate. To the others, *i.e.* those who were lucky enough to be at the meeting (hopefully) these pictures will remind of the pleasant days. Further these sets of photographs will have a historical value in the future — at least one will be able to watch how the individual professors and students are aging.

Unfortunately this approach is not original. Rembrandt did the same with his selfportraits quite a few years ago.

Fig. 1. A look into the meeting room with Professors Zare and Karger in the front.

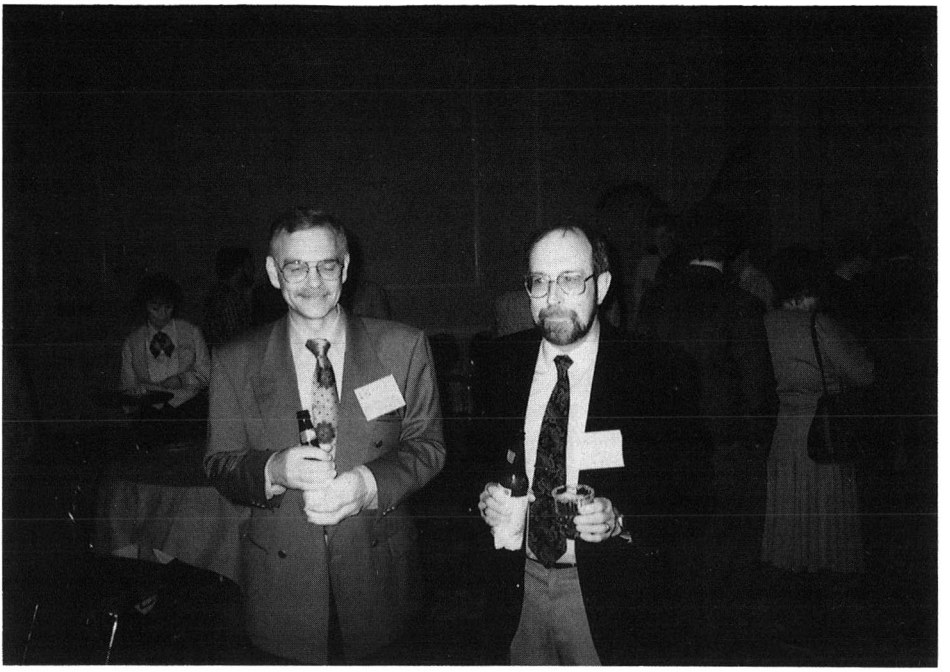

Fig. 2. Dr. Verheggen and Professor Everaerts getting a drink to get all the strength needed for organizing the next HPCE meeting in 1992.

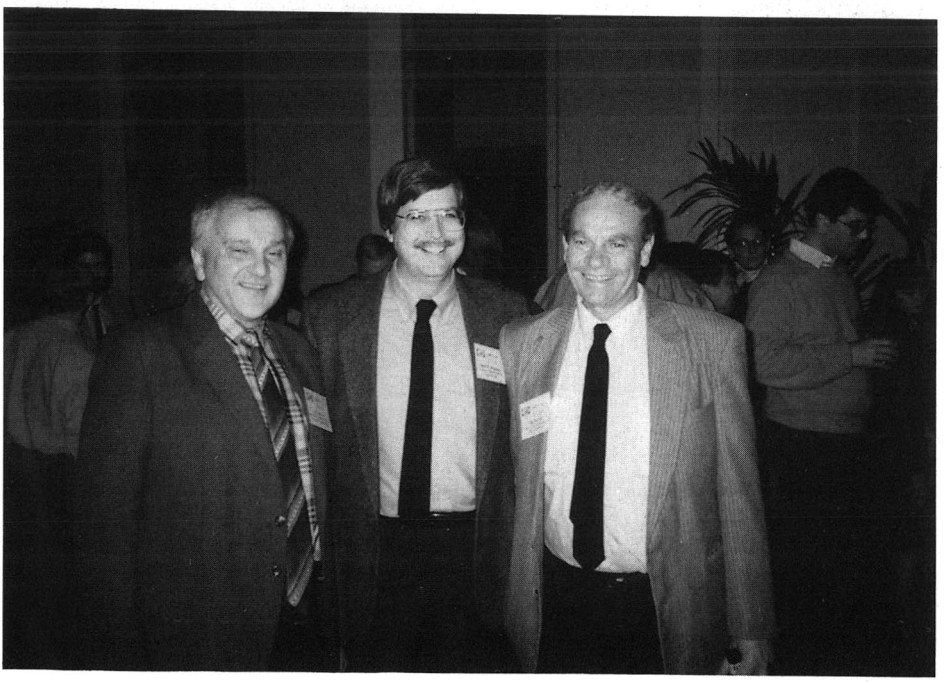

Fig. 3. A group of laughing good guys—from the left: Dr. Bocek, Professor Jorgenson and Professor Jellum.

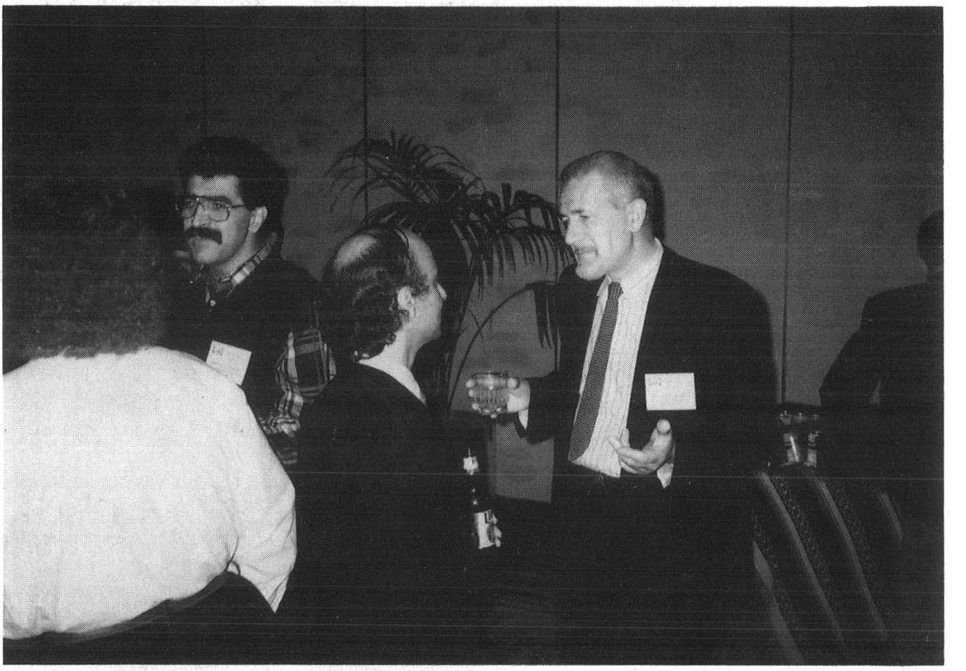

Fig. 4. In depth discussion—Dr. Cohen (left) and Professor Righetti (right).

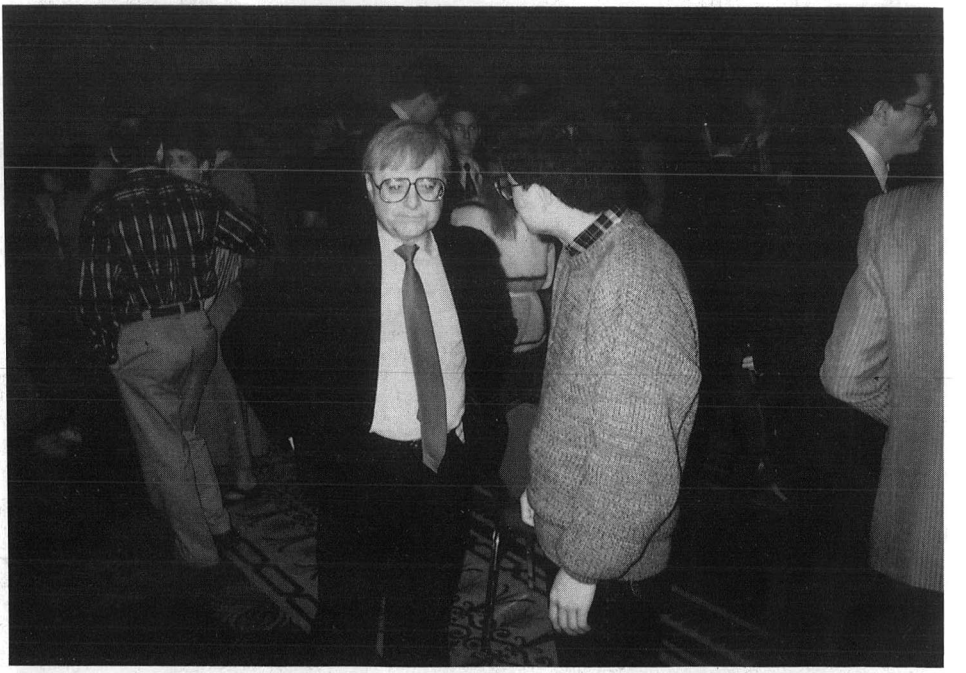

Fig. 5. ... and another one, this time with Professor Regnier in the centre.

PUBLICATION SCHEDULE FOR 1991

Journal of Chromatography and Journal of Chromatography, Biomedical Applications

MONTH	D 1990–M 1991	J	J	A	S	O	N	D
Journal of Chromatography	Vols. 535–545/1	545/2 546/1 + 2 547/1 + 2	548/1 + 2 549/1 + 2 550/1 + 2	552/1 + 2 553/1 + 2 554/1 + 2 555/1 + 2	556/1 + 2 557/1 + 2 558/1	558/2 559/1 + 2		
Cumulative Indexes, Vols. 501–550				551/1 + 2				
Bibliography Section	560/1	560/2			561/1			561/2
Biomedical Applications	Vols. 562–566	567/1	567/2 568/1	568/2	569/1 + 2 570/1	570/2	571/1 + 2	572/1 + 2

The publication schedule for further issues will be published later

INFORMATION FOR AUTHORS

(Detailed *Instructions to Authors* were published in Vol. 558, pp. 469–472. A free reprint can be obtained by application to the publisher, Elsevier Science Publishers B.V., P.O. Box 330, 1000 AH Amsterdam, The Netherlands.)

Types of Contributions. The following types of papers are published in the *Journal of Chromatography* and the section on *Biomedical Applications:* Regular research papers (Full-length papers), Review articles and Short Communications. Short Communications are usually descriptions of short investigations, or they can report minor technical improvements of previously published procedures; they reflect the same quality of research as Full-length papers, but should preferably not exceed six printed pages. For Review articles, see inside front cover under Submission of Papers.

Submission. Every paper must be accompanied by a letter from the senior author, stating that he/she is submitting the paper for publication in the *Journal of Chromatography*.

Manuscripts. Manuscripts should be typed in double spacing on consecutively numbered pages of uniform size. The manuscript should be preceded by a sheet of manuscript paper carrying the title of the paper and the name and full postal address of the person to whom the proofs are to be sent. As a rule, papers should be divided into sections, headed by a caption (*e.g.*, Abstract, Introduction, Experimental, Results, Discussion, etc.). All illustrations, photographs, tables, etc., should be on separate sheets.

Introduction. Every paper must have a concise introduction mentioning what has been done before on the topic described, and stating clearly what is new in the paper now submitted.

Abstract. All articles should have an abstract of 50–100 words which clearly and briefly indicates what is new, different and significant.

Illustrations. The figures should be submitted in a form suitable for reproduction, drawn in Indian ink on drawing or tracing paper. Each illustration should have a legend, all the *legends* being typed (with double spacing) together on a *separate sheet*. If structures are given in the text, the original drawings should be supplied. Coloured illustrations are reproduced at the author's expense, the cost being determined by the number of pages and by the number of colours needed. The written permission of the author and publisher must be obtained for the use of any figure already published. Its source must be indicated in the legend.

References. References should be numbered in the order in which they are cited in the text, and listed in numerical sequence on a separate sheet at the end of the article. Please check a recent issue for the layout of the reference list. Abbreviations for the titles of journals should follow the system used by *Chemical Abstracts*. Articles not yet published should be given as "in press" (journal should be specified), "submitted for publication" (journal should be specified), "in preparation" or "personal communication".

Dispatch. Before sending the manuscript to the Editor please check that the envelope contains four copies of the paper complete with references, legends and figures. One of the sets of figures must be the originals suitable for direct reproduction. Please also ensure that permission to publish has been obtained from your institute.

Proofs. One set of proofs will be sent to the author to be carefully checked for printer's errors. Corrections must be restricted to instances in which the proof is at variance with the manuscript. "Extra corrections" will be inserted at the author's expense.

Reprints. Fifty reprints of Full-length papers and Short Communications will be supplied free of charge. Additional reprints can be ordered by the authors. An order form containing price quotations will be sent to the authors together with the proofs of their article.

Advertisements. Advertisement rates are available from the publisher on request. The Editors of the journal accept no responsibility for the contents of the advertisements.

There's more to our CE autosampler than automation.

On the new Model 270A-HT High Throughput Capillary Electrophoresis System, a unique sample cooling system minimizes sample degradation. Our special design eliminates evaporation. Ion replenishment can be fully automated with the multiple buffer system. The software makes it easy to custom-tailor analysis parameters to each sample...Whether you need unattended overnight operation on 50 samples or just a few, optimal performance is ensured. The Model 270A-HT High Throughput Capillary Electrophoresis System. Higher sensitivity, greater reliability and more performance than ever. Contact Applied Biosystems today.

Applied Biosystems

oster City, U.S. Tel: (415) 570-6667. Telex: 470052 APBIO UI. Fax: (415) 572-2743.
ississauga, Ca Tel: (416) 821-8183. Fax: (416) 821-8246.
arrington, U 0925-825650. Telex: 62'611 APBIO G. Fax: 0925-828196.
eiterstadt, C Tel: 06151-87940. Telex: 4197318 Z ABI D. Fax: 06151-84899.
aris, France '8 65 24 44. Telex: 230458 ABIF. Fax: (1) 48 63 22 82.
ilan, Italy. 9404561. Fax: (0)2 8321655.
aarssen, Th ands. Tel: (0) 3465-74868. Telex: 70896. Fax: (0) 3465-74904.
urwood, Au el: (03) 808-7777. Fax: (03) 887-1469.
okyo, Japan. 699-0700. Fax: (03) 699-0733.